1122-21

14c

JOURNAL OF
COLLOID SCIENCE

Editor-in-Chief
Victor K. La Mer, Columbia University, New York

Advisory Board

C. O. Beckmann
K. F. Bonhoeffer
J. A. Christiansen
M. L. Corrin
P. J. W. Debye
John T. Edsall
I. Fankuchen
John D. Ferry
Wilfried Heller
John G. Kirkwood
E. C. Lingafelter
L. G. Longsworth
S. G. Mason
J. Th. G. Overbeek
R. Ruyssen
E. K. Rideal
William Seifriz
Leo Shedlovsky
Theodore Shedlovsky
Robert Simha
R. H. Smellie
Jacinto Steinhardt
The Svedberg
Hugh S. Taylor
Arne Tiselius
Robert D. Vold
Bernard Vonnegut
Ralph W. G. Wyckoff
Bruno H. Zimm

VOLUME 10
1955

ACADEMIC PRESS INC.—PUBLISHERS
NEW YORK, N. Y.

DYNAMIC MECHANICAL PROPERTIES OF PLASTICIZED POLYVINYL ACETATE[1]

Malcolm L. Williams[2] and John D. Ferry

Department of Chemistry, University of Wisconsin, Madison, Wisconsin

Received October 18, 1954

Introduction

Although numerous studies of the dynamic mechanical properties of concentrated polymer solutions have been described, very few have extended to high enough frequencies or low enough temperatures to encompass the transition (as a function of frequency) from soft and rubberlike to glass-like consistency (1). Such measurements are reported here for a 50% solution (by volume) of polyvinyl acetate in tri-*m*-cresyl phosphate. The same polymer sample has been extensively studied in the undiluted state (2), as well as in solution under conditions corresponding to the plateau and terminal regions of the relaxation spectrum (3–5). To correlate the latter with the new measurements in the transition region, the steady-flow viscosity of the 50% solution in tri-*m*-cresyl phosphate has also been determined.

Materials and Methods

The polyvinyl acetate was an unfractionated sample of grade AYAX, lot 1232, furnished through the kindness of Mr. A. K. Doolittle of Carbide and Carbon Chemicals Company. Its properties have been described in the preceding paper (2) and elsewhere (3–5). The tri-*m*-cresyl phosphate was practical grade, from the Eastman Kodak Company. The solution (50% by volume, calculated 50.5% by weight) was mixed in an arrangement designed by Mr. D. J. Plazek; a flask containing a Teflon-covered piece of magnetized iron imbedded in the mixture was very slowly rotated between the poles of a powerful magnet, while warmed to approximately 60°C. by an infrared lamp.

Steady-flow viscosities were measured by the falling-cylinder apparatus of Fox and Flory (6) as modified in this laboratory (7). Measurements of

---

[1] Part XVII of a series on Mechanical Properties of Substances of High Molecular Weight.

[2] Union Carbide and Carbon Fellow in Physical Chemistry, 1952–1954.

TABLE I

Steady-Flow Viscosities

Temp., °C.	Log η
−0.5	10.14
7	9.41
17	8.39
25	7.77
34	7.02
41	6.49

the complex shear compliance ($J^* = J' - iJ''$) were made with the double transducer of Fitzgerald and Ferry (8), as modified by Fitzgerald (9).

STEADY-FLOW VISCOSITIES

Logarithms of the steady-flow viscosity at six temperatures are given in Table I. These values, plotted against $1/T^2$, where T is the absolute temperature, gave a straight line, thus conforming to the relationship previously found empirically for undiluted polyisobutylene (6); the slope was 1.1×10^6 deg.², about twice that for polyisobutylene (6, 9). The viscosity of the solvent at 25°C. was 0.57 poise[3]; thus the logarithm of the relative viscosity of the polymer solution at this temperature was 8.02. This fits in reasonably with values at lower concentrations in different solvents (10), on the basis that the relative viscosity is approximately a function of volume concentration alone.

DYNAMIC MEASUREMENTS

For the transducer measurements, three pairs of disc-shaped samples were employed. Samples 42 had dimensions of $^{11}/_{16}$ in. (diameter) by $^{1}/_{32}$ in. (thickness) and, after compression, a sample coefficient (8) of 67.5 cm. at 25°C. Samples 40, $^{11}/_{16}$ in. by $^{3}/_{32}$ in., had a nominal coefficient of 20.1, and samples 41, $^{11}/_{32}$ in. by $^{3}/_{16}$ in., a nominal coefficient of 3.19, both at 25°C.

Check runs following any temperature sequence below 30°C. agreed well with initial measurements; but after samples 42 had been taken to higher temperatures, check runs at 25°C. gave values of J' and J'' about 10% lower than the original. Since the J''/J' ratios were unchanged, this deviation was attributed to sag, and the data reported for 35.1°C. and 40.0°C. may therefore be somewhat less precise than at the other temperatures.

The nominal sample coefficients for 40 and 41 were adjusted by empirical corrections of +11% and −7.7%, respectively, to bring the values of J' and J'' into coincidence with those for samples 42; in the former case the deviation was attributed to sag during mounting of the samples, and in the latter to bulging.

---

[3] We are indebted to Mr. Donald M. Stern for this value.

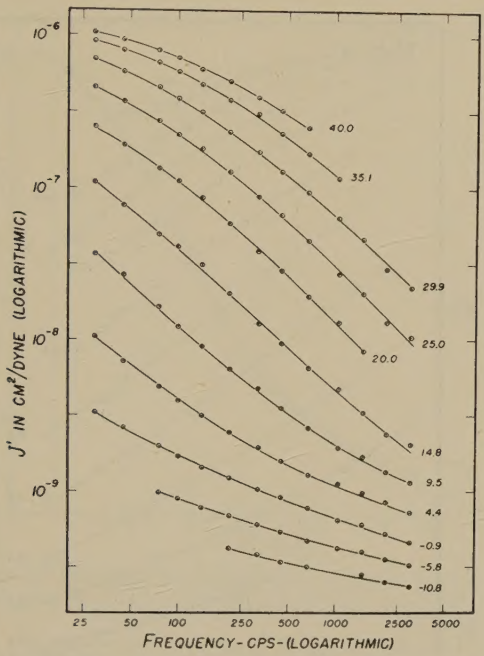

FIG. 1. Variation of the real part of the dynamic shear compliance, J', with frequency for polyvinyl acetate plasticized by tri-*m*-cresyl phosphate (50% by volume) at eleven temperatures as indicated.

Sample coefficients at temperatures other than 25°C. were calculated, as usual, on the assumption that the sample thickness remained constant. The thermal expansion was calculated from measurements of density (ρ), which could be approximated by the equation $\rho = 1.183 - 0.86 \times 10^{-3} (t - 25)$, where t is Centigrade temperature.

Values of J' and J'' at eleven temperatures from -11°C. to 40°C. are shown as double logarithmic plots against frequency (from 30 to 4500 cycles per second) in Figs. 1 and 2. Where data on different samples were taken at the same frequencies and temperatures, the values have been averaged. Complete numerical data are recorded elsewhere (11). Over this range of temperatures and frequencies, J' varies from $10^{-6.0}$ to $10^{-9.6}$, and J'' from $10^{-6.3}$ to $10^{-10.0}$.

For application of the method of reduced variables, the usual double logarithmic plots of J'_p and J''_p were prepared (2, 9), using 298°K. as the reference temperature, with J_∞ estimated as 1.5×10^{-10} cm.²/dyne. Values of log a_T, the reduction factor expressing the change of all retardation times with temperature, obtained from J'_p and J''_p were in good agreement; they are listed in Table II.

Values of J'_p and J''_p plotted against ωa_T (where ω is the circular fre-

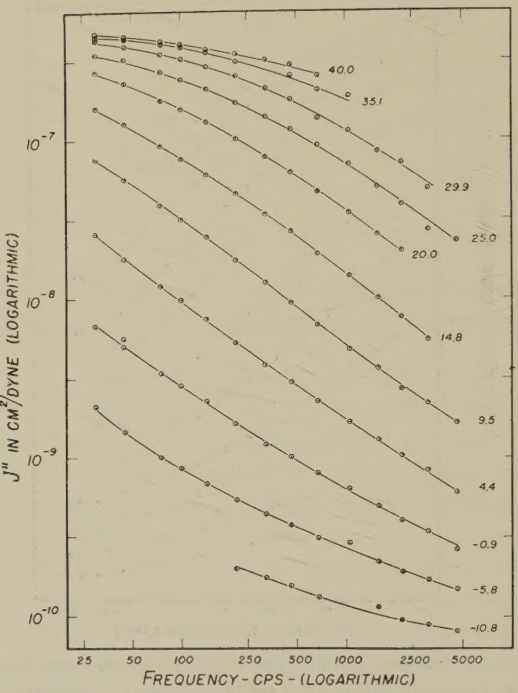

FIG. 2. Variation of the imaginary part of the dynamic shear compliance, J'', with frequency for polyvinyl acetate plasticized by tri-*m*-cresyl phosphate at eleven temperatures as indicated.

TABLE II

Reduction Factors

Temp., °C.	Log a_T	Temp., °C.	Log a_T
−10.8	4.54	20.0	0.42
−5.8	3.57	25.0	0.00
−0.9	2.80	29.9	−0.35
4.4	2.10	35.1	−0.65
9.5	1.48	40.0	−0.90
14.8	0.93		

quency), with double logarithmic scales, are shown in Figs. 3 and 4. Data at all temperatures and frequencies superpose to give composite curves representing J' and J'' at 25°C. from $10^{1.4}$ to $10^{9.1}$ sec.$^{-1}$. From these curves, G' and G'', the components of the complex rigidity, and η', the real part of the complex viscosity, have been calculated; they are shown in Fig. 5, again using double logarithmic scales, at the standard temperature of 25°C.

The shapes of all these curves are rather similar to those previously given for the undiluted polymer (2). However, the loss tangent $J''/J' = G''/G'$,

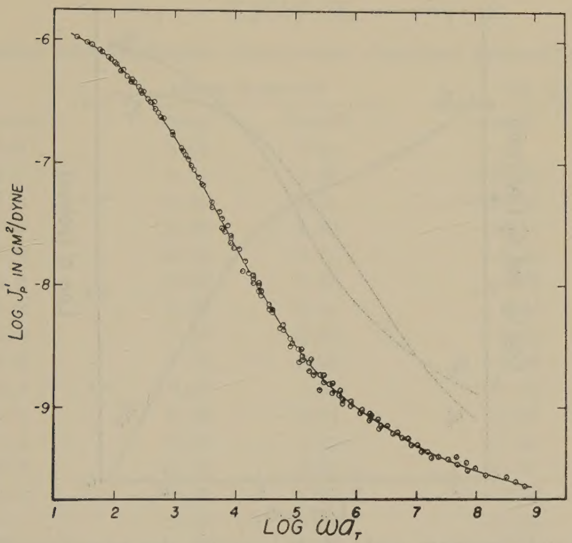

FIG. 3. Real part of the complex compliance reduced to 25°C., plotted logarithmically against reduced frequency. Temperature key same as in Figs. 1 and 2.

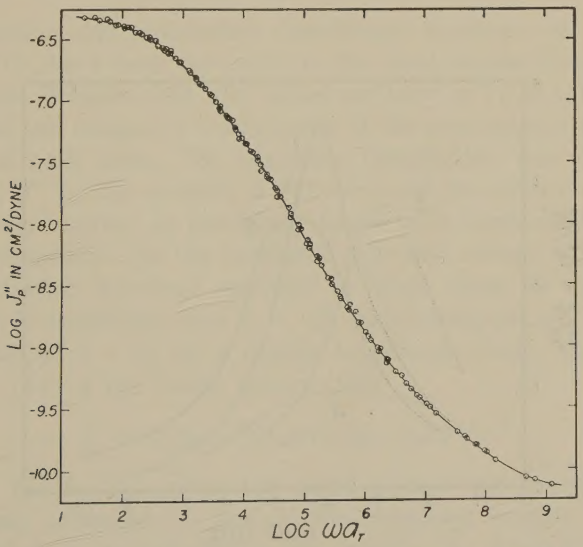

FIG. 4. Imaginary part of the complex compliance reduced to 25°C., plotted logarithmically against reduced frequency. Temperature key same as in Figs. 1 and 2.

in which small differences are more obvious, shows a somewhat broader and lower maximum in the plasticized polymer; a similar and more marked broadening by diluent is shown also in comparing polystyrene with a 62% solution of the latter in decalin (Fig. 6).

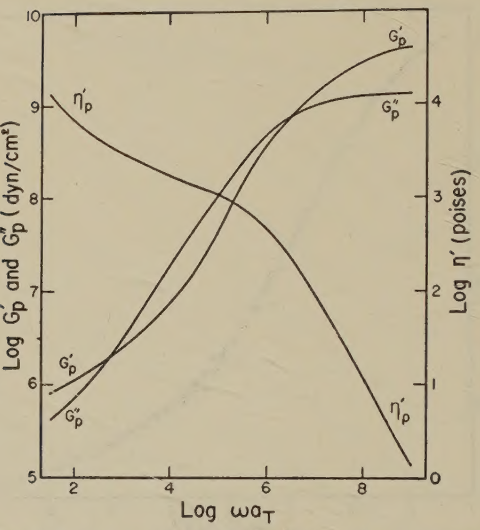

FIG. 5. Real and imaginary parts of the complex shear modulus, G' and G'', and the real part of the complex viscosity, η', reduced to 25°C., plotted logarithmically against reduced frequency.

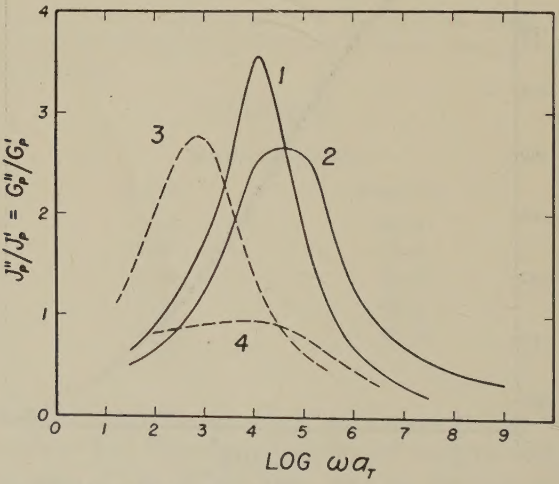

FIG. 6. Loss tangents ($J''/J' = G''/G'$), plotted logarithmically against reduced frequency for (1) polyvinyl acetate, reduced to 75°C., (2) 50% (by volume) solution of polyvinyl acetate in tri-*m*-cresyl phosphate, reduced to 25°C., (3) polystyrene, reduced to 125°C., and (4) 62% solution (by weight) of polystyrene in decalin, reduced to 25°C.

TABLE III

Relaxation and Retardation Distribution Functions Reduced to 25°C.

	Log Φ_p (dyne/cm.^{2})		Log L_p (cm.^{2}/dyne)	
Log τ_p (sec.)	From G'	From G''	From J'	From J''
−9.0	8.61	8.94	—	−10.31
−8.5	8.74	8.93	−10.45	−10.28
−8.0	8.80	8.91	−10.33	−10.15
−7.5	8.80	8.89	−10.17	−9.98
−7.0	8.81	8.78	−9.94	−9.80
−6.5	8.60	8.65	−9.70	−9.59
−6.0	8.32	8.44	−9.46	−9.37
−5.5	7.96	8.06	−9.26	−9.10
−5.0	7.43	7.50	−8.89	−8.78
−4.5	6.84	7.05	−8.39	−8.45
−4.0	6.45	6.64	−7.91	−7.87
−3.5	6.17	6.26	−7.38	−7.41
−3.0	5.91	5.97	−6.97	−7.01
−2.5	5.69	5.67	−6.67	−6.74
−2.0	5.42	5.46	−6.53	−6.52
−1.5	5.20	5.27	−6.55	−6.52

DISTRIBUTION FUNCTIONS

The relaxation and retardation distribution functions, Φ_p and L_p, reduced to 25°C., have been calculated in the usual manner from our second approximation formulas (12), and values are listed in Table III. The values from the real and imaginary components of the measurements are in good agreement in both cases. The relaxation distribution was also obtained from G' and G'' by the method of Schwarzl and Staverman (13); the results were very similar, as previously found in a comparison of the two methods of calculation for the undiluted polyvinyl acetate (2).

The distribution functions resemble in shape those for the undiluted polymer (2); in particular, near $\Phi = 10^6$ both relaxation spectra have the theoretical slope of $-\frac{1}{2}$ on a double logarithmic scale, specified by a modification (14) of the Rouse theory (15):

$$\Phi = (1/2\pi\sqrt{6})(a\rho N_0/M_0)(\zeta_0 kT)^{\frac{1}{2}}\tau^{-\frac{1}{2}}$$

where $a = (\overline{r_0^2}M_0/M)^{\frac{1}{2}}$, $\overline{r_0^2}$ is the mean square end-to-end separation of the polymer molecule, M_0 and M the molecular weights of monomer unit and polymer, respectively, ρ the density, N_0 Avogadro's number, ζ_0 the monomeric friction coefficient, and k Boltzmann's constant. For a solution, ρ is replaced by c, the concentration in g./ml. The effect of plasticization on the friction coefficient can thus be calculated, if the spectra for both undiluted and plasticized systems are reduced to a common temperature.

For the undiluted polymer, the mechanical measurements do not ex-

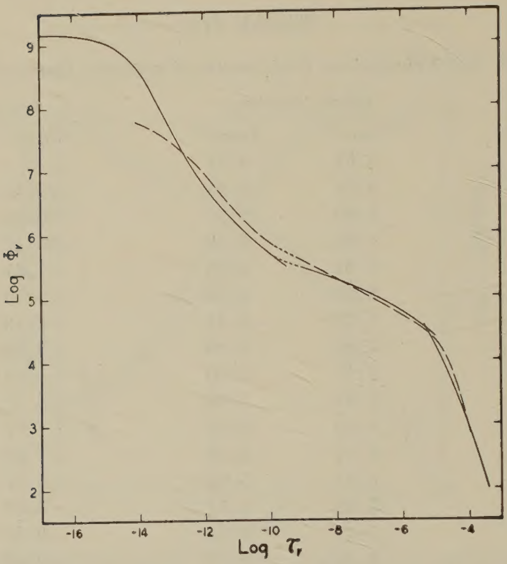

FIG. 7. Distribution function of mechanical relaxation times (Φ_r) reduced to unit density and unit steady-flow viscosity at 25°C. Solid curve: left of short dashes, polyvinyl acetate in tri-*m*-cresyl phosphate; right of short dashes, polyvinyl acetate in trichloropropane. Dashed curve: polystyrene in decalin. Short dashes indicate no experimental measurements in this region.

tend below 50°C., but the electrical reduction factor b_T is available at lower temperatures, permitting comparison of the two systems at 40°C.; the identity of a_T and b_T at higher temperatures (2) justifies this procedure. From the data of the preceding paper (2), Δ log a_T for the interval from 75°C. to 40°C. for the undiluted polymer is 4.85, whereas from Table II for the 50% solution it is -0.90 for the interval from 25°C. to 40°C. The value of a should be close to that of the polymer in a Θ-solvent (16), which from the data of Shultz (17) is estimated to be 2.8 A. for polyvinyl acetate. By interpolating values of τ for Φ/ρ and $\Phi/c = 10^6$, we find log ζ_0 (in dyne sec./cm.) at 40°C. to be 2.53 for the undiluted polymer and -4.47 for the 50% solution. Thus the introduction of the diluent diminishes the monomeric friction coefficient by a factor of about 10^7.

To correlate the transition zone of the relaxation spectrum in Table III with the plateau and terminal zones previously studied in concentrated solutions (in 1,2,3-trichloropropane), the former must be reduced to a reference state of unit viscosity and concentration, using the relations $\Phi_r = \Phi_p/c$ and $\tau_r = \tau_p c/\eta$, where η is the steady-flow viscosity at 25°C. The function thus reduced is plotted in Fig. 7; it fits in quite well with the plateau (3, 4) and terminal (5) zones, which are also shown. The

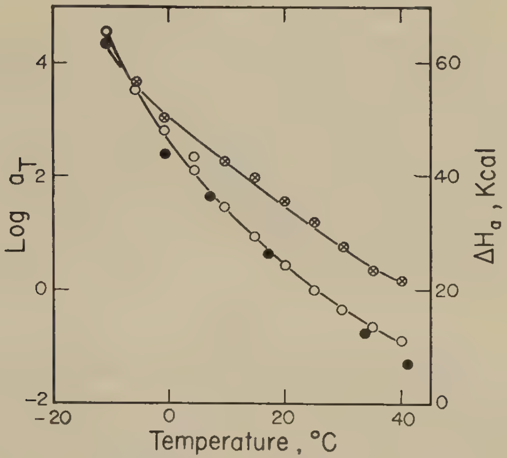

FIG. 8. Logarithm of reduction factor a_T and apparent energy of activation ΔH_a plotted against temperature. Key to points: open circles, log a_T from dynamic measurements; solid circles, log a_T from steady-flow viscosity; crossed circles, ΔH_a.

minimum numerical slope of the log-log plot in the plateau region is 0.15; as in solutions of other vinyl polymers of similar molecular weight, the plateau is not horizontal. The whole composite function is very similar to that previously found for concentrated polystyrene solutions (1), shown as a dashed curve. These two polymer samples are of closely similar weight-average molecular weight (polyvinyl acetate 420,000, polystyrene 370,000) and are fairly similar in number-average (140,000 and 197,000, respectively); the close coincidence of their relaxation spectra when reduced to standard reference states is further support for the view that the mechanical behavior of such polymers depends almost entirely on the backbone structure and not on the nature of the side chains.

TEMPERATURE DEPENDENCE OF MECHANICAL PROPERTIES

According to the method of reduced variables, the reduction factor a_T should be obtainable not only from empirical shifts of the dynamic data but also from the temperature dependence of $\eta; a_T = \eta T_0 c_0/\eta_0 T c$, where η and c refer to the temperature of measurement and η_0 and c_0 to the reference temperature (here 25°C.). Values of a_T from both sources are plotted in Fig. 8; they agree quite well, although those from viscosity change somewhat less rapidly with temperature.

The apparent activation energy for relaxation processes, $\Delta H_a = R d\ln a_T/d(1/T)$, is also plotted in Fig. 8, and shows the usual rapid increase with decreasing temperature. Interrelation of such curves for different polymer systems will be discussed in a future communication.

ACKNOWLEDGMENTS

This work was part of a program of research on the physical structure and properties of cellulose derivatives and other polymers supported by the Allegany Ballistics Laboratory, Cumberland, Maryland, an establishment owned by the United States Navy and operated by the Hercules Powder Company under Contract NOrd 10431. It was also supported in part by a grant from Research Corporation and by the Research Committee of the Graduate School of the University of Wisconsin from funds supplied by the Wisconsin Alumni Research Foundation. The fellowship in Physical Chemistry given by Union Carbide and Carbon Corporation is gratefully acknowledged. We are much indebted to Mrs. J. C. Alexander for assistance in calculations.

SUMMARY

The real and imaginary components of the complex compliance have been measured between 30 and 4500 cycles per second in the temperature range −11°C. to 40°C. for a 50% (by volume) solution of polyvinyl acetate in tri-*m*-cresyl phosphate. Results at all temperatures and frequencies superpose by the method of reduced variables to give the components at 25°C. over 7.5 decades of frequency, corresponding to the transition from rubberlike to glasslike consistency at this temperature. Values of the steady-flow viscosity have been measured between 0° and 41°C. and found to give nearly the same temperature reduction factors as found empirically from the dynamic measurements. Relaxation and retardation distribution functions have been calculated. By reducing these data to a common temperature for both plasticized and undiluted polymer, it is concluded that the presence of 50% diluent reduces the monomeric friction coefficient by a factor of 10^7. By reducing the data to a hypothetical reference state of unit density and unit steady-flow viscosity and combining them with previous data on solutions of the same polymer in 1,2,3-trichloropropane, the distribution function of mechanical relaxation times can be obtained at 25°C. over 13.5 decades of time. The distribution function is found to be similar in shape and location on the time scale to that obtained for polystyrene in decalin previously studied in this laboratory.

REFERENCES

1. GRANDINE, L. D., JR., AND FERRY, J. D., *J. Appl. Phys.* **24,** 679 (1953).
2. WILLIAMS, M. L., AND FERRY, J. D., *J. Colloid Sci.* **9,** 479 (1954).
3. SAWYER, W. M., AND FERRY, J. D., *J. Am. Chem. Soc.* **72,** 5030 (1950).
4. FERRY, J. D., SAWYER, W. M., BROWNING, G. V., AND GROTH, A. H., JR., *J. Appl. Phys.* **21,** 513 (1950).
5. FERRY, J. D., WILLIAMS, M. L., AND STERN, D. M., *J. Phys. Chem.* **58,** 987 (1954).
6. FOX, T. G., AND FLORY, P. J., *J. Am. Chem. Soc.* **70,** 2384 (1948).
7. FERRY, J. D., GRANDINE, L. D., JR., AND UDY, D. C., *J. Colloid Sci.* **8,** 529 (1953).
8. FITZGERALD, E. R., AND FERRY, J. D., *J. Colloid Sci.* **8,** 1 (1953).
9. FERRY, J. D., GRANDINE, L. D., JR., AND FITZGERALD, E. R., *J. Appl. Phys.* **24,** 911 (1953).

10. Ferry, J. D., Foster, E. L., Browning, G. V., and Sawyer, W. M., *J. Colloid Sci.* **6,** 377 (1951).
11. Williams, M. L., Ph.D. Thesis, University of Wisconsin, Madison, 1954.
12. Williams, M. L., and Ferry, J. D., *J. Polymer Sci.* **11,** 169 (1953).
13. Schwarzl, F., and Staverman, A. J., *Appl. Sci. Research* **A4,** 127 (1953).
14. Ferry, J. D., Landel, R. F., and Williams, M. L., *J. Appl. Phys.* (in press).
15. Rouse, P. E., Jr., *J. Chem. Phys.* **21,** 1272 (1953).
16. Flory, P. J., *J. Chem. Phys.* **17,** 303 (1949).
17. Shultz, A. R., *J. Am. Chem. Soc.* **76,** 3422 (1954).

A COMPARISON PHOTOMETER TO MEASURE LIGHT SCATTERING OF AEROSOLS AND GASES, USING THE LATTER AS LIGHT-SCATTERING STANDARDS

Frank T. Gucker, Jr., and Axel H. Peterson[1]

Contribution No. 662 from the Chemical Laboratory of Indiana University, Bloomington, Indiana

Received August 21, 1952; revised October 20, 1954

Abstract

This article describes the design and operation of an extremely sensitive instrument for automatic measurement of light scattered from aerosols and gas molecules. The lower limit of measurement with aerosols is determined by the scattering from the air molecules in which the particles are dispersed. The scattered light and a suitably attenuated portion of the direct light fall successively upon a photomultiplier tube, the anode current of which passes through a high resistor to give an *IR* drop which is measured in a comparison voltmeter. The high-voltage supply of the photomultiplier is adjusted to give a constant *IR* drop with the attenuated direct light on the photomultiplier, so as to compensate for changes in the photomultiplier sensitivity and largely offset changes in the lamp brightness. If the scattering due to the air is maintained constant, the lower limit of measurement can be reduced to the background noise, which is about 1.5% of the air scattering. This corresponds to the light scattered by a sample containing about 3×10^{-11} g./l. of a dioctyl phthalate aerosol of 0.3μ diameter.

Since the instrument is sensitive to the molecular scattering due to gases, they may provide a convenient scattering standard for aerosol measurements, which can then be expressed as the ratio of the light scattering of the aerosol to that of the standard gas. Since gases vary widely in their light-scattering ability, such measurements also would find application in gas analysis.

Introduction

Several years ago the senior author, Hugh B. Pickard, and Chester T. O'Konski described a photoelectric instrument for comparing the concentrations of very dilute aerosols (1), sensitive to 10^{-9} g./l. of dioctyl phthalate smoke of 0.3 μ diameter. Since that time, the photomultiplier tube has proved superior to the vacuum phototube in the measurement of extremely low light levels, and the present work was undertaken in order to develop an instrument of improved sensitivity, suitable for measuring and controlling the concentration of dilute aerosols. The availability of improved photomultiplier tubes and their use at low current levels enabled

---

[1] Present address: Mellon Institute, Pittsburgh 13, Pennsylvania.

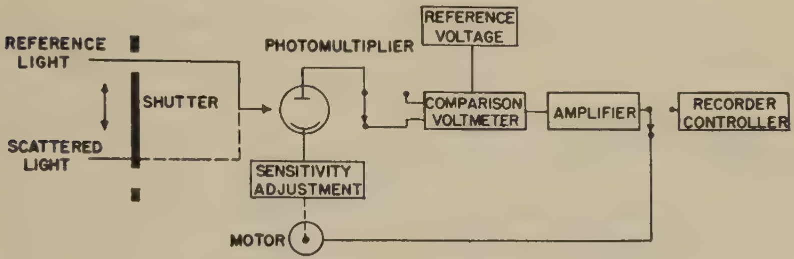

FIG. 1. Block diagram of instrumental operation.

us to achieve this objective through a fairly simple resistance-matching circuit connected to a standard industrial recording controller. The resulting apparatus is considerably more sensitive than the previous instrument and is suitable for continuous automatic measurement as well as control. It responds to the light scattered by gases as well as by aerosol particles, and the former may serve as convenient scattering standards for aerosol measurement

APPARATUS

Figure 1 shows a block diagram of the instrument. It operates on the principle of comparing light scattered from the aerosol with reference light which is an attenuated portion of the beam illuminating the aerosol. The two light beams fall successively upon the photomultiplier tube. Its anode current, passing through a suitable high resistor, produces an IR drop which is balanced against a reference voltage by means of a comparison voltmeter. This comparison of scattered and reference light, if made frequently enough, compensates for any change in the sensitivity of the photomultiplier tube and amplifier system, and largely compensates for small changes in the brightness of the lamp.

In the apparatus, the two light beams are focused alternately on the same portion of the photomultiplier cathode. In the standardizing part of the cycle, the shutter and switches are both in the *down* position shown, the reference light falls on the photomultiplier tube, its output is connected to the comparison voltmeter through a suitable anode resistor, and the amplifier output is connected to a motor which controls the sensitivity adjustment. The standardizing process consists in matching the reference voltage, 6 v. in this instrument, with that developed by the photomultiplier current passing through the anode resistor. Any difference in voltage appears at the output of the comparison voltmeter and passes through the amplifier to a reversible motor connected to the sensitivity adjustment, a rheostat which controls the high voltage supplied to the photomultiplier tube. The balancing takes place in 2 seconds, after which the cycle-control motor (not shown) automatically turns the shutter to allow the scattered

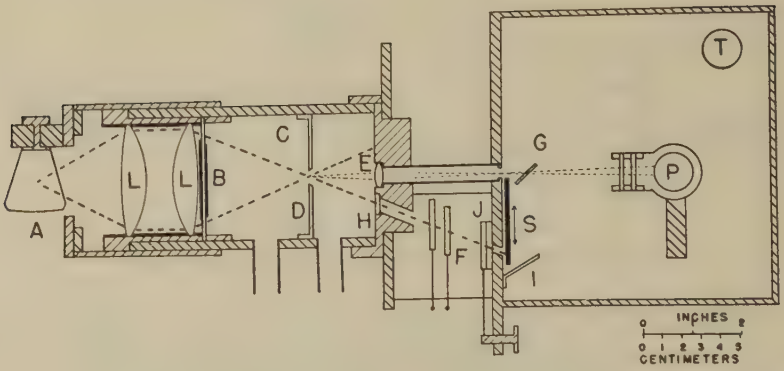

Fig. 2. Smoke cell and optical system of photometer.

light to fall upon the photomultiplier tube for 58 seconds. At the same time relays (also not shown) switch the photomultiplier to the upper input connection of the comparison voltmeter, and the amplifier output to the recorder-controller. This either records the voltage unbalance due to the scattered light or operates a controller to change the mass concentration of the aerosol generator and thus reduce this unbalance to zero.

Optical and Mechanical System

Figure 2 shows the optical and mechanical system. The dark-field illumination is similar to that devised in 1941 by Victor K. La Mer, David Sinclair, and S. Hochberg (2), and used by the senior author, Chester T. O'Konski, Hugh B. Pickard, and James N. Pitts, Jr., in their photoelectronic counter for colloidal particles (3, 4). The light source *A* is a 50 cp. automobile headlight. The pair of aspheric condenser lenses *L L*, each with a focal length of about 5.7 cm. and a diameter of 6.35 cm., brings the light to a focus at the diaphragm *D* in cell *C*. The glass plate *B* has a central disc of black paper on each side which throws a conical shadow slightly larger than the viewing lens *E*. This lens collects the light scattered between about 15° and 30° of the forward direction from a small volume in the aperture of *D*, and brings it to a focus in the plane of the stop at the right end of the tube contaning *E*.[2] When the shutter *S* is in the position shown, the light passes through a piece of plane glass *G* and falls on the photomultiplier *P*, mounted in a box containing also the amplifier tube *T* and its associated circuits.

A small fraction of the direct light passes through the glass window *H* and filters F. If the shutter S is moved up from the position shown, the scattered light is cut off and the reference light is reflected from the mirror I and falls upon G, where a small percentage of it is reflected onto the same part of the cathode of the photomultiplier P struck by the scattered light. The proper optical attenuation of the direct light is obtained with the two neutral filters F which can be slid into the beam to give attenuation factors of approximately 10, 100, and 1000, and two polarizing discs J, one of which can be rotated over a graduated scale for continuous interpolation.

---

[2] Since this work was done, a superior dark-field illuminating system has been described by Frank T. Gucker, Jr., and Donald G. Rose (5), in which the dark stop is placed in front of the first condensing lens and its image focused in the plane of the collecting lens *E*. The size of this image may be brought so close to that of the entrance pupil of *E* that light can be collected within 1° of the forward angle.

The combination of tungsten lamp and 1P21 photomultiplier tube with an S-4 photosurface gives a bell-shaped spectral response curve lying between 3000 and 7000 A, and having a maximum at 5100 A.

Electronic System

This system was designed to overcome instabilities associated with the photomultiplier tube, its high-voltage supply, the lamp and its voltage supply, and the amplifier. Since the errors associated with some of these components can be very high if uncompensated, the design of the circuit was based on a detailed study of the different components, and we will describe briefly some of their characteristics which are of general importance in connection with this and other similar circuits.

Photomultiplier. This tube can deliver up to 1000 μa., but an output of 20 μa. may fall off as much as 30% per hour owing to aging. Our experience with five selected 931A tubes and two 1P21 tubes showed that stability of the order of 0.1% per hour is possible with an anode current of 0.1 μa. or less. Since the characteristics of these tubes vary widely, each one should be checked before it is incorporated into the circuit. The dark current should not exceed a few thousandths of a microampere, and the sensitivity should be comparable with that of other good tubes.

High-Voltage Supply. Since the photomultiplier output varies approximately as the fifth power of the voltage applied to the tube, a well-regulated voltage supply is essential. Most high-voltage supplies depend upon gaseous voltage-regulator tubes. We have found that these tubes may hold the voltage constant to 0.01% for a period of hours; more frequently they are responsible for erratic jumps of several tenths of a per cent, and they change as much as 1% during a 1-hour warm-up period. While selected tubes will give better performance, high-voltage dry batteries supplying very low currents are preferable as reference elements. These also must be selected, since some are erratic, but in general they fluctuate less than the voltage-regulator tubes. Many batteries have been found to give a voltage constant to within 0.001% or less per hour at constant temperature, with a noise level less than one part in 10^7, as measured with this apparatus under suitable conditions. High-voltage batteries should be chosen to have a noise level of less than 10 p.p.m. Small mercury batteries have given excellent results.

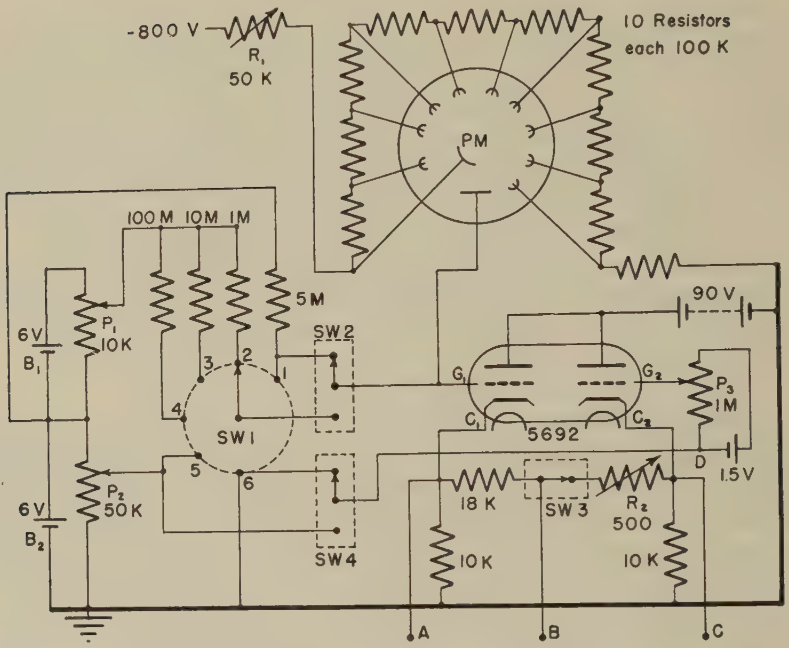

FIG. 3. Electronic circuit of comparison voltmeter.

Lamp Voltage Supply. The 50-cp. automobile headlight requires 6 amp. at 6 v. When connected to a 100–amp.-hr. storage battery, the voltage of which decreased 0.5% per hour, the light of the lamp decreased 2.5% per hour. In general, the light intensity changes five times as much as the voltage applied to the lamp. The peak-to-peak noise level of the battery voltage was 0.01%, and that of the lamp was 0.05%. When the lamp was operated from a rectifier connected through a stepdown transformer to a Sorensen Model 2000 A.C. (electronic) Voltage Regulator, its voltage drifted less than 0.1% over a period of a week, with a peak-to-peak voltage noise level of 0.05%. This noise probably could be reduced considerably by "floating" a battery in parallel with the rectifier, to act as a filter.

Comparison Voltmeter. The d.-c. circuit shown in Fig. 3 proved to be one of the most stable portions of the system, with a peak-to-peak noise level of less than 0.001%, measured with a 1-second full-scale response time, and a drift normally less than 0.002% per hour with full battery operation. All resistances were wire-wound, except for the 1-megohm carbon voltage divider P_3. The heaters were grounded, although this is not shown in Fig. 3, since the location of the ground connection is not critical. The use of regulated a. c. on the heaters increased the peak-to-peak noise level to 0.005% but did not affect the drift. The twin-triode tube was shock-mounted. The 5692, a mechanically strengthened version of the 6SN7, was found preferable because the latter occasionally gave erratic changes amounting to several millivolts input. For these tubes, the input impedance of grid G_1 was between 10,000 and 1,000,000 megohms over a range from 0 to 6 v. A plot of output vs. input voltage deviated only 0.6 % from linearity over the same range. The grid current usually was less than 10^{-10} amp.

The circuit of the comparison voltmeter functions as a differential cathode follower. The advantage of this circuit as an impedance-matching device for adapting high-resistance circuits to low-resistance recorders has been discussed elsewhere (6). Any difference in the voltage of grids G_1 and G_2 causes a corresponding difference in voltage between the cathodes C_1 and C_2. The potentiometer P_3 connected to G_2 serves to adjust the zero of the amplifier and to compensate for the dark current of the photomultiplier tube PM. The switch $SW1$ primarily serves to vary the resistance in the photomultiplier anode circuit. $SW2$, in the up position shown, selects a 5-megohm anode resistor during the standardization and, in the down position, any resistor chosen by $SW1$ during the operating cycle. Potentiometer P_1 provides a bucking voltage from B_1 to compensate for stray light. Potentiometer P_2 is a ten-turn Helipot used to vary the bias from B_2 applied to G_2 for scale (or zero) suppression. A reduction in the grid bias on G_2 can be made to compensate for most of the voltage developed in the anode resistor by the photocurrent, and allows the output recorder to be used as a partial deflection instrument with a much higher sensitivity than would be possible if the whole photocurrent voltage were read on the scale. For example, if a 4.5-v. signal is measured on the recorder alone, the latter might be adjusted to give full-scale deflection for 5 v. If P_2 is adjusted to reduce the grid bias on G_2 by 4.00 v., the difference in potential at the recorder input will be reduced correspondingly and the recorder sensitivity may be increased to 1 v. full scale. It will read 0.5 full scale for 4.5 v., with a sensitivity five times that of the first arrangement.

Normally the recorder is connected between contacts B and C, and its sensitivity is adjusted by changing the resistor R_2. For highest sensitivity, $SW3$ is opened and the recorder is operated between A and C.

Recorder and Standardizing Circuit. Both of these functions were performed by a Brown Electronik Potentiometer Pyrometer Circular Chart Recorder modified as shown in Fig. 4. Connections were made to the four right-hand terminals of the strip beneath the slide wire so that $SW5$ could switch the amplifier output from the recorder-balancing motor M_1 to a similar sensitivity-adjusting motor M_2 during the 2-second standardizing period. The terminal connections are designated W, Y, R, G, for the white, yellow, red, and green color-coded wires. A synchronous motor, not shown in the diagram, cycled $SW4$ (the left-hand section of which is shown in Fig. 3), $SW5$, and $SW2$ (Fig. 3) with the beam shutter attached to it. All of these are in the standardizing position in these diagrams. During this

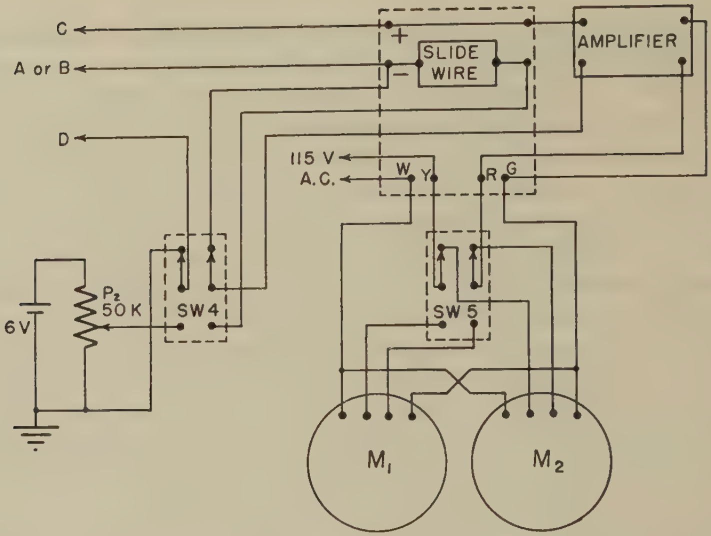

FIG. 4. Switching connections for recorder and sensitivity adjusting motor.

portion of the cycle, the left-hand pole of *SW*4 disconnects P_2 and grounds *D*, while the right-hand pole of *SW*4 disconnects the recorder slide wire and connects *A* or *B* direct to the amplifier which drives M_2. This motor, as shown in Fig. 1, is connected to the sensitivity adjustment, a variable resistance R_1 (Fig. 3) in series with the photomultiplier power supply.

Operation of the Instrument

The zero adjustment in the amplifier is made by putting *SW*1 (Fig. 3) in position 5, with *SW*2 and *SW*4 each in the down position, and setting P_2 at 0 (*i.e.*, with the slider at the junction with P_1), and adjusting P_3 to give zero output to the recorder, reversing the polarity of the 1.5-v. battery if necessary. Next the cycling motor is turned manually to the standardizing position, which connects the photomultiplier anode to the 5-megohm resistor, grounds G_2 except for the small bucking potential, and throws the reference beam on the photomultiplier. The amplifier then drives the sensitivity-adjusting motor, which varies the high-voltage supply to the photomultiplier tube until the voltage drop of the anode current across the 5-megohm resistor brings the potential of grid G_1 to that of G_2. The cycling motor is then turned manually to the operating position and the aerosol is introduced into the cell. With the scattered light on the photomultiplier tube, P_2 is varied and the recorder sensitivity is adjusted until a suitable deflection is produced on the recorder. If the aerosol is dilute and the scattered light is small, *SW*1 may be turned from position 2 to 3 or 4, where the sensitivity of the instrument is increased by factors of 10 and 100, respectively. In these positions the stray light may be important in comparison with the scattered light and must be compensated. This is done by sweeping the aerosol out of the cell with filtered air and adjusting P_1 until the voltage drop due to the stray light current is matched and the recorder reads 0 on the scale on which it will be used.[3] When these adjustments have been completed, the cycling motor is started, the aerosol is passed through the cell, and the system automatically standardizes itself and records or controls aerosol light scattering.

Experimental Results

A careful study of the performance of the instrument was made to determine its reliability. Since it was found sensitive to the light scattered by filtered air at room temperature and pressure, we also briefly studied molecular light scattering from several gases in order to investigate the possibility of using them as standards, thus avoiding the difficulties of generating and analyzing standard aerosols. These experimental results are summarized below.

Photometer Performance

The measurements in the next few paragraphs are given in terms of the background light of the instrument with air in the cell. The *background light* is the sum of the *stray light* (scattered by the solid parts of the cell) and the light scattered by the gas in the cell. The fluctuations (noise) associated with this background light set the lower limit of photometric measurement. In our apparatus, the stray light was about 30 times that scattered by air in the cell, and considerable increase in sensitivity could be obtained by reducing it to, or below, the light scattered by air. The limiting factors in measuring larger amounts of light are lamp stability and eventually the photomultiplier, if its anode current exceeds about 0.1 μa.

Noise Level. This was about 0.05% (of background) peak-to-peak when the lamp was supplied from a lead-acid automobile storage battery. This noise was measured with a recorder taking 25 seconds for full-scale travel, expanding the scale so that a 5% light change caused full-scale travel. When the lamp was operated on rectified a. c. from a step-down transformer connected to a Sorensen Model 2000 A.C. (electronic) Voltage Regulator, the noise level rose to about 0.25% peak to peak.

Microphonics. These effects were less than the noise level (0.05% peak to peak) when the instrument was mounted on a light table.

---

[3] If the adjustment is made with SW1 on 4, automatic compensation could be achieved also in positions 3 and 2 by adding a voltage-dividing circuit like that in our earlier penetrometer (1), to reduce the compensating voltage by factors of 10 and 100, respectively.

Lamp Stability. This is the limiting factor in most measurements with the present system. When the lamp was operated at 6 amp. from a 100-amp.-hr. storage battery, the response decreased about 2.5% per hour without automatic standardization. This change is reduced but not completely eliminated by standardization against the reference beam. Thus a 10% change in lamp voltage causes a 1% change in reading with ammonium chloride smoke and a 3% change with cigaret smoke, when measured against ethyl chloride as a standard. This may be due to the color change of the filament with voltage and to the fact that the two optical paths are different, with one involving direct transmission and the other scattering, which varies with the wavelength of the light. The effect probably could be corrected by using a filter to restrict the measurement to a narrow band of light, and this point would require further study before using gases as accurate absolute standards.

Temperature Effects. These were not accurately measured, but we estimate a change of about 0.5% per °C. for the stray light. No data are available for the case where automatic standardization was used.

Contamination by Sample. This was tested on three occasions by drawing room air through the instrument at the rate of several liters per minute for 12 hours, causing a change of less than 1%.

Sensitivity of Photometer for Aerosols. A dioctyl phthalate aerosol containing 0.05 μg./l. of 0.3 μ diameter was found to scatter an amount of light equal to the background. The sensitivity of the instrument, as determined by its peak-to-peak noise level, therefore corresponds to $0.05 \times 0.0005 = 0.00003$ μg., or 3×10^{-11} g./l. of this aerosol.

Molecular Light Scattering

We made measurements with helium, air, carbon dioxide, methyl bromide, and ethyl chloride in the cell. Our results with the first three gases were reproducible when they were obtained from various sources, filtered free of suspended matter in a number of different ways, and put through the cell at widely different flow rates. In general, the scatter on the recorder chart was close to the noise level of the measurement of air scattering, which is about 1.5%. However, methyl bromide and ethyl chloride were much less satisfactory, since the scattered light increased in an erratic way after they had stood in the cell for a few minutes, possibly because of the formation of a fog with these materials, which boil only slightly below room temperature.

Our initial readings corresponded to the light scattered by the gas plus the considerably larger stray light scattered by the stops and other solid parts of the cell. The latter can be measured most directly after evacuating the cell, provided the whole system is vacuum-tight and the stray light is independent of changes in pressure which might distort the cell. The stray

TABLE I

Light Scattering of Gases Relative to Air

Gas	$10^6(n-1)$	$\frac{(n-1)^2}{(n_a-1)^2}$	Observed scattering	
			This work (15°–30°)	Literature (90°)
He	35	0.014	—	—
Air	293	1.000	1.0	1.0
CO_2	449	2.35	2.4	2.6
CH_3Br	964	10.8	13	—
C_2H_5Cl	1179	16.2	17	16

light also can be determined from measurements with the cell filled successively by two different gases of known and widely different scattering powers. As a first approximation, we may calculate the scattering of any gas relative to air at the same molecular concentration from the simple Rayleigh law for isotropic molecules (neglecting depolarization):

$$\frac{I}{I_a} = \frac{(n-1)^2}{(n_a-1)^2},$$

where I and I_a are the scattering intensities of the gas and air, respectively, and n and n_a are the corresponding indices of refraction. In the second and third columns of Table I we have collected some refractive indices for gases at S.T.P. illuminated by green light of about 5100 A. (7) and listed the corresponding relative scattering values calculated from the Rayleigh equation. The 1.4% calculated relative scattering for helium is less than the 1.5% noise level and therefore should be negligible in our apparatus, and we corrected all our results for stray light by subtracting the scattering observed with helium from that with the other gas in the cell. The results were divided by that for air to give the ratios listed in the fourth column of Table I. The agreement with Rayleigh's equation in the case of the other gases justifies our conclusions about helium. Our results also agree satisfactorily with those collected from the literature by S. Bhagavantam (8) and listed in the last column of Table I, although the earlier workers measured transverse instead of forward scattering and frequently used the sun as a source of light, with photographic or visual methods of comparing intensities, instead of a tungsten source with a receiver having an S-4 photosurface.

Standardization with Gases

As a result of our experiments with molecular light scattering from gases, we recommend standardization of the instrument by measurements at atmospheric pressure with helium or air, together with carbon dioxide gas, which is readily available in pure form compressed in cylinders, evaporated from dry ice, or made by the interaction of acids with carbonates and dried before use. The standard would then be the scattering from carbon dioxide at a molecular concentration corresponding to S.T.P. To illustrate the method of standardization, we may consider the following example:

The electronic circuits of the instrument were turned on and allowed to warm up. With the lamp off, the Helipot P_2 (Fig. 3) was set at zero, and the recorder balanced to zero by adjusting P_1 to compensate for the photomultiplier dark current, about 2% of the stray light current. The cell then was filled with filtered air at 24°C. and 740 mm. Hg, the lamp turned on, and P_2 adjusted to a reading of 73.5 H (Helipot divisions) to balance the recorder. This reading corresponds to the stray light plus air scattering. Next carbon dioxide gas (obtained from dry ice) was introduced at 24°C. and 740 mm. Hg. With the Helipot fixed, the recorder deflections were 32.5, 31.1, 31.8, 32.0, 32.0, averaging 31.9 R (recorder divisions). Since we had found 1 R = 0.0909 H, this corresponded to 2.90 H for the difference between the scattering due to CO_2 and air under the same conditions. The scattering of CO_2 had been found to be 2.4 relative to air (Table I); therefore we can write:

$$S_{CO_2} - S_{air} = S_{CO_2} - S_{CO_2}/2.4 = 2.90\ H$$

Hence the scattering due to CO_2 under the experimental conditions is $2.90 \times (2.4/1.4) = 4.97\ H$, and that at S.T.P. is $4.97 \times (760/740) \times (299/273) = 5.59\ H$. Finally a test aerosol was run into the cell and P_2 was turned to 864.0 to balance the recorder. The scattering due to the aerosol therefore was $864.0 - 73.5 = 790.5\ H$, or $790.5/5.59 = 141$ relative to carbon dioxide.

A convenient secondary standard for aerosol measurements is the *background scattering* (stray light plus air scattering). In this case, the aerosol scattering is $790.5/73.5 = 10.76$ relative to background scattering. The instrument could be used safely for some time, without restandardization with helium and carbon dioxide, by adjusting the photomultiplier gain to give a background scattering of 73.5 H when the cell is filled with air at the same molecular concentration.

These measurements illustrate the use of the photometer as a partial-deflection instrument for small changes over a total range of 80 recorder divisions (equivalent to 7.2 H), or as a null instrument for larger changes, over a total range of 1000 H.

References

1. Gucker, F. T., Jr., Pickard, H. B., and O'Konski, C. T., *J. Am. Chem. Soc.* **69**, 429–438 (1947).
2. La Mer, V. K., and Sinclair, D., OSRD Report 1857 (1943), available through Office of Publication Board, U. S. Department of Commerce, as Report No. 944; also Part V of OSRD Report No. 865 (September 4, 1942).

3. Gucker, F. T., Jr., O'Konski, C. T., Pickard, H. B., and Pitts, J. N., Jr., *J. Am. Chem. Soc.* **69,** 2422–2431 (1947).
4. Gucker, F. T., Jr., and O'Konski, C. T., *Chem. Revs.* **44,** 373–388 (1949).
5. Gucker, F. T., Jr., and Rose, D. G., *Brit. J. Appl. Phys., Supplement* No. 3, pp. S138–S143 (1954).
6. Gucker, F. T., Jr., and Peterson, A. H., *Anal. Chem.* **25,** 1577 (1953).
7. "International Critical Tables," V, pp. 5–10. McGraw-Hill Book Co., New York, 1930.
8. Bhagavantam, S., "Scattering of Light and the Raman Effect," pp. 56–58. Chemical Publishing Co., Inc., Brooklyn, 1942.

THE VISCOSITY OF SUSPENSIONS OF SPHERES

Clyde Orr, Jr., and H. G. Blocker

The Georgia Institute of Technology, Engineering Experiment Station, Atlanta, Georgia

Received October 12, 1954

Abstract

Particle size distribution, often suggested as a factor influencing the viscosity of suspensions, is considered quantitatively. By an analysis of previously reported data, the viscosity of suspensions of spheres from the lowest to the highest concentration is shown to be described in terms of the viscosity of the pure liquid, the volume fraction of solids, the packed sediment volume of solids, and the geometric standard deviation for the solids.

Introduction

In 1906 Einstein showed that, as the concentration of solid particles approaches zero, the viscosity of a suspension of spherical particles is described by

$$\frac{\eta - \eta_0}{\eta_0} = 2.5c, \qquad [1]$$

where η is the suspension viscosity, η_0 the viscosity of the pure liquid, and c the volume fraction particles.

Numerous relations for concentrated suspensions have been suggested. For example, Hess (1), assuming a simple arrangement for the particles in a fluid flowing in a capillary, arrived at

$$\frac{\eta - \eta_0}{\eta} = lc, \qquad [2]$$

where l is a constant numerically greater than one. Robinson (2, 3), for glass spheres in a variety of liquids, proposed

$$\frac{\eta}{\eta_0} = \frac{1 + bc}{1 - c_0}, \qquad [3]$$

where c_0 is the volume of the sediment obtainable from unit volume of suspension, and b is a constant tentatively described as a frictional coefficient. The term c_0 sets the upper limiting value, the condition at which sufficient numbers of particles are in contact with other particles for the apparent suspension viscosity to approach infinity.

Examination of the experimental data available indicates that the relative viscosity of suspensions of spheres increases exponentially with suspension concentration. Experimental values (4, 5) for the Einstein constant have been found to vary between 1.5 and 35. These observations suggest that an equation might be written

$$\frac{\eta - \eta_0}{\eta} = ac^k \qquad [4]$$

where a and k are functions which depend on suspension properties.

The constants of Eq. [4] may be evaluated if the equation is put in the form

$$\log\left(1 - \frac{\eta_0}{\eta}\right) = \log a + k \log c. \qquad [5]$$

The slope and intercept when $c = 1$ of the experimental straight line resulting when the left side of the equation is plotted against log c are equal to the values of the constants k and log a, respectively.

The physical significance of a and k may now be discussed. Particle size need not be considered. Reiner (6) and others have shown that particle size of itself cannot affect suspension viscosity. However, Kruyt (7) and Hermans (8) have pointed out that size distribution is definitely involved. Robinson (2, 3), as mentioned above, suggested the use of a limiting concentration. Orr (9) and Orr and DallaValle (10) used this limiting concentration and in addition used the term $1 - \frac{c}{c_0}$ raised to an empirical power to describe the viscosities of certain suspensions. Blocker (11) showed that this power was related to the size distribution of the powders composing the suspensions. Thus it is suggested that a is related to c_0 and k to the geometric standard deviation, σ_g, a measure of size distribution.

DATA

Values of c_0 and σ_g are given as such in the technical literature by few investigators of suspension viscosity. Reasonably satisfactory values may sometimes be estimated from the information which is given, however. In the case of c_0 estimation may be made from the packed sediment volume, the centrifuged sediment volume, or from the limit which experimental viscosity data indicated. In the case of σ_g, estimation may be made from the limits of particle size, if these data are included.

The viscosity data given by Eilers (12), Robinson (2, 3), Ward and Whitmore (4), and Blocker (11) were found to be sufficient for the analysis herein proposed. Representative data plotted in accordance with Eq. [5] are presented in Fig. 1. It may be observed that, in general, rather straight lines are obtained. The slopes and intercepts are thus easily established

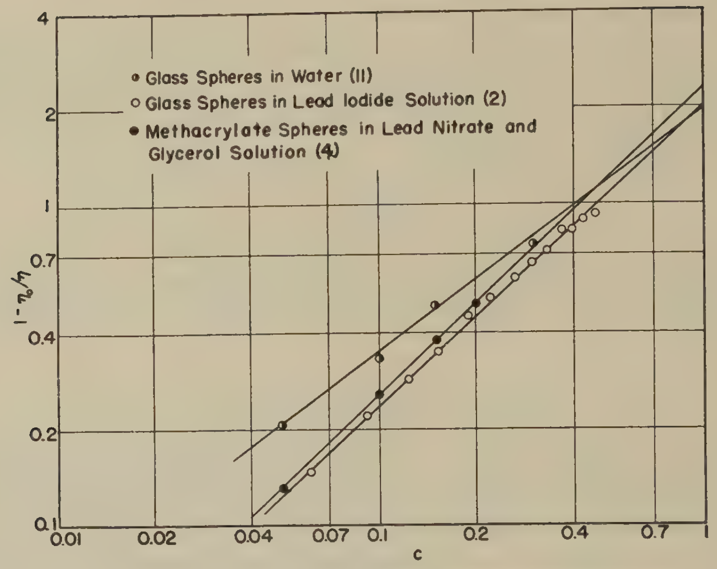

Fig. 1. Plot of the experimental data of several investigators.

and a and k are readily evaluated. It was observed that the values obtained for a and k were approximately equal to the reciprocals of c_0 and σ_g, respectively.

Results

Table I presents data in a form suitable for comparing c_0 with $1/a$ and $1/\sigma_g$ with k. The limiting volume fraction, c_0, as indicated by several methods of evaluation, is included. When a plot of apparent viscosity versus solids concentration was not given in the original source of the data, such a plot was constructed in order to estimate the limiting concentration. When particle size distribution was not specifically stated, σ_g was estimated by assuming 2% of the particles to be smaller than the smallest size indicated and 2% larger than the largest size indicated. These values were then plotted on log-probability paper and σ_g was determined as the 84.13% size divided by the 50% size, as explained by DallaValle (13).

Examination of the results in the table indicates that k is indeed closely related to $1/\sigma_g$ and that $1/a$ is related to c_0. The correct value for c_0 seems to lie generally between those indicated by sedimentation and by centrifugation. This result is not surprising; the sedimentation value would be expected to represent a minimum value and the centrifugation value a maximum.

From the evidence presented herein it appears that the viscosity of suspensions of spheres from the lowest to the highest concentration can be described by a relatively simple equation the individual terms of which have a distinct physical significance.

TABLE I

Comparison of Suspension Properties with Terms Obtained from Viscosity Measurements

Suspension and source	c_0			$1/a$	Size distribution	$1/\sigma_g$	k
	By sedimentation	By centrifugation	From plot of viscosity data[a]				
Bitumen emulsion (12)	—	—	0.75	0.73	$25\% < 3.4\mu$; $25\% < 6.0\mu$	0.654	0.695
Glass spheres in glucose (3)	0.315	0.508	0.45	0.450	3 to 4μ	0.935	0.877
Glass spheres in glucose (3)	0.389	0.553	0.50	0.515	4 to 10μ	0.800	0.813
Glass spheres in glucose (3)	0.520	0.588	0.58	0.575	10 to 30μ	0.760	0.758
Glass spheres in No. 30 motor oil (2)	—	—	0.55	0.625	10 to 30μ	0.760	0.720
Glass spheres in No. 50 motor oil (2)	—	—	0.50	0.625	10 to 30μ	0.760	0.720
Glass spheres in castor oil (2)	—	—	0.47	0.610	10 to 30μ	0.760	0.728
Glass spheres in corn sirup (2)	—	—	0.49	0.625	10 to 30μ	0.760	0.660
Glass spheres in glycol (2)	—	—	0.51	0.585	10 to 30μ	0.760	0.658
Glass spheres in sucrose (2)	—	—	0.40	0.562	10 to 30μ	0.760	0.701
Glass spheres in lead iodide sol'n (2)	0.51	0.51	—	0.575	5 to 8μ	0.893	0.889
Glass spheres in lead iodide sol'n (2)	0.51	0.51	0.42	0.513	5 to 8μ	0.893	0.923
Methacrylate spheres in lead nitrate and glycerol sol'n (4)	—	—	0.40	0.465	$-152 + 177$ B.S.S.	0.869	0.954
Methacrylate spheres in lead nitrate and glycerol sol'n (4)	—	—	0.40	0.263	$-147 + 208$ B.S.S.	0.961	1.16
Methacrylate spheres in lead nitrate and glycerol sol'n (4)	—	—	0.40	0.311	$-76 + 208$ B.S.S.	0.953	0.988
Methacrylate spheres in lead nitrate and glycerol sol'n (4)	—	—	0.40	0.263	83.5% within $-27.5 + 49.5$ B.S.S.	0.971	1.01
Glass spheres in water (11)	0.456	0.560[b]	—	0.541	$\sigma_g = 1.42$	0.704	0.719

[a] Approximate values.
[b] Previously unreported.

ACKNOWLEDGMENT

The authors wish to thank Prof. J. M. DallaValle for his suggestions and helpful criticism.

REFERENCES

1. HESS, W. R., *Kolloid-Z.* **27**, 1–11 (1920).
2. ROBINSON, J. V., *J. Phys. & Colloid Chem.* **53**, 1042–1056 (1949).
3. ROBINSON, J. V., *J. Phys. & Colloid Chem.* **55**, 455–464 (1951).
4. WARD, S. G., AND WHITMORE, R. L., *British J. Appl. Phys.* **1**, 286–290 (1950).
5. MCBAIN, J. W., "Colloid Science." D. C. Heath and Company, Boston, 1950.
6. REINER, M., "Deformation and Flow." H. K. Lewis and Co., Ltd., London, 1949.
7. KRUYT, H. R., "Colloid Science," Vol. I. Elsevier Publishing Company, Amsterdam, 1952.
8. HERMANS, J. J., "Flow Properties of Disperse Systems." Interscience Publishers, Inc., New York, N. Y. 1953.
9. ORR, C., JR., "The Transference of Heat between a Pipe Wall and a Liquid-Solid Suspension Flowing Turbulently Inside the Pipe. The Thermal Conductivity and Viscosity of a Liquid-Solid Suspension." Ph.D. Thesis, Georgia Institute of Technology, Atlanta, Georgia, December 1952.
10. ORR, C. JR., AND DALLAVALLE, J. M., Heat-Transfer-Research Studies for 1954, *Chem. Eng. Progr. Symposium Ser.* **50** (No. 9), 29–45 (1954).
11. BLOCKER, H. G., "An Investigation of Factors Affecting the Viscosities of Liquid-Solid Suspensions." M.S. Thesis, Georgia Institute of Technology, Atlanta, Georgia, June 1954.
12. EILERS, H., *Kolloid-Z.* **97**, 313–21 (1941).
13. DALLAVALLE, J. M., "Micromeritics." Pitman Publishing Co., New York, N. Y., 1948.

THE RHEOLOGY OF PRINTING INKS.

III. STUDIES OF SIMPLE DISPERSIONS[1]

A. C. Zettlemoyer and G. W. Lower

National Printing Ink Research Institute, Lehigh University, Bethlehem, Pennsylvania

Received July 31, 1954; revised October 15, 1954

Abstract

One of the most important factors underlying the rheological properties of printing inks is the interaction between the pigment and the vehicle. The complicated formulations of most inks, however, make it difficult to make a detailed study of this factor, and very little attention has been given it in the past. For this reason a simple system of calcium carbonate in polybutene oil was chosen for the study reported here. With this system, quantitative information on the nature of the pigment-vehicle interaction has been obtained. An understanding of simple systems, such as this one, is essential before we can hope to understand the much more complicated systems present in commercial printing inks.

The particle size of the pigment has been found to have a marked effect on the viscosity: *i.e.*, the smaller the particle size, the greater the viscosity at a given loading. This effect has been explained on the basis that there is a shell of immobilized vehicle on the surface of each pigment particle and in the narrow portions of the interstices of agglomerates. This immobilized vehicle increases the effective pigment volume to an extent proportional to the amount of pigment surface present. This increase of effective pigment volume can be treated quantitatively so that data on similar pigments of different particle size can be correlated.

Particle-size distribution in the range of 0.1 to 0.4 μ has no effect on the viscosity. The addition of a surface-active agent, *i.e.*, stearic acid, has been found to reduce the viscosity by localizing the pigment-vehicle interaction and thus decreasing the thickness of the shell of adsorbed vehicle.

These results add to our understanding of the many factors which contribute to the rheological properites of printing inks and which, in turn, control their printing properties.

Introduction

The seat of the complex rheological properties of printing inks is the interface between pigment and vehicle. Pigment surfaces in general are characterized by residual valence forces which result in interactions with the vehicle. This interaction in printing inks is complex, because the surface of the pigment is usually heterogeneous and because the vehicle is almost always a mixture of many compounds. Another factor which complicates printing ink rheology is the variation in particle size together with the wide particle-size distribution which most pigments possess. A third factor which assumes more prominence in some systems than in others is the interaction among particles leading to agglomeration. All of these factors have a significant influence on the nature of the flow curve (the stress versus rate of shear curve), which is the most commonly employed representation of rheological data. Whether the behavior of inks during printing can be depicted completely by flow curves is still in question; however, the fundamental knowledge of adsorbed films, agglomeration, and other disturbances introduced by pigmentation has been useful in explaining some of the technological phenomena.

---

[1] Presented as paper No. 22 before the Division of Paint, Varnish and Plastics Chemistry, A.C.S., at the Milwaukee Meeting, April 1, 1952.

The work reported here was designed to single out some of the more complicated variables so that they could be dealt with in turn to increase our understanding of the behavior of printing inks. More specifically it was aimed at the clarification of the effect of pigment particle size, with other conditions kept constant and as simple as possible. Later the effect of a simple vehicle additive was also studied. For this simplified approach, dispersions of calcium carbonate in polybutene oil were chosen.

The four calcium carbonate pigments employed in this work were specially prepared by repeated fractionation of the same precipitated batch so that four fractions varying only in average particle size were obtained; therefore, the only difference between the samples was particle size. Polybutene oil was chosen as the vehicle because it represents the simplest fluid with which printing ink consistencies could be obtained. This vehicle is a hydrocarbon possessing no functional groups such as acid or hydroxyl groups.

Much work has been reported in the literature heretofore on the viscosity of suspensions. Although many theoretical and empirical equations have been developed for the viscosity of suspensions, Einstein's simple equation (1) for dilute suspensions of spherical particles remains the most basic one. This equation merely states that the specific viscosity η_{sp} is proportional to the pigment loading expressed as the volume fraction V.

$$\eta_{sp} = KV \qquad [1]$$

where: η_{sp} is the specific viscosity of the suspension,

K is a proportionality constant theoretically equal to 2.5 for spherical particles, and

V is the pigment concentration expressed as volume fraction.

This equation has been found to apply well to several systems, but only at very low particle concentrations (2–5). It has been extensively modified in an attempt to extend its application to higher concentrations (6–12). The usual approach in such attempts has been to add terms containing higher powers of V; another approach which has been taken is to make use of an exponential relation such as was done first by Arrhenius (13):

$$\eta_r = (exp)kc \qquad [2]$$

where: η_r is the relative viscosity of the suspension,
k is a constant, and
c is the concentration in grams per milliliter of vehicle.
Modifications of this equation have also been suggested (14–16).

None of these equations is entirely successful. Whereas a given equation may apply to one system, it often fails when tried with another. Particle size and particle-size distribution have not often been considered, and, furthermore, the vehicle used was often water or a complex mixture. At any rate, none of the equations in the literature fits the data obtained here for the calcium carbonate-polybutene system.

Mention has been made qualitatively in the literature by Hatschek (17) and by others (18–20) of the possibility that pigment-vehicle interaction produces an adsorbed shell which increases the effective volume of the pigment. This concept has been applied quantitatively in this study, and has been developed along lines amenable to other concepts of immobilization resulting from extremely fine division of particles as long as pigment area is the controlling factor.

Experimental

In most of the reported work on the viscosity-concentration relationship of suspensions, the systems were so complex as to render difficult any analysis of the effect of a particular variable such as particle size. In the present investigation, both the pigment and the vehicle were as simple and basic as possible.

Vehicle

The vehicle chosen was Polybutene No. 12, manufactured by the Oronite Chemical Company. The two batches of this vehicle used had viscosities of about 11 poises at 30°C., and thus printing ink consistencies could be obtained. It consisted of a mixture of homologous branched-chain hydrocarbons with an average molecular weight of 530 and a density of 0.87 g./ml. The molecules were essentially linear hydrocarbons with short methyl and ethyl side chains. Therefore, there were no functional groups present in the vehicle which might have exerted some complex effect on the viscosity of the suspensions.

Pigments

For the study of the effect of particle size and size distribution on the viscosity of the suspensions, a series of four closely fractionated calcium

TABLE I

Characteristics of Calcium Carbonate Fractions

Fraction	Surface area, *m.*^{2}/*g.*	Mean particle diameter *d*, *microns*
A	16.2	0.13 ± 0.08
B	12.2	0.18 ± 0.09
C	8.9	0.23 ± 0.10
D	5.2	0.39 ± 0.28

carbonates (calcite, density 2.71 g./ml.) was obtained from the Diamond Alkali Company. All pigment samples were prepared from the same precipitated batch by repeated fractionation by air elutriation until the particle-size distribution within each fraction was very narrow. The surface areas in square meters per gram and the corresponding mean particle diameters, *d*, in microns were determined from nitrogen adsorption measurements by using the BET method as described by Brunauer (21). Uniformity of particle size was of secondary consideration in this work; nevertheless, examination of electron photomicrographs of these materials showed the particles to be quite smooth, regular, and uniform in size. It also showed that the magnitudes of these particle sizes were correct, and that a threefold range of size and area had been covered.

The properties of the various pigment fractions are summarized in Table I. The ranges of the particle sizes include 95% of the several hundred particles measured from each electron photomicrograph; the majority of the particle sizes in each sample were much closer to the indicated values than the ranges suggest.

Preparation of Suspensions

First the pigment was dried at 110°C. at 20 mm. pressure for 24 hours to remove most of the adsorbed water. It was then made into a paste containing 10% to 20% pigment by volume. This paste was given two passes over a three-roll mill and diluted with the pure vehicle to give suspensions of the required concentrations. These diluted suspensions were given two more passes over the mill to insure complete dispersion. The mill setting could be reproduced by means of hydraulic gages so that each of the suspensions could be subjected to the same amount of mechanical dispersing action.

Analysis for Pigment Content

A direct analysis for pigment content was made on each suspension by vaporizing the vehicle over a low gas flame and igniting the pigment in a muffle furnace at 1000°C. The ignited residue was weighed as CaO and calculated to the weight of calcium carbonate. From this result and the pigment density the volume per cent of pigment was determined. The precision of this analysis was about 1.0%.

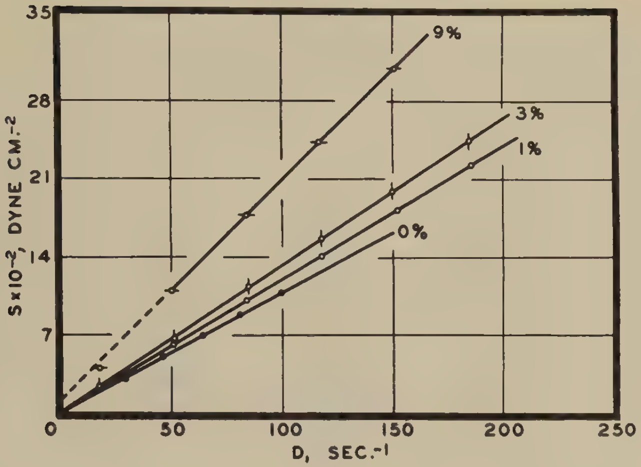

FIG. 1. Flow curves for calcium carbonate C in polybutene No. 12.

Viscosity Determination

The viscosities were determined at 30.0°C. from the slope of the isothermal stress versus rate of shear curves, henceforth referred to as S-D flow curves, as described by Lower, Walker, and Zettlemoyer (22). Fortunately, the viscosities of the suspensions did not change with age; this indicated that the dispersions did not absorb appreciable quantities of water from the air. Upon long standing the pigment settled, but it could be readily redispersed by stirring. For low pigment concentrations the dispersions were Newtonian; that is, the flow curves were linear and passed through the origin. At higher concentrations definite curvatures set in at low shearing stresses, but the curves were linear at higher stresses. For these suspensions the plastic viscosities were calculated from the slope of this linear portion of the curve. Representative samples of these flow curves are shown in Fig. 1 for calcium carbonate C in polybutene No. 12, in which Newtonian behavior was observed up to nearly 9% pigment.

Dielectric constant measurements were also made by Voet (23) on several of these suspensions to determine if agglomeration was an important factor in producing the measured viscosities. Unfortunately, the results were inconclusive because the particles were nonconductive.

The results of the viscosity determinations for the calcium carbonate-polybutene suspensions are shown in Tables II to V and summarized in Fig. 2. In these tables, V is the volume fraction of the pigment or the fraction of the total volume of the suspension which is occupied by the pigment (these volume fractions can be converted to weight per cents by multiplying by 300); η, the viscosity of the suspension; η_r, the relative viscosity of the suspension; and η_{sp}, the specific viscosity. The significance of the last column of each table will be explained later.

TABLE II

Viscosity of Calcium Carbonate A in Polybutene No. 12

Surface area = 19.2 m.^{2}/g.

V, $CaCO_3$ volume fraction	η or U, *poises*	η_r	η_{sp}	$(1 + kA)V$ Corrected volume fraction
0.00	11.05	1.00	0.00	0.00
0.0115	12.10	1.095	0.095	0.0165
0.0200	12.92	1.169	0.169	0.0288
0.0304	13.82	1.251	0.251	0.0437
0.0404	14.80	1.339	0.339	0.0581
0.0508	16.24	1.470	0.470	0.0731
0.0612	17.63	1.595	0.595	0.0880
0.0652	17.89	1.619	0.619	0.0938
0.0819	20.80	1.882	0.882	0.118
0.0911	22.44	2.027	1.027	0.131

TABLE III

Viscosities of Calcium Carbonate B in Polybutene No. 12

Surface area = 12.2 m.^{2}/g.

V, $CaCO_3$ volume fraction	η or U, *poises*	η_r	η_{sp}	$(1 + kA)V$ Corrected volume fraction
0.00	11.05	1.00	0.00	0.00
0.0104	12.03	1.089	0.089	0.0138
0.0196	12.59	1.139	0.139	0.0261
0.0290	13.50	1.222	0.222	0.0386
0.0498	15.09	1.366	0.366	0.0663
0.0699	17.27	1.563	0.563	0.0931
0.0896	19.80	1.792	0.792	0.119

TABLE IV

Viscosities of Calcium Carbonate C in Polybutene No. 12

Surface area = 8.9 m.^{2}/g.

V, $CaCO_3$ volume fraction	η or U, *poises*	η_r	η_{sp}	$(1 + kA)V$ Corrected volume fraction
0.00	11.05	1.00	0.00	0.00
0.0118	11.97	1.083	0.083	0.0146
0.0303	13.28	1.202	0.202	0.0376
0.0407	14.19	1.284	0.284	0.0505
0.0499	14.95	1.353	0.353	0.0619
0.0698	16.85	1.525	0.525	0.0866
0.0913	19.25	1.742	0.742	0.113
0.121	24.00	2.172	1.172	0.150

The variation in viscosity with concentration is shown graphically in Fig. 2 for each of the four pigments. As can be seen from the relative positions of the curves, the viscosity is higher the smaller the particle size or the larger the surface area of the suspended pigment. The early linear nature of the curves indicates that the viscosity increase is directly proportional to the concentration up to a volume fraction of about 0.04.

TABLE V

Viscosities of Calcium Carbonate D in Polybutene No. 12

Surface area = 5.2 m.^{2}/g.

V, $CaCO_3$ volume fraction	η or U, *poises*	η_r	η_{sp}	$(1 + kA)V$ Corrected volume fraction
0.00	11.05	1.00	0.00	0.00
0.0128	12.00	1.086	0.086	0.0146
0.0196	12.42	1.124	0.124	0.0224
0.0302	13.18	1.193	0.193	0.0345
0.0414	13.99	1.266	0.266	0.0472
0.0455	14.08	1.274	0.274	0.0519
0.0706	16.32	1.477	0.477	0.0806
0.0914	18.49	1.673	0.673	0.104
0.122	22.72	2.056	1.056	0.139

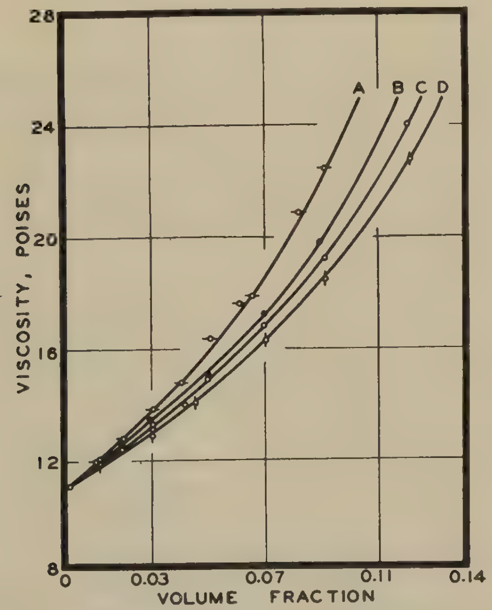

FIG. 2. Viscosity-concentration curves for the calcium carbonate-polybutene No. 12 system.

A—calcium carbonate A
B—calcium carbonate B
C—calcium carbonate C
D—calcium carbonate D

Above this point the viscosity rises more rapidly than would be predicted on the basis of a direct proportionality between η_{sp} and V.

INTERPRETATION OF DATA

The Einstein equation (Eq. [1]) predicts a linear relationship between η_{sp} and V. Furthermore, this equation indicates that the viscosity should

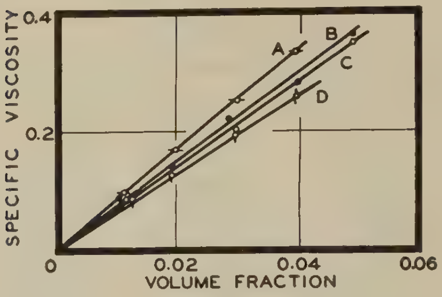

FIG. 3. Specific viscosity-concentration curves for the calcium carbonate-polybutene No. 12 system.

A—calcium carbonate A
B—calcium carbonate B
C—calcium carbonate C
D—calcium carbonate D

not depend on the particle size but only on the volume fraction of particles, and that the shear rate should have no effect on viscosity. This equation has been verified experimentally for systems which obey the rigid conditions demanded in the derivation, that is, at low concentrations and for systems which exhibit no particle-vehicle interaction. The factor 2.5 has been found to vary slightly with particle shape, and is a maximum for long rod-shaped particles.

The values of K for the systems examined here are equal to the slopes of the lines in Fig. 3. It is readily seen that the factor varies from fraction to fraction, and furthermore, K is always of the order of 6 to 8. Since the four calcium carbonate pigments have essentially the same particle shape, it is not likely that a shape factor alone is responsible for the divergence. Instead, immobilization of vehicle has been postulated. The only variable in these systems to which the divergence can be attributed is the particle size or surface area. Robinson (10) and Gourlay (24) have modified the Einstein equation by adding a correction factor for the sedimentation volume, but neither of these approaches was found applicable to the data presented here. The failure of all previously suggested modifications of the Einstein equation apparently lies in the fact that the particle size, and consequently the particle area, has not been taken into account.

If entrainment by aggregates or adsorption of the vehicle is the chief cause of immobilization, the pigment with the smaller size should produce aggregates containing a large number of small interstices, and its larger surface area should adsorb proportionately more vehicle. This immobilized vehicle tends to increase the effective volume fraction of the pigment. This point of view can be put into mathematical form by recognition of the fact that both effects produce the same end result and hence may be interpreted on the basis of either one. The mechanism of adsorption has been chosen in this case, giving:

$$V' = kA \qquad [3]$$

where: V' = volume of vehicle immobilized per ml. of pigment
A = surface area of the pigment in m.^{2}/g.
k = a constant for a given pigment and vehicle with the units of g./m.^{2}. The value of k is the product of the pigment density in g./cc. times the thickness of the adsorbed film in microns.

The volume of this adsorbed layer increases the effective volume of the particles to $V_p + kAV_p$, where V_p is the actual pigment volume and kAV_p is the volume of the adsorbed vehicle. If this effective volume is substituted for the pigment volume in the general Einstein equation, the following equation is obtained:

$$\mathrm{n}_{\mathrm{sp}} = K \frac{(V_p + kAV}{V_T} \qquad [4]$$

where K is the usual constant and V_T is the total volume of the suspension. This equation may be written:

$$\eta_{sp} = K(1 + kA)V, \qquad [5]$$

where $V = V_p/V_T$ and is the volume fraction of pigment alone. This equation has been found useful in interpreting the data reported here for Newtonian dispersions.

In order to evaluate the constants k and K of Eq. [5] it is necessary to plot η_{sp} against V. This plot is shown in Fig. 3, where only the low concentrations are plotted, since it is the linear region of the viscosity curves that is to be used. The slope of the η_{sp} vs. V curve for each pigment fraction must equal $K(1 + kA)$ according to Eq. [5]. By determining the slopes graphically from Fig. 3 and substituting the corresponding values for the areas, four equations were obtained as follows:

$$\begin{aligned}
(A)\ 8.36 &= K(1 + 16.2k) \\
(B)\ 7.39 &= K(1 + 12.2k) \\
(C)\ 7.06 &= K(1 + 8.9k) \\
(D)\ 6.46 &= K(1 + 5.2k).
\end{aligned}$$

When the above equations were solved by the method of averages, the values for the constant were determined to be:

$$\begin{aligned}
K &= 5.68 \\
k &= 0.0271 \text{ g./m.}^2.
\end{aligned}$$

If the assumptions made are correct, the viscosity-concentration curves should coincide if η_{sp} is plotted against the corrected volume fraction, $(1 + kA)V$. These corrected volume fractions are shown in the last columns of Tables II to V for the various pigment fractions.

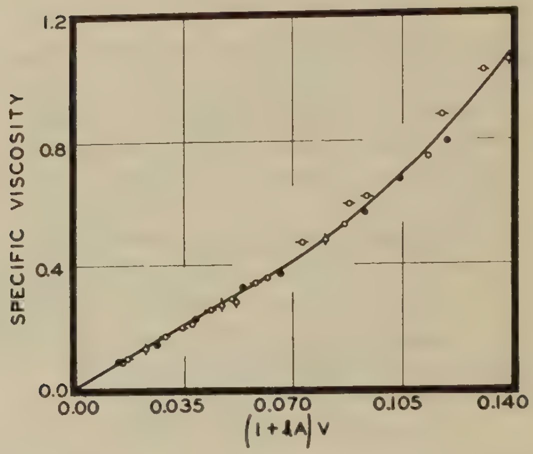

Fig. 4. Specific viscosity-corrected concentration curves for the calcium carbonate-polybutene No. 12 system.

-○-—calcium carbonate A
●—calcium carbonate B
○—calcium carbonate C
ϕ—calcium carbonate D

The results are shown in Fig. 4, where η_{sp} is plotted against $(1 + kA)V$. The points all fall very close to the same general curve over a volume fraction range of 0.00 to 0.14. There is a slight deviation for calcium carbonate A at the higher concentrations where the system was non-Newtonian.

These results show that the particle size of the pigment has a definite effect on the viscosity and that this effect can be explained by taking the immobilization of the vehicle into account. When the proper correction is made, the viscosity-concentration curves for this system coincide and are independent of the area. The greater increase in viscosity at higher concentrations can be explained by recognition that high shear rates within the body of the bulk fluid are attained at moderate calculated rates based on the geometry of the viscometer, and that the local shearing stresses may be sufficiently large to remove part of the adsorbed layers or to break up agglomerates.

In order to represent the curvature at higher concentrations, an attempt was made to apply equations, including logarithmic and power series, to the viscosity-concentration curves. No simple equation was found to represent the data.

Calcium carbonate A, with the highest surface area and smallest particle size, exhibited a yield value at a volume concentration of about 4%, whereas calcium carbonate D, with a low area, did not until a 9% concentration was reached. Since the Einstein equation cannot account for pseudo-

TABLE VI

Mixed Particle-Size Sample

Viscosities of calcium carbonates A + D in polybutene No. 12

Average area 8.9 m.^{2}/g.

V, volume fraction	η, *poises*	η_r	η_{sp}
0.00	11.64	1.00	0.00
0.0109	12.55	1.078	0.078
0.0200	13.02	1.119	0.119
0.0299	13.91	1.195	0.195
0.0402	14.84	1.275	0.275
0.0502	15.82	1.359	0.359

plastic behavior, the upper limits of concentration imposed by the first appearance of anomalous behavior were lower for the high area pigments than for the coarser ones. Apparently, however, factors other than adsorption are at work in this system because no correlation could be found between area and yield value.

Particle-Size Distribution

In order to determine the effect of particle-size distribution on viscosity, a series of suspensions of different concentrations were prepared using a mixed pigment. This mixed pigment was prepared by mixing a weighed amount of calcium carbonate A (16.2 m.^{2}/g.) with calcium carbonate D (5.2 m.^{2}/g.) to give a mixture with an area equal to that of calcium carbonate C (8.9 m.^{2}/g.). This mixture was then dispersed in the polybutene oil in the same manner as was used for the other suspensions. The viscosities of a series of suspensions of this mixed pigment were then determined and the results are tabulated in Table VI.

Figure 5 shows the viscosity-concentration curve of this mixed pigment compared with that of calcium carbonate C. The curves coincide. Since the mixed sample was prepared from two pigments with mean particle sizes differing by a factor of three and the calcium carbonate C sample has a narrow particle-size range at 0.23 μ, the particle-size distribution apparently has little effect in this system within the range studied.

Apparent Thickness of Adsorbed Film

Since the value of k in Eq. [5] might be expected to be related to the thickness of the adsorbed films, this quantity was calculated from the determined value of k. Since the value of k has been found to be 0.0271 g./m.^{2} and since k is equal to the product of the pigment density times the film thickness in microns, the thickness of the adsorbed film is 0.0271/2.93 or 0.00925 μ, which is 92.5 A.

This thickness would account for three to four layers if oriented per-

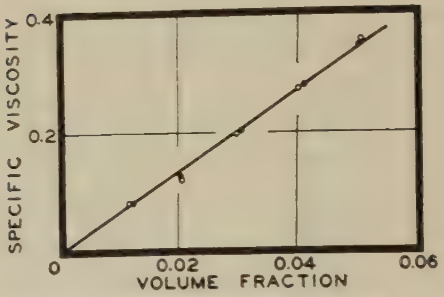

FIG. 5. Specific viscosity-concentration curves for mixed pigment and for calcium carbonate C in polybutene No. 12 system.

●—mixed pigment
○—calcium carbonate C

pendicular to the surface, and considerably more layers if oriented parallel to the surface, or randomly as might be expected. That the depth of the adsorbed film could be almost 100 A. in this system seems unlikely. Therefore, immobilization of vehicle in the interstices of structural units larger than the ultimate pigment particles appears to make a considerable contribution to the flow properties.

Stearic Acid Addition

It is well known that small additions of a surface-active agent often have a considerable effect on the flow of suspensions. The agent is partly adsorbed on the pigment surface where it can alter the pigment-vehicle interaction and affect the amount of aggregation. These effects in turn alter the flow characteristics of the dispersion.

In order to determine the effect of the addition of a small amount of a surface-active agent to the system under study, stearic acid was added to the calcium carbonate-polybutene suspensions. This expedient introduced a small amount of a highly polar substance into a vehicle which previously had been nonpolar. The stearic acid was added to the polybutene oil before the addition of the pigment. The paste was milled, diluted to the required concentrations with pure polybutene, and remilled in the same manner as described for the previous suspensions.

The samples were prepared in this manner with calcium carbonate A as the pigment and polybutene No. 12 as the vehicle. The amounts of stearic acid to be added were calculated using Harkins' (25) value of 21 A.^{2} for the cross-sectional area of a stearic acid molecule. One dispersion contained only enough acid to cover half of the pigment surface (0.0170 g. acid/g. pigment) and the other contained enough to produce two layers on the pigment surface if all the acid were adsorbed (0.0728 g. acid/g. pigment).

TABLE VII

Viscosity of Suspensions with Stearic Acid Added

Calcium carbonate A stearic acid–polybutene No. 12

Series S (½ monolayer)

0.0170 g. acid/g. pigment

V, volume fraction	g. acid left/g. vehicle	g. acid adsorbed/g. pigment	η_0, *poises*	η, *poises*	η_r	η_{sp}
0.0098	0.000	0.0170	11.75	12.45	1.060	0.060
0.0183	0.000	0.0170	11.75	13.22	1.125	0.125
0.0278	0.000	0.0170	11.75	14.14	1.203	0.203
0.0382	0.000	0.0170	11.75	15.01	1.277	0.277
0.0479	0.000	0.0170	11.75	16.44	1.399	0.399

TABLE VIII

Viscosity of Suspensions with Stearic Acid Added

Calcium carbonate A stearic acid–polybutene No. 12

Series S-1 (2 monolayers)

0.0728 g. acid added/g. pigment

V, volume fraction	g. acid left/g. vehicle	g. acid adsorbed/g. pigment	η_0, *poises*	η, *poises*	η_r	η_{sp}
0.0100	0.0012	0.0358	11.66	12.33	1.057	0.057
0.0197	0.0023	0.0386	11.58	12.86	1.111	0.111
0.0294	0.0033	0.0410	11.50	13.52	1.176	0.176
0.0391	0.0044	0.0412	11.42	14.35	1.257	0.257
0.0494	0.0052	0.0428	11.37	15.54	1.367	0.367

Since not all of the acid was adsorbed by the pigment in the second dispersion, analyses had to be made to determine the amounts remaining in the vehicle. Then, the viscosities of the vehicle containing the determined amounts of acid could be interpolated from Fig. 6. In this predetermined graph, viscosity of the vehicle versus concentration of stearic acid is plotted.

The viscosity-concentration curves in Fig. 7 indicate that stearic acid decreases the specific viscosities of these suspensions and that the higher the concentration of acid the greater is the reduction in the viscosities. In series S practically all of the acid added was adsorbed by the pigment. Therefore, the reduction in viscosity of these suspensions must be attributed to the adsorption of the stearic acid on the surface of the pigment. In series S-1 between 50% and 60% of the acid present was adsorbed. The remaining free acid contributes to the reduction in viscosity of the vehicle. This effect has been taken into account, however, as described earlier. Therefore, the reduction in viscosity of this series also must be attributed to the adsorbed acid.

The change in viscosity due to the adsorbed stearic acid cannot be accounted for by an increase in the effective volume of the particles. An

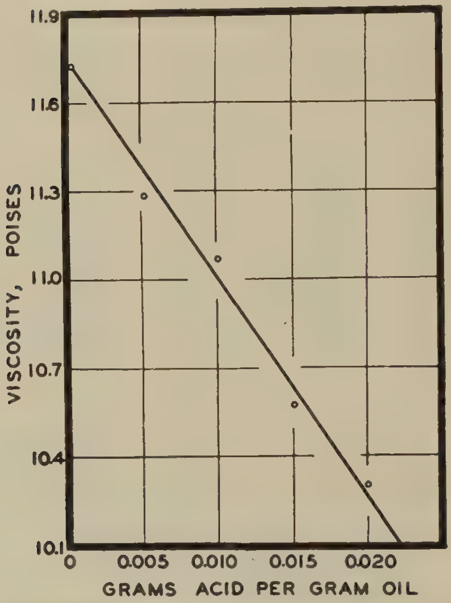

FIG. 6. Viscosity-concentration curve for stearic acid in polybutene No. 12 system.

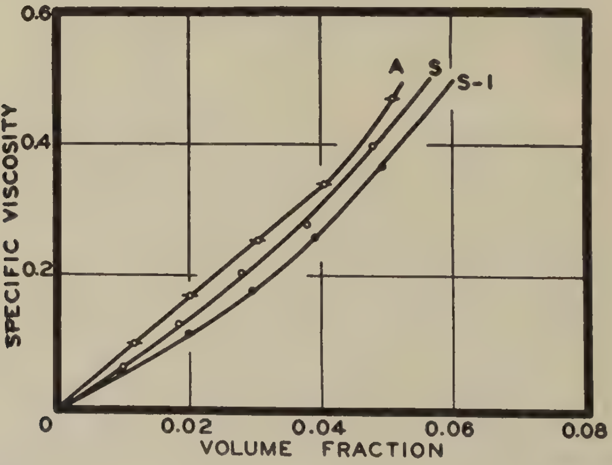

FIG. 7. Viscosity curves for the calcium carbonate A-stearic acid-polybutene No. 12 system.

A—calcium carbonate A
S—calcium carbonate A + 0.0170 g. acid/g. pigment
S-1—calcium carbonate A + 0.0728 g. acid/g. pigment

TABLE IX

Summary of Adsorbed Layer Volume Calculations

Calcium carbonate A–polybutene No. 12

Curve	Stearic acid layers	Slope	kA	cc. Ads./g. pigment	
				Calc.	Stearic acid by analysis
A	0	8.36	0.437	0.149	0.0000
S	½	6.96	0.224	0.0764	0.0196
S-1	2	5.88	0.0344	0.0117	0.0422 to 0.0505

examination of the data taken on the pure polybutene systems and with added stearic acid shows that K is dependent upon the chemical nature of the pigment-vehicle system and is not merely a factor determined by the shape of the pigment particle, as has been claimed in the past (1). The addition of stearic acid changed the nature of the vehicle but did not affect the particle shape, and yet the value of K did not remain constant. This is true regardless of whether one calculates K from the simple Einstein Eq. [1] or from the modification, Eq. [5].

It can be shown also that if K is assumed not to change with the addition of stearic acid, the values of k obtained from Eq. [5] are absurd. If K is a constant dependent only on the particle size and particle shape, the value 5.68 obtained for the pure polybutene system may be used. By using this value of K and the values of m given above, the values of kA and the volumes of the adsorbed layers can be calculated. The results of these calculations are summarized in Table IX.

These figures indicate definitely that the addition of stearic acid decreased either the volume of the adsorbed layer or the interstitial space. Regardless of the mechanism, the calculated total volume of the adsorbed layer cannot be less than the volume of the stearic acid known to be adsorbed. Since the amount of acid adsorbed was actually about three to four times greater than that calculated from Eq. [5], however, the value of K could not be the same for this system as for the pure polybutene system. This further indicates that K is not merely a shape factor but depends also on the nature of the relationship between the pigment surface and the external phase.

It is possible that the effect of stearic acid on the viscosity is due to a neutralization of the force field between the solid particles (26) and, consequently, to a reduction in aggregation tendencies. A reasonable assumption is that the acid is adsorbed with the polar group oriented towards the pigment. The polar carboxyl group could then partially counteract the fields around the pigment particles so that the particles would have less tendency to attract each other. A decrease in aggregation would have the same effect as a decrease in adsorption, namely, a reduction in viscosity.

ACKNOWLEDGMENTS

The authors are grateful to Drs. E. Gamble, R. R. Myers, and W. C. Walker of this Laboratory for many helpful discussions.

SUMMARY

1. The viscosity of the calcium carbonate-polybutene system increases with an increase in the surface area of the pigment, concomitant with a decrease in particle size.

2. The effect of the surface area may be attributed to the immobilization of vehicle and the corresponding increase in the fraction of the volume effectively occupied by the pigment.

3. This increase in effective volume may be handled at low volume concentration by adding a correction factor to the Einstein equation, making it:

$$\eta_{sp} = K(1 + kA)V,$$

where K is constant for a system of given chemical constitution, k is another constant, A is the area of the pigment so that kA is the volume of the adsorbed layer of vehicle, and V is the volume fraction of pigment.

4. At higher concentrations the correction for the adsorbed layer explains the differences in behavior of the pigments used here, but the data do not fit a linear relationship.

5. Particle-size distribution in the range from 0.1 to 0.4 μ has no effect on the viscosity of this system.

6. The lower the surface area of the carbonate pigment the greater the concentration must be before the suspension exhibits non-Newtonian flow and thixotropy.

7. The reduction of the viscosity by the addition of stearic acid as a surface-active agent may be attributed to adsorption of the acid by the pigment. The adsorbed acid appears to localize the interaction between vehicle and pigment so that the immobilized volume is decreased.

8. The constant K in the Einstein equation has been shown to be dependent upon the chemical nature of the system rather than only on the particle shape as was previously believed.

REFERENCES

1. EINSTEIN, A., *Ann. Physik* **19,** 289 (1906); *ibid.* **34,** 591 (1911).
2. BANCELIN, J., *Compt. rend.* **152,** 1582 (1911).
3. ODEN, S., *J. Physik. Chem.* **80** (709) (1912), *Nova Acta Regiae Soc. Sci. Upsaliensis* **3,** 4 (1913).
4. EIRICH, F., BUNZYL, M., AND MARGARETHA, H., *Kolloid-Z.* **79,** 236 (1936); *ibid.* **81,** 7 (1937).
5. BROUGHTON, G., AND WINDEBANK, C. S., *Ind. Eng. Chem.* **30,** 407 (1938).
6. GUTH, E., AND SIMHA, R., *Kolloid-Z.* **74,** 266 (1936).

7. Mark, H., "Physical Chemistry of High Polymeric Systems," Vol. 2, p. 279. Interscience Publishing Co., Inc., N. Y. (1940).
8. Vand, V., *J. Phys. & Colloid Chem.* **52,** 300 (1948); *ibid.* **52,** 314 (1948); *Nature* **155,** 364 (1945).
9. Vand, V., *J. Phys. & Colloid Chem.* **52,** 277 (1948).
10. Robinson, J., *J. Phys. & Colloid Chem.* **53,** 1082 (1949).
11. Brailey, R. H., Calco Tech. Report No. 901, American Cyanamid Co., N. J.
12. Kienle, R. H., Calco Tech. Report No. 901, American Cyanamid Co., N. J.
13. Arrhenius, C., *Z. physik. Chem.* **1,** 285 (1887).
14. Weltmann, R., and Green, H., *J. Applied Phys.* **14,** 569 (1943).
15. Droste, W. H., *Farben, Lacke, Anstrichstoffe* **3,** 61 (1949).
16. Traxler, R. N., Schweyer, H. E., and Moffatt, L. R., *Ind. Eng. Chem.* **29,** 489 (1937).
17. Hatschek, E., *Kolloid-Z.* **9,** 280 (1912).
18. Siesholtz, H., and Cohan, L. H., *Ind. Eng. Chem.* **41,** 390 (1949).
19. Lyttleton, D. V., and Traxler, R. N., *Ind. Eng. Chem.* **40,** 2115 (1948).
20. Mills, H., *J. Oil and Colour Chemists' Assoc.* **29,** 128 (1946).
21. Brunauer, S., "The Absorption of Gases and Vapors," Vol. 1. Princeton University Press, 1943.
22. Lower, G. W., Walker, W. C., and Zettlemoyer, A. C., *J. Colloid Sci.* **8,** 116 (1953).
23. Voet, A., private communication; see also Voet, A., and Suriani, L. R., *J. Colloid Sci.* **7,** 1 (1952); Preprint Booklet, ACS Division of Paint, Plastics and Printing Ink Chemistry, September 1953, p. 297.
24. Gourlay, J. S., *J. Oil and Colour Chemists' Assoc.* **34,** 385 (1951).
25. Harkins, W. D., and Anderson, T., *J. Am. Chem. Soc.*, **59,** 2189 (1937).
26. Hutchinson, E., *Trans. Faraday Soc.* **43,** 435, 439, 443 (1947).

THE LIESEGANG PHENOMENON.

I. SOL PROTECTION AND DIFFUSION

R. Matalon and A. Packter[1]

Received July 29, 1954

Abstract

The phenomenon of rhythmic precipitation is reviewed, and quantitative data are presented for four insoluble metal salt systems in gelatine and agar.

The conditions for which the precipitated zones appear, and their periodicity, have been analyzed in terms of the concentrations of the reacting ions and other factors.

The results show that the rhythmicity obeys a simple relation similar to that obtained theoretically from diffusion laws by previous investigators; but that absorption onto the sol formed in the gel medium is the predominant factor.

Among the theories proposed to explain the Liesegang phenomenon, that of Dhar and Chatterjee fits best the results obtained.

Introduction

Rhythmic precipitation was first observed by Liesegang (1). When a drop of concentrated silver nitrate solution is placed on a layer of gelatine gel, impregnated with potassium chromate solution, silver chromate is precipitated in the gelatine, not as a continuous precipitate, but in a series of concentric rings, separated by clear gel. The positions of the rings follow a geometric progression law, $x_n = ak^n$; where x_n is the distance of the nth ring from the origin of diffusion; a and k are constants, k being known as the spacing coefficient.

The phenomenon has since been examined by a large number of investigators, for a wide range of insoluble materials. S. Veil (2, 3) has presented a comprehensive range of the substances that have led to rhythmicity and stratification in gel media.

Although prior work has been primarily of a qualitative nature, it is known that several factors affect rhythmicity. S. Veil (2) has noted the effects of the gel medium on the phenomenon. The results indicate that silver and cuprous salts are rhythmically precipitated in gelatine, but not in agar; whereas lead iodide showed rhythmicity only in the latter medium. On the other hand, most cupric salts are rhythmically precipitated in silica gels.

---

[1] Present address: F. W. Berk & Co., Clay Development Laboratory, London Colney, England.

Foster (4) and Schleussner (5) have found that a trace of chloride ion in a previously dialyzed gelatine results in the appearance of clearly defined chromate rings. Liesegang (6) and other investigators remarked that for clear definition, a trace of free amino-solids in the gelatine is important, and gelatose, a hydrolyzed gelatine, has been added to the gel medium for this purpose.

The rhythmicity of silver chromate, lead iodide, etc., is modified by the *p*H of the gel medium; and it is well known that potassium dichromate leads to more defined rhythmicity than potassium chromate (Bradford (7), Kohler (8), Stansfield (9)).

Values for the spacing coefficient are rarely given in the literature, and workers in this field have generally based their observations on counting the visible rings (*cf.* Serb-Serbina (10), Holmes (11)). This is due to the fact that in most cases precipitation leads to blurred zones which do not lend themselves to quantitative recording. Although the silver chromate-gelatine system is well known for its rhythmicity, a quantitative correlation between the spacing coefficient and the relative concentrations of the reagents is, however, only vaguely found in the work of Lakhani and Mathur (12). These workers investigated the rhythmicity over a very narrow range of concentrations, and their experimental relation has received no mathematical support.

Two main hypotheses have been put forward to explain the Liesegang phenomenon. The supersaturation hypothesis of W. Ostwald (13) postulates that the material formed by metathesis, *e.g.*, silver chromate, is originally present as a highly supersaturated metastable *solution*, and only precipitates after a high degree of supersaturation or a supersolubility product has been reached. The main supporter of this theory has been van Hook (14).

According to the coagulation hypothesis of Dhar and Chatterjee (15), the insoluble material is first produced as a metastable *colloidal dispersion*, and not as a supersaturated *solution*. Precipitation then occurs, as a result of the coagulation of this dispersion by an excess of the diffusing ions.

More recently the authors (16) have investigated in detail the stability of insoluble metal salt sols in solutions of organic acids, and in gelatine, and have presented quantitative data in support of a coagulation hypothesis. Silver and complex copper salts sols are protected by gelatine, etc., by adsorption onto the surface of the sol particle, through free undissociated carboxyl groups.

In both cases, however, it is obvious that the "stability" of the sol, or of the supersaturated solution, in the gel medium is one important factor in this phenomenon.

Several authors have studied the possible role of diffusion (17, 18). In recent papers, Neumann and Costeanu (19) and Wagner (20) have deduced the geometric progression relation from diffusion laws, and, neglecting the effect of the gel medium, concluded that $(k - 1)$ should vary as the reciprocal of the initial concentration of the diffusing solution. As yet, no experimental evidence has been put forward to support these conclusions.

This work is an investigation into the quantitative aspects of rhythmic precipitation. The effects of various factors are considered—the gel medium, the nature and concentration of precipitated substance, as well as the influence of various impurities, which modify the substance precipitated and its rhythmicity. Among these, the effects of chloride ion and of *p*H have been investigated in detail. The substances studied are silver chromate and dichromate, trisilver arsenate, and disilver hydrogen arsenate, copper pyridine thiocyanate, and lead iodide. These systems have been selected since they readily give periodic precipitates in gels of gelatine or agar.

The rhythmic precipitation has been followed by free diffusion of a solution of the cation into the gel containing the anion. It is shown that the relationship $(k - 1) = A + B/C_0$ is verified, where k is the constant in the geometric progression law. The value of A depends on the gel medium and plays an important role in determining the periodicity, generally far greater than that of diffusion. For a series of silver salts, at constant anion concentration, A increases in the inverse order to the peptization ratio (as defined by Packter and Matalon (16)) observed for the corresponding sol in aqueous gelatine solution.

The value of B depends on the substance precipitated.

The presence of traces of chloride ion in the gelatine is known to affect markedly the periodicity of silver chromate. This effect is shown to be due to the flocculation of the positively charged silver chromate by negatively charged chloride ions.

Diffusion experiments have also been carried out in order to establish the cation-anion ratio along the diffusion path. It is shown that:

1. this ratio is a constant quantity for the position of the last ring, regardless of the time allowed for diffusion and of other factors to be outlined in detail.

2. this ratio varies, however, with the anion concentration according to a Freundlich law.

Experimental and Results

1. *Diffusion into Set Gels*

Whenever periodic precipitation is observed, this phenomenon is determined essentially by the cation-anion ratio present along the diffusion path. Diffusion experiments have therefore been carried out in the first instance on a solute diffusing into a gel, and then on the solute diffusing into a gel containing a precipitant.

A given volume of an aqueous solution of a reagent was left to stand over a gel contained in a test tube of standard cross section, for periods of time up to 96 hours. The average concentration of the diffused material at varying depths in the gel was obtained by determining the concentration present in slices of 0.5 cm. thickness along the gel. The method used for separating the gel from the glass tube prior to the slicing consisted in immersing the tube for about 10 seconds in a water bath heated to 60°C. The gel cylinder was then tipped over onto a filter paper and sliced with a razor blade. Titration of the reagents was carried out on aqueous dispersions of the slices at 30°C., using standard volumetric methods.

With silver nitrate, it was found that the ratio C_x/C_0 is independent of the initial concentration, C_0, of the diffusing solute within the range 1.00 M to 0.20 M; C_x is the concentration of diffusing cation at distance x from the origin of diffusion. Neither the type of gelatine used (*i.e.*, dialyzed photographic or undialyzed Coignet) nor the pH affected the ratio C_x/C_0. The ratio C_x/C_0 was, however, affected by the volume of the diffusing solution; and we adopted as standard a volume of 1 c.c. of solution diffusing into a gel cylinder of 15 c.c.

The diffusion of simple inorganic salts such as silver nitrate, copper sulfate, and lead nitrate has been followed, using gelatine with the first two salts and agar with the latter salt. The diffusion rate in all cases was found to obey the diffusion relation:

$$\frac{C_x}{C_0} = \frac{1}{f(t)} \exp \frac{-x^2}{\phi(t)}$$

where $f(t)$ and $\phi(t)$ are functions of the time of diffusion, t. Figure 1 shows the results obtained for silver nitrate for various values of t; similar graphs were obtained for copper sulfate and lead nitrate.

In all three cases,

$$\log \frac{C_x}{C_0} = \log M - Nx^2$$

or

$$\frac{C_x}{C_0} = Me^{-Nx^2}$$

M and N are shown to decrease as the time, t, before the gel is sliced, is increased.

2. Diffusion and Rhythmic Precipitation

When a reagent R diffuses into a gel containing a precipitant Q, a sol is first observed in the gel, followed sooner or later by the appearance of a ring of precipitated material, or of isolated crystals, arranged at a well-defined distance from the origin of the diffusion. As the time of contact

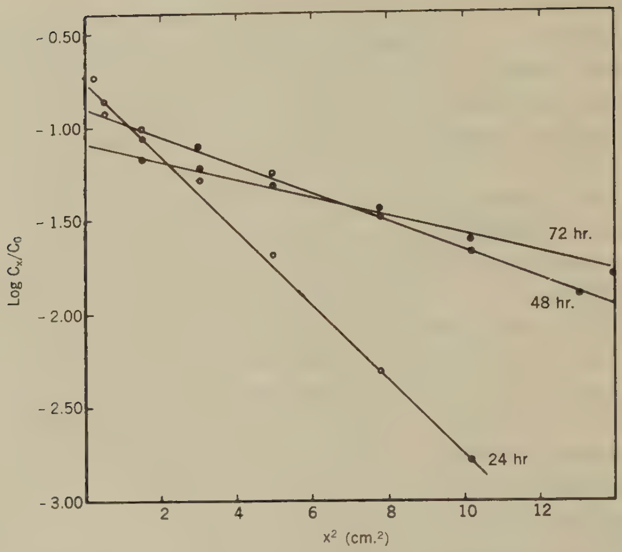

FIG. 1. Diffusion of 1 c.c. M silver nitrate into 5% gelatine gels. Variation in C_x/C_0 with distance.

increases and diffusion proceeds further into the gel, the number of rings gradually increases. Eventually, the number of rings obtained reaches a limit which is imposed by the relative concentrations of the reagents R and Q and by the nature of the precipitated material.

The following experiments have been carried out in order to establish the definite ratio of R to Q for which a periodic precipitation is obtained, as well as that for which finely dispersed sols of the material form in the gel.

The solution of the reacting cation was allowed to diffuse into a set gel containing the reacting anion.

It was found that diffusion was not affected by the presence of a reacting anion resulting in precipitation; thus the rhythmic precipitation is only a minor disturbance in the diffusion process.

The values of C_x obtained from such experiments are used in the latter part of this work to determine the cation-anion concentration ratios at the position of the last ring.

3. *Rhythmic Precipitation*

The method adopted here consisted in allowing the reacting cation to diffuse into the gel containing the reacting anion. This method results in a well-defined periodicity, as opposed to that of anion diffusion, which generally results in peptized sols.

A series of experiments were carried out in order to define quantitatively

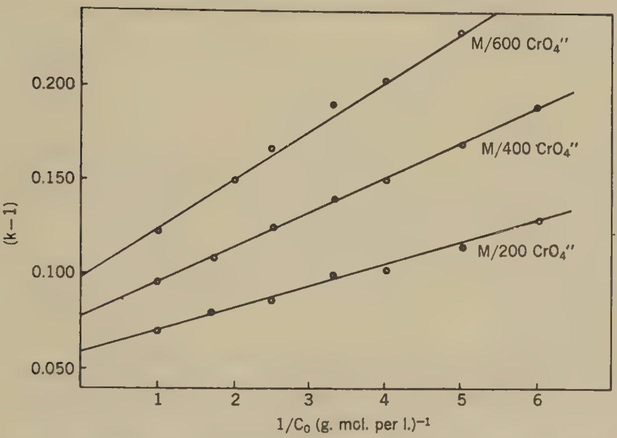

FIG. 2. Direct precipitation of silver chromate in 5% Coignet gelatine gels (pH 5.2). Variation in spacing with Ag^+ ion concentration.

the k values in the geometric progression law, $x_n = ak^n$ (Jablczynski (17)) as well as to study the effect of various factors such as pH, relative concentration ratios, and the properties of the gel medium which affect the rhythmic behavior. In the following certain experimental conditions will be described under which we have found rhythmicity to be well defined and quantitative analysis possible.

Rhythmic precipitation was studied by measuring in a cathetometer the distance between respective rings. The value of k was obtained from an average of at least ten rings with an experimental error of 2% to 5%.

(*a*) *Effect of the Cation Concentration in the Diffusing Solution.* A series of experiments were carried out on silver chromate, disilver hydrogen arsenate, copper pyridine thiocyanate in gelatine at pH 5.2 (and containing a trace of chloride in the case of silver chromate), and on lead iodide in agar in order to determine the effect of the concentration of the diffusing solution on the rhythmic precipitation. The results obtained (Figs. 2, 3, 4, and 5) show that in all cases

$$(k - 1) = A + B/C_0,$$

where C_0 is the initial concentration of the diffusing solution, and A and B are constants.

(*b*) *Effect of the Anion Concentration in the Gel.* A series of experiments were carried out on the effect of anion concentration in the gel. The results obtained for the various systems are presented in Figs. 2, 3, 4, and 5. In the case of copper pyridine thiocyanate, it was found possible to obtain clear periodicity only at one anion concentration.

In all cases at constant cation concentration, increasing the anion concentration has the effect of decreasing the values of both A and B.

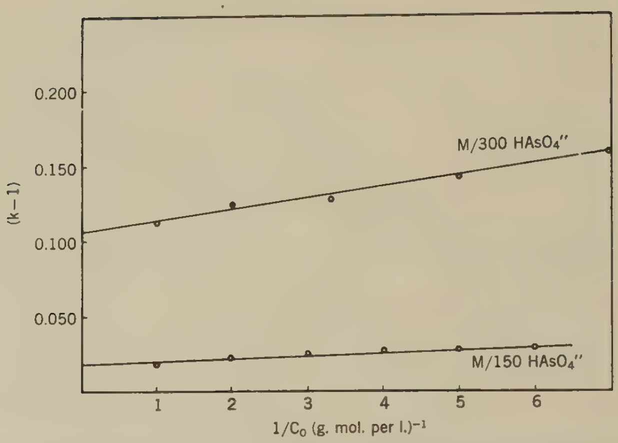

FIG. 3. Direct precipitation of silver arsenate in 5% dialyzed gelatine gels (pH 5.2). Variation in spacing with Ag^+ ion concentration.

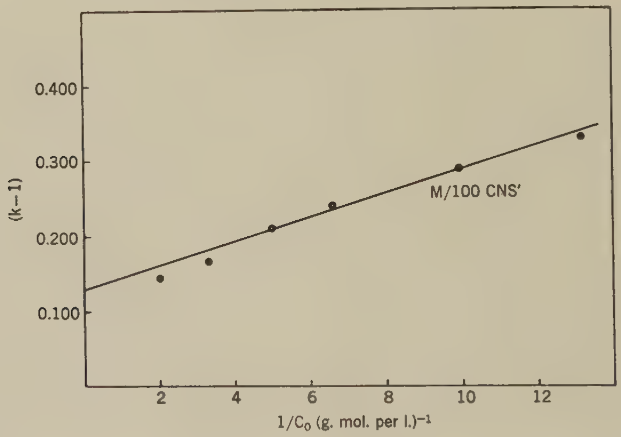

FIG. 4. Direct precipitation of copper pyridine thiocyanate in 5% dialyzed gelatine gels (pH 6.4). Variation in spacing with Cu^{2+} ion concentration.

The value of A varies with the anion concentration (C_Q), according to the relation

$$A = a\left[\frac{1}{C_Q}\right]^n,$$

where n is a constant, generally greater than unity. The values of n, determined from the results available, are 0.2, 1.1, 1.3, and 2.7 for lead iodide, silver chromate, copper pyridine thiocyanate, and silver hydrogen arsenate, respectively.

(c) *Effect of pH*. The phenomenon of rhythmicity was studied over pH

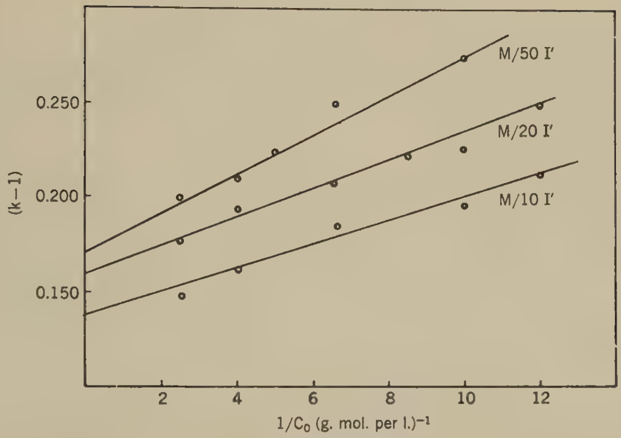

FIG. 5. Direct precipitation of lead iodide in 1% agar gels (*p*H 6.8). Variation in spacing with Pb^{2+} ion concentration.

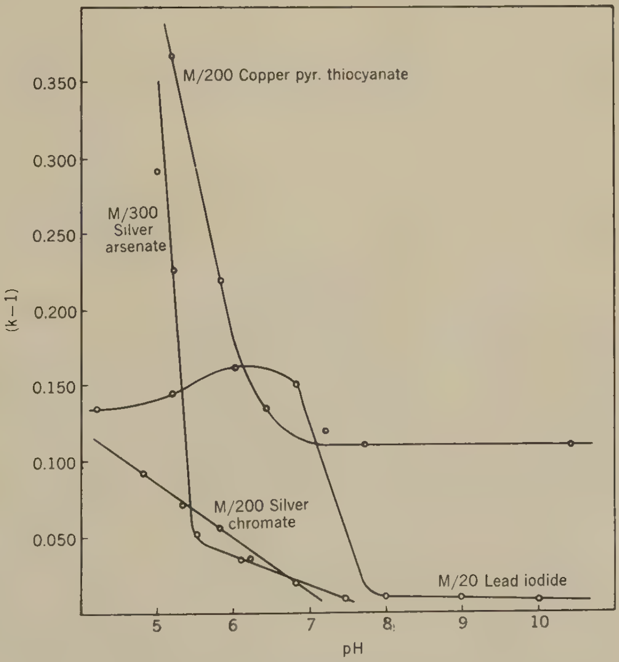

FIG. 6. Direct precipitation of metal salts. Variation in spacing with *p*H of the gel medium.

values ranging from 3.5 to 12 by addition of acetic acid or ammonia to the gel medium.

The results obtained for the various salts are represented in Fig. 6. For copper pyridine thiocyanate, it was found that, on varying the *p*H between 11 and 6, the value of k remained practically constant. At pH values below 6, however, k showed signs of increasing and peptization was observed at pH 5.2, preventing further quantitative measurements with the cathetometer.

It is interesting to note that, whereas in the case of silver chromate $(k - 1)$ is directly proportional to the pH over the range 6.8 to 4.8, a definite change in behavior is observed for silver arsenate and lead iodide at well-defined pH values. With the silver arsenate system, a marked change in the slope of the curve is observed around pH 5.4. A similar change is observed with lead iodide at pH 6. For both salts, flocculation is observed in alkaline medium, whereas peptization occurs in acid medium. The critical pH values at which a marked change in the rhythmic behavior is observed is indicative of a radical change in the composition of the precipitated material. With arsenate salts, the disilver hydrogen arsenate is precipitated at pH values lower than 5.4, and the trisilver arsenate at pH's greater than 5.4. This result is in agreement with the pK value of the arsenate salts reported in the literature (Blanc (21)). With lead iodide, basic salts are precipitated at pH values higher than 6. This is in agreement with the known properties of this lead salt at these pH values (Demassieur (22)).

A series of experiments has been carried out on the 0.005 M silver chromate system in Coignet gelatine in order to investigate the effect of the pH of the gel medium on the values of the constants A and B. The results obtained show that the value of B remains constant over the pH range 6.8 to 4.8 (beyond which peptization occurs), whereas the value of A increases with decrease in the pH (Table I).

(*d*) *Effect of the Gel Medium.* The rhythmic behavior of silver chromate depends to a great extent on the type of gelatine used.

Table II shows the $(k - 1)$ values obtained at pH 5.2 in gelatines at constant chloride ion concentration of 0.003 M.

In this table the free acidity of various gelatines is also presented. These results show that as the free carboxylic groups available are increased in the gelatine used, the value of k is also increased.

TABLE I

Variation of A with pH

0.005M K_2CrO_4 in 5% Coignet Gelatine

pH	A
6.6	0.002
6.2	0.028
5.8	0.045
5.3	0.058
4.8	0.065
4.4	0.100

TABLE II

Effect of the Gel Medium on k − 1 Values

Gelatine	$0.0025M$ CrO_4''	$0.005M$ CrO_4''	Free acidity expressed as cc. N soln. per 100 g.
Photographic (dialyzed)	0.047	0.017	14.9
Coignet (not dialyzed)	0.130	0.070	24.4
Spa (not dialyzed)	Peptized sol	Peptized sol	40.4

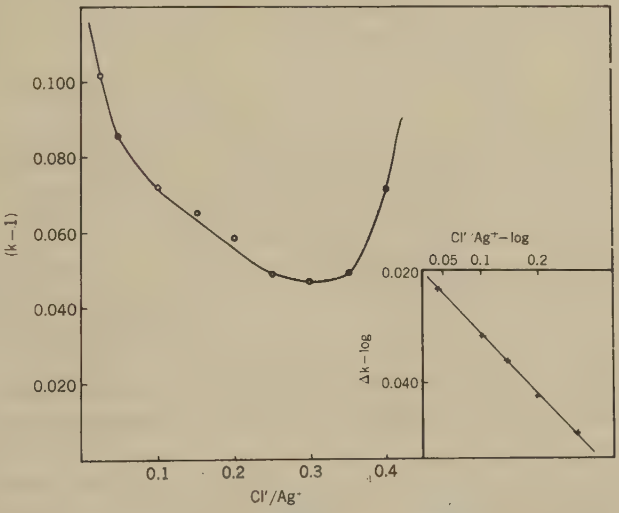

FIG. 7. Direct precipitation of 0.0025 M silver chromate. (1 c.c. M Ag^+ into 5% dialyzed gelatine gels. pH 5.2) Variation in spacing with chloride-silver concentration ratio.

This result suggests that the rhythmic behavior is governed, among other factors, by the structure of the gel medium and, in particular, by the available polar groups which are reacting with the silver ions.

(*e*) *Effect of Chloride Ions.* In the examples already cited we have indicated that a constant chloride ion concentration was added when necessary to the gel medium. A series of experiments have been carried out on silver chromate precipitation in dialyzed gelatine, and a study of the effect of chloride has been made. The results are shown in Fig. 7. It is found that, whereas the gelatine in absence of chloride ion leads to a peptized sol, the presence of a minute amount of chloride leads to a well-defined rhythmicity. The values of k decrease continuously up to a maximum chloride-silver ratio, after which further increase in chloride ion concentration leads to an increase in k.

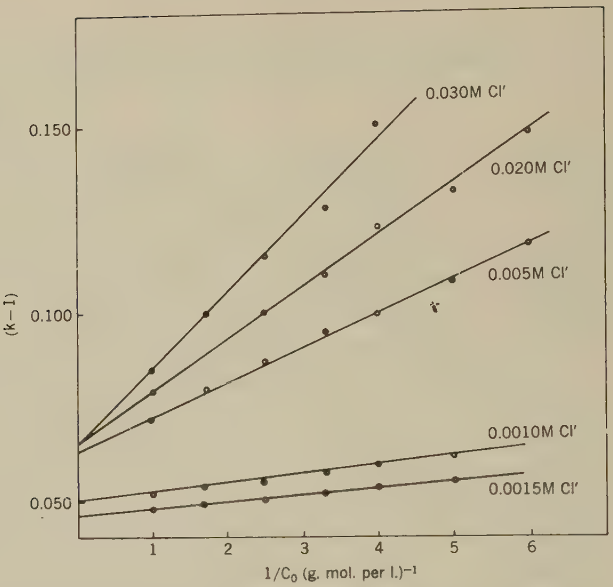

FIG. 8. Direct precipitation of 0.0025 M silver chromate in 5% dialyzed gelatine gels (pH 5.2). Variation in spacing with Ag^+ ion concentration. Addition of chloride ion.

The linearity observed, between log Δk and log $[Cl']/[Ag^+]$ indicates that the chloride ion is absorbed on the silver chromate sol, according to a Freundlich isotherm.

The presence of chloride ion is not essential in the silver arsenate system. With the copper pyridine thiocyanate system, it was found to have no effect on the rhythmicity.

(*f*) *Effect of Cation Concentration at Varying Chloride Ion Content.* A series of experiments has been carried out on the system 0.0025 M Ag_2CrO_4 in dialyzed gelatine, in order to investigate the effect of chloride ion concentration on the values of A and B. The results are presented in Fig. 8. It is shown that with increasing Cl'/Ag^+ ratio the values of A and B both decrease, the fall in B being very marked. With further increase in the chloride ion concentration and consequent repeptization, there is an increase in both the A and B values.

4. Importance of the Cation-Anion Ratio in Determining Rhythmic Behavior

Several experiments were carried out on the systems previously studied in order to define the cation-anion ratio at various distances along the gel medium where peptization, periodic precipitation, and flocculation were observed. (This ratio is a constant quantity for the position of the last

TABLE III

The Effect of Anion Concentration on Cation-Anion Ratios for Silver Chromate

A. 5% Coignet Gelatine, *p*H 5.2, $0.003M$ Cl′[a]

	$0.001M$ CrO_4''	$0.0025M$ CrO_4''	$0.005M$ CrO_4''
Flocculation	50.0	26.0	9.0
Periodic precipitate	12.0	3.5	1.0
Peptized Sols	1.0	0.5	0.2

B. 5% Dialyzed Gelatine, *p*H 5.2, No Cl′

	$0.001M$ CrO_4''	$0.0025M$ CrO_4''	$0.005M$ CrO_4''
Flocculation	100	100	14.0
Periodic precipitate	70.0	20.0	3.0
Sol	0.5	0.2	0.1

[a] Present as an impurity ($CaCl_2$) in the gelatine.

TABLE IV

The Effect of pH on Cation-Anion Ratios for Silver Chromate and Silver Arsenate

A. Silver Chromate, $0.005M$ K_2CrO_4 in 5% Coignet Gelatine

	5.2	6.8
Flocculation	9.0	10.0
Periodic precipitate	1.0	1.0
Peptized sols	0.2	0.2

B. Silver Arsenate, $0.0033M$ Na_2HAsO_4 in 5% Dialyzed Gelatine

	4.2	4.8	5.0	5.2	5.5	6.1	6.8	7.7
Periodic precipitate (brown crystals)	100	100	40.0	10.0	1.5	0.5	0.2	0.1
Periodic precipitate (black crystals)	30.0	30.0	2.0	1.0	0.05	0.05	0.05	0.05

ring, irrespective of the time of diffusion.) The results obtained for the silver chromate system are summarized in Tables III, IV, and V.

(*a*) *Effect of Anion Concentration.* The results are presented in Table III.

As the cation-anion ratio is decreased, the reaction product varies from the flocculated state to a finely dispersed sol, the periodic precipitation representing the intermediate stage. As a general rule, the cation-anion ratios for which the various states are observed decrease as the anion concentration is increased, according to the relation

$$\frac{C_R}{C_Q} = \alpha \left[\frac{1}{C_Q}\right]^n.$$

Similar results have been obtained with the other systems investigated.

TABLE V

The Effect of Chloride Ion on Cation-Anion Ratios for Silver Chromate

$0.0025M$ K_2CrO_4 in 5% Dialyzed Gelatine

		$0.00025M$		$0.0005M$	
	No addition	$0.001M$ Cl′	to $0.0005M$ Cl′	$0.004M$ Cl′	$0.005M$ Cl′
Periodic precipitate	20.0	4.0	1.5	1.5	1.5
Sols	0.2	0.1	0.2	0.1	0.3

The values of C_R/C_Q may be compared with the cation-anion ratios for rapid coagulation of the corresponding metal salt sols in aqueous solutions of gelatine and agar (16). In every instance, rapid coagulation occurs at a far lower cation-anion ratio in the aqueous solution.

(*b*) *Effect of pH*. The results are given in Table IV.

Similar results as in Table IV, *B*, have been observed with the other systems. Increasing the *p*H values generally tends to decrease the various ratios at which the reaction leads to flocculation, periodic precipitation or sol formation.

(*c*) *Effect of Chloride Ion.* The effect of chloride ion on the ratios previously determined was followed for the silver chromate system in dialyzed gelatine (Table V).

It is found that on addition of chloride the critical value of the silver-chromate ratio at which the rings are formed decreases very rapidly and soon reaches a minimum constant value.

DISCUSSION

1. The Spacing Law

We have noted that the Liesegang phenomenon is characterized by a geometric progression law governing the position of consecutive rings, and a similar geometric law is obeyed for the time necessary for the appearance of the rings (Morse and Pierce (23)).

The spacing coefficient, according to Wagner (20), obeys the relation

$$(k - 1) = B/C_0,$$

where C_0 is the initial concentration of the diffusing solution, and B is directly dependent on the supersaturation.

The present work demonstrates that, provided a certain cation-anion concentration ratio is reached, periodicity is observed in the precipitation. The position along the tube at which this minimum cation concentration, *i.e.*, the minimum sol concentration, C_R is reached, depends, however, not only on diffusion but also on the adsorption occurring with the gel medium.

As a result of adsorption, the effective cation concentration at any point along the gel is reduced by an amount $C_0 . KC_G{}^m$, where C_G is the concentration of the gel medium, and K and m are constants. Hence Wagner's relation should be expressed as

$$(k - 1) = \frac{C_R + KC_G{}^m C_0}{C_0} = \frac{C_R}{C_0} + KC_G{}^m.$$

The experiments carried out indicate, in fact, a spacing law,

$$(k - 1) = A + B/C_0,$$

and $A(=KC_G{}^m)$ demonstrates the adsorption effect of the gel medium. When C_0 is large ($>0.5\ M$), the spacing is determined by this factor. The adsorption effect was neglected by Wagner, whose relation was based on diffusion alone.

The value of the constant K depends, in turn, on the interaction between the gel medium and the substance precipitated, and A, for a specific gel concentration, varies with the concentration of the precipitate, C_Q, according to a Freundlich law,

$$A = a\left[\frac{1}{C_Q}\right]^n.$$

A large value of n shows that the stabilizing effect of the gel medium falls rapidly as the amount of precipitate is increased; whereas the small value observed for lead iodide indicates that agar is an excellent stabilizing agent for this material over a wide range of concentration.

For a series of silver salts at constant C_Q, the values of A increase in the *inverse* order to the peptization ratios (16) observed for the corresponding sol, in aqueous gelatine suspension:

Arsenate > chromate > oxalate > chloride.

The constant B, according to Wagner, is directly dependent on the "supersaturation." The experimental results obtained show that the values of B are, in fact, essentially determined by the minimum cation concentration, C_R, at which precipitation occurs. The value C_R, in turn, is dependent on the concentration of the precipitated material and the *p*H of the gel medium, and in the case of silver chromate, on the presence of traces of chloride ion. In these latter systems, the variation of B with the Cl'/Ag^+ ratio is very marked, and the spacing coefficient is very much affected by traces of chloride ion.

2. *The Mechanism of Protection*

Rhythmic precipitation observed in gels is a highly specific phenomenon, depending on the nature of the material precipitated in the gel medium as well as on those factors which by their presence modify the actual precipitation mechanism. The values of A have in fact been observed to vary with the concentration and structure of the precipitated material.

The gel medium not only acts in slowing down the rate of diffusion, thereby retarding the precipitation reaction, but also acts as a protecting agent bringing about the initial formation of a more or less stable sol. Gelatine and related amino acids have been found excellent protecting agents for silver arsenate, silver chromate, and copper pyridine thiocyanate sol in aqueous solution (16), and agar and other polysaccharides are powerful peptizers for lead iodide. It is significant that when the gel medium is a poor protecting agent for the precipitated substance (as with silver oxalate and chloride) (16), A is very low and no rhythmicity is observed. Protection is not due to the withdrawal of, for example, free Ag^+ ions to form a silver ion-gelatine complex, as proposed by van Hook (24); but the Freundlich type of relation between (C_R/C_Q) and C_Q indicates that the protection is due to an adsorption mechanism. Precipitation in gel media is caused by the coagulation of the protected sol, by the flocculating ion. The authors (16) have indeed obtained similar results for the protection of insoluble metal salts in gelatine solutions. The higher cation concentration required for coagulation of a sol of particular concentration indicates that other factors are occurring in the gel medium.

3. The Effect of Chloride Ion

The material rhythmically precipitated in gelatine is initially stabilized in the sol form by the positively charged gelatine, $^+NH_3G \cdot COOH$. Negatively charged ions destabilize the sol and lead to rapid coagulation. This effect has been demonstrated with the chloride ion. The presence of minute traces of this ion in gelatine brings about a marked change in the precipitation behavior of silver chromate in set gels. Stable sols give rhythmic rings of precipitate in the presence of traces of chloride ion. The spacing coefficient decreases with the concentration of chloride ion, according to a Freundlich type of isotherm, $\Delta k = a(C_{\mathrm{Cl'}})^n$, suggesting a preferential adsorption of the negatively charged ion, on the silver-chromate sol.

A similar flocculation process has been observed in aqueous sols, of this material.

4. The Mechanism of Precipitation

Two main theories have hitherto been proposed to account for the Liesegang phenomenon. The quantitative data obtained in this work all tend to confirm a coagulation theory.

According to the law of mass action, one would expect the following results: (1) the peptization ratios for a series of silver salts should be stoichiometric, independent of the concentration of reacting ions, and vary directly as the solubilities in water;[2] (2) the "supersolubility product" for a particular metal cation and gel system should be independent of the concentration and nature of the salt precipitated.

The cation concentrations at which precipitation occurs are, in many instances, not in accordance with the law of mass action and tend to vary with the nature and concentration of the salt precipitated. The ratio C_R/C_Q in fact varies with C_Q, according to a Freundlich-type law.

CONCLUSIONS

It is shown that adsorption on to the sol, formed in gel media, is a predominant factor in the Liesegang phenomenon. The conditions for which the precipitated zones appear and their periodicity have been analyzed in terms of the relative ratios of the reacting ions, and of the adsorption of the gel medium on to the initial sol.

The results obtained show that simple relations are obeyed for the periodicity of the type proposed by Wagner from diffusion laws. An additional effect of importance in determining the spacing coefficient is the nature of the gel, which influences the stability and the growth of the precipitate.

Among the theories hitherto proposed, that of Dhar and Chatterjee fits best the results obtained. The conclusion is reached that for every salt considered the interaction with the gel medium is a specific one, not necessarily determined by the interaction with any one of the single ions of the salt.

ACKNOWLEDGMENTS

We wish to express our thanks to Professor Sir Eric Rideal for his continuous interest and helpful suggestions; and to Crookes Laboratories, Ltd., for a grant to one of us (A. P.).

REFERENCES

1. LIESEGANG, R., *Z. physik. Chem.* **23,** 365 (1897).
2. VEIL, S., "Les Periodicités de Structure." Paris, 1935.
3. VEIL, S., *Bull. soc. chim. France* [5] **17,** 212 (1949).
4. FOSTER, J., *J. Phys. Chem.* **23,** 145 (1919).
5. SCHLEUSSNER, R., *Kolloid-Z.* **31,** 347 (1922).
6. LIESEGANG, R., *Z. physik. Chem.* **88,** 1 (1914).
7. BRADFORD, J., *Biochem. J.* **10,** 169 (1916).
8. KOHLER, A., *Kolloid-Z.* **19,** 65 (1916).
9. STANSFIELD, R., *Am. J. Sci.* **43,** 1 (1917).

---

[2] This statement is not in accord with the findings of La Mer and Dinegar, *J. Am. Chem. Soc.* **73,** 380 (1951) who find that the critical limiting supersaturation in the absence of colloid is a specific reproducible number depending upon the salt precipitated. (Editor)

10. Serb-Serbina, N. N., *Kolloid-Z.* **62,** 79 (1933).
11. Holmes, H. N., *J. Am. Chem. Soc.* **40,** 1187 (1936).
12. Lakhani, K., and Mathur, N., *Kolloid-Z.* **67,** 59 (1936).
13. Ostwald, W., *Z. physik. Chem.* **27,** 265 (1897).
14. van Hook, A., *J. Phys. & Colloid. Chem.* **42,** 1191 (1938).
15. Dhar, N. R., and Chatterjee, A. C., *Kolloid-Z.* **31,** 15 (1922).
16. Packter, A., and Matalon, R., *Discussion Faraday Soc.,* in print, 1954.
17. Jablczynski, K., *Bull. soc. chim. France* [4] **33,** 592 (1923).
18. Schleussner, R., *Kolloid-Z.* **34,** 338 (1924).
19. Neumann, K., and Costeanu, V., *Kolloid-Z.* **84,** 130 (1940).
20. Wagner, C., *J. Colloid Sci.* **5** (1), 85 (1950).
21. Blanc, E., *J. chim. phys.* **18,** 28 (1920).
22. Demassieur, N., *Compt. rend.* **189,** 428 (1929).
23. Morse, H. W., and Pierce, G. W., *Z. physik. Chem.* **45,** 589 (1907).
24. van Hook, A., *J. Phys. & Colloid Chem.* **45,** 422 (1941).

STUDIES IN WATER-IN-OIL EMULSIONS.

IV. THE INFLUENCE OF THE EMULSIFYING AGENT ON THE VISCOSITY OF WATER-IN-OIL EMULSIONS OF HIGH WATER CONTENT

P. Sherman

Gestetner Ltd., Tottenham, London, N. 17, England

Received July 29, 1954; revised September 23, 1954

Abstract

The role of the emulsifying agent in determining the viscosity of water-in-oil emulsions of identical high volume concentration disperse phase has been investigated. Ten nonionic emulsifying agents were examined. The relative viscosity of the emulsions prepared from six of these were of the same order, but appreciable divergences from the mean were exhibited by the remainder. It is concluded that the chemical constitution of the emulsifying agent does affect the resultant emulsion viscosity, presumably through the physical state of the film formed at the interface and its relationship to the two phases.

Introduction

Equations defining the viscosity of dilute solid dispersions (1) or emulsions (2) generally indicate a dependence on the viscosity of the continuous medium and the volume concentration of disperse phase, whereas the nature of the emulsifying agent itself is not taken into account. In the more complex case of concentrated dispersions, or emulsions where it is assumed that the particles are small enough to be considered as rigid spheres (3), the equations are modifications of the classical Einstein equation. In these due allowance is made for the various phenomena involving the dispersate particles, *e.g.*, interaction between the particles (4), presence of an electric charge on their surface (5), increase in the over-all dimensions due to hydration (6), and nonspherical shape (7). In the case of water-in-oil emulsions Schulman and Cockbain (5) observed that the water droplets were of irregular shape and attributed this to the rigid nature of the interfacial film. They also assumed "that the state of the interfacial film as observed at the air-water interface i.e. solid, viscous, or liquid, is reflected in the nature of the resultant emulsion being respectively a grease, viscous, or a liquid emulsion." No quantitative data were provided.

Few observations have been reported in the literature on the specific influence of the emulsifying agent when working with emulsions of identical volume concentration disperse phase, and those which are to be found relate solely to oil-in-water emulsions. Thus Gabriel (8), investigating asphaltic bitumen emulsions, noticed that their viscosity varied considerably, but this was attributed to variation in the degree of water absorption by the different bitumens. Broughton and Squires (3) working with olive oil, benzene, and Nujol as the oil phase and with sodium oleate, saponin, and triethanolamine oleate as emulsifying agents, showed the influence of the emulsifying agent in determining emulsion viscosity, and found that the most efficient stabilizers were those which gave the emulsions of lowest viscosity. Toms (9) prepared emulsions of 50% volume concentration disperse phase, using sodium and potassium laurates, myristates, palmitates, stearates, and oleates as emulsifiers, and various organic liquids as dispersates. The emulsions differed appreciably in viscosity, those stabilized by oleates being found to be less viscous than those stabilized by the other soaps. It was concluded that these variations were explainable on the basis of interaction at the oil-water interface between the emulsifying agent and the two phases. Sumner (10) observed that at the same volume concentration the emulsions of lowest viscosity showed least tendency to flocculate; he also stressed the importance of the interfacial complex.

In the present work water-in-oil emulsions of the same volume concentration have been prepared with various emulsifying agents, and the influence of the latter on the viscosity and flow properties investigated. The ten surface-active agents examined were all of the nonionic type.

EXPERIMENTAL

The emulsion composition was maintained constant throughout:

Aqueous phase:
- 6.5% Glycerine (pale straw grade).
- 65.5% Distilled water.

Oil phase:
- 2.8% Emulsifying agent.
- 25.2% Mineral oil ($\eta_{21^\circ} = 0.136$ poise).

The values quoted are all weight percentages. The emulsifiers were all readily soluble in the mineral oil, and no heating was necessary to effect their solution. The emulsions were prepared at room temperature by carefully adding the aqueous solution to the oil phase with efficient stirring; they were then passed twice through a pentacreme homogenizer. In this manner very homogeneous emulsions of small particle size (approximately 2 μ) were obtained in all but two cases. Blown soya oil gave a wide range of particle size distribution, and in both this emulsion and that prepared from soya lecithin many multiple emulsion droplets were observed. Polyethylene glycol (200) monooleate emulsified spontaneously, but propylene glycol monooleate, blown soya, and glyceryl polyricinoleate did not promote smooth emulsification, and very vigorous agitation was necessary.

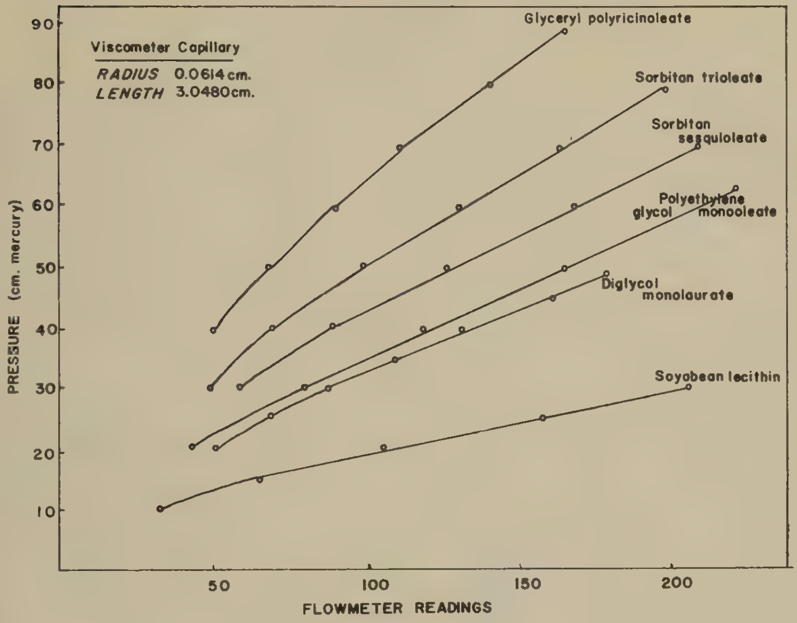

FIG. 1. Flow curves of some emulsions.

Emulsion viscosity measurements were carried out with the use of a variable-pressure capillary plastometer in the manner indicated in a previous paper of this series (11). Once again the reciprocal mobility was adopted as the nearest approximation to the viscosity (η). Figure 1 illustrates the shear behavior with varying stress of some of the emulsions preprepared. In all cases there is a decrease in the "apparent" viscosity with increasing rate of shear, the graphs eventually becoming linear.

Determination of the viscosity of the oil phase (η_0) was carried out with an Ostwald viscometer of the conventional pattern. The dimensions were such that the kinetic energy (12) and surface tension (13) correction factors could be neglected. Owing to slight variation in the density of the oil phase in some cases, the volume concentration (ϕ) showed a slight deviation from the value of 0.686, but it was small enough to be of no consequence.

The viscometric data are shown in Table I. All determinations were carried out at 21.0° ± 0.1°C.

The calculated volume concentration ($\phi_{\text{calculated}}$) was derived from the Hatschek relationship for concentrated emulsions (3)

$$\phi = \frac{(\eta - \eta_0)^3}{\eta^3}$$

The volume factor $h = \phi_{\text{calculated}}/\phi_{\text{observed}}$.

Emulsion stability tests were performed by transferring samples to

TABLE I

Viscosity Measurements

Emulsifying agent employed	Reciprocal mobility η (poises)	Intercept yield value	η_0	η/η_0	ϕ observed	ϕ calculated	Volume factor h
Soya lecithin	1.10	807	0.168	6.55	0.688	0.609	0.89
Sorbitan sesquioleate	2.60	1766	0.176	14.77	0.687	0.811	1.18
Sorbitan monooleate	2.67	1456	0.176	15.14	0.687	0.815	1.19
Sorbitan trioleate	3.22	1922	0.169	19.03	0.686	0.850	1.24
Polyethylene glycol (200)[a] monooleate	2.10	1214	0.151	13.91	0.686	0.799	1.17
Diglycol monolaurate	2.14	1221	0.144	14.86	0.686	0.811	1.18
Propylene glycol monooleate	2.20	1614	0.149	14.76	0.686	0.810	1.18
Blown soya bean oil	2.72	3229	0.184	14.78	0.686	0.811	1.18
Glyceryl polyricinoleate	4.21	2825	0.358	11.76	0.686	0.766	1.12
Polyethylene glycol polyricinoleate	3.90	2371	0.939	4.15	0.686	0.437	0.64

[a] The 200 refers to the molecular weight of the polyethylene glycol chain.

graduated stoppered cylinders which were maintained at 35°C. for eight weeks. The diglycol monolaurate emulsion broke down within 24 hours, the emulsifying agent being precipitated as a solid flocculate. In all other cases there was no visible water separation at the end of the aging period, although "creaming" occurred in one or two cases; consequently the samples were centrifuged at 6000 r.p.m. for 10 minutes and the degree of water separation estimated. The results are given in Table II. Also included are the ranges of particle size within the aged emulsions. It was observed that the lecithin emulsion showed an appreciable increase in the number of multiple emulsion droplets on aging, the structure now being similar to that of an inferior-quality groundnut lecithin emulsion.

Parallel with the above work an evaluation was made of the technique suggested by Cockbain and McRoberts (14) with a view to developing a fairly rapid method for the determination of emulsion stability. Seven emulsifying agents were examined at 0.5% weight concentration in the oil phase, and the constants obtained are indicated in Table III. Owing to slow adsorption in some cases, the interfaces were aged for 1 hour prior to investigating the rate of drop coalescence. Drop stabilities were determined at 24.0° to 25.0°C. As the stability of water drops at the oil-water interface greatly exceeds that of oil drops, it was found more convenient to determine

TABLE II

Results of Emulsion Stability Tests

Emulsifying agent employed	Oil separation after 8 weeks* (*ml.*)	Water separation on centrifuging† (*ml.*)	Particle size range in aged emulsion (μ)
Soya lecithin	34	0.2	Normal drops 10–48. Multiple drops 80–110
Sorbitan sesquioleate	1	Nil	Very homogeneous; not greater than 3.5
Sorbitan monooleate	Nil	0.1	Very homogeneous; not greater than 4.5
Sorbitan trioleate	1	0.06	Very homogeneous; not greater than 4.5
Polyethylene glycol (200) monooleate	3	Nil	Mainly 3–6
Diglycol monolaurate	Unstable; broke down within 24 hours		
Propylene glycol monooleate	25	1.5	Mainly 20–27
Blown soya bean oil	3	0.1	Normal drops 3.0–7.0. Multiple drops 20.0–27.0
Glyceryl polyricinoleate	3	0.1	Very homogeneous; not greater than 4.5. A few multiple droplets
Polyethylene glycol polyricinoleate	Nil	Nil	Very homogeneous; not greater than 3.5

* Volume of emulsion stored in each cylinder was 150 ml.

† Capacity of centrifuge tubes was 6.2 ml.

TABLE III

The Stability of Emulsion Drops

Emulsifying agent	Average volume per drop (*ml.*)	Coalescence rate constant k (*min.*$^{-1}$)	Half-life time of drops $\tau_{1/2}$ (*min.*)	Drainage time t_D (*min.*)
Soya lecithin	0.012	1.20	0.21	0.09
Sorbitan sesquioleate	0.004	0.33	0.65	0.45
Sorbitan monooleate	0.005	0.43	0.60	0.42
Polyethylene glycol (200) monooleate	0.004	0.23	0.78	0.22
Diglycol monolaurate	0.009	2.38	0.17	0.09
Propylene glycol monooleate	0.008	1.54	0.22	0.14
Glyceryl polyricinoleate	0.010	0.95	0.64	0.43

the lifetime of the latter, thus permitting numerous observations in a conveniently short period of time as a routine test. Simultaneously interfacial tension measurements could be made when desired.

Results and Discussion

The emulsifying agent exerts a profound influence on the viscosity of emulsions of high disperse phase concentration. This effect is not likely to be so pronounced in more dilute dispersions, and at such concentrations that the mean free path between the dispersed globules is equal to, or greater than, the diameter of the globules, the effect will be negligible.

Reference to Table I indicates that the relative viscosities of the emulsions prepared from the ten emulsifying agents examined vary over a wide range. Six of these fall within the limits 13.9 to 15.2, whereas of the other four, three gave values falling below the mean. The low viscosity of the soya lecithin emulsion is probably accounted for by the fact that a gaseous type of film is formed at the oil-water interface (15); further complications arise through the formation of multiple emulsion droplets. Woodman (16) attributed this latter phenomenon to the presence in lecithin of opposite-type emulsifiers each exerting its own influence independently of the other. Qualitative observation indicated that the glycol esters yielded interfacial films much more rapidly, but of lesser rigidity, than the other emulsifiers examined. This is reflected in the lower viscosity of the former. The two polyricinoleates examined show low relative viscosities, but this may be due to the very slow interfacial adsorption observed which results in the emulsion viscosity not remaining constant but rising progressively to a maximum over a period of a few days after preparation (17). This would also result in the "Volume factor" h increasing proportionately. The polymerized derivatives raise the viscosity of the oil phase to a much greater extent than do the other emulsifying agents; this is to be expected on the basis of their high molecular weight and complex structure. In addition, the relationship of η_0 to η is reflected in the conformance of the majority of the emulsions with the Sibree modification of the Hatschek equation, h lying in the region of 1.2.

The precise interpretation of "yield value" data, which is obtained by extrapolation of the straight-line region of the plastometer curve, is still a subject for much speculation. Most theories approximate to the view that it defines the shearing stress at which the attractive forces ("internal friction") between the dispersed particles have been overcome and laminar flow prevails. In this instance the highest "yield values" and viscosities are exhibited by the emulsions prepared with the surface-active molecules containing several carboxylic acid radicles, viz., sorbitan trioleate, the polyricinoleates, and blown soya oil. With all these agents a greater degree of aggregation should be possible by the interlocking of the hydrocarbon chains than is feasible with the mono-esters. A higher shearing stress would then be required to effect "deflocculation" in the former case prior to the exhibition of Newtonian-type flow.

Comparison of the results in Tables II and III shows good agreement in the relative order of emulsion stabilities, although a direct quantitative relationship is not apparent. Contrary to the observations of Broughton and Squires, it was not found that the emulsions of lowest viscosity were necessarily the most stable. Thus, of the glycol esters, only polyethylene glycol (200) monooleate gave an emulsion of the same order of stability as those prepared from sorbitan esters and the polyricinoleates.

Pink (18) ascribes the stability of water-in-oil emulsions to interfacial precipitation of emulsifier from the oil phase, in the form of hydrated soap, in the presence of a small amount of water. This is attributed to the penetration of water into the interior of the molecules at the interface and attachment to the polar groups. Alexander (19) also is of the opinion that stabilization is effected by a three-dimensional interfacial film, i.e., by a system analogous to emulsion stabilization with solid powders. It is highly probable, therefore, that when an emulsifying agent is present in excess of critical concentration for micelle formation a polymolecular film is formed. Since all the emulsions investigated were of the same volume concentration, variations in viscosity are attributable only to the influence of the different emulsifying agents used in their preparation, with particular reference to the stabilizing films formed at the interface. Two factors may possibly account for these variations.

1. The physical nature of the interfacial film and its rheological properties. This will affect globular resistance to deformation on the application of a shearing stress to the system, and its magnitude will be reflected in the derived viscosity.

2. The "volume factor," as influenced by precipitation at the interface. A high rate of adsorption will increase the dimensions of the dispersed globules appreciably and result in increased viscosity. Table I shows that a low relative viscosity is accompanied by a low "volume factor," and in fact there appears to be a curvilinear relationship between the two constants, where $h = \log_{10} \frac{\eta}{\eta_0} + c$, and $c = 0.06$. The reason why the polyethylene glycol polyricinoleate emulsion shows a "volume factor" lower than unity is not readily apparent.

The orientation of the emulsifying agent at the interface will be of major importance in these considerations and will be influenced by the relative hydrophilic and lipophilic affinities of the polar and nonpolar groups, respectively. In addition, interfacial film development will modify the nature and magnitude of the oil phase-water droplets forces, and will also modify the forces of cohesion between dispersate globules in concentrated emulsions where the condition of hexahedral packing is approached.

SUMMARY

Water-in-oil emulsions of the same volume concentration disperse phase have been prepared using various nonionic emulsifying agents. Differences in their relative viscosities and stabilities have been found which can be accounted for only by interfacial phenomena involving the emulsifying agents. Two possible contributory factors are discussed.

ACKNOWLEDGMENT

The author would like to thank the Board of Directors of Gestetner Ltd. for permission to publish this paper.

REFERENCES

1. EINSTEIN, A., *Ann. Physik* **19,** 289 (1906); *ibid.* **34,** 591 (1911).
2. TAYLOR, G. I., *Proc. Roy. Soc.* (*London*) **A138,** 41 (1932).
   LEVITON, A., AND LEIGHTON, A., *J. Phys. Chem.* **40,** 71 (1936).
3. HATSCHEK, E., *Kolloid-Z.* **8,** 34 (1911); *ibid.* **11,** 284 (1912); *ibid.* **12,** 238 (1913); *Trans. Faraday Soc.* **9,** 80 (1913).
   RICHARDSON, E. G., *Kolloid-Z.* **65,** 32 (1933).
   BROUGHTON, J., AND SQUIRES, L., *J. Phys. Chem.* **42,** 252 (1938).
   EILERS, H., *Kolloid-Z.* **97,** 313 (1941).
4. GUTH, E., AND SIMHA, R., *Kolloid-Z.* **74,** 266 (1936).
   EIRICH, F., BUNZL, M., AND MARGARETHA, H., *Kolloid-Z.* **74,** 276 (1936); *ibid.* **75,** 20 (1936).
   DE BRUIJN, H., *Rec. trav. chim.* **61,** 863 (1942); *Proc. Intern. Rheol. Congr.* **2,** 95 (1948).
   VAND, V., *J. Phys. & Colloid Chem.* **52,** 277, 300 (1948).
   MOONEY, M., *J. Colloid Sci.* **6,** 162 (1951).
5. VON SMOLUCHOWSKI, M., *Bull. Acad. Sci. Cracovie,* p. 182 (1903).
   VERWEY, E. J. W., *Hydrophobic Colloids Symposium, Utrecht,* p. 58 (1937); *Trans. Faraday Soc.* **36,** 192 (1940).
   VERWEY, E. J. W., AND OVERBEEK, J. TH. G., "Theory of the Stability of Lyophobic Colloids." Elsevier, Amsterdam, 1948.
   CHEESMAN, D. F., AND KING, A., *Trans. Faraday Soc.* **36,** 241 (1940).
   DICKINSON, W., *Trans. Faraday Soc.* **37,** 140 (1941).
   SCHULMAN, G. H., AND COCKBAIN, E. G., *Trans. Faraday Soc.* **36,** 651, 661 (1940).
6. SIBREE, J. O., *Trans. Faraday Soc.* **26,** 26 (1930); *ibid.* **27,** 161 (1931).
7. EIRICH, F., AND SIMHA, R., *Monatsh. Chem.* **71,** 67 (1937).
   SIMHA, R., *J. Research Natl. Bur. Standards* **42,** 409 (1949); *J. Colloid Sci.* **5,** 386 (1950).
8. GABRIEL, L. G., "Technical Aspects of Emulsions," p. 140. London, 1935.
9. TOMS, B. A., *J. Chem. Soc.* **1941,** 542.
10. SUMNER, C. G., *Trans. Faraday Soc.* **36,** 272 (1940); "Clayton's Theory of Emulsions and Their Technical Treatment," 5th ed., p. 221. Churchill, London, 1954.
11. SHERMAN, P., *J. Soc. Chem. Ind.* (*London*) **69,** S70 (1950).
12. DE JONG, O., "First Report of Viscosity and Plasticity," Ch. 3. Amsterdam, 1935.
13. JONES, G., AND FORNWALT, H. J., *J. Am. Chem. Soc.* **60,** 1683 (1938).
14. COCKBAIN, E. G., AND MCROBERTS, T. S., *J. Colloid Sci.* **8,** 440 (1953).
15. ALEXANDER, A. E., AND TEORELL, T., *Trans. Faraday Soc.* **35,** 727 (1939).
16. WOODMAN, R. M., *J. Soc. Chem. Ind.* (*London*) **54,** 70T (1935).
17. SHERMAN, P., *J. Colloid Sci.* **8,** 35 (1953).
18. PINK, R. C., *Trans. Faraday Soc.* **37,** 180 (1941).
19. ALEXANDER, A. E., *Advances in Colloid Sci.* **3,** 85 (1950).

PRIMARY SALT EFFECTS WITH SOME PARAFFIN-CHAIN SALT SOLUTIONS[1, 2, 3]

J. A. Erikson[4] **and E. C. Lingafelter**

The Department of Chemistry, University of Washington, Seattle, Washington

Received August 24, 1954

ABSTRACT

The primary salt effect of tetramethylammonium dodecanesulfonate, tetramethylammonium tetradecanesulfonate, and sodium decanesulfonate all at 25°C. and sodium dodecanesulfonate and tetramethylammonium tetradecanesulfonate at 40°C. on the displacement reaction between thiosulfate and bromoacetate ions has been studied. It was found that the measured rate constant from a paraffin-chain salt solution containing micelles had nearly the same value that it had in a solution containing an equivalent amount of simple, completely dissociated electrolyte. Since it is well established that a considerable number of gegenions are attached to the micelle, the above result indicates that the micelle has a rather large ionic effect. This effect compensates for the decrease in ionic effect brought about by the decrease in simple ion concentration due to the aggregation of the simple ions to form micelles.

INTRODUCTION

This paper is concerned with the ionic catalysis of an ionic reaction, the thiosulfate-bromoacetate displacement reaction, by some paraffin-chain salts, the sodium and tetramethylammonium salts of decane-, dodecane-, and tetradecanesulfonates. A previous experiment (1) indicated that the rate constant at 40°C. was increased as reactants were replaced by sodium dodecanesulfonate. This was found to be true here, but to a much smaller magnitude. The previous results are in error mainly owing to the use of an inadequate calculation method. This will be discussed later.

Paraffin-chain salts are ionic compounds which have paraffin chains incorporated in one or both ions. Because of the hydrophobic nature of the paraffin-chain part there exists a threshold concentration of paraffin-chain

---

[1] Taken from a thesis submitted by J. A. Erikson to the University of Washington in partial fulfillment of the requirements for the Ph.D. degree, June, 1954.

[2] Presented before the Division of Physical and Inorganic Chemistry at the Northwest Regional American Chemical Society Meeting, Richland, Washington, June, 1954.

[3] A part of this work was carried out under United States Army Ordnance Corps Basic Research Contract No. DA-04-200-ORD-236.

[4] Procter and Gamble research fellow 1950–1951. Present address: Department of Petroleum Refining, Colorado School of Mines, Golden, Colorado.

ions in aqueous solution, called the critical micelle concentration, above which the excess paraffin-chain ions associate to form aggregates of colloidal dimensions. The electrical charge of this aggregate is partially neutralized by an "atmosphere" of simple ions whose charge is of the opposite sign to the charge of the micelle. These simple ions are called gegenions and the resulting aggregate of paraffin-chain ions and gegenions is called a micelle.

One of the many questions concerning micelles is the question concerning the effect of the micelle charge on the activity coefficients of simple ions. An analysis of the values of the activity coefficients of gegenion and micelle has been given by Hartley (2). Activity coefficients which may behave more rationally and therefore may be simpler to discuss are those of simple ions whose charges are of the same sign as the micelle charge. No method exists to determine such activity coefficients individually, but a value for a group of some of these coefficients may be determined by studying the primary salt effect. The rate constant of the thiosulfate-bromoacetate reaction,

$$S_2O_3^{=} + BrCH_2COO^{-} \rightarrow (\text{Activated Complex})^{\equiv} \rightarrow Br^{-} + S_2O_3CH_2COO^{=} \qquad [1]$$

is related to the activity coefficients ν_T, ν_B and ν^* of the thiosulfate, bromoacetate, and activated complex ions, respectively, by

$$k_{\text{exp}} = k_0 \frac{\gamma_T \gamma_B}{\gamma^*}. \qquad [2]$$

Equation [2] has been tested many times (3) and shown to be correct. Where anomalies were found, these anomalies were shown to be due to side reactions between associated ions (4), orientation effects (5), or anomalies in the activity coefficients (6). If the activity coefficients in Eq. [2] depend upon the charge of the corresponding ions and on the common environment in a manner no more complicated than the Debye-Hückel dependence, then a study of the variation of the experimental rate constant may yield an effective ionic strength for this environment.

EXPERIMENTAL

Materials

Sodium dodecanesulfonate was prepared by refluxing a Halogen Chemical Co. dodecyl bromide, an analytical-grade sodium sulfite, and water for several days until the bromide layer disappeared. A weighed amount of the recrystallized material was diluted to the mark of a liter volumetric flask and the concentration computed, taking into account the water content of the material, which was determined by drying a sample in a vacuum oven.

The tetramethylammonium alkanesulfonates were made from the corresponding sodium alkanesulfonates by first converting them to the silver alkanesulfonates and then reacting these with tetramethylammonium chloride. Solutions were made in the same manner as the sodium dodecanesulfonate solutions and also by preparing a solution of the approximate concentration and then drying a sample of this solution to constant weight in a vacuum oven.

Sodium decanesulfonate was already in stock and was recrystallized before being used.

A reagent-grade potassium hydrogen phthalate was dried at 100°C. in a vacuum oven, without any previous purification. A weighed amount was diluted to volume in a volumetric flask.

Carbonate free sodium hydroxide was prepared by filtering a 50% solution into a liter of cooled, boiled, distilled water. The solution was protected as completely as possible from the air by two drying tubes filled with Ascarite, one on a piece of tubing through a rubber stopper on the bottle, and the other on the end of the pipet, which also went through the stopper of the bottle. The pipet was used to transfer the solution.

An Eastman 10% solution of tetramethylammonium hydroxide was diluted to an approximate concentration with cooled, boiled, distilled water. The hydroxide solutions were standardized against the standard acid phthalate solutions, with a Beckman *p*H meter used to detect the end point.

A reagent-grade bromoacetic acid was recrystallized three times from benzene, and then once from acetone. It was stored in a desiccator over phosphorus pentoxide. An approximate amount was quickly transferred to a weighed weighing bottle, and weighed. The bromoacetic acid was rinsed into a beaker and transferred to a liter volumetric flask. The solution was standardized against the hydroxide with the *p*H meter to detect the end point. The normality obtained from the initial weight of the bromoacetic acid was used as a check on the experimental technique and on the purity of the compound.

The bromoacetic acid solution and the appropriate hydroxide solution were mixed to form the corresponding bromoacetate solution by adjusting the *p*H of the mixture to the standardization end point *p*H.

A reagent-grade potassium iodate was dried at 150°C., weighed, and diluted to volume in a 2-liter volumetric flask. The solutions were approximately 0.005 N.

An approximate amount of reagent-grade sodium thiosulfate was placed in a liter pyrex bottle, which had just been rinsed with boiling, distilled water. A liter of boiling, distilled water was added, and the bottle was stored to permit the solution to cool. The solution was standardized by the potassium iodate solution; the dead-stop technique was used to detect the end point.

Tetramethylammonium thiosulfate was prepared from tetramethylammonium sulfate and barium thiosulfate. The tetramethylammonium sulfate was prepared from silver sulfate and tetramethylammonium chloride, and the barium thiosulfate was prepared from sodium thiosulfate and barium chloride. Solutions were prepared and standardized in the manner described above for solutions of sodium thiosulfate.

A reagent-grade sodium nitrate was dried at 110°C., and a weighed amount was diluted to volume in a liter volumetric flask. Sometimes, as a check, the solution was standardized by evaporating a known volume to constant weight.

Tetramethylammonium nitrate was prepared from tetramethylammonium chloride and silver nitrate.

Iodine solutions containing 4% potassium iodide were prepared in the usual manner. They were filtered through a sintered glass filter to remove any small crystals of iodine. Concentrations varied, but most solutions were approximately 0.005 *N*.

Iodine solutions containing 5% tetramethylammonium iodide were prepared by dissolving the iodine in a hot solution of the required amount of the iodide and then allowing the solution to cool. Any tetramethylammonium iodide or tetramethylammonium tri-iodide was removed by filtration. The concentration of iodine was limited to less than 0.002 *N* because of the insolubility of the tetramethylammonium tri-iodide (7). Iodine would not dissolve in the cold solution of tetramethylammonium iodide because the crystals of iodine became coated with the insoluble tri-iodide. Both iodine solutions were standardized against the calculated initial concentrations of thiosulfate salt present in the kinetic solutions. Sometimes the iodine solutions were checked against the potassium iodate solution by employing a thiosulfate solution of a comparable concentration as an intermediate standard.

The Dead-Stop Titration

The end point of the iodine-thiosulfate reaction was determined by a dead-stop technique (8). A potential difference of about 10 mv. was used. A 10-cm. deflection of the galvanometer indicated an iodine concentration 3×10^{-6} *N*. The end point was almost always noted before the deflection attained 1 cm., but in a number of titrations the variation of the galvanometer deflection was measured and graphed versus the volume of iodine solution so that all the readings could be extrapolated back to zero deflection.

Apparatus

The 500-ml. Erlenmeyers in which the runs were performed were thermostated in a 20-liter water bath, regulated by a Sargent zero current relay. The temperature was regulated to ±0.1°C. All the temperatures were adjusted with the same 0° to 50°C. thermometer. The sampling pipets were left in the Erlenmeyers according to an arrangement described by Hahn (9). Volumetric glassware was calibrated at 25°C. and computed corrections were applied when the glassware was used at 40°C. Time was measured with a stop watch.

Experimental Procedure

The solutions used in the kinetic experiments were assembled by various methods by adding stock solutions to volumetric flasks by means of burets and pipets. Usually solutions of thiosulfate salt and other electrolytes were made and thermostated. To these were added aliquots of the stock solution of the bromoacetate salt. The time at the addition was observed. Samples of 50 ml. each were titrated with standard iodine. The reaction was stopped by adding the sample to an amount of iodine solution, delivered from a buret, which was insufficient to react with all of the thiosulfate in the sample. The titration was completed using the dead-stop technique to detect the end point. The time was recorded when the 50-ml. sample was released from the pipet. Two drops of 0.1 *N* acetic acid were added initially to the iodine solution to suppress the formation of hypoiodite.

CALCULATIONS

Three methods were used in the calculations of the rate constants. The magnitude of the difference between the reactant concentrations in a run determined which method was to be employed for that run.

If the reactant concentrations were equal, the equation

$$kt = \frac{1}{a - x} - \frac{1}{a} \qquad [3]$$

was used with the following modification. Since

$$[\mathrm{I_2}]M = (a - x)V, \qquad [4]$$

where M is the volume of iodine required for a sample of volume V, Eq. [3] became

$$\frac{1}{M} = \frac{[\mathrm{I_2}]k}{V}t + \frac{1}{M_0} \qquad [5]$$

so that the rate constant, k, could be obtained from the slope, $[\mathrm{I_2}]\,k/V$, of the graph of $1/M$ versus t. The intercept $1/M_0$ was used together with the initial concentration of the thiosulfate to calculate the normality of the iodine. A normality of the iodine solution was calculated from each intercept and an average value was found from all the runs using the same iodine solution, and this average was used to calculate the rate constants.

The equation for the unequal reactant concentration case

$$\frac{(a - b)kt}{2.303} = \log\frac{a - x}{b - x} - \log\frac{a}{b} \qquad [6]$$

was modified using Eq. [4] and

$$D = \frac{V}{[\mathrm{I}_2]}(a - b) \qquad [7]$$

to give

$$\log \frac{M}{M - D} = -\frac{[\mathrm{I}_2]Dk}{2.303V}\, t + \log \frac{M_0}{M_0 - D}. \qquad [8]$$

It was thought that D could be chosen to give the straightest line for a graph of $\log \frac{M}{M - D}$ versus t. Roughly this was true, but usually there was a range of D where the curvature was obscured by the experimental deviations. D was calculated from the initial concentrations of the reactants and the normality of the iodine solution; the latter value was obtained from runs having equal reactant concentrations.

When D was small, but not zero, it was found that Eq. [5] was not accurate, and Eq. [8] was too cumbersome. Equation [8] was therefore rearranged by expanding $\log \frac{M}{M - D}$, that is,

$$\log \frac{M}{M - D} = \frac{D}{2.303M}\left\{1 + \frac{1}{2}\left(\frac{D}{M}\right) + \frac{1}{3}\left(\frac{D}{M}\right)^2 + \frac{1}{4}\left(\frac{D}{M}\right)^3 + \cdots\right\} \qquad [9]$$

and simplified to

$$\frac{1}{M} F\left(\frac{D}{M}\right) = \frac{[\mathrm{I}_2]k}{V}\, t + \frac{1}{M_0} F\left(\frac{D}{M_0}\right) \qquad [10]$$

where

$$F\left(\frac{D}{M}\right) = 1 + \frac{1}{2}\left(\frac{D}{M}\right) + \frac{1}{3}\left(\frac{D}{M}\right)^2 + \frac{1}{4}\left(\frac{D}{M}\right)^3 + \cdots \qquad [11]$$

To facilitate the computations, a large graph of $F(D/M)$ versus D/M was drawn. D was computed from Eq. [7] as before, and the rate constant was computed from the slope of a graph of $(1/M)F(D/M)$ versus t.

For all runs, the method of averages was used to calculate all slopes and intercepts directly from the co-ordinates of the points. Deviations of the points from this average straight line were calculated and compared. Points with too large a deviation were investigated for mistakes, and if an error could not be found, the point was discarded from the data.

ACCURACY AND PRECISION OF THE RESULTS

If the required volumes of iodine solutions were calculated for a hypothetical run using reactant concentrations which differed slightly, and a rate constant were calculated from these data on the assumption that the reactants had equal concentrations, two results were apparent. First, the usual reciprocal volume of iodine solution versus time graph was a slightly curved line, and, therefore, the average deviation from the best average line was no longer zero and, second, the calculated rate constant from the slope of this best average line no longer agreed with the assumed rate constant. The curvature of the data or the average deviation of the data from a straight line, the difference in the reactant concentrations, and the change in the rate constant were all related. Thus it was found by calculation that a 2.8, 5.5, and 11 % decrease in the bromoacetate concentration gave curves concave downwards, whose average deviations were 0.052, 0.11, and 0.30 %, respectively, and whose "slopes" yielded rate constants which were too small by 4.5, 10, and 20 %, respectively.

It should be emphasized that these curves all appeared approximately straight. The actual magnitude of the per cent average deviation in an actual run does not mean too much, since any curvature probably would be obscured by the random scatter of the titration values. Thus a small average deviation, although desirable, did not necessarily mean that the rate constant was accurate.

The errors in the rate constants are primarily due to the errors in the concentrations of the solutions employed, and secondarily due to the error in setting the temperature of the water bath. The change in the rate constant with temperature, dk/dt, at 25°C. and an ionic strength of 0.014 M is 0.034 min.^{-1} degree^{-1}. A tenth of a degree temperature change corresponds to a 1 % error in the rate constant. However, the effect on the rate constant due to the variation in temperature during a 3000-minute run will be averaged to a smaller value than this, and the relative error of the rate constants from runs produced at the same time will likewise be smaller than this, but rate constants compared from runs produced at different times or compared to literature values will be influenced proportionally by any error in the temperature. It is reasonable to assume that the thiosulfate concentration is known to 0.5 %, while the bromoacetate is known to 1 %, twice as much because two standard solutions had to be made to make the one bromoacetate solution.

The error in the rate constants is accordingly about 3 %. The precision of the rate constant values in an experiment where the same stock solutions were used and the same temperature setting of the bath was used for all the runs, is much better, and the agreement and reproducibility are about 1 %.

Errors due to other causes are negligible.

RESULTS

The results are tabulated in Table I. The concentrations are expressed in millimoles per liter. The concentration sum, used here and on some of

TABLE I

Experimental Results

Run number	Paraffin-chain salt concentration (mm./l.)	Nitrate salt concentration (mm./l.)	Thiosulfate salt concentration (mm./l.)	Bromoacetate salt concentration (mm./l.)	Concentration sum (millimoles/l.)	Square root of the concentration sum	Experimental rate constant (l./mole minute)
Experiment 2. 25°C. $(CH_3)_4N$ $C_{14}H_{29}SO_3$, Fig. 8							
1	0.0	10.12	0.854	1.19	13.9	0.118	0.408[a]
2	0.20	9.92	"	"	"	"	0.410
3	0.41	9.72	"	"	"	"	0.408
8	0.61	9.51	"	"	"	"	0.411
5	0.81	9.31	"	"	"	"	0.411
6	1.02	9.11	"	"	"	"	0.410
4	2.03	8.10	"	"	"	"	0.408
11	4.05	6.07	"	"	"	"	0.397
9	5.06	5.06	"	"	"	"	0.394
10	6.07	4.04	"	"	"	"	0.394
7	8.09	2.03	"	"	"	"	0.397
13	10.12	0.0	"	"	"	"	0.385
Experiment 3. 40°C. Na $C_{12}H_{25}SO_3$							
4	0.0	0.0	5.50	5.46	22.0	0.148	1.58[b]
1	20.3	0.0	0.488	0.428	22.2	0.149	1.60
Experiment 4. 25°C. $(CH_3)_4N$ $C_{12}H_{25}SO_3$, Fig. 7							
8	0.0	21.61	0.92	0.91	25.3	0.159	0.480[a]
1	0.0	17.86	0.89	0.88	21.4	0.146	0.458[a]
2	6.77	11.07	"	"	"	"	0.462
9	6.77	11.06	"	"	"	"	0.451
3	8.91	8.94	"	"	"	"	0.449
4	11.07	6.81	"	"	"	"	0.454
5	13.21	4.65	"	"	"	"	0.445
6	15.71	2.16	"	"	"	"	0.442
7	17.83	0.0	"	"	"	"	0.433
Experiment 5. 40°C. Na $C_{12}H_{25}SO_3$, Fig. 4							
6	0.0	0.0	5.38	5.37	21.5	0.147	1.53[b]
5	0.0	"	5.38	5.37	21.5	"	1.52[b]
4	6.25	"	3.84	3.84	21.6	"	1.54
3	11.92	"	2.44	2.44	21.7	"	1.55
2	17.90	"	0.98	0.98	21.8	"	1.57
1	19.59	"	0.46	0.46	21.4	0.146	1.58

[a] These data are illustrated on Fig. 1.

[b] These data are illustrated on Fig. 2.

TABLE I—*Continued*

Run number	Paraffin-chain salt concentration (mm./l.)	Nitrate salt concentration (mm./l.)	Thiosulfate salt concentration (mm./l.)	Bromoacetate salt concentration (mm./l.)	Concentration sum (millimoles/l.)	Square root of the concentration sum	Experimental rate constant (l./mole minute)
Experiment 6. 25°C. $(CH_3)_4N$ None							
7	0.0	11.73	0.99	0.99	15.7	0.125	0.434[a]
Experiment 7. 25°C. $(CH_3)_4N$ $C_{14}H_{29}SO_3$, Fig. 9							
7	0.0	8.13	1.23	1.22	13.0	0.114	0.418[a]
5	0.81	7.32	"	"	"	"	0.422
8	4.05	4.05	"	"	"	"	0.410
10	6.08	2.02	"	"	"	"	0.404
4	8.11	0.0	"	"	"	"	0.398
4′	0.0	16.22	"	"	21.1	0.145	0.476[a]
2	0.81	15.38	"	"	"	"	0.472
3	4.05	12.17	"	"	"	"	0.464
8′	16.21	0.0	"	"	"	"	0.434
5′	11.05	36.78	1.11	1.11	19.2	0.139	0.433
Experiment 8. 25°C. $(CH_3)_4N$ $C_{14}H_{29}SO_3$, Fig. 6							
10	0.0	0.0	1.09	1.08	4.35	0.066	0.361[a]
7	0.85	"	"	"	5.19	0.072	0.373
8	1.70	"	"	"	6.04	0.078	0.379
2	2.54	"	"	"	6.89	0.083	0.382
5	4.24	"	"	"	8.59	0.093	0.396
6	7.04	"	"	"	11.38	0.107	0.404
4	25.44	"	"	"	29.79	0.173	0.471
3	50.88	"	"	"	55.2	0.235	0.548
Experiment 9. 25°C. $(CH_3)_4N$ None							
2	0.0	0.0	1.21	1.21	4.83	0.0695	0.346[a]
6	"	"	2.22	2.21	8.87	0.0942	0.378[a]
8	"	"	2.22	2.21	8.86	0.0941	0.378[a]
4	"	"	2.66	2.65	10.62	0.1031	0.389[a]
10	"	"	3.80	3.80	15.20	0.1233	0.415[a]
Experiment 11. 40°C. $(CH_3)_4N$ $C_{14}H_{29}SO_3$, Fig. 10							
5	0.0	11.59	1.65	1.65	18.2	0.135	1.59[b]
1	2.33	9.26	"	"	"	"	1.56
6	5.80	5.79	"	"	"	"	1.50
3	11.61	0.0	"	"	"	"	1.44
7	0.0	23.17	"	"	29.8	0.173	1.84[b]
8	2.32	20.94	"	"	"	"	1.80
2	11.61	11.59	"	"	"	"	1.70
10	23.22	0.0	"	"	"	"	1.57
9	46.43	0.0	"	"	53.0	0.230	1.79
4	68.49	0.0	"	"	75.1	0.274	1.93

TABLE I—*Continued*

Run number	Paraffin-chain salt concentration (mm./l.)	Nitrate salt concentration (mm./l.)	Thiosulfate salt concentration (mm./l.)	Bromoacetate salt concentration (mm./l.)	Concentration sum (millimoles/l.)	Square root of the concentration sum	Experimental rate constant (l./mole minute)
Experiment 12. 25°C. Na $C_{10}H_{21}SO_3$, Fig. 3							
4	0.0	0.0	0.92	0.92	3.68	0.060	0.325[a]
5	9.18	"	"	"	12.9	0.113	0.408
7	18.37	"	"	"	22.1	0.149	0.462
9′	18.37	"	"	"	22.1	0.149	0.459
6	22.04	"	"	"	25.7	0.160	0.481
10′	36.74	"	"	"	40.4	0.201	0.531
2′	55.12	"	"	"	58.8	0.243	0.562
4	0.0	"	"	"	3.68	0.060	0.325[a]
3′	"	"	"	"	3.68	0.060	0.325[a]
7′	"	"	1.66	1.67	6.66	0.082	0.352[a]
9	"	"	1.84	1.83	7.34	0.086	0.351[a]
4	"	"	0.92	0.92	3.68	0.060	0.325[a]
2	"	7.02	"	"	10.7	0.104	0.388[a]
6′	"	7.02	"	"	10.7	0.104	0.385[a]
1	"	14.05	"	"	17.7	0.133	0.429[a]
8	"	19.67	"	"	23.4	0.153	0.459[a]
1′	"	0.0	1.07	3.33	6.53	0.081	0.356[a]
4′	"	"	1.39	2.50	6.66	0.082	0.352[a]
7′	"	"	1.66	1.67	6.66	0.082	0.352[a]
8′	"	"	1.94	0.83	6.66	0.082	0.338[a]
10	"	"	0.92	4.58	7.35	0.086	0.357[a]
9	"	"	1.84	1.83	7.34	0.086	0.351[a]
3	"	"	2.14	0.92	7.34	0.086	0.356[a]
Experiment 13. 25°C. $(CH_3)_4N$ $C_{14}H_{29}SO_3$							
4′	0.0	0.0	0.62	0.61	2.46	0.050	0.318[a]
4	"	"	1.28	1.22	5.05	0.071	0.342[a]
Experiment 14. 40°C. Na $C_{12}H_{25}SO_3$							
3	0.0	0.0	0.33	0.33	1.31	0.036	1.11[b]
8	"	"	1.63	1.64	6.53	0.081	1.25[b]
8″	"	"	3.27	3.28	13.07	0.114	1.44[b]
2	11.65	"	0.33	0.33	13.0	0.114	1.50

the figures, is defined to be equal to the sum of the concentrations of paraffin-chain salt, nitrate salt, and bromoacetate salt plus three times the concentration of the thiosulfate salt. In the absence of micelles the concentration sum is equivalent to the ionic strength.

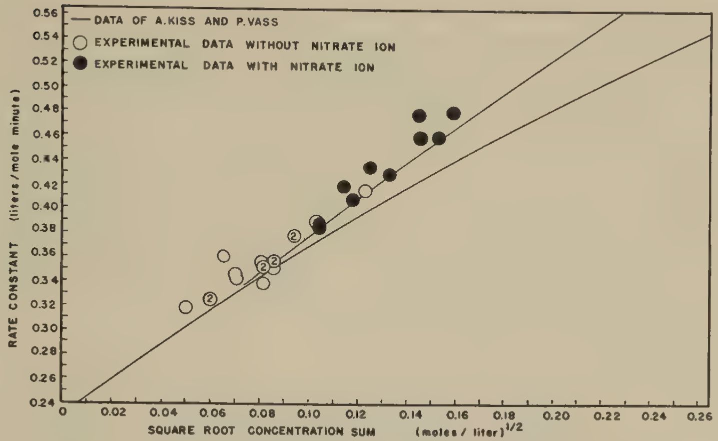

FIG. 1. Rate constants for reactants with and without nitrate ion at 25°C.

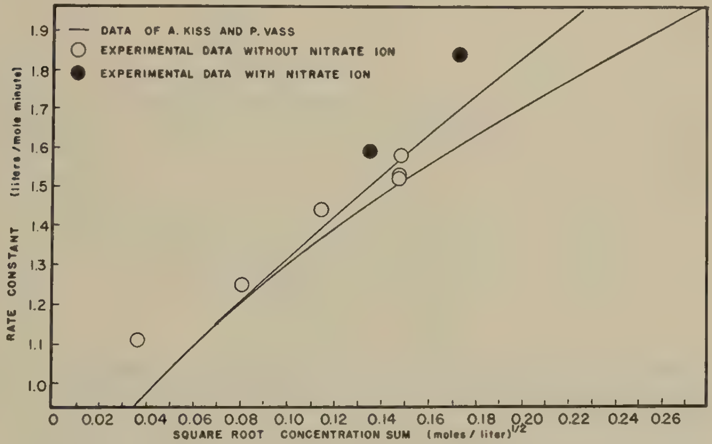

FIG. 2. Rate constants for reactants with and without nitrate ion at 40°C.

Reactants and Simple Ions

One or more runs of each experiment contained no paraffin-chain salt. When the results from these runs were compared with each other on a single rate constant versus ionic strength graph, the average spread of the results was about 3% (Figs. 1 and 2). The lower solid curve represents the results of Kiss and Vass (10) using solutions which contained only reactants. The upper solid curve represents their results where increasingly larger amounts of nitrate salt were added to a constant (0.00125 M) concentration of reactants. The reactant concentrations employed here for all the runs indicated by black dots were not the same, although most of the reactant concentrations were nearly the same (0.001 M).

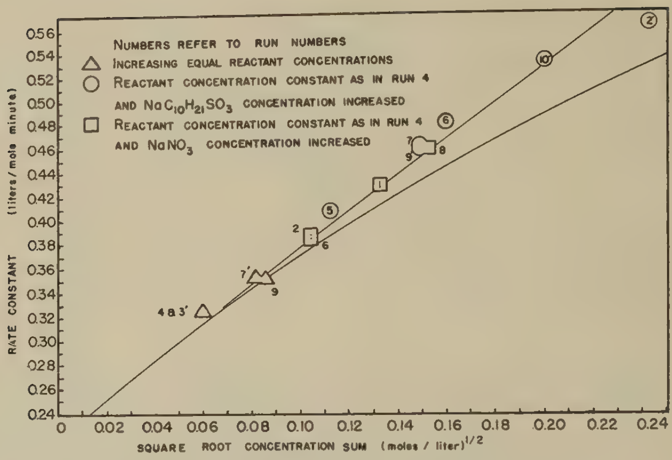

FIG. 3. Comparison of the rate constants from solutions containing decanesulfonate ion and similar solutions containing nitrate ion.

Reactants with Paraffin-Chain Ions

In solutions of paraffin-chain salts which did not contain micelles, especially with sodium decanesulfonate (Fig. 3), no change in the rate constant was observed if paraffin-chain ion were substituted for nitrate ion. This indicated that in spite of the very different nature of the paraffin-chain ion compared with the nitrate ion, these singly charged ions influence the thiosulfate-bromoacetate reaction in the same manner.

Reactants with Micelles

Three experiments, 3, 5, and 14, demonstrated that the rate constant at 40°C. was slightly increased as reactants of equal concentrations were re-

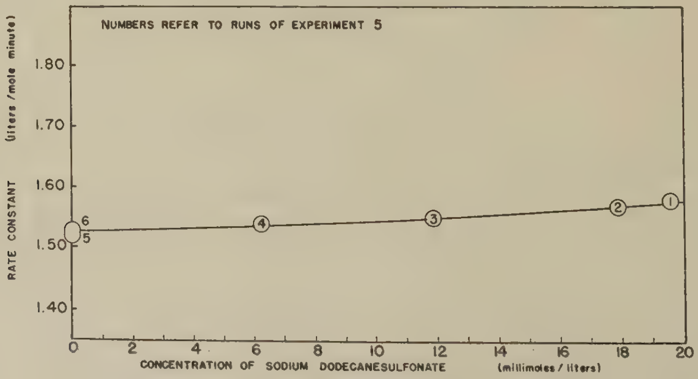

FIG. 4. Variation of the rate constant when reactants are replaced by sodium dodecanesulfonate at 40°C.

placed by an ionic strength equivalent amount of sodium dodecanesulfonate. The results from the more elaborate experiment are shown on Fig. 4.

An earlier experiment (1) likewise indicated this increase, but the results are in error and the increase should not be as much as is recorded. The corrected results and the old results are shown together on Fig. 5.

The primary error was caused by calculating the rate constants with the method for equal reactant concentrations, even though the reactant concentrations were slightly different. This method has been recommended for this situation by Daniels, Mathews, and Williams (11). The corrected rate

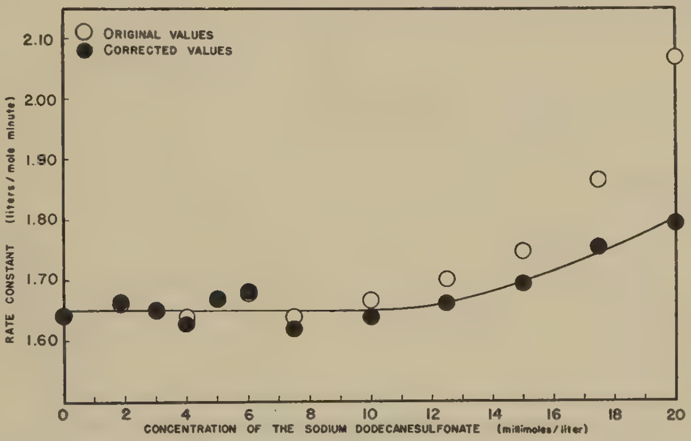

FIG. 5. Variation of the rate constant when reactants are replaced by sodium dodecanesulfonate at 40°C.

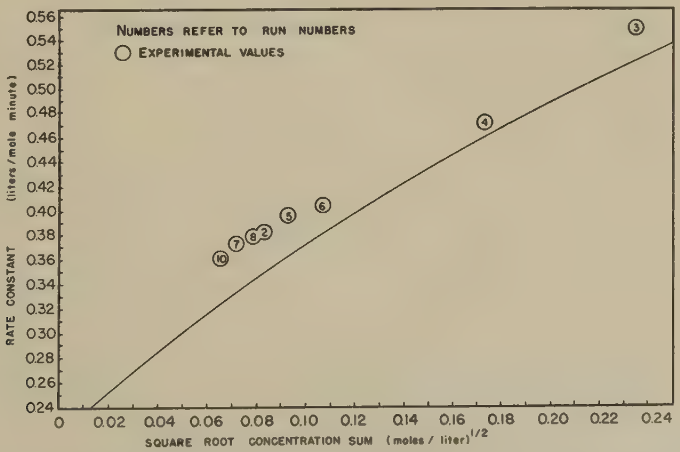

FIG. 6. Rate constants at 25°C. for various solutions of $(CH_3)_4NC_{14}H_{29}SO_3$ containing a constant amount of reactants.

constants have been recalculated taking into account this slight difference in reactant concentrations by the method already described.

The addition of tetramethylammonium tetradecanesulfonate to a constant amount of reactants resulted in an increase in the rate constant which, from a comparison with the results of Kiss and Vass, appeared to be nearly the same as if an ionic strength equivalent amount of equal concentration reactants had been added instead. This was demonstrated by experiment 8 (Fig. 6) and also by runs 3, 10, 9, and 4 of experiment 11. Within experimental error, these data are in agreement with the above-mentioned slight increase in the rate constant produced by replacing reactants with paraffin-chain salt.

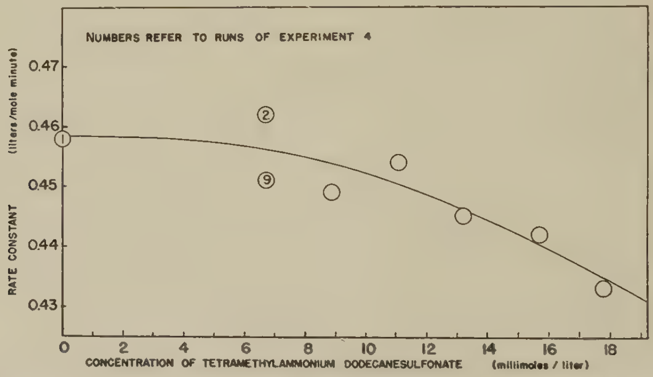

FIG. 7. Variation of the rate constant when nitrate ion is replaced by dodecanesulfonate ion at 25°C.

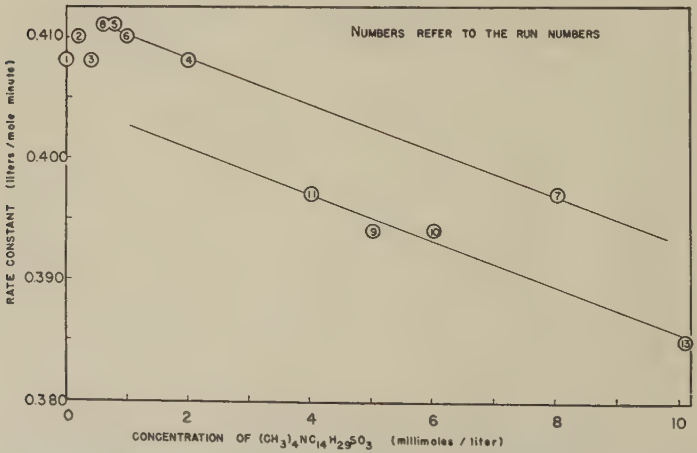

FIG. 8. The rate constant when NO_3^- is replaced by $C_{14}H_{29}SO_3^-$ at 25°C. in experiment 2.

Nitrate Ion with Micelles

If nitrate salt were replaced by the equivalent amount of paraffin-chain salt, the rate constant decreased; the decrease was somewhat more than the increase noted above. This was observed with tetramethylammonium dodecanesulfonate at 25°C. (Fig. 7) and with tetramethylammonium tetradecanesulfonate at both 25°C. (Figs. 8 and 9) and 40°C. (Fig. 10). These data are not in disagreement with the data in which an increase was observed, since the primary salt effect produced by nitrate salt is greater than the effect produced by an ionic strength equivalent amount of reactants. The difference of 0.0075 min.$^{-1}$ between the two groupings of the results in ex-

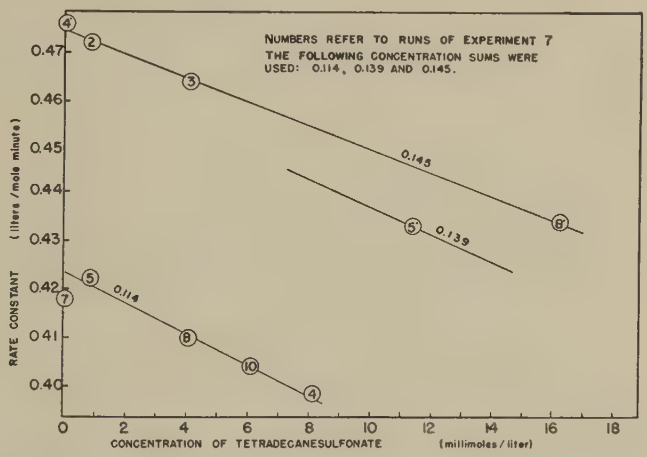

FIG. 9. Variation of the rate constant when nitrate ion is replaced by tetradecanesulfonate ion at 25°C.

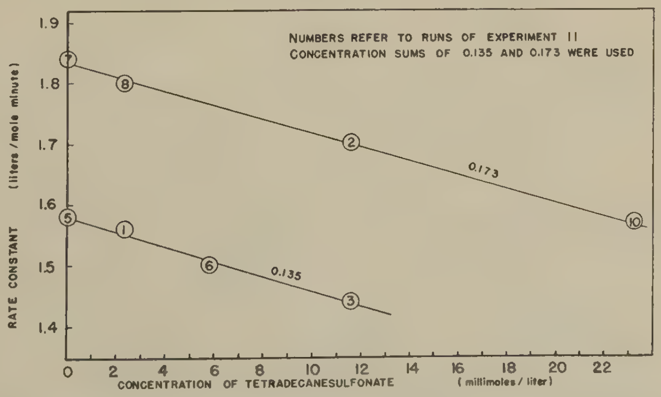

FIG. 10. Variation of the rate constant when nitrate ion is replaced by tetradecanesulfonate ion at 40°C.

periment 2 (Fig. 8) is believed due to a systematic error, since the lower group of runs was performed two days after the higher group.

DISCUSSION

The indifference of the rate constant to the presence of micelles, in solutions containing micelles, can be crudely predicted from the theoretical behavior of the rate constant in solutions containing simpler complexes. Since theoretically the rate constant is a function of the ionic strength, it will be sufficient to calculate only the ionic strength of solutions containing singly, doubly, triply, etc., charged ions in various degrees of association. In order to keep the calculations simple, only two ionic species will be considered to be present in each solution; the singly charged positive ions, and the complex anions containing singly charged positive and negative ions. In the case of a solution containing a neutral aggregate, only the neutral aggregate will be present.

A solution will, therefore, contain either the ions M^+ and $M_nA_m^{n-m}$, or the neutral molecules M_mA_m; where m is 1, 2, 3, . . . , n is 0, 1, 2, . . . , and for each solution n is equal to, or less than, m. It will be assumed that all the solutions can be constructed from a single solution, 0.02 M in MA. The concentration of the $M_nA_m^{n-m}$ complex is $(0.02)(1/m)$, and the concentration of the M^+ ion is $0.02(1 - n/m)$. The ionic strength for a given solution is

$$u = (0.01)\,(1/m)\,(m - n)\,(1 + m - n). \qquad [12]$$

The degree of neutralization of the charge of the complex ions is given by n/m.

Figure 11 is a graph of the square root of the ionic strength for various degrees of association of the "monomer," dimer, trimer, etc. The lines

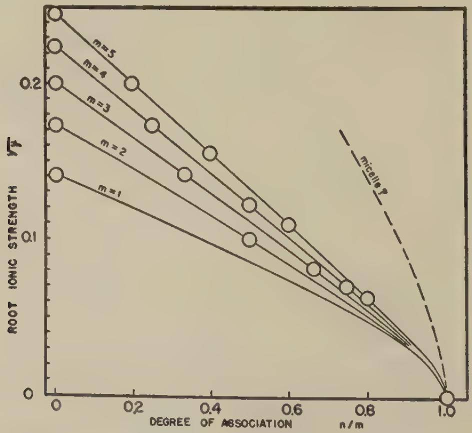

FIG. 11. Theoretical ionic strengths for solutions 0.02 M of MA, where the reaction $A_m^{-m} + mM^+ \rightarrow M_nA_m^{n-m} + (m - n)M^+$ has gone to completion.

result from considering n as a continuous variable, but only the points represent physically possible solutions. An empirical line correlating an "ionic strength" for a micelle containing approximately 50 or 60 paraffin-chain units is assumed to be in the location labeled "micelle?". This particular location is assumed in order to correlate the effective ionic strength of a micelle having a degree of association of approximately 0.8 to 0.9 with the results of this research: that the rate constant of the reaction in a solution containing micelles, is comparable to the rate constant of the reaction in a hypothetical solution containing the same amount of completely dissociated paraffin-chain salt. This line does not appear out of position when compared with the lines for the simple ions, even though the ionic strength principle is not valid in this region.

McBain (12, 13) regarded the charges on the exterior of the micelle to be too widely spaced to exert a mutual and therefore large effect, and concluded that ionic effects of solutions of micelles would not be much different from those of uni-univalent electrolytes. The conclusion drawn from the experiments of this research regarding the ionic effects of paraffin-chain salt solutions is that the ionic effects of the charged micelles are quite large, at least large enough to compensate for the decrease in ionic effect due to the simple ions that have associated to form micelles. The net effect of this compensation is that the influence of these paraffin-chain salt solutions containing micelles on the ionic reaction is approximately the same as if the paraffin-chain salt were behaving as a uni-univalent electrolyte.

It appears, therefore, that the activity coefficients of simple ions of charge of the same sign as the micelle charge, in solutions of paraffin-chain salts which contain micelles, have a value which is not much different from the value that they would have in a hypothetical solution containing a completely dissociated paraffin-chain salt of the same stoichiometric concentration.

REFERENCES

1. ERIKSON, J. A., AND LINGAFELTER, E. C., *J. Colloid Sci.* **4,** 591 (1949).
2. HARTLEY, G. S., *Trans. Faraday Soc.* **31,** 31 (1935).
3. LA MER, V. K., *J. Am. Chem. Soc.* **51,** 3341, 3678 (1929).
4. WYATT, P. A. H., AND DAVIES, C. W., *Trans. Faraday Soc.* **45,** 774 (1949).
5. LA MER, V. K., *J. Am. Chem. Soc.* **53,** 2832 (1931).
6. LA MER, V. K., AND FESSENDEN, R. W., *J. Am. Chem. Soc.* **54,** 2351 (1932).
7. RAY, S. K., AND BHATTACHARYA, R. R., *J. Indian Chem. Soc.* **13,** 456–463 (1936).
8. BRADBURY, J. H., *Trans. Faraday Soc.* **49,** 304 (1953).
9. HAHN, F. L., *Anal. Chim. Acta* **4,** 573 (1950).
10. KISS, A., AND VASS, P., *Z. anorg. u. allgem. Chem.* **217,** 305 (1934).
11. DANIELS, F., MATHEWS, J. H., AND WILLIAMS, J. W., "Experimental Physical Chemistry," 3rd ed., p. 169. McGraw-Hill Book Co., New York and London, 1941.
12. MCBAIN, J. W., *J. Am. Chem. Soc.* **50,** 1639 (1928).
13. MCBAIN, J. W., AND BETZ, M. D., *J. Am. Chem. Soc.* **57,** 191 (1935).

THE STRUCTURE OF "VISCOELASTIC SOLUTIONS" OF COLLOIDAL ELECTROLYTES

P. A. Winsor

Shell Petroleum Company Limited, Thornton Research Centre, Chester, England

Received June 10, 1954; revised received September 2, 1954

INTRODUCTION

In the course of the preparation of a series of systems for the investigation of electrooptical effects shown by liquid crystalline solutions of colloidal electrolytes (*cf.* succeeding paper), a number of observations were made which appear to afford insight into the structure of "viscoelastic solutions" of colloidal electrolytes.

The nature of the intermicellar equilibria and phase changes encountered in solutions of colloidal electrolytes has been discussed in previous papers (1, 2) and is recapitulated in Fig. 1.

In dilute aqueous solutions of the higher amphiphilic salts (and in more concentrated solutions of those of lower molecular weight) the amphiphilic ions are "molecularly dispersed" as shown on the left of Fig. 1.

At higher concentrations isotropic micellar solutions are produced in which the amphiphilic C region (which is in equilibrium with nonmicellar salt) has mainly the S_1 form (convex towards water). However, owing to thermal fluctuations, regions of planar and S_2 form will also be present in equilibrium.

At still higher concentrations (depending on the nature of the amphiphilic salt) and in certain multicomponent systems (1, 2) smectic liquid crystalline solutions are produced. These appear to contain only one form of micelle, the G micelle, which is potentially coextensive with the solution itself.

Under other conditions, as in certain of the aqueous "S_2" solutions discussed below, in multicomponent systems (1, 2), or in solutions of amphiphilic salts (*e.g.*, Aerosol OT) in hydrocarbons, isotropic solutions in which the micelles are predominantly of S_2 form arise.

The distinction between the isotropic S_1 and S_2 solutions is only in the balance of the intermicellar equilibrium within them, and it is often possible to pass continuously from one to the other. The liquid crystalline phase, on the other hand, is a distinct phase with definite limits (composition and/or temperature) of stability.

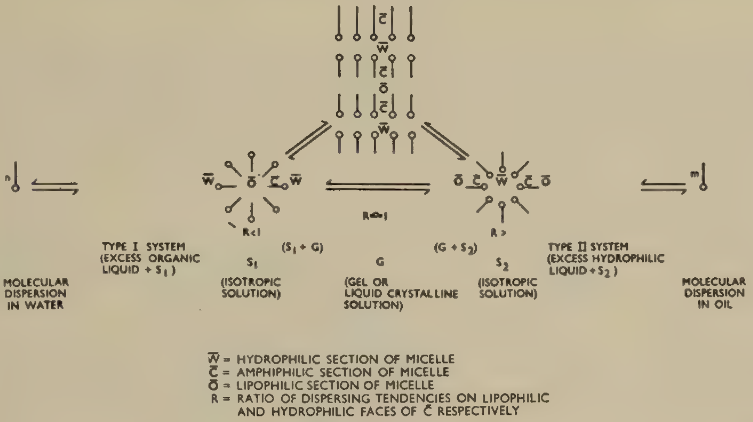
W̄
C̄
Ō
n
m
R<1
R≏1
R>
TYPE I SYSTEM (EXCESS ORGANIC LIQUID + S₁)
(S₁ + G)
(G + S₂)
TYPE II SYSTEM (EXCESS HYDROPHILIC LIQUID + S₂)
MOLECULAR DISPERSION IN WATER
S₁ (ISOTROPIC SOLUTION)
G (GEL OR LIQUID CRYSTALLINE SOLUTION)
S₂ (ISOTROPIC SOLUTION)
MOLECULAR DISPERSION IN OIL
W̄ = HYDROPHILIC SECTION OF MICELLE
C̄ = AMPHIPHILIC SECTION OF MICELLE
Ō = LIPOPHILIC SECTION OF MICELLE
R = RATIO OF DISPERSING TENDENCIES ON LIPOPHILIC AND HYDROPHILIC FACES OF C̄ RESPECTIVELY

FIG. 1. Intermicellar equilibrium and associated phase changes shown by certain series of solubilized systems.

EXPERIMENTAL

A particularly convenient series of systems for the study of the phase changes and intermicellar equilibrium discussed above is that derived from undecane-3 sodium sulfate/cyclohexylammonium chloride/water (3). This series gives rise, even in the liquid crystalline region, to pourable solutions which are readily manipulated and whose compositions may be simply determined volumetrically (see below). Further, the intermicellar equilibrium and associated phase changes (Fig. 1) may readily be regulated at will. This may be done:

1. By altering the position of equilibrium in the balanced action

$$RSO_4Na + C_6H_{11}\cdot NH_3Cl \rightleftharpoons RSO_4\cdot NH_3\cdot C_6H_{11} + NaCl$$

by varying the proportions of the reactants.

2. By dilution.

According to (1), displacement of the chemical equilibrium to the right by addition of cyclohexylammonium chloride displaces the intermicellar equilibrium to the right.

According to (2), dilution with water of a mixture containing a particular $RSO_4Na/C_6H_{11}\cdot NH_3Cl$ ratio displaces the intermicellar equilibrium to the left. This is a general effect of dilution on aqueous amphiphilic salt solutions.

Examples of these procedures used for the preparation of experimental samples are shown in Tables I, II, and III.

The following points may be noted concerning certain of the systems shown in Tables I, II, and III.

TABLE I

Displacement of Intermicellar Equilibrium and Associated Phase Changes to the Right by the Addition of a 48.6% (by Weight/Total Volume) Solution of Cyclohexylammonium Chloride to 25 ml. of a 4% (by Weight/Total Volume) Solution of Undecane-3 Sodium Sulfate at Room Temperature (21°C.)

Sample	Vol. cyclohexylammonium chloride solution added ml.	Condition of system	Remarks
A	<0.8	S_1	Water-clear, isotropic
B	0.8	$S_1 + G$	Phases separate overnight
C	0.85	G	Fluid liquid crystalline solutions; slightly opalescent; no indication of more than one type of liquid crystalline solution
D	0.925	G	
E	1.0	G	
F	1.075	G	
G	1.15	G	
H	1.175	$G + S_2$	These settle overnight (temperature about 19° ± 2°C.) into two phases, one isotropic, one liquid crystalline. Shaking gives clear, slightly opalescent dispersions of the two phases which show streaming birefringence between crossed polaroids. This disappears at once on cessation of flow, the dispersions appearing isotropic when at rest
I	1.20	$G + S_2$	
J	1.25	$G + S_2$	
K	1.30	Probably a stable ($S_2 + G$) emulsion (see below)	Isotropic; clear with slight opalescence; shows streaming birefringence
L	1.40	Type II	Upper layer 5 ml.; on shaking, a clear solution is obtained. On resting, this at once becomes turbid and separation into bulk phases is almost complete in ¼ hour

1. *Effect of Shear on Phase Miscibility*

The Type II systems, L in Table I and I and J in Table II, become clear and homogeneous on gentle stirring, rapidly clouding and separating into layers when allowed to rest. These systems therefore provide rather striking examples of the effect of rate of shear on the miscibility of conjugate liquid phases. This phenomenon, which is frequently observed in systems containing amphiphilic compounds (4), has recently also been recorded for systems containing macromolecular solutes (5).

2. *Effect of Change of Temperature on Phase Changes and Intermicellar Equilibria*

On cooling the systems in Tables I, II, and III the intermicellar equilibrium and phase changes (Fig. 1) are displaced to the left. Thus in Table I,

TABLE II

Displacement of Intermicellar Equilibrium and Associated Phase Changes to the Right by the Addition of a 48.6% (by Weight/Total Volume) Solution of Cyclohexylammonium Chloride to 50 ml. of a 2% (by Weight/Total Volume) Solution of Undecane-3 Sodium Sulfate at 20°C.

Sample	Vol. cyclohexylammonium chloride solution added, ml.	Condition of system	Remarks
A	0.67	S_1	Water-clear, isotropic
B	0.80	S_1	Water-clear, isotropic
C	0.93	Probably $S_1 + G$	Opalescent; isotropic but birefringent on streaming. S_1 and G phases do not separate on standing
D	1.07	Probably $S_1 + G$	
E	1.20	G	Opalescent; stable birefringence
F	1.33	G	
G	1.47	Probably $G + S_2$	Opalescent; birefringent on streaming; S_2 and G phases do not separate on standing
H	1.60	Probably $G + S_2$	
I	1.73	Type II	Two isotropic phases, upper 10 ml.
J	1.87	Type II	Two isotropic phases, upper 17 ml.

on cooling the Type II system L to 0°C. it gave a system similar to K at room temperature. On cooling the ($S_2 + G$) systems H, I, and J, permanently birefringent G systems were obtained. On cooling the ($S_1 + G$) system B it was converted to a single water-clear isotropic phase S_1.

3. Variation in Stability of (S + G) Emulsions with Concentration of Amphiphilic Salt

It appears from Tables I, II, and III that the stability of the emulsions of ($S_1 + G$) and of ($G + S_2$) increases with diminishing alkyl sulfate concentration. The study of the interface present in these emulsions, viz., anisotropic liquid/isotropic liquid, has not yet been recorded in the literature, and its theoretical and experimental investigation should be of much interest. The interface S/G should presumably be characterized by two interfacial tensions. In such emulsions, even when at rest, it may well be that the form of the particles of the disperse phase (either S or G) is not spherical.

It appears that, in Tables I, II, and III, the clear, apparently isotropic, single-phase systems which show streaming birefringence are probably to be regarded as stable (S + G) emulsions.

Although several of the dispersions designated ($S_2 + G$) in Table I separated into S_2 and G phases on standing at room temperatures, under closer temperature control (thermostat at 19°C.) separation (except over

TABLE III

Alternate Displacement of Intermicellar Equilibrium and $S_1 - G$ Phase Change to the Right by Addition of a 48.6% (by Weight/Total Volume) Solution of Cyclohexylammonium Chloride and to the Left by Addition of Water to Initially 10 ml. of 20% (by Weight) Undecane-3 Sodium Sulfate Solution at 20°C.

Total volume cyclohexylammonium chloride solution added, ml.	Total volume of water added, ml.	Condition of system	Remarks
0	0	S_1	Water-clear; isotropic
0.9	0	$S_1 + G$	Cloudy; phases separate on standing
1.05	0	G	Opalescent liquid crystal
1.05	10	S_1	Water-clear; isotropic
1.15	10	$S_1 + G$	
1.25	10	G	
1.25	20	S_1	
1.35	30	$S_1 + G$	
1.4	20	G	
1.4	20	$S_1 + G$	
1.55	30	G	
1.55	40	$S_1 + G$	
1.65	40	G	
1.65	60	$S_1 + G$	
1.75	60	G	
1.75	80	$S_1 + G$	Opalescent, birefringent on streaming. No evidence of separation of phases on standing
2.1	80	$S_1 + G$	
2.3	80	G	Stable birefringence

an exceedingly narrow range of composition) did not occur. The effect of variation in temperature in promoting separation is probably due to its influence in shifting the limits of the narrow range of composition over which (at a particular temperature) separation occurs. The samples which show phase separation are thus brought within the zone of instability from time to time.

Where separation is observed, the differences between the refractive indices and densities of the phases are small and the interfacial tension between the phases is extremely low. Where separation does not occur, it seems possible that one, or more probably both, of the interfacial tensions S/G may have reached zero, leading to the production of clear, thermodynamically stable dispersions of the two phases. If the interfacial tensions were finite (unless the densities of the phases were equal), the dispersions would necessarily be thermodynamically unstable. Further, since the two phases are so similarly composed, material transfer from the smaller to the larger droplets of the disperse phase would be very easy and rapid separation of the phases (such as is actually found even with those Type II systems in Tables I and II which become truly homogeneous on shaking) would be expected to occur. The coexistence of two equilibrium phases

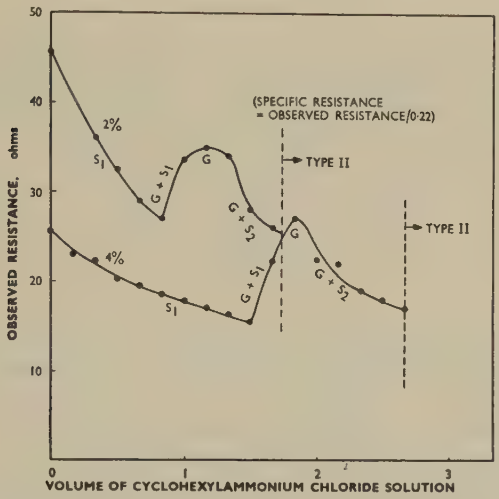

FIG. 2. Changes in electrical resistance observed on addition of cyclohexylammonium chloride (48.6% by weight/total volume) to 50 ml. of undecane-3 sodium sulfate solution.

with zero interfacial tension is difficult to visualize, but it appears possible that such phenomena do occur, *e.g.*, in the critical region for the transformation liquid/gas (6).

4. Electrical Resistance Changes

The two resistance/composition curves in Fig. 2 are closely similar to one another and to that determined earlier (3) at a higher alkyl sulfate concentration (10%). Thus, although bulk phase separation occurs readily at 10%, slowly at 4%, and not at all at 2%, similar resistance/composition curves are obtained in all three cases. This supports the view that the inflections in the resistance curves accompany similar phase changes in all three cases, but that the stability of the emulsions formed from the separating phases increases progressively with dilution.

5. Compositions of S and G Phases in Equilibrium

Some analytical figures for equilibrium S and G phases selected from Table I are given in Tables IV and V. RSO_4^- was determined by titration with cetyl pyridinium bromide, $C_6H_{11}\cdot NH_3^+$ by titration with alcoholic potassium hydroxide using phenolphthalein as indicator, and Cl^- by Volhard's method. Na^+ was calculated from the above results and the condition for electrical neutrality of the phases. The figures for RSO_4^- and $C_6H_{11}\cdot NH_3^+$ in both Tables IV and V indicate a considerable enrichment of the liquid crystalline phase in both these species in either $(S_1 + G)$ or $(G + S_2)$ sys-

TABLE IV

Analysis of Equilibrium S_1 and G Phases Produced When 1.5 ml. of Cyclohexylammonium Chloride Solution (48.6% Weight/Total Volume) Was Added to 50 ml. of Undecane-3 Sodium Sulfate Solution (4% by Weight/Total Volume) at 19°C.

Phase separation (in a thermostat) required about three days

	Phase volume, ml.	$C_{11}H_{23}\cdot SO_4^-$, millimoles per ml.	$C_6H_{11}\cdot NH_3^+$, millimoles per ml.	Cl^-, millimoles per ml.	Na^+, millimoles per ml.
S_1 phase (upper)	35.5	0.084	0.063	0.113	0.134
G phase (lower)	16.0	0.276	0.188	0.10	0.190

tems. This recalls the results for the phase analysis in the anhydrous hydrocarbon/oleic acid/monoethanolamine system reported earlier (3).

6. Nature of "Viscoelastic Solutions" of Amphiphilic Salts

Typical S_1 and S_2 solutions of amphiphilic salts such as those considered above are isotropic and mobile Newtonian liquids.

Liquid crystalline (G) solutions of amphiphilic salts are characterized by their anisotropy. They are frequently highly viscous (*e.g.*, 20% aqueous solutions of tetradecane-7 sodium sulfate or Aerosol OT) but in some instances are readily pourable as with the liquid crystalline (sodium + cyclohexylammonium) undecane-3 sodium sulfate solutions shown in Tables I, II, and III.

In addition to these well-defined types of solution, whose properties are qualitatively satisfactorily accounted for on the basis of micellar theory, there is a series of aqueous "viscoelastic soap solutions" (7) which are less well defined and whose properties have not, as yet, been satisfactorily accounted for. A characteristic of these "solutions" is that they show structural viscosity, their rheological behavior being strongly dependent on mechanical conditions. Some examples of such "solutions" are as follows.

Viscoelastic solutions of ammonium oleate (1.5 ml. oleic acid + 50 ml. ammonia (specific gravity 0.88) + 950 ml. water, *i.e.*, $0.0048N$ ammonium oleate + 15.3 g./l. excess ammonia) were examined by Hatschek and Jane (8) using a Couette viscometer. They found that when the outer cylinder was rotated at a constant angular velocity the torque on the inner one, after a short period of normal magnitude, increased to an irregularly fluctuating value many times greater. When such a viscoelastic solution is stirred round in a glass beaker and stirring is interrupted, the solution comes to rest much more rapidly than an ordinary solution and then reverses its direction of motion, often for about a complete revolution.

In contrast to solutions of ammonium oleate, dilute solutions of the more hydrophilic potassium oleate are normal mobile isotropic liquids. However, viscoelastic properties similar to those of the ammonium oleate solutions appear on addition of a soluble potassium salt. Thus the addition of 1.1 ml.

TABLE V

Analysis of Equilibrium S_2 and G Phases Produced When 2.39 ml. of Cyclohexylammonium Chloride Solution (48.6% Weight/Total Volume) Was Added to 50 ml. of Undecane-3 Sodium Sulfate Solution (4% by Weight/Total Volume) at (19° ± 3°C.)

Phase separation required about 14 days and occurred only when some variation in temperature was permitted

	Phase volume, ml.	$C_{11}H_{23}\cdot SO_4^-$, millimoles per ml.	$C_6H_{11}\cdot NH_3^+$, millimoles per ml.	Cl^-, millimoles per ml.	Na^+, millimoles per ml.
S_2 phase (upper)	35.0	0.125	0.153	0.164	0.136
G phase (lower)	17.4	0.170	0.185	0.165	0.151

of a solution containing 100 g. potassium acetate/100 ml. solution to 25 ml. of a 1% solution of potassium oleate gives a viscoelastic solution similar to the solution of ammonium oleate described by Hatschek and Jane. Conversely, addition of 1 equivalent of potassium hydroxide to the latter solution (*i.e.*, replacement of NH_4^+ by K^+) destroys its viscoelasticity and also eliminates the slight turbidity which is evident with the viscoelastic ammonium oleate solution.

When a concentrated solution of potassium acetate or carbonate is added to a mobile isotropic 10% solution of potassium oleate (S_1), a thick, apparently isotropic jelly is formed. This jelly, however, shows marked birefringence if held between crossed polaroids and stirred with a glass rod.

It was suggested by Lawrence (9) and further by Hartley (7) that viscoelastic properties such as those discussed above are due to the production of "secondary micelles" or aggregates of Hartley micelles (S_1) through the formation of a crystal type of lattice between the polar groups on the surface of adjacent micelles, thus giving rise to (virtually) chains of liquid droplets. Such incipient crystallization of highly soluble salts, often at high dilution, seems, however, unlikely. It is more probable that the behavior of viscoelastic "solutions" is due to their constitution as intimate emulsions of S and G phases such as have already been considered in connection with Tables I, II, and III above. The emulsions in these tables, as well as the S and G phases themselves, were, however, all of low viscosity.

The formation of liquid crystal G from an isotropic S_1 solution of an alkali metal soap may, in suitable circumstances, be brought about by:

1. Fall in temperature.
2. Increase in concentration.
3. Substitution of alkali metal by a more lipophilic cation.
4. Addition of inorganic salt.

The progressive operation of any of these processes at first results in the production of S_1 + G phases in equilibrium (*cf.* Tables I, II, and III). The equilibrium phases in certain instances, *e.g.*, in Tables I and III, or with "solutions" of tetradecane-6 and -7 sulfate of appropriate over-all concentration, separate fairly readily, but in other cases (*cf.*, *e.g.*, Tables II and

III) they form stable emulsions. The phases of these emulsions, besides differing little in specific gravity, are close to one another in refractive index so that the emulsions may appear clear or only slightly turbid. The rheological properties of these emulsions will depend on the phase ratio, on the droplet size distribution, on the form of the emulsion, *i.e.*, S_1 in G or G in S_1, on the viscosity of the phases (particularly of the continuous phase), and on the interfacial tensions which, in such systems, are invariably low. In the systems shown in Tables II and III the S and G phases and their emulsions are all rather mobile liquids.

The behavior of the dilute ammonium oleate "solution" described above suggests that on stirring it forms a finely dispersed emulsion S_1 in G which reverts to a coarser (possibly multiple) dispersion of S_1 and G on standing. The viscosity of the G-phase formed in solutions of alkane-1 salts is always high.

The appearance of anisotropy when the jelly formed from the 10% potassium oleate solution and potassium carbonate (p. 95) is agitated is paralleled by the behavior of the S_1 + G and G + S_2 emulsions recorded in Tables I, II, and III. When such an emulsion is at rest, the particles of liquid crystal are in equilibration with the surrounding isotropic regions and, owing to the process of rotational diffusion, show no preferred orientation. The emulsion as a whole therefore appears isotropic. On stirring, orientation of the liquid crystal particles may occur and anisotropy becomes apparent. This disappears more or less rapidly on removal of the disturbance.

On settling out of the less stable (S + G) emulsions in Table I the lower phase (G) shows strong birefringence between crossed polaroid sheets,

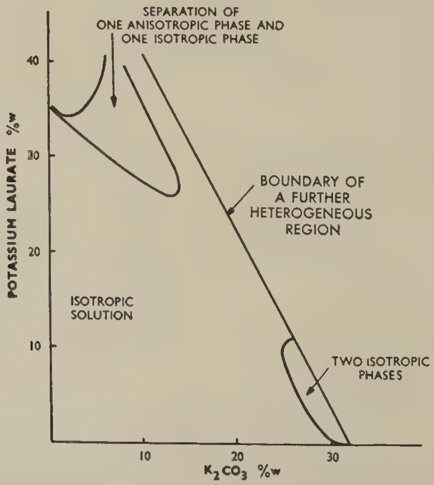

FIG. 3. Phase diagram for potassium laurate/water/potassium carbonate system (after D. G. Dervichian, M. Joly, and R. S. Titchen (10)).

whereas the upper phase (S_1 or S_2) is isotropic. Presumably, orientation of regions of the bulked G phase occurs during settling. On reagitating the settled phases, an almost clear, apparently isotropic emulsion is again obtained which shows streaming birefringence.

The interpretation given in the preceding paragraphs receives support from an extensive study by D. G. Dervichian, M. Joly, and R. S. Titchen (10) of the rheological and optical properties of potassium laurate/water systems containing potassium carbonate or potassium chloride. Their results for the systems containing potassium carbonate are reproduced in Figs. 3, 4, and 5. The contour lines of equal viscosity have been plotted on a logarithmic scale indicating the very large effects observed.

According to these authors "there is an exact correspondence between the four regions defined by viscosity and the four regions defined by streaming birefringence. . . . With the systems studied the regions of Newtonian flow and of absence of streaming birefringence coincide. At the same time streaming birefringence only appears with systems showing non-Newtonian laminar flow."

It is suggested by Dervichian and collaborators that these "variations in properties of the isotropic phase of the soap/salt water systems may be the manifestation of "transformations of higher order" within this phase." It seems, however, that the behavior described is probably to be interpreted in terms of emulsions of S (S_1 or S_2) and G phases as already suggested

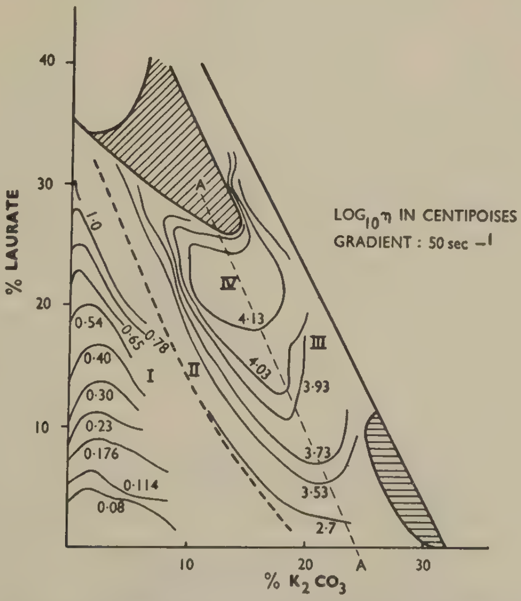

Fig. 4. Contours of equal viscosity for systems in Fig. 3 (after D. G. Dervichian, M. Joly, and R. S. Titchen (10)).

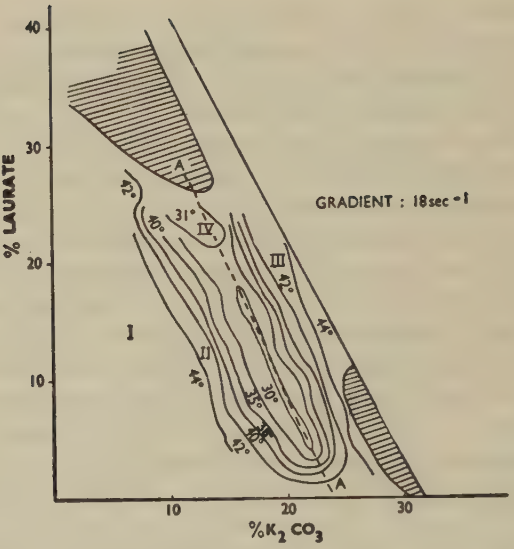

FIG. 5. Contours of equal extinction angles for systems in Fig. 3 (after D. G. Dervichian, M. Joly, and R. S. Titchen (10)).

above. At higher soap concentrations these emulsions are unstable and actual phase separation occurs as indicated in Fig. 3. At lower soap concentrations (as in Tables I and II) more stable emulsions are obtained and give rise to the phenomena under consideration. In Figs. 3, 4, and 5, on this interpretation, region I corresponds to an S_1 soap solution ($R < 1$, *cf.* Fig. 1), region II to a stable emulsion $S_1 + G$ (R in $S_1 < 1$), region IV to a stable emulsion of ($G + S_1$ or S_2) (R in S phase $\simeq 1$), region III to a stable emulsion of ($G + S_2$). The "nigre lye bay" at the lower right-hand corner of Fig. 5 corresponds to precipitation as a Type II system as in Table II (I and J). In the rather critical type of mixtures which probably occurs in region IV, rate of shear might be expected to exert a considerable effect on the actual phase ratio and construction of the phases just as in the case of the Type II systems in Tables I and II (p. 90 and 91). These effects may account for certain curious aspects of behavior noted for this region by Dervichian, Joly, and Titchen, concerning which reference to their original paper should be made.

The effects of added water-soluble and water-insoluble (but polar) organic liquids on the viscosity changes occurring when potassium chloride is added to an aqueous solution of sodium oleate have been studied by Bungenberg de Jong and van Alphen (11). Some of their results are reproduced in Fig. 6.

It is clear that addition of the water-soluble organic liquids displaces the line corresponding to *AA* (Fig. 4) to the right (and thus displaces the intermicellar equilibria (Fig. 1) to the left), whereas the water-insoluble liquids exert the opposite effect. Similar effects are produced with regard to the formation of Type II systems. These results are those to be expected, on the theory given above, from the general influence of water-soluble and water-insoluble organic liquids on the intermicellar equilibrium (*cf.*, *e.g.*, Winsor (4, 12).

It is clearly difficult to distinguish experimentally between a stable S/G emulsion and a single-phase system, and it appears likely that the identification of rather stable (S_1 + G) emulsions as systems of a single phase may have occurred in certain cases described in the literature. This seems, for example, to be probable with the "visibly turbid solutions" of *n*-hexadecyl trimethyl ammonium bromide investigated by Debye and Anacker by methods of light scattering (13) and would necessitate considerable modification of their theoretical conclusions. In more recent work of a similar nature by Anacker (14), dilute aqueous systems containing decyl trimethyl ammonium and octyl and decyl sulfonates were actually identified as emulsions of greater or less stability. Although an investigation of the nature of the separating phases has not yet been made, these probably correspond to S and G. If this supposition is correct and is also applicable to the "visibly turbid" *n*-hexadecyl trimethyl ammonium bromide "solutions," the optical results obtained by Debye and Anacker and the dynamo-optical experiments of Backus and Scheraga (15, 16) should be reinterpreted in terms of

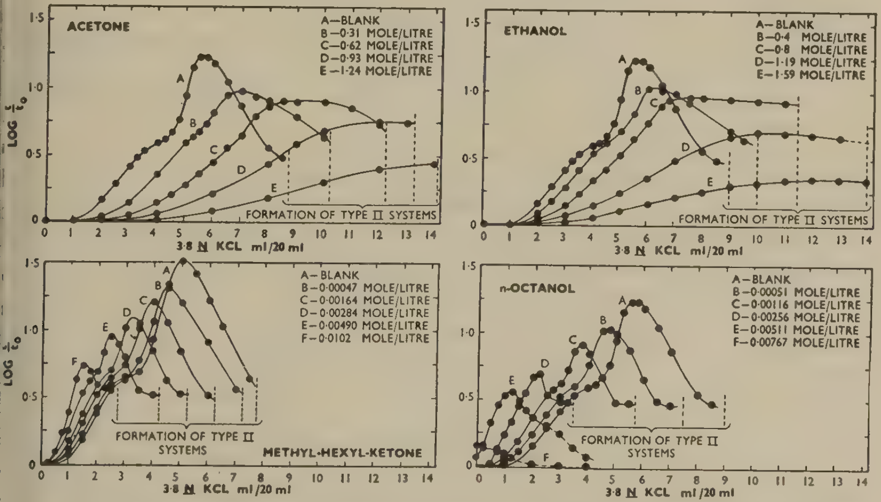

FIG. 6. Changes in relative viscosities occurring when "*a*" ml. of 3.8 *N* KCl are added o solutions containing 5 ml. sodium oleate stock solution (40 g. sodium oleate + 000 ml. water + 200 ml. 2 *N* KOH), "*b*" ml. organic liquid, and (15 − (*a* + *b*)) ml. ater (after H. G. Bungenberg de Jong and G. W. H. M. van Alphen (11)).

particle size and shape in S/G emulsions. However, to make such an interpretation one would presumably first need a determination of particle composition. This might possibly be achieved by X-ray measurements (2).

ACKNOWLEDGMENT

The author wishes to thank the Directors of the Shell Petroleum Company Limited for permission to publish this paper.

SUMMARY

The phase equilibria and the underlying intermicellar equilibria in the system undecane-3 sodium sulfate/cyclohexylammonium chloride/water are discussed. Observations are described which are used as the basis for a general theory of the nature of "viscoelastic soap solutions."

REFERENCES

1. *cf.*, *e.g.*, LUMB, E. C., AND WINSOR, P. A., *Ind. Eng. Chem.* **45,** 1086 (1953).
2. WINSOR, P. A., *J. Phys. Chem.* **56,** 391 (1952).
3. BROMILOW, J., AND WINSOR, P. A., *J. Phys. Chem.* **57,** 889 (1953).
4. WINSOR, P. A., *Trans. Faraday Soc.* **44,** 376 (1948).
5. SILBERBERG, A., AND KUHN, W., *Nature* **170,** 450 (1952); *J. Polymer Sci.* **68,** 21 (1954).
6. MAYER, J., "Changements de phases," p. 35. Société de Chimie Physique, Paris, 1952.
7. HARTLEY, G. S., "Paraffin-Chain Salts." Hermann et Cie., Paris, 1936.
8. HATSCHEK, E., AND JANE, R. S., *Kolloid-Z.* **38,** 33 (1926).
9. LAWRENCE, A. S. C., *Trans. Faraday Soc.* **30,** 189 (1935).
10. DERVICHIAN, D. G., JOLY, M., AND TITCHEN, R. S., "Changements de phases," p. 152. Société de Chimie Physique, Paris, 1952.
11. BUNGENBERG DE JONG, H. G., AND VAN ALPHEN, G. W. H. M., *Proc. Acad. Sci. Amsterdam* **50,** 849, 1011, 1227 (1947).
12. WINSOR, P. A., *Trans. Faraday Soc.* **46,** 762 (1950).
13. DEBYE, P., AND ANACKER, E. W., *J. Phys. Chem.* **55,** 644 (1951).
14. ANACKER, E. W., *J. Colloid Sci.* **8,** 402 (1953).
15. SCHERAGA, H. A., AND BACKUS, J. K., *J. Am. Chem. Soc.* **73,** 5108 (1951).
16. BACKUS, J. K., AND SCHERAGA, H. A., *J. Colloid Sci.* **6,** 508 (1951).

ELECTRICAL-OPTICAL EFFECTS IN LIQUID CRYSTALLINE SOLUTIONS CONTAINING AMPHIPHILIC SALTS

P. A. Winsor

Shell Petroleum Company, Limited, Thornton Research Centre, Chester, England

Received June 10, 1954; revised received September 2, 1954

INTRODUCTION

Investigations by electrical conductivity measurements of a variety of solutions containing amphiphilic salts have been described previously (1, 2). In those investigations a high-frequency alternating source of current was used as in the many measurements of the conductivities of aqueous amphiphilic electrolyte solutions published in the literature (3). The investigation of aqueous solutions of amphiphilic electrolytes using a continuous potential difference has also been reported in the literature in connection with the measurement of transport numbers (3).

The present paper records experiments to determine whether evidence may be detected of distortion (or orientation) under the influence of an applied potential difference of the various micellar forms present in solutions of amphiphilic salts. Electrooptical effects have been found with liquid crystalline solutions containing amphiphilic salts (4).

THEORY

It has been shown previously (1, 2, 5, 6) that the behavior and phase equilibria observed with solutions of amphiphilic salts (whether they contain water, water-soluble organic solvent (*e.g.*, ethylene glycol), water-insoluble organic solvents (*e.g.*, hydrocarbon), or mixtures of these in the most varied proportions) may be accounted for on the basis of the balance within them of an intermicellar equilibrium which may be represented diagrammatically as in Fig. 1 of the preceding paper.

The following considerations may be advanced on the deformation effects which might be expected with each of the idealized micellar forms shown, under the influence of a sufficiently strong electrical field.

1. S_1-Micelle. This form of micelle is perhaps most typically developed n the mobile isotropic aqueous solutions of amphiphilic electrolytes at concentrations not too greatly above the "critical micelle concentration" (7). The micelle carries a net electrical ionic charge and should therefore migrate n an electrical field. This migration has been demonstrated by measurements of transport numbers (3, 7). The resting micelle is isotropic, but since it is of a fluid character (7), if migrating sufficiently rapidly it is conceivable that it would be distorted by shear and become elongated, orientated, and anisotropic. It should be remarked, however, that streaming birefringence does not appear to occur with most isotropic solutions o amphiphilic electrolytes.

2. G-Micelle. These micelles form the liquid crystalline solutions or gel (G) of amphiphilic salts which may be obtained in water, in organic solvent or in mixtures of these (1, 2). The micelles have the same composition as the solution as a whole (8) and are potentially coextensive with it. However except in so far as uniform orientation by flow has taken place, the orientation of regions of the micelles within the solution will vary.

Consider two regions of liquid crystal arranged as at I(*a*) and I(*b*) (Fig 1) between two electrodes. If a potential difference is now applied to the electrodes, these regions will be affected differently.

(i) In the case of I(*a*) some alteration in the mean alignment of the (liquid) hydrocarbon chains relative to the polar surfaces within the liquid crystal might be expected, producing II(*a*). With I(*b*) no such change would be likely (II(*b*)). Since the hydrocarbon chains differ in refractive index along and across their long axes, a change in refractive index along *XY* would occur at (*a*) but not at (*b*). This differential change might produce turbidity.

(ii) The transport numbers of the amphiphilic ion and counter ions relative to the electrodes would probably be different for regions of liquid crystal such as I(*a*) and I(*b*) (Fig. 1), which are differently aligned with respect to the applied field. On continued application of a potential difference (p.d.) this might lead to local heterogeneity and thus produce turbidity.

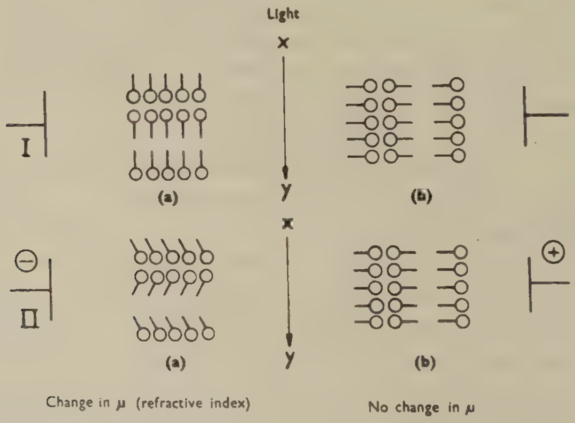

FIG. 1. Possible effect of an applied p.d. on differently oriented regions of liquid crystal (4).

EXPERIMENTAL

A. Qualitative Experiments

The following preliminary experiments were carried out to see what evidence for the effects suggested above could be obtained qualitatively.

1. S_1-Micelles. It was thought that the most readily deformable S_1 micelles might be found in S_1 solutions whose composition was close to that at which the phase transition $S_1 \rightarrow (S_1 + G)$ occurs (Fig. 1 in preceding paper). With this composition R is approaching unity, and it might be expected that a convex micellar surface could readily be deformed towards the planar form under the influence of shear. For these reasons a solution was prepared containing undecane-3 sodium sulfate (10% by weight/volume) to which cyclohexylammonium chloride (48.3% by weight/total volume) had been added until the transition $S_1 \rightarrow (S_1 + G)$ was almost reached (2). This solution, contained in a narrow-bore U-tube, was electrolyzed between platinum electrodes using a rectifier generating potential differences (p.d.) up to 700 v. With the p.d. adjusted to give vigorous gassing at the electrodes, no sign of birefringence could be obtained when the experimental sample was observed between crossed polaroid sheets. It was therefore concluded that in this system and under these conditions the possible appearance of anisotropy visualized under (1) "*Theory*" above is not realized.

2. G-Micelles. The following liquid crystalline solutions were investigated: (i) Tetradecane-7 sodium sulfate 20% by weight. (ii) Tetradecane-7 potassium sulfate 20% by weight. (iii) Pentadecane-8 sodium sulfate 3.1% by weight. (iv) Aerosol OT 20% by weight. (v) A series of liquid crystalline solutions obtained by adding cyclohexylammonium chloride solution (48.6% by weight/total volume) to aqueous solutions of undecane-3 sodium sulfate of 1%–10% concentration. (vi) The liquid crystalline solution (6) containing undecane-3 sodium sulfate (5 ml. 20% by weight), hydrocarbon B (5 ml.), and octanol-1 (1.2 ml.).

In all cases a turbidity appeared at once on applying a potential difference of 20–40 v./cm.

If the p.d. was applied only for a short time (*e.g.*, a fraction of a second) the turbidity disappeared when the p.d. was removed. If the p.d. was applied for a longer time (*e.g.*, half a minute), on its removal the main turbidity disappeared at once as before, but there was also a residual turbidity which was more persistent. It seems possible that the less persistent turbidity may be accounted for according to 2(i) under "*Theory*," whereas the more persistent turbidity may arise according to 2(ii). There is, however, an element of doubt about the completeness of this interpretation since the turbidity still appears in regions where, on other grounds, it is thought that uniform orientation of the liquid crystalline solution occurs. Thus if a layer of a liquid crystalline solution from the series under (v) above is included between a cover slip and microscope slide, it is highly probable that the lamellae become oriented parallel to the plane glass surfaces. Application of a p.d. at opposite edges of the cover slip (*i.e.*, as at II(*a*), Fig. 1) produces turbidity. The change I(*a*) to II(*a*) would correspond to a change from a uniaxial to a biaxial liquid crystal, but it is not clear how such a change could result in the appearance of turbidity.

When in the example described, the continuous p.d. was replaced by a similar alternating p.d. from the mains supply (50 cycles per second) no turbidity appeared. No visible turbidity was produced when isotropic S_1 and S_2 solutions were subjected to a continuous p.d., even when the isotropic phase formed the upper layer of a conjugate pair of S + G phases in equilibrium. In this case production of turbidity was confined to the liquid crystalline phase.

When subjected to shear, liquid crystalline solutions readily become orientated. The orientation is evident in X-ray diagrams (9) or in samples held between crossed polaroid sheets (10) and is semipermanent. From observation between crossed polaroid sheets of liquid crystalline solutions under the influence of a continuous p.d., it appears unlikely that the resulting turbidity was accompanied by any rearrangement of the orientation of the liquid crystals within major tracts of the solution.

3. S_2-Solutions. The experimental method was similar to that used with S_1 solutions. Results obtained were again negative.

B. Quantitative Experiments

Because of the qualitative results obtained with the liquid crystalline solutions described above, further more quantitative experiments were made using the undecane-3 sodium sulfate/cyclohexyl ammonium chloride/water system discussed in the preceding paper.

1. Relation between Applied Potential Difference and Turbidity. Rate of Decay of Turbidity. These relationships were investigated using the liquid crystalline solution obtained from 100 ml. undecane-3 sodium sulfate solution (10% by weight) and 7 ml. cyclohexylammonium hydrochloride solution (48.6% by weight/total volume). To permit measurements of the turbidity produced, a cell (Fig. 2) was used which could be inserted on the E.E.L. absorptiometer (Evans Electroselenium Ltd., Harlow, Essex). The approximate constant of this cell was 28 and its resistance when charged with the above solution was about 3000 ohms. Some results obtained are shown in Fig. 3. The potential differences (from a high-tension battery) were applied for a period of 30 seconds only, since this was found sufficient to reach the approximate maximum turbidity. Longer application resulted in undue heating of the experimental samples.

The rate of growth of turbidity was too rapid for accurate observation. It is, however, by no means instantaneous. This was shown by reversing the applied potential difference, varying the frequency of reversal using a

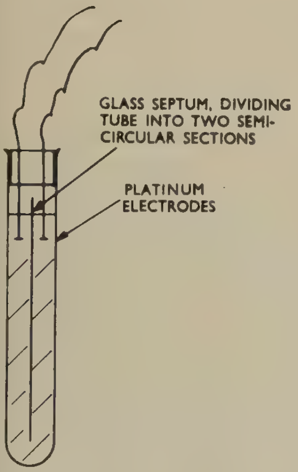

FIG. 2

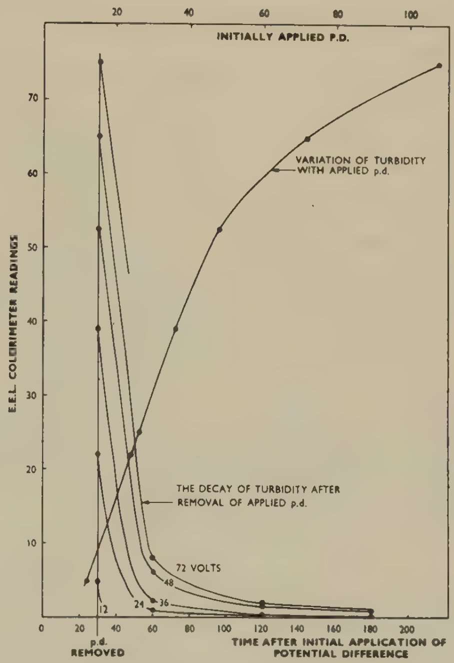

FIG. 3

FIG. 2. Cell for observation of turbidity; for use in conjunction with E.E.L. colorimeter.

FIG. 3. Turbidities produced on application of potential differences (p.d.) to a liquid crystalline solution containing undecane-3 sodium sulfate (10% by weight, 100 ml.) cyclohexylammonium chloride (48.6% by weight/total volume, 7 ml.).

Marconi beat frequency oscillator with a Telephone Mfg. Co. Ltd. relay Tube 5PA 18A connected to two high-tension batteries of suitable (equal) voltage. To ensure that there was no net unidirectional passage of current a condenser (capacity 8 μf.) was included in series with the cell for frequencies above 20 cycles per second. For lower frequencies this condenser was omitted.

Using ±48 v., frequencies above about 10 cycles per second gave no measurable turbidity on the E.E.L. colorimeter. With +48-v. half cycles (100/second), a maximum deflection of 15 was obtained, while with 48 v. applied continuously a maximum deflection of 35 was reached. By direct visual observation a just perceptible turbidity occurred at ±48v. at 50 cycles per second. At ±120 v. there was a just perceptible turbidity at about 150 cycles per second.

3. Relation between Micellar Constitution and Production of Turbidity. The systems in Table II (previous paper) represent a rather closely related series in which the intermicellar equilibrium and phase changes are gradually displaced to the right.

Using an applied potential difference of 120 v.: A and B gave no turbidity.

C gave a turbidity rising to about 16 units.
D “ “ “ “ “ “ 33 “ .
E “ “ “ “ “ “ 45 “ .
F “ “ “ “ “ “ 25 “ .

G on first application of a p.d. gave a maximum deflection of 45 units, but on reapplication gave no deflection. However a deflection similar to the original was obtained after cooling on reapplication of the p.d.

H, I, and J gave no measurable turbidity.

These results demonstrate clearly how specific the electrooptical effect is for the liquid crystalline phase. The two different successive results with sample G (which were obtained on a rather cool morning) must be attributed to the effect of the heat produced by the applied current in displacing the intermicellar equilibrium and phase changes to the right. The effect of cooling confirms this view. On cooling sample G it shows permanent birefringence, and in this condition alone it shows a marked electrooptical effect. In emulsified systems containing G and S_1 or S_2 one would expect the turbidity generated on application of a p.d. to be regulated by the proportion of the current carried by the G phase. This will be governed by the emulsion type (S_1 in G or G in S_1), by the form of the dispersed phase, and by the relative conductivities of the two phases. In the above series, whereas the $S_1 + G$ emulsions give marked turbidity on application of the potential difference, the $G + S_2$ emulsions remain clear.

Acknowledgment

The author wishes to thank the Directors of the Shell Petroleum Company Limited for permission to publish this paper.

Summary

Electrical-optical effects are described which are shown specifically by liquid crystalline solutions of colloidal electrolytes. Theoretical speculations are advanced concerning the origins of the observed effects.

References

1. Winsor, P. A., *Trans. Faraday Soc.* **46,** 762 (1950).
2. Bromilow, J., and Winsor, P. A., *J. Phys. Chem.* **57,** 889 (1953).
3. *cf., e.g.,* McBain, J. W., "Colloid Science." D. C. Heath & Co., Boston, 1950.
4. Winsor, P. A., *Nature* **173,** 81 (1954).
5. Winsor, P. A., *Trans. Faraday Soc.* **44,** 376 (1949).
6. Lumb, E. C., and Winsor, P. A., *Ind. Eng. Chem.* **45,** 1086 (1953).
7. Hartley, G. S., "Paraffin-Chain Salts." Hermann et Cie., Paris, 1936.
8. Philippoff, W., and McBain, J. W., *Nature* **164,** 885 (1949).
9. *cf., e.g.,* McBain, J. W., and Marsden, S. S., *J. Phys. Chem.* **52,** 10 (1948).
10. Schulman, J. H., Matalon, B., and Cohen, M., *Discussions Faraday Soc.* **11,** 117 (1951).

THE STATISTICAL ELECTRIFICATION OF AEROSOLS BY IONIC DIFFUSION

Ross Gunn

Physical Research Division, United States Weather Bureau, Washington, D. C.

Received November 27, 1954

ABSTRACT

A quantitative investigation of the diffusion of atmospheric ions onto spherical particles is reported. Special emphasis is given to random charging processes. The analysis shows that in typical cases about half of the particles are positively charged and the other half negatively charged. Nearly every particle carries at least one electronic charge and some twenty or more. Expressions are developed for the statistical distribution of the fractional number of droplets in relation to their charge. When particle collisions are infrequent, the average free charge of the positive and negative *fractions* depends only on the square root of the radius and the mean thermal energy of each droplet. It is shown that *an equipartition is established* between the *electrical* potential *energy* of each drop and its thermal *kinetic energy*. Typical particle electrification somewhat increases the coagulation rate normally attributable to diffusion alone. *Systematic* droplet electrification of a selected sign is superimposed on this random charging if the positive and negative light ion conductivities of the environment have appreciably different values. The calculated distribution and average charge magnitude agree with those observed on silica dust and new measurments on cloud particles.

I. INTRODUCTION

A number of the basic problems of modern atmospheric physics are related to the electrical charges normally observed on cloud droplets, dust, and rain. The origin of this electrification has been obscure and the magnitude and distribution of the charges uncertain. It is well established that many solid dusts dispersed in the atmosphere are highly electrified and that this electrification plays some part in determining the effective coagulation rates. It has been surmised that cloud droplets have similar properties. However, the frictional contact usually invoked to describe the origin of charges on solid dusts does not appear applicable to cloud droplets, and appeal to direct measurement is required. Preliminary measurements of the charge on individual cloud partices are reported herein, and these correspond roughly with earlier measurements on solid aerosols. It is a fair inference, therefore, that the basic electrification processes have a common origin and are not related to frictional contacts between colliding elements. The present investigation shows that the mechanism principally responsible for the electrification of small non-associating cloud droplets and for *aged* aerosols is the diffusion of natural atmospheric ions onto the suspended particles. The electromechanics of the larger cloud droplets is more complex.

With the object of establishing a better understanding of droplet charging mechanisms in the atmosphere, a theoretical and experimental study of the systematic diffusion of ions onto droplets has recently been completed (2). Reliable expressions for the average charge on atmospheric droplets were obtained which show a dependence upon the ionic characteristics of the environment, the droplet size, and the rate of fall. This theoretical investigation also provided expressions for the rate of combination of ions with suspended drops that now permit a calculation of the statistical distribution of droplets in relation to the net electrical charge that they carry. The earlier paper, which worked out the *systematic charge* transferred to droplets by ionic diffusion, and the present one, that examines the distribution of the accumulated *random charge*, both assume (1) that the space charge outside the droplet is so disperse that its influence on the ionic motions may be neglected; (2) that every ion striking the surface of a droplet or particle will be held by the image forces, and, therefore, the droplets may discharge only by capturing an ion of the opposite sign; and (3) that selective capture due to quasicrystalline double layers may be ignored. Assuming the well-established laws of diffusion and ion motions in an electric field, the average *systematic* charge carried by a spherical droplet in the atmosphere was shown to be given by

$$Q_0 = [1 + F(aVe/2\pi kTu)^{1/2}] \left[\frac{akT}{e} \ln \frac{N_+u_+}{N_-u_-}\right] [1 - \exp - (4\pi e(N_+u_+ + N_-u_-)t)] \qquad [1]$$

where

$$u = \frac{N_+u_+ + N_-u_-}{N_+ + N_-}. \qquad [2]$$

In these relations, N_+ and N_- are the ionic densities of the positive and negative light ions in the environment, u_+ and u_- are their mobilities, a is the droplet radius, V is its velocity of fall, e is the electronic charge, k is the Boltzmann constant, T is the absolute temperature, t is the time, and F is a dimensionless constant closely approximating unity. Equations [1] and [2] have been checked experimentally (3). For reasons outlined in reference 2, Q_0 in Eq. [1] can never exceed $4kTa^2/\pi\ eL$, where L is the mean free path.

The effective charging time, τ, for a droplet by Eq. [1] is approximately

$$\tau = 1/4\pi e(N_+u_+ + N_-u_-). \qquad [3]$$

In ordinary air the charging time is of the order of 400 seconds.

II. The Random Electrification of Cloud Droplets in an Ionized Environment

It is well known that the electrical conductivity of the air is maintained by cosmic rays or radioactivity which systematically produce a continuous supply of ion pairs. Assume that these new ions maintain N_+ and N_- positive and negative light ions per unit volume in a given region and that their average thermal velocity is C_+ and C_-, respectively. Now, if there are a number of cloud droplets present, it is clear that, as a result of thermal agitation and diffusion, the number of positive ions striking a droplet in a given time will be proportional to $N_+ C_+$, and the number of negative ions colliding will be proportional to N_-C_-. Suppose that the number of positive ions striking a group of droplets is exactly equal to the number of negative ions striking them. Then, many of the droplets will remain neutral, but this is purely a result of chance. The laws of probability show that many ions of a single sign will collide with a fraction of the droplets and hence build up charges of considerable magnitude. Some of the droplets will be positively charged and an equal number will be negatively charged. A distribution of droplet numbers in relation to their charge is ultimately established.

It has been found possible to work out in detail this distribution of droplet frequency in relation to the charge they carry, provided the number of collisions of ions with the droplets is very large. This requirement is fully met by drops or dust particles immersed in the ionized air of the earth. It should also be clear that if the ionic density of one type of ion exceeds that of the other, or if its thermal velocity is greater than the other, so that ions of a single sign collide oftener with a given droplet than do those of opposite sign, then the distribution curve of charge will be displaced towards the sign of the ion that collides most frequently.

A mathematical investigation that considers the probability of an ion striking a given droplet and the influence of the drop charge on this probability leads to the conclusion that the resulting distribution of drops and charges approximates the normal Gaussian Law. To avoid a tedious mathematical discussion, it is convenient here to assume that a Gaussian distribution is established and work out the constants for the distribution by a direct comparison with the physical requirements.

According to the Gaussian distribution law, the frequency of occurrence, F_x, or number of droplets or solid particles in a given class width, w, is expressible in terms of the total frequency or number of droplets, F_t, by

$$F_x = \frac{F_t w}{\sqrt{2\pi\sigma^2}} \exp\left[\frac{-(x-y)^2}{2\sigma^2}\right] \qquad [4]$$

where $x - y$ is the deviation of the independent variable from its mean value y, and σ is a constant known as the standard deviation. Since we are interested in finding the fraction of cloud droplets that carry a given number of elementary charges, it is natural to identify x with the number of positive elementary charges carried by a droplet, and y with the average number of elementary charges carried on all the droplets. Accordingly, the class width, w, is taken as unity, and the droplet charge as xe. Thus, from Eq. [4], the ratio of the number of droplets carrying $x + 1$ elementary charges to the number carrying x charges can be written as

$$\frac{F_{x+1}}{F_x} = \frac{\exp\left[\frac{-1}{2\sigma^2}(x^2 + 2x + 1 - 2xy - 2y + y^2)\right]}{\exp\left[\frac{-1}{2\sigma^2}(x^2 - 2xy + y^2)\right]}, \qquad [5]$$

which may be rearranged and partly expanded to yield

$$\frac{F_{x+1}}{F_x} = \left[1 - \frac{2x + 1}{2\sigma^2} + \frac{(2x + 1)^2}{8\sigma^4} \cdots\right]\left[\exp\left(\frac{y}{\sigma^2}\right)\right] \qquad [6]$$

where σ^2 and y are constants yet to be evaluated from the basic physical interpretation.

By good fortune, one may also calculate the ratio given in Eqs. [5] and [6] from the combination coefficients of atmospheric ions on spherical particles. In order to do this, it is noticed that the distribution of droplets carrying different numbers of elementary charges represents a steady state and, hence, does not change with the time. Under such circumstances, one may appeal to the principle of detailed balancing at equilibrium that is frequently employed in statistical mechanics (4). This principle requires that in a given interval of time, the number of cloud droplets or particles that capture a *negative* ion and, hence, *move out* of the group of droplets carrying $(x + 1)$ elementary charges and into the group carrying x elementary charges, must be exactly equal to the number of droplets carrying a charge xe which is moved *into* the group carrying a charge $(x + 1)e$, by the capture of a *positive* ion. This requirement is obviously a statistical one, and instantaneous deviations normally occur.

In an immediately preceding paper, the rate of capture of ions diffusing onto a spherical particle carrying an arbitrary charge has been derived and is immediately applicable to the problem before us (2). Thus, directing attention to the numbers of ions and drops in a unit volume, one may write from the above principle:

$$\left(\frac{dN_+}{dt}\right)_x = \eta_{+x} N_+ F_x = \left(\frac{dN_-}{dt}\right)_{(x+1)} = \eta_{-(x+1)} N_- F_{(x+1)} \qquad [7]$$

where F_x and F_{x+1} are the number of droplets per unit volume carrying x and $(x + 1)$ elementary charges, respectively, and η_{+x} and $\eta_{-(x+1)}$ are the combination coefficients for the positive and negative ions, respectively, when combining with droplets carrying charges of xe and $(x + 1)e$. Using the relatively exact expressions for these combination coefficients as given by reference 2, one may write

$$\frac{4\pi kTau_+N_+F_x}{e\left[1 + \frac{x}{2}\left(\frac{e^2}{akT}\right) + \frac{x^2}{6}\left(\frac{e^2}{akT}\right]^2 + \cdots\right]} = \frac{4\pi kTau_-N_-F_{x+1}}{e\left[1 - \frac{(x+1)}{2}\left(\frac{e^2}{akT}\right) + \frac{(x+1)^2}{6}\left(\frac{e^2}{akT}\right)^2 \cdots\right]} \tag{8}$$

The distribution of droplets as a function of the number of elementary charges may be directly deduced from this relation by a step by step development. However, it is more convenient to divide one series by the other and compare it with the Gaussian relation of Eq. [6]. Thus, rewriting Eq. [8], one has

$$\frac{F_{x+1}}{F_x} = \frac{N_+u_+}{N_-u_-}\left[1 - \frac{2x+1}{2\left(\frac{akT}{e^2}\right)} + \frac{\left(4x^2 + \frac{14}{3}x + \frac{4}{3}\right)}{8\left(\frac{akT}{e^2}\right)^2} \cdots\right]. \tag{9}$$

Now, a comparison of this expression with that of Eq. [6] shows that the equilibrium is essentially Gaussian and a very good approximation, provided $akT/e^2 >> 1$. Moreover, the relations show that the undetermined constants, σ and y, should be replaced by

$$\sigma^2 = \frac{akT}{e^2} \tag{10}$$

and

$$\exp\left(\frac{y}{\sigma^2}\right) = \exp\left[\frac{ye^2}{akT}\right] = \frac{N_+u_+}{N_-u_-} = \frac{\lambda_+}{\lambda_-} \tag{11}$$

where λ_+ and λ_- represent the positive and negative light ion conductivities, respectively. A brief examination will show that this latter relation is equivalent to Eqs. [1] and [2] when the droplets are cloud- or dust-like and the velocity of fall, V, approaches zero. It is apparent, therefore, that the Gaussian equation is directly applicable to cloud and dust electrification problems.

According to Eq. [4] and the requirements of the above relations, the distribution of the number of droplets having charges of x elementary units and immersed in an environment in which the positive and negative ion conductivities are λ_+ and λ_-, respectively, is given by

$$F_x = \frac{F_t e}{\sqrt{2\pi akT}} \exp\left[\frac{-\left(x - \left(\frac{akT}{e^2}\right)\ln\frac{\lambda_+}{\lambda_-}\right)^2}{2\left(\frac{akT}{e^2}\right)}\right]. \qquad [12]$$

This is the fundamental relation of cloud droplet and aerosol electrification and includes both the statistical and systematic charging effects. The character of these estimated distributions is evident in Fig. 1, where curves are given for droplets of different radii.

A number of important quantities may be estimated from the above distribution function. For example, the fraction of all droplets carrying zero charge is, evidently,

$$\frac{F_0}{F_t} = \sqrt{\frac{e^2}{2\pi akT}} \exp\left[\frac{-\left(\left(\frac{akT}{e^2}\right)\ln\frac{\lambda_+}{\lambda_-}\right)^2}{\frac{2akT}{e^2}}\right]. \qquad [13]$$

Thus, in a cloud where the positive and negative conductivities are equal ($\lambda_+ = \lambda_-$), one finds that the fraction of drops that are neutral is the coefficient of Eq. [13], and this may be compared directly with observations. For example, the reader may verify, by substituting appropriate quantities, that 99% of the atmospheric droplets of radius greater than 10^{-2} cm. will carry at least one elementary charge. On the other hand, a droplet or dust particle of radius 10^{-6} cm. will seldom carry even a single elementary charge.

Another quantity that is important in the investigation of dust and raindrop charging is the average number of elementary charges carried by the positively charged droplet fraction. Now, if the positive and negative ion conductivities are equal, the average number of elementary charges on the positive droplets, $\bar{x}_+$, is numerically the same as that on the negatives and both are given by

$$\bar{x}_+ = \bar{x}_- = \frac{1}{F_0}\int_0^\infty F_x\,dx = \int_0^\infty \exp\left[\frac{-x^2e^2}{2akT}\right]dx = \sqrt{\frac{\pi akT}{2e^2}}, \qquad [14]$$

where F_0 is the number of droplets that carry zero charge. This corresponds to the coefficient of Eq. [13]. The average charge carried by both the positive and negative fractions of the cloud drops is, therefore,

$$\bar{q}_+ = \bar{q}_- = \sqrt{\frac{\pi akT}{2}}. \qquad [15]$$

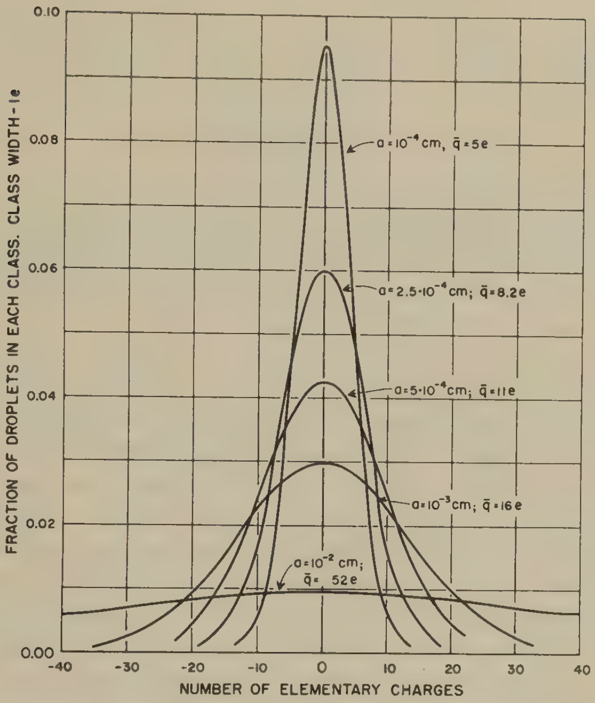

FIG. 1. Distribution of the fractional number of droplets in relation to their charge and radius as estimated from Eq. [12] with $\lambda_+ = \lambda_-$. $\overline{q}$ is the mean statistical charge, irrespective of sign, calculated from Eq. [15] and expressed in terms of the elementary electronic charge.

This relation is an exceedingly simple, but important, result, since it shows that the mean statistical charge on a nonassociating atmospheric particle depends only on the square root of the radius of the particle and its mean thermal energy. It should be noted that Eq. [15] assumes that the positive and negative ionic conductivities are equal. If they are not equal, the distribution curve will be displaced in such a way that $\bar{q}_+ \neq \bar{q}_-$, and the mean random charges must be calculated directly from Eq. [12] by a series integration.

As an interesting corollary of the investigation, one may write Eq. [15] as

$$\frac{1}{2}\frac{\bar{q}_+^{\,2}}{a} = \frac{\pi}{4}kT. \qquad [16]$$

Since a is essentially the electrical capacity of the droplet, the terms on the left-hand side represent the droplet's stored electrical energy, while kT is its probable thermal kinetic energy. Thus, there is an equipartition between the electrical and mechanical energies of the droplets when equilibrium is reached.

The charge per unit mass on cloud drops is of some importance in describing raindrop charges. Therefore, by use of Eq. [15], one finds

$$\frac{\bar{x}_+ e}{m} = \frac{\bar{q}_+}{m} = \sqrt{\frac{9kT}{32\pi a^5 d}} = \frac{\bar{q}_-}{m}, \qquad [17]$$

where $\bar{q}_+/m$ is the average specific charge carried by the positive cloud droplets, and d is the bulk density of the droplet or particles. By substituting numerical values in Eqs. [15] and [17], it is found that a typical cloud droplet of radius $5 \cdot 10^{-4}$ cm. carries 11 elementary charges, and this corresponds to a specific charge of nearly 11 esu/g. Such charges will be shown elsewhere to be important in describing raindrop electrification.

The above discussion emphasizes the electrification transferred to a large number of cloud droplets by the random collision of positive and negative ions known to exist in the atmosphere. These ions are constantly replenished at a rate of something like 10 ion pairs/cm.^{3}/sec. by cosmic rays and radioactivity. Therefore, the process of droplet or dust electrification is a continuing one, and a large amount of free charge is transferred to a cloud in an hour or so. A large fraction of the free charge separated by the cosmic rays is neutralized by the random character of the collision of the ions with the droplets. On the other hand, the above arguments indicate that a considerable fraction of the separated free charges appears as a mixture of positive and negative droplets constituting the cloud.

III. The Initial Coagulation Rate for Small Electrified Particles

A complete analysis of the coagulation mechanics of electrified particles is quite beyond the scope of this paper. It appears that the controlling processes depend critically upon the particle size and the degree of size uniformity. At least three different regimes are evident, and one considers here only the simplest case where the particles are uniform in size and smaller than 2×10^{-4} cm. radius, but larger than the mean free path. Under these special conditions, one may work out the coagulation constant. Expressions for the rate of combination of ions with spherical droplets have been derived in reference 2 and used in Eq. [8] above. These expressions are related to those derived long ago by Townsend (5) but are complete and have been freed of his limiting boundary assumptions. These relations are applicable to the transport of charged particles of an aerosol, provided diffusion and particle space gradients play a significant role. From Eq. [37] of reference 2, one may write

$$-\frac{dN_\pm}{dt} = \frac{8\pi kTuaN_\pm^2}{q\left(1 + \frac{1}{2}\frac{Qq}{akT} + \frac{1}{6}\left(\frac{Qq}{akT}\right)^2 + \text{etc.}\right)} \qquad [18]$$

where Eq. [37] has been doubled because the relative mobility of two identical particles is twice that of a massive particle interacting with a single one. It may be noticed that when Q and q are of opposite sign, the terms in the series alternate in sign. Moreover, since the magnitude of Qq on an average particle is given by Eq. [15], one may substitute its value in the series which yields immediately a convergent numerical series. When ions of the same sign interact, the value of the series approximates 2.42, but if they are of opposite sign, the series has the value 0.50. Thus, if η' is the viscosity of air, the mobility of the particles is

$$u = \frac{q}{6\pi a\eta'}. \quad [19]$$

Substitution of this in Eq. [18] leads to the well-known Smoluchowski expression for the coagulation rate when the particles are not electrified, or

$$-\frac{dN}{dt} = \frac{4kT}{3\eta'} N^2. \quad [20]$$

For interacting particles carrying electrical charges of the same sign, Eq. [18] leads to

$$-\frac{dN_\pm}{dt} = 0.41 \left[\frac{4kT}{3\eta'}\right] N^2_\pm \quad [21]$$

and for interacting particles of opposite sign,

$$-\frac{dN}{dt} = 2.0 \left[\frac{4kT}{3\eta'}\right] N_+ N_-. \quad [22]$$

The reader may verify from Eq. [13] that nearly all the particles will carry a charge so that $N_+ = N_- = N/2$, nearly. Therefore,

$$-\left(\frac{dN}{dt}\right)_t = 1.2 \left(\frac{4kT}{3\eta'}\right) N^2. \quad [23]$$

The electrification of the particles therefore, increases the coagulation rate by about 20%. By considering the basic equations, one may demonstrate that the coagulation due to electrical forces alone is

$$-\frac{dN}{dt} = \frac{\pi}{4} \left(\frac{4kT}{3\eta'}\right) N^2. \quad [24]$$

Since the electrical coagulation constant is approximately the same size as that due to diffusion, it will be seen that particle electrification plays some part in the coagulation of aerosols. A more detailed study of the phenomena in actual clouds will appear in another paper.

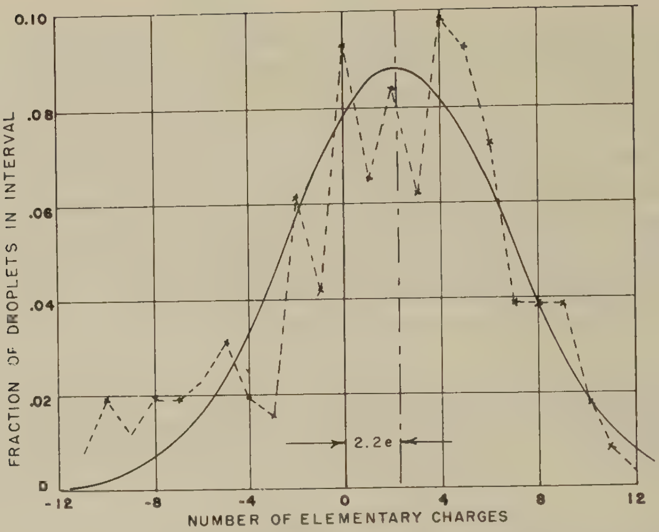

FIG. 2. Distribution of the fractional number of droplets in relation to their charge. Observed data on 250 cloud droplets given by dashed curve. Solid curve is calculated from Eq. [12].

IV. OBSERVED ELECTRIFICATION OF CLOUD DROPLETS AND POWDERED SILICA

Measurements of the electrical charges carried by some 250 laboratory-produced cloud droplets are summarized in Fig. 2. This curve was made available through the kindness of Mr. Russell H. Woessner of this Division, who will report presently on a more complete set of data. The droplets of Fig. 2 were produced in an experimental cloud chamber where the ionization of the air was maintained by radium at a sufficiently high level to insure that equilibrium charges were established on all droplets. The dashed curve represents the observed data, and the solid line is plotted according to Eq. [12]. The average charge on the positive droplets was 5.15 e, while that on the negatives was 5.21 e. More positive droplets were observed than negatives, and the mean excess positive charge was 2.2 e. The average radius of the droplets, as determined from their individual falling velocities, was 1.15×10^{-4} cm. The relation of these data to the theoretical values shown in the solid curve will be discussed in a later paragraph.

While cloud droplet data are particularly suited to test any theory of particle electrification, numerous other measurements of the charge distribution for silica dust dispersed in the air are available. For example, Gillespie and Langstroth (1) have reported on the charge distribution resulting from the dispersal of some 30,000 powdered Vycor particles having a "median diameter less than 1 micron." They give information

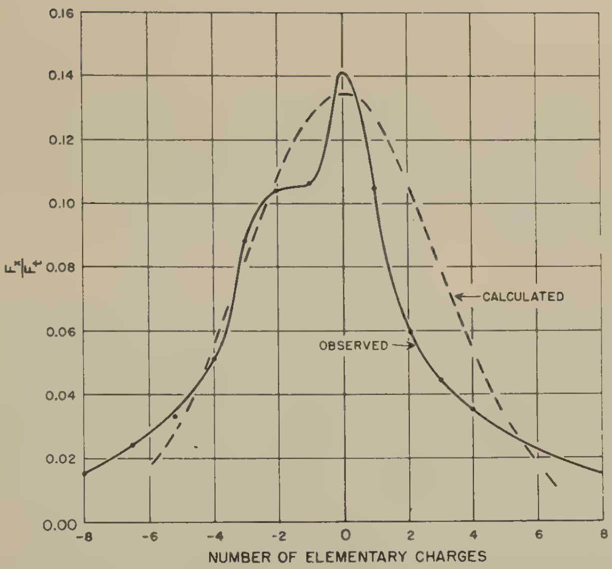

FIG. 3. Silica dust particle distribution in relation to the electrical charge (from Gillespie and Langstroth, ref. 1). Solid curve represents their observations. Dashed curve is calculated from Eq. [12].

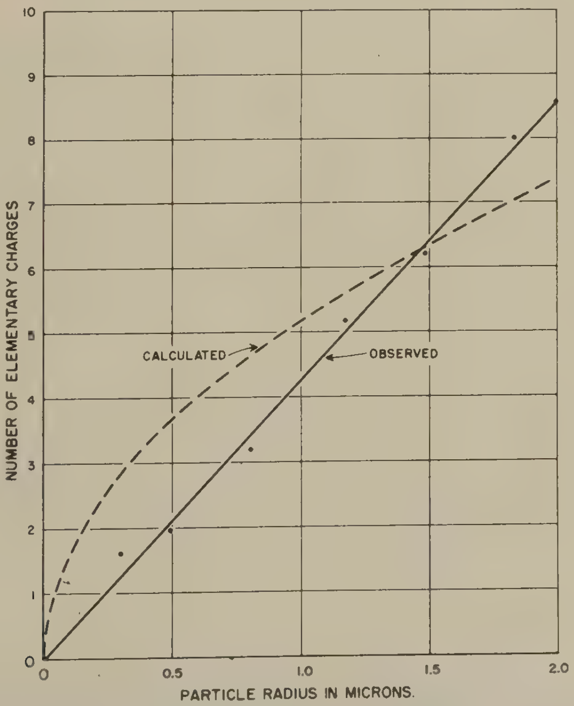

FIG. 4. Mean charge, irrespective of sign, for particles of different radii. Solid line from ref. 1. Broken curve from Eq. [15].

on the distribution for various ages, but because the electrification due to the method of dispersal might persist for more than an hour, the data reproduced here for comparison are for dust that has been aged more than 3 hours. These data are shown in the solid line in Fig. 3. In a similar way, their determination of the relation between apparent radius and the average charge is given by the solid line in Fig. 4.

V. Discussion

An examination of the curves of Fig. 1, which are plotted directly from Eq. [12], assuming equal positive and negative conductivities, shows that the distribution of charges are symmetrical and that the fraction carrying zero charge increases notably as the droplet radius decreases. For example 90% of the cloud droplets of radius 10^{-4} cm. carry at least one elementary charge, while the mean charge irrespective of sign is 5 e. Charges of such magnitude will obviously modify the collision processes when one droplet approaches another. Moreover, a short calculation shows that this random electrification plays an important role in determining the electrical properties of rain formed by the association of many cloud particles. This complex subject will receive quantitative examination in contemporary meteorological publications.

The frictional or collision processes, usually invoked to describe the electrification of dusts, cannot be used to describe the electrification of water and cloud droplets because such collisions would result in association, and, hence, precipitation. However, it is interesting to note that simple ionic diffusion can transfer ions to any kind of an aerosol, and, indeed, if the aerosols are so dispersed that collision between particles is infrequent, then the only obvious way that charge can be maintained on an aged aerosol is by some such ionic transfer process. Because of this situation, it is of interest to compare the estimated electrification that seems applicable to cloud droplets with the charges normally observed on dusts.

The solid curve of Fig. 2 describes the distribution of charged droplets in a cloud according to Eq. [12]. Because of the small size of the sample, the observational scatter about the computed value is large. The mean estimated random charge is found to be 5.6 e. Superimposed upon this random charge is a systematic one of 2.2 e, suggesting that ionization processes in the cloud chamber and diffusion of ions to the wall maintain an excess positive conductivity of about 12%. There is little doubt but that a larger sample would have given better agreement with the theory, but the general agreement is considered satisfactory.

Data on cloud droplet charges are difficult to obtain experimentally, and it seems worth while, therefore, to compare the theory leading to Eq. [12] with available silica dust data. The image forces acting on ions close to a silica particle are known to be smaller than those on a water droplet, but a short calculation will show that at atomic distances the attachment energies are much greater than the thermal energy, and therefore, ions are not at all likely to be re-emitted from a silica particle (Eq. [30], ref. 2). Except for the departure of dust particles from a spherical shape, every other requirement of the analysis appears to have been met, so one might reasonably expect the above theory to agree with Gillespie and Langstroth's measurements. In Fig. 3, the solid line is a plot of their measurements and the dashed curve is the value calculated by Eq. [12], assuming a mean diameter of 1 μ ($a = 5 \times 10^{-5}$ cm.). The agreement with observation is satisfactory. One notices, however, that the observed curve is displaced toward negative charges by about one elementary charge. This is to be anticipated, since Eq. [12] predicts such a displacement when the ionic conductivities are not exactly equal. It may be recalled that *ion pairs* are always produced in any ionization process and that in clear dry air the mobility of the negative ion is some 40% greater than that of the positive. Thus, in clear air, the negative conductivity could exceed that of the positive ions by 40%, and the distribution would be displaced toward negative values by about 5.5 units. Even though many dust particles are present to capture both ions, it is not unreasonable to expect that a slight asymmetry of conductivity will still persist. A 12% excess of negative conductivity within the silica dust cloud will account for the observed displacement toward negative values.

As a final test of the present analysis, the observed relation between the effective radius of the silica particles and their mean random charge has been plotted in Fig. 4. Gillespie and Langstroth plot a linear solid curve connecting the quantities. However, it may be seen that the dashed curve representing Eq. [15] gives nearly as good a representation. Indeed, one of their published curves for dust particles, not so aged, shows a relation just like that estimated.

The comparison between the present analysis and actual measurement is favorable to the belief that clouds of water droplets smaller than 2×10^{-4} cm. in radius and dispersed dusts of solid material acquire a random distribution of free charges by ionic diffusion. If this is correct, then it follows that the electrification of particulate matter in the atmosphere is a universal, widespread phenomenon, bearing directly on a number of basic weather processes. Some of these matters will be discussed in subsequent papers.

REFERENCES

1. Gillespie, T., and Langstroth, G. O., *Can. J. Chem.* **30**, 1056–1068 (1953).
2. Gunn, R., *J. Meteorol.* **11**, 339–347 (1954).
3. Phillips, B. B., and Gunn, R., *J. Meteorol.* **11**, 348–351 (1954).
4. Tolman, R. C., "Principles of Statistical Mechanics." Oxford Press, 1938.
5. Townsend, J. S., "Electricity in Gases." Oxford Press, 1914.

ERRATA TO "VISCOSITY AND ELECTROVISCOUS EFFECT OF THE AgI SOL. II. INFLUENCE OF THE CONCENTRATION OF AgI AND OF ELECTROLYTE ON THE VISCOSITY" (1)

Mr. P. Mukerjee of the University of Southern California has drawn our attention to an error in Table III (p. 76) of the above-mentioned paper (1). The calculated values of the correction factor *f* from the modified Einstein equation

$$\eta_{\mathrm{rel}} = 1 + 2.5\,\varphi\,(1 + f) \qquad [1]$$

as given in columns 4–7 of Table III should be multiplied by about 100. The correct values are given below, calculated for an average particle radius of 170 A, other data being those mentioned in the paper (1).

TABLE III (CORRECTED)

Equilibrium solution no.	$1/\kappa$ A.	Electrolyte content, *millimoles/l.*	Correction factor *f* according to Smoluchowski (2)		Correction factor *f* according to Booth (3)	
			ζ = 200 mv.	ζ = 100 mv.	ζ = 200 mv.	ζ = 100 mv.
1	500	0.035	158	39	1.04	0.26
2	278	0.12	54	13.6	0.78	0.20
3	138	0.49	16	4.0	0.57	0.14
4	64	2.3	2.5	0.62	0.42	0.11
6	25	15.0	0.53	0.13	0.24	0.06

Our experimental results when extrapolated to infinite dilution of the colloidal particles can be expressed by

$$\eta_{\mathrm{rel}} = 1 + K\,\varphi \qquad [2]$$

in which K has the value 3.55, with an uncertainty of about 3%. The difference between 3.55 and the Einstein value 2.5 is considered not to be an electroviscous effect in the sense of Smoluchowski and Booth, because it is independent of the electrolyte content. It is ascribed to the fact that silver iodide particles are not truly spherical (4). The experimental electroviscous effect at infinite dilution is thus smaller than the uncertainty in K, say smaller than 0.1, which is below the calculated values, considering that the ζ-potentials of the silver iodide sols are certainly above 75 mv. and probably above 100 mv.

We are inclined to ascribe the difference between the experiments and Booth's theory to the fact that Booth gives only the first term of a series expansion in ζ and that for a ζ-potential of about 100 mv. more terms of the series should be considered. The range of applicability of Smoluchowski's theory (very thin double layers) has probably not yet been reached even at the highest electrolyte content.

References

1. Harmsen, G. J., van Schooten, J., and Overbeek, J. Th. G., *J. Colloid Sci.* **8,** 72 (1953).
2. Smoluchowski, M. von, *Kolloid-Z.* **18,** 194 (1916).
3. Booth, F., *Proc. Roy. Soc.* (*London*) **A203,** 533 (1950).
4. Another possible explanation has been proposed by Harmsen, G. J., van Schooten, J., and van der Waarden, M., *J. Colloid Sci.*

Van't Hoff Laboratory,
University of Utrecht,
Netherlands

G. J. Harmsen
J. van Schooten
J. Th. G. Overbeek

Received December 2, 1954

EFFECT OF SWELLING OR OF AN ADSORBED LAYER ON THE VISCOSITY OF A SUSPENSION OF SPHERICAL PARTICLES

In an article, "Flow of Concentrated Suspensions," by P. S. Williams (1), some data are reported on the relative viscosity of some suspensions of small glass spheres in glycerol-water solutions. One interpretation of the results was given in terms of a theoretical equation published by one of the present writers (2), the equation being

$$\ln \eta_r = 2.5\varphi/(1 - \lambda\varphi) \qquad [1]$$

where η_r is the relative viscosity, φ is the volume fraction of the suspended spheres, and λ is a parameter which measures the crowding interaction of the spheres with each other. The systems were not precisely monodisperse; and λ must therefore be interpreted as an average value, since the crowding effect varies with the ratio of the sphere diameters.

The values of λ computed by Williams vary with φ, the range in λ being roughly from 1.5 to 3.5. Such a wide variation casts doubt on the theory. However, suspended particles of colloidal dimensions may carry rigidly adsorbed layers of the liquid which are commensurable with the particle diameter. If allowance is made for such an adsorbed layer, the effective hydrodynamic volume being thereby increased by a factor f, the theoretical equation then becomes

$$\ln \eta_r = 2.5f\varphi/(1 - \lambda f\varphi). \qquad [2]$$

To test this equation it is convenient to write it in the form

$$1/\varphi = f\lambda + 2.5f/\ln \eta_r\,. \qquad [3]$$

Thus the theory predicts that $1/\ln \eta_r$ will be a linear function of $1/\varphi$. When Williams' data for his spheres of nominal diameters 4, 8, and 12 μ are plotted as thus indicated, it is found that the data for each diameter do lie approximately on a straight line. Furthermore, the three lines are nearly identical. Graphical solution for f and λ gives the values in the following Table I.

The last column of the table gives the thickness, δ, of the adsorbed layer corresponding to the listed value of f. This computation was made by the equation

$$\delta = (f - 1)\Sigma n_i D_i^3 / 6\Sigma n_i D_i^2$$

n_i being the number of spheres of diameter D_i, as given in Williams' Table III.

TABLE I

Values of mean crowding factor, λ, and effective volume increase, f, computed from Williams' data for suspensions of spheres up to concentration $\varphi = 0.5$

Nominal sphere diameter, μ	f	λ	δ, μ
4	1.32	0.99	0.20
8	1.32	0.99	0.40
12	1.29	1.09	0.66

With regard to the computed values of δ, it is to be noted, first, that they are larger than might be expected, and, second, that they are roughly proportional to the nominal particle diameter, being approximately 5% of it in all three cases. These two facts concerning the values of δ suggest that the increase in effective volume of the suspended material is not due primarily to an adsorbed layer of liquid on each sphere, but more likely to a degree of agglomeration, with effective solidification of the liquid trapped within the agglomerates. This interpretation of Williams' viscosity measurements is given support by Williams' observation that a suspension of spheres less than 1 μ in diameter formed a gel on standing 24 hours.

Williams' viscosity measurements on mixtures of 4μ and 12μ spheres might conceivably permit calculation of the particular λ values for these two diameter ratios 3 and 1/3; but the attempt failed, probably because of the relatively large value and variability of f.

Equation [3] was developed independently by each of the two authors of this letter; and it has been found by one of us (W. A. Hermonat) to be applicable to many colloidal systems and solutions.

References

1. Williams, P. S. *J. Appl. Chem.* **3,** 127 (1953).
2. Mooney, M. *J. Colloid Sci.* **6,** 162 (1951).

Contribution #133
From General Laboratories,
United States Rubber Company
Received December 27, 1954

M. Mooney
W. A. Hermonat

BOOK REVIEWS

Statistical Analysis in Chemistry and the Chemical Industry. By CARL A. BENNETT (Chief Statistician, General Electric Company, Richland, Washington) and NORMAN L. FRANKLIN (Lecturer in Chemical Engineering, University of Leeds, England), Wiley and Sons, Inc., New York, 1954. XVI + 724 pp. Price $8.

It should be stated at the outset that the book under review is a particularly complete and authoritative treatise on statistics. Its authors, one of whom is a mathematical statistician and the other a chemist, were selected by the Committee on Applied Mathematical Statistics of the National Research Council for the task of preparing a "comprehensive book on applied mathematical statistics with illustrative examples and material from chemistry and the chemical industry." This task the authors have accomplished with distinction, using no mathematics beyond calculus. Their style is clear and precise, the notation adequate, and numerous tables assist the reader in grasping the reasoning as well as the computational details of the methods presented.

The question arises as to the type of reader for whom this book is intended. Few chemists will have the leisure and patience to work their way through as systematic a study as is presented in this book, even though a rich reward is assured for those who will. It seems fair to state that the present book is primarily useful to the young chemist in a college or in an industrial concern who, having seen the very real advantages of experimenting in accordance with statistical principles, is willing (and encouraged by management) to spend considerable time and mental effort in the study of this field. Those chemists who have read and been stimulated by Youden's book and wish to progress further in a "painless" way will have to wait for a simpler book. Such a book would not proceed systematically through the mathematics of statistics but approach the entire field from the viewpoint of the immediate need of the chemist.

JOHN MANDEL, Washington, D. C.

Monomolecular Layers, a symposium presented on December 27, 1951, at the Philadelphia meeting of the American Association for the Advancement of Science. Edited by HARRY SOBOTKA. Published by The American Association for The Advancement of Science, Washington, D. C., 1954. 207 pp. Price $3.75 to members, $4.25 retail.

Despite the increasing importance of surface phenomena in the field of fundamental research as well as industrial applications, very few treatises have been devoted to this branch of physical chemistry. We are therefore indebted to Harry Sobotka for having edited *Monomolecular Layers* following a symposium held in Philadelphia in December, 1951, under the auspices of the American Association for the Advancement of Science. The nine articles included here illustrate the problems with which American specialists on surface films are concerned.

H. J. Trurnit's discussion of modern techniques for study of surface layers is too brief, although he describes some ingenious apparatus that he built himself.

E. Mishuck and F. Eirich have an apparatus able to detect a surface pressure of 0.01 dyne/cm. They apply the perfect-gas law with protein films to measure their molecular weights. We appreciate this work, but the sensitivity of their apparatus falls somewhat short of a more desirable value.

The mechanical properties of surface films considered by A. P. Brady and M. G. Brown are: (1) static and dynamic surface tensions, (2) surface viscosity, (3) gas permeability. After an intensive study, the authors conclude that a pure detergent forms an adsorbed film of "gaseous" type on the surface of aqueous solutions; impurities considerably modify the mechanical properties of the film.

J. K. Dixon, C. M. Judson, and D. G. Salley use radioactive substances to study the adsorption of surface-active molecules at the water-air interface. This method is excellent and permits, in particular, a discussion of the validity of Gibbs' equation. The built-up monolayers of Langmuir-Blodgett can serve as a radioactive source of uniformly distributed activity and reproducible density if, like D. E. Beicher, one utilizes stearic acid monolayers containing C_{14} for this purpose.

E. G. Shafrin and W. A. Zisman study hydrophobic monolayers and consider their adsorption from aqueous solutions. E. Hutchinson gives a survey of the properties of films at the oil-water interface. The Editor and S. Rosenberg describe several chemical reactions occurring in surface films. Finally, E. Havinga similarly studies the mechanism of chemical reactions at the air-water interface using surface potentials measurements. A theory is advanced to explain the differences in activity between molecules on the surface as compared with molecules in the bulk of the solution.

On the whole, this book constitutes an interesting collection for all those who are interested in the physical chemistry of surfaces.

Henri L. Rosano, New York, New York

INTERACTION OF SERUM ALBUMIN WITH BUILT-UP MONOMOLECULAR LAYERS OF FATTY ACIDS[1, 2]

Irving H. Sher and Harry Sobotka

Department of Chemistry, The Mount Sinai Hospital, New York

Received December 13, 1954

ABSTRACT

The specific removal of built-up oligomolecular films of stearic acid and its lower homologs by dilute serum albumin solutions is described. The influence on this reaction of temperature, pH, concentration of albumin, and presence of buffer salts is discussed. The specificity of the underlying formation of water-soluble complexes in respect to both reactants is emphasized. The occurrence of skeletonization and penetration phenomena is noted.

INTRODUCTION

The investigation of reactions of monomolecular layers with substances in adjacent phases increases the knowledge of the two-dimensional state and contributes to the understanding of reaction mechanisms in general. As one of the reactants is in a fixed position, such reactions fall into the category of heterogeneous reactions; diffusion rates become important and molecular orientation plays a major role.

The "monomolecular" reactant may be spread on a liquid hypophase or it may be deposited on a solid body, while the bulk reactant may be in a liquid or a gaseous phase. Interesting studies of the adsorption of monolayers from a gas phase have been reported by Hayes and Dean (1). Some reactions of floating monolayers ("H-layers") with molecules in the hypophase have been reviewed by Havinga (2) and by Sobotka and Rosenberg (3). The former authors show amongst other phenomena the signal increase of the rate of lactonization due to the apparent thousandfold increase of acidity at the boundary; the latter authors discuss the effect of molecular shape and position on the oxidation of cholestenone, oleic acid, and aliphatic sulfur compounds.

When proteins are involved in "two-dimensional" reactions the investigation may at the same time shed light on problems of protein structure. Experiments by Rothen on reactions of protein-protein couples, mostly of immunochemical nature, have defied orthodox explanations. Trurnit (4)

---

[1] This work was carried out under U. S. Public Health Service Grant C-1791.

[2] We wish to thank Miss Pham Thi Thu for able assistance.

has studied the system chymotrypsin vs. serum albumin with the substrate built up by the Blodgett-Langmuir technique in mono- or oligomolecular layers. His interesting observations of the enzymatic reaction chymotrypsin-serum albumin are complicated by the competing adsorption of the enzyme onto the slide and by the fact that the diffusion of the reaction products influences the kinetics of the reaction.

We have selected a system of relative simplicity, the reaction of serum albumin with built-up long-chain fatty acid films, which yields water-soluble complexes. This system does not involve spread protein molecules, which are an interesting laboratory artifact but whose properties and reactivities are not as closely related to those of the native proteins as is often tacitly assumed (5). The stripping of stearic acid films by serum albumin was observed by Trurnit (4, footnote 13). We have studied the conditions of this reaction and shall describe and discuss in the following section the effect of the thickness of the fatty acid layers and of the albumin concentration, the kinetics of the reaction and the total amount of turnover, the effect of temperature, of the hydrogen ion concentration, and of the concentration, ionic strength, and chemical nature of various buffer salts, and finally the specificity of the reaction in reference to both reactants. The implications of our results for the subfractions of serum albumin and, in turn, the significance of these subfractions for crystallizability and coagulation temperature of albumin, and finally, the changes of these properties in disease will be reported separately.

Methods and Materials

Glass microscope slides, 25 by 75 mm., were used which had been chromium coated on one side by vacuum deposition. The glass cell in which the reactions were carried out was 30 mm. square and 60 mm. high.

Stirrers were made by flattening a length of glass tubing of outside diameter 9.5 mm., inside diameter, 8 mm. The resulting ribbon was twisted to give a spiral with one revolution per 12 mm.; the direction of the twist was such that the solution was thrown downward. The heating element consisted of a spiral of Nichrome wire around a core of small-bore glass tubing. This was inserted in a glass tube of slightly larger bore, which had been sealed off flat at the bottom. One lead came out between the two tubes and the other through the center of the core. This unit required 10 to 20 additional ohms in series with a Variac rheostat for good temperature control.

When assembled, the heating unit was placed at the far left-hand corner of the cell as viewed from above. The stirrer was placed dead center and rotated clockwise, and the slide was set flush against the near cell wall as far as possible to the right. The uniformity of this arrangement is essential for the reproducibility of the results.

The chromium glass slides were rubbed down with ferric stearate, leaving a monolayer adhering to the slide. A monomolecular layer of the lipid under study was then formed by spreading its benzene solution on a buffered hypophase, containing 1 ml. 0.1 *M* barium acetate and 2.5 ml. 0.1 *M* phosphate, of pH 7.2, per liter of distilled water. The phosphate solution was prepared in the usual manner from Na_2HPO_4 and KH_2PO_4. The final solution was then 10^{-4} *M* for barium acetate and 2.5×10^{-4} *M* for phosphate; the pH was 7.45.

The temperature of the hypophase was 23°–27°C. unless otherwise stated. The appropriate pressure, usually 29.5 dynes/cm., was applied to the film by means of a barrier-pulley-weight apparatus (6). Two of the slides, held back to back, were dipped by hand into the film at a steady rate of about 3 seconds per dip and 3 seconds per withdrawal. For most of the work the slides were dipped 20 times to a depth of 15 mm. to form a base step of 41 layers. They were then dipped to successively lower depth so as to make 10 steps differing one from another by one dip or two layers. The apparent thickness of the slide was then determined from an empirical curve, using a simple tilt-table interferometer with a sodium vapor lamp as the monochromatic source (7).

The reaction cell was prepared by introducing 30 ml. minus the volume of the reactant into the cell and bringing it to the desired temperature while stirring. The slide was then placed in the solution (with the back flush against the wall of the cell where it was held by capillary action). The solution of the reactant, such as albumin in distilled water, was introduced immediately from a pipet and the stop watch started. Constant temperature within ±0.2°C. was maintained by adjustment of the Variac during the time of the run. The stirrer and stop watch were started and stopped simultaneously and the slide removed from the cell and rinsed once very gently with a little distilled water.[3] The apparent thickness of the lipid deposit was measured once again in the interferometer, and the amount of material lost or gained by the treatment was calculated.

Unless otherwise noted, the conditions for the reaction were standardized as follows: an area of 25 × 25 mm. was covered with a 40-layer (20 dips) base of stearic acid-barium stearate as obtained on a hypophase of pH = 7.45. Upon this were added a number of steps of two layers each. The volume of the solution in the cell was 30 ml.; it was 0.0167 *M* for phosphate buffer of pH = 7.2 and 0.0133 *M* for Na_2SO_4 and contained 0.0167% crystalline bovine serum albumin.

It was shown that stirring is necessary for the removal of stearic acid. Figure 1 illustrates the effect of the rate of stirring on an 0.0167% solu-

---

[3] It had been shown that no protein was deposited as the slide was withdrawn through the surface; for there was no difference in comparison with controls in which the cell contents were flushed out with distilled water prior to withdrawal.

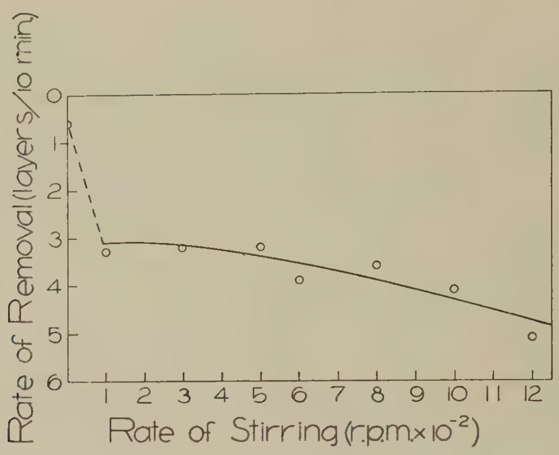

FIG. 1. Effect of stirring on removal of stearic acid.

tion of bovine serum albumin. The removal rate was constant between 100 and 500 r.p.m.; at about 1000 r.p.m. the solution started to foam, and we ascribe the increase in removal rate at the higher stirring rates to secondary effects. The rate of stirring in all the following experiments was uniformly 500 r.p.m.

The standard conditions, described above, were modified in an appropriate manner to study the effect of thickness and area of the slides, and of the albumin and buffer concentration. In the experiments on specificity, the lipid and the protein components were modified as indicated. The albumin used was in most instances crystalline bovine serum albumin.[4] In the experiment on individual albumin fractions we used horse serum which was fractionated with ammonium sulfate according to the procedure of Michel (8). The first albumin fraction was separated into a crystalline and a noncrystalline portion. The subsequent two fractions were both crystalline, and the fourth fraction was amorphous at the time of this study but crystallized upon prolonged standing in the cold. All fractions were dialyzed against water before use. Polylysine was obtained from Prof. K. G. Stern, Polytechnic Institute of Brooklyn, to whom we wish to express our thanks. For the isoarachidic acid we are indebted to Dr. Weitkamp of the Standard Oil Company of Indiana.

The dye-binding equilibria were measured by the technique of Klotz using methyl orange (9). The lipid content of the protein fractions was estimated by the method of Swahn (10).

---

[4] We are indebted to Dr. Lachat of Armour and Company, Chicago, for various samples of this material.

EXPERIMENTAL RESULTS AND DISCUSSION

Thickness of Slide

We have compared the influence of the number of stearic acid layers upon the rate of the "ripping-off" reaction. In order to keep within the most critical range for the interferometric observation with light of wavelength 590 mμ, plates were prepared which gave purple interference colors of the first, second, and third order. Table I shows the rate of removal in numbers of layers over a 20-minute period at 36°C. There appears to be a slight decrease of the effect on thicker slides, which may be due to greater cohesion of thicker films.

Area of Slide

Film areas of 350, 663, and 965 mm.^{2} of stearic acid, 45 layers thick, were exposed under identical conditions to 5 mg. of albumin in 30 ml. of phosphate solution for 10 minutes. As expected, the rate of removal was the same for the three slides, namely, 3.4, 3.7, and 3.5 layers. The rate of removal is within wide limits a function of the concentration of the protein and not of the proportion of total albumin in solution to stearic acid exposed.

Kinetics

The initial rate of removal follows a linear course. Figure 2 shows that the reaction in the case of bovine serum albumin remains linear for the first 20%–40% of its course. This percentage is computed on the basis of the saturation equilibrium.

Saturation

The amount of stearic acid which may form a water-soluble complex with albumin must be in a given ratio to the protein. This saturation level is a figure of importance for various experiments in the present investigation. Its value for different albumin fractions and preparations

TABLE I

Thickness of Film and Rate of Removal

Number of layers of stearic acid	Number of layers removed in 20 min. (corrected for blank)
43	7.2
45	7.6
45	6.8
137	6.1
137	6.3
145	6.4
245	5.6

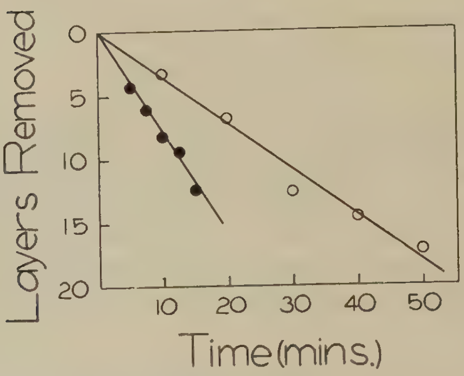

FIG. 2. Rate of stearic acid removal. Saturation of albumin with stearic acid in these experiments would be reached after removal of *ca.* 50 layers.

will not necessarily run parallel to the reaction rate. Although the latter is easier to determine, we have endeavored also to establish the molecular ratio stearic acid/albumin at the point of saturation.

A quantitative consideration shows that the number of stearic acid molecules in 1 cm.^{2} (100 mm.^{2}) of a monomolecular layer is *ca.* 4.5×10^{14} molecules or 7.5×10^{-10} moles. An equal number of albumin molecules of molecular weight 69,000 will be contained in 0.052 mg. of albumin. Under our experimental conditions, the upper limit of film area with which we may operate is about $25 \times 25 = 625$ mm.^{2}. On the other hand, the rate of the reaction and the accuracy of the determination require a protein concentration not much below 0.01 % and a reaction volume of 30 ml. In the examples given in Fig. 3 we used 2.0 and 1.96 mg. of various batches of bovine serum albumin, *i.e.*, concentrations of 0.0067 % and 0.0065 %. The exposed areas were 350 and 625 mm.^{2}, respectively. Thus, the amount of albumin, if combining with stearic acid on a mole per mole ratio, would take up approximately 10 and 6 complete layers of stearic acid, respectively.

For reasons detailed below in the section on skeletonization and also because we wished to remain within an interferometrically sensitive zone of thickness, we used more than one slide for each experiment. Each successive point on the curves in Fig. 3 indicates the use of a new slide; the maximum number of layers removed from a single slide never exceeded eight. Thus, we are assured that the removal is measured under optimal conditions. The ordinate gives the molecular ratio of stearic acid removed/albumin. The curves flatten out at a molar ratio of 2/1 and approach equilibrium rates of 2.3/1 and 2.7/1. It will be noted that the higher end value is found with an albumin preparation of slower reactivity. To evaluate the significance of these data, it is necessary to know the original lipid content of the albumin preparation (see below).

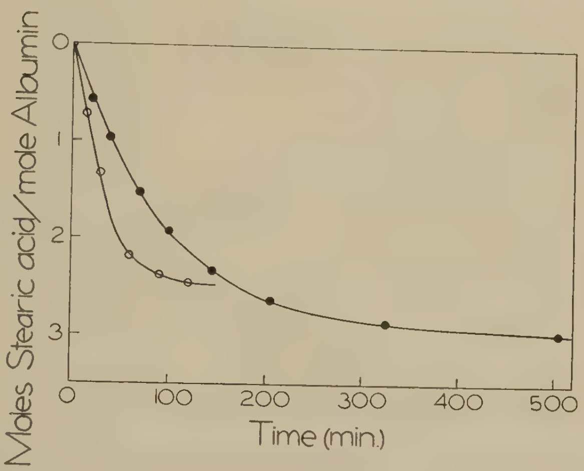

FIG. 3. Kinetics of stearic acid removal.

Albumin Concentration

The rate of removal of stearic acid is in linear proportion to the albumin concentration up to 0.03% or *ca.* 4 × 10^{-6} *M* albumin. Above this value the rate rises less steeply and flattens out towards a maximum which is presumably governed by the rates of diffusion of the albumin towards the slide and of the reaction product in the opposite direction (Fig. 4).

Temperature

The reaction rate increases with temperature over the range investigated. The upper limit of the observations is reached at a temperature where the film changes in appearance by gradual obliteration of the in-

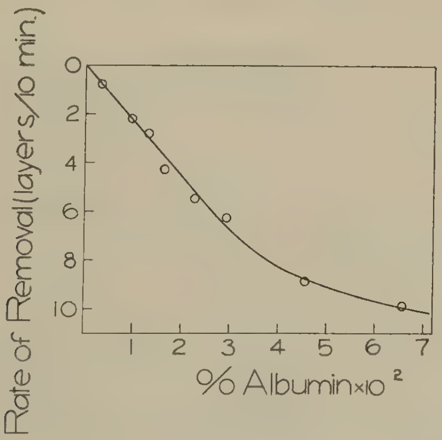

FIG. 4. Influence of serum albumin concentration on stearic acid removal.

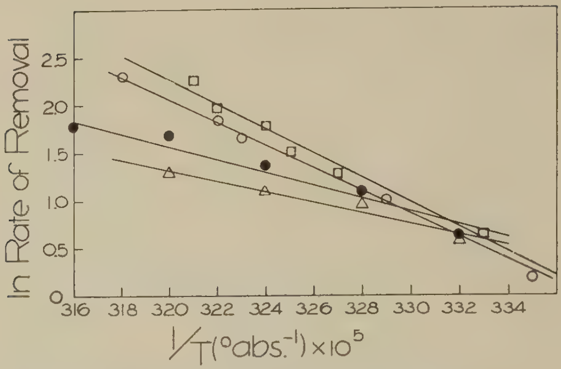

FIG. 5. Effect of temperature on removal rate.

dividual steps on the plate. At this point, which may correspond for the two-dimensional built-up state to the melting point in the three-dimensional state, the ripping-off reaction loses its specificity, and even buffer solution without albumin will now remove stearic acid. This upper temperature limit (*cf.* Table III) varies from one fatty acid to another. Its distance on the temperature scale from the melting point of the substance in bulk varies considerably, not only between saturated and unsaturated acids, but even within the length of the chain. The nature of the underlying surface may also influence the cohesion of monomolecular layers (11).

The effect of temperature on reaction rate in the case of stearic acid is illustrated in Fig. 5, which shows the natural logarithm of the rate as ordinate plotted against the reciprocal of the temperature in degrees Kelvin. The points from individual experiments fall on straight lines. The gradient of these lines appears to be a function of the protein concentration within the range of our observations.

Effect of Buffers

The rate of stearic acid removal depends on the presence of buffer salts. The effect of albumin in distilled water is rather low; it is considerably enhanced by neutral salts such as potassium chloride or sodium sulfate, but the highest rates are observed with phosphate solutions. This effect of phosphate ion upon the mobility of molecules in a two-dimensional array parallels the effect of phosphate on protein penetration through organic layers observed by Trurnit (12). The phosphate effect on the removal of stearic acid reaches its maximum at a phosphate molarity of 0.005 and continues on a constant level at least to 0.05 molarity. The effect of other buffers, as shown in Table II, decreases in the order phosphate, citrate, and ethylene diamine tetraacetate, veronal, and maleate. The relationship between this effect and the molarity and ionic strength of

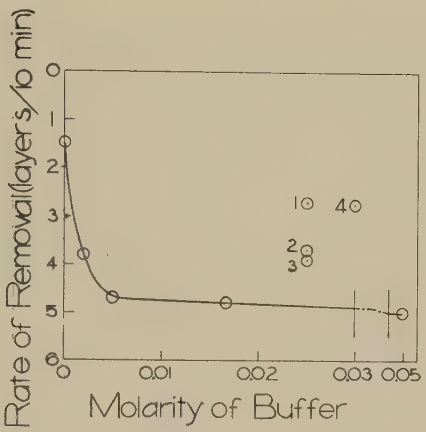

FIG. 6. Effect of nature and concentration of buffers on removal rate.

the buffers remains to be investigated. The pH dependency of the reaction is illustrated in Fig. 7. Phosphate buffers were used in a range of concentration which does not influence the reaction rate (see above). There is no removal of stearic acid below pH 6. The effect shows a sharp rise to pH 6.6 at 36°C., where it reaches a maximum value; this value is maintained constant up to pH 8. The effect is not influenced by changes in ionic strength. At 36°C. and at 40°C. the curves run a similar course. At the lower temperature, the curve is smoothed out; at 40°C. it shows a higher maximum further over to pH 6.9 and slight decrease towards higher pH values. The limb to the acid side of the maximum reflects the increasing ionization of the reactive cationic groups of the albumin; the value of the flat branch on the alkaline side appears again to be limited by diffusion rates. This limiting factor is higher at higher temperatures.

Removal Rate of Various Fatty Acids

Films of various fatty acids were deposited on slides at 25°C. and usually under a lateral pressure of 29.5 dynes/cm. on the standard hypophase. The reacting solution contained 0.0167% albumin in 0.025 *M*

TABLE II

Rate of Removal of Stearate Film by Serum Albumin in the Presence of Various Buffers at pH = 7.2 and 35°C.

Number curve	Buffer	Molarity	Ionic strength × 10^2	Number of layers removed in 10 min.
	Phosphate	0.0167	4.1	4.8
1	Maleate	0.025	7.3	2.7
2	Versene	0.025	14.3	3.7
3	Citrate	0.025	14.9	3.9
4	Veronal	0.033	0.49	2.75

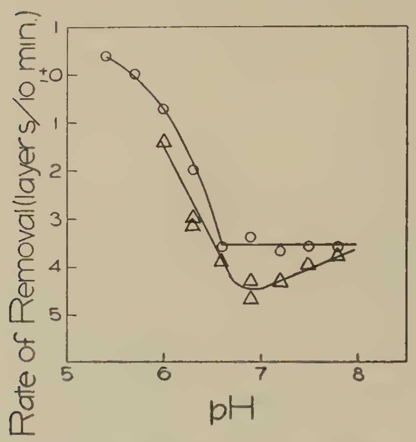

FIG. 7. Effect of pH on removal rate.

phosphate buffer of pH 7.2. The slides were run for 10 minutes at the temperature given. Table III summarizes the results, showing the apparent number of layers removed (minus) or gained (plus). The temperature where the appearance of the slides has changed so as to preclude readings is indicated by an asterisk. The last column to the right gives the melting points of the pure compounds. The results show that the effect is specific for palmitic and stearic acid, whereas the higher members of the saturated series are not attacked by albumin solutions. The effect of albumin on the transethylenic elaidic acid with 18 carbon atoms and on isoarachidic acid with a carbon chain of 19 atoms and a branched group on the penultimate carbon is questionable. Cholesterol is not removed at

TABLE III

The Number of Apparent Layers Removed (−) or Gained (+) by Albumin Acting on Slides of Various Lipids at the Temperatures Shown

* = Lipid melts and blurs.

Lipid	26°	32°	35°	40°	45°	50°	55°	Melting point of bulk phase
Palmitic acid	−5.6	−7.4	*					64.0
Stearic acid	−1.5	−2.6	−3.0	−3.6	*			69.4
Arachidic acid			0	−0.3		−1.0	−0.4	76.3
Behenic acid			+0.1		−0.1	0		80.7
Lignoceric acid						+0.5		81.0
Elaidic acid	−1.1		*					51.5
Brassidic acid			+0.3	+0.6		*		61.5
Isoarachidic acid			−1.2	−0.9				75.0
Cholesterol			0					148.5

all. The difference between palmitic and stearic acid, on the one hand, and the higher normal acids, on the other hand, is striking; it cannot be explained by the few degrees difference in their melting points.

Reactions with Proteins Other than Albumin

That the reaction is specific for serum albumin was shown in experiments with serum globulin (0.0167%), ovalbumin (0.0334%), and pepsin (0.0334%), all of which did not change the thickness of stearic acid under conditions where serum albumin (0.0167%) removed 3.7 layers within 10 minutes; a 1.67×10^{-3} M solution of arginine had no clear-cut effect under the same conditions, whereas polylysine (0.008%) became adsorbed on the stearic acid plate and increased its apparent thickness by the equivalent of 4.0 layers.

Influence of Other Substances

A number of other substances were tried, none of which acted on stearic acid layers by itself. When used in conjunction with albumin, the ripping-off capacity of the latter remained unchanged in the presence of iodoacetate and acetyltryptophan, nor could we observe any effect of heparin and of chondroitin sulfuric acid within the limits of the method. But the albumin effect is substantially reduced by the presence of azorubin and of the sodium salts of lower fatty acids. It would appear that the former group of compounds, when they react with albumin, select other sites on

TABLE IV

The Reaction of Various Chemicals with Stearate Slides and Their Action in Conjunction with Albumin

Reaction time 20 minutes (except for experiments marked with *, which were run for 10 min.).

Reactant	Concentration	Change in Thickness in 10 min. (a)	Layers removed (−) in presence of albumin (b)	Difference (b) − (a)	Layers removed (−) in albumin control
Sodium caproate	$8.33 \times 10^{-4}M$	+0.5	−5.6	−6.1	−7.4
Sodium caprylate	$8.33 \times 10^{-4}M$	+0.4	−3.4	−3.8	−7.4
Sodium caprate	$8.33 \times 10^{-4}M$	+0.3	−0.2	−0.5	−7.4
Iodoacetate	$1.67 \times 10^{-3}M$	+0.5	−7.4	−7.9	−7.4
Acetyltryptophan	$1.67 \times 10^{-3}M$	+1.3	−6.4	−7.7	−7.4
*Chondroitin sulfuric acid	0.0167%	+0.9	−2.4	−3.3	−3.7
*Heparin	0.0167%	+0.9	−0.8	−1.7	−2.0
Azorubin	$1.67 \times 10^{-5}M$	+0.3	−4.1	−4.4	−7.4
Azorubin	$6.70 \times 10^{-5}M$	+0.3	−2.2	−2.5	−7.4
Azorubin	$11.7 \times 10^{-5}M$	+0.7	−2.0	−2.7	−7.4

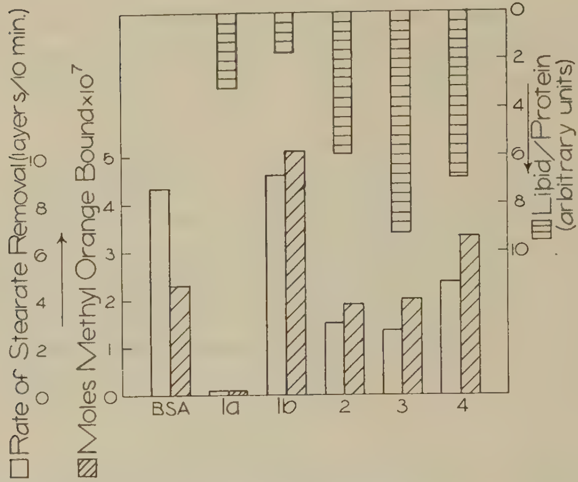

FIG. 8. Comparison of removal rate of stearic acid and adsorption of methyl orange on various fractions of horse serum albumin.

the surface of the albumin molecule; on the other hand, fatty acid anions and anionic dyes compete with stearic acid for the same sites.

When serum albumin was saturated with powdered stearic acid by nonturbulent agitation with an excess for 3 hours at 28°C., the centrifuged supernatant took up 1.5 layers within 10 minutes of stearic acid under standard conditions against 4.4 layers for the untreated albumin.

The rate of stearate removal for individual albumin fractions runs parallel to their adsorptive power for dyestuffs. Figure 8 illustrates this relationship for the various fractions of horse serum albumin. The height of the diagonally hatched columns gives the amount of methyl orange adsorbed, whereas the unhatched columns show the rate of the ripping-off reaction. The horizontally hatched columns above illustrate the lipid content of the original albumin fractions as obtained by Swahn's colorimetric method. Similar results showing the parallelism of affinity for azorubin and stearic acid were obtained with human serum albumin.

Skeletonization and Penetration

The ripping-off reaction does not remove the film monolayer by monolayer, but skeletonizes the stearic acid-barium stearate film by selective removal of the stearic acid molecules. This phenomenon parallels skeletonization of films by organic solvents such as benzene, which likewise preferentially remove the free stearic acid. The fact that the albumin treatment results in skeletonized films may be proved by refilling the holes on the film. In contrast to films skeletonized by organic solvents, refilling with hexadecane is not possible because of the oleophobic nature of the

TABLE V

Removal of Stearic Acid Monolayers by Albumin through a Blanket of Cholesterol Monolayers in 10 Min. at 36°C.

Number of stearic acid layers	Number of cholesterol layers	Total decrease (corrected for blank)
0	50	0
50	0	−3.3
40	6	−5.2
34	10	−3.9
30	14	−4.7
28	20	Slides Smear

surface, owing to adsorption of small amounts of albumin. However, we had found previously that skeleton films may be refilled with water. In the present case the surface is wettable and the water fills the holes left by removal of stearic acid. Restitution of the original interference color is not quite complete because of the lower refractive index of water.

The cohesion of mono- and oligo-molecular films is diminished in comparison to the same substance in bulk. The two-dimensional m.p. has been found lowered for stearic acid (13), and we ascribe the disorganization of crystalline films, described in the section on "Removal Rate of Various Fatty Acids," at least in part to this lowering of the melting point. One should also point in this connection to the observation of Havinga and De Wael (14), who found by X-ray diffraction that stearic acid films have a hexagonal structure at room temperatures, while the hexagonal form of the stearic acid in bulk is stable only a few degrees below its "three-dimensional" melting point. This diminution of cohesion alters the penetrability of a substance to such an extent that the film of a few layers thickness can not be treated as semipermeable membrane. One has not to assume specific holes and faults in a monolayer to explain its penetrability, but must consider this as an intrinsic property of the two-dimensional state.

We have been able to illustrate this situation by covering stearic acid films with up to 20 layers of cholesterol, keeping the sum of the two kinds of layers between 44 and 50 to facilitate optical observation. When these films were subject to albumin solutions under standard conditions, the ripping-off reaction proceeded right across a blanket of 6–14 monolayers of cholesterol with unabated speed. Moreover, the refilling of the skeletonized film with water is likewise apparently not impeded by the cholesterol blanket.

REFERENCES

1. HAYES, K. E., AND DEAN, R. B., *J. Am. Chem. Soc.* **73,** 5584 (1951).
2. HAVINGA, E., *in* "Monomolecular Layers," p. 192. A publication of the American Association for the Advancement of Science, 1954.

3. Sobotka, H., and Rosenberg, S., *in* "Monomolecular Layers," p. 175. A publication of the American Association for the Advancement of Science, 1954.
4. Trurnit, H. J., *Arch. Biochem. and Biophys.* **47,** 251 (1953); *ibid.* **51,** 176 (1954).
5. Kaplan, J. G., Andrews, D. H., and Fraser, M. J., *J. Colloid Sci.* **9,** 203 (1954).
6. Sher, I. H., and Chanley, J. D., *Rev. Sci. Instr.*, in press, 1955.
7. Sobotka, H., *in* "Medical Physics" (Otto Glaser, ed.), Vol. 2, p. 550. Yearbook Publ., Chicago, 1950.
8. Michel, A., *Sitzungsberichte der Wuerzburger physik. med. Ges.* **29,** 117 (1895).
9. Klotz, J. M., Burkhard, R. K., and Urquhart, J. M., *J. Am. Chem. Soc.* **74,** 202 (1952).
10. Swahn, B., *Scand. J. Clin. & Lab. Invest.* **5,** Suppl. 9, 7 (1953).
11. Karagounis, G., *Helv. Chim. Acta* **37,** 805 (1954).
12. Trurnit, H. J., *Science* **111,** 1 (1950).
13. Beischer, D. E., *in* "Monomolecular Layers," p. 107. A publication of the American Association for the Advancement of Science, 1954; *Science* **115,** 682 (1952).
14. Havinga, E., and de Wael, J., *Chem. Weekblad* **34** (No. 43) (1937).

MICELLE FORMATION BY SULFONATES IN A NONPOLAR SOLVENT

Samuel Kaufman and Curtis R. Singleterry

Naval Research Laboratory, Washington 25, D. C.

Received November 5, 1954; revised January 4, 1955

ABSTRACT

The micellar properties of oil-soluble sulfonates in benzene have been studied by the fluorescence depolarization method. In moist benzene, the dinonylnaphthalene sulfonates of barium and sodium aggregate to form micelles of 7 to 8 and 12 to 13 monomers, respectively; the size of these micelles is not sensitive to water concentration. The critical range for micelle formation of these sulfonates is estimated at 1×10^{-6} to 1×10^{-7} formula weight per liter. A barium petroleum sulfonate was found to aggregate in micelles of 34 to 35 monomers. The difference between the sizes of micelles of the two types of sulfonates is explained in terms of the geometries of the respective monomers. The formation of Rhodamine B-sulfonate complexes has been observed, requiring a slight revision of previously developed methods for treatment of the data. The micellar nature of these substances in nonpolar solvents supports a previously published explanation of their effectiveness in reducing the corrosion potentials of acids in lubricating oils.

INTRODUCTION

High molecular weight petroleum sulfonates have been used for many years to impart rust-inhibiting and detergent properties to lubricants (1). A variety of sulfonates have been used, but few data are available concerning the micellar nature of these substances in nonpolar environments.

Mattoon and Mathews (2) investigated pure sodium bis(2-ethylhexyl) sulfosuccinate (Aerosol OT) in *n*-dodecane. They interpreted their data to indicate spherical micelles whose radii may be at least doubled by saturation with water, and they found micelles to persist down to a weight concentration of 5%. Subsequently, Mathews and Hirschhorn (3) studied the same system over a wide range of concentrations viscometrically and by means of the ultracentrifuge. In dispersions of moderate moisture content, they interpreted their data to support the previously suggested spherical micelle whose size increased with increasing water content, but for the anhydrous system they proposed a platelike micelle. For both moist and anhydrous conditions, however, their viscometric data (extrapolated to infinite dilution) are in striking agreement with the Einstein equation for flow of suspended spheres. A series of naphtha sulfonates in a number of hydrocarbon solvents was investigated viscometrically by van der Waarden (4) who concluded that these sulfonates formed platelike micelles.

Studies of oil-soluble carboxylate soaps in nonpolar media have established the micelle size and critical concentration region (5, 6, 7), and the dependence of micelle shape and size (8, 9) upon water content. Observations of moist and of anhydrous systems of sodium dinonylnaphthalene sulfonate in benzene revealed no viscosity difference that would denote a change from linear to spherical units such as that found with the sodium phenylstearate system (9, 10).

The increasing use of sulfonates as lubricant additives, detergents, and dispersing agents for both general and naval applications has stimulated this laboratory to study their properties in detail. As salts of strong bases and a relatively strong acid they are insensitive to hydrolysis, and their superior performance as rust inhibitors has been established. Baker, Singleterry, and Solomon (11) have studied the action of synthetic sulfonates of known and reproducible compositions which had been found comparable in rust inhibition with commercially available petroleum sulfonates. They have proposed mechanisms based on the micellar nature of these substances to explain their rust-inhibiting and acid-deactivating properties. The fluorescence depolarization study reported here was undertaken as a parallel phase of the same problem; it demonstrates and explores the micellar nature which is the basis for solubility and certain other useful properties of these additives, which are dispersible in an unusually wide variety of solvents.

Experimental Methods

A. *Materials*

Dinonylnaphthalene sulfonic acid (HDNNS), especially synthesized for research use, was received as a 45% solution in petroleum naphtha. The neutral equivalent weight of the acid was 463 (theory, 460.7). The supplier stated that the substance was a mixture of isomers resulting from the sulfonation of a dinonylnaphthalene, prepared by alkylation of naphthalene with a propylene trimer. The alkylated hydrocarbon was fractionally distilled to isolate the dinonyl fraction. The acid was tested for the presence of mono- or tri-alkyl species by partitioning a sample in approximately equal portions between petroleum ether and a suitable isopropanol-water blend. The equivalent weights of the two fractions were found to be identical.

Barium dinonylnaphthalene sulfonate ($Ba(DNNS)_2$) was prepared by neutralizing a solution of the acid in a benzene-isopropanol-water (200/50/1) mixture with an excess of solid barium hydroxide, and subsequently back titrating to the bromthymol blue end point, found externally. The solvents were removed by distillation at reduced pressure; the residual alcohol, water, and naphtha were swept from the residue by additions of benzene during the distillation. The residue was taken up in benzene, filtered through a fine glass frit, divided into ampoules, frozen, and dried in the frozen state at reduced pressure (*ca.* 0.2 mm. Hg). Final traces of moisture and solvent were removed at 95°C. and a pressure of 5 μ Hg. The ampoules were sealed and refrigerated until used. The dry material was a porous, brittle, white solid containing 13.04% barium (theory 13.00).

Neutral sodium dinonylnaphthalene sulfonate (NaDNNS) was received from the manufacturer as a 20% solution in benzene. It was prepared for use by drying from the frozen solution as described for $Ba(DNNS)_2$, after dilution with benzene. The dry compound was similar in appearance to the $Ba(DNNS)_2$, but faintly darker. It contained 4.57% sodium (theory 4.76), but tests indicated the absence of free acid. The discrepancy in the analysis is attributed to inert unsulfonated hydrocarbons.

Barium petroleum sulfonate was prepared as follows: Sodium petroleum sulfonate in di(2-ethylhexyl) sebacate was twice treated with an excess of 30% aqueous $BaCl_2$ at 100°C., and was washed with water at 100°C. until the washings yielded a negative test for chloride. The diester solution of the barium sulfonate was diluted with benzene, and the sulfonate was twice precipitated with acetone, in which it is insoluble. The precipitate was dissolved in benzene, filtered, divided into ampoules, frozen, and dried as described for the $Ba(DNNS)_2$. The dry solid, which contained 13.2% barium, was similar in appearance to the synthetic sulfonates described above, except for its buff color. The analysis indicates an average molecular weight of 1040.6, corresponding to an acid of molecular weight 452.6.

Benzene was percolated through activated silica gel over a fine glass frit to remove polar impurities and water. It was stored over sodium until used.

Rhodamine B was purified chromatographically. Benzene-extracted Rhodamine B hydrochloride was converted to the base, dissolved in benzene, and transferred to a column of activated alumina. The dye was eluted with 1/1 acetone-benzene solution, which separated the Rhodamine B and its impurities into discrete bands, of which Rhodamine B was the foremost. The elutriate was acidified with HCl, dried first with a stream of dry nitrogen, and finally *in vacuo* ($10\ \mu$ Hg) at 80°C. A saturated solution of this dye in benzene was centrifuged before use. Its concentration (3.45×10^{-5} moles/liter) was determined spectrophotometrically in aqueous solution prepared from an evaporated aliquot of the benzene solution. Qualitative paper chromatograms indicated that the treated dye was of appreciably higher purity than the starting material.

B. *Measurements*

Fluorescence measurements were made with a modified Brice-Speiser light-scattering photometer (12). The general experimental procedures used have been described (6, 7). Spectral absorption measurements were made with a Beckman DU spectrophotometer, modified to accommodate the same 30 × 30 mm. cell used for the fluorescence measurements. This modification eliminated the uncertainties attending the examination of two separate specimens intended to be identical in properties and composition. The cell compartment of the spectrophotometer was fitted with reflectors, so that the beam made four passes through either the reference or test cell. The long path length was especially advantageous for measuring the weak absorption of the dye in the more dilute sulfonate solutions.

The absorption peak of the dye in these systems was subject to a drift of wave length due to an interaction with the glass of containing vessels. To minimize this interference, the solutions were prepared in volumetric flasks internally coated with Teflon, which is more inert than glass (13). In such flasks the sulfonate-dye solutions were found to be stable for 2 days or longer. The more concentrated solutions developed their equilibrium optical properties rapidly, and measurements were made within 4 hours of their preparation. The solutions containing 10^{-5} mole or less of sulfonate approached equilibrium over a period of several hours; measurements on such solutions were made after about 24 hours.

Apparent densities of the sulfonates were computed from the specific gravities of benzene and benzene solutions of the sulfonates. Measurements were made with an analytical balance and a plummet. The density of Rhodamine B crystals was estimated by observing their buoyancy in liquids of various densities. For the limited considerations requiring this datum, the assumption was made that the apparent density in solution was equal to the density of the crystals.

RESULTS

Benzene dispersions of $Ba(DNNS)_2$ examined ranged in concentration from 2×10^{-3} to 5×10^{-7} formula weight (F.W.) per liter, and those of NaDNNS from 1×10^{-3} to 2×10^{-6} F.W. per liter. Water-solute ratios (F.W. H_2O/F.W. solute) of 1.0 and 3.0 were maintained for $Ba(DNNS)_2$ and NaDNNS, respectively. Enough additional water was added to saturate the free benzene to the extent of 15%. Under these conditions the compositions were considered insensitive to fluctuations in atmospheric humidity. The Rhodamine B dye concentration was held constant (1.72×10^{-7} mole per liter) for the barium salt compositions, but because of the lower level of color development in the dispersions of NaDNNS, more dye was used, and the amount was increased with decreasing concentration of the sulfonate. Only one dispersion of the barium petroleum sulfonate (1.14×10^{-3} F.W. per liter) was examined. The water-solute ratio in this case was 1.0, and enough additional water was present to saturate the free benzene to the extent of 10%. Dry dispersions of $Ba(DNNS)_2$ and of NaDNNS were studied for comparison purposes.

Results of the measurements appear in Table I. Values of V were computed from F. Perrin's equation (6, 14) for the depolarization of fluorescence as a function of rotational diffusion,

$$V = \frac{p(3 - p_0)\tau RT}{3(p_0 - p)\eta}, \qquad [1]$$

where V is the hydrodynamic gram-molecular (or -micellar) volume of the mobile unit from which the fluorescence is emitted, p is the polarization of its fluorescence, p_0 is the polarization of completely immobilized dye molecules, τ is the excited lifetime, R is the gas constant, T is the absolute temperature, and η is the viscosity of the solution.

Values of τ for computations of V were obtained from the relation (6, 15),

$$\frac{\tau}{q} = \frac{\tau'}{q'}, \qquad [2]$$

where q is the ratio of fluorescence intensity ($I_{z\,\mathrm{av}}$) in arbitrary units to the extinction coefficient ($1/l \log_{10} 1/T$) at 546 mμ. From a plot of τ'/q' *vs.* peak absorption wave length for Rhodamine B solutions in methanol and glycerol, τ'/q' was interpolated at the wave length of maximum absorption of each specimen.

TABLE I

Micelle Size of Sulfonates in Benzene by Fluorescence Depolarization Method

Sulfonate concentration, *F.W./l.*	Fluorescence polarization (p)	Fluorescence intensity ($I_{z\,\mathrm{av}}$) arbitrary units	546 mμ Extinction coefficient $\left(\frac{1}{l}\log_{10}\frac{1}{T}\right)$	Total dye concentration, μ mole/l.	Apparent gram-micellar volume (V), *cc.*
Sodium Dinonylnaphthalene Sulfonate Apparent density at 25°C. = 1.100; F.W. = 482.7; 3.0 moles H_2O/F.W. NaDNNS. Benzene 15% saturated with H_2O.					
2.16×10^{-6}	0.074	0.0249	0.00370	1.	1420
5.39×10^{-6}	0.085	0.0394	0.00495	0.7	2020
1.08×10^{-5}	0.084	0.0608	0.00642	0.7	2350
1.08×10^{-4}	0.124	0.0230	0.00188	0.7	4420
3.56×10^{-4}	0.129	0.0827	0.00633	0.7	5500
7.22×10^{-4}	0.140	0.0537	0.00425	0.3	5540
1.08×10^{-3}	0.137	0.0872	0.00704	0.3	5500
Barium Dinonylnaphthalene Sulfonate Apparent density at 25°C. = 1.217; F.W. = 1046.7; 1.0 mole H_2O/F.W. $Ba(DNNS)_2$. Benzene 15% saturated with H_2O.					
5.00×10^{-7}	0.082	0.0196	0.00216	0.172	2080
1.00×10^{-6}	0.091	0.0310	0.00292	0.172	2770
5.00×10^{-6}	0.122	0.0367	0.00329	0.172	4240
1.00×10^{-5}	0.127	0.0540	0.00444	0.172	4770
1.00×10^{-4}	0.138	0.1561	0.01147	0.172	6220
1.00×10^{-3}	0.138	0.2109	0.01472	0.172	6620
2.01×10^{-3}	0.142	0.2116	0.01555	0.172	6560
1.00×10^{-3} [a]	0.136	0.2371	0.01617	0.172	6680
Barium Petroleum Sulfonate Apparent density at 25°C. = 1.192; F.W. = 1040.6; 1.0 mole H_2O/F.W. sulfonate. Benzene 10% saturated with H_2O.					
1.14×10^{-3}	0.3521	0.1114	0.01094	0.34	30300

[a] Anhydrous system.

DISCUSSION

The micelle sizes of NaDNNS (aggregation number 12 to 13) and $Ba(DNNS)_2$ (aggregation number 7 to 8) at concentrations in the plateau region of Fig. 1 indicate aggregations of the fewest monomers reported for metallic salts except the laurates (of Fe, Mg, Cu and Zn) and the zinc carboxylates in boiling toluene studied by Nelson and Pink (16). The contrasting size of the barium petroleum sulfonate micelle (aggregation number 34 to 35) is attributed to the difference between the geometries of monomers of the two types of sulfonates studied here. The gram-micellar volumes found for $Ba(DNNS)_2$ and NaDNNS at concentrations above 5×10^{-4} F.W. per liter are 6600 and 5500 c.c., respectively. This close comparability of micelle sizes indicates that the acid residue has a strong influence upon the extent to which these aggregates can grow, whereas the perceptible difference between their sizes suggests a secondary influence of the metallic radical. The larger gram-micellar volume (30,000 c.c.) and corresponding aggregation number for the barium petroleum sulfonate are indicative of molecules whose geometry permits the accommodation of more hydrocarbon tails about the compact polar core of the micelle. This accommodation will occur if the hydrocarbon section immediately adjacent to the sulfonate group is less bulky than the naphthalene nucleus, even though the two sulfonates have comparable equivalent weights. The fact that the petroleum sulfonate represents a variety of molecular structures may also contribute to the packing of more monomers into a single aggregate.

Micelles as small as those reported here must be approximately isodimensional because of the molecular arrangement required to shield the cores from mutual interaction to form larger aggregates. This conclusion is confirmed by the results of a viscometric study of NaDNNS in benzene (10), which indicated a limiting value of 2.5 ± 0.2 for η_{sp}/ϕ, in conformity with the Einstein equation for suspended spheres. The volumes calculated from the depolarization measurements correspond to spherical micelles having radii of 13.8 A. and 13.0 A. for $Ba(DNNS)_2$ and NaDNNS, respectively. Since the average length of the fully extended DNNS radicals is estimated from the Fischer-Hirschfelder model to be about 17 A., it would appear that the two nonyl substituents occupy average positions in which they are appreciably folded or bent toward the micelle. This would be expected if the hydrocarbon portions of the molecule can accommodate themselves to occupy the available space nearest the micelle, for which they are more probable competitors than the freely diffusing solvent molecules. A molecule whose structure places the major hydrocarbon bulk farther away from the polar core could occupy a smaller solid angle in the micelle, resulting in a larger aggregation number and effective radius. The sphere radius calculated for the barium petroleum sulfonate micelle is 22.4 A., which is a reasonable value, although the possibility that the micelle is in this case an ellipsoid of low eccentricity is not excluded (17).

In the dilute range of the dinonylnaphthalene sulfonate systems, the fluorescence polarization (Table I) decreases with decreasing stoichiometric concentration. A superficial consideration of this fact would suggest that the true micelle volume (which is directly proportional to the true aggregation number) follows the same trend. This inference could be derived from Perrin's equation (6, 14).

A similar trend of polarization with soap concentration has been observed with Acridine Orange as the tagging dye for calcium xenylstearate micelles (7). However, when micelles of this soap were tagged with Rhodamine B the polarization remained constant throughout the entire concentration range, indicating a constant micelle size. It was found that the discrepancy was due to a distinct difference between the properties of the two dyes. Rhodamine B is slightly soluble and colorless in benzene; when solubilized in the micelle it is spectrally absorbing and brilliantly fluorescent. Although likewise only slightly soluble in benzene, Acridine Orange was both spectrally absorbing and fluorescent in the absence of micelles, where the polarization of its fluorescence was 0.01. However, when solubilized in the micelle, the polarization was 0.29. In view of the constant micelle size indicated by Rhodamine B, it was evident that the trend of polarization with concentration was a composite effect resulting from the simultaneous fluorescence of Acridine Orange in two distinct micro environments.

In the present study the trend is similar, but the details of its interpretation are necessarily different. Since Rhodamine B is neither spectrally absorbing nor fluorescent in pure benzene, the low values of polarization are not attributed to free molecules of the dissolved dye. However, if some agent smaller than a micelle could interact with a dye molecule to convert it to a chromatically active state, the consequent polarization of its fluorescence would be less than that expected from the dye solubilized in a micelle. It is proposed that the activating agent is the sulfonate monomer.

Figure 1 is a plot of *apparent* aggregation number *vs.* stoichiometric concentration for the dinonylnaphthalene sulfonate systems. This apparent aggregation number is computed from V (Eq. [1]), the formula weight, and the apparent density of the sulfonate. In the concentration range studied, the apparent aggregation number reaches a plateau, which is taken to represent true aggregation number or micelle size at all stoichiometric concentrations studied. Since the apparent aggregation number is derived from a composite polarization value, it approaches the true aggregation number when the micelle-borne dye molecules far outnumber those in the monomer-dye complex.

Figure 1*a* is an enlarged plot of the dilute region of Fig. 1. Here an attempt is made to extrapolate the apparent aggregation number to infinite dilution. Although there is too much curvature to permit exact extrapolation, it is a reasonable estimate that the value is between 1.5 and 2 in

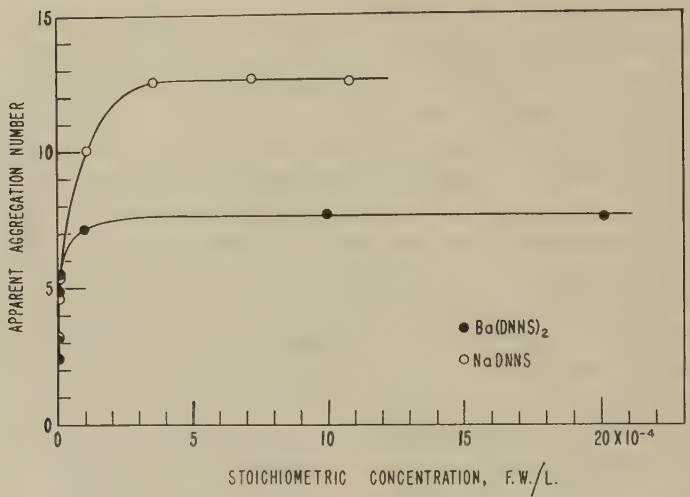

FIG. 1. Influence of concentration on apparent aggregation numbers of dinonylnaphthalene sulfonates.

both cases. The plots of Figs. 1 and 1*a* are consistent with the view that micelles and their independent monomers coexist (18, 19), and that a 1/1 dye-sulfonate monomer complex is the nonmicellar fluorescent unit in both systems.

At infinite dilution micelles should be expected to vanish. Then the anticipated values of apparent aggregation numbers for 1/1 complexes of Rhodamine B (F.W., 479; $d^{25^\circ\mathrm{C.}}$, 1.2) and sulfonate should be approximately 1.5 for $Ba(DNNS)_2$ (F.W., 1057; $d^{25^\circ\mathrm{C.}}$, 1.217), and 1.7 for NaDNNS (F.W., 483; $d^{25^\circ\mathrm{C.}}$, 1.100), when the aggregation number is computed on the basis of the formula weights and apparent densities of the respective sulfonates alone. These values fall in the range of the extrapolation described above. There is independent support in the literature for the existence of dye-detergent complexes; Mukerjee and Mysels (20) isolated a pinacyanol-sodium lauryl sulfonate species, insoluble in water, but soluble in nonpolar solvents, and Subrahmanya *et al.* (21) interpreted their colorimetric data to indicate the formation of complexes of crystal violet with Igepon T and Aerosol OT in aqueous systems.

In the light of evidence for two states of dispersion for Rhodamine B in these systems, a further analysis of the $Ba(DNNS)_2$ system was made, based on the equation (7),

$$R\frac{Q_m}{Q_s} = R\frac{q_m}{q_s} = \frac{p_c - p_s}{p_m - p_c} \times \frac{3 - p_m}{3 - p_s}, \qquad [3]$$

where R is the ratio of dye in micelles to that in monomer-dye complexes, Q is the quantum fluorescence efficiency, p is the fluorescence polariza-

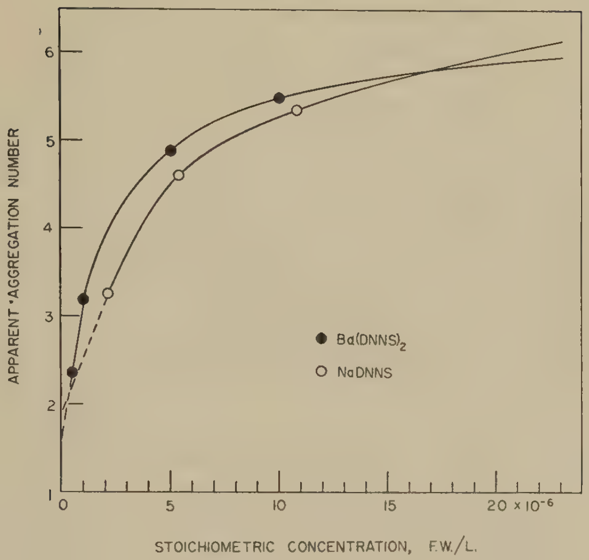

FIG. 1*a*. Extrapolation of apparent aggregation numbers to infinite dilution of dinonylnaphthalene sulfonates.

tion, and the subscripts *c*, *m*, and *s* refer to the composite, the micellar, and the monomer-dye complex emissions of Rhodamine B, respectively. Figure 2 is a plot derived from the data of the $Ba(DNNS)_2$ system. The extrapolation (7) to $R = 0$ estimates the location of the critical range for micelle formation, which is taken in this case to be 4×10^{-7} F.W. per liter. This value should be understood to indicate primarily an order of magnitude, since it is based on several unavoidable approximations and assumptions.

The computation of R requires the assignment of appropriate numerical values for the quantities in Eq. [3]. Of these, p_c is directly measured (Table I), and p_m and q_m are taken as equal to the average of the measured polarizations and efficiencies for the two most concentrated $Ba(DNNS)_2$ dispersions, in which micellar dye preponderates. This leaves p_s and q_s to be established. Estimates of these quantities by extrapolation of p_c and q_c to infinite dilution are unsatisfactory, and possibly theoretically unjustified. A more appropriate solution involves the relation between the observed excited life, τ_c, and the actual excited lives, τ_s and τ_m, when the dye exists in two states of dispersion in the same system:

$$\tau_c = \frac{R}{1+R}\,\tau_m + \frac{1}{1+R}\,\tau_s. \qquad [4]$$

The simultaneous solution of Eqs. [1], [2], [3], and [4] established the values of p_s and q_s used to compute R. For this treatment, Eqs. [1] and [2] were used to describe the relation of p_s, q_s, and τ_s for the dye-monomer complex ($\tau = \tau_s$, $q = q_s$, and $p = p_s$), whose hydrodynamic volume, V, was computed from the formula weights and apparent densities of the dye and $Ba(DNNS)_2$; Eqs. [3] and [4] were

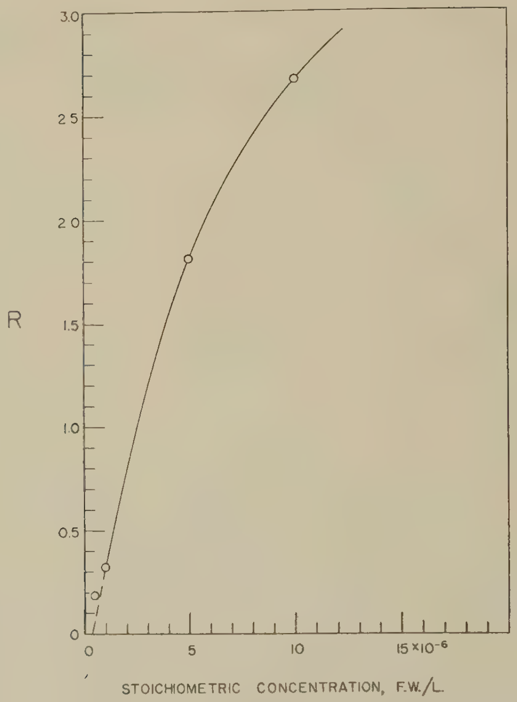

FIG. 2. Extrapolation to the critical concentration for micelle formation of barium dinonylnaphthalene sulfonate.

applied to the data from the most dilute $Ba(DNNS)_2$ dispersion (5×10^{-7} F.W. per liter). The use of data from the most dilute solution is preferred because the results are then less sensitive to uncertainties in p_m.

In the case of Acridine Orange the ratio, R, of dye in micelles to dye in true solution was in theory nearly a linear function of the micelle concentration, but in the present instance R is the ratio of micelle-borne dye to dye in the sulfonate monomer-dye complex, and because of the more complex equilibria involved it may not be as nearly proportional to the micelle concentration. However, R and the micelle concentration approach zero simultaneously. Hence, a short extrapolation of R should furnish an estimate of the location of the critical range which is less exact than that obtained in the simpler Acridine Orange case only to the extent that the curvature of the plot reduces the reliability of the extrapolation.

No weight is given to the lowest point in the extrapolation. Although it is significant in indicating the continuity of the data, this point should be expected to lie to the left of the extrapolation locus because it is so near the critical range.

The concavity of the plot toward the horizontal axis may be an indirect result of the unusually small micelles involved. For such small micelles the monomer concentration required to satisfy the equilibrium between micelles and monomer is an increasing function above the critical range, rather than the nearly constant function described for systems of larger micelles (17). Thus the monomer concentration increases several fold as the stoichiometric concentration rises from 10^{-6} to 10^{-3}. At high stoichiometric concentrations the increasing monomer concentration thus enhances the probability of (*1*) the monomer rather than the dye entering the micelle and (*2*) the formation of the monomer-dye complex. Both effects will reduce the value of R at high sulfonate concentrations.

The data for the NaDNNS system suggest an order of magnitude for the critical range similar to that found for $Ba(DNNS)_2$. However, the same treatment of data for the NaDNNS system is unwarranted because of the lower consistency of these data. Rhodamine B, in the presence of NaDNNS, was extraordinarily sensitive to color shifts arising from disturbances of the acid-base equilibrium by contact with the glass of the reagent vessels and optical cells. $Ba(DNNS)_2$ systems were more stable in this respect than those of NaDNNS. Such difficulties were not encountered with the carboxylates previously studied, perhaps because the latter should be expected to buffer the system, whereas these sulfonates could not be expected to do so.

The micelle size for the anhydrous $Ba(DNNS)_2$ system was not markedly different from that found for the moist system, as is indicated by the data in Table I. Exploratory measurements with a dry dispersion of NaDNNS also indicated that micelle size was not sensitive to water content.

SUMMARY

Sodium and barium dinonylnaphthalene sulfonates form unusually small spherical micelles (aggregation numbers 12 to 13 and 7 to 8, respectively) in benzene, and the moisture content of these systems does not seriously affect the micelle size. The critical range for micelle formation by these substances lies between 1×10^{-7} and 1×10^{-6} formula weight per liter. The barium petroleum sulfonate studied formed micelles (aggregation number 34 to 35) of several times the size observed for the dinonylnaphthalene sulfonates. The difference in size is explained in terms of the geometries of the respective monomers.

Observations reported here are consistent with the theory that micelles and free monomer coexist.

The demonstration of the micellar nature of barium and sodium sulfonates in benzene dispersions supports the solubilization mechanism proposed earlier to explain the reduced corrosion potential of acids in lubricating oils containing a neutral sulfonate additive.

A new phenomenon affecting the fluorescence depolarization method has been observed, namely, the formation of complexes between Rhodamine B and certain amphipathic molecules. With a slight revision of previously developed theory, the data from systems containing these complexes now can be interpreted.

Some refinements in the experimental techniques of studying micelles and some sources of error not previously encountered or recognized have been discussed.

ACKNOWLEDGMENTS

The authors wish to acknowledge the courtesy of John G. Honig in supplying unpublished viscosity data, and the cooperation of King Organic Chemicals, Inc., of Norwalk, Connecticut, in making available supplies of dinonylnaphthalene sulfonic acid and its sodium salt.

REFERENCES

1. PRITZKER, G. G., *Natl. Petroleum News* **37,** R-793 (1945).
2. MATTOON, R. W., AND MATHEWS, M. B., *J. Chem. Phys.* **17,** 496 (1949).
3. MATHEWS, M. B., AND HIRSCHHORN, E., *J. Colloid Sci.* **8,** 86 (1953).
4. VAN DER WAARDEN, M., *J. Colloid Sci.* **5,** 448 (1950).
5. ARKIN, L., AND SINGLETERRY, C. R., *J. Am. Chem. Soc.* **70,** 3965 (1948).
6. SINGLETERRY, C. R., AND WEINBERGER, L. A., *J. Am. Chem. Soc.* **73,** 4574 (1951).
7. KAUFMAN, S., AND SINGLETERRY, C. R., *J. Colloid Sci.* **7,** 453 (1952).
8. ARKIN, L., AND SINGLETERRY, C. R., *J. Colloid Sci.* **4,** 537 (1949).
9. HONIG, J. G., AND SINGLETERRY, C. R., *J. Phys. Chem.* **58,** 201 (1954).
10. HONIG, J. G., AND SINGLETERRY, C. R., unpublished data.
11. BAKER, H. R., SINGLETERRY, C. R., AND SOLOMON, E. M., *Ind. Eng. Chem.* **46,** 1035 (1954).
12. BRICE, B. A., HALWER, M., AND SPEISER, R., *J. Opt. Soc. Amer.* **40,** 768 (1950).
13. KAUFMAN, S., unpublished work in progress.
14. PERRIN, F., *J. phys. radium* [VI] **7,** 390 (1926).
15. PRINGSHEIM, P., "Fluorescence and Phosphorescence," p. 317. Interscience Publishers, Inc., New York, 1949.
16. NELSON, S. M., AND PINK, R. C., *J. Chem. Soc.*, p. 1744 (1952); *Nature* **169,** 620 (1952).
17. SINGLETERRY, C. R., paper presented before meeting of American Oil Chemists' Society, Minneapolis, Minn., October 11–13, 1954.
18. JONES, E. R., AND BURY, C. R., *Phil. Mag.* **4,** 841 (1927).
19. ALEXANDER, A. E., AND JOHNSON, P., "Colloid Science," Vol. 2, p. 672. Oxford, New York, 1949.
20. MUKERJEE, P., AND MYSELS, K. J., paper presented at the 126th meeting of the American Chemical Society, New York, September 17, 1954.
21. SUBRAHMANYA, R. S., RAO, M. R. A., AND DOSS, K. S. G., *Proc. Indian Acad. Sci.* **34A,** 324 (1951).

THE BAR VISCOMETER

D. Tollenaar and M. C. Bisschop

Research Institute T.N.O. for Printing and Allied Industries, Amsterdam

Received November 5, 1954

Rotational Viscometers

One of the principal conditions to be met in the determination of a plasticity diagram is that a homogeneous field of stress must exist in the material to be measured. So long as one has to deal with a Newtonian liquid, this condition is of no importance; however, as soon as there is no longer a proportionality between the shearing stress τ and the rate of shear D, a D–τ diagram can be determined unequivocally only in a homogeneous field.

Such a field is obtained in rotational viscometers, at least if the clearing between bob and cup is small with respect to the diameter of the bob. Though the simple types of MacMichael and Stormer viscometers meet this demand, they usually do not allow of measurements at high shearing stresses. If it is desired to use shearing stresses as high as 10^6 dynes/cm.^{2}, it is in most cases necessary to employ very expensive instruments. This, however, involves another drawback, namely, the difficulty of obtaining effective temperature control. For the heat developed at these high shearing stresses, also in the case of oils of only some tens of poises, leads to a perceptible increase of temperature, sometimes even as high as 5°C. (1). Henry Green (2) and Green and Weltmann (3) regarded the resulting decrease in viscosity as a deviation from Newtonian behavior, and they based their thixotropy theory on the appearance of a hysteresis loop in the plasticity diagram.

These views were afterwards partly retracted by Weltmann (4), as it became clear that it was the temperature increase due to internal friction which might be responsible for hysteresis loops.

The occurrence of such marked temperature rises is associated with the fact that the heat developed in a homogeneous field of stress is the same throughout the liquid bulk, in contrast to the heat developed in the capillary viscometers, where the shearing stress, and therefore also the heat development, is greatest along the wall, as no heat is developed in the axis of the capillary. In this type wall cooling is therefore more effective than in the case where the shearing stresses are distributed homogeneously.

The Band Viscometer

In 1940 Wacholtz and Asbeck (5) constructed a band viscometer in which a homogeneous field of stress is created in a slit through which a band is drawn. This apparatus permits shearing stresses up to 10^5 dynes/cm.^{2}. The slit walls can be cooled to the desired temperature, just as the outer cylinder can be cooled in the rotational viscometer. The band passes through the liquid in the middle of the slit without particular constructions being necessary. Every other position of the band during operation leads to correction stresses, which force the band to the center. The band, therefore, adjusts itself.

The band viscometer has one drawback of a practical nature: it is difficult to make not only an 80-cm. band of constant thickness but also, for that matter, an even metal slit. If it is desired to obtain high shearing stresses at not too short falling times, it is necessary to keep the distance between band surface and slit wall small. In this case the band thickness and slit width must have very small tolerances (6).

The Bar Viscometer

The bar viscometer is already an old instrument. In 1903 Segel (7) gave a description of a cylinder which coaxially moves through a slightly wider hollow cylinder. Between the two surfaces there is the liquid the viscosity of which is to be measured. As with the rotational viscometer, a homogeneous field of stress is obtained by giving the clearing between the two cylinder surfaces a small width with respect to the cylinder radius. The shearing stress at the wall of the inner cylinder is:

$$\tau = \frac{P}{2r\, lR_1}$$

the rate of shear being:

$$D = \frac{v}{R_1 \ln \dfrac{R_2}{R_1}}$$

where P = load in dynes,
l = length of outer cylinder in cm., and
v = rate of fall in cm./sec.

If $R_2/R_1 = 1 + \Delta$, where Δ is a small figure, the rate of shear becomes:

$$D = v/R_1\Delta = v/(R_2 - R_1).$$

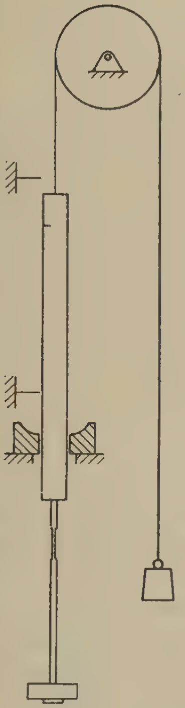

FIG. 1

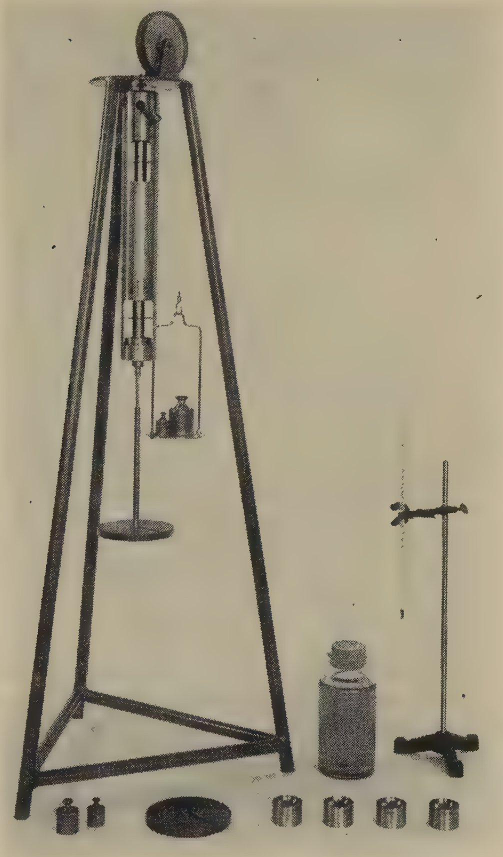

FIG. 2

FIG. 1. Bar and ring of the bar viscometer.
FIG. 2. Bar viscometer.

The bar viscometer is relatively simple in construction. An accurately machined and polished bar, with a length of 38.00 mm. and a diameter of 19.988 mm. is suspended in a holder, which itself is mounted to the stand by means of a spherical hinge. When the bar is released it can be balanced by means of a counter weight. The lower end of the bar projects through a ring with a height of 20.0 mm. and a diameter of 20.048 mm., fixed in the holder. The liquid to be measured is between the bar and the ring. The free end of the bar is now loaded, after which it falls through the ring. During the fall the weight of the bar is balanced by the counter weight and the internal friction of the liquid. The ring can be replaced by rings of slightly larger diameter, by means of which it is possible to control the

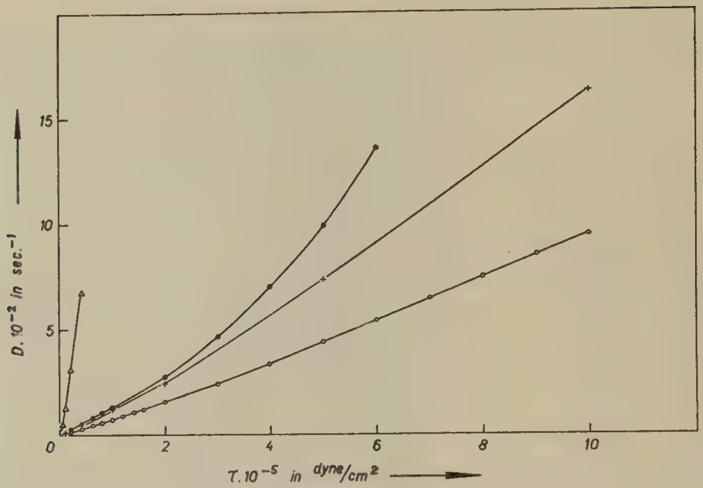

FIG. 3. D–τ diagrams measured with the bar viscometer.
○ mineral oil
× offset ink
● linseed oil varnish
△ news ink

rate of fall at constant load. By using a narrow ring and a high load a shearing stress of 10^6 dynes/cm.^{2} for highly viscous oils (*e.g.*, 1000 poises) can be reached.

The apparatus can be calibrated with oils of known viscosity. It has been found that using the O. B. oil of the National Bureau of Standards the calibration factors differ by only a few per cent from the values calculated.

In the measurement of reference oils straight lines were obtained in the D–τ diagrams up to a shearing stress of 10^6 dynes/cm.^{2}. Other mineral oils also showed purely Newtonian flow. The risk of high shearing stresses leading to a measurable rise of temperature is much less with the bar than with the rotational viscometer, since the temperature effects due to heat generation are suppressed largely by using a narrow slit. A complete discussion of the temperature differences and the heat transfer in a liquid layer sheared between coaxial cylindrical surfaces has been published by Weltmann and Kuhns (4). The heat capacity of the bar and the ring are large with respect to the heat of friction, while the heat conduction in the metal is more favorable than in the plastic material of the band viscometer. A drawback of the above construction is that no water bath can be fitted. As a result, the measurements have to take place in a room of constant temperature.

In general, this bar viscometer is not suitable for the measurement of shearing stresses lower than 10^4 dynes/cm.^{2}. Substances such as typographic inks and offset inks often show structure viscosity and sometimes hysteresis phenomena. These are most pronounced at shearing stresses much lower than 10^4 dynes/cm.^{2}. In this case the plasticity diagram must be supplemented with measurements by the rotational viscometer.

The drawbacks of the rotational viscometer are usually negligible at these low shearing stresses.

REFERENCES

1. MILL, C. C., AND GATES, E. R., *Anal. Chem.* **25,** 1390 (1953).
2. GREEN, H., *Anal. Chem.* **14,** 576 (1942).
3. GREEN, H., AND WELTMANN, R. N., *Anal. Chem.* **15,** 201 (1943).
4. WELTMANN, R. N., AND KUHNS, P. W., *J. Colloid Sci.* **7,** 218 (1952).
5. WACHOLTZ, F., AND ASBECK, W. K., *Kolloid-Z.* **93,** 280 (1940).
6. HULL, H. H., *J. Colloid Sci.* **7,** 316 (1952).
7. SEGEL, M., *Physik. Z.* **4,** 493 (1903).
8. POCHETTINO, A., *Nuovo Cimento* **8,** 77 (1914).
9. PUGH, B. H. L. D., *J. Sci. Instr.* **21,** 177 (1944).

MOLECULAR AREAS OF ADSORBATES

J. J. Kipling

The University, Hull, England

Received October 26, 1954

In the study of adsorption at solid surfaces, attention is increasingly paid to the orientation of the adsorbed molecules. The orientation is usually deduced by comparing the experimental value for the area occupied by the adsorbed molecule with the values expected for the several possible orientations. For this purpose, reference is often made to data obtained experimentally for insoluble condensed films on liquid surfaces, such as are recorded by Adam (1). The importance of these data is that they were obtained with a high degree of accuracy on a surface which can be taken as smooth even on the molecular scale. Such data, however, should not be used uncritically as criteria of orientation. An illustration from the recent literature may make this clear.

It has been assumed (2, 3) that aliphatic alcohols are adsorbed on carbon surfaces with a vertical orientation. In a recent paper, Kipling and Tester (4) estimated that ethyl alcohol occupied 17.9 A.^{2}/molecule when adsorbed on an active charcoal. This attracted the adverse comment (5) that the value is considerably smaller than that of 21.6 A.^{2}/molecule obtained by Adam (1) for films of long-chain alcohols on aqueous substrates. In the solid state, however, docosanol occupies an area (perpendicular to the axis of the hydrocarbon chain) of 18.5 A.^{2}/molecule (6), which is the same as is found in crystals of a long-chain hydrocarbon (7). This would be expected from a study of molecular models, as the oxygen atom is slightly smaller than the carbon atoms, and the —OH group therefore falls within the boundaries of the —CH_2 chain. At one time, it would have seemed natural to accept Adam's figure as the appropriate standard, as it is close to the value (20.5 A.^{2}/molecule) which was obtained for so many other long-chain molecules (fatty acids, esters, amides, methyl ketones, ureas) that it was regarded as a property of the hydrocarbon chain. More recently, however, it has been shown for fatty acids that the value of 20.5 A.^{2}/molecule (instead of the value of 18.4 expected from the X-ray results for the hydrocarbon chain) is obtained in close-packed films only because the carbonyl group projects beyond the boundaries of the hydrocarbon chain (8, 9). It seems likely that this explanation can similarly be applied to all other substances recorded by Adam (1) as having this molecular area, with the exception of amines on alkaline substrates.

In the latter case, the amines are presumably present to a substantial extent in the hydrated form (as -aminium hydroxides), and the incorporation of bound water in the surface film would account for an apparent molecular area greater than corresponds to that of the hydrocarbon chain. Such hydration by hydrogen-bonding would be expected to be more extensive with alcohols, which do, indeed, show a higher apparent molecular area than the amines.

If this explanation is valid, it is clearly not always appropriate to use data from work on such films as criteria for assessing the orientation on hydrophobic surfaces (such as charcoal) especially in the absence of aqueous media. When alcohols and amines are adsorbed on hydrophobic surfaces, the value of 18.4 A.^{2}/molecule seems to be the appropriate reference figure. This is subject to an important qualification. The values for long-chain compounds are for films designated as "solid." For short-chain compounds, more often the subject of investigation on solid surfaces, the films, even when close-packed, are usually regarded as "liquid" films. The latter would be expected to have a considerably higher coefficient of thermal expansion than the former, and there is some experimental evidence that this is the case. Comparisons with reference values should therefore be made with considerations of temperature in mind.

In the light of the above argument, the agreement between the experimental value of 17.9 and the expected value of 18.4 A.^{2}/molecule for ethyl alcohol adsorbed on charcoal is reasonable. There is, however, evidence (10) that the lower fatty acids are adsorbed on the same charcoal with the major axis parallel, and not perpendicular, to the solid surface. The orientation of ethyl alcohol on the charcoal may not, therefore, be regarded as firmly established. The major point, however, that the surface molecular areas derived from studies on aqueous substrates do not always provide valid criteria for judging orientations on solid surfaces, is of much wider significance.

REFERENCES

1. ADAM, N. K., "The Physics and Chemistry of Surfaces," 3rd ed., Table III. London, 1941.
2. HANSEN, R. S., FU, Y., AND BARTELL, F. E., *J. Phys. & Colloid Chem.* **53,** 769 (1949).
3. INNES, W. B., AND ROWLEY, H. H., *J. Phys. & Colloid Chem.* **51,** 1154 (1947).
4. KIPLING, J. J., AND TESTER, D. A., *J. Chem. Soc.* **1952,** 4123.
5. HANSEN, R. S., AND HANSEN, R. D., *J. Colloid Sci.* **9,** 1 (1954).
6. MARWICK, T. C., *Proc. Roy. Soc. (London)* **131A,** 621 (1931).
7. MÜLLER, A., *Proc. Roy. Soc. (London)* **120A,** 437 (1928).
8. VOLD, M. J., *J. Colloid Sci.* **7,** 196 (1952).
9. KIPLING, J. J., AND NORRIS, A. D., *J. Colloid Sci.* **8,** 547 (1953).
10. KIPLING, J. J., AND BLACKBURN, A., unpublished work.

THE ELECTRICAL DISPERSION OF LIQUIDS AS AEROSOLS[1]

Vadim G. Drozin

Department of Chemistry, Columbia University, New York

Received September 16, 1954

Abstract

The dispersibility of a series of liquids at high electric potentials was investigated experimentally and theoretically. Large electrostatic pressure plays a predominant part in the process of dispersion and is a function of dielectric constant and radius of curvature of the liquid in the capillary. Nonpolar organic liquids having small dielectric constants could not be dispersed. Prediction of the dispersibility of a liquid can be made from knowledge of the value of its dielectric constant.

Introduction

When one applies a high potential to certain liquids contained in a glass tube ending in a fine capillary, the liquid issues from the capillary in the form of threads and, under certain conditions, as a highly dispersed aerosol consisting of drops of relatively uniform size. This formation of water threads was discovered by George Mathias Bose in 1745 and ascribed later to the reduction of surface tension by an electric field. In 1914 John Zeleny (1) rediscovered this phenomenon and investigated it from the point of view of an electrical discharge from a liquid point. The experiments carried out by Burton and Wiegand (2) with electrified (up to 800 v.) streams of water drops showed that the electrified water thread split up into narrower jets while the large electrified drops split up into smaller ones. The effect was attributed to the repulsion between the similarly charged drops.

Macky (3) investigated the behavior of single water drops of radius 0.085–0.26 cm. in a strong electric field and found that elongated drops, at a definite field strength, became unstable and a filament became drawn out from the end of the drop. The critical field strength at which the drops became unstable is a function of the radius of the drop and of its surface tension. The drop size, therefore, decreased, so that there was a limit for the maximum-sized drops which could exist in a strong field. Recently, the electrical dispersion of liquids has again been investigated by Vonnegut and Neubauer (4). They suggest that this method be applied to the production of monodispersed liquid aerosols, since they observed Higher Order Tyndall Spectra. Our interest stems from this suggestion.

---

[1] This research was supported by Contract At(30-1)-1434 between the Atomic Energy Commission and Columbia University and was carried out in 1952–53.

No satisfactory quantitative explanation of this phenomenon has been suggested to date.

Experimental

By increasing the applied potential from zero to 12 kv. we have observed the stages of dispersion shown in Fig. 1.

When a low potential was applied, the rate of production of droplets increased (B), and the droplets then became elongated (C) until a steady thread (D) was formed (at about 6 kv.); this thread separated into several smaller threads at a few centimeters from the capillary tip, the point of division approaching the tip (E) with increasing voltage. On further raising of the voltage, a cloud of fine droplets appeared in addition to three or four individual threads (F). Finally, the last thread disappeared (G), leaving a cloud of very fine droplets, visible in a dark room by transmitted light. This cloud also exhibited faint Higher Order Tyndall Spectra (HOTS).

The potential at which the cloud first appears without threads depends on the capillary characteristics (radius, shape, wall thickness), on the field gradient, and on the liquid to be dispersed. No cloud of water could be produced at a voltage of 12 kv. by a capillary which formed droplets

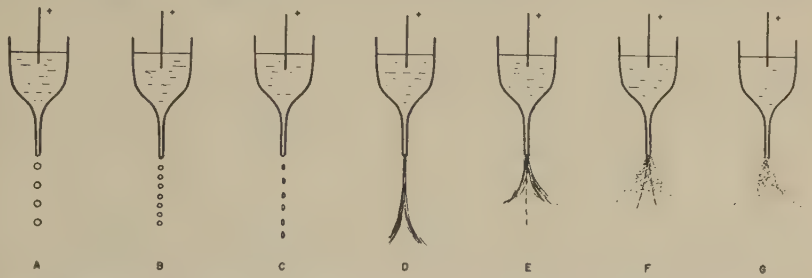

FIG. 1. Stages of dispersion observed by increasing the applied potential.

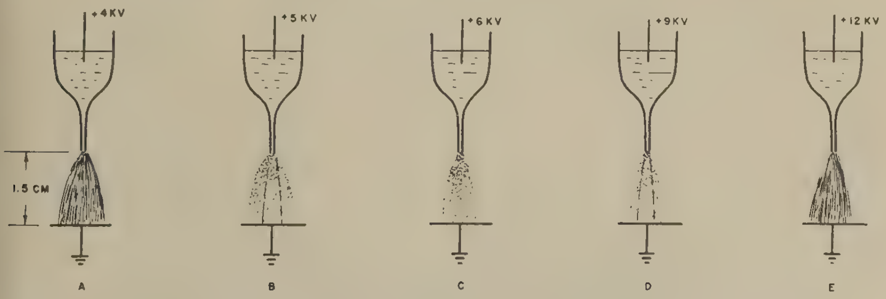

FIG. 2. Stages of dispersion observed when a grounded plate was placed 1.5 cm. from the capillary tip.

TABLE I

	σ	γ	$\epsilon_0 = n^2$	ϵ	$\eta \cdot 10^{18}$	$C.f(\epsilon)$	Dispersibility
1. Water	1×10^{-6}	73	1.76	81	1.84	257	Fine dispersibility obtained at high potentials
2. Glycerin	6×10^{-8}	65	2.17	56.2	2.66	110.5	
3. Methyl alcohol	2×10^{-7}	22	1.77	31.2	1.68	35.6	
4. Acetone	6×10^{-8}	24	1.85	21.5	2.80	16.75	
5. Ethyl nitrate	5×10^{-7}	—	1.92	19.7	2.91	13.4	
6. Acetic acid	1×10^{-7}	24	1.88	6.3	1.73	1.0	
7. Chloroform	2×10^{-8}	27	2.09	5.1	1.10	0.36	Fine threads of liquid appear after high potential is applied
8. Ether	4×10^{-13}	16	1.82	4.4	1.15	0.35	
9. Xylol	1×10^{-15}	27	2.27	2.4	0.36	0.11	It was not possible to disperse these liquids even at high potentials up to 30 kv.
10. Toluene	1×10^{-14}	27	2.25	2.34	0.37	0.11	
11. Benzene	1×10^{-18}	29	2.25	2.24	0.08	0.11	
12. Carbon tetrachloride	4×10^{-18}	26	2.13	2.25	0.00	0.09	
13. Microcrystalline wax (melted)	10^{-14}–10^{-18}	—	2.1	2–2.5	—	0.08–0.05	

Specific conductivity σ in cm.$^{-1} \times \Omega^{-1}$, surface tension γ in dynes/cm., square of refractive index $n^2 = \epsilon_0$, dielectric constant ϵ, dipole moment $\eta \times 10^{18}$ in dynes$^{1/2}$ cm.^{2}, coefficient $C.f(\epsilon)$ from Eq. [5] for the electrostatic pressure as a criterion for the dispersibility of a number of substances. (Most of the data for σ, γ, n, ϵ, and η are taken from I.C.T.)

larger than about 3 mm. in diameter at zero voltage. In the case of an asymmetrical capillary tip or the presence of some conductor in the vicinity of the capillary, disturbances of the threads or cloud were observed.

When the field gradient was altered by the presence of a ground at a distance of 1.5 cm. from a capillary tip of 0.05 cm. diameter, the previously described stages were observed at lower voltages than without an applied ground, as shown in Fig. 2. When the voltage was raised beyond that required to produce the cloud, the stages were reversed, *i.e.*, the smaller streams reappeared and the cloud disappeared entirely. Increasing the distance to the grounded plate from 1.5 to 4 cm. has the effect of increasing the voltage required to produce the cloud from 6 to 8 kv.

If the capillary is placed in an insulated glass flask and a voltage applied, drop or stream formation ceases after a few seconds, apparently owing to the setting up of space charges. If a grounded wire is introduced into the flask, the fine spray is accompanied by droplets, which creep up the outside capillary walls and then fly off at almost right angles towards the nearest walls of the flask at a distance of about 2 cm. Again, the fine spray disappears after a short time.

The dispersibility of some liquids and their physical constants are given in Table I. All liquids used for dispersion in this work were of C.P. grade. To find out the relative dispersibility of the liquids listed in Table I, the same capillary at constant distance (~10 cm.) from the ground was used. The diameter of the capillary was approximately 0.06 mm. Therefore, the curvature of the liquid surface in the capillary was very large and hydrostatic pressure was completely negligible (no drop formation on the tip of the capillary).

Calculation of Electrostatic Pressure

The following pressures exist on a drop at the tip of a capillary: (*1*) pressure due to surface tension (which is inversely proportional to the radius of the droplet), (*2*) hydrostatic pressure (which can be eliminated by using a very fine capillary), (*3*) excess vapor pressure on the curved surfaces (which can be neglected because of the relatively large radius of curvature of the liquid surface), and (*4*) electrostatic pressure on the surface of the liquid where the latter forms a boundary with air or another nonpolarizable medium.

The electrostatic pressure, p, exerted by a liquid on a nonpolarizable boundary is given by the equation (5):

$$p = \frac{1}{8\pi}(\epsilon - 1)[E^2 + (\epsilon - 1)E_n^2] - \frac{1}{8\pi}E^2\frac{d(\epsilon - 1)}{d\rho}\rho, \qquad [1]$$

where E and E_n are the field strength and its normal component, respectively, ϵ is the dielectric constant, and ρ is the density of the liquid.

The first term of this equation represents the force perpendicular to the surface of the insulator where the latter forms the boundary with vacuum ($\epsilon = 1$) or another nonpolarizable medium (like air [$\epsilon \cong 1$]). This force tries to pull the insulator into the nonpolarizable medium. In our case, the force is applied on the surface of a drop at the tip of the capillary, *i.e.*, in the surface formed by the surface tension forces and having appreciable curvature providing sufficient field strength for dispersion.

The second term represents the effect of electrostriction.

The following assumptions are made in the derivation:

1. The liquid is an insulator, *i.e.*, has a negligible electrolytic conductivity. It was found experimentally that the successful dispersion was possible if the specific conductivity of the liquid was less than $10^{-5}\Omega^{-1}\text{cm.}^{-1}$ (6).

2. The dielectric constant on the boundary between liquid (having dielectric constant ϵ) and air (with dielectric constant 1) changed continuously in the surface layer of the liquid. The thickness of this layer can be reasonably assumed to be equal to the dipole length.

If we assume that the drop formed at the tip of the capillary is an ideal hemisphere, we can neglect the tangential component E_τ of the field strength in the formula $E^2 = E_n^2 + E_\tau^2$ and substitute E_n for E in Eq. [1]:

$$p = \frac{1}{8\pi} E_n^2 \left[\epsilon(\epsilon - 1) - \frac{d(\epsilon - 1)}{d\rho} \rho \right] \qquad [2]$$

or, more generally,

$$p = Cf(\epsilon)E_n^2 \qquad [3]$$

Therefore, to calculate the electrostatic pressure, p, it is necessary to have an expression for the dielectric constant as a function of density. Such expressions given by Onsager (7) and by Henriquez (8) will be considered.

To make relative estimates of the electrostatic pressure possible, the field strength must be determined. As a first approximation, $E_n = U/r_c$, where U is the applied potential and r_c, the radius of the capillary. This assumption makes it possible to compare electrostatic pressures for different liquids under a given applied potential. The actual radius of curvature of the local fluctuation of the liquid surface (and therefore the field strength) is difficult to determine.

A capillary so fine that no liquid will issue from it without application of some potential was used.

1. *Onsager's Equation:* Onsager's (7) theory of polarization of dipolar liquids in a constant electric field gives the following equation, which is in good agreement with the experimental data in the case of liquids with a weak polarity.

$$\frac{(\epsilon - \epsilon_0)(2\epsilon + \epsilon_0)}{\epsilon} = c\rho, \qquad [4]$$

where $c = (4\pi\eta^2/9kT)(\epsilon_0 + 2)^2$, η is the dipole moment, and $\epsilon_0 = n^2$. From Eq. [4]

$$p = \frac{1}{8\pi}\frac{U^2}{r_c^2}\left[\epsilon(\epsilon - 1) - \frac{\epsilon^2(\epsilon - \epsilon_0)(2\epsilon + \epsilon_0)}{2\epsilon^2 + \epsilon_0^2}\right]. \qquad [5]$$

The calculations give the following values for $Cf(\epsilon)$ (Eq. [3]): for toluene 0.11 and for benzene 0.11.

2. *Henriquez' Equation* (8): The measured value of dipole moments for a number of substances with both strong and weak polarity and those calculated from the Henriquez' equation are in good agreement. This agreement justified the use of the Henriquez' equation for the calculation of the electrostatic pressure. The equation is:

$$\frac{(\epsilon - 1)(\epsilon + 4)}{8\epsilon + 7} = a\rho + b, \qquad [6]$$

where $a = (4\pi\eta^2/9kT)$ and $b = (\epsilon_0^2 - 1)(\epsilon_0^2 + 4)/8\epsilon_0^2 + 7$ (if ϵ is greater than 20, a term $(\epsilon - 1)^3 \times 1.7 \times 10^{-3}$ must be added to the denominator of Eq. [6]).

The factor $Cf(\epsilon)$ (see Eq. [3]) calculated from this equation is given in Table I for several substances.

Discussion

The distortion of the falling water droplets in a strong uniform electric field observed by Macky (3) may now be explained by applying the above considerations. At each end of the polarized droplet, a certain electrostatic pressure exists which is in equilibrium with the surface tension. But, when the field is sufficiently strong, the surface disrupts at some segment and causes a decrease in the radius of curvature in that area. This increases the electrostatic pressure ($p \sim 1/r^2$), causing a filament from the end of the droplet to be drawn out. The end part of the filament, being unstable, disintegrates into very fine droplets. It is interesting to point out that only the positively induced end of the droplet shows this behavior; the negatively induced end does not. In other experiments with liquids in capillaries, *fine* dispersion also occurred only if positive potential was applied (4). The explanation may be related to the fact that, as shown by English (9), there is a certain difference also between positive and negative corona, especially at larger curvature of the liquid surface.[2]

The same explanation as given above for Macky's experiments is applicable to the dispersion of liquids in capillaries; in this case, the field strength on the places where local fluctuations of the surface curvature occurred becomes high and, therefore, the threads of the liquid shoot out at a high velocity. Zeleny (1) has measured the velocity of a thread of about 4 μ in diameter to be about 8m./sec. This means that the threads are emitted at very high pressures. They are stable owing to inertia, surface tension, and the presence of a field of like charges around them. At the critical potential for the start of fine dispersion (monodisperse aerosol formation), the surface tension forces are overcome by electrical forces of mutual repulsion and the main thread splits up into many symmetrically distributed thin threads, which become unstable and immediately disintegrate into very fine charged droplets.

---

[2] The reason for the local fluctuation in the curvature of the liquid surface is as yet not known; maybe it is small irregularities on the liquid surface such as electrolyte products, dust, etc.

The following conclusions can be drawn from a comparison of the data (for specific conductivity, dipole moment, and refractive index) given in Table I with the results of our experiments:

1. Substances with specific conductivity lower than $10^{-13}\ \Omega^{-1}\text{cm.}^{-1}$ and higher than $10^{-5}\ \Omega^{-1}\text{cm.}^{-1}$ (6) (inorganic acids, salts) cannot be dispersed.

2. Substances with dipole moments smaller than $\sim 1 \times 10^{-18}$ dyne$^{1/2}$ cm.^{2} cannot be dispersed. Substances with larger dipole moments can be dispersed if their specific conductivity is not larger than $10^{-5}\ \Omega^{-1}\text{cm.}^{-1}$; otherwise the electrolytic conductivity cannot be neglected in the derivation of the electrostatic pressure.

3. If the coefficient $Cf(\epsilon)$ of Eq. [3] calculated for a given liquid from Henriquez' equation is $\geqq 1$, the liquid can be dispersed.

The experiments also gave (indirect) proof that the surface tension is, at least for nonpolar ($\eta \approx 0$) liquids, not influenced by the applied potential; substances with almost the same surface tension (such as toluene and acetone) behave completely differently with regard to dispersion.

ACKNOWLEDGMENTS

I am indebted to Professor Victor K. La Mer, Director of the Contract, for suggesting this problem, for his continued interest in its prosecution, and for assistance in the preparation of the manuscript.

Thanks are extended to Mr. Pui-Kum Lee for valuable assistance in performing some phases of the experimental work and for the drawings.

REFERENCES

1. Zeleny, J., *Phys. Rev.* **3,** 69 (1914); *ibid.* **10**(2), 1 (1917); *ibid.* **16**(2), 102 (1920); *Proc. Cambridge Phil. Soc.* **18,** 71 (1915).
2. Burton, E. F., and Wiegand, W. B., *Phil. Mag.*, 1912, published by the University of Toronto.
3. Macky, W. A., *Proc. Roy. Soc.* (*London*) **133,** 565–587 (1931).
4. Vonnegut, B., and Neubauer, R. L., *J. Colloid Sci.* **7,** 616 (1952).
5. Abraham, M., and Becker, R., "The Classical Theory of Electricity and Magnetism," p. 101. Blackie & Son, Ltd., London, 1946.
6. Neubauer, R. L., and Vonnegut, B., *J. Colloid Sci.* **8,** 851 (1953).
7. Onsager, L., *J. Am. Chem. Soc.* **58,** 1486 (1936).
8. Henriquez, P. C., *Rec. trav. chim.* **54,** 574 (1935).
9. English, W. N., *Phys. Rev.* **74,** 179 (1948).

A CONE-AND-PLATE VISCOMETER[1]

H. Markovitz, L. J. Elyash, F. J. Padden, Jr., and T. W. DeWitt

Mellon Institute, Pittsburgh, Pennsylvania

Received October 18, 1954

Abstract

A weight-driven cone-and-plate viscometer is described. It has a simpler construction and can be used over a wider range than some other instruments of this type. Liquids with viscosities from 1 to 50,000 poises have been investigated, and rates of shear from 0.0002 to 9000 sec.$^{-1}$ have been achieved with this instrument. With one filling of the viscometer, a 1000- to 30,000-fold range of rates of shear can usually be covered. With concentrated polymer solutions, it is practically always possible to determine the zero shear viscosity.

I. Introduction

A great variety of instruments and techniques have been used to study the steady-state flow properties of non-Newtonian liquids as a function of rate of shear. In recent years, the advantages of the conical surface in a rotation-type viscometer have been exploited by several workers (1–7). The instrument to be described here shares with some of these the advantages of a practically uniform rate of shear throughout all of the material, simple operation, easy filling and cleaning, direct calculation of results, and the requirement of a relatively small sample. It, however, is constructed more simply and can be used over a wider range of viscosities and rates of shear than many of them. Viscosities from 1 to 50,000 poises have been measured and rates of shear from 0.0002 to 9000 sec.$^{-1}$ have been achieved with this instrument. With one filling of the viscometer, a 1000- to 30,000-fold range of rates of shear can usually be investigated. In concentrated polymer solutions, it is practically always possible to determine, and to know that one has determined, the zero shear viscosity. In designing this instrument, simplicity of design, ease of operation, and range of usefulness were prime considerations. Since the main purpose was to cover a wide range of conditions, an accuracy of a few per cent was considered sufficiently good.

---

[1] The work discussed herein was performed as part of the research project sponsored by the Reconstruction Finance Corporation, Office of Synthetic Rubber, in connection with the Government Synthetic Rubber Program.

II. DESCRIPTION OF THE APPARATUS

A schematic diagram of the instrument is shown in Fig. 1. The liquid is sheared in the gap between the stationary truncated cone (1) and the rotating flat plate (4). A known torque is applied to the plate and the resulting angular velocity is measured.

The cone is accurately positioned when the conical surfaces of its integral shaft are held against the bearing surfaces of the spindle in the headstock (2) of a vertically mounted watchmaker's lathe (3). It is kept from rotating by inserting the pin (12) into one of the 60 holes of the indexing head (13). Almost flat cones with angles of approximately ½°, 2°, and 4° were machined. Each was then truncated at the plane 0.0015 inch from its vertex. This made it comparatively easy to position the plate with respect to the cone and eliminated the danger of having the two elements in contact through a small error in positioning. Theoretical and experimental justification for removing the tip of the cone to this extent will be given later. Cones of two different diameters, 4 and 9 cm., are available. Since the inherent error in using the larger cones is less, they are used in most cases. (See next section.) They have the additional advantage, at low shearing stresses, that the ratio of torque due to the viscosity of the liquid to that due to friction is larger, the larger the cone. The advantage of the smaller size cones is that higher rates of shear can be achieved with lower weights.

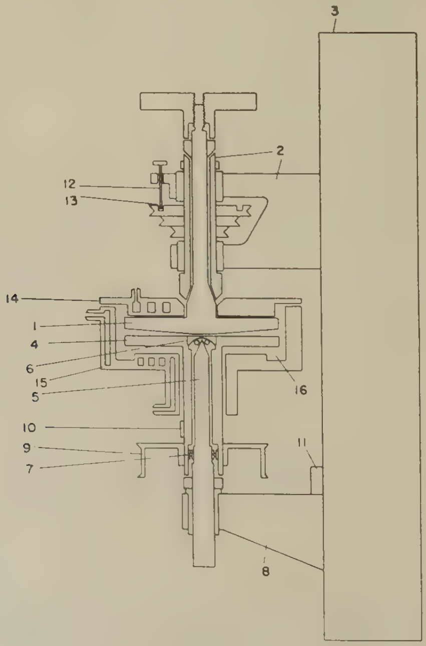

FIG. 1. Schematic diagram of cone-and-plate viscometer.

The flat plate and its integral hollow shaft can turn with very little friction on the pivot shaft (5) which is held in the tailstock (8) of the lathe. The plate assembly is supported and positioned by the miniature pivot (6) and radial (7) bearings. A known torque is applied to the plate by hanging a weight (0.05 g. to 1000 g. are used) on a string which, after being led over a pulley, is wrapped around the cylindrical drum (9). Viscosities have also been determined on this instrument by driving the cone with a motor and measuring the resulting torque on the plate with either a balance or strain gauge. The present method of operation, however, is preferable because it provides a wide range of speeds (from 10^{-6} to 10 r.p.s.) without the use of complicated and expensive constant-speed and torque-measuring devices. The motion of the plate is followed by reflecting the light of a galvanometer lamp from the mirror (10). For the slowest speeds, a traveling microscope is used to follow the reflection of the cross hairs of the galvanometer lamp. For the fastest speeds, a photoelectric setup is used. The light beam traverses a slit in front of a photoelectric tube and the resultant signals are amplified and recorded as pips on a Brush Development Company oscillograph. The speed of rotation is determined from the known chart speed and the distance between pips. For intermediate speeds, the light is allowed to fall on a ground glass scale and the time for 1, 0.03, 0.003, or 0.0006 revolutions is measured. The light from the mirror can always be made to fall on the scale by rotating the cone and plate as a unit and then fixing the headstock in an appropriate position through the use of the indexing head. This method is preferable to merely turning the plate because in this way the material in the gap is not sheared and one need not worry about letting the material relax again before resuming measurements.

In filling the viscometer, the material is placed on the plate, which is then raised and clamped in its correct position. Very viscous liquids are transferred from their jars with the use of a hypodermic syringe, cut off at the bottom of the barrel so that the plunger can go all the way through. This allows the viscometer to be filled quickly and without the inclusion of air bubbles. The plate is brought into position by moving the tailstock against a stop (11) fixed to the lathe bed. The stop is adjusted so that a 0.0013-inch gauge will slip through the gap between the flat surface of the truncated cone and the plate easily, while a 0.0016-inch gauge will not go through at all.

To control the temperature, water from a thermostated bath is circulated through the labyrinthine channels of a tripartite jacket. A disc-shaped part (14) rests on the top of the cone, and two symmetrical parts (15) enclose the plate, gap, and sides of the cone. The latter, supported by rods attached to the lathe mount, can be moved aside to gain admittance to the gap and to allow the plate to be moved up and down. The temperature can be determined by inserting a thermocouple into either the liquid or holes provided in each of the cones.

To overcome friction in the plate assembly, a minimum torque must be applied. In this instrument, the amount of the frictional torque varies from less than 0.025 up to 0.3 gramweight cm. It is, however, constant within one run, as is attested to by the fact that, for a Newtonian liquid, the applied torque is a linear function of the speed of rotation of the plate. In a given run, the friction can be determined as long as low enough rates of shear can be achieved so that such plots are linear and can be extrapolated to zero speed. By using this technique, it has proved possible to use effective driving torques down to 0.05 gramweight cm.

III. SOME DESIGN CONSIDERATIONS

For design purposes, it is necessary to calculate the errors introduced by various types of misalignment. In these computations, the assumptions of a simple laminar type of flow and negligible contribution of inertia will be made. These assumptions should at least be valid at the low speeds of rotation and small total displacements at which most of the data are taken.

The torque on the element of surface of the plate bounded by the circular arcs r and $r + dr$, and the lines ϕ and $\phi + d\phi$, is $f(r, \phi)\eta\ \Omega r^2 dr d\phi$, and the total torque, L, on the plate is given by

$$L = \eta\Omega \int_0^R \int_0^{2\pi} f(r, \phi) r^2 \, dr \, d\phi, \qquad [1]$$

where r and ϕ are the usual polar coordinates in the plane of the plate, η is the viscosity at the given rate of shear, Ω is the angular velocity of the plate, and $\Omega f(r, \phi)$ is the velocity gradient at the point (r, ϕ).

If we have perfect alignment, as illustrated in Fig. 2*a*, $f(r, \phi)$ is simply $1/\theta$, and

$$L = 2\pi\eta\Omega R^3/3\theta \qquad [2]$$

where θ is the angle between the plate and the generator of the cone, and R is the radius of the plate. It is assumed that $\theta = \sin\theta = \tan\theta \ll 1$.

If, as in Fig. 2*b*, the apex of the cone is at a distance h above the plate, $f(r, \phi)$ is $r/(h + \theta r)$ and, if $h/\theta R \ll 1$,

$$L = (2\pi\eta\Omega R^3/3\theta)[1 - (3h/2\theta R)]. \qquad [3]$$

If, as in Fig. 2*c*, the axis of the cone is tilted at an angle $\beta(\ll 1)$ with respect to the axis of the plate, but the two axes intersect at the center of the plate,

$$f(r, \phi) \cong 1/(\theta + \beta \sin\phi), \qquad [4]$$

where the line $\phi = \pi/2$ is taken to be the line on the plane of the plate formed by the intersection of that plane with the plane determined by the axes of the plate and cone. Substituting Eq. [4] into [1], we find

$$L = 2\pi\eta\Omega R^3/3\theta[1 - (\beta/\theta)^2]^{1/2}$$

or if $\beta \ll \theta$

$$L = (2\pi\eta\Omega R^3/3\theta)[1 + \tfrac{1}{2}(\beta/\theta)^2]. \qquad [5]$$

If, as in Fig. 2*d*, the axis of the cone is parallel to that of the plate, but displaced a distance b from it,

$$f(r, \phi) = r/\theta(r^2 + 2br\cos\phi + b^2)^{1/2},$$

where $\phi = 0$ is the line formed by the intersection of the plane of the plate and the plane determined by the two parallel axes. If $b \ll R$,

$$L = (2\pi\eta R^3\Omega/3\theta)[1 + (7b^2/3R^2)]. \qquad [6]$$

If, as in Fig. 2*e*, the cone is truncated so that its plane surface is a circle of radius ρ positioned at a height l above the plate so that the apex would have been located at the center of the plate,

$$L = (2\pi\eta\Omega/l)\int_0^\rho r^3\,dr + (2\pi\eta\Omega/\theta)\int_\rho^R r^2\,dr$$

$$= (2\pi\eta\Omega R^3/3\theta)[1 - (\rho^3/4R^3)].$$

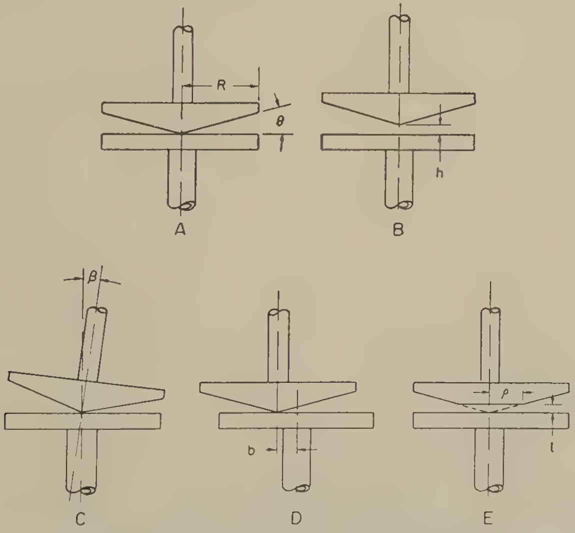

FIG. 2. Types of misalignment that may be encountered in viscometer: (*A*) correctly aligned; (*B*) vertically displaced; (*C*) tilted axes; (*D*) horizontally displaced; (*E*) truncated cone.

For a cone with $R = 4$ cm. and $\theta = 2°$, the following values for the above deviations will change the torque by 1% and thereby cause an error of 1% in the calculated value of the viscosity: $h = 0.0010$ cm., $\beta = 20$ minutes $= 0.005$ radian, $b = 0.26$ cm., and $\rho = 1.36$ cm. The actual values of these quantities in this instrument are at worst $h = 0.0005$ cm., $\beta = 0.6$ minutes, $b = 0.005$ cm., and $\rho = 0.11$ cm. (for the 2° cone). It is thus seen that these misalignments should cause an error less than 1% in the 2° cone and about 3% with the ½° cone.

The viscosity at a given rate of shear is calculated by using the following equation, which can be deduced directly from Eq. [2]:

$$\eta = (3\theta ga/4\pi^2R^3)Tm,$$

where g is the acceleration of gravity, a is the radius of the cylindrical drum on which the string is wound, R is the radius of the base of the cone, T is the period of revolution, and m is the mass of the driving weight in excess of that needed to overcome the frictional torque. The rate of shear is simply $2\pi/\theta T$.

IV. Experimental Results

Newtonian Liquids: For such materials, a plot of applied weight versus rate of shear should be a straight line through the origin with a slope

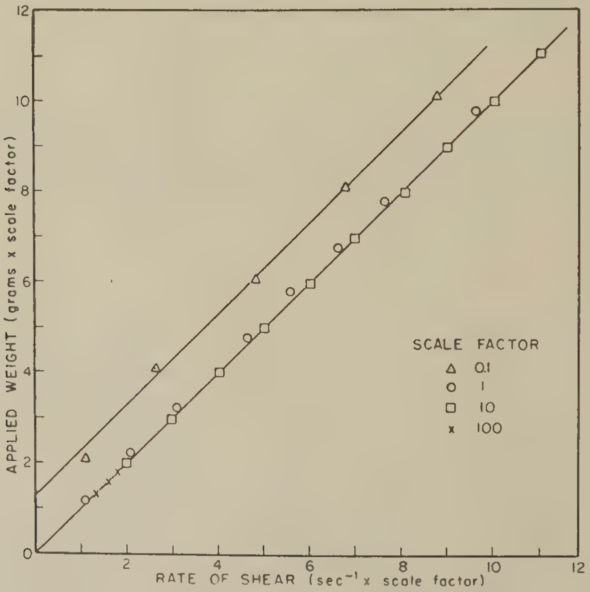

FIG. 3. Plot of applied force against rate of shear for a Newtonian liquid—NBS oil N-16.

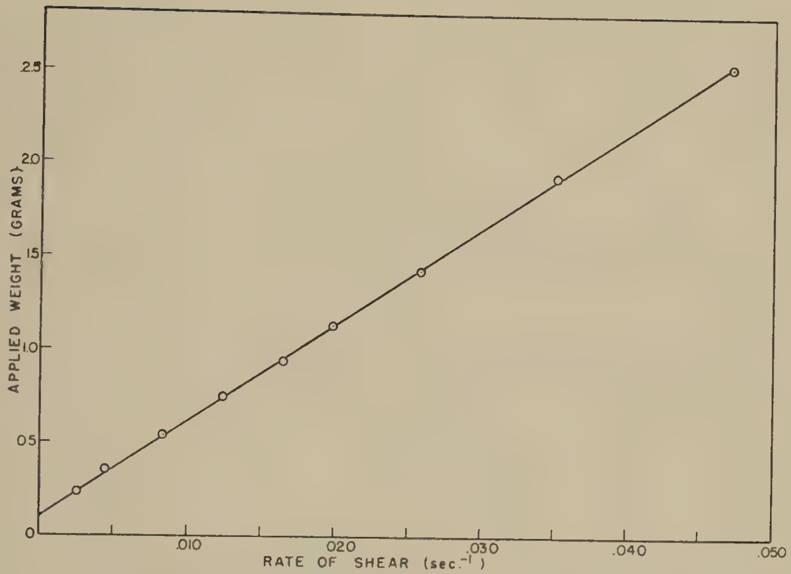

FIG. 4. Plot of applied force at low rates of shear for a non-Newtonian liquid—a 4% solution of polyisobutylene in decalin.

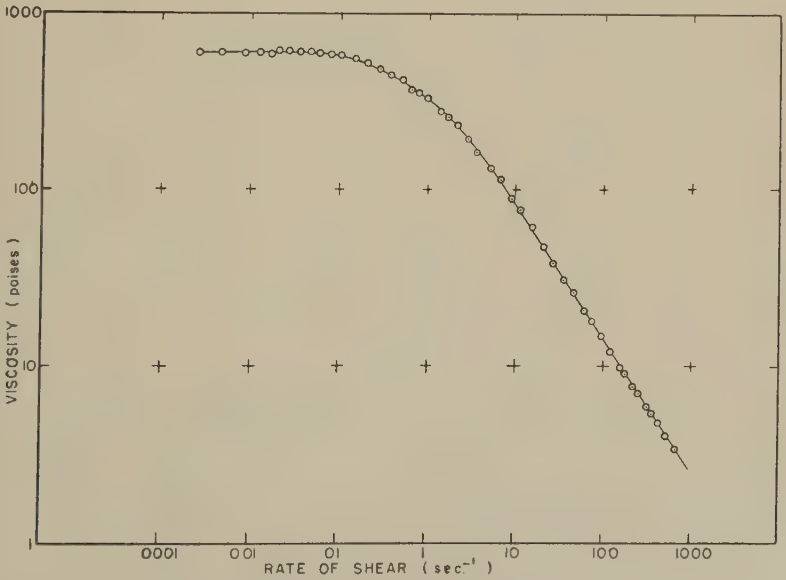

FIG. 5. Plot of apparent viscosity against rate of shear for a non-Newtonian liquid—a 4% solution of polyisobutylene in decalin.

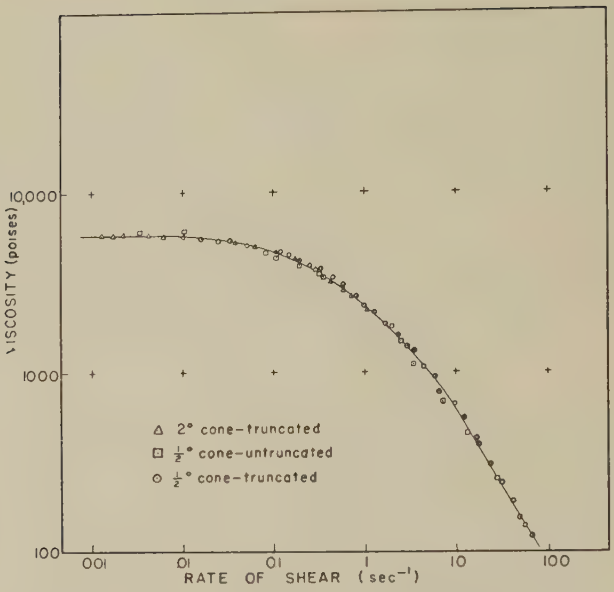

FIG. 6. A comparison of results obtained with different cones for a 13% solution of polyisobutylene (Vistanex B-100) in decalin.

proportional to the viscosity. Actually, owing to friction, the experimental results yield a linear plot with an intercept on the weight axis of about 0.15 g. or less corresponding to a torque of 0.3 gram weight cm. or less. An example of such a plot is shown in Fig. 3. The liquid was a sample of National Bureau of Standards Oil N-16, whose viscosity was 11.3 poises. The graph shows results taken over more than a thousandfold range of rates of shear as the speeds of rotation varied from 0.0006 to 1 r.p.s. The intercept of 0.13 g. on the "0.1" scale corresponds to 0.26 gram weight cm. of frictional torque, but it is to be noted that the line on this scale is parallel to those obtained at higher weights and speeds. The viscosity calculated from the slope of the line and the dimensions of the instrument is 11.5 poises.

Non-Newtonian Liquids: At sufficiently low rates of shear, such materials behave as Newtonian liquids. A plot of applied weight versus rate of shear for a 4% solution of a polyisobutylene fraction in decalin illustrates this. (See Fig. 4.) The zero shear viscosity obtained from this line is 609 poises, while that obtained on a torsion pendulum instrument is 620 poises. The range of data available with one filling of the viscometer is indicated in Fig. 5 where the data on this same solution are shown as a plot of apparent viscosity as a function of rate of shear. More than 5.5 decades of rates of shear were covered. This is a rather favorable case. In most cases, only about four decades are covered.

Figure 6 shows data obtained with various cones on one non-Newtonian liquid — a 13 % solution of Vistanex B-100 in decalin. It is seen that cones of two different angles as well as the truncated and untruncated cones all give results in rather good agreement.

REFERENCES

1. Mooney, M., and Ewart, R. H., *Physics* **5**, 350 (1934).
2. Piper, G. H., and Scott, J. R., *J. Sci. Instr.* **22**, 206 (1945).
3. Weissenberg, K., *Proc. Intern. Congr. on Rheology, Holland* **1948**, II—114 (1949).
4. Higginbotham, R. S., *J. Sci. Instr.* **27**, 139 (1950).
5. Pollett, W. F., and Cross, A. H., *J. Sci. Instr.* **27**, 209 (1950).
6. Roberts, J. E., *Proc. Second Intern. Congr. on Rheology, Oxford* **1953**, 91 (1954).
7. McKennell, R., *Proc. Second Intern. Congr. on Rheology, Oxford* **1953**, 350 (1954).

CONCENTRATION DEPENDENCE OF THE RHEOLOGICAL BEHAVIOR OF THE POLYISOBUTYLENE–DECALIN SYSTEM[1]

T. W. DeWitt, H. Markovitz, F. J. Padden, Jr., and L. J. Zapas

Mellon Institute, Pittsburgh 13, Pennsylvania

Received October 18, 1954

Abstract

The dynamic moduli and dynamic viscosities, as well as the apparent steady-state viscosities, in the polyisobutylene–decalin system have been studied in considerable detail. It is found, above about 8% concentration, that it is necessary to assume that moduli are proportional to the square of the concentration, rather than to the first power, in defining reduced variables. With this assumption, data for solid polymer satisfactorily superpose on master curves with those of concentrated solutions. The same procedure achieves superposition for the apparent steady-state viscosities. The latter, when plotted as a function of reduced rates of shear, yield curves closely similar to, but not quantitatively identical with, those of the dynamic viscosities as a function of the frequency. It is suggested that in concentration ranges where c^2 is required in the reduced variables, and in the solid polymer, a temporary gel structure exists as a result of bimolecular association between monomer units in the polymer chains. The primary data are compared with the results of two recent molecular theories of viscoelastic behavior.

I. Introduction

It has become customary to describe the dynamic behavior of viscoelastic systems, such as concentrated polymer solutions, by recording a dynamic modulus and a dynamic viscosity as a function of frequency and to interpret these quantities in terms of a mechanical model consisting of springs and viscous dashpots. A single element in such an array is characterized by a modulus and a viscosity coefficient, or by a relaxation time given by the ratio of the viscosity coefficient to the modulus. Since no real system is adequately described by a single element, nor by several, it is current practice to assume an infinite parallel set of Maxwell-type elements, each of which consists of a spring and a viscous dashpot in series, and to compute from the data the distribution of relaxation times, or strengths, necessary to describe the mechanical behavior of the system under consideration. In spite of its purely phenomenological character, the mechanical model approach has provided a very successful framework for the correlation of a great deal of data. Ferry (1) has shown that simple and reasonable assumptions about the dependence of the moduli and relaxation times on temperature and concentration lead to the definition of reduced variables, in terms of which data at widely differing frequencies, temperatures, and concentrations may be incorporated into master curves characteristic of the material. Although Ferry's reduced variables have been notably successful, they are not applicable over the whole concentration range, since it is known that reduced data for solutions cannot be extrapolated to solid polymer (2). It has been further shown that a suitable modification (3) of the Maxwell model permits the inclusion of the apparent steady-flow viscosities and the associated Weissenberg effects in the same scheme. Reduced variables of the same form can be defined for these latter phenomena, and they can be interpreted in terms of the same moduli, relaxation times, and distribution function as the dynamic data. Some preliminary data bearing on these equations have been published elsewhere (4).

---

[1] The work discussed herein was performed as part of the research project sponsored by the Reconstruction Finance Corporation, Office of Synthetic Rubber, in connection with the Government Synthetic Rubber Program.

Until recently there has been no molecular foundation for these procedures, and it has not been possible to assign physical reality with any degree of confidence to the moduli and relaxation times employed. This situation has been materially improved by the appearance of two theories (5, 6) based on a detailed, though necessarily still approximate, analysis of the motion of long-chain molecules in a viscous medium. Though they differ in detail, both theories describe a viscoelastic material in terms of a modulus and a characteristic relaxation time. The modulus is found to be proportional to the number of effective chains per unit volume and to the absolute temperature. The relaxation time is determined primarily by the zero shear viscosity but also is inversely proportional to the concentration of effective chains and to the absolute temperature. These are just the assumptions introduced by Ferry (1) and on which his reduced variables are based, if the number of effective chains per unit volume is set proportional to the concentration.

In spite of continuing activity in this field, systematic data relating to the above discussion are somewhat scarce, particularly in the very low frequency, or low rate of shear, region. The present work was undertaken to aid in filling some of these gaps. Particular attention is paid to the slow end of the mechanical spectrum, both dynamic and steady-state, when long relaxation times predominate. There is also special interest in the relationship between the dynamic and the apparent steady-state viscosity and in the possibility of applying reduced variables to the latter.

II. EXPERIMENTAL

A commercial polyisobutylene, Vistanex B-100, with a number-average molecular weight of 370,000 and a weight-average molecular weight of 1.06×10^6 was used throughout. Decalin, of C.P. Grade, was used as a solvent. Concentrations of 3, 5, 7, 8, 10, 13, 17, and 20% by weight were studied. They were rotated for several days at elevated temperature to achieve homogeneity. Low frequency measurements were made in the range of 5×10^{-2} to 1.5 cycles per second with the use of a torsion pendulum instrument which will be described more fully elsewhere (7). The instrument consists essentially of a cylindrical bob which is driven by a coil in a magnetic field. The coil is supplied with a sinusoidal current from a mechanically driven generator. The bob dips into a cylindrical cup containing the sample or, more conveniently, is just immersed in the sample in its jar container. Provision is made for independently measuring the amplitude and mechanical phase angle of the bob relative to the driving signal. From these data and the dimensions of the bob and container, the real and imaginary parts of the complex modulus, and the dynamic viscosity, are calculated. Measurements at frequencies of from 5 to 100 cycles per second were made on a mechanically driven instrument (8). Apparent steady-flow viscosities were determined in a cone-and-plate viscometer which will be described in detail in a forthcoming paper. The lower part of this instrument is a horizontal circular plate mounted on low friction ball bearings and free to turn under a torque supplied by weights. Mounted coaxially above this plate is a fixed cone which makes an angle of ½° (or 2° or 4°) with the plate. The apex of the cone almost touches the plate and the sample is placed between the two. The apparent viscosity is computed from the speed of rotation of the lower plate produced by the application of a known torque. The particular virtue of this type of viscometer is the virtually constant rate of shear that is obtained over the whole radius of the instrument. The apparent viscosities of the system under investigation are severely dependent on the rate of shear, and interpretation is greatly simplified if measurements can be made at a uniform rate of shear. In most cases, falling ball viscosities were obtained on the solution by dropping a small steel ball through the liquid contained in a test tube. The Faxen correction was made in each case. All measurements were taken at temperatures close to room temperature and the data corrected to 25°C., by means of the experimentally determined temperature coefficient of viscosity. The dynamic moduli and viscosities of the solid polymer were obtained at three temperatures, using the torsion pendulum instrument modified for solids. These data were reduced to the equivalent curves at 25°C., with the use of the reduced variables of Ferry (1). The zero shear viscosities of the solid polymer, necessary for this reduction, were obtained from the equation:

$$\log \eta = -15.70 + \frac{0.515 \times 10^6}{T^2} + 3.40 \log M$$

given by Leaderman (9). Here η is the zero shear viscosity, T the absolute temperature, and M the weight-average molecular weight.

III. RESULTS

Considerable attention was devoted to obtaining reliable zero shear viscosities which are needed for the reduction of the raw data to master curves. It was found that falling ball viscosities were not always reliable for solutions with concentrations lower than about 8%, apparently because the effective rate of shear for the smallest steel ball available ($\frac{1}{32}$-inch diameter) was too high. Most reliance was placed on results from the cone-and-plate viscometer, which is capable of giving very low rates of shear. A region of rates of shear could nearly always be found where, in this instrument, the viscosity was independent of rate of shear for a decade or more. The corresponding viscosity then was taken as the zero shear viscosity. It was also found, for all but the higher concentrations, that the torsion pendulum apparatus could be operated at frequencies sufficiently low so that the dynamic viscosity became independent of frequency and was in reasonably good agreement with the steady-state cone-and-plate results. Table I compares the zero shear viscosities obtained by different methods for the several concentrations. A log-log plot of zero shear viscosity against concentration is shown in Fig. 1. Above 3%, the plot is a straight-line with a slope of 5. This agrees with the result of Ferry (10), who found the viscosity of comparable solutions to depend on the fifth power of the concentration.

The primary data for the dynamic moduli, the dynamic viscosities, and the apparent steady-state viscosities of the solutions are shown in Figs. 2, 3, and 4, respectively, and the data (reduced to 25°C.) for the solid polymer in Fig. 5. The torsion pendulum dynamic data in the very low frequency region for the 7% solution is shown on an enlarged scale in Fig. 6 in order that the behavior of the modulus and viscosity in the low-frequency range may be better observed. The rigidity, which has been successfully measured as low as tenths of a dyne per square centimeter,

TABLE I

Concentration	Temperature	Viscosity, *poises*		
		Torsion pendulum	Falling ball	Cone-and-plate viscometer
(*% by weight*)	(*°C.*)			
3.0	25.1	6.33	6.04	7
5.0	24.8	56.0	59.2	58.0
7.0	25.0	291	277	
8.0	25.0	600	427	597
9.0	24.1		1,030	1,100
10.0	25.6	1,620	1,700	1,760
13.0	25.0	6,260	6,170	6,200
17.0	25.0	20,800	19,300	
20.0	24.9		53,100	54,600

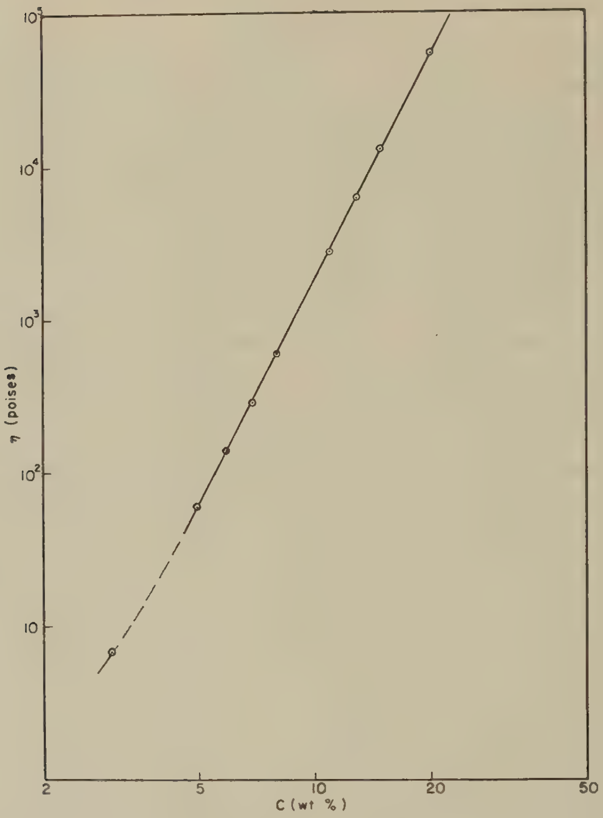

FIG. 1. Plot of steady-flow viscosity against concentration.

virtually disappears at frequencies where the dynamic viscosity has become, within experimental accuracy, independent of frequency and equal to the steady-state zero shear viscosity.

In Fig. 4, the dynamic viscosity curves, taken from Fig. 3, are plotted as dashed curves (with the rate of shear taken equal to the frequency) for comparison with the steady-state viscosities of the same solutions. It has been predicted (3), as a result of using a rotating coordinate system for the recoverable strain, that the apparent steady-state viscosity should be the same function of the rate of shear as the dynamic viscosity is of the angular frequency. This is seen to be not quite true. The shapes are the same, but the steady-state curve is displaced about a factor of 1.5 to the right. Since these data were obtained in the cone-and-plate viscometer, in which the rate of shear is constant, there is no ambiguity about the proper rate of shear to use, and it must be concluded that rate of shear is not quite quantitatively equivalent to frequency.

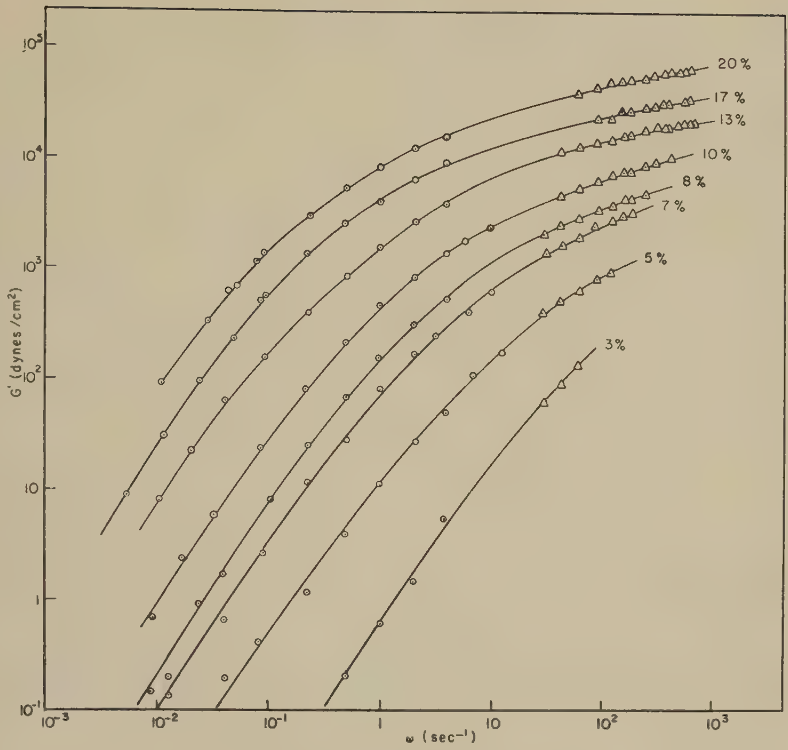

FIG. 2. The dynamic moduli as a function of frequency for solutions of various concentrations.

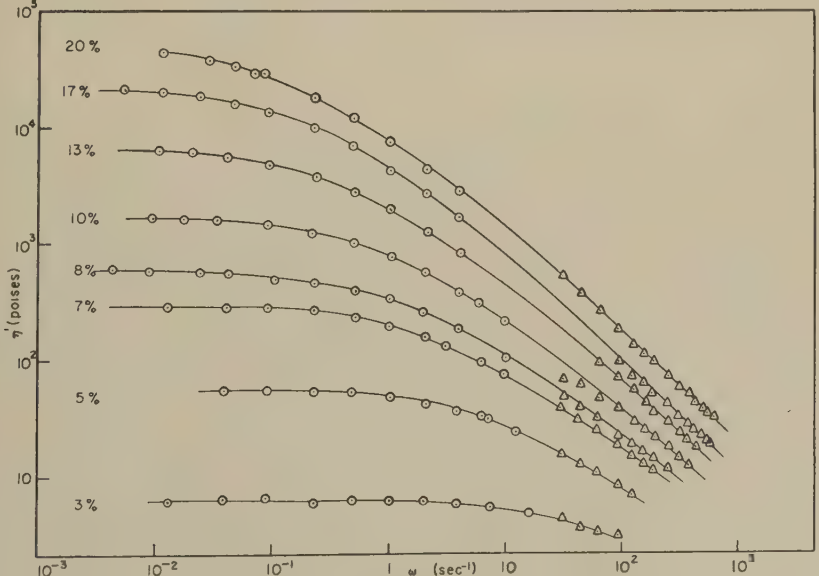

FIG. 3. The dynamic viscosities as a function of frequency for solutions of various concentrations.

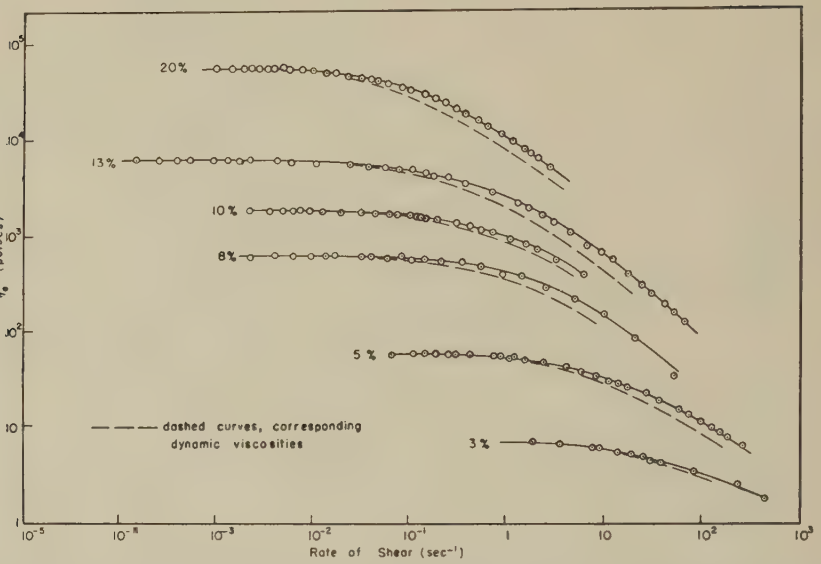

FIG. 4. The steady-state apparent viscosities as a function of rate of shear for solutions of various concentrations. The dashed curves are the corresponding dynamic viscosities.

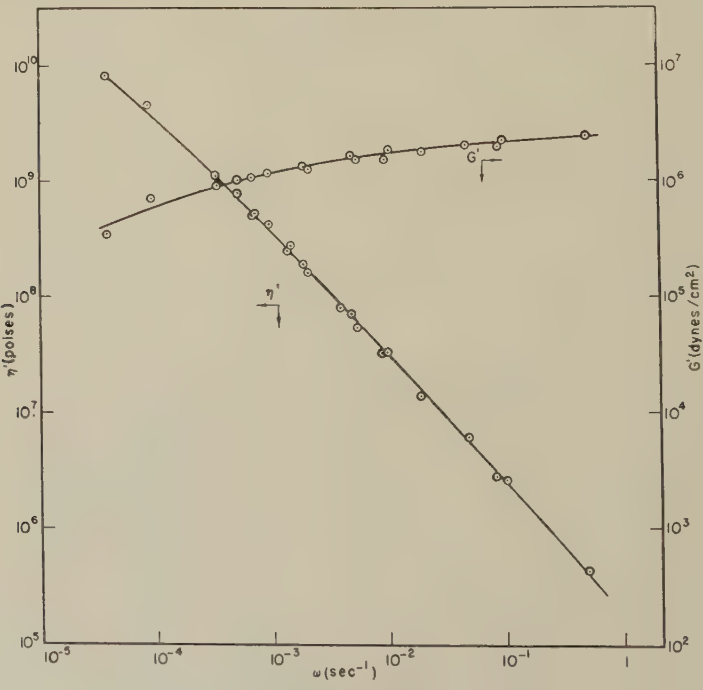

FIG. 5. The dynamic viscosity and rigidity as a function of frequency for solid polyisobutylene.

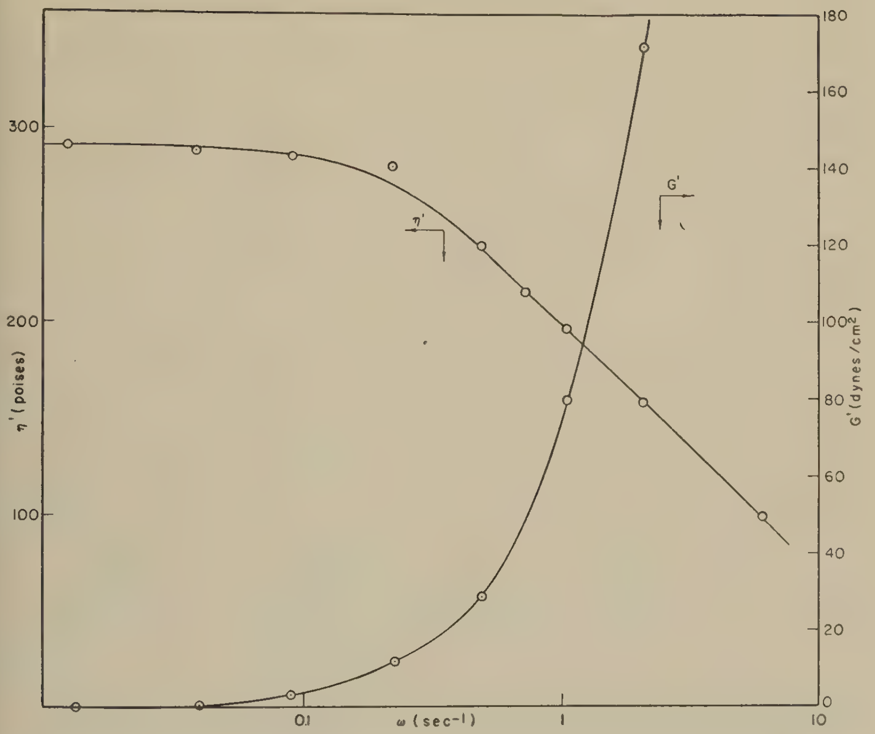

FIG. 6. The low-frequency behavior of the dynamic rigidity and viscosity of a 7% solution of polyisobutylene in decalin.

IV. THE SUPERPOSITION OF DATA

It is apparent from Figs. 2, 3, and 4 that the curves for the dynamic moduli, the dynamic viscosities, and the steady-state viscosities are, in each case, of the same shape for the different concentrations. Each set could be composed into a single curve by appropriate translations along the axes. With the assumptions that the concentration and temperature dependence of all the relaxation times is the same and measured by the zero shear viscosity, and that the moduli depend linearly on concentration and temperature, reduced variables (due to Ferry (1)) which summarize the necessary shifts can be defined. These are $G_r' = G'(T_0c_0/Tc)$, $\eta_r = \eta'/\eta$, and $\omega_r = \omega(\eta T_0 c_0/\eta_0 Tc)$ where G' is the dynamic modulus, η' is the dynamic viscosity, η is the zero shear viscosity, T is the absolute temperature, c is the concentration in grams per unit volume, ω is the angular frequency, and c_0, T_0, and η_0 refer to an arbitrary reference state. This reference state is usually chosen so that η_0 and c_0 are unity. When these reduced variables were used with the data in Figs. 2, 3, and 4, they were found to be inadequate. The curves at low concentration superposed, but those at higher concentrations tended to be displaced progressively in

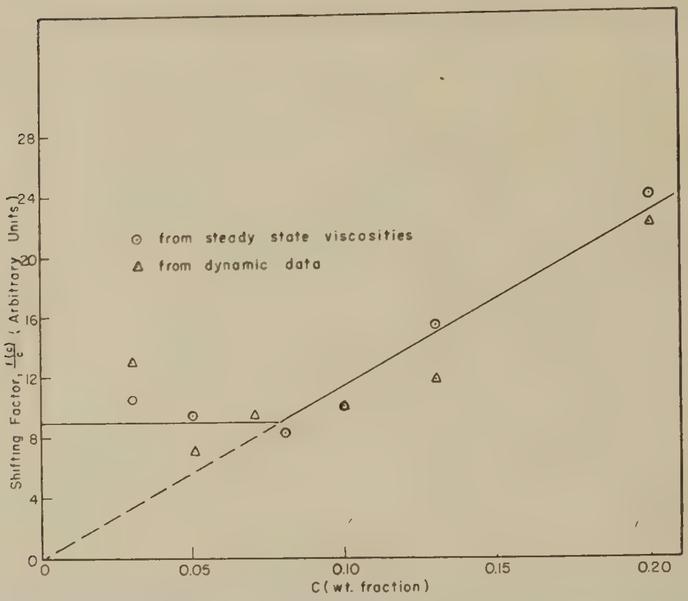

FIG. 7. A plot of the shifting factors required to achieve superposition of data for solutions of different concentrations.

the direction of higher frequencies, or rates of shear. The assumption concerning the concentration dependence of the moduli can be modified to achieve superposition. All of the reduced variable treatment was retained except that c was replaced by $f(c)$ and $f(c)$ determined empirically from the shifts required to bring the curves into coincidence. Values of $f(c)$ thus obtained were plotted against c. The first such plot suggested that c^2 might be involved. A plot of the function $f(c)/c$ can be used to distinguish among various possibilities. If this is constant, the dependence is linear; if it is linear in c and goes through the origin, the function $f(c)$ is proportional to c^2; and if it is linear but has an intercept different from zero, $f(c)$ can be represented by $ac + bc^2$, where a and b are constants. A plot of the quantities $f(c)/c$ against c is shown in Fig. 7. Of the several possibilities, a combination of the first two seems to best agree with the data. Up to about 8%, the concentration dependence of the moduli appears to be approximately linear; above this concentration they are more nearly proportional to c^2. Although a certain latitude in curve shifting makes it difficult to reach an unambiguous conclusion, it is at least quite clear that $f(c)/c$ is not constant over the concentration range. The data in Fig. 7 could be considered as defining two separate lines, one horizontal (moduli linear in c), and one passing through the origin and linear in c (moduli proportional to c^2). The intersection of the two establishes the place where the concentration dependence changes and is judged to be about 8%. The form

TABLE II

Concentration, *wt. %*	η_0, *poises*	G'_r/G'	ω_r/ω
3	6.5	2.66	17.3
5	58	1.6	93
7	290	1.17	3.3×10^2
8	6×10^2	1.00	6×10^2
10	1.75×10^3	6.4×10^{-1}	1.12×10^3
13	6.2×10^3	3.79×10^{-1}	2.35×10^3
17	2.3×10^4	2.21×10^{-1}	5.08×10^3
20	5.2×10^4	1.6×10^{-1}	8.3×10^3
100	3.8×10^{10}	6.4×10^{-3}	2.5×10^8

$f(c) = ac + bc^2$ cannot be firmly excluded, but reconstituted master curves using the resulting reduced variables were not quite as good as those based on the above assumption.

On the basis of this interpretation of the results given in Fig. 7, new reduced variables were defined. The arbitrary reference state was chosen for convenience as a solution at 25°C. with unit viscosity and a concentration of 0.08 (*i.e.*, $c_0 = 0.08$). For solutions of 8% concentration and below, the reduced variables are $G_r' = (G'T_0\, 0.08)/(Tc)$, $\eta_r' = \eta'/\eta$, and $\omega_r = \omega\eta T_0\, 0.08/Tc$. For concentrations of 8% and above, the reduced variables are $G_r' = G'T_0(0.08)^2/Tc^2$, $\eta_r' = \eta'/\eta$, and $\omega_r = \omega\eta T_0(0.08)^2/Tc^2$. The reduced variables G_r' and ω_r, computed using this prescription, are listed in Table II for each of the concentrations, including solid polymer. For the latter, a figure of 3.8×10^{10} was used for η at 25°C.

The dynamic data thus reduced are plotted in Fig. 8. It is particularly gratifying that the data for the solid polymer fit in so well on this plot in spite of the long extrapolation from 20% to 100% concentration. What discrepancy there is, is probably within some possible uncertainty for the zero shear viscosity of this sample. For comparison, the position that the 20% and 100% viscosity data would have occupied relative to the main curve, if a linear dependence of moduli on concentration had been retained, is also shown. Likewise the position the 3% viscosity data would have occupied, if a square dependence had been used throughout, is shown. The c^2 factor for reduced variables also seems to give a better reduced plot than the c factor used on data recently reported (11) on solutions of another sample of polyisobutylene in decalin.

The reduced frequencies in Table II, which were used in constructing Fig. 8, were then used for the steady-state viscosity data of Fig. 4. The superposition thus achieved, with η_r now given by η_a'/η, where η_a is the apparent steady-state viscosity at a given shear rate and where the rate of shear is substituted for the frequency, is shown in Fig. 9. In order to avoid confusion, only a few representative experimental points are shown for each concentration. The excellent result confirms the contention that reduced variables are as applicable to steady-state viscosities as to dy-

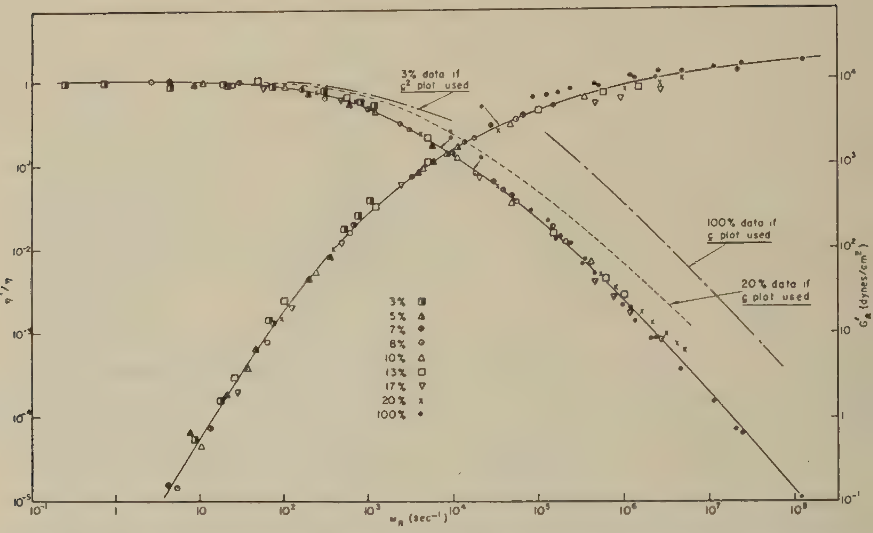

FIG. 8. The superposition of data achieved for different concentrations through the use of the proposed reduced variables. The lack of agreement that results from the use of variants on these variables is indicated by the dashed and dotted lines.

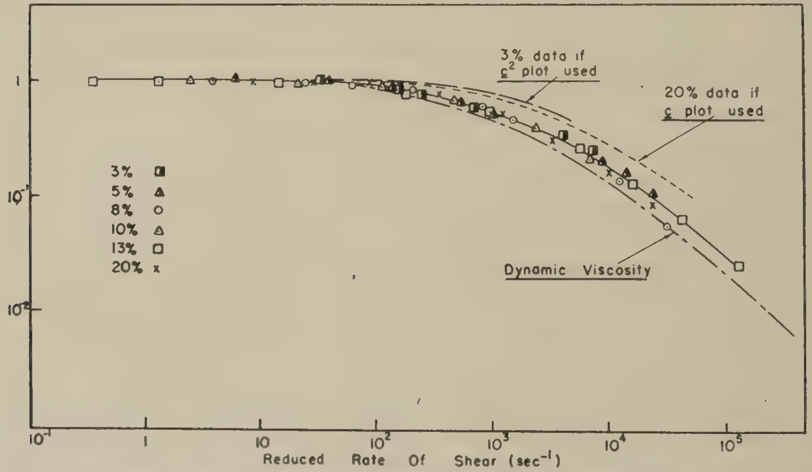

FIG. 9. The superposition of data achieved for the steady-state viscosities when the reduced apparent viscosity and the reduced rate of shear are used as variables.

namic data. The displacement that would have occurred had the 20% data been reduced using a linear concentration dependence, or the 3% data using the square of the concentration, is shown and is seen to be quite comparable to that obtained in the case of the dynamic data. The reduced dynamic viscosity curve from Fig. 8 is also included. As expected from the comparison in Fig. 4, based on the primary data, it has the same shape as the steady-state data but is displaced slightly.

V. Discussion

The success achieved using a c^2 dependence for the constituent moduli at the higher concentrations permits an interesting, though speculative, interpretation. It suggests the presence of a temporary gel structure resulting from a coupling between molecules. If this coupling originates in a bimolecular association between monomer links, it would be expected that the number of coupling points would vary as the square of the concentration of monomer units. The molecular weight between couples would increase and the number of effective chains per unit volume, to which the modulus is proportional, would decrease with the square of the concentration as the polymer is diluted. At some point in the dilution, less than one couple per molecule will exist, the effect of the gel structure will disappear, and the effective number of chains per unit volume will be determined by the concentration and molecular weight of the polymer. The existence of a gel structure as a result of coupling between monomer units is consistent with the tendency of high molecular weight, but uncrosslinked, polymers to show a modulus plateau in the rubbery region. For polyisobutylene this plateau occurs at about 3×10^6 dynes/cm.^{2} (12). This is a value which the simple theory of rubber-like elasticity would associate with a cross-linked network with a molecular weight of about 8300 (in this case, 148 monomer units) between cross-links. If this is taken at its face value, it says that about one out of 74 monomer units in the solid polymer is involved in a coupling point (the fractional number of such units, $\rho_0 = 0.0135$), where $\rho_0 (= 0.0135)$ is the fraction of monomer units involved in "cross-links" at $c = 1$ and ρ is that at any other concentration c. Gelation theory (13) says that the gel point should occur when $y_w = (1/\rho)$, where y_w is the weight-average degree of polymerization of the primary molecules. If we take $y_w = 1.06 \times 10^6/56 = 1/\rho_0 c = 1/0.0135\, c$, we should be able to calculate the concentration at which the "gel point" would occur. Above this concentration, we might expect the c^2 dependence of the moduli to become dominant. Solving this equation, we find $c = 0.064$ the empirical choice of 0.08 for this critical concentration based on curve shifting. It is further to be noted that coupling of this sort plays an important role in the rather successful theory of the melt viscosity of polymers proposed by Bueche (14). Indeed, he considers a reasonable figure for the number of coupled chains to be of the order of one every several hundred chain atoms, which is the same order of magnitude as that deduced here from the value of the modulus plateau.

The composite curves in Fig. 8 permit the approximate calculation of a relaxation distribution function, Φ, such that $\Phi\, d \ln \tau$ represents the contribution to the elastic reaction of relaxation times between $\ln \tau$ and $\ln \tau + d \ln \tau$. This function has been calculated using the second approximation method of Ferry (15) from both the modulus and viscosity curves. The results thus obtained from the data of Fig. 8 have been reduced to solid

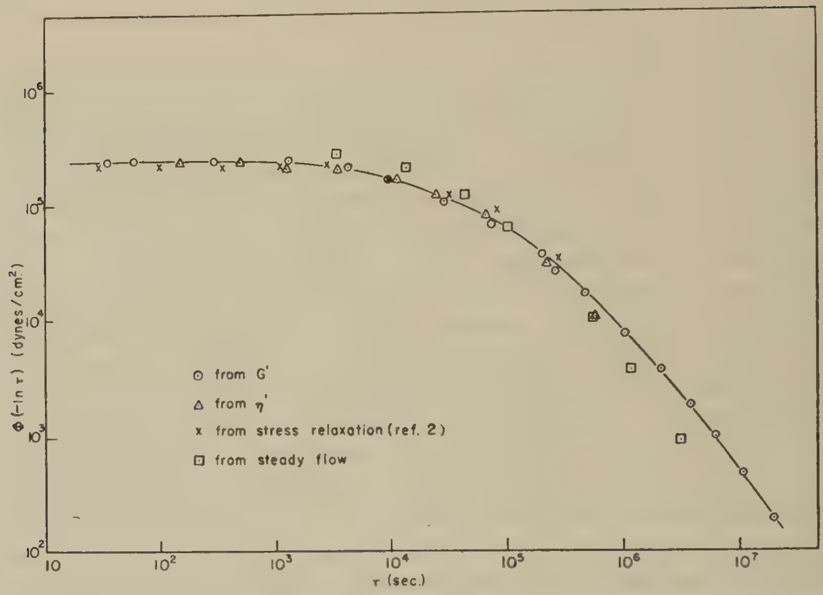

FIG. 10. The relaxation distribution function obtained from the dynamic rigidity, the dynamic viscosity, the steady-flow viscosity, and stress relaxation (2).

polymer using the relations $\Phi_r = \Phi(T_0/Tc^2)$ and $\omega_r = \omega(T_0/T)(\eta/\eta_0c^2)$, where η_0 is the zero shear viscosity of the solid polymer, taken as 3.8×10^{10} poises. The reduced data which now represent the distribution function for solid polymer are plotted in Fig. 10. The solid points show the same function calculated by Ferry (2) (and taken from Fig. 7 of the cited paper) from stress relaxation data (16). The excellent agreement further justifies the use of c^2 in the reduced variables. It thus becomes possible to infer the dynamic behavior of the solid polymer from data on solutions for this system.

It should also be possible to approximate the distribution function from the steady-state viscosity data. It has been shown that this can be written in the same form as is customary for the dynamic viscosity (3), but with the rate of shear in place of the frequency, *i.e.*,

$$\eta_a = \sum(G_i\tau_i)/(1 + \tau_i^2\Omega^2)$$

where η_a is the apparent steady-state viscosity and Ω is the rate of shear. It is readily seen that exactly the same procedure can be applied to the steady-state viscosity as to the dynamic viscosity for the derivation of the distribution function. This has been done and the result plotted as indicated in Fig. 10. The distribution function thus obtained is displaced from that for the dynamic data to the extent expected from the fact that, as noted in Figs. 4 and 9, the steady-state viscosity is equivalent to the dynamic viscosity at a frequency which is a constant factor times the rate of shear.

The low frequency data reported in this paper on the dynamic rigidity and viscosity are particularly useful for a comparison with two recent molecular theories of viscoelastic behavior. The theories of Rouse (5) and Bueche (6) both predict a relaxation spectrum, discrete at long times, as a result of different modes of cooperative movement of long-chain coiling molecules. Each furthermore yields an expression for a characteristic time that has no arbitrary parameters and which is determined primarily by the zero shear viscosity of the solution. Although they were derived for dilute solutions, there would appear to be no basic reason for their not being at least approximately applicable to more concentrated solutions. In the case of Rouse's theory, this time is given by:

$$\tau = (6\eta)/(\pi^2 nRT);$$

Bueche's differs from this only by being twice as large. Here η is the zero shear viscosity of the solution, n is the number of moles per unit volume, R is the gas constant, and T the absolute temperature. If n is set equal to c/M, where c is the concentration in grams per unit volume and M is the molecular weight, we have:

$$\tau = (6\eta M)/(\pi^2 cRT)$$

or

$$\tau = (12\eta M)/(\pi^2 cRT)$$

for the theories of Rouse and Bueche, respectively. The relaxation times have been calculated using the above expressions for an 8% solution of a

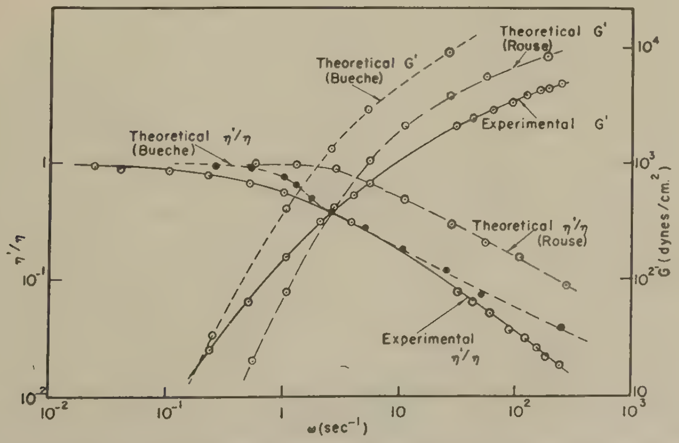

FIG. 11. A comparison of experimental data with the theoretical predictions of the theories of Rouse and Bueche for an 8% solution of polyisobutylene in decalin.

polymer of weight-average molecular weight (the polyisobutylene used in this work) 1.06×10^6, and are found to be 0.19 or 0.39 second. From this, and the expressions given by the respective authors for η'/η and G' as a function of $\omega\tau$, theoretical curves were computed for the 8% solution. The results are compared with the experimental data for this solution in Fig. 11. When it is considered that neither theory contains any adjustable parameters, the agreement must be considered extraordinarily good. Bueche's viscosity curve shows almost perfect agreement in the neighborhood of $\omega\tau = 1$ but has a peculiar inflection just before this. The shape of Rouse's curve is more nearly that of the experimental data but is somewhat displaced from it. In both cases, the theoretical decrease more slowly at higher frequencies than do the experimental data, which seem to have a high-frequency slope of about unity. The theoretical moduli also show excellent agreement with the data, although the shapes differ somewhat. The primary difference in this respect is the low frequency behavior, where the theoretical curves both rise approximately with the square of the frequency. The experimental data, down to the lowest measurable moduli of below 1 dyne/cm.^{2}, never seem to rise faster than with about the three halves power of the frequency. These discrepancies may be associated either with the presence of a wide molecular weight distribution in the sample or with the fact that the theories, which were derived only for the case of dilute solutions, are being compared with data obtained at relatively high concentrations.

REFERENCES

1. FERRY, J. D., *J. Am. Chem. Soc.* **72,** 3746 (1950).
2. FERRY, J. D., FITZGERALD, E. R., JOHNSON, M. F., AND GRANDINE, L. D., JR., *J. Appl. Phys.* **22,** 717 (1951).
3. DEWITT, T. W., *J. Appl. Phys.*, in press.
4. PADDEN, F. J., AND DEWITT, T. W., *J. Appl. Phys.* **25,** 1086 (1954).
5. ROUSE, P. E., JR., *J. Chem. Phys.* **21,** 1272 (1953).
6. BUECHE, F., *J. Chem. Phys.* **22,** 603 (1954).
7. MORRISSON, T. E., ZAPAS, L. J., AND DEWITT, T. W., *Rev. Sci. Instr.*, in press.
8. MARKOVITZ, H., YAVORSKY, P. M., HARPER, R. C., JR., ZAPAS, L. J., AND DEWITT, T. W., *Rev. Sci. Instr.* **23,** 430(1952).
9. LEADERMAN, H., *J. Polymer Sci.* **13,** 371 (1954).
10. JOHNSON, M. F., EVANS, W. W., JORDAN, I., AND FERRY, J. D., *J. Colloid Sci.* **7,** 498 (1952).
11. FERRY, J. D., JORDAN, I., EVANS, W. W., AND JOHNSON, M. F., *J. Polymer Sci.* **14,** 261 (1954).
12. Unpublished data from this laboratory; also, TOBOLSKY, A. V., AND MCLAUGHLIN, J. R., *J. Polymer Sci.* **8,** 543 (1952).
13. STOCKMAYER, W. H., *J. Chem. Phys.* **12,** 125 (1944).
14. BUECHE, F., *J. Chem. Phys.* **20,** 1959 (1952).
15. FERRY, J. D., FITZGERALD, E. R., GRANDINE, L. D., JR., AND WILLIAMS, M. L., *Ind. Eng. Chem.* **44,** 703 (1952).
16. ANDREWS, R. D., HOFMAN-BANG, N., AND TOBOLSKY, A. V., *J. Polymer Sci.* **3,** 669 (1948).

ON THE "ACTIVE CENTERS" FOUND ON METAL SURFACES[1]

Shigeto Yamaguchi

Scientific Research Institute, Ltd., Hongo, Tokyo, Japan

Received December 27, 1954

ABSTRACT

The contact surfaces of metals of cubic structure, produced by chemical etching are composed frequently of the (111) planes. The facets of metal crystals formed by etching are chemically more active than the edges and corners of the crystals. The area of the active zone found on an etched surface amounts to approximately 80% of the area of the contact surface. These experimental results were obtained by means of oxide replicas in electron microscopy.

INTRODUCTION

It is well known that there are "active centers" on the surface of a catalyst. The real forms of the active centers found on metals have been investigated by means of oxide replicas in the present study.

OCTAHEDRAL PLANES ON AN ETCHED SURFACE

1. Electron Microscopy

The iron single crystal here used was a wire (2 mm. diameter) prepared by repeated wire-drawing and annealing. The test piece of nickel single crystal was a disk (10 mm. diameter, 2 mm. thickness). The surface of the disk was oriented mechanically parallel to the (111) planes. These single crystals were prepared by S. Kaya.[2] The test piece of Permalloy single crystal (Ni, 81.5%) was cut from an ingot prepared by R. M. Bozorth and his co-workers (1).

The single crystals of these metals were etched with an ethanol solution of bromine. The oxide replica films formed on these etched surfaces and isolated from them were observed by means of electron microscopy (2). The three micrographs obtained from iron, Permalloy, and nickel show octahedral figures regularly oriented (see Figs. 1, 2, and 3).

The octahedral figures are also found on the etched surfaces of aluminum,

---

[1] Partly presented at the 13th International Congress of Pure and Applied Chemistry, Group 13: Surface Chemistry, Stockholm, Sweden, July 30, 1953.

[2] Prof. J. Horiuti (Hokkaido University, Japan) and Dr. T. Nakayama (Waseda University, Japan) lent the author these test pieces.

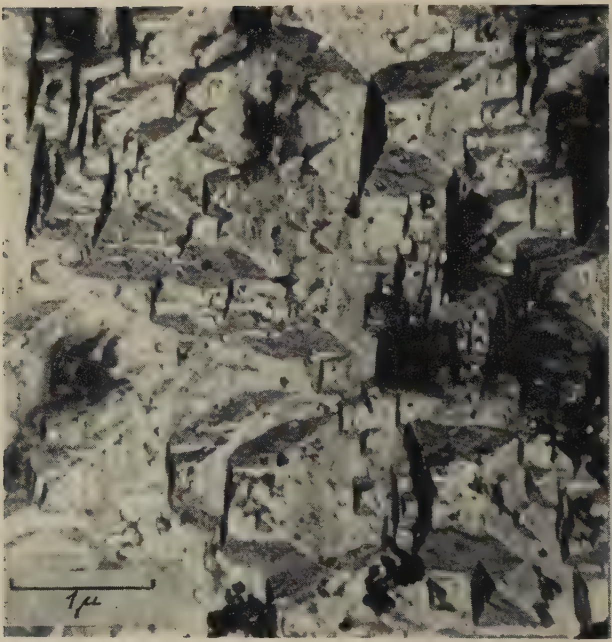

FIG. 1. Micrograph of the oxide replica formed on the etched surface of an iron single crystal. The octahedral figures regularly oriented are seen here. It can be seen that the oxide films are thinner at the reprinted crystal edges and corners than on the crystal facets.

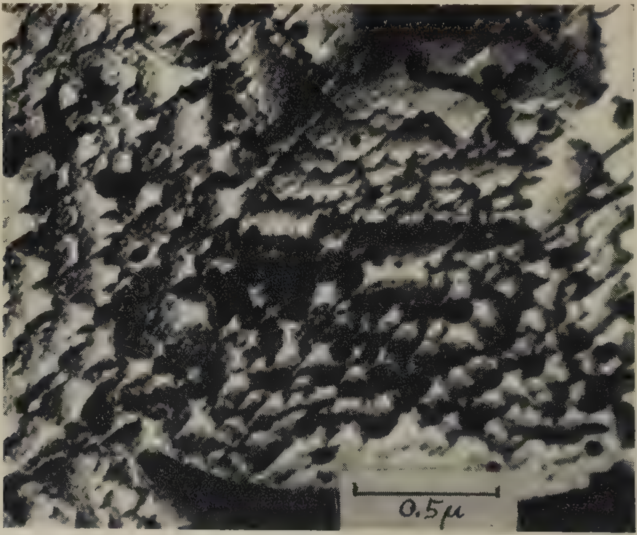

FIG. 2. Micrograph of the oxide replica formed on the etched surface of a Permalloy single crystal. The octahedral figures regularly oriented are seen here. It can be seen that the oxide films are thinner at the reprinted crystal edges and corners than on the crystal facets.

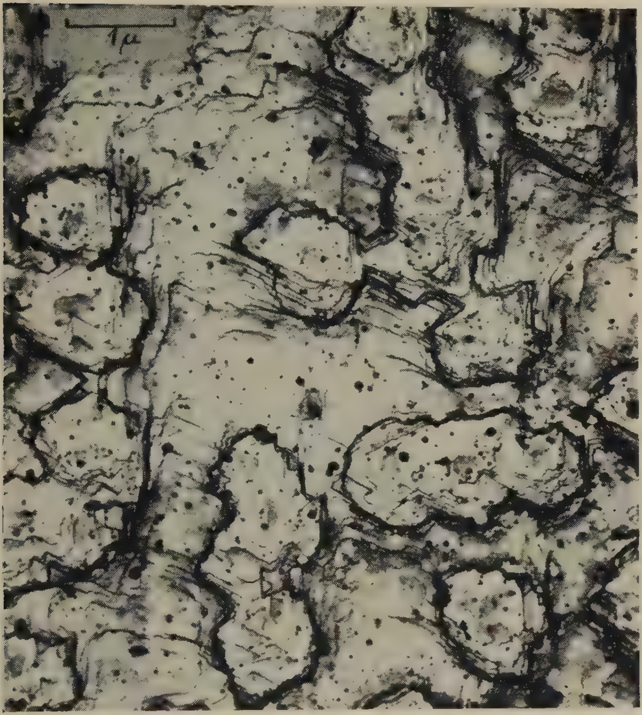

FIG. 3. Micrograph of the oxide replica formed on the etched surface of a nickel single crystal. The octahedral figures are reprinted in this oxide replica.

stainless steel, etc. (2, 3). Figures other than the octahedral are sometimes found on the etched surfaces of metals (3, 4). For iron and nickel suitable as catalysts the frequency of the appearance of the octahedral etch figure is considerably higher than that of the other figures.

2. Electron Diffraction

The etched surfaces of the same test pieces as for microscopy were observed by means of electron diffraction. The diffraction patterns obtained inform us of the orientations of the macroscopic surfaces of the test pieces. Figure 4 is the reflection pattern obtained from the etched surface of the iron single crystal. The orientation determined in Fig. 4 was compared with that observed in the micrograph of Fig. 1. The inclination (about 55 degrees) of the (001) planes to the macroscopic surface in Fig. 4 is roughly equal to that estimated in the micrograph of Fig. 1. The diffraction patterns obtained from the etched surfaces of Permalloy and nickel were compared with the micrographs of Figs. 2 and 3. In this way it was concluded that the etched surfaces of the metals of cubic structure are composed frequently of the (111) octahedral facets.

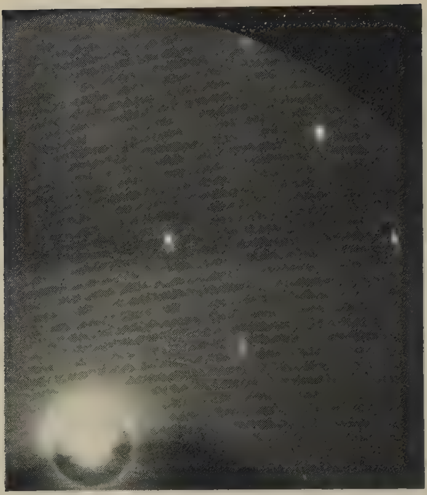

FIG. 4. Diffraction pattern from the etched surface of the same iron single crystal in Fig. 1. The incident beam is parallel to the (001) and (110) planes of the body-centered cubic crystal (*i.e.*, along a $[\bar{1}10]$ zone axis). The inclination angle between the (001) plane and the macroscopic surface is approximately equal to that estimated in Fig. 1.

CHEMICAL ACTIVITY OF CRYSTAL FACETS

The *facets* of the metal crystals produced by etching are chemically more active than the crystal *edges* and *corners*. This is concluded readily from the electron micrographs of the oxide films observed in the present study.

It is remarked in the micrographs of the oxide replicas that the oxide films are thinner at the reprinted crystal edges and corners than on the crystal facets (see Figs. 1 and 2, ref. 5). The thickness of the former films is roughly estimated to be 100 A., whereas that of the latter films is about 300 A. (6). This fact means that the crystal facets are about three times more active than the crystal corners and edges actually produced by etching. This phenomenon is always recognizable in the oxide replicas formed on the etched surfaces of metals (3, 4), and independent of the types of the etch figures found on metals.

ACTIVITY COEFFICIENT OF CONTACT SURFACE AREA

The ratio (α) of the active area to the contact area is roughly estimated from the micrographs of the oxide replicas observed.

$$\alpha = \frac{S}{S + \sigma} \cong \left(1 - \frac{\sigma}{S}\right),$$

where S denotes the area of one crystal facet and σ denotes the area of one crystal edge of an octahedron found in Fig. 1. The symbol α denotes, as it were, the activity coefficient of contact surface area. If σ/S is 0.2, as may be measured in Fig. 1, α is 80%. The value of the activity coefficient is approximately constant among the micrographs of the oxide replicas taken by several microscopists (5). The summarized active area found on a metal surface is equal to the summarized contact area reduced by the activity coefficient. The summarized contact area may be estimated by means of physical adsorption. The conception of the activity coefficient here defined will be applicable to the results of catalysis experiments carried out with coiled wires of nickel and iron chemically etched.

SUMMARY

1. In the discussion of the contact surfaces of metallic catalysts, it is reasonable to employ the (111) plane of cubic lattice as the contact net plane.

2. The facets of the metal crystals produced by etching are about three times more active than the edges and corners of the crystals.

3. The area of the active zone found on an etched surface amounts approximately to 80% of the contact surface area.

ACKNOWLEDGMENTS

The present study has been carried out with the financial aid of the Heavy Industry Bureau, Ministry of International Trade & Industry of Japan. Sincere thanks are expressed to Prof. L. G. Sillén (Royal Institute of Technology, Sweden), who gave the author an opportunity to present this paper.

REFERENCES

1. WALKER, J. G., WILLIAMS, H. J., AND BOZORTH, R. M., *Rev. Sci. Instr.* **20,** 947 (1949).
2. MAHLA, E. M., AND NIELSEN, N. A., *J. Appl. Phys.* **19,** 378 (1948).
3. MAHL, H., "Metallurgical Application of the Electron Microscope." *Inst. Metals (London) Monograph and Rept. Ser.* **No. 8,** 37 (1950).
4. COSSLETT, V. E., "Practical Electron Microscopy," p. 228. Butterworths Scientific Publications, Ltd., London, 1951.
5. YAMAGUCHI, S., *J. Appl. Phys.* **23,** 935 (1952).
6. HEIDENREICH, R. D., AND NESBITT, E. A., *J. Appl. Phys.* **23,** 352 (1952).

THE EFFECT OF ALIPHATIC DETERGENTS ON THE MECHANICAL STABILITY OF POLYSTYRENE LATEX[1]

Charles P. Roe and P. D. Brass

Received February 15, 1955

Abstract

1. The mechanical stability of polystyrene emulsions is greatly affected by the nature and surface concentration of adsorbed ionic detergents.

2. The electrokinetic potential of the particles in soap-protected polystyrene emulsions is not affected by surface concentration of adsorbed soap.

3. The variation of mechanical stability of polystyrene emulsions with adsorbed soap may probably be largely accounted for by steric interference of the adsorbed carbon chains.

4. Work with a nonionic emulsifier indicates that mechanical stability of a protected lyophobic colloid probably depends on both steric and electrical factors.

Introduction

The stability of a colloidal system is a term which refers to the capacity of the system to persist in an unaltered state of dispersion. Certain factors which limit colloidal stability, such as sedimentation and flocculation, lend themselves to precise analysis. Other factors, such as mechanical treatment, chemical, thermal, and electrical conditions, also exert important effects on colloidal stability, but usually these factors do not lend themselves to precise analysis. Such factors are frequently of great practical importance, however, and this fact has stimulated the development of test methods for the evaluation and control of several aspects of stability which do not yield to complete theoretical treatment. Despite the fact that many of these methods are semiempirical, the results obtained by them possess theoretical as well as practical interest. The present contribution is based upon study of a specific instance of this sort, namely, the reaction of a certain type of aqueous lyophobic dispersion to the turbulence produced by high-speed stirring. This reaction is commonly referred to as the mechanical stability of the dispersion.

Numerous attempts have been made to account for the stability of lyophobic colloids on the basis of electrostatic repulsion, and in recent years a substantial advance along this line has been made by Verwey and Overbeek in their quantitative theoretical treatment of double-layer interaction (1). However, spontaneous flocculation due to Brownian motion is the only process contemplated by these authors, and application of their results has been made principally to unprotected inorganic colloids, such as silver iodide and the metal oxide sols.

---

[1] Contribution No. 144 from the general Laboratories of the United States Rubber Company, Passaic, New Jersey.

There is an important class of lyophobic dispersions, of which the hydrocarbon polymers are typical, which are strongly stabilized by adsorption of surface-active solutes at the polymer-water interface. Heretofore no purely electrical theory has been found adequate to account for the known behavior of these dispersions. One of the purposes of this contribution is to supply data which elucidate the reason for this inadequacy of the electrostatic interaction theory in dealing with the stability of protected colloids.

A different approach to the problem of stabilization of colloidal dispersions has been advanced by Mackor and van der Waals (2). They have considered an example in which no electrostatic effects can be involved, namely, a dispersion of carbon in liquid paraffins with adsorbed dodecyl benzene as a stabilizer. In this case flocculation is assumed to be hindered by mutual interference of the hydrocarbon chains of the adsorbed alkyl benzene, and the free-energy change resulting from the crowding of chains necessary to permit flocculation can be calculated.

It seems reasonable that both types of stabilizing influence may have significant effects in the case of aqueous polymer dispersions containing ionic surfactants adsorbed at the polymer-water interface. The measurement of mechanical stability has been adopted as a tool to study this possibility in carefully prepared aqueous polystyrene dispersions stabilized with either potassium palmitate or potassium laurate. Some discussion of similar dispersions stabilized by a nonionic surfactant is also included.

We have investigated this matter by finding out how the amount of soap adsorbed at the polymer-water interface affects (1) the stability of a dispersion and (2) the double-layer potential at the interface. For information about stability we have had recourse to the mechanical stability test; for data on the double-layer potential we have depended on electrophoretic mobilities. Experimental results of this sort are significant only if they are obtained under properly controlled conditions, and we shall accordingly discuss an essential requirement.

The stability of aqueous colloidal dispersions is in general affected by the nature and concentration of the ionic atmosphere in the aqueous phase. A similar assertion is valid with regard to the adsorption of surfactants and the double-layer potential at an interface. Recently it has been shown (3) that in a salt-bearing solution of an ionic surfactant the concentration of gegen-ions plays a very important role in determining the adsorption equilibrium at the air-water interface, whereas the concentration and valence of ions having the same sign as the surfactant ions have a negligible effect on adsorption. There is reason to believe that a similar importance attaches to the gegen-ion concentration in an aqueous dispersion protected by an adsorbed surfactant. Thus in our polystyrene dispersions, which were protected by either K-palmitate or K-laurate, care was taken to control the total concentration of K+ dissolved in the aqueous phase, but the nature of the surface-inert anions, which usually were confined to carbonate, bicarbonate, and persulfate, was regarded as being of minor importance, except for effects on pH, which was maintained at 10.5 by means of a carbonate-bicarbonate buffer. Since it has been shown (3) that gegen-ions and surfactant ions are adsorbed in approximately equal numbers at the air-water interface, it was assumed that a similar equivalence prevails in the adsorbed layer at the polymer-water interface, and that the adsorbed gegen-ions make no contribution to the concentration of dissolved gegen-ions in the aqueous phase. Control of the gegen-ion concentration along lines indicated in this paragraph was a distinctive feature of all our experiments, and was essential to interpretation of the results.

Methods and Materials

The Mechanical Stability Test

For our purpose in this paper the mechanical stability of a polymer dispersion is defined as the number of seconds required to produce complete flocculation by high-speed stirring of a 60-ml. specimen of the dispersion containing 24% by volume of solid polymer. The specimen was contained in a square 8-ounce glass sample bottle, and the stirring rate was 14,000 r.p.m. A special perforated blade ¾ inch in diameter was used. No temperature control was imposed.

The test as described in the preceding paragraph possesses several arbitrary features, but no apology is offered for them, since the test is not known to have any absolute significance. Reproducibility of results was highly satisfactory in the dispersions here tested. This was all that was required of the test, since we used it only to inquire how the stability changed as we varied certain conditions.

Perhaps the selection of complete flocculation to indicate the end point deserves comment. Most of our experiments were performed on polystyrene dispersions stabilized with potassium palmitate at surface concentrations insufficient to saturate the polymer-water interface. No trouble with foaming was caused by stirring in palmitate-stabilized systems, and the end points were sharp and easily recognized. However, in potassium-laurate–stabilized dispersions foaming trouble was encountered, and the results were less precise.

Electrophoresis

Electrophoresis measurements on polymer dispersions were made by use of the moving boundary method due to Tiselius (4). All measurements were made in potassium palmitate solutions below the critical micelle concentration, and equilibration of the dispersion and its bounding solution was accomplished by dialysis. Density differences and current densities were such that sharp boundaries could be maintained without resorting to the low-temperature feature of the Tiselius method. Movement of the boundaries was followed by direct observation with a cathetometer.

Surface Tension

The drop-weight method was employed, using the corrections of Harkins and Brown (5).

Soaps

Potassium palmitate and potassium laurate were prepared by careful neutralization of the free acids in the best grade supplied by the Eastman Kodak Company.

All other reagents were of analytical grade and were used as supplied.

Particle Size

Statistical data on average particle size and specific area of the polymer dispersions were obtained from electron photographs.

RESULTS AND DISCUSSION

In presenting experimental data we have reported adsorption in terms of the molar surface concentration of soap, and have confined ourselves to the region of surface concentrations below the saturation level. This means that in the palmitate-stabilized dispersions only a negligible fraction of the soap was dissolved in the water phase, and also that the concentration of soap in the water phase was negligible with respect to the concentration of buffer salt used. The circumstances were different in the laurate-stabilized samples, and the equilibrium concentration of soap had to be taken into account in reckoning both the adsorption and the total gegen-ion concentration. This was done with the aid of a previously established adsorption isotherm of potassium laurate on polystyrene at the appropriate gegen-ion concentration.

Electrophoresis and Mechanical Stability of a Polystyrene Dispersion Stabilized with Potassium Palmitate

The dispersion was originally produced with potassium palmitate as the sole surfactant in the polymerization recipe, and no cations other than potassium were introduced at any time.

Specimens of this dispersion were prepared for electrophoresis by adjusting the polymer contents to 1% at various desired soap levels and by adjusting the total K+ concentration in the serum to 0.1 molar with the aid of a buffer mixture of K_2CO_3 and $KHCO_3$ at pH = 10.5. Each 1%

dispersion was dialyzed for 20 hours against the solution which was subsequently employed as the bounding solution in the electrophoresis cell. In order to test the effectiveness of dialysis in securing equilibration with respect to soap, surface tension measurements were made on both the dispersion and the bounding solution. Since the electrolyte concentration and pH level were the same in all solutions and since the dissolved soap content was negligible by comparison to the total electrolyte, the surface tension could be interpreted unambiguously as a measure of the dissolved soap concentration. Complete data on the surface tension and electrophoresis measurements are given in Table I, in which the following symbols are employed:

s = surface concentration of soap in moles/cm.^{2} at polymer-water interface.
γ_1 = surface tension of bounding solution in dynes/cm.
γ_2 = surface tension of 1% polystyrene dispersion in dynes/cm.
H_1 = electrophoretic mobility of advancing boundary in cm.^{2}/volt sec.
H_2 = electrophoretic mobility of receding boundary in cm.^{2}/volt sec.
$\bar{H}$ = average electrophoretic mobility of the particles in cm.^{2}/volt sec.

Specimens for mechanical stability testing were derived from the same latex and were adjusted to the desired soap levels and to 24% polymer by volume. Gegen-ion concentration in the serum was adjusted to 0.1 molar with the aid of a K_2CO_3-$KHCO_3$ buffer at pH = 10.5. Results of the stability tests are listed in Table II.

Inspection of Tables I and II discloses that the amount of soap adsorbed has no effect on electrophoretic mobility. However, mounting soap adsorption in the same range causes an increase of mechanical stability which

TABLE I

Electrophoretic Mobility of Polystyrene Dispersions Stabilized with K-Palmitate

[K+] = 0.1 Mole/liter; pH = 10.5

$10^{10}s$ *(moles/cm.^{2})*	γ_1	γ_2	10^4H_1	10^4H_2	$10^4\bar{H}$
0.4	62.6	63.7	−6.65	−6.50	−6.57
1.0	52.0	51.5	−6.95	−6.30	−6.62
3.4	38.0	38.5	−6.20	−6.10	−6.15

TABLE II

Mechanical Stability vs. Surface Concentration of Potassium Palmitate

$10^{10}s$ *(moles/cm.^{2})*	*t (sec.)*
0.52	4
0.76	12
1.04	55
1.30	186
1.57	504
1.83	>1000

amounts to several orders of magnitude. Thus it becomes clear that in a dispersion protected by an ionic surfactant mechanical stability may be affected strongly without altering the electrokinetic potential. This does not imply that the electrokinetic potential is without effect on stability, but it does demonstrate that this potential is not the exclusive or even the dominant factor in controlling stability.

Before entering upon a detailed discussion of the significance of this result we shall present a more extensive set of data on mechanical stability.

Mechanical Stability: Dependence on Soap Adsorption and Length of Carbon Chain

We shall first consider a set of dispersions prepared with potassium palmitate as the sole stabilizer and with no cations other than K+. The first member of the set was produced in a manner very similar to that indicated in the preceding section. The second member of the set was prepared by use of the first member as a seed. Thus the average particle diameter was increased without initiating any new particles. The third member of the series was prepared by use of the second as seed, and so on.

Each finished dispersion was subjected to a determination of mechanical stability at three desired levels of surface concentration of adsorbed soap. Specimens for stability determinations were prepared by adjusting the polymer contents to 24% by volume and by adjusting the serum electrolyte contents to 0.1 in K+ with a K_2CO_3-$KHCO_3$ buffer mixture at pH = 10.5. Data are listed in Table III and are graphed in Fig. 1.

We shall also consider a set of dispersions stabilized solely with potassium laurate. The upper members of this set were also prepared by seeding. Ad-

TABLE III

Mechanical Stability Data on Polystyrene Dispersions at Various Average Particle Sizes vs. Adsorbed K-Palmitate

Dispersion #	10^5a (*cm.*)*	$10^{10}s$ (*moles/cm.*^{2})	*t* (*seconds*)
1	0.99	0.81	9
		1.07	61
		1.33	427
2	1.63	1.07	6
		1.57	146
		1.81	492
3	3.12	1.40	11
		1.79	149
		2.17	1012
4	5.30	1.93	13
		2.26	96
		2.48	325

* Area average particle diameter.

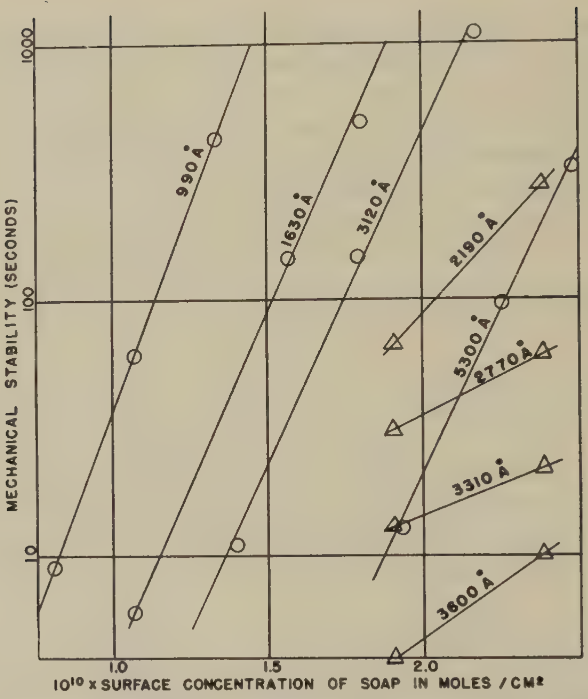

FIG. 1. Mechanical stability of polystyrene dispersions vs. surface concentrations of adsorbed soap. ○ K-palmitate-stabilized; △K-laurate-stabilized.

TABLE IV

Mechanical Stability Data on Polystyrene at Various Average Particle Sizes vs. Adsorbed K-Laurate

Dispersion #	10^5a (*cm.*)	$10^{10}s$ (*moles/cm.*^{2})	t (*seconds*)
5	2.19	1.91	67
		2.38	280
6	2.77	1.91	31
		2.38	61
7	3.31	1.91	13
		2.38	22
8	3.60	1.91	4
		2.38	10

justments of polymer contents and serum electrolyte were made as before. Owing to trouble with foaming, which obscured the end point, the data cover a smaller range of adsorptions and exhibit less precision than in the case of the palmitate-stabilized dispersions. Data are listed in Table IV and are also graphed in Fig. 1.

Reference to Fig. 1 shows that the data on the palmitate-stabilized dispersions exhibit the following features:

1. The logarithm of t is a linear function of s.

2. The slope of the log t vs. s curves is independent of average particle size.

3. The numerical value of stability decreases with increasing particle size.

Of these, the first two lend themselves to analysis, whereas dependence of stability on particle size does not appear to do so.

Data on the laurate-stabilized dispersions are less definite, largely because of a lower degree of precision. These data imply, however, that K-laurate is a less effective stabilizer than K-palmitate. There also appears to be little question that the slopes of the curves are smaller in the laurate system than in the palmitate.

Discussion of Slopes of Stability Curves in Figure 1—Palmitate-Stabilized Systems

We have shown that the surface concentration of adsorbed soap at the polymer-water interface affects the mechanical stability of a dispersion without producing any change in the electrokinetic potential. We shall now inquire whether the entropy change caused by the crowding of adsorbed hydrocarbon chains when two protected surfaces impinge on one another is sufficient to account for the observed dependence of mechanical stability on surface concentration of adsorbed soap. The method of calculation used in pursuing this inquiry is rather crude and ignores several factors which would probably have important effects on the final result. Nevertheless it is felt to be of some interest to determine whether this entropy effect makes a substantial contribution to the total effect. The mode of approach was suggested by the work of Mackor and van der Waals (2).

The rate of a chemical process is expressed by the Arrhenius equation

$$-dN/dt = Af(N) \exp(-E/RT), \qquad [1]$$

where N is the number of molecules reacting.

$f(N)$ is some algebraic function of N.
E is the activation energy of the process.
T is absolute temperature.
R is the molar gas constant.
A is a constant.
t is time.

We can now integrate [1] and obtain

$$t = -\frac{1}{A} \exp(E/RT) \int_{N_0}^{N} \frac{dN}{f(N)}, \qquad [1a]$$

where the lower and upper limits are the initial and final numbers of molecules involved.

Taking the logarithm of both sides of [1*a*] and differentiating with respect to s, we obtain

$$d \log t/ds = (1/RT)\,(dE/ds). \qquad [1b]$$

We shall now assume that a flocculating dispersion is analogous to a chemical reaction in which the molecules are replaced by dispersion particles. We may then identify $d \log t/ds$ of Eq. [1*b*] with the slope of the logarithmic stability curve, and we may further identify E with the free-energy change resulting from the coagulation process. For our purposes we are neglecting terms in E which may be due to heat effects, desorption effects, and electrical effects, and are retaining only the term which arises from the entropy of crowding as two protected surfaces approach each other. We proceed to make use of a formula given by Guggenheim (6), after Huggins (7), to calculate the free energy corresponding to this process, neglecting heat effects and volume changes.

The Guggenheim-Huggins formula expresses the free-energy change which occurs when a long-chain molecule dissolves in a small molecule solvent. Since heat effects and volume changes are treated as negligible, the only surviving term is that due to the change in entropy. The equation given by Guggenheim reads

$$\frac{\Delta_m F}{RT} = \frac{N_1}{N_1 + N_r} \ln \frac{N_1}{N_1 + rN_r} + \frac{N_r}{N_1 + N_r} \ln \frac{rN_r}{N_1 + rN_r} + \frac{z}{2}\frac{N_1 + qN_r}{N_1 + N_r} \ln \frac{N_1 + rN_r}{N_1 + qN_r} - \frac{z}{2}\frac{qN_r}{N_1 + N_r} \ln \frac{r}{q}, \qquad [2]$$

where F = free energy per mole.
N_1 = mole fraction of solvent.
N_r = mole fraction of solute (long-chain molecules).
r = volume of 1 mole of solute/volume of 1 mole of solvent.
z = a factor whose value is 6 for an open-chain molecule.
q = $(1/z)\,[r(z - 2) + 2] = (1/3)\,(2r + 1)$ when $z = 6$.
T = absolute temperature.
R = molar gas constant.

This equation was deduced from consideration of a nonpolar polymer dissolving in a nonpolar solvent. The subscript m in the left member signifies that the free-energy change refers to 1 mole of solution.

It is recognized that it is not strictly valid to utilize Eq. [2] in a discussion of the behavior of adsorbed soap molecules at a polymer-water interface, inasmuch as this system fails to conform to several assumptions which were made in deducing the equation. It is clear that we are ignoring heat effects, orientation effects, and volume changes, which in our system almost certainly contribute to the total value of the activation energy of coagulation. We must emphasize that our sole reason for employing Eq. [2] is to inquire whether or not the entropy of crowding is an important term in the activation energy appearing in Eq. [1*b*]. We shall be satisfied if Eq. [2] predicts the right order of magnitude for the slopes of the curves in Fig. 1.

Equation [2] may be rewritten so as to give ΔF for 1 mole of soap by multiplying both sides by $(N_1 + N_r)/N_r$.

$$\frac{\Delta F}{RT} = \frac{N_1}{N_r} \ln \frac{N}{N_1 + rN_r} + \ln \frac{rN_r}{N_1 + rN_r} + \frac{z}{2}\frac{N_1 + qN_r}{N_r} \ln \frac{N_1 + rN_r}{N_1 + qN_r} - \frac{zq}{2} \ln \frac{r}{q}. \qquad [2a]$$

We now restrict attention to a layer at the polymer-water interface and consider that this layer is of sufficient thickness to contain the adsorbed soap molecules. The space not taken up by soap is occupied by water molecules at the normal density of liquid water. Let

n = the number of moles of water per cm.^{2} of adsorbed layer in absence of soap;

then $N_1 = n - rs,$

$N_r = s,$

and Eq. [2*a*] becomes

$$\frac{\Delta F}{RT} = \frac{n}{s}\left(1 - \frac{rs}{n}\right) \ln \left(1 - \frac{rs}{n}\right) + \ln \left(\frac{rs}{n}\right) - \frac{z}{2}\frac{n}{s}\left(1 - \frac{r-q}{n}s\right) \ln \left(1 - \frac{r-q}{n}s\right) - \frac{zq}{2} \ln \frac{r}{q}. \qquad [2b]$$

We assume that on coagulation the surface concentration of soap is doubled in the area of contact, and that hence the free energy per mole of soap in the region of contact is given by replacing s with $2s$ in Eq. [2*b*]. The change of free energy per mole of soap due to coagulation is

$$\frac{\Delta F(2s)}{RT} - \frac{\Delta F(s)}{RT} = \frac{n}{2s}\left(1 - \frac{2rs}{n}\right) \ln \left(1 - \frac{2rs}{n}\right) - \frac{n}{s}\left(1 - \frac{rs}{n}\right) \ln \left(1 - \frac{rs}{n}\right) + \ln 2 - \frac{zn}{4s}\left(1 - 2\frac{r-q}{n}s\right) \ln \left(1 - 2\frac{r-q}{n}s\right) + \frac{zn}{2s}\left(1 - \frac{r-q}{n}s\right) \ln \left(1 - \frac{r-q}{n}s\right). \qquad [3]$$

We may now calculate numerical values of the left member of [3] for various values of s in the range which is of interest according to Fig. 1. The thickness of the adsorbed layer has been taken to be 18 A, and n is thus fixed at 10^{-8} mole/cm.^{2}; r is set equal to 17; c equals 11.7. Table V

TABLE V

$10^{10}s$	$2.3\,(1/RT)\,[\Delta F(2s) - \Delta F(s)]$	$2.3\,(1/RT)\,[\Delta F(2s) - \Delta F(s)]$ per cm.^{2}
0.5	0.553	0.276×10^{-10}
1.0	0.869	0.869×10^{-10}
1.5	1.291	1.940×10^{-10}

shows the results of calculation, after conversion to logarithms to the base 10, for a few values of s.

We now identify $[\Delta F(2s) - \Delta F(s)]$ per cm.^{2} of Table V with the activation energy E of Eq. [1b]. Setting $2.3\ (1/RT[\Delta F(2s) - \Delta F(s)]$ per cm.^{2} equal to G, we find that the mean slope of the G vs. s relation is given by

$$\frac{dG}{ds} = 2 \times (0.869 - 0.276) = 1.18 \text{ in the interval } 0.5 \leqq s \times 10^{10} \leqq 1;$$
$$= 2 \times (1.940 - 0.869) = 2.14 \text{ in the interval } 1 \leqq s \times 10^{10} \leqq 1.5.$$

The experimental slope of the stability curves obtained from the palmitate-stabilized latices is 2.7. The agreement in order of magnitude is thus satisfactory, and we infer that the change in entropy due to crowding of adsorbed soap molecules makes a significant contribution to the free energy of the coagulation process.

Effect of a Nonionic Stabilizer

A dilute dispersion of polystyrene was made with nonionic detergent of the polyethylene oxide class, with an oleyl group at one end of the chain. Despite the presence of an excess of detergent this dispersion was very unstable and flocculated completely after a few hours of standing. An electrophoresis experiment disclosed that the particles had zero electrophoretic mobility. This is a significant observation, since it indicates that the interference of adsorbed hydrocarbon chains is not in this case sufficient to impart any great degree of stability.

The same nonionic detergent was found to be capable of completely displacing adsorbed potassium palmitate from the polystyrene-water interface. This was demonstrated with the aid of a technique in which radioactive soap was adsorbed and displaced from the interface between water and a thin film of polystyrene. Details of the method have been previously published by the writers (3).

Despite the apparently complete removal of adsorbed soap by the nonionic detergent, a polystyrene latex containing both soap and the nonionic was more stable mechanically than in the presence of either detergent alone. Furthermore in the presence of both detergents the particles exhibited a finite electrophoretic mobility less than that in absence of the nonionic, but greater than that in the absence of soap.

From these observations we infer that stability in this system requires a certain degree of cooperation between electrical and steric factors. Although the precise nature of the balance which is required between the two is little understood, it is evident that neither one alone is adequate to account for the observed facts.

REFERENCES

1. VERWEY, E. J., AND OVERBEEK, J. TH. G., "Theory of the Stability of Lyophobic Colloids." Elsevier, Amsterdam, 1948.
2. MACKOR, E. L., AND VAN DER WAALS, J. H., *J. Colloid Sci.* **7,** 535 (1952).
3. ROE, C. P., AND BRASS, P. D., *J. Am. Chem. Soc.* **76,** 4703 (1954).
4. TISELIUS, A., *Trans. Faraday Soc.* **33,** 524 (1936); LONGSWORTH, L. G., *J. Am. Chem. Soc.* **61,** 529 (1939).
5. HARKINS, W. D., AND BROWN, F. E., *J. Am. Chem. Soc.* **41,** 499 (1919).
6. GUGGENHEIM, E. A., "Mixtures," p. 195, equation (10.09.3). Oxford Press, 1952.
7. HUGGINS, M. L. *Ann. N. Y. Acad. Sci.* **43,** 9 (1942).

ANALYSIS OF THE VALIDITY OF THE GOUY-CHAPMAN THEORY OF THE ELECTRIC DOUBLE LAYER

G. H. Bolt

Department of Agronomy, Cornell University, Ithaca, New York

Received January 3, 1955

INTRODUCTION

With the advancement of colloid science the interest in the precise structure of the electric double layer has increased considerably. Until recently the theoretical description of the double layer formed on planar interfaces has been based entirely on the theory of Gouy-Chapman (5, 7, 13). It is well known that this theory involves the assumption of a number of idealizing conditions (13) which mainly center around the acceptance of ideal behavior of the ions in the double layer. In addition the dielectric saturation of the medium and the polarization energy of the ions are neglected.

Some attempts to examine the validity of these assumptions have been published (1, 6, 9, 14, 16). All these proposed improvements of the double-layer theory were, in general, concerned with only one of the shortcomings of the Gouy theory. Since the effects of the different assumptions involved will tend to offset each other to a certain degree, it is necessary to consider simultaneously all the approximations inherent in the Gouy theory.

The expanded double-layer equation must contain appropriate expressions for the energies of interaction and polarization of the ions and should allow for the functional dependence of its dielectric constant on the local field strength. Insofar as exact expressions are available for these factors, substitution of these expressions in the double-layer equation renders the latter insolvable by ordinary mathematical means. Since the purpose of the following treatment is mainly to determine the order of magnitude of the effects caused by the acceptance of Gouy's assumptions, certain approximations will be used in deriving the secondary energy terms to be introduced in the corrected double-layer equation. This will bring the double-layer equation on the level of a first-order correction; the next step to be considered will be the introduction of secondary corrections to the first-order correction terms. In all probability, however, the first-order corrections will, in many cases, be small enough to warrant the neglect of secondary-correction terms.

The corrected double-layer equation obtained in this way can be solved very simply if the double layer under consideration contains only counterions of one kind. Although, in general, at least one species of co-ions[1] is present, the neglect of the co-ions is warranted if either the equilibrium dialyzate of the colloid suspension is dilute or the interaction between the colloidal particles is sufficiently high to limit the relative amount of the co-ions present. Many colloidal suspensions can be brought under one of these categories. Finally, since the corrections proposed will be of considerable magnitude only close to the colloid surface, a good extrapolation of the results obtained to suspensions falling outside the categories mentioned, seems possible.

Derivation of the Extended Double-Layer Equation

The fundamental differential equation of the electric double layer on planar interfaces is obtained by the combination of the Poisson and Boltzmann equations, which leads to:

$$\frac{d^2\psi}{dx^2} = -\frac{4\pi}{\epsilon}\sum_i \nu_i n_{0_i} \exp\left(-E_i/kT\right) \qquad [1]$$

in whch ψ = electric potential, x = distance coordinate, ϵ = dielectric constant, n_0 = bulk concentration of the ions, k = Boltzmann constant, T = absolute temperature, and E = work needed to bring an ion from the bulk solution to the location under consideration.

The energy term E consists of several components, of which the most important one, E_1, is the potential energy of the ion in the electric field resulting from the colloidal plate and the average volume density of charge. In addition, several other energy terms should be considered, viz., E_2, the energy resulting from the Coulombic interaction between the ions themselves; E_3, the energy of polarization of the ion in the electric field; E_4, the (repulsive) energy caused by short-range non-Coulombic interaction between the ions; and E_5, the non-Coulombic short-range interaction between ion and particle surface (e.g., nonionic chemical bonds). All these energy terms, except for the last one, are dependent upon the electric field strength and/or the local concentration of ions. In addition, the dielectric constant appearing in Eq. [1] depends upon the local concentration of ions and the field strength.

In a paper devoted to the effects of dielectric saturation on the structure of the electric double layer, Grahame (9) proposed the use of an empirical equation for the relation between the dielectric constant and the electric field strength of the form:

$$D = \frac{\epsilon_0 - \epsilon_\infty}{1 + q(dy/dx)^2} + \epsilon_\infty \qquad [2]$$

---

[1] The term "co-ions" is used to indicate the ions which carry a charge equal in sign to the charge of the colloid particles.

in which $D = \frac{\partial \epsilon (dy/dx)}{\partial (dy/dx)}$, $y = e\psi/kT$ (reduced electric potential), ϵ_∞ = dielectric constant at infinite field strength, ϵ_0 = dielectric constant at zero field strength, and q is a constant ($\simeq 0.75 \times 10^{-16}$ cm.^{2}). This expression can be substituted directly into Eq. [1]. If the field strength, dy/dx, does not exceed 10^8 cm.$^{-1}$, an approximation can be used:

$$D \simeq \frac{\epsilon_0}{1 + q(dy/dx)^2}. \qquad [2a]$$

Equation [2] also provides the means to calculate the dielectric constant in the immediate vicinity of an ion. Such a calculation is necessary in order to obtain the polarizability of the ion and the surrounding layer of oriented water molecules (the hydrated ion). The polarizability in turn forms the basis of the calculation of the polarization energy of the ion in the double layer.

A plot of the dielectric constant of water surrounding an ion, against the distance from the center of the ion (2), shows that the dielectric constant remains virtually constant from infinity to approximately 5 A. from the center and then drops off very sharply to a low value of 3–6. This behavior of the dielectric constant makes it possible to describe the ion in solution in first approximation as a spherical cavity with a dielectric constant of 3–6 and a radius of about 2 or 3 A. With the use of this model an estimate of the polarization energy of the ion in the dielectric field can be given as a function of the field strength.

Following Böttcher (4) one finds for this case:

$$E_3 = -\frac{a^3}{6} \cdot \frac{3\epsilon_0(\epsilon_i - \epsilon_0)}{2\epsilon_i + \epsilon_0} \cdot (d\psi/dx)^2 \qquad [3]$$

in which ϵ_i is the dielectric constant inside the spherical "ion cavity," ϵ_0 is the dielectric constant of water at zero field strength, and a is the radius of the ion cavity.

Defining $p = -\frac{a^3}{6} \cdot \frac{3\epsilon_0(\epsilon_i - \epsilon_0)}{2\epsilon_i + \epsilon_0} \cdot \frac{kT}{e^2}$, Eq. [3] can be written:

$$E_3/kT = p(dy/dx)^2. \qquad [4]$$

For the purpose of calculation two values were used for p, viz., $p = 0.37^5 \times 10^{-16}$, and $p = 0.75 \times 10^{-16}$ cm.^{2}, which values correspond to ionic radii of 2.3 and 2.9 A., respectively. In considering these figures it should be kept in mind that the ionic radius referred to in fact corresponds to the radius of the hydrated ion, the hydration hull being taken as the zone over which the dielectric constant of water is materially reduced.

In applying Eq. [4] to the double-layer equation [1] the assumption is introduced that the field strength can be taken as constant over the region that is occupied by the ion. Close to the particle wall this might result in an appreciable error, the polarization energy term being underestimated. For this reason two different values of the constant p were employed which together should cover a sufficient range to allow an estimate of the influence of this term. The limit of applicability of formula [4] is again a field strength, dy/dx, of around 10^8 cm.$^{-1}$.

The energy resulting from Coulombic interaction, E_2, between the ions can be calculated according to Loeb's approach (14). In accordance with Debye-Hückel's limiting law one finds:

$$E_2/kT = -\frac{\nu^2 e^2 \tilde{K}}{2\epsilon kT} \cdot \frac{(1 - \exp(-2\tilde{K}x))}{2\tilde{K}x} \qquad [5]$$

in which $\tilde{K} = \sqrt{\frac{8\pi\nu^2 e^2 n/2}{\epsilon kT}}$, ν = valence, e = electronic charge, and x = distance of ion to the particle surface.

The first term of the right-hand part of this equation refers to the energy of interaction proper, the second term signifies the influence of the planar discontinuity in the dielectric, caused by the presence of the colloidal plate, on this interaction (image effect). The form presented here refers to colloidal plate which can be regarded as a perfect insulator. It can easily be proved (2) that this image term is smaller than 15% of the interaction term if the ion under consideration is at a distance of at least 4 A. from the particle wall, assuming the charge density of the colloid surface to be at least 10 μ Coulombs/cm.^{2}. Since the structure of the double layer in the first few Angstrom units adjacent to the colloid surface is hardly accessible to calculation at all, one feels satisfied to omit the image term entirely, with the understanding that the calculations performed do not apply directly to the first few Angstrom units of the double layer. In practice this first layer is taken care of by the introduction of a distance of closest approach between the ion and the colloid surface (*cf.* discussion of E_5).

This simplification leads to the equation:

$$E_2/kT \simeq -\frac{\nu^2 e^2 \tilde{K}}{2\epsilon kT}. \qquad [5a]$$

Introducing the constant t, according to:

$$t = \frac{e^3\sqrt{\pi N_{Av}/1000}}{(\epsilon kT)^{3/2}} = 0.82(\text{l./mole})^{\frac{1}{2}}$$

this can be written:

$$E_2/kT = -t\nu^3\sqrt{c}. \qquad [5b]$$

This equation is comparable with the Debye-Hückel expression:

$$\ln \gamma = \frac{-A\nu^2\sqrt{\mu}}{1 + aB\sqrt{\mu}}, \qquad [6]$$

in which μ = ionic strength, A, a, and B are constants. Except for the denominator, Eqs. [5*b*] and [6] are identical. The concentration c appearing in [5*b*] refers to the (variable) concentration of the single counter-ion considered, which explains that the constants t and A differ by a factor $\sqrt{2}$.

The absence of the denominator in Eq. [5*b*] is the result of the use of a boundary condition in the derivation of this equation which differs from the one used in the Debye-Hückel derivation. In the latter case the charge of an individual ion is balanced by a local excess of oppositely charged ions in the immediate surroundings of the ion. This countercharge, which is numerically equal to the charge of the central ion, must be located outside the distance of closest approach of the positive and negative ions. This condition limits the energy gain due to the regrouping of the ions and leads to the presence of the denominator in Eq. [6].

Applying the same theory to the double layer, which contains virtually only ions of like sign, the excess charge of the central ion is now balanced by a local deficit of equally charged ions. The creation of this deficit is not limited at all by a distance of closest approach between the ions, which explains the absence of the denominator in Eq. [5*b*].

The high values of the concentrations occurring in the double layer make it necessary to apply a second correction for the ionic interaction. This correction term, E_4, corresponds to the short-range non-Coulombic repulsion between the ions. A similar term is present in the extended Debye-Hückel equation for "neutral electrolytes," which equation reads:

$$\ln \gamma = \frac{-A\nu^2\sqrt{\mu}}{1 + aB\sqrt{\mu}} + C\mu \qquad [7]$$

The values of the constant C given in the literature, however, refer to the mutual repulsion of cation and anion. In the case of a single ionic solution one should expect to find somewhat larger values of C, since ions of equal sign are both surrounded by water molecules polarized in the same direction with respect to the center of the ion. Upon approach this would cause a greater repulsion than is the case for oppositely charged ions. Since experimental data concerning the values of C to be used in single ionic solutions are not available, a number of values were employed in the following calculations.

Defining the short-range repulsion by:

$$E_4/kT = sc \qquad [8]$$

the values of s used in the calculations are 0.06, 0.09, and 0.15 l./mole, respectively. The values of C, given in the literature, are 0.05 l./mole for KCl and 0.12 l./mole for NaCl (12). It is to be expected that s is roughly proportional to the volume of the hydrated ion involved.

It is of interest to note that a completely different approach based on Stern's theory of the double layer leads to comparable results. According to Stern the Boltzmann equation should be modified with a statistical factor, which is related to the volume available for the ion. In its simplest form this equation becomes (*cf.* Stern, reference 15):

$$c = c_0 \frac{(z - c)}{(z - c_0)} \cdot \exp(-E/kT) \qquad [9]$$

in which z is the reciprocal of the molar volume of the ion. This Stern equation can be transformed into:

$$c = c_0(1 - c/z) \exp(-E/kT) \qquad [9a]$$

assuming that c_0/z is very much smaller than 1. For moderate concentrations this equation is identical with the expression obtained by series expansion of the exponential of E_4/kT, present in the extended Boltzmann equation, viz.:

$$c = c_0(1 - sc) \exp(-E'/kT)$$

in which E' signifies the energy term, excluding the short-range interaction. It should be mentioned that the "molar volume" s to be used in the following calculations corresponds to an interaction volume of the ion of 100–250 A.^{3}, which seems a reasonable value for the volume of the hydrated ion.

The energy term resulting from short-range interaction between the ion and the colloid, E_5, cannot be generalized. There will always exist a short-range repulsion analogous to the repulsion between the ions themselves. This effect, which amounts to the introduction of a distance of closest approach between the ion and the wall (*cf.* Stern, reference 15), can easily be taken care of by a shift in the distance coordinate in the double-layer equation, as will be shown later. In addition, specific attraction forces between ion and surface might exist. The structure of the surface and the size of the ion will be of decisive importance for this interaction. It is expected, however, that the interaction energy will be of considerable magnitude only if dehydration of the ion would occur close to the surface. In the case of cations as counter-ions, this does not seem probable, in general, unless the dielectric constant of the colloid exceeds that of water (*cf.* Grahame, reference 10). In the following calculations E_5 was neglected for that reason, except for the allowance for a distance of closest approach.

A combination of equations [1], [2*a*], [4], [5*b*], and [8] now leads to the extended double-layer equation:

$$\frac{1}{1 + q(dy/dx)^2} \cdot \frac{d^2y}{dx^2} = -\frac{4\pi\nu e^2 N_{Av} c_0}{1000\epsilon kT} \qquad [10]$$

$$\cdot \exp\{-\nu y + \nu^3 t\sqrt{c} - sc - p(dy/dx)^2\}$$

in which c = concentration in moles/l.

SOLUTION OF THE EXTENDED DOUBLE-LAYER EQUATION

Defining:

$$\nu^2\beta = \frac{8\pi e^2 \nu^2 N_{Av}}{1000\epsilon kT} = \nu^2 \times 1.06 \times 10^{15} \text{ cm./mmole at } 25°\text{C.}$$

and $z = dy/dx$, Eq. [10] can be rewritten:

$$\frac{\exp(pz^2)}{1 + qz^2} \cdot dz^2 = -\nu\beta c_0 \exp(-\nu y + \nu^3 t\sqrt{c} - sc) \cdot dy. \qquad [11]$$

For comparison the Gouy-Chapman equation for a similar system be given here:

$$dz^2 = -\nu\beta c_0 \exp(-\nu y) \cdot dy. \qquad [11a]$$

In working out Eq. [11] it seems permissible to replace the concentration c appearing in the correction terms in t and s by a quantity c', defined as $c' = c_0 \exp(-\nu y + \nu^3 t\sqrt{c'} - sc')$. In effect this means the neglect of the factor $\exp(pz^2)$ in the expressions to be used for the correction terms in the right-hand part of Eq. [11], since $c = c' \exp(pz^2)$. This is justifiable if the value of z remains smaller than 10^8 cm.$^{-1}$, which was already assumed in the derivation of the energy term E_3.

Accepting this approximation, the equation [11] can be integrated immediately. This is done most conveniently by substituting:

$$-\nu dy = (d \ln c' - d\nu^3 t\sqrt{c'} + dsc')$$

in Eq. [11]. Using the boundary condition: $z = 0$ when $c' = c'_c$ (at the central plane between the colloidal plates) this integration leads to:

$$\frac{\exp(-p/q)}{q}\left[\ln(1 + qz^2) + \frac{p/q(1 + qz^2)}{1.1!} + \frac{(p/q)^2(1 + qz^2)^2}{2.2} + \cdots\right]_0^z \qquad [12]$$
$$= \beta[c' - \tfrac{1}{3}\nu^3 tc'^{3/2} + \tfrac{1}{2}sc'^2]_{c'_c}^{c'}.$$

Defining:

$$b = c_0 \exp(-\nu y) = c' \exp(-\nu^3 t\sqrt{c'} + sc')$$

this equation can be written symbolically:

$$f_1\left[\frac{(d \ln b/dx)^2}{\nu}\right] = f_2\left[f_3\left(\frac{\ln b}{\nu}\right)\right] \qquad [13]$$

or:

$$\frac{\nu\, dx}{d \ln b} = \frac{1}{\sqrt{f_{-1}\left[f_2\left\{f_3\left(\frac{\ln b}{\nu}\right)\right\}\right]}}. \qquad [14]$$

Graphical integration of $\dfrac{dx}{d \ln b}$, plotted against ($\ln b$), will yield x as a function of $\ln b$. This last quantity equals the electric potential except for the constant $\ln c_0$. Such a graphical integration cannot be performed with accuracy, however. Therefore, Eq. [14] is compared with the corresponding equation derived from the Gouy-Chapman equation, which reads:

$$\frac{\nu\, dx}{d \ln b} = \frac{1}{\sqrt{\beta(b - b_c)}} \qquad [14a]$$

in which b is now identical with the concentration.

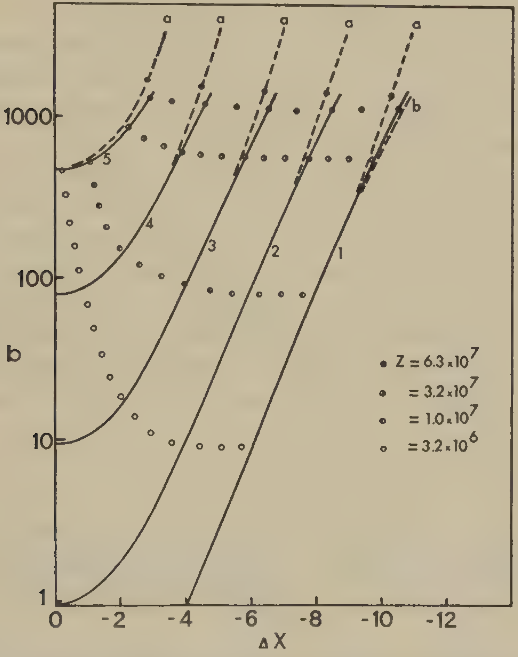

FIG. 1. Correction Δx (in Angstroms), to be applied to the distance coordinates of the Gouy-Chapman double-layer equation, as a function of b (in millimoles per liter).

Curves 1–5: $p = q = 0.75 \times 10^{-16}$ cm.^{2}, $s = 0.06$ l./mole.

$1a$–$5a$: ditto, $s = 0.15$ l./mole.

$1b$: $p = q/2 = 0.37^5 \times 10^{-16}$ cm.^{2}, $s = 0.06$ l./mole.

The values of b_c are, respectively, 0.099 (1), 0.97 (2), 9.2 (3), 77.6 (4), 467 (5) millimoles/l.

Subtracting the equations [14] and [14a] one finds:

$$\Delta\left(\frac{\nu\, dx}{d \ln b}\right) = \frac{1}{\sqrt{f_{-1}\left[f_2\left\{f_3\left(\frac{\ln b}{\nu}\right)\right\}\right]}} - \frac{1}{\sqrt{\beta(b - b_c)}}. \qquad [15]$$

Furthermore:

$$\nu \Delta x = \int_{b_c}^{b} \Delta\left(\frac{\nu\, dx}{d \ln b}\right) \cdot d \ln b. \qquad [16]$$

In this equation Δx signifies the correction to be applied to the distance coordinate of the potential and concentration curves obtained from the Gouy-Chapman equation. Since the right-hand part of Eq. [15] can be calculated numerically for any given value of b, the integration is now reduced to the graphical integration of a calculated correction function.

The results of calculations[2] and corresponding graphical integrations, based on the described method, are presented in Fig. 1. In this figure the corrections, Δx, to be applied to the Gouy-Chapman curves are plotted against $b = c_0 \exp(-\nu y)$, using different values of the constants p, q, s, t, and b_c. By interpolation the corrections to be applied in other cases can easily be estimated.

---

[2] All calculations were performed by the Cornell Computing Center.

With the help of this graph the construction of the concentration-distance curve becomes very simple indeed. For this purpose the Gouy-Chapman curve is constructed first. The correction, Δx, to be applied for every value of b (or c) can be read from the graph. The new curve can now be fitted to applicable boundary conditions. In case of a known potential of the surface of the colloid, the constructed curve is simply terminated at this potential. If the surface density of charge of the colloid, Γ, is known, the position of the surface on the new curve is found from the relation:

$$\Gamma = \frac{\sqrt{2}}{\beta\sqrt{q}} \operatorname{arc\,tan}(\sqrt{q}\cdot z_s) \text{ meq/cm.}^2 \qquad [17]$$

in which $z_s = (dy/dx)_{\text{surface}}$. The corrected double layer curve represents the relation between $b(= c_0 \exp - \nu y)$ and the distance. This curve can be transferred to a corrected concentration-distance curve with help of the relation:

$$b \exp(pz^2) = c \exp(-\nu^3 t\sqrt{c} + sc). \qquad [18]$$

Since z is a function of b, which function was already evaluated in the first part of the calculation performed, the relation between b and c can be obtained by equating both sides of this equation graphically. An example of a corrected curve is given in Fig. 2.

The above procedure can be used to derive a corrected relation between the concentration in the central plane between colloidal plates and the distance between the plates. According to the Gouy-Chapman theory this relation is, in case of low concentration of the co-ions, given by:

$$b_c = c_c = \frac{\pi^2}{\nu^2\beta(d + x_0)^2} \qquad [19]$$

in which $2d$ = distance between the colloidal plates, and

$$x_0 = \frac{2}{\nu\sqrt{\beta c_c}} \operatorname{arc\,tan} \frac{2\sqrt{c_c}}{\Gamma\sqrt{\beta}} \qquad \text{[cf. ref. 2]}$$

The corrected relation cannot be given explicitly but is plotted in Fig. 3, together with Eq. [19]. The lines correspond to the Gouy theory and the corrected double-layer theory for the case in which the charge density equals 10^{-7} me/cm.^{2}. The difference between the corrected and uncorrected curve is certainly very small.

In addition to the corrections applied so far, the distance of closest approach between ion and surface has to be considered in order to obtain the correct relation between distance of the plates and the central con-

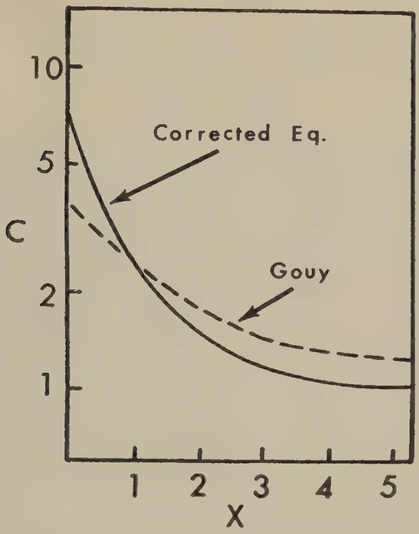

FIG. 2. Relation between the concentration c (in moles per liter) and the distance x (in Angstroms) measured from the surface of a colloidal particle. The density of charge of the surface is 10^{-7} me/cm.^{2}; the distance between the particles equals 10.7 A. (high interaction).

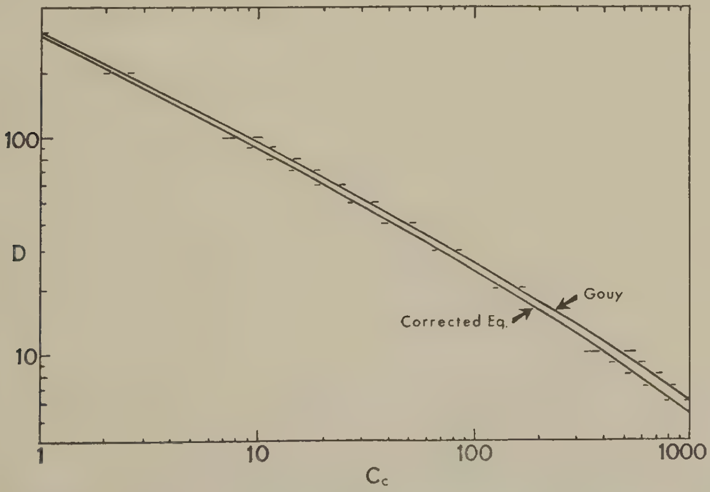

FIG. 3. Relation between the concentration in the central plane c_c (in millimoles per liter) and the distance $2d$ (in Angstroms) between colloidal plates. The surface density of charge is 10^{-7} meq/cm.^{2}.

centration. The effect of this last correction is a shift of the concentration-distance curve over a distance equal to the distance of closest approach. Such a shift (approximately 1–2 A.) brings the corrected curve even closer to the Gouy curve, which leads to the conclusion that the Gouy relations will provide a very dependable basis for the calculation of the concentration in the central plane between colloidal plates.

DISCUSSION

The four corrections introduced in the foregoing treatment, viz., dielectric saturation, polarization of the ion, Coulombic interaction of the ions, and short-range repulsion between the ions have a tendency to balance each other. Dielectric saturation and ionic polarization seem to offset each other almost completely if the field strength does not exceed 5×10^6 volts/cm. ($z = 2 \times 10^8$ cm.$^{-1}$). Since this is roughly equal to the maximum value of the field strength occurring in the double layer formed on plates with a charge density of 2×10^{-7} meq/cm.^{2} ($= 20\ \mu$ Coulomb/cm.^{2}), one can conclude that both effects can be neglected safely for colloids with a charge density equal to or smaller than 2×10^{-7} meq/cm.^{2}. Since the polarization is dependent upon the size of the ion, this term should still be considered if the ratio of different ions present in the double layer is the purpose of the calculation.

For colloids with a charge density exceeding 2×10^{-7} meq/cm.^{2}, the polarization term will increase very rapidly, leading to ionic concentrations much lower than would be expected from the Gouy-Chapman calculations. The applicability of the approximations used in the derivation of the polarization term becomes doubtful in this region, and, therefore, no accurate predictions can be made for this case.

The two other correction terms again tend to balance each other. In this case, however, the Coulombic interaction exceeds the influence of the short-range repulsion probably up to concentrations of 1 or 2 molar. If the concentration exceeds this value, the short-range repulsion will increase very rapidly, eventually limiting the concentration that can exist in the single-ionic solution to a definite ceiling value. A reasonable estimate for this maximum concentration seems 10 to 15 molar. Since the concentration close to a surface carrying a charge density of 10^{-7} meq/cm.^{2} according to Gouy-Chapman is only 2.5 molar, the Coulombic interaction of the ions will be the main correction factor in these systems, although the effect of this correction is partly offset by the short-range repulsion. If the charge density exceeds the value of 10^{-7} meq/cm.^{2} (*e.g.*, 3×10^{-7} meq/cm.^{2}), the short-range repulsion will exceed the influence of the Coulombic interaction in the region close to the particle surface. For even higher values of the charge density the limiting value suggested above will determine the properties of the double layer to a large extent. The balancing effect of the two interaction terms again causes the simple and corrected double-layer theories to be in close agreement, if the charge density does not exceed 2–3 $\times 10^{-7}$ meq/cm.^{2}.

In addition to the above considerations it should be kept in mind that the boundary conditions imposed on the double layer also tend to influence the effect of the proposed corrections. If the charge of the colloid is kept constant, the effects will be somewhat smaller than is the case when the surface potential remains constant. In the specific case of $\Gamma = 10^{-7}$ meq/cm.^{2}, it can be proved that the difference between the concentration in the central plane derived from the Gouy theory and that calculated from the corrected double-layer equation varies between 10 and 30%, depending upon the degree of interaction of the double layer (Figs. 2 and 3).

If, in addition to the effects discussed above, allowance is made for a distance of closest approach between the ions and the colloid surface [which means the acceptance of the outer Helmholtz plane (Grahame, reference 8) as the boundary of the diffuse layer], the difference between the Gouy theory and the corrected double-layer theory becomes even smaller.

The concentration close to the surface is always about doubled as a result of the corrections. This last effect is, however, limited to a very small region (about 1 A.) adjacent to the particle surface.

As to the influence of the corrections on measurable properties of the double layer, the osmotic pressure will be influenced in the same manner as the concentration in the central plane is influenced. The changes to be expected are accordingly small. The capacity of the double layer will be increased slightly, the increase passing through a maximum around a surface density of charge of about 2×10^{-7} meq/cm.^{2}. Above that value the capacity will tend to decrease again, all changes being very small unless excessively high-charge densities are involved. Both conclusions are borne out by practical observations. The measurement of the osmotic pressure of illicit suspensions ($\Gamma = 3 \times 10^{-7}$ meq/cm.^{2}), as described elsewhere (3), gave results in close agreement with the Gouy-Chapman theory. Capacity measurements by Grahame (11) showed that Gouy-Chapman calculations provide a dependable basis for the estimation of the capacity.

In one respect the introduced corrections are of extreme importance. According to the Gouy theory the ratio of ions of equal valence adsorbed in a double layer equals the ratio of these ions in the bulk solutions. Of the introduced correction terms, both the polarization energy and the short-range repulsion between the ions themselves and between the ions and the colloid surface are highly dependent upon the size of the hydrated ion. These correction terms will, therefore, essentially determine the ratio of the adsorbed ions. This effect might conceivably introduce deviations from the Gouy-Chapman theory of the order of a factor 5. Such factors have been observed in the study of the exchange equilibrium in clay systems (2). A careful analysis of the data obtained from these experiments should cast some light on the correctness of the proposed corrections. In addition, these experiments could be used advantageously to obtain information about special cases of short-range attraction between ions and colloid surface, which attraction has been neglected so far. Experiments with clay systems suggest that such interactions occur between K and certain clays.

SUMMARY

Approximate expressions for the influence of dielectric saturation, polarization of ions, and ionic interactions on the structure of the electric double layer were derived and were incorporated in a generalized Poisson-Boltzmann differential equation for the electric double layer. The solution of this extended equation in terms of a correction function, to be applied to the standard Gouy-Chapman treatment of the double layer, showed that in the case of colloid suspension with a low concentration of co-ions (relative to the concentration of counter-ions) these corrections are small, provided the surface density of charge of the colloid does not exceed 2×10^{-7} meq/cm.^{2} (= 20 μ Coulomb/cm.^{2}). Especially the effects of dielectric saturation and polarization of the ions, being opposite in sign, balance each other rather closely. The effect of ionic interaction can be of some magnitude, the maximum effect probably occurring around the mentioned charge density of $2\text{–}3 \times 10^{-7}$ meq/cm.^{2}. Above this value the short-range repulsion will start to exceed the effect of the Coulombic interaction, and eventually lead to a uniform concentration of ions over some distance from the plate. It is expected, therefore, that if the charge density of a colloid does not exceed 2×10^{-7} meq/cm.^{2}, the Gouy-Chapman theory will give fairly reliable results, especially if the charge density of the colloid under consideration is constant.

The conclusions drawn are in agreement with certain experimental observations.

REFERENCES

1. Bikerman, J. J., *Phil. Mag.* [7] **33,** 384 (1942).
2. Bolt, G. H., Physico-chemical properties of the electric double layer on planar surfaces. Ph.D. Thesis, Cornell University, 1954.
3. Bolt, G. H., and Miller, R. D., *Soil Sci. Soc. Am. Proc.*, in print.
4. Böttcher, C. J. F., "Theory of Electric Polarization." Elsevier, Amsterdam, 1952.
5. Chapman, D. L., *Phil. Mag.* [6] **25,** 475 (1913).
6. Conway, B. E., Bockris, J. O., and Ammar, I. A., *Trans. Faraday Soc.* **47,** 756 (1951).
7. Gouy, C., *J. Phys.* **9**(4), 457 (1910).
8. Grahame, D. C., *Chem. Revs.* **41,** 441 (1947).
9. Grahame, D. C., *J. Chem. Phys.* **18,** 903 (1950).
10. Grahame, D. C., *J. Electrochem. Soc.* **98,** 343 (1951).
11. Grahame, D. C., *J. Am. Chem. Soc.* **76,** 4819 (1954).
12. Harned, H. S., and Owen, B. B., "The Physical Chemistry of Electrolytic Solutions." Reinhold, New York 1943.
13. Kruyt, H. R., "Colloid Science," Vol. I. Elsevier, Amsterdam, 1952.
14. Loeb, A. L., *J. Colloid Sci.* **6,** 75 (1951).
15. Stern, O., *Z. Elektrochem.* **30,** 508 (1924).
16. Williams, W. E., *Proc. Phys. Soc.* (*London*) **66,** 372 (1953).

PROPERTIES OF SODIUM ABIETATE FROM AMERICAN COLOPHONY

From Experiments of J. W. McBain's Students (1923–1926)
reported by M. E. L. McBain

Palo Alto, California

Received February 14, 1955

Abstract

The conductivity and osmotic activity of a series of solutions of sodium abietate from colophony have been measured at 90°C., at which temperature they are homogeneous and isotropic. The results indicate that sodium abietate is a colloidal electrolyte.

There was little known of the physicochemical properties of rosin up to 1923, although it was an important component of household soap. It was known to consist largely of abietic acid, whose formula Fahrion (1) concluded was $C_{20}H_{30}O_2$. However, he believed that colophony contained at least two acids, and in 1903 Tschirch (2) isolated three which he designated as α, β, and γ acids. From Ruzicka's (3) work in 1922 "it seems clear that the acid melting at 158° is the one actually present in colophonium and the higher melting acids are formed from it by the action of heat." The fact, as found by us and other investigators, that melting is not sharp but takes place over a range of temperature, supports Ruzicka's conclusion.

After the publication of Steele's (4) method of preparation of crystalline abietic acid in 1922, work was begun in the Bristol laboratories to determine the physicochemical characteristics of the sodium salt. The work is briefly summarized here. Though Ostwald (5) likewise started similar investigations on the abietates in 1923, no other worker, even now, has carried out experiments at 90°C. Harva (6) of the Abo Academy has made a comprehensive study of the properties of Tall Oil Rosin soap at temperatures up to 60°C.

At room temperature the abietate solutions from 1.0 N_w down to 0.15 N_w are heterogeneous, but at 90°C. the higher concentrations remain clear and homogeneous, though the concentrations below 0.05 become turbid and cloudy owing to hydrolysis.

The abietic acid was prepared by Steele's method from American water-white colophony (grade WW) and was finally obtained as pale yellow crystals melting at 158°–161°C. (Steele likewise found the melting point not to be sharp, his value being 158°–162°C.). The molecular weight of the crystals was found to be 300.2 (theory 302.2). A normal solution of sodium abietate was obtained by adding the requisite amount of sodium hydroxide made from sodium drippings and boiled-out water (7). Other concentrations were made from this by adding weighed quantities of water.

The conductivity was measured with a Leeds & Northrup drum bridge, using a telephone as a null-point instrument, standard post office resistances, induction coil, and oil thermostat.

Table I gives the conductivity measurements made by H. H. Kamil.

TABLE I

Equivalent Conductivity and Density Data for Sodium Abietate Solutions at 90.0°C.

Conc., N_w	D_{90}^{90}	D_{4}^{90}	λ
1.00	1.0538	1.0107	81.21
0.50	1.0322	0.9963	113.0
0.2488	1.0236	0.9881	161.0
0.20	1.0175	0.9831	168.7
0.159	1.0145	0.9800	178.7
0.10	1.0110	0.9763	189.7
0.07	1.0087	0.9733	199.2
0.05	1.0067	0.9718	212.9

It will be noticed that the conductivity is high, comparable to other fatty acid soaps. (1.0 N sodium palmitate is 84.66 mhos at 90°C.) Similarly the curve rises with dilution but shows no maximum or minimum. The abietate more closely resembles the caprate or caprylate that likewise show smooth curves.

The osmotic data were obtained from the lowering of vapor pressure using the dew-point method of McBain and Salmon (8). Table II also gives results for sodium oleate included for comparison.

TABLE II

Osmotic Coefficient "g" of Sodium Abietate and Sodium Oleate at 90°C. from Dew-Point Lowering[a], θ

Sodium abietate[b]			Sodium oleate[c]		
Conc., N_w	Dew-Point lowering, °C.	g	Conc., N_w	Dew-Point lowering, °C.	g
1.0	0.42	0.44	0.8	0.12	0.16
0.75	0.33	0.45	0.6	0.16	0.28
0.50	0.28	0.55	0.4	0.13	0.35
	0.26[c]	0.53	0.2	0.08	0.45

[a] $g = \theta/2m \times 1.858$.

[b] Experiments by H. H. Kamil in 1925.

[c] Experiments by H. I. Bull in 1927 with new material.

In evaluating these results, it is interesting to note that the osmotic coefficients of sodium laurate correspond very closely to those of the abietate; the values from published data being 0.35, 0.43, and 0.53 for the 1.0, 0.75, and 0.5 N_w concentrations. The combination of fairly low osmotic activity and fairly high conductivity indicates that sodium abietate also belongs to the class of colloidal electrolytes. This, however, is not as strikingly evident as in the case of the highly colloidal sodium oleate.

Harva draws attention to the fact that Pohle (9) found the surface tension of rosin soap solutions to be more like those of sodium laurate than of other fatty acid soaps.

The sodium abietate solutions here studied showed definite changes with time. Thus the melting point of the abietic acid changes over a period of five months from 158°–162°C. to 145°–149°C. The higher value was restored by recrystallization. Likewise, when the optical rotation was taken at the beginning of an experiment it was $[\alpha]_D^{17.5} = -52.53$, but after two weeks it was $(\alpha)_D^{17.5} = -49.28$.

The implication is that isomeric changes are being reflected in these changing values.

The change with time in conductivity of the solutions was also noticeable, but is not as pronounced. Unlike other soaps, conductivity of sodium abietates increases with time. Thus in Kamil's experiment, the resistance dropped slowly for 8 days, from 237.92 to 224.8 mhos, but thereafter remained constant. As a check on this observation Miss Grant repeated the experiment using 1.0 N_w sodium abietate made by the addition of sodium ethylate in alcohol to crystals obtained from grade I American colophony. She likewise found the resistance to drop during the first 25 hours and thereafter remain practically constant dropping from 229.3 mhos after 2 hours to 224.4 after 25 hours, where it remained during a further 68 hours. The final values of specific conductance obtained by these two experimenters are in good agreement, namely, 0.06218 and 0.06200 mhos.

Harva in his investigation of Tall Oil Rosin soap also found changes of conductivity with time. He attributed it to autoxidation and to the slowness in attaining hydrolytic equilibrium, since he found that hydrogenated rosin soaps r remained constant throughout the 257 hours he studied them.

On cooling the normal solution of sodium abietate two layers separated, the upper being isotropic between crossed Nicols and the lower being anisotropic with a positive angle of extinction. (Microphotographs, using Zeiss Phoku attachment and Gutmann heating stage were made, but the plates are no longer available.) Observations were made of the temperatures at which freshly prepared heterogeneous abietate solutions became homogeneous. Some results are collected in Table III.

TABLE III

Temperature of Homogeneity of Sodium Abietate Solutions

Conc., N_w	1.0	0.5	0.25	0.20	0.15	0.10
Temp., °C.	89.0	61	45	41	35	Room temperature

Again it was noticed that if these temperatures were read after the solutions had been used in the foregoing experiments, they were all lower. The refractive index curve plotted against concentration for fresh solutions is a straight line, whereas for aged and previously used solutions it is concave to the concentration axis.

REFERENCES

1. Fahrion, W., *Z. angew. Chem.* **14,** 1197, 1252 (1901).
2. Tschirch, A., and Studer, B., *Arch. Pharm.* **241,** 495 (1903).
3. Ruzicka, L., and Meyer, J., *Helv. Chim. Acta* **5,** 315 (1922); see also *C.A.* **16,** 2500 (1922).
4. Steele, L. L., *J. Am. Chem. Soc.* **44,** 1333 (1922).
5. Ostwald, W., and Lorenz, R., *Kolloid-Z.* **32,** 119, 195 (1923).
6. Harva, O., Thesis of the Abo Akademie, 1951.
7. Bunbury, H. M., and Martin, H. E., *J. Chem. Soc.* **105,** 418 (1914).
8. McBain, J. W., and Salmon, C. S., *J. Am. Chem. Soc.* **42,** 426 (1920).
9. Pohle, W., *Oil & Soap* **17,** 150 (1940).

NOTE ON THE CONDUCTIVITY OF DILUTE SOLUTIONS OF MYRISTYL SULFONIC ACID

In 1939 a paper (1) reporting on the conductivity of paraffin chain sulfonic acids commented that "the measurements of the most dilute solutions of C_{11} and C_{14} may possibly be affected by some systematic error." With this in mind, the writer repeated the experiments with myristyl sulfonic acid, using more carefully prepared conductivity water and very lightly platinized electrodes. Though a dozen years have elapsed since the work was done, it is worth reporting that one error lay undoubtedly in the sorption by the walls of the cell. It was found that the first reading of each series was always higher than subsequent ones and many samples had to be used before results were obtained which were consistently high and which remained constant.

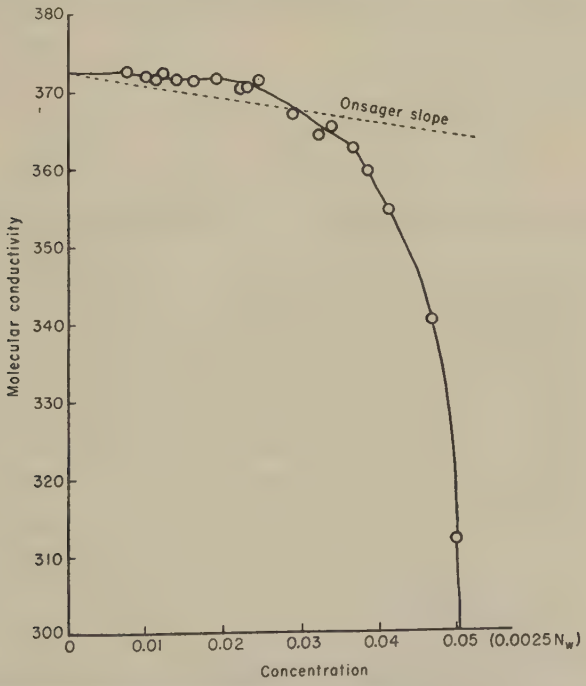

The results for these dilute solutions are plotted above. The greatest dilution used, $0.0000577N_w$, gave an equivalent conductivity of 372.4 mhos, compared with Mr. Dye's 360.5 for his most dilute solution, $0.001089N_w$.

The graph also shows the Onsager slope, calculated from the latest value for myristyl ion, 371.6 (2). It will be seen that the conductivity in this dilute region rises above its infinite dilution value, "a phenomenon which seems to admit of no other interpretation than the formation of (probably small) micelles" (3). This conclusion was also reached in the paper to which this experimental work is an extension. It would probably be found true for all colloidal electrolytes if special care were given to the study of the most dilute solutions.

References

1. McBain, E. L., Dye, W. B., and Johnson, S. A., *J. Am. Chem. Soc.* **61**, 3210 (1939).
2. Gonick, E., *J. Phys. & Colloid Chem.* **50**, 291 (1946).
3. Quoted from Hartley, G. S., Collie, B., and Samis, C. S., *Trans. Faraday Soc.* **32**, 796 (1937).

Stanford University, California
M. E. L. McBain

Received March 1, 1955

THEORY OF THE STABILITY OF LYOPHOBIC COLLOIDS

In 1948 a monograph (1) with the above title appeared from our hand. Recently Professor B. V. Derjaguin drew our attention to a number of papers (2, 3) published by him on the same subject which were not quoted in our monograph. These papers, especially the 1941 paper by Derjaguin and Landau, contain already the essential elements of the theory as treated in our monograph, notably a combination of Van der Waals' attraction with double-layer repulsion for high potentials, applied especially to the deduction of the Schulze-Hardy rule.

We regret greatly to have overlooked these publications, and this note is published to recognize explicitly Derjaguin's and Landau's priority. Professor Derjaguin's earlier publications on the repulsion between weakly charged double layers are of course well known, among them the first calculation of the repulsive force (4) and the first indication of thermodynamically and statistically correct methods for calculating the corresponding free energy (5).

We feel that we may be partly excused for overlooking the papers because all the work for our monograph was performed during the war (*cf.* Preface to the monograph) when we were cut off from all Allied information by the occupation of our country by the German army. The papers (2, 3) were published during this period.

In order to show that our work, although later than Professor Derjaguin's, was performed independently, we wish to point to the existence of a number of publications (6–11) prior to our monograph (1); the 1944 publication, in particular (of which the 1945 one is a nearly literal translation), contains already all the essentials of our work. Moreover the treatment in the monograph is more extended than that by Derjaguin and Landau and often runs along completely different lines. On the other hand, their publication contains remarks that do not figure in our monograph, *e.g.*, a theoretical derivation of Ostwald's rule of activity coefficients (AK Satz).

References

1. Verwey, E. J. W., and Overbeek, J. Th. G., "Theory of the Stability of Lyophobic Colloids." Elsevier, Amsterdam, 1948.
2. Derjaguin, B., *Trans. Faraday Soc.* **36,** 730 (1940).
3. Derjaguin, B., and Landau, L., *Acta Physicochim. U. R. S. S.* **14,** 633 (1941); *J. Exptl. Theoret. Phys.* (*U. S. S. R.*) **11,** 802 (1941); *J. Exptl. Theoret. Phys.* (*U. S. S. R.*) **15,** 662 (1945). This is a second printing of the paper in Russian of (1941).
4. Derjaguin, B., *Bull. acad. sci. U. R. S. S. Classe math. nat., Sér. chim.* (*Russ.*), **5,** 1153 (1937); *Acta Physicochim. U. R. S. S.* **10,** 333 (1939).
5. Derjaguin, B., *Trans. Faraday Soc.* **36,** 203 (1940).
6. Verwey, E. J. W., *Chem. Weekblad* **39,** 563 (1942) (in Dutch).
7. Verwey, E. J. W., Tweede Symposium over sterke electrolyten en over de electrische Dubbellaag, Utrecht, 3 and 4 July 1944, pp. 111–132 (in Dutch).
8. Verwey, E. J. W., *Philips Research Repts.* **1,** 33 (1945) (in English).
9. Overbeek, J. Th. G., Grenslaagverschijnselen, Symposium 5 and 6 July 1946. *Verhandel. Koninkl. Vlaam. Acad. Wetenschap. Belg., Kl. Wetenschap.*, pp. 130–156 (1947) (in Dutch).
10. Verwey, E. J. W., and Overbeek, J. Th. G., *Trans. Faraday Soc.* **42B,** 117 (1946).
11. Verwey, E. J. W., *J. Phys. & Colloid Chem.* **51,** 631 (1947).

Philips Research Laboratories, Eindhoven,
van't Hoff Laboratory, University of Utrecht
E. J. W. Verwey
J. Th. G. Overbeek

Received February 4, 1955

DROPWISE CONDENSATION OF VAPORS AND HEAT TRANSFER RATES

The condensation of saturated vapor on a colder surface is commonly "filmwise." Water condensate, under some conditions, fails to wet metallic surfaces and forms discrete droplets, "dropwise condensation." Dropwise condensation of water on metal has been achieved in the past (1) by coating the metal with stearic acid, benzyl mercaptan, or similar materials. These promoters of dropwise condensation are dissolved and removed by the condensate after a relatively brief time, but so long as they are effective, heat transfer rates an order of magnitude greater than those expected during filmwise condensation are observed.

We have been able to prepare stable surfaces of sufficiently low surface energy so that steam and also three different organic vapors were condensed in the dropwise manner. Some details of the condensation are given below. This appears to be the first demonstration of the dropwise condensation of organic liquids (low–surface-energy liquids). Heat transfer coefficients have not yet been measured for this process, but it is expected that the improvement in heat-transfer rates in the dropwise condensation of organic vapors may give this technique commercial interest.

The low-energy surfaces were prepared by coating clean polished brass with a commercial "Teflon" finish, the DuPont "Teflon" Primer for Aluminum (850-202). This is a dispersion containing about 50% of tetrafluoro-ethylene. One part of the primer was diluted with 80 of distilled water containing 0.8 part of a wetting agent, Aerosol OT (clear 25%). The coatings prepared were about 20,000 Ångstrom units thick.

We have condensed the following compounds, as dropwise films; the condensing temperature and corresponding surface tension of the liquid are indicated: water (100°C., 58.9 dynes/cm.), ethylene glycol (120°C., 37.8 dynes/cm.), nitrobenzene (110°C., 33.3 dynes/cm.), aniline (110°C., 32.5 dynes/cm.). Benzene (80°C., 21.3 dynes/cm.) condensed as a continuous film.

This work has been supported by a grant from Research Corporation.

Reference

1. McAdams, W. H., "Heat Transmission." McGraw-Hill, New York, 1954.

Department of Chemical Engineering
The Johns Hopkins University
Baltimore, Maryland

Leonard Topper
Eric Baer

Received January 19, 1955; revised received February 25, 1955

PHASE-CONTRAST MICROSCOPY OF NATURAL RUBBER LATICES (MORPHOLOGY OF THE RUBBER PARTICLES IN NATURAL LATICES)

The possibilities of phase-contrast microscopy for the investigation of rubber and plastics have already been mentioned in the book of Bennet and co-workers on "Phase Microscopy" (1). Nevertheless these authors have so far not been able to establish results with regard to the structure of rubber hydrosols by this experimental method.

Of course the resolving power of the electron microscope is much higher than that of the phase-contrast microscope, but with the latter studies can be made on a liquid object (hydrosol) without difficulty, thus permitting in many cases completion of investigations on colloidal systems by light scattering (2, 3).

To obtain maximum resolving power with a normal light microscope one must, according to Gottschewski (4), use a dark-field condensor and a phase-contrast objective.

The present authors used the Ortholux, made by Leitz company, with the dark-field condensor D 120 17, phase-contrast objective Pv 90/115, in combination with periplane 10× for the investigation of the latices of the following plants: *Hevea brasiliensis*, *Ficus elastica*, *Ficus Nekbudu*, *Manihot dichotoma*, *Castilloa nicoyensis*, *Manilkara balata*, *Cryptostegia grandiflora*.

Some of the larger spherical particles in these latices seemed, even in the fresh state, to be built up from other spherical particles of much smaller diameter, but it was difficult to record this photographically because of the vigorous Brownian movement of the particles.

Checking of the movement by addition of agar led to the structure's becoming less clearly visible and disappearing into the strong light with time.

Following the method used by Brown (5) in the investigation of G.R.S. latex and the experimental procedure of Bradford (6), the latex, after purification, was fixed by bromination. This showed up the above-mentioned morphological structure in almost all clearly visible spherical, oval, and pear-shaped particles.

It was subsequently found, that by adding 1%–2% NaOH to the latex the grapelike arrangement also becomes clearly visible after a few days (probably because of hydrolysis of the proteins on the particles surface) and could thus be recorded photographically.

From these findings the authors conclude that:

1. All rubber particles in natural rubber latices with a diameter of more than approximately 400 A. are secondary colloidal particles, built up from smaller spherical particles.

The secondary particles are for the greater part spherical, pear-shaped, or oval, but in one case (*Manihot*) spherical particles form linear secondary particles.

2. By coagulation processes the different secondary particles may disappear again, the structure of the hydrogel being determined more or less only by the smaller particles, but it has not yet been possible to establish that these are really primary particles. Possibly these are an intermediate size of relatively stable secondary particles.

3. As the same holds for polyvinyl-acetate latex it may be concluded with some caution that the existence of secondary particles is a common building principle in colloidal systems of the Sol-type. One can assume

that in many cases the real primary colloidal particle will be the polymeric molecule.

4. A possible explanation for the existence of stable secondary particles, especially in latices, is that the polymerization center of the plant (perhaps the vacuole of the lutoids) becomes completely filled up by primary rubber particles. The skin of the vacuole remains as a protective layer on the surface of the secondary particles so formed, thus stabilizing them until this layer becomes removed by hydrolysis of the protoplasma with acids, NaOH, enzymes, or otherwise and so effecting coagulation of the latex.

References

1. Bennet, A. H., Osterberg, H., Jupnik, H., and Richards, O. W., "Phase Microscopy." John Wiley & Sons, Inc., New York, 1951.
2. Debye, P., *J. Appl. Phys.* **15,** 338 (1954); *ibid.* **17,** 392 (1946).
3. La Mer, V. K., *J. Phys. & Colloid Chem.* **52,** 65 (1948).
4. Gottschewski, G. H. M. *Z. wiss. Mikroskop.* **61,** 185 (1953).
5. Brown, W., *J. Appl. Phys.* **18,** 273 (1947).
6. Bradford, E. B., *J. Appl. Phys.* **23,** 609 (1952).

A manuscript with photographs was received by the editor August 9, 1954, part of which will be published in a German journal and part, in the Archives of Rubber Cultivation.

Foundation for Rubber
Research and Development
Bogor, Indonesia

Th. G. F. Schoon
K. L. Phoa

Received August 9, 1954;
revised December 20, 1954.

Book Reviews

Adhesion and Adhesives. Fundamentals and Practice. Papers read at a Symposium held at Case Institute of Technology in Cleveland, Ohio, and a Conference held in London, England. Edited by Clark, Rutzler, and Savage (mentioned on the binding only, not on the title page). John Wiley & Sons, New York, 1954. 229 pp., Price $9.75.

In April 1952 two conferences on adhesion were held. The papers presented at the British conference were preprinted and reached American shores over two years ago. Now they appear combined with those read in Cleveland and supplemented by discussion reports. It is not stated in the book which paper belongs to which symposium but, presumably, this omission won't worry the future historian of our science.

I believe that these future historians will be fascinated by the book. It fixes, for posterity to see, the deplorable state of our ideas on the nature of adhesion and the function of adhesives. When the main problems of adhesive joints are settled, the scientists of those days will be able to judge the progress achieved by contrasting their knowledge with our groping.

Will this progress be accelerated by the publication under review? Perhaps—if the discrepancies in the book don't frighten away a potential leader in the adhesives research.

The book consists of two parts: "Fundamentals" includes 14 contributions and "Practice" has 29. Some of the "fundamental" papers have no apparent relation to the "practice" treated in the second part. The most common fallacies (*i.e.*, statements which the reviewer believes to be false) of the theoretical part are: (1) it is mplicitly assumed that the strength of an adhesive joint is determined by the molecular attraction between adhesives and adherends, and (2) experimental values of a failing load are trusted as if they were material constants, independent of the method and the instrument used.

The "practical" part brings a host of interesting but, naturally, disconnected observations. A detailed comment on these would be out of place in a review.

The book has neither a subject nor an author index.

J. J. Bikerman, New York, N. Y.

Synthetic Rubber. Editorial Board: G. S. Whitby (ed. in chief), C. C. Davis, and R. F. Dunbrook. John Wiley & Sons, Inc., New York, and Chapman & Hall, Ltd., London, 1954. 1044 pp. Price $18.00.

The development of the synthetic rubber industry was certainly one of the major echnical achievements forced upon the United States by World War II and here eceives fitting commemoration in a volume prepared under the auspices of the Division of Rubber Chemistry of the American Chemical Society. Although the rganization of the topics has been in the hands of an editorial board, ably headed by Professor G. S. Whitby of the University of Akron, the actual writing has been by some 38 specialists in the field of synthetic rubber technology. This has permitted a particularly broad coverage of all technical aspects of the field. Thus the book not only covers such expected topics as synthetic rubber manufacture, testing, procssing, and uses, it also treats the related subjects of butadiene and styrene manufacture and contains accounts of German synthetic rubber manufacture and some of the surveys carried out of other types of diene polymers and copolymers investigated on an experimental basis during the war and subsequently.

To the reader not immediately concerned with some phase of rubber technology, probably the most fascinating feature is the history and chronology of synthetic rubber development which appears in the first two chapters and is amplified in the opening paragraphs of many of the specialized sections. As far as I know, all this material has never been brought together before and should be of lasting interest not only to scientists but to students of the interaction of government and industry during the war period.

Inevitably in such an encyclopedic production by a number of authors, some topics receive more attention than others, and if anything is slighted it is the basic theory underlying free radical and emulsion polymerization processes, which is treated only rather cursorily in Chapter 8. Although such information is available elsewhere, as in P. J. Flory's *Principles of Polymer Chemistry*, the important contributions to basic scientific knowledge coming from synthetic rubber research seem to merit more notice than they receive. On the other hand, Marvel and Baumgarten have given a rather detailed discussion of the chemical structure of synthetic rubber and diene polymers in general, which has not been assembled elsewhere.

In summary, this book serves really two purposes, as a permanent memorial to the wartime synthetic rubber program and as a current guide to synthetic rubber technology, and should be of real value to readers interested in either of these fields.

CHEVES WALLING, New York, New York

Errata

Volume 9, Number 6, "Viscosity Behavior of Sodium Carboxy Methyl Cellulose in Water at High Dilutions," by H. Fujita and T. Homma

Page 595, legend to Figure 1, "30°C." should read "25°C."

Page 600, line nine from bottom, "30°C." should read "25°C."

ELECTROSTATIC FORCES BETWEEN NONIDENTICAL COLLOIDAL PARTICLES

Arthur Bierman[1]

Fellow of the National Foundation for Infantile Paralysis, Columbia University, Zoology Department, New York City

Received February 11, 1955; revised April 11, 1955

Abstract

The Verwey-Overbeek theory is extended to nonidentical particles and shown to e in need of revision. This revision is carried through by introducing an interaction ependent ψ_0. It is shown that attractive forces can arise between nonidentical lates at small distances. The conditions for this attraction and the range of this orce are calculated. It is shown that the range can be as large as a few hundred Angtroms.

Notation

$\psi(x, y, z)$ = electrostatic potential

D = dielectric constant

ρ = charge density per unit volume

ϵ = elementary charge

ν_i = valence of the i'th ion

$_i(x, y, z)$ = number of ions of the i'th species per unit volume at x, y, z

n_{i_0} = number of ions of the i'th species per unit volume at infinity

k = Boltzmann constant

T = absolute temperature

P = pressure

F = force

σ_i = charge density per unit area of the i'th surface

μ = chemical potential

N_i^* = total number of sites available per unit area of the i'th surface to the cation

S_i^* = total number of sites available per unit area of the i'th surface to the anion

c_{0_i} = isoelectric medium concentration of the cation for the i'th surface

$\underline{c}_{0_i}$ = isoelectric medium concentration of the anion for the i'th surface

---

[1] Present address: Physics Department, Columbia University, N. Y. City.

c = cation concentration in the medium
$\underline{c}$ = anion concentration in the medium
N_{0_i} = isoelectric concentration of the ion on the i'th surface
$\bar{\mu}$ = molarity of the medium ions
$M = \sum_{i=1}^{n/2} n_{i_0}$

One of the important problems of colloid science is the determination of the nature and magnitude of forces involved in the interaction of highly charged lyophobic colloids immersed in an electrolytic solution.

The theory of this interaction was placed on a firm footing by Verwey and Overbeek (1), who limited themselves, however, to a consideration of identical particles. In this paper we shall extend the theory to nonidentical particles.

I. THEORETICAL FUNDAMENTALS

Lyophobic colloids consist of macromolecular particles in an electrolytic medium, which particles have no affinity for the solvent. Solvation plays therefore no significant role, and the electrostatic potential becomes the main focus of investigation.

If we have an arbitrary, charge-bearing surface in a medium containing charges, the electrostatic potential ψ can be calculated from the Poisson equation:

$$\nabla^2\psi = -\frac{4\pi}{D}\,\rho(x, y, z). \qquad [1]$$

When the system is in equilibrium, the charge density ρ can be calculated from:

$$\rho(x, y, z) = \sum_i \epsilon\nu_i n_i(x, y, z) = \sum_i \epsilon\nu_i n_{i_0} e^{-(E(x,y,z)/kT)} \qquad [2]$$

The energy $E(x, y, z)$ in the Boltzmann distribution consists of a number of terms, the most important of which is the electrostatic energy $\epsilon\nu_i\psi(x, y, z)$. If all other contributions are ignored, Eq. [1] becomes:

$$\nabla^2\psi = -\frac{4\pi\epsilon}{D}\sum_{i=1}^{n} \nu_i n_{i_0} e^{-(\epsilon\nu_i\psi/kT)} \qquad [3]$$

Equation [3] is the Poisson-Boltzmann (P.B.) equation and represents the foundation of a good part of the theory of the interaction of colloidal particles.

Limiting ourselves to one dimension, [3] becomes:

$$\frac{d^2\psi}{dx^2} = -\frac{4\pi\epsilon}{D}\sum_{i=1}^{n} \nu_i n_{i_0} e^{-(\epsilon\nu_i\psi/kT)}, \qquad [4]$$

which can be immediately integrated as follows:

$$\frac{d\psi}{dx}\frac{d^2\psi}{dx^2} = -\frac{4\pi\epsilon}{D}\sum_{i=1}^{n} \nu_i n_{i_0} \frac{d\psi}{dx} e^{-(\epsilon\nu_i\psi/kT)}. \tag{5}$$

Hence:

$$\left(\frac{d\psi}{dx}\right)^2 = \frac{8\pi kt}{D}\sum_{i=1}^{n} n_{i_0} e^{-(\epsilon\nu_i\psi/kT)} + C_1. \tag{6}$$

The second integration follows from [6]:

$$\int \frac{d\psi}{\sqrt{\dfrac{8\pi kT}{D}\sum_{i=1}^{n} n_{i_0} e^{-(\epsilon\nu_i\psi/kT)} + C_1}} = \pm\int dx + C_2. \tag{7}$$

If C_1 and C_2 are evaluated from the boundary conditions, ψ can be solved for from Eq. [7]. A detailed discussion of the above for the case $n = 2$ can be found in the treatise by Verwey and Overbeek.

Our main interest, on the other hand, does not lie in the calculation of the potential but in the determination of the *force* between two charge-bearing surfaces. There exist various ways of accomplishing this, and we shall in particular consider the case of two infinite parallel plates, one at $x = 0$, the other at $x = l$.

For every volume element of solution between these plates to be in equilibrium, the pressure gradient and electrostatic force must cancel:

$$\frac{dP}{dx} + \rho\frac{d\psi}{dx} = 0. \tag{8}$$

Equation [8] can be integrated, using Eq. [1]. We find:

$$P - \frac{D}{8\pi}\left(\frac{d\psi}{dx}\right)^2 = C_3. \tag{9}$$

Hence, at every point in solution the difference between the pressure and Maxwell's stresses is a constant. This constant must be the force pushing the plates apart. It is counteracted by the pressure which the solution exerts in back of each plate and is equivalent to the pressure at infinity. Hence, the force is given by:

$$F = P(x) - P_\infty - \frac{D}{8\pi}\left(\frac{d\psi}{dx}\right)_x^2. \tag{10}$$

From Eq. [8]:

$$\begin{aligned} P(x) - P_\infty &= \int_\infty^x dP = \int_x^\infty \rho\, d\psi \\ &= \sum_{i=1}^{n} \epsilon\nu_i n_{i_0} \int_x^\infty e^{-\epsilon\nu\psi/kT}\, d\psi, \end{aligned}$$

and, since $\lim_{x\to\infty}\psi(x) = 0$:

$$P(x) - P_\infty = kT\sum_{i=1}^{n} n_{i_0}(e^{-\epsilon\nu_i\psi/kT} - 1). \qquad [11]$$

The force becomes then:

$$F = kT\sum_{i=1}^{n} n_{i_0}(e^{-\epsilon\nu_i\psi/kT} - 1) - \frac{D}{8\pi}\left(\frac{d\psi}{dx}\right)_x^2. \qquad [12]$$

Equation [12] can also be derived from an extension of an argument due to Langmuir (2). As is well known, the existence of a charged surface in an electrolytic medium gives rise to a diffuse double layer. This leads to a difference in osmotic pressure between the solution in front of and behind the charged surface. It is given by:

$$\begin{aligned} P &= kT[n(x) - n_\infty] \\ &= kT\sum_{i=1}^{n} n_{i_0}[e^{-\epsilon\nu_i\psi(x)/kT} - 1]. \end{aligned} \qquad [13]$$

This is the force exerted from this volume element at x against the plates, tending to push them apart. On the other hand, each volume element containing a charge density ρ also experiences a force $\frac{D}{8\pi}\left(\frac{d\psi}{dx}\right)^2$ drawing it toward the plate; hence a force of equal magnitude is exerted on the plate charges by the charges in that volume element. The total repulsive force, therefore, exerted per unit volume, on the plates, is:

$$F = kT\sum_{i=1}^{n} n_{i_0}[e^{-\epsilon\nu_i\psi(x)/kT} - 1] - \frac{D}{8\pi}\left(\frac{d\psi}{dx}\right)^2. \qquad [14]$$

Equation [14] is identical with [12].

We can now use Eq. [6] in [14], resulting in:

$$F = -\frac{D}{8\pi}C_1 - kT\sum_{i=1}^{n} n_{i_0}. \qquad [15]$$

Equation [15] will now be evaluated for two simple cases treated already by Verwey and Overbeek.

1. If we are dealing with a single plate, ψ as well as $d\psi/dx$ are zero at infinity. Hence, from Eq. [6]:

$$C_1 = -\frac{8\pi kT}{D}\sum_{i=1}^{n} n_{i_0}, \qquad [16]$$

and the force becomes zero, as expected.

2. If we have two identical plates, i.e., $\psi(0) = \psi(l)$, the potential will then have a minimum at $x = l/2$; $d\psi/dx$ is therefore zero at $l/2$, and, from [6]

$$C_1 = -\frac{8\pi kT}{D}\sum_{i=1}^{n} n_{i_0} e^{-(\epsilon\nu_i/kT)\psi(l/2)}. \qquad [17]$$

This results in:

$$F = kT\sum_{i=1}^{n} n_{i_0}[e^{-(\epsilon\nu_i/kT)\psi(l/2)} - 1]. \qquad [18]$$

If we are dealing with a single species of electrolytes, $n = 2$, $\nu_1 = -\nu_1$, Eq. [18] reduces to:

$$F = 2kTn_0\left[\cosh\frac{\epsilon\nu\psi(l/2)}{kT} - 1\right], \qquad [19]$$

which is the expression developed by Verwey and Overbeek, Langmuir, etc. It is always a repulsive force.

The above considerations enable us now to proceed to an examination of the forces between nonidentical particles.

II. NONIDENTICAL PARTICLES

The evaluation of the force requires the proper determination of the constant C_1, which in turn means the proper determination of boundary conditions. Verwey and Overbeek discussed the relative advantages of settling upon either ψ_0 or σ as being independent of interaction, and concluded that it was physically preferable to consider the surface potential ψ_0 as a constant of l. This can be justified by the following thermodynamic argument.

The charge on the particle surface has its origin in the adsorption of potential determining ions from the solution onto the surface. There must exist therefore a drop in the chemical potential between solution and surface. This migration of ions is opposed by an electric potential $\epsilon\nu\psi_0$. At equilibrium the two must balance:

$$\epsilon\nu\psi_0 + \Delta\mu = 0. \qquad [20]$$

The chemical potential difference depends on two factors: the ion concentration c in solution and its concentration on the surface. If we assume, as a first approximation, that the latter contribution is negligible, ψ_0 becomes:

$$\psi_0 = \frac{kT}{\epsilon\nu}\ln\frac{c}{c_0}. \qquad [21]$$

Hence, Verwey and Overbeek conclude that ψ_0 is independent of the interaction distance l.

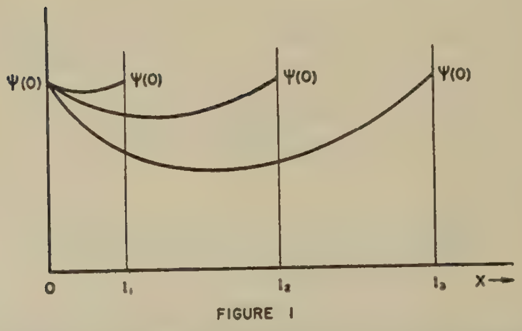

FIG. 1. The family of curves $\psi(x)$, for various l, for two identical particles.

Since they limited themselves to a consideration of identical particles, the argument with its boundary conditions led to proper conclusions. But if an extension of the theory to nonidentical particles is attempted, it becomes at once apparent *that neither σ nor ψ_0 can be selected as constant without ending up with physically impossible results.*

This can be seen from the following argument. The P.B. equation gives us $\psi(x)$ as a function of the interaction distance l between two plates. For two identical particles, a family of curves results as shown in Fig. 1. It is seen that the minimum of $\psi(x)$ increases with increasing interaction and that the curve approaches a horizontal line in the limit as l approaches zero. From Gauss's law, therefore, the charge densities on the two plates approach zero for large interaction.

But if we now fix $\psi(0) \neq \psi(l)$ and cause these two *nonidentical* plates to approach, $\psi(x)$ must clearly acquire a larger and larger slope which will ultimately become infinite for zero distance. The charge densities become therefore also infinite—a physically absurd conclusion. The above physical argument (represented in Fig. 2) can be confirmed in a straightforward manner by an examination of the first and second integrations of the P.B. equation.

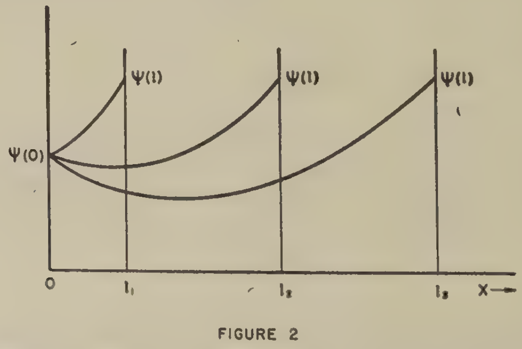

FIG. 2. The family of curves $\psi(x)$, for various l, for two nonidentical particles.

The need for a revision of the theory is clearly indicated. In particular, the artificial constancy of ψ_0 must be removed. This means, more specifically, that we must find some reasonable physical argument whereby ψ_0 can be determined as a function of the interparticle distance l, or of some other l-dependent function.

We also know from the above arguments that this functional dependence of $\psi(0)$ and $\psi(l)$ on l must have the property that, as l approaches zero, $\psi(0)$ and $\psi(l)$ must become identical. For otherwise an infinite charge density is again indicated.

It is not very difficult to find the physical conditions which can determine ψ_0. All we need to do is to remember that the l independence of ψ_0 was established by a thermodynamic argument which ignored the contribution of the surface chemical potential. It is therefore immediately suggested that we include the surface chemical potential in the equilibrium determination of ψ_0. This inclusion leads directly to the revised theory.

III. THE REVISED THEORY

Consider a surface of an infinite plate immersed in an electrolytic medium. A given kind of cation can migrate from the solution and be adsorbed on open sites of the surface. The plate has also a given negative charge density which is assumed here to be independent of the ions in solution. (This latter approximation can be removed without affecting the argument or its conclusions.) Let N^* be the total number of these sites available per unit area to the cation, let N_0 be the number of these sites filled when the surface is neutral, and let c_0 be the ion concentration in solution at infinity when the plate is isoelectric. Further, let N and c represent the surface and medium concentration, respectively, of the ion for some arbitrary state of the system. We shall further assume that the ions do not interact in any way on the surface except for the crowding effect. The chemical potentials of the ion on the surface and in solution are given by:

$$\begin{aligned} \mu(\text{surface}) &= \mu_{0_s}(T, P) + kT \ln \frac{N}{N^* - N} \\ \mu(\text{medium}) &= \mu_{0_m}(T, P) + kT \ln c. \end{aligned} \qquad [22]$$

The surface potential in [22] can be derived quite simply from statistical mechanical considerations and amounts to introducing a Langmuir-type adsorption isotherm.

If N sites are filled at an ionic concentration c, $\Delta\mu$ is given by:

$$\Delta\mu = \mu_{0_s} - \mu_{0m} + kT \ln \frac{N}{c(N^* - N)}$$

or, considering the definition of c_0 and N_0:

$$\Delta\mu = kT \ln \frac{c_0 N(N^* - N_0)}{c N_0(N^* - N)}. \qquad [23]$$

From Eqs. [20] and [23],

$$\psi(0) = \frac{kT}{\epsilon\nu}\left[\ln \frac{c}{c_0} - \ln \frac{N(N^* - N_0)}{N_0(N^* - N)}\right]. \qquad [24]$$

This is now the required relationship between ψ_0 and l, since N is a function of l from Gauss's law.

IV. APPLICATION OF THE THEORY TO NONIDENTICAL PARTICLES

To apply the theory to nonidentical particles it is necessary to establish the over-all shape of the $\psi(x)$ curves between such particles, for various l. As was shown in Fig. 1, in the case of two identical particles the curve drops to a minimum halfway between the two plates. It seems reasonable to assume that if two nonidentical particles are some distance apart, the curve will also have a minimum, although probably not in the central plane.

But what happens at close distance? We must remember here that electro-neutrality has to be preserved in the limit as l approaches zero. Hence the two charge densities are either zero or of equal magnitude but opposite in sign for maximum interaction. If the two charge densities are zero, the minimum will keep rising as l decreases, but will remain a minimum for all l, regardless how small. This would also be made feasible by the physical requirement that the two surface potentials come closer and closer to each other for large interaction. If, on the other hand, $\lim_{l\to 0} \sigma_1 = -\sigma_2$, the curve must lose its minimum at some small l and rise from one surface to the other. In that case, then, the charge density on one plate will have reversed its sign and the two plates will be oppositely charged from that point on.

These two alternatives can be evaluated from a consideration of Eq. [24]. If the charge densities become zero, then N_i becomes N_{i_0} at $l = 0$, and hence:

$$\lim_{l\to 0} \begin{array}{l} \psi_{0_1} = \dfrac{kT}{\epsilon\nu} \ln \dfrac{c}{c_{0_1}} \\ \psi_{0_2} = \dfrac{kT}{\epsilon\nu} \ln \dfrac{c}{c_{0_2}}. \end{array} \qquad [25]$$

But we must also require that $\lim_{l\to 0} \psi_{0_1} = \psi_{0_2}$; therefore, a minimum can exist for all l only if $c_{0_1} = c_{0_2}$. This is of course a very special case for two nonidentical plates, and we can conclude that if the isoelectric points of two nonidentical plates are *not* the same, there will exist a certain l^* for which $\psi(x)$ ceases to have a minimum and rises from the surface with the smaller potential to that with the larger. This in turn means an electrostatic attraction which could conceivably become larger than the repulsive osmotic pressure.

Without solving for C_1, which is a function of l, we can use Gauss's law.

$$\begin{aligned} \sigma_1 &= -\frac{D}{4\pi}\left(\frac{d\psi}{dx}\right)_0 \\ \sigma_2 &= \frac{D}{4\pi}\left(\frac{d\psi}{dx}\right)_l \end{aligned} \qquad [26]$$

and hence, from [6]:

$$\begin{aligned} \sigma_1 &= -\frac{D}{4\pi}\sqrt{\frac{8\pi kT}{D}\sum_{i=1}^{n} n_{i_0} e^{-\epsilon\nu_i\psi_0/kT} + C_1} \\ \sigma_2 &= \frac{D}{4\pi}\sqrt{\frac{8\pi kT}{D}\sum_{i=1}^{n} n_{i_0} e^{-\epsilon\nu_i\psi(l)/kT} + C_1} \end{aligned} \qquad [27]$$

It can be seen from [27] that σ_1 becomes $-\sigma_2$ in the limit as l approaches zero. Furthermore, this resultant symmetry is independent of the parameters of the two plates.

We turn now to Eq. [24], in order to establish its physical validity; this must be shown in the identity of $\psi(0)$ and $\psi(l)$ for $l = 0$.

Assume that the condition is not satisfied. Then the slope will become increasingly large for small l, and therefore also the charge density on the first plate will become increasingly negative. But, as soon the charge density takes on the finite value $-N_{1_0}$ (for which N_1 is zero), the potential ψ_0 becomes infinite. Since this occurs for a finite value of the slope, this result is mathematically unacceptable. Hence, Eq. [24] must satisfy the physical requirement of the identity of the two potentials for maximum interaction.

We shall now investigate the conditions for which short-range attractive forces can arise between nonidentical particles. There are two ways of doing so. One is to examine the force at maximum interaction, i.e., $l = 0$. This follows from [12]:

$$F(0) = kT\sum_{i=1}^{n} n_{i_0}\left[e^{-\epsilon\nu_i\psi(0)/kT} - 1\right] - \frac{2\pi}{D}\sigma^2. \qquad [28]$$

If [28] is negative the force is attractive; it can be evaluated by using the conditions:

$$\left.\begin{aligned} \psi(0) &= \psi(l) \\ \sigma_1 &= -\sigma_2 \end{aligned}\right\} \quad \text{for} \quad l = 0. \qquad [29]$$

This procedure, although simple, involves extensive calculations and will not be attempted here.

We shall instead investigate the possibility of an attractive force from the standpoint of the conditions permitting the force to become zero at some finite l^*. For all l smaller than this, the force is attractive, and hence the above procedure enables us also to determine the range of attraction. For these purposes we shall simplify the model to some extent by assuming that $|\nu_i| = |\nu_j|$ for all i, j. Hence:

$$\begin{aligned}\sum_{i=1}^{n} n_{i_0} e^{-\epsilon\nu_i\psi/kT} &= 2\left(\sum_{i=1}^{n/2} n_{i_0}\right)\cosh\frac{\epsilon\nu\psi}{kT} \\ &= 2M\cosh\frac{\epsilon\nu\psi}{kT}.\end{aligned} \qquad [30]$$

Setting $z_1 = \dfrac{\epsilon\nu\psi(0)}{kT}$, $z_2 = \dfrac{\epsilon\nu\psi(l)}{kT}$, $\Omega_i = \dfrac{cN_{0_i}}{c_{0_i}(N^*_i - N_{0_i})}$, and using Eqs. [24], and [26]:

$$e^{z_i} = \frac{\Omega_i[\epsilon\nu(N^*_i - N_{0_i}) - \sigma_i]}{\sigma_i + \epsilon\nu N_{0_i}}. \qquad [31]$$

Solving for σ_i:

$$\sigma_i = \frac{\epsilon\nu N_{0_i}\left[\dfrac{c}{c_{0_i}} - e^{z_i}\right]}{\Omega_i + e^{z_i}}. \qquad [32]$$

From Eqs. [26], [32], and [6] C_1 can be determined.

$$\begin{aligned}C_1 = {} & \frac{16\pi}{D^2(e^{z_i} + \Omega_i)^2} \\ & \cdot\left\{\pi\epsilon^2\nu^2 N_{0_i}^2\left[\frac{c}{c_{0_i}} - e^{z_i}\right]^2 - kTDM\cosh z_i(e^{z_i} + \Omega_i)^2\right\}.\end{aligned} \qquad [33]$$

If there exists an l^* for which the force becomes zero, the constant C_1 must then have the value of:

$$C_1 = -\frac{16\pi kT}{D}M. \qquad [34]$$

Substituting [34] into [33] results in:

$$\pi\epsilon^2\nu^2 N_{0_i}^2\left[\frac{c}{c_{0_i}} - e^{z_i}\right]^2 - kTDM(\cosh z_i - 1)(e^{z_i} + \Omega_i)^2 = 0. \qquad [35]$$

Furthermore, Eq. [34] also enables us to integrate [7] from $x = 0$ to $x = l$. It leads to:

$$\int_0^l dx = \frac{kT}{\epsilon\nu}\sqrt{\frac{D}{16\pi kTM}}\int_{z_1}^{z_2}\frac{dz}{\sqrt{\cosh z - 1}} \qquad [36]$$

which in turn can be evaluated:

$$l^* = \sqrt{\frac{DkT}{8\pi M\epsilon^2\nu^2}} \ln \frac{\tanh z_2/4}{\tanh z_1/4}. \quad [37]$$

To examine this more concretely, we select $z_1 = 0.5$ volt, $z_2 = 5$ volts, and set M equal to $\bar{\mu}N$, where N is Avogadro's number. The coefficient $\bar{\mu}$ is then the molarity of the ions in solution. Substituting these values into [37] results in:

$$l^* = 1.5 \times 10^{-9} \text{ cm.}/\sqrt{\bar{\mu}}. \quad [38]$$

If $\bar{\mu} = 10^{-4}$, $l^* = 15$ A; if $\bar{\mu} = 10^{-6}$, $l^* = 150$ A.

It can also be established by simple substitution that the above values for z_i and M are compatible with Eq. [32], if N_i^* and c/c_{0_i} obey certain specified relations. In particular, for $z = 5$ volts, $c/c_{0_2} > 148$, since σ_2 is positive.

We can also evaluate σ_2; if $\bar{\mu} = 10^{-4}$, we find that

$$\sigma_2 = 6.85 \times 10^4 \text{ e.s.u./cm.}^2$$

$$= 1.4 \times 10^{14} \text{ charges/cm.}^2.$$

Similar operations can be carried out for the first plate, and restrictions are again found for the various parameters. In particular it is required that $c/c_{0_1} < 1.6$.

The above indicates that an attractive force is possible between non-identical plates, but that it depends upon very large differences in the isoelectric concentrations.

One other interesting question is the dependence of the force on the ionic strength of the medium. This can be examined most easily from [28]. Since σ and $\psi(0)$ are here independent of the ion concentration, the only relation enters via Σn_{i_0}. This indicates that the repulsive part of the force is directly proportional to the ionic concentration.

V. EXTENSION OF THE THEORY TO MORE THAN ONE IONIC SPECIES

Equation [24] was developed on the basis that only one given ion was adsorbed on open sites; the surface charges of the other sign were assumed to be independent of the medium. This is clearly a special case of the more general situation where both positive and negative charges adsorb from the medium.

Furthermore, one uncomfortable aspect of the theory as developed until now is the heavy dependence of the attractive force and its range on very large differences in the isoelectric concentrations. We therefore examine the more general theory of multiple adsorption with the hope that the conditions of attraction will prove here to be less rigid.

The extension of the theory is quite straightforward as long as we assume that the adsorption of these ions are independent of each other, except in so far as there are a limited number of sites available per unit area for the cation as well as for the anion. Equation [24] is therefore still valid, but [31] and [32] no longer hold.

To be specific: let S_i^* be the total number of available sites for the anion per square centimeter on the i'th plate, let S_i be the actual number of such sites filled, and $\underline{c}_i$ the anion concentration in the medium. The charge density is then given by:

$$\sigma_i = \epsilon\nu(N_i - S_i) \qquad [39]$$

on the assumption that the valence of the cation and that of the anion are identical in magnitude. At the isoelectric point, $N_i = S_i = N_0$; the corresponding medium concentrations are c_{0_i} and $\underline{c}_{0_i}$ for the cation and anion, respectively.

There are now two separate equations for the equilibrium potential ψ_0 , as given by [20]. One relates to the $\Delta\mu$ of the cation and yields Eq. [24]. The other is

$$\Delta\bar{\mu} - \epsilon\nu\psi_0 = 0, \qquad [40]$$

where $\Delta\bar{\mu}$ is the change in chemical potential of the anion. Using the same reasoning as with respect to the cation we find the second equation for ψ_0 :

$$\psi_0 = \frac{kT}{\epsilon\nu}\left[\ln\frac{S_i}{S_i^* - S_i} + \ln\frac{\underline{c}_{0_i}(S_i^* - N_{0_i})}{N_{0_i}\underline{c}}\right]. \qquad [41]$$

Equation [41] can now be solved for S_i . Setting $\zeta_i = \dfrac{\underline{c}_{0_i}(S_i^* - N_{0_i})}{N_{0_i}\underline{c}}$, we find:

$$S_i = \frac{S_i^* e^{z_i}}{\zeta_i + e^{z_i}}. \qquad [42]$$

After some manipulation of the above equations, we finally conclude that:

$$e^{z_i} = \frac{\Omega_i[(\zeta_i + e^{z_i})(\epsilon\nu N_i^* - \sigma_i) - \epsilon\nu S_i^* e^{z_i}]}{\sigma_i(\zeta_i + e^{z_i}) + \epsilon\nu S_i^* e^{z_i}} \qquad [43]$$

and hence:

$$\sigma_i = \frac{\epsilon\nu\{\Omega_i N_i^*(\zeta_i + e^{z_i}) - S_i^* e^{z_i}(e^{z_i} + \Omega_i)\}}{(\zeta_i + e^{z_i})(\Omega_i + e^{z_i})}. \qquad [44]$$

Equations [43] and [44] are the equations analogous to [31] and [32]. In particular, the dependence on c/c_{0_i} can be seen in [32]: the charge density of the positive plate must be larger than exp (z_i). An inspection of [44] discloses that no such rigid dependence exists. In particular, if σ_i is positive, [44] demands that:

$$\underline{c}_{0_i} < \frac{e^{z_i} N_0 \underline{c}(e^{z_i} + \Omega_i)}{\Omega_i N_i^*} \tag{45}$$

and

$$S_i^* > \frac{N_{0_i} \Omega_i N_i^* (\underline{c} e^{z_i} - \underline{c}_{0_i})}{e^{z_i} N_{0_i} \underline{c}(e^{z_i} + \Omega_i) - \Omega_i N_i^* \underline{c}_{0_i}}. \tag{46}$$

If σ_i is to be negative, $\underline{c}_{0_i}$ can have any value as long as:

$$S_i^* < \frac{N_{0_i} \Omega_i N_i^* (\underline{c} e^{z_i} - \underline{c}_{0_i})}{e^{z_i} N_{0_i} \underline{c}(e^{z_i} + \Omega_i) - \Omega_i N_i^* \underline{c}_{0_i}}. \tag{47}$$

We can therefore conclude that a multiple adsorbing system can give rise to attraction between nonidentical plates without imposing very rigid demands upon any one given parameter, in particular, the isoelectric concentration.

VI. Application of This Theory to Coagulation of Colloidal Mixtures[2]

As we have seen, nonidentical particles can attract each other over short range. Further, even if the force does not become attractive, the repulsive force decreases over some interval for large interaction. It has also been shown that the magnitude of this attraction depends upon the *difference* of the plates; i.e., the more nonidentical, the greater the attractive force.

Suppose now we have a mixture of different colloids in solution. From the above it follows that those colloids which are most different will have the greatest chance of attracting and hence coagulating. We will obtain therefore a precipitation of those colloids falling at the tail ends of the distribution curve, leaving the colloids in the middle of this curve in solution. It would seem then that by properly controlling the composition of the colloid mixture, as well as the salt concentrations, one should be able to use this approach to precipitate out those colloids from a mixture which are undesirable, leaving the desired ones behind.

VII. Discussion

The above considerations indicate that as long as we are dealing with the interaction of identical particles, the boundary conditions of Verwey and Overbeek (i.e., the independence of the surface potential of the interaction distance l) are physically adequate and give correct results. This means that it is possible to ignore the contribution of surface crowding to the chemical potential difference.

---

[2] This idea was suggested to me by Dr. N. Rashevsky.

But if we extend the theory to deal with the interaction of nonidentical particles, the Verwey and Overbeek theory is no longer justified, because it leads to the physically absurd conclusion that the charge densities become infinite for $l = 0$. This conclusion arises exactly because crowding is ignored, and hence no limitation is put upon the possible number of adsorbed charges.

In the revised theory the surface potential is included in the total chemical potential, and hence crowding is taken into account. This in turn means that both the charge density and the electrostatic surface potential become functions of l. This revision has no effect on the formal expression for the forces between identical particles; it does greatly affect the theory of forces between nonidentical particles. In particular, it points up the possibility of attractive forces arising at short range between particles both of which are positively charged at large distances from each other.

The physical basis of these attractive forces is clear. It is well known that two approaching positively charged particles drive charges off each other's surfaces. If they are identical, the charge density simply goes to zero in a symmetrical manner. If they are nonidentical, one surface will become neutral and then negative when the other is still positive. In this region two forces exist: an electrostatic attraction between the two oppositely charged particles, and a repulsive force due to the affinity of the potential determining ions in solution for the plate surface. These ions attempt to migrate back to their sites (with an affinity which increases with decreasing charge density) and hence exert an influence causing the plates to move apart. Under certain specified conditions the net force becomes attractive in this region.

We find therefore in the revised theory that it is no longer necessary to resort to London-van der Waals forces in order to account for short-range attraction between nonidentical particles. This of course in no way rules out the probable importance of these forces.

It is also of interest that the direction of the force depends very much on the identity or nonidentity of the interacting particles. The above might conceivably be of some use in explaining the behavior of large charged molecules (proteins, nucleic acids) in living systems.

VIII. SUMMARY

1. A consideration of nonidentical particles necessitates a revision of the Verwey-Overbeek theory; the electrostatic surface potentials must be made functions of the interaction.

2. An inclusion of the crowding effect in the chemical potential provides the physical basis for the interaction dependence of ψ_0.

3. Suitable expressions are found for the case where (a) a single ion is adsorbed, providing the positive charge on the surface; and (b) two ions

of different sign are adsorbed. This system is less rigid with respect to its requirements for attraction.

4. Identical particles experience only repulsive electrostatic forces in agreement with the theory of Verwey and Overbeek.

5. The surface potentials of the two nonidentical plates become identical at $l = 0$.

6. The charge densities of two nonidentical plates bearing net charges of the same sign at large distance become equal and opposite at $l = 0$.

7. If certain conditions are met there will exist a distance l^* at which the repulsive force between two nonidentical plates becomes zero and is attractive for smaller l.

8. The magnitude of the repulsive part of the force at $l = 0$ is directly proportional to the ionic strength of the medium.

9. The range of the attractive force can be of the order of a few to a few hundred Angstroms.

10. Since the magnitude and range of the attractive force depends upon the nonidentity of particles, it suggests that in a mixture of colloids, the most nonidentical particles will precipitate out, leaving the more identical portion in solution.

Note: In a previous paper, (3), a somewhat different presentation was given of the same idea. In particular, the force was calculated via the free energy; Eq. [28] was derived and formed the basis of discussion. Since the method used in this paper is very much shorter and more general, we have refrained from discussing the other approach. The interested reader is referred to reference 3.

REFERENCES

1. VERWEY, E. J. W. AND OVERBEEK, J. TH. G., "Theory of the Stability of Lyophobic Colloids." Elsevier Publishing Co., Amsterdam, 1948.
2. LANGMUIR, I., *J. Chem. Phys.* **6**, 893 (1938).
3. BIERMAN, A., *Proc. Natl. Acad. Sci. U. S.* **41**, 245 (1955).

THE DIFFUSION BATTERY METHOD FOR AEROSOL PARTICLE SIZE DETERMINATION[1]

Jess W. Thomas

Health Physics Division, Oak Ridge National Laboratory, Oak Ridge, Tennessee

Received July 27, 1954; revised March 21, 1955

Abstract

The diffusion battery consists of a number of long, narrow, parallel channels through which the fluid moves in streamline flow. Measurement of the fractional penetration of a homogeneous, sub-micron aerosol through the battery allows the determination of its diffusion constant and particle size. The object of this work was to investigate the validity of the diffusion method.

Circular tube batteries were used to determine diffusion coefficients of gaseous molecules; satisfactory agreement with previous values was obtained. Two parallel plate batteries were used for aerosol particle size measurement in the 0.15- to 0.40-μ radius range; data were extrapolated to zero flow rate through the battery. Results checked those obtained by the gravity settling method and standard optical methods in the 0.15- to 0.30-μ radius range. Above 0.30-μ radius, the batteries gave low results.

The diffusion battery is applicable for determining particle size from atomic dimensions to radii of about 0.3μ. Battery construction difficulties, however, essentially limit the method to particles under 0.1-μ radius.

Introduction

At present very few methods are available for measurement of aerosol particle sizes below 0.1-μ radius. If the particles are liquid, the "growing" technique developed by La Mer, Inn, and Wilson (1) applies. Solid aerosols may be measured by use of the electron microscope and, indirectly, by use of the ultramicroscope. However, the measurement of particle size by the electron microscope is slow and expensive.

Very small aerosols are characterized by relatively high diffusion rates, and it is possible to utilize this property for measurement of the particle size. The first application of the diffusion method to aerosol particle size determination was made by Nolan and Guerrini (2) in 1935. They found the radii of atmospheric condensation nuclei to be about 0.03 μ. Later work was done by Nolan and Nolan (3), Nolan and Kennan (4) and Radushkevich (5). During World War II, the method was used by Rode-

---

[1] The initial work on this project was supported jointly by the Army Chemical Corps and Oak Ridge National Laboratory. ORNL is operated by Carbide and Carbon Chemicals Company for the U. S. Atomic Energy Commission.

bush, Holley, and Lloyd (6) to determine particle sizes in conjunction with filter paper tests.

Following Rodebush *et al.* (6) the apparatus is called a "diffusion battery," and consists of 19 or 20 long parallel channels, 0.1 mm. wide and 12.7 cm. high, in which gravity has a negligible effect on particles of radius below 0.3 μ. As the aerosol moves, in streamline flow, through the long narrow rectangular channels, the random Brownian movement of the particle causes it to displace from its original position in the air flow streamline. The most probable displacement from a streamline is zero, but the average displacement is proportional to the square root of the travel time. Consequently, some of the particles are displaced sufficiently to reach the walls of the battery. It is assumed that once the particle reaches the battery wall, it will adhere. Therefore, a fraction F of the influent particles appear in the battery effluent. Since the magnitude of the Brownian movement increases with decreasing particle size, the smaller the particle size, the lower the value of F. From the value of F, the diffusion constant D of the aerosol may be obtained and the particle size calculated.

Townsend (7), using channels of circular cross section, was probably the first to develop the theory of mass transfer by diffusion in channels. His "diffusion battery" consisted of several metal tubes, 10 cm. long and 0.3 cm. in diameter, arranged in parallel. His objective was to determine the diffusion coefficients of ions in air and in various gases. The gaseous ions were sorbed by the wall of his diffusion tube while en route through it, analogous to the removal of aerosol particles by a battery wall. The equation developed by Townsend was rederived in 1948 by Gormley and Kennedy (8). They obtained

$$F = 0.819e^{-\alpha} + 0.0975e^{-6.1\alpha} + 0.0325e^{-16\alpha} + \cdots; \qquad [1]$$

$$\alpha \equiv \frac{3.66\pi\, Dz}{Q}.$$

The symbol D is the diffusion constant of the diffusing aerosol or gas, z the length of the diffusion tube, and Q the volumetric flow rate. The equation applies for values of F below 0.78. For values of F above 0.78 another equation applies (8).

In 1935 Timoney, working with Nolan and Guerrini (2), developed an equation for the parallel plate battery (rectangular cross section). This type of battery is more suitable than the circular type for work with relatively large particles (~ 0.01- to 0.5-μ radius). The equations developed at that time by Timoney were later corrected by Gormley in an appendix to a paper by Nolan and Nolan (3).

$$F = 0.910e^{-\alpha} + 0.053e^{-11.4\alpha} + \cdots; \qquad [2]$$

$$\alpha = \frac{3.77\, bDz}{aQ}.$$

In this case Q is the volumetric flow rate through one channel, $2a$ the spacing between the parallel plates, and b the height of the channels perpendicular to the direction of air flow. The quantities D, F, and z have the same meaning as in the case of the circular diffusion tube.

Recently, at this laboratory (9), this basic equation was rederived with the following result:

$$F = 0.915e^{-\alpha} + 0.059e^{-11.8\alpha} + 0.026e^{-80\alpha}, \qquad [3]$$

$$\alpha = \frac{3.77\ bDz}{aQ}.$$

Equations [2] and [3] check very closely. For values of F under 0.90, there is a difference of less than 1% in F for the same value of D in both equations. Rodebush *et al.* (6) used the coefficient 0.99 instead of 0.915 or 0.91 in the first term of the equation. Equation [3] is considered reliable, and it is used in the present work.

To obtain the particle size of the aerosol from diffusion constant measurements, the Einstein diffusion equation is used, with Millikan's correction (10) for the application of the equation to a nonhomogeneous medium:

$$\begin{aligned} D &= \frac{kT}{6\pi\eta\, r}\left(1 + A\,\frac{\lambda}{r}\right) \\ A &= A_0 + Be^{-C\frac{r}{\lambda}} \end{aligned} \qquad [4]$$

A, B, and C are empirical constants; λ is the mean free path of an air molecule; and r is the radius of the diffusing particle. Millikan (10) obtained his corrections for values of λ/r ranging up to 134. Since λ is about 6×10^{-6} cm. for air at room temperature and pressure, this equation may be expected to hold for oil drops as small as 0.0005 μ in radius.

The values of A_0, B, and C used in Eq. [4] depend on the value selected for the mean free path. The values corresponding to the presently accepted mean free path of 6.53×10^{-6} cm. (760 mm., 23°C.) are $A_0 = 1.25$, $B = 0.44$, $C = 1.09$. These values were obtained by changing the values summarized by Rodebush, Langmuir, and La Mer (11) to correspond to $\lambda = 6.53 \times 10^{-6}$ cm. There is a variation in the value of A with the nature of the droplet (10, 12).

Equation [4] does not apply accurately to particles as small as gas molecules; but the equation gives values which are good approximations. Substitution of the diffusion constant of oxygen, 0.2 cm.^{2}/sec., into Eq. [4] yields 2.5 Å. as the radius of the oxygen molecule; the collision radius of the oxygen molecule (13) is about 1.8 Å. For hydrogen, Eq. [4] gives 1.6 Å.; the collision radius (13) is 1.35 Å.

OBJECTIVE AND EXPERIMENTAL APPROACH

It is difficult to construct a diffusion battery which will measure particle sizes in the range covered by the standard light-scattering methods (<0.1-μ radius), but it was believed essential to confirm the method by a standard technique, despite the battery construction difficulties. At the other extreme, it is possible to check the battery equations and methods using the ultimate in small "particles," that is, gas molecules. Since gas molecules have relatively large diffusion constants, this experiment is easily done.

The objectives of this work were to check the diffusion battery method by (*1*) measuring known gas diffusion constants and (*2*) using particles of about 0.1- to 0.5-μ radius.

Determination of Gas Diffusion Constants

The air-gas mixture was passed at several flow rates through a 3.5-cm. inside diameter glass tube lined with an absorbent paper. The gas component, present in small proportion, diffuses to the wall during transit and is absorbed by the impregnated paper. To maintain streamline flow in the diffusion tube, auxiliary calming sections of tubing were used, 80 cm. long at the entrance and 45 cm. long at the exit.

Diffusion constants were determined for two gases, SO_3 and NH_3. The absorbing paper was impregnated with oleic acid for the SO_3 test and with saturated copper sulfate solution for the NH_3 test, allowing complete absorption of all SO_3 or NH_3 molecules contacting the paper. The gas concentrations were in the range of 1 to 10 mg./l. The SO_3 gas concentration was obtained by passing the inlet air over fuming sulfuric acid containing 20% free SO_3, and the NH_3 gas concentration by passing the air over 0.25 *N* ammonium hydroxide. In both tests, Ascarite was used to remove CO_2, and in addition for the SO_3 test, the inlet air was dried to prevent aerosol formation. Bubblers were used to sample the gas influent and effluent to the diffusion tube. In the SO_3 test, it was necessary to fit the inlet tube to the bubbler with a medium porosity glass disc, to prevent aerosol formation in the bubbler. Water was used as the absorber for SO_3. The SO_3 concentration and penetration samples were analyzed by titration against 0.05 *N* sodium hydroxide, using phenolphthalein as an indicator. For the NH_3 test, the bubblers contained 25.0 ml. of 0.05 *N* H_2SO_4 in 400 ml. water. After absorption of the ammonia gas, the bubbler solutions were titrated to pH 6.5.

The results of the experiments are summarized in Table I. The diffusion constant of SO_3 as determined experimentally was about 30% higher than the value calculated from empirical equations (14, 15) in the literature. However, the empirical equations are not accurate, as may be seen from the graph given by Sherwood (14). The diffusion constant of NH_3 was found to be 8% lower than the experimental value given by Andrussow (15).

TABLE I

Diffusion Constant Determinations

Temperature, 24 ± 2°C. Pressure, 740 mm. Hg

Gas used	Inlet concentration, *mg./liter*	Diffusion tube length, *cm.*	Flow rate, *l./min.*	Gas penetrating, %	Diffusion constant, *cm.²/sec.*	
SO_3	6.75	14.6	0.950	17.4	0.147	0.146
SO_3	5.59	14.6	1.960	37.6	0.152	
SO_3	5.19	14.6	0.950	19.1	0.138	
NH_3	2.40	14.6	0.947	9.2	0.207	0.203
NH_3	2.07	14.6	1.950	34.9	0.165	
NH_3	2.08	5.8	0.947	31.4	0.229	
NH_3	1.77	5.8	1.950	53.2	0.210	
NH_3	2.19	5.8	0.500	16.6	0.200	
NH_3	2.04	5.8	0.750	27.4	0.206	

It was concluded that the equation for the circular battery is correct, or very nearly correct. The method for determination of the diffusion coefficient of gases and vapors described above may be, in many cases, a more convenient method than the standard methods.

Diffusion Batteries

Two batteries were made, each having channels 0.01 cm. wide by 12.7 cm. high. The larger battery, 47.3 cm. long, had 20 parallel rectangular channels; the small battery, 5.08 cm. long, had 19 channels. The pressure drop at 1 l./min. air flow rate was 7.5 cm. H_2O for the large battery, 0.8 cm. H_2O for the smaller battery.

A very fine grade of graphite was used to make the battery plates. This was relatively easy to machine to the close tolerance necessary (±0.00015 in. in thickness over an area of about 125 sq. in.). The channels were made by machining out a layer of graphite 0.01 cm. thick from each battery plate, leaving shims in the center and at the edges for spacers. Two heavy stainless steel plates were placed on both sides of the battery, and the assembly bolted together. Two end pieces of about 1-l. capacity were provided to direct the air stream from the battery channels into a $\frac{3}{8}$-in. pipe.

The spacings ($2a$) of the channels in the battery were measured with a microscope. The values obtained were averaged to give the following: Large battery, $2a = 0.0095$ cm.; small battery, $2a = 0.0092$ cm. By these measurements the most probable deviation of each channel width from the average width was 0.0004 cm. for either battery.

The channel spacings were also calculated from pressure drop measurements. By these calculations, $2a$ for the large battery was 0.00994 cm.; small battery, $2a = 0.00970$ cm. Since the existence of end effects would tend to lower the value for $2a$ determined in this manner, the values of $2a$

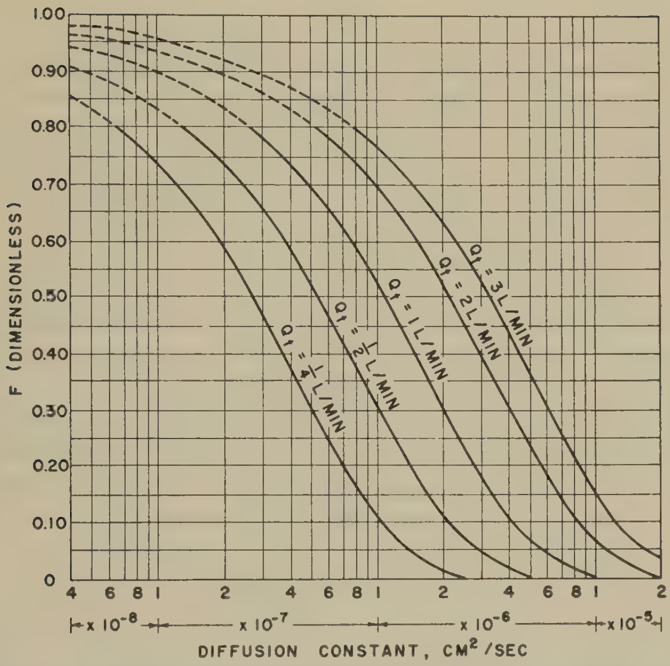

FIG. 1. Theoretical large battery penetration vs. diffusion constant as a function of air flow rate.

were taken to be 0.0100 cm. for the large battery, 0.0098 cm. for the small battery. The large battery was designed specifically for measuring particles of about 0.2-μ radius. Figure 1 shows a plot of theoretical fractional penetration versus diffusion constant at several different flow rates through the large battery. Q_t is the total flow through the battery, l./min.

Determination of Aerosol Diffusion Constants

An apparatus of the type described by La Mer, Inn, and Wilson (1) was used to generate a di-2-ethylhexylphthalate (DOP) aerosol. Nitrogen was used as a carrier gas when the boiler temperature exceeded 125° C. Condensation nuclei were usually supplied by a heated sodium chloride coated nichrome wire (16). Nuclei were also obtained by passing N_2 over several grams of sodium chloride maintained at 550° to 580° C. in a muffle furnace. The nichrome wire method permits relatively rapid changes in particle size; the muffle furnace method has the advantage of stability. Aerosol concentrations influent and effluent to the batteries were measured by the NRL E-3 Smoke Penetration Meter described by Knudson and White (17).

Particle sizes were measured by gravity settling in a convection free chamber, and by the optical methods described by Sinclair and La Mer

(18). Aerosol stability was checked by isolating a sample of smoke in the penetration meter, and observing the rate of change of the intensity of the scattered light with time. Smoke from the generator was drawn through either the large battery, small battery, or bypass, then through the penetration meter, and then on through a capillary flow meter to the vacuum line. The fractional penetration of aerosol through the batteries was measured for several flow rates and the particle size calculated after making corrections for entrance effects.

It was known from preliminary investigations that an entrance effect existed, owing to mass transfer of particles to the battery surfaces at the battery inlet by mechanisms other than diffusion through a parabolic air velocity gradient. This problem was attacked by use of the two batteries, which were essentially alike except for their length z. The length of the small battery is 5.08 cm. compared to 47.3 cm. for the long battery. The other battery constants are essentially the same for the two batteries; if they were exactly the same, the effective length of the small battery would be

$$5.08 \times \frac{0.100}{0.098} \times \frac{19}{20} = 4.92 \text{ cm.}$$

It was assumed that the same aerosol mass transfer to the battery wall occurs in the first 4.92 cm. of the large battery as occurs in the entire length of the small battery. Therefore, at a point 4.92 cm. down the large battery in the z-direction, the influent aerosol concentration will be the same as the concentration at the exit of the small battery. Designating as F_c the fraction of the aerosol penetrating the last $(47.3 - 4.9) = 42.4$ cm. of the large battery, the following relation holds:

$$F_c = \frac{F(\text{large battery})}{F(\text{small battery})}.$$

F_c then represents the penetration through a battery 42.4 cm. long, corrected for entrance effects. Since this battery has a different z value, Fig. 1 does not directly apply. However, for a given F_c and Q_t, D values may be read from Fig. 3 and multiplied by the factor $1.11 = \left(\frac{47.3}{42.4}\right)$.

RESULTS—DISCUSSION

Figure 2 shows typical experimentally determined aerosol diffusion constants, corrected for battery entrance effects, plotted against flow rates through the battery. As the flow rate decreases, the apparent diffusion constant as determined by the battery decreases. Since mass transfer by turbulence, etc., would decrease with decreasing flow rate, the plot was extrapolated to zero flow to obtain the best value of the diffusion constant of the aerosol.

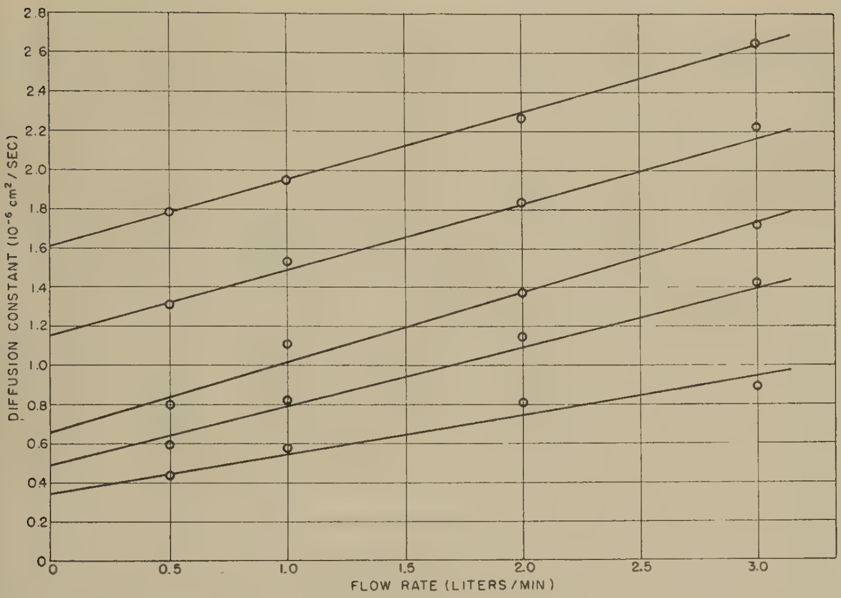

FIG. 2. Extrapolation of experimentally determined diffusion coefficients to zero flow rate.

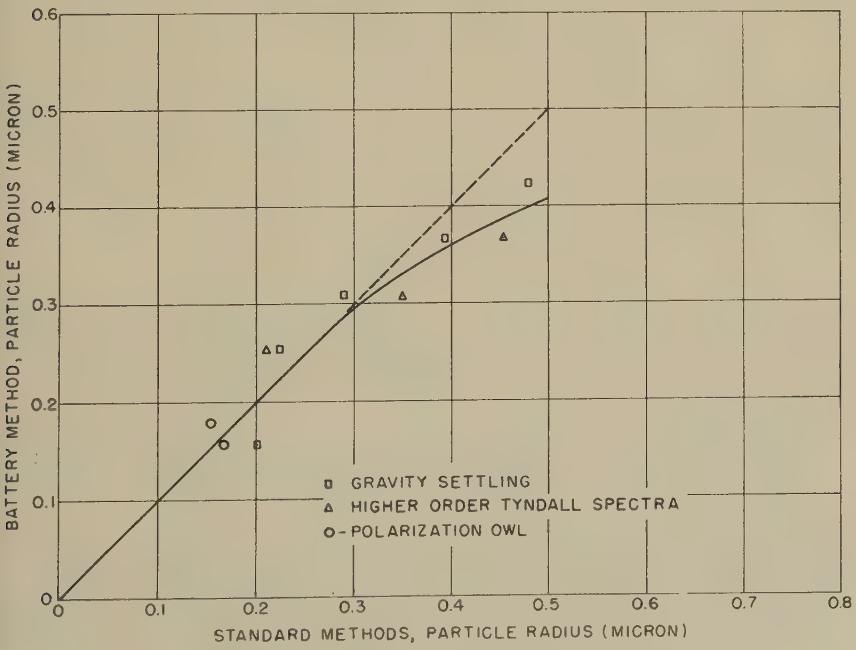

FIG. 3. Comparison of battery method with standard methods.

Penetrations through both batteries were determined for flow rates of ½, 1, 2, and 3 l./min. for six different particle sizes ranging from 0.15-μ radius to 0.40-μ radius. The corrected penetration, F_c, was determined at each flow rate and the apparent diffusion constant calculated. The apparent diffusion constants were then extrapolated to zero flow and the corresponding particle size obtained. Results (Fig. 3) show that the diffusion method is confirmed by standard methods to within the precision of the data (about $\pm 10\%$), in the 0.15- to 0.30-μ radius range. Above 0.30-μ radius, the battery method becomes increasingly inaccurate.

The cause for the discrepancy, i.e., higher diffusion constants with higher flow rates, has not been determined. Since the aerosols exhibited distinct higher order Tyndall spectra, they were reasonably homogeneous. It would require a very inhomogeneous aerosol to explain the apparent observed rate of change of diffusion constant with flow rate. Calculations made on the effect of slight irregularities in the battery spacing, coagulation of the aerosol, etc., showed these effects to be relatively minor. In the gas diffusion experiments, there was no tendency for the measured diffusion constant to increase with flow rate, indicating that the diffusion theory is not in error. It is possible that the discrepancy is due to entrance effects existing beyond 5 cm. in the battery inlet; or to exit effects.

The diffusion battery is best adapted for measuring particles of about 0.05-μ radius or lower. For example, a battery adapted to the size range 0.002-μ to 0.02-μ radius could be easily made by using 20 channels 50 cm. long by 10 cm. high, with a 2.5-mm. spacing between the plates; using moderate flow rates of about 1 l./min. through the battery. Since the battery method was confirmed for particle radii in the range 0.15 to 0.30 μ, and also for gas molecules, it seems established that the method is good for the entire particle size spectrum below 0.3-μ radius.

REFERENCES

1. LA MER, V. K., INN, E. C. Y., AND WILSON, I. B., *J. Colloid Sci.* **5,** 471 (1950).
2. NOLAN, J. J., AND GUERRINI, V. H., *Proc. Roy. Irish Acad.* **43A,** 5 (1935).
3. NOLAN, J. J., AND NOLAN, P. J., *Proc. Roy. Irish Acad.* **45A,** 47 (1939).
4. NOLAN, P. J., AND KENNAN, E. L., *Proc. Roy. Irish Acad.* **52A,** 171 (1949).
5. RADUSHKEVICH, L. V., *Acta Physicochim. U.R.S.S.* **6,** 161 (1937); **11,** 265 (1939).
6. RODEBUSH, W. H., C. E. HOLLEY, JR., AND B. A. LLOYD, OSRD Report 2050 (1943). (Available as Report PB-99669, Office of Technical Service, Department of Commerce, Washington, D. C.).
7. TOWNSEND, J. S., *Trans. Roy. Soc. (London)* **193A,** 129 (1900).
8. GORMLEY, P. G., AND KENNEDY, M., *Proc. Roy. Irish Acad.* **52A,** 163 (1949).
9. DEMARCUS, W. C., AND THOMAS, J. W., ORNL Report 1413 (1952). (Available from Office of Technical Services, Department of Commerce, Washington, D. C.).
10. MILLIKAN, R. A., *Phys. Rev.* **22** [2nd s.], 1 (1923).

11. Rodebush, W. H., Langmuir, I., and La Mer, V. K., OSRD Report 865 (1942). (Available as Report PB-32203, Office of Technical Service, Department of Commerce, Washington, D. C.).
12. Wasser, V. E., *Physik. Z.* **34,** 257 (1933).
13. Glasstone, S., "Textbook of Physical Chemistry," 2nd ed., p. 282. Van Nostrand, New York, 1946.
14. Sherwood, T. K., "Absorption and Extraction," 1st ed., pp. 16–18. McGraw-Hill, New York, 1937.
15. Andrussow, L., *Z. Electrochem.* **54,** 566 (1950); **55,** 51 (1951).
16. La Mer, V. K., NYO Report 512, Columbia University, New York 27, New York (1951).
17. Knudson, H. W., and White, L., Naval Research Lab., Report P-2642, September 14, 1945.
18. Sinclair, D., and La Mer, V. K., *Chem. Revs.* **44,** 245 (1949).

AN ELECTRON MICROSCOPE STUDY OF SODIUM CHLORIDE PARTICLES AS USED IN AEROSOL GENERATION

James P. Lodge and Barbara J. Tufts*

Cloud Physics Project, University of Chicago, Chicago 37, Illinois

Received Oct. 21, 1954; revised March 25, 1955

Abstract

The effects of temperature, moisture, and filament age on sodium chloride particles evaporated from the hot-wire source used in the La Mer generator were studied with the RCA EMU-2E electron microscope. The size appears to vary with temperature and filament age, and concentration seems to be a function of temperature. The shape of the sodium chloride crystals is related to the amount of moisture present. The variation of particle size with filament age appears to yield smooth curves, implying an orderly change. This is attributed to crystal growth in the coating of the hot wire.

Introduction

Although laboratory aerosols have been generated upon nuclei of evaporated salts for several years, little has been known about the dependence of size and concentration of the nuclei on various parameters. The most common method of generation of these particles is evaporation from a hot wire, as developed by La Mer (2, 5). With the use of the electron microscope, much can be discovered about such nuclei. In a study of methods of preparing finely divided sodium chloride, Craig (1) noted that the salt on evaporation *in vacuo* was amorphous and chainlike in appearance, changing to the cubic form on exposure to room air. McLaughlin *et al.* (3) also pointed out the change in appearance which took place when the sodium chloride which had been evaporated *in vacuo* was exposed to room air. In the La Mer generator, air or some other gas must be present; however, atmospheric humidity, which is the most likely cause of these morphologic changes, can be reduced at will.

In this study the effects of temperature, moisture, and filament age on the size and concentration of particles from this type of particle source were examined with the RCA type EMU-2E electron microscope.

Experimental

The final form of the apparatus used, designed to overcome the difficulty of the extreme sensitivity to moisture, is shown schematically in Fig. 1. It

---

* The research reported in this paper has been sponsored by the Geophysics Research Directorate of the Air Force Cambridge Research Center, Air Research and Development Command, under Contract AF19(604)-618.

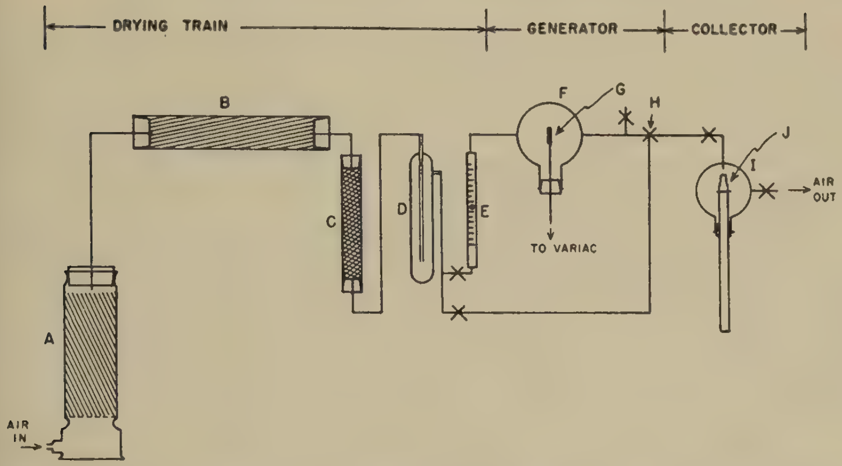

FIG. 1. Schematic diagram of the apparatus, including drying train, generator, and collector.

consists of a drying train and an arrangement for generation and collection of the salt. The drying train was composed of a Drierite tower, *A*, a phosphorus pentoxide tube, *B*, a filter tube packed with glass wool, *C*, and a cold trap, *D*, which was inserted into a Dewar flask filled with liquid nitrogen during collection. The air from the cold trap was then led through a rotameter, *E*. The generator was constructed of a 1-l. round-bottomed flask, *F*. Into the neck of this flask was inserted the salt filament, *G*. The air was led out of the chamber through a three-way stopcock, *H*. The collector, *I*, constructed from a 500-ml. round-bottomed flask, was connected to the stopcock by a short length of rubber tubing which could be sealed off. In the neck of the collector was placed a copper rod, *J*, 2 cm. in diameter, with the inserted end tooled to receive an RCA electron microscope specimen holder with a specimen screen. The lower end of the rod was immersed in a Dewar flask of dry ice and acetone during collection, thus causing a thermal gradient between the specimen holder in close contact with the rod, and the air, which was slightly above room temperature. This caused thermal precipitation of a portion of the salt particles onto the specimen screen. The collector was provided with air cutoffs at both the inlet and outlet, permitting the chamber to be sealed at the conclusion of collection, so that the whole flask could be removed from the apparatus and carried to the microscope. The specimen could then be placed rapidly in the microscope with as little exposure to room air as possible. A bypass permitted air from the cold trap to be diverted through the stopcock, *H*, thus allowing the collector to be flushed with air which had not passed through the generator, while the air flow through the latter was bled off through the auxiliary stopcock to the left of *H*.

The filament was prepared by repeatedly dipping in hot, saturated salt solution a coil 20 mm. long, of 26-gauge nichrome wire containing eight turns approximately 8 mm. in diameter. The total resistance of the coil was 1.8 ± 0.1 ohms. An attempt was made each time to place a coating of salt about 1½ mm. thick on the wire. This was difficult to reproduce and varied from time to time and also over the length of a single filament, representing probably the largest source of error in this study.

When first prepared, the filament surface was comparatively smooth and dull white, and each coil of the filament was outlined by the salt coating. After a few hours of heating, the whole surface was "feathery" and crystalline in appearance, and the filament was uniformly covered, with none of the wire turns visible in outline. These changes point up the difficulty of assigning a meaningful temperature to the filament, since they indicate that the actual site of the evaporation changes with time.

To study the effects of temperature changes on emission of the salt, collections were made using two different applied filament voltages in the apparatus as described above. Arbitrarily, 6 volts and 8 volts, representing incipient and low red heat, respectively, were chosen. A thermocouple on the surface of a typical salt coating measured 298° C. and 324°C. at the two settings. Collections could not be taken any oftener than once an hour since at least ½ hour was needed for the copper rod to equilibrate with the dry ice-acetone mixture, and collection times at 6 and 8 volts were ½ hour and 15 minutes, respectively. The air flow was kept constant during both equilibration and collection at 2 l. min^{-1}. Continual air flow was necessary owing to the tendency of the specimen holder and grid to ice over if not bathed in moving dry air.

The collections were assumed to be true aliquots of the total sample, on the basis of the following reasoning. The size distribution of salt particles would be expected to be relatively constant across the jet of air entering the collector. The specimen grid was in the approximate center of this jet, and the velocities involved were too low for centrifugal size separation to be important. Efficiency of thermal precipitation is independent of particle size. Thus, the measured distribution should be representative and the number of particles in a collection should represent a constant, if unknown, fraction of the total sample.

Several micrographs were made of each collection and these photographs were then examined by projection from an enlarger. Micrographs of particles of known size, Dow-polystyrene latex, lot No. 580-G, were used as a standard of magnification. It was discovered that the first hour's collection of salt showed large particles which were cubic in shape. With increasing time, but only under rigorously dry conditions, the particles lost their cubic shape, tending instead to become round or oval. Increasing filament age showed a corresponding decrease in particle size. Many of the particles from the first hour collection were in the micron range, some

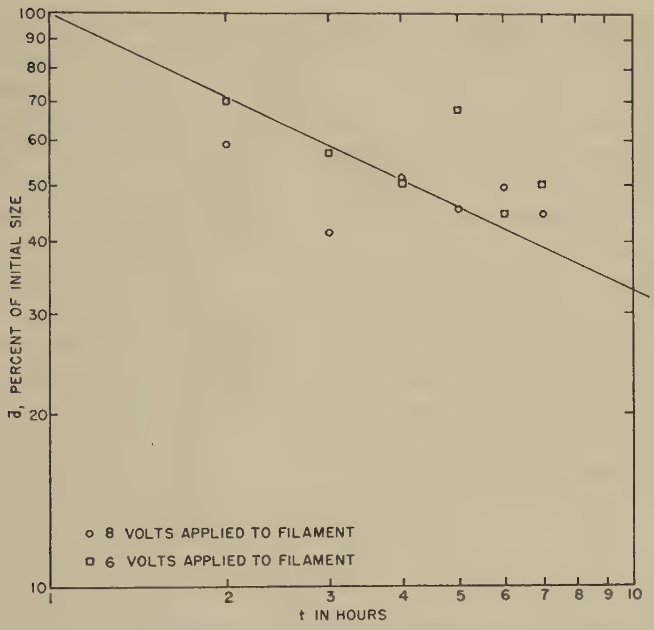

FIG. 2. Relationship between filament age and mass mean diameter expressed as per cent of the mass mean diameter at 1 hour. The line represents the equation $\bar{d} = 100\ t^{-0.5}$.

of them being as large as 3.5μ.[1] The particles from the last collection, i.e., after 5 to 7 hours, varied from 300 to 100 Å.

DISCUSSION

One hundred particles from each collection were counted and sized. A preliminary analysis of the resulting data utilized the relative mass mean diameters, compared with the first hour collection, taken as 100%. Figure 2 represents the resulting relative sizes $\bar{d}$ as a function of filament age, t. There appears to be some justification for the assumption of a linear log-log relationship; the best least-squares line has the equation $\bar{d} = 100\ t^{-0.5}$. It will be noted that this relationship is independent of filament voltage.

However, quite aside from the very large scatter of points in this representation, a statistical analysis showed that the residual variances were non-normal. Since the scatter was primarily due to the large contribution of a few large particles to the mass mean, another representation of the size distribution was sought. It was suggested that a nonparametric technique be employed. Therefore, the upper 80% tolerance limit for each collection was determined by the method of Murphy (4). This limit, d_{80}, is interpreted to mean that one may state, to a confidence level of 0.90, that 80% of all particles are smaller than the given size. An upper limit only was used because virtually all collections contained particles as small as 100 Å. Figure 3 shows the resulting plot; to a fair approximation it may be seen that log d_{80} is linear with the inverse of the time. The lines represent least-squares solution; the residual variances are normal in this model. Here the absolute size difference caused by the higher temperatures (applied voltage) shows clearly.

---

[1] Particle dimensions in this paper refer either to the length of the side of a cube or to equivalent particle diameter, whichever is applicable.

A study of the effect of filament age on particle concentration was made by counting all the particles in an area of standard size and position for each run. The number thus obtained was assumed to be directly proportional to the concentration, on the basis of the reasoning outlined in the experimental section. An analysis of variance of the less complete 6-volt data gave, for five series for which hours 1, 3, and 5 were measured, a

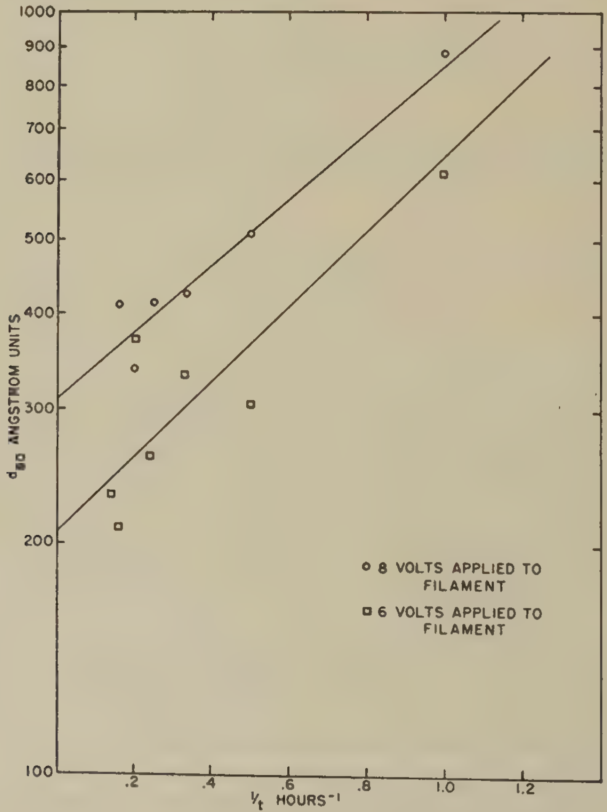

FIG. 3. Relationship between filament age and upper 80% tolerance limit. Lines represent least-squares solutions of the equation log $d_{80} = \mu + \beta/t$.

mean concentration number of 17.8 ± 15.0 with no significant effect either of time or of the individual filament. The more complete 8-volt data contained six series with all measurements for hours 1 through 6. Here the lumped mean concentration was 57.2 ± 40.8, corrected for the same sampling period. The larger number of samples here showed no significant variation with time by F-test, but a significant difference from one filament to another. It is probable that a larger number of samples would show the same effect with the 6-volt data. Application of the t-test to these means gave $t = 6.55$ for 49 degrees of freedom; hence, the chance that the two means are in fact identical, despite the large standard deviation, is vanishingly small. Thus it seems permissible to state that the increase in concentration produced by increasing filament voltage from 6 to 8 volts is roughly threefold. Hence particle concentration is found to be a function of filament temperature (and of the individual filament which may, in the absence of a really good method of measuring surface temperatures, be the same thing), but is independent of filament age despite the enormous changes in particle diameter.

A possible physical explanation is the following: Aging of the filament has been observed to cause the salt coating to rearrange slowly into larger crystals, thus diminishing the total emitting surface. The heated filament is surrounded by a layer of salt vapor, at a partial pressure dependent only on filament temperature. The only effect, then, that a decrease in emitting area could have would be to decrease the thickness of this layer. The rate of self-nucleation in this layer is therefore constant, since it is determined by concentration and temperature. The final particle size, however, is related to the time of growth, which is controlled by the thickness of this layer.

Weyl (6) has hypothesized that, on the early stages of condensation from a supersaturated atmosphere, particles are formed which are nonstoichiometric in composition, and hence charged. It seemed possible that the application of an external field might move particles out of the condensation zone more rapidly or hold them in it for longer periods, depending on the sign of the field, thus permitting still further control of size. To test this theory, a 21-gauge nichrome wire was wound into a helix of a larger diameter than the salt filament, which was secured within it. This grid was so connected that it could be heated by alternating current, and simultaneously held at any desired D.C. level. The heating avoided the possibility of the grid itself acting as a thermal precipitator owing to the difference between its temperature and the temperature of the heated salt filament. Potentials up to 300 volts, positive or negative (a field of *ca.* 600 volts cm.^{-1}), and changes in separation between the filament and the grid produced no effect, probably owing to the very small area of supersaturation and the high speed of the condensing particles.

SUMMARY

The final results show relationships between filament age and particle size, between the amount of moisture and the shape. The shape of the particles is sensitive to virtually undetectable amounts of moisture. However, the spheroidal or oval shape of the dry particles is readily reproducible under extremely anhydrous conditions. Particle size was shown to decrease in an orderly fashion with filament age and to increase with increasing filament temperature. A change in filament potential from 6 to 8 volts was shown to produce an increase in particle concentration of about threefold.

ACKNOWLEDGMENTS

Suggestions and assistance by Dr. Roscoe R. Braham, Jr., of this laboratory and by Dr. James E. McDonald, formerly of this laboratory, are gratefully acknowledged, as well as assistance by Dr. William Kruskal and associates of the Committee on Statistics of the University of Chicago, and by Dr. Worth H. Rodebush, Department of Chemistry, University of Illinois.

REFERENCES

1. CRAIG, A., AND MCINTOSH, R., *Can. J. Chem.* **30,** 448 (1952).
2. LAMER, V. K., AND SINCLAIR, D., N.D.R.C. Report, July, 1941.
3. MCLAUGHLIN, T. A., SENNETT, R., AND SCOTT, G. D., *Can. J. Research* **A28,** 530 (1950).
4. MURPHY, R. B., *Ann. Math. Stat.* **19,** 581 (1948).
5. SINCLAIR, D., AND LA MER, V. K., *Chem. Revs.* **44,** 245 (1949).
6. WEYL, W. A., *J. Colloid Sci.* **6,** 389 (1951).

STUDIES ON POLYELECTROLYTES. VII. GUM TRAGACANTH

Sadhan Basu and Anil K. Sircar

Indian Association for the Cultivation of Science, Calcutta-32, India.

Received November 18, 1954; revised March 28, 1955

In two previous communications (1, 2) it has been shown that the free acids and their sodium salts from both arabic and agar gums behave as polyelectrolytes. In the present paper the results of measurements on the free acid and its sodium salt of gum tragacanth are reported. The method of preparation of free acid and its sodium salt was exactly the same as described in the case of gum arabic (1). Removal of calcium from the gum was effected in a way described for gum agar (2). The equivalent weight of free tragacanth acid was 550. The molecular weight of the free acid and its sodium salt was in the range of 80,000 to 100,000, as determined osmometrically in the presence of HCl and NaCl, respectively. On an average there are about 180 dissociable groups per molecule.

As will be evident from Fig. 1, the viscosity measurements with solutions of free acid in water showed a rapid rise in reduced viscosity with dilution. In the presence of HCl, η_{sp}/c vs. c curve showed a maximum which shifted to higher concentrations of gum acid with increase in the free HCl concentration and ultimately became linear at sufficiently high concentration of free acid. All these clearly indicate the polyelectrolyte nature of the free acid and the linear character of the molecule.

When, however, viscosity measurements were extended to the sodium salt of the gum acid, certain peculiarities were noted (Fig. 2). The reduced viscosity diminished with diminishing concentration of sodium salt, contrary to what has been noticed in the case of gum acid. The η_{sp}/c vs. c curve was not linear as with neutral polymers. Addition of sodium chloride caused an over-all lowering of the viscosity of the solution at all concentrations measured and the η_{sp}/c vs. c curves became linear.

At any particular concentration, however, the reduced viscosity of the sodium salt is higher than that of the free acid. Since reduced viscosity is a measure of the hydrodynamic volume unit of the dissolved molecules, the sodium salt must have a more extended structure than the free acid, or in other words, the COOH groups are less dissociated than the COONa groups. Measurements of pH of the solution of sodium salt showed that the

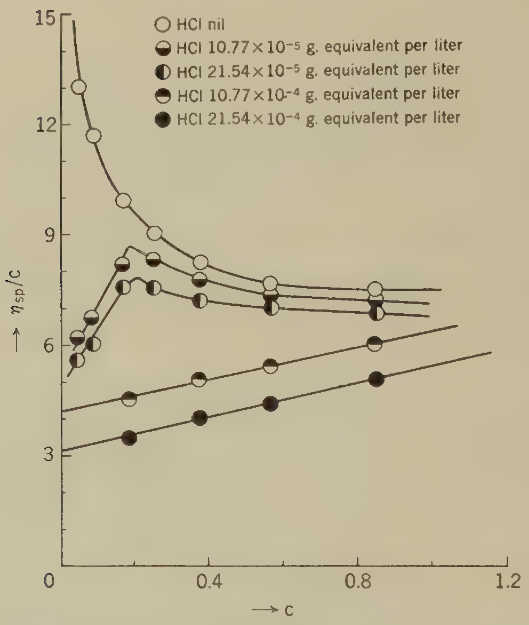

FIG. 1. Change of reduced viscosity with concentration in presence of HCl.

○ HCl nil
◒ HCl 10.77 × 10^{-5} gram-equivalent per liter
◐ HCl 21.54 × 10^{-5} gram-equivalent per liter
◓ HCl 10.77 × 10^{-4} gram-equivalent per liter
● HCl 21.54 × 10^{-4} gram-equivalent per liter

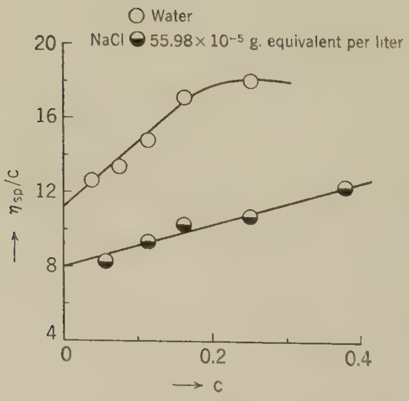

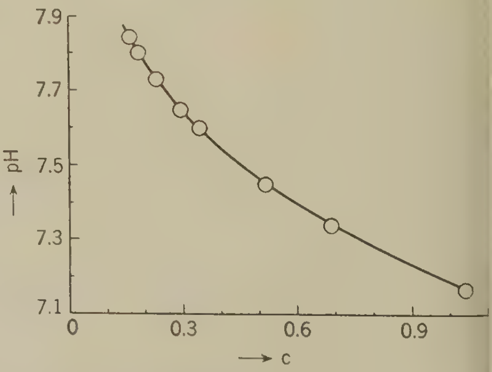

FIG. 2 (left). Viscosity of sodium tragacanth.
FIG. 3(right). Change of pH with dilution of sodium tragacanth.

pH increases with dilution (Fig. 3). This can only be due to hydrolysis of the sodium salt with dilution. Since the acid groups are less dissociated, hydrolysis will tend to lower the viscosity of the solution with dilution. The relative importance of this factor compared to the uncoiling effect with dilution may be responsible for the viscosity behavior of the solutions of the sodium salt and for the apparent indication of its nonpolyelectrolytic nature.

ACKNOWLEDGMENTS

Thanks are due to Dr. S. R. Palit for laboratory facilities and to the Council of Scientific & Industrial Research, India, for a fellowship to one of us (A. K. S.).

REFERENCES

1. BASU, S., DASGUPTA, P., AND SIRCAR, A. K., *J. Colloid Sci.* **6**, 539 (1951).
2. BASU, S., AND SIRCAR, A. K., *J. Colloid Sci.* **9**, 574 (1954).

ON THE ADHESION OF DROPS AND PARTICLES ON IMPACT AT SOLID SURFACES. I.

T. Gillespie[1]

Chemical Defence Experimental Establishment, Porton, near Salisbury, Wiltshire, England

Received December 1, 1954; revised April 12, 1955

I. Introduction

A recent unpublished analysis, by the author, of the data available for the penetration of uncharged homogeneous La Mer-Sinclair generator aerosols through "mechanical" type filters has indicated that many of the anomalous results may be interpreted as being due to the nonadherence of some of the aerosol particles and drops which come in contact with the filter fibers. For example, the observation of Ramskill and Anderson (1) and La Mer *et al.* (2) that it is often more difficult to filter a heavy spherical particle or drop than a lighter one of the same radius can be explained on this basis. Since the filtration process is so complex, there may be other as yet unrealized factors responsible for anomalous results; in consequence an attempt was made to investigate this question in a more direct manner.

A horizontal stream of aerosol particles was directed towards a single earthed metal cylinder of small diameter. Counts were made of the number of particles of a given size deposited at various positions on the surface of the cylinder. The distribution was compared with the type to be expected from theory in each case. It was hoped that such a comparison would help to decide whether nonadherence on contact is likely in practical cases, particularly when the cylinder had been treated so as to change its surface.

The results obtained were compatible with the hypothesis that the aerosol particles did not necessarily adhere to the cylinder on contact. It was possible to calculate from the data the "slippage coefficient," i.e., the fraction of the particles which did not adhere on contact in any particular case. Some indication of the variation of this quantity with changes in the air velocity has been obtained.

It would appear that the effectiveness of a cylinder for collecting a specific aerosol may be increased by appropriate surface treatment of the cylinder.

---

[1] Present address: Department of Physical Chemistry, King's College, University of London.

Evidence is also cited which suggests that the presence of electric charges on some of the particles increases their chances of adhering to the cylinder on contact.

II. EXPERIMENTAL

A horizontal stream of aerosol particles was drawn at a known velocity past a small vertical cylinder of blue tempered spindle steel in the apparatus illustrated in Fig. 1. The internal diameter of the main brass tube was 8.5 cm. The distance from the entrance of the tube to the collecting cylinder was approximately 60 cm. The total length of the tube was 100 cm. Since the Reynolds number for the flow in the tube was less than 2000 even at the highest velocity used, the flow of the air was believed to be nonturbulent. At an average velocity of 5.8 cm./sec. in the tube the Reynolds number past a collecting cylinder of radius 150 μ was 1.7.

The time of exposure of the cylinder to the aerosol stream was kept small enough in each experiment to prevent one particle's being deposited on top of another. Since previous work (3) indicates that electric effects might play a part in such experiments, the cylinder was connected to the tube and both were earthed. In most of the experiments an attempt was made to remove a large fraction of the charged particles from the aerosol stream by passing it through two vertical electrodes 32 cm. long maintained at a D.C. potential difference of 4000 volts/cm.

After exposure the central portion of the tube (Fig. 1) which held the collecting cylinder was removed and the deposit examined with the aid of an optical microscope. Transmitted light, a 12X eyepiece, and a 40X objective were used. The cylinder could be rotated about its axis and the angle at which measurements were made determined from a 360 degree graduated disc attached to the hand vice which held the cylinder in place. The number of particles per unit length, n, deposited at any angle was determined by bringing into sharp focus the edge of the cylinder and counting the number

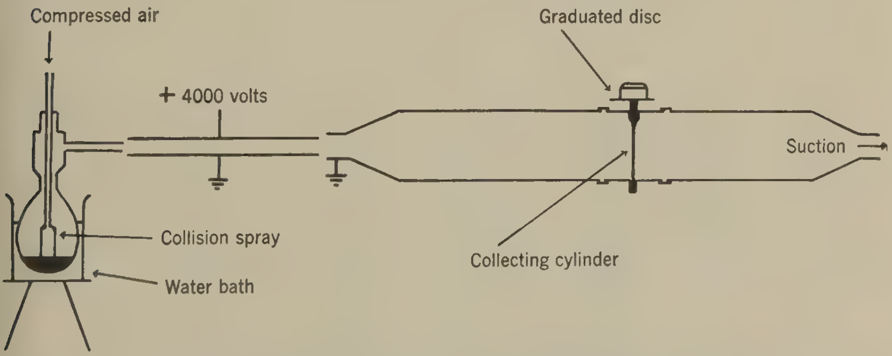

FIG. 1. Diagram of apparatus for assessing deposition on a cylinder.

of the particles of a given size which were then in focus along a strip of the cylinder at a known position along its length. The portion of the cylinder chosen for assessment was the central part extending 5 mm. from either side of the center. At zero angle, the number of particles per unit length was usually a maximum (n_0).

The effect of treating the surface of the blue steel cylinders was investigated. Silicone fluid DC 1107 supplied by Midland Silicones Ltd., London, was wiped on a "clean" cylinder and it was then baked for 2 hours at 200°C. The wiping procedure was repeated and the cylinder baked for a further 8 hours at 200°C. Other cylinders were treated by dipping them in glycerol. The glycerol collected in beads. Since the distribution of these beads was uniform, it was possible to assess the distribution of the aerosol particles on the parts of the cylinder between the beads.

In a set of subsidiary experiments lycopodium spores (spherical solid particles of 15-μ radius) dispersed in the atmosphere by mechanical means

TABLE I

Angular Distribution of Aerosol Particles Colleted by a 150-μ Radius Steel Cylinder
(Values in the body of the table are of n/n_0.)

Aerosol[a]	*Stearic Acid*							
Expt. No.	1	2	3	4	5	6	7	8
Radius (μ)	1.1	1.1	1.8	1.1	1.1	1.8	1.1	1.8
V_0 (*cm./sec.*)	5.8	5.8	20.4	20.4	20.4	20.4	5.8	5.8
θ (degrees)								
0	1.0	1.0	1.0	1.0	1.0	1.0	1.0	1.0
2.5	—	—	—	—	—	—	—	—
5	1.29	1.26	1.1	0.85	0.86	0.94	0.92	—
10	0.82	0.55	0.71	0.81	0.58	0.64	0.89	0.87
15	—	—	—	—	—	—	—	—
18	—	—	—	—	—	—	—	—
20	0.77	0.78	0.67	0.77	0.37	0.36	0.91	1.02
25	—	—	—	—	—	—	—	—
30	0.86	0.76	0.71	0.73	0.58	0.43	0.82	0.82
40	0.65	0.75	0.63	0.56	0.37	0.25	0.56	0.63
50	0.74	0.87	0.42	0.49	0.44	0.18	0.70	0.73
60	0.86	0.76	0.42	0.35	0.25	0.11	0.51	0.73
70	0.61	0.80	0.17	0.28	0.28	0.07	0.46	0.31
80	0.60	0.56	0.17	0.17	0.12	0.04	0.35	0.24
90	0.54	0.52	0.08	0.11	0.07	0.04	0.29	0.24
100	0.39	0.37	0	0.06	0.06	0	0.24	0
110	0.37	0.31	0	0.06	0.04	0	0.10	0
120	0.05	0.25	0	0.06	0.03	0	0.04	0
130	0.23	0.24	0	0.05	0.05	—	0.10	—
140	0.05	0.16	0	0.12	0.04	—	0.05	—
150	0.09	0.18	0	0.04	0.03	—	0	—
160	0	0.11	0	0.04	0.04	—	0.01	—
170	0.09	0.08	0	0.04	0.03	—	0	—
180	0	0.12	0	0.04	0.04	—	0	—

[a] All data were obtained with apparatus for removing charged particles except for experiments 1 to 4 inclusive.

Aerosol	*Stearic Acid*				*Paraffin Wax*			
Expt. No.	9	10	11	12	13	14	15[b]	16[c]
Radius (μ)	1.1	1.1	1.1	1.1	1.1	1.8	1.1	1.1
V_0 (*cm./sec.*)	11.6	8.7	16.1	26.3	11.6	11.6	11.6	11.6
θ (degrees)								
0	1.0	1.0	1.0	1.0	1.0	1.0	1.0	1.0
2.5	—	—	0.85	—	—	—	—	—
5	0.91	1.02	0.65	0.91	—	—	—	—
10	0.76	0.84	0.61	1.01	0.96	0.87	1.02	0.95
15	0.52	0.83	—	—	—	—	—	—
18	—	—	—	—	—	—	—	0.90
20	0.45	0.79	0.62	0.80	0.65	0.73	1.00	0.63
25	—	0.86	—	0.94	—	—	—	—
30	0.38	0.63	0.57	0.62	0.69	0.41	0.92	0.47
40	0.17	0.43	0.53	0.63	0.38	0.36	0.71	0.32
50	0.14	0.31	0.43	0.29	0.23	0.23	0.45	0.37
60	0.14	0.30	0.19	0.22	0.23	0.41	0.43	0.16
70	0.05	0.26	0.10	0.19	0.08	0.23	0.29	0.16
80	0.02	0.16	0.05	0.10	0.12	0	0.22	0.10
90	0	0.04	0	0.02	0.08	0	0.10	0.05
100	0	0.04	0	0	0	—	0.06	0
110	0	0.02	—	0	—	—	0	0
120	0	0.03	—	—	—	—	0	—
130	—	0.04	—	—	—	—	—	—
140	—	0	—	—	—	—	—	—
150	—	0	—	—	—	—	—	—
160	—	0	—	—	—	—	—	—
170	—	—	—	—	—	—	—	—
180	—	—	—	—	—	—	—	—

[b] Cylinder treated with silicone fluid.

[c] Cylinder dipped in glycerol.

were collected on an untreated cylinder without attempting to remove the charged particles beforehand, largely because of the difficulty of collecting any at all when the charged particles were removed. The deposit was viewed under a microscope, and particles were seen to leave the surface when clean air was drawn past the cylinder. This effect was quantitatively assessed in the following manner. Lycopodium spores were deposited on a cylinder at a stream velocity of 17.4 cm./sec. The deposit was assessed as above. Clean air was drawn past the cylinder for a specific time at the same velocity and in the same direction as used for collecting. The deposit was reassessed. This procedure was repeated several times. All of the exposures to the clean air were for 1 min. except the last, which was for 5 min. In a second experiment the above procedure was repeated except that the velocity of the clean air flow was increased for each new exposure, which lasted 2 min. The collection velocity was 5.8 cm./sec.

III. EXPERIMENTAL RESULTS

Most of the experimental results are given in Table I, and typical examples of the data are illustrated in Figs. 2, 3, 4, 5, and 6. Since the deposits

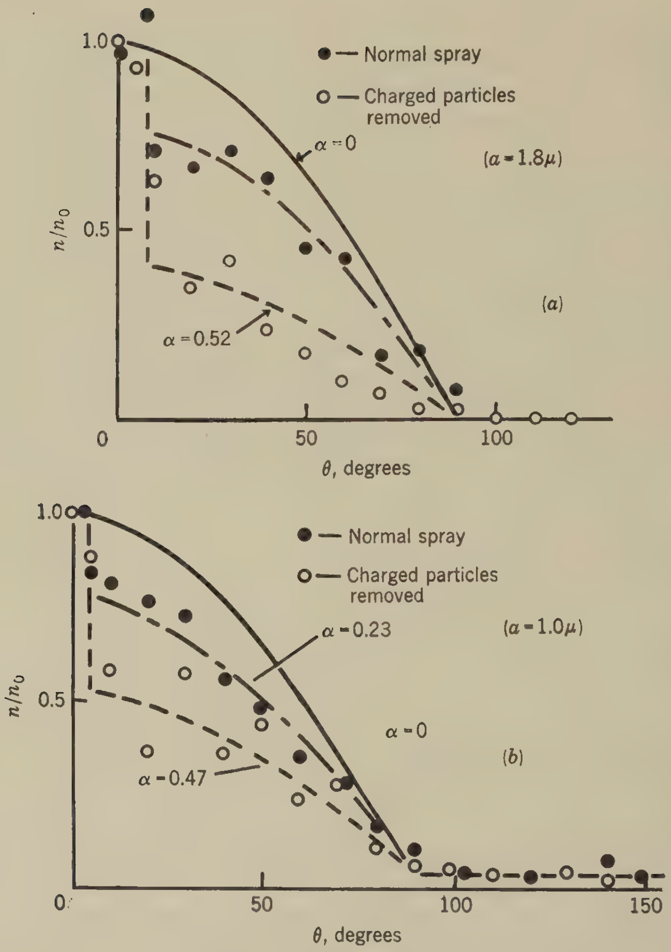

FIG. 2. The distribution of stearic acid particles collected on a 150-μ radius steel cylinder. The plotted lines were calculated for the "slippage coefficients" as indicated. (V_0 = 20.4 cm./sec.)

on the cylinders were symmetrical with respect to the direction of the aerosol stream, the results for corresponding angles on either side of the cylinder were averaged; the results in Table I are the results so obtained.

Figure 2 illustrates the deposits observed with and without the use of electrodes for removing electrically charged particles from the stream. Figure 3 illustrates the effect of surface treatment of the cylinder upon the distribution of the collected particles. It should be mentioned that in the case of the glycerol-treated cylinder the data given refer only to that part of the surface between the globules of glycerol. Figure 4 illustrates the difference in the deposits collected at different flow rates, and Figs. 5 and 6

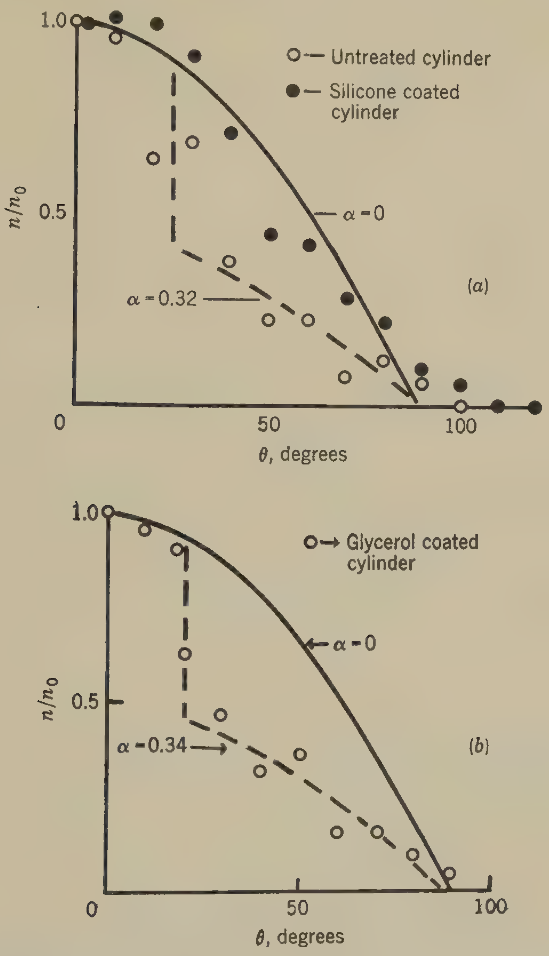

FIG. 3. The distribution of 1-μ paraffin wax particles collected by a 150-μ radius steel cylinder. (V_0 = 11.6 cm./sec., and the charged particles were removed.)

illustrate the results obtained in the subsidiary lycopodium spore experiments. The effect illustrated in Fig. 5 has not been observed for any other aerosol particles.

IV. ANALYSIS OF THE RESULTS

In a previous article (3) the effective radius of a cylinder, R_{eff}, for the interception of aerosol particles in the absence of electrical effects was given as

$$R_{\mathrm{eff}} = \left(R + a - \frac{R^2}{R + a}\right) \sin \theta_0 , \qquad [1]$$

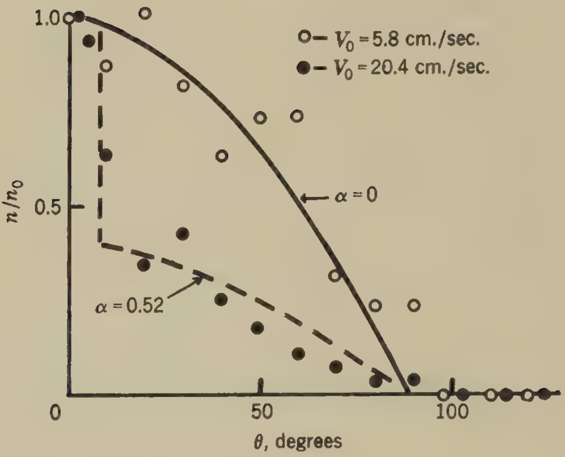

FIG. 4. The distribution of uncharged 1.8-μ radius stearic acid particles collected by a 150-μ radius steel cylinder at different flow rates.

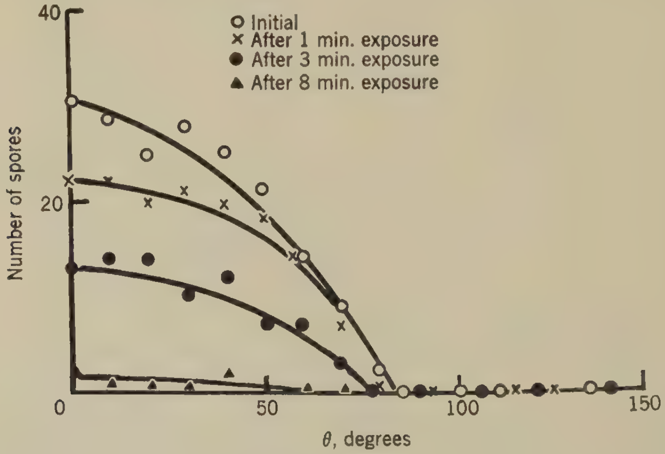

FIG. 5. The effect of clean air at the collection velocity upon a deposit of lycopodium spores on a 150-μ radius steel cylinder.

where R denotes the cylinder radius, a is the particle radius, and θ_0 is the greatest angle measured from the direction of the air flow at which aerosol particles are intercepted. The number of particles, n/cm., deposited in a small arc at an angle θ would be given by

$$n = n_0 \cos \theta, \qquad [2]$$

where n_0 denotes the number of particles/cm. deposited in the same small arc at $\theta = 0$. Equations [1] and [2] are based on the assumption that all the particles which graze the cylinder adhere to it. The unpublished analysis of filtration data referred to previously suggests that if this assumption were

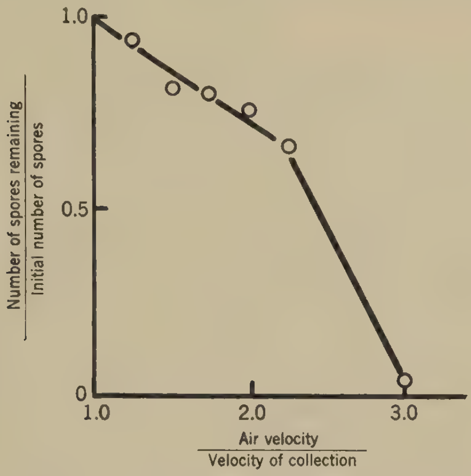

FIG. 6. The removal of collected lycopodium spores by clean air.

not valid, θ_0 would be reduced for a fraction $1 - f$ of the particles and the reduced angle θ_0' may be interpreted as the angle where "slippage" begins. Hence

$$n = n_0 \cos \theta, \quad \theta < \theta_0' : \tag{3}$$

$$n = fn_0 \cos \theta, \quad \theta > \theta_0' . \tag{4}$$

The presence of an essentially uniform deposit of particles on the cylinder at angles of greater than 90 degrees has been interpreted as due to diffusion or electric effects. The presence of such a deposit alters Eqs. [3] and [4] to

$$n = (n_0 - n_D) \cos \theta + n_D , \quad \theta < \theta_0' ; \tag{5}$$

$$n = f(n_0 - n_D) \cos \theta + fn_D , \quad \theta > \theta_0' , \tag{6}$$

where n_D is a constant and denotes the number of particles deposited at any angle greater than 90 degrees. In most cases n_D was very small and could be neglected.

The "slippage coefficient" α, defined as the fraction of the contacts of the aerosol particles with the cylinder which are not effective, is given by

$$\alpha = (1 - f)(1 - \sin \theta_0') \tag{7}$$

The values of the "slippage coefficient" determined from the experimental data are summarized in Table II. Figure 7 illustrates the variation of α with velocity for uncharged stearic acid particles of 1-μ radius and an untreated cylinder of 150-μ radius. The use of Eqs. [1] to [7] is based on the assumption that inertial deposition is a very minor factor. The results of previous work (4, 5) indicate that under the conditions of the present experiments such an assumption is valid. No attempt was made to analyze the lycopodium spore experiments.

TABLE II

Summary of the Slippage Data

Aerosol	a, μ	V_0 (cm./sec.)	f	$\frac{n_D}{n_0}$	θ_0' (degrees)	α	Treatment of cylinder
Stearic acid[a]	1.1	5.8	—	0.05	—	0	None
Stearic acid[a]	1.1	5.8	—	0.10	—	0	None
Stearic acid[a]	1.8	20.4	0.77	0	8	0.20	None
Stearic acid[a]	1.1	20.4	0.75	0.04	5	0.23	None
Stearic acid	1.1	20.4	0.5	0.04	4	0.47	None
Stearic acid	1.8	20.4	0.4	0	8	0.52	None
Stearic acid	1.1	5.8	—	0.03	—	0	None
Stearic acid	1.8	5.8	—	0	—	0	None
Stearic acid	1.1	11.6	0.44	0	10	0.46	None
Stearic acid	1.1	8.7	0.5	0.02	30	0.25	None
Stearic acid	1.1	16.1	0.67	0	2	0.32	None
Stearic acid	1.1	26.3	0.46	0	35	0.23	None
Paraffin wax	1.1	11.6	0.44	0	25	0.32	None
Paraffin wax	1.8	11.6	0.55	0	15	0.33	None
Paraffin wax	1.1	11.6	—	0	—	0	Coated with silicone fluid
Paraffin wax	1.1	11.6	0.48	0	20	0.34	Dipped in glycerol

[a] Aerosol from the normal spray. In all other cases the apparatus for removing electrically charged particles was operating.

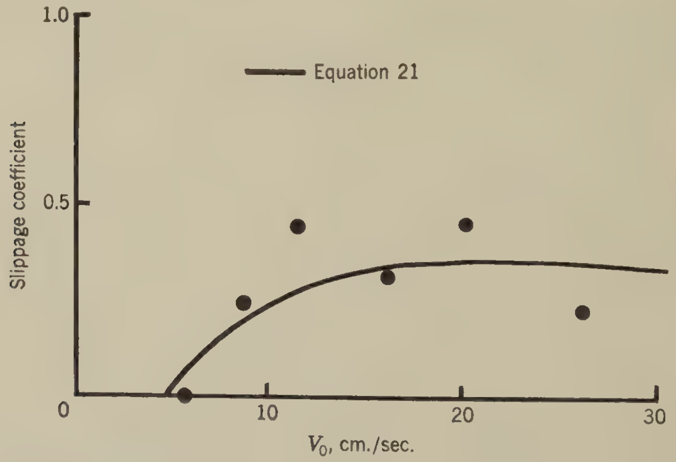

FIG. 7. Variation of the "slippage coefficient" with velocity for uncharged 1-μ radius stearic acid particles.

V. DISCUSSION OF THE EXPERIMENTAL RESULTS

The results of these experiments are apparently compatible with the hypothesis that not all aerosol particles adhere to solid surfaces on contact. Figure 2 indicates that the presence of electric charges on some of the particles enhances their chances of adhering to the cylinder on contact. Figure 3 indicates that a particular surface may be treated in such a way as to increase the chances of adherence on contact. It is believed that treatment of the blue steel cylinders with silicone fluid DC 1107 rendered the surface more oleophilic. The contact angle of the molten wax particles was smaller on the treated surfaces than the untreated. This is in agreement with the greater ease with which the wax particles were captured. Treatment of the steel cylinders by dipping them in glycerol had no apparent effect on the portion of the cylinder surface which was not covered with glycerol globules. Very few particles were observed on the surface of these globules, but this aspect of glycerol treatment was not investigated owing to the many uncontrollable factors which might be involved.

Figure 7 indicates that at very small velocities the chances of "slippage" occurring are small. Nonadherence becomes more apparent as the velocity is increased, and there is a tendency for it to decrease at large velocities. This is the same effect that was revealed in the unpublished analysis of filtration data previously mentioned. In the following section a brief summary of that analysis is given.

VI. ANALYSIS OF FILTRATION DATA

1. *Calculation of the "Slippage Coefficient" from Filtration Data*

The method of calculating the "slippage coefficient" for a given experiment was as follows. First the true index of filtration, Δx_0, was calculated from

$$\Delta x_0 = -\ln P, \qquad [8]$$

where P denotes the penetration of a homogeneous aerosol expressed as a fraction. Since Δx_0 is proportional to the probability of a particle's being captured when an aerosol stream passes a single fiber (3)

$$\alpha = 1 - \frac{\Delta x_0}{\Delta x}, \qquad [9]$$

where Δx is the index of filtration to be expected on the basis that all of the particles which graze the fibers in the filter adhere. For Δx a value was calculated in each case from previous results (3) based on the concept of an ideal filter. Although such a procedure might not yield numerically correct values of the "slippage coefficient," the relative differences in this quantity for different materials should be real. The expression previously developed (3) for Δx neglects inertia effects, and since much larger velocities were to be considered in this study, it was necessary to modify the expression to include possible inertia effects. Previous work (6, 7, 8, 9, 10) would suggest that the effective radius of a fiber for the deposition of aerosol particles by inertia alone is given at low Reynolds numbers by

$$R_{\mathrm{eff}}\ (\text{inertia alone}) = C_1\left(\frac{2}{9}\rho\frac{a^2V_0}{\eta}\right) - C_2 \qquad [10]$$

where ρ and a denote the particle density and radius, respectively. μ is the viscosity of air, and V_0 is the mean velocity of the air flow through the filter. C_1 and C_2 are constants for the values of $\rho a^2 V_0$ considered. The values of C_1 and C_2 proposed by previous workers are not consistent. The latest work (8) suggests that $C_2 = 0$ and $C_1 = 0.04$. Using these values

$$\Delta x = \frac{L}{A}\left[\bar{R} + a - \frac{\bar{R}}{\bar{R} + a} + \left(\frac{kT}{6\eta a \gamma V_0} + \frac{0.018\rho a^2 V_0}{\eta}\right)\left(1 + \frac{C\lambda}{a}\right)\right] \quad [11]$$

L = the total length of fiber in the filter.
A = the cross sectional area of the filter.
$\bar{R}$ = the mean fiber radius.
k = Boltzmann's constant.

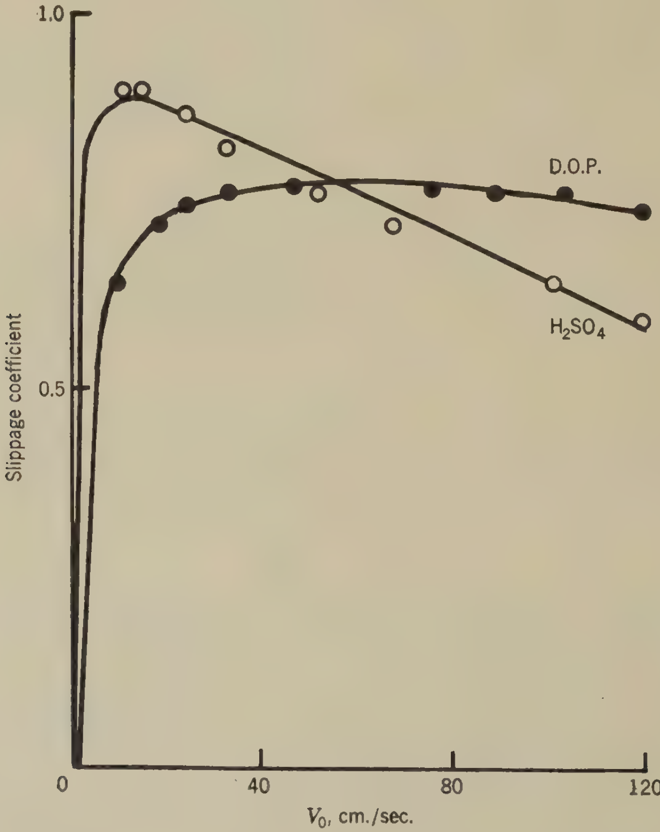

FIG. 8. Variation of the "slippage coefficient" with velocity illustrating the difference in behavior of D.O.P. and sulfuric acid aerosols ($a = 0.15\ \mu$). Points ● and ○ refer to data calculated from the filtration results of Ramskill and Anderson for a viscose filter and for D.O.P. and sulfuric acid aerosols, respectively. The full lines were plotted using Eq. [21] and the constants given in the text.

T = the temperature.
C = Cunningham's constant.
λ = the mean free path of air.
γ = a factor depending upon the mean distance between the filter fibers.

The methods of calculating γ, $\bar{R}$, and L have been given previously (3, 7, 11).

A typical result of calculations using Eqs. [9] and [11] is given in Fig. 8 and illustrates the difference in behavior of dioctyl phthalate and sulfuric acid aerosols observed by Ramskill and Anderson (1) for a viscose filter. The data required to calculate Δx for these and other experiments were kindly supplied by Dr. E. A. Ramskill.

A comparison of Fig. 8 with the results obtained in studying the deposition of particles on a single cylinder (Fig. 7) indicates that in both cases the chances of nonadherence on contact appear to be restricted to a range of velocities below and above which adherence is more likely. When all of the filtration data for the experiments which have been reported were analyzed the same phenomenon was observed. In Figs. 7 and 8 the solid lines were plotted from a semiempirical theory of the effect developed to facilitate further research. An abridged and simplified version of the considerations leading to an experimental expression for "slippage" follows.

2. The "Slippage Coefficient"

Consider a spherical aerosol particle of radius a which has come in contact with a filter fiber of radius R, as illustrated in Fig. 9. Without suggesting the mechanism responsible for the lack of adhesion we may say that the particle (or a drop) will be removed from the surface of the fiber just after contact if

the viscous drag
$$\geqslant \sigma F_A , \qquad [12]$$

where F_A denotes the force of adhesion, and σ is a constant. Assuming that

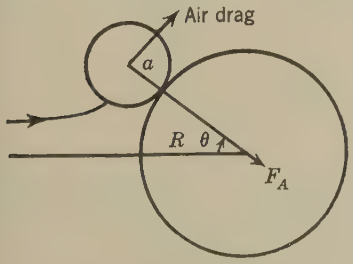

FIG. 9

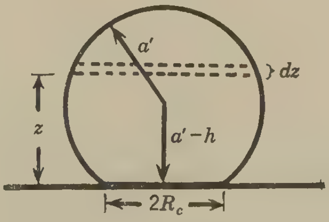

FIG. 10

FIG. 9. An aerosol particle in contact with a filter fiber.

FIG. 10. A flattened spherical particle on a flat plate.

the velocity near the fiber is given by the solution of the viscous flow equations (7) and the drag is given by an approximate use of Stokes' law, the angle θ_0' above which particles would be removed on impact is given by

$$C_\theta V_0 \sin \theta_0' = \sigma F_A \tag{13}$$

where
$$C_\theta = 1.5(1 - \beta)\phi \left[\frac{6\pi\eta a}{\left(1 + \frac{C\lambda}{a}\right)} \right] \cdot \left[1 - \left(\frac{R}{R + a}\right)^2 + 2 \cos \left(1 + \frac{a}{R}\right) \right], \tag{14}$$

$$\phi = \frac{1}{-\ln \beta + 2\beta - \frac{\beta^2}{2} - \frac{3}{2}} \tag{15}$$

and β is the packing density (3). Since the effective radius of the fiber is proportional to $\sin \theta_0'$,

$$\alpha = 1 - \frac{\sigma F_A}{C_\theta V_0}, \tag{16}$$

Equation [16] should give the correct value of the slippage coefficient provided all parts of the fiber were similar and electrical effects were absent. In practical cases neither of these conditions would be strictly fulfilled. Examination of filter fibers which had been exposed to aerosol particles indicated spots where there was a tendency for the particles to accumulate in some cases. The particles were not removed by rather rough handling of the fibers. We may therefore suggest that in a practical case a fraction, f, of the contacts between aerosol particles or drops and filter fibers are always effective, regardless of the velocity of impact. This is in approximate agreement with the results obtained in the study of the deposition of particles on a single cylinder (Table II). The slippage coefficient which would be determined experimentally is given by

$$\alpha = (1 - f)\left(1 - \frac{\sigma F_A}{C_\theta V_0}\right). \tag{17}$$

To apply this expression to slippage data from filtration experiments or other sources it was essential to determine F_A and particularly the manner in which it varies with the velocity of impact.

3. *The Force of Adhesion*

If $a \ll R$, the adhesive force between a spherical particle or drop in contact with a cylindrical fiber may be calculated by considering the force between a flattened particle and a flat plate, as illustrated in Fig. 10. With the method of Bradley (12) and Hamaker (13) F_A was calculated on the basis that the attraction was due to Van der Waals forces and the force pulling a single molecule to the plate from a distance r was C_3/r^4. The result was

$$F_A = \pi C_3 N_1 \left[-\frac{(a')^2}{3z^3} + \frac{1}{z} - \frac{\delta}{z^2} + \frac{\delta^2}{3z^3} \right]_{r_0}^{2a'-h+r_0}, \qquad [18]$$

where N_1 is the number of molecules in unit volume of the drop or particle and r_0 denotes the shortest distance between the molecules of the drop or particle and the flat plate which are in contact. The other symbols are illustrated in Fig. 10 and $\delta = a' - h + r_0$. For $r_0 \ll 2a' - h$ and $h \ll a'$

$$F_A = \frac{\pi C_3 N_1 a}{r_0^2}\left(1 + \frac{R_C^2}{3ar_0}\right), \qquad [19]$$

where R_C is the radius of the circular area of contact (Fig. 10). If ϵ_A is the energy of adhesion per unit area of contact,

$$F_A = 6\pi\epsilon_A a\left(1 + \frac{R_C^2}{3ar_0}\right). \qquad [20]$$

The force of adhesion therefore depends on the velocity of impact, in as much as the velocity of impact would affect the area of contact. This question is discussed in detail in the second article of this series, where the mechanism responsible for the lack of adhesion is considered. In applying Eq. [20] to slippage data it was found that all the results were in agreement with the hypothesis that R_C was proportional to V_0. This leads to

$$\alpha = (1 - f)\left[1 - \frac{6\pi\epsilon_A a\sigma}{C_\theta}\left(\frac{1}{V_0} + \frac{V_0}{V_m^2}\right)\right], \qquad [21]$$

where V_m denotes the velocity at which slippage is a maximum. This is the equation from which the data for the solid lines in Figs. 7 and 8 were calculated. In Fig. 7 $V_m = 26$ cm./sec., $f = 0.45$, and $6\pi\epsilon_A a\sigma/C_\theta = 4.5$. In Fig. 8 for the D.O.P. aerosol $V_m = 55$ cm./sec., $f = 0.2$, and $6\pi\epsilon_A a\sigma/C_\theta = 2.1$; for the sulfuric acid $V_m = 9.4$ cm./sec., $f = 0.1$, and $6\pi\epsilon_A a\sigma/C_\theta = 0.26$.

4. Discussion

The values of V_m, f, and $6\pi\epsilon_A a\sigma/C_\theta$ for the data available on the filtration of aerosols produced in La Mer-Sinclair generators have been included in an unpublished British Ministry of Supply report. They have not been reproduced at this time, since the filtration experiments were not designed to investigate the possibility that drops and particles do not always adhere to filter fibers on impact, and in consequence the data, although encouraging, are far from being complete. Since La Mer-Sinclair generators are in operation in many laboratories, it is to be hoped that appropriate steps will be taken to fill these gaps in the future, since such results would be of interest in other physical chemical problems where the impact of drops and particles with surfaces may not always result in adhesion.

VII. SUMMARY

1. The deposition of particles on the surface of a thin cylinder exposed to a low-velocity aerosol stream has been studied. The experimental results may be interpreted if we reject the common assumption that aerosol particles always adhere to surfaces on contact.

2. The presence of electric charges on some of the aerosol particles enhances their chances of adhering to a surface.

3. Coating of a cylinder may affect the chances of specific aerosol particles' adhering to it.

4. Many of the discrepancies between the actual performance of filters and that which would be expected from theory may be rationally explained by taking into account the possibility that not all the particles or drops which graze the surface of the fibers adhere.

5. Nonadherence on impact would appear to be limited to a range of particle or drop velocity and to depend upon the physical properties of the drop or particle as well as the collecting surface.

ACKNOWLEDGMENTS

This paper is published with the permission of the Chief Scientist, British Ministry of Supply. The author appreciates the interest shown by Mr. H. L. Green and Professor Sir Eric Rideal.

REFERENCES

1. Ramskill, E. A., and Anderson, W. L., *J. Colloid Sci.* **6,** 416 (1951).
2. La Mer, V. K., Gendron, I., and Gruen, R., *Nuclear Science Abstracts* **5,** No. 775 (1951).
3. Gillespie, T., *J. Colloid Sci.* **10,** 299 (1955).
4. Taylor, G. I., Aeronautical Research Committee. Report No. 4350, D.W.T.3, 1940.
5. Glauert, M. A., Aeronautical Research Committee. Report No. 4805, D.W.T.7, 1940.
6. Davies, C. N., *Inst. Mech. Engs.* (*London*) *Proc.* B, **1B,** 185 (1952).
7. Langmuir, I., O.S.R.D. Report No. 865, 1942.
8. Albrecht, F., *Physik. Z.* **32,** 48 (1931).
9. Sell, W., *Forschungsheft* **347,** 1 (1931).
10. Landahl, H. D., and Herrmann, R. G., *J. Colloid Sci.* **4,** 103 (1949).
11. Davies, C. N., Reprint from the Ninth International Congress on Industrial Medicine, 1949.
12. Bradley, R. S., *Phil. Mag.* **13,** 853 (1932).
13. Hamaker, H. C., *Physica* **4,** 1058 (1937).

ON THE ADHESION OF DROPS AND PARTICLES ON IMPACT AT SOLID SURFACES. II.

T. Gillespie and Sir Eric Rideal, F.R.S.

Department of Physical Chemistry, King's College University of London

Received December 1, 1954; revised April 12, 1955

I. Introduction

In the first article of this series (1) evidence was presented which indicated that many of the anomalous results which have been obtained in studies of the filtration of aerosols by fibrous filters may be explained on the basis that the drops and particles do not always adhere to the filter fibers on contact. An experimental study of the distribution of particles deposited on a cylinder exposed to an aerosol stream and an analysis of all the filtration data available led to the conclusion that there is usually a range of particle and drop velocities where there may be a lack of adhesion. Both above and below this range adhesion occurs on contact. In studying the effects of turbulence on the coagulation of an ammonium chloride aerosol Gillespie and Langstroth (2) found an indication of a similar process. In "still air" the rate of coagulation was compatible with the assumption that the particles adhered on contact. As the degree of turbulence was increased the coagulation rate did not increase as would be expected, but the aerosol appeared to coagulate less readily. At higher degrees of turbulence the rate of coagulation increased rapidly. These results are in agreement with the hypothesis that the chance of a particles adhering to a solid surface is dependent on the velocity of approach and that there exists a range of velocities where adhesion on contact is not certain. Because of the complex nature of filtration and coagulation experiments this evidence which suggests a lack of adhesion is not conclusive; in consequence we have attempted to examine the conditions under which particles or drops would exhibit this interesting velocity effect.

A detailed examination of the oblique impact of a jet of aerosol drops onto a microscope slide and a high-speed photographic study of the impact of large drops onto a flat glass surface combined with a semiquantitative analysis has led to a deeper understanding of an experimental relationship previously derived for the conditions under which adhesion on contact is not certain in filtration and other experiments (1). It appears that the mechanism responsible for the velocity effects referred to above is as follows.

When a particle or drop collides with a solid surface, there is an elastic reaction and the apparent area of contact is determined by the velocity of impact. The real area of contact is usually less than the apparent and depends upon the maximum pressure on impact. If the aerodynamic shearing forces are large enough and the real area of contact small enough, the joint will be broken by shear in the case of particles and by a "necking" out process in the case of drops. At very small velocities the aerodynamic forces are unable to do this, whereas at large velocities the area of contact is sufficiently great to ensure adhesion. This accounts for the fact that there appears to be a range of velocities in which adhesion does not always occur on contact.

Although the analysis of this complex effect was of necessity rather qualitative, the forces required to remove drops from a flat surface seemed to be so small that an attempt was made to measure the force required to detach drops from a solid surface with the aid of an ultracentrifuge. The results indicated that in this case too a "necking" out process occurred and the force necessary to detach a drop was very much less than would be required if this were not so.

II. The Oblique Impaction of Aerosol Drops

1. Apparatus and Procedure

The apparatus used to investigate the oblique impaction of aerosol drops is illustrated in Fig. 1. The liquid to be sprayed (dibutyl phthalate) was placed in the atomizer. With stopcocks *A* and *B* open an aerosol was generated using a compressed air supply of 2 lbs./in.^{2} pressure for 30 sec.,

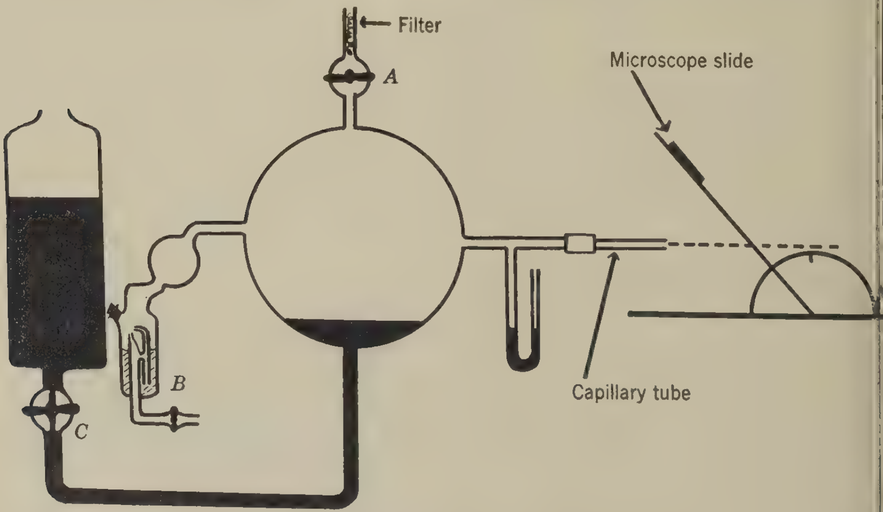

Fig. 1. Aerosol impaction apparatus.

thus ensuring that the liter flask used as an aerosol chamber was filled with a dilute, well-mixed aerosol. After closing stopcocks *A* and *B* the aerosol was allowed to settle for 1 min. Stopcock *C* was then opened and a jet of aerosol drops was pushed out of the horizontal capillary tube at a known velocity. The capillary tube normally used was 4 cm. long and 1 mm. internal diameter. Tubes up to 10 cm. long were used in check experiments without affecting the size distribution of the drops in the jet. The velocities used were such that a thin ribbon of apparently uniform diameter was extruded for a distance always greater than 5 cm. from the orifice. A microscope slide was placed on the inclined plane, which had its central portion cut away so that the slide was supported on guides which extended 1 cm. from each end. The slide was pulled through the jet at a known velocity, controlled by a system of elastic bands. The distance between the jet orifice and the spot where the jet struck the slide was 2.5 cm. to prevent small differences in this distance from affecting the results (3). Several samples were often taken on the same slide, side by side. The samples were kept sufficiently sparse to prevent one drop's falling on top of another. The total sampling time for a given aerosol was less than 2 min., which should have prevented coagulation and surface loss effects from substantially changing the aerosol during sampling. Before refilling the aerosol chamber for the next test it was thoroughly cleaned by introducing a stream of clean compressed air.

Each deposit obtained by this sampling procedure was assessed using a microscope with a 40× objective and a 15× eyepiece and substage illumination. The apparent radii of the drops were measured with the aid of a scale in the eyepiece. The mass of a given drop was determined by measuring the focal length of the lens formed by the drop and calculating the mass in a manner similar to that described by May (4). Since it was found that there was only a small variation in the focal length of the drops of a given area of contact regardless of the velocity or angle of impact, it was the custom in a good many assessments to measure only the apparent radii of the drops and to supplement this with a few focal length observations as a check. The nearly constant relation between the focal length and the area of contact indicated among other things that the procedure used in cleaning the slides, namely, washing in hot chromic acid, rinsing first in distilled water, then in acetone, and wiping with a clean cloth resulted in similar surfaces for each experiment. The size distribution of the drops in the jet was determined as required by trapping a sample in the space between two horizontal microscope slides and assessing the sedimented sample.

2. *Experimental Results*

Below a critical velocity depending upon the angle of impaction no aerosol drops were collected on the slides. Above this velocity the deposits were thin streaks of width approximately 1 mm. or less. There were no drops deposited outside this limit. At small angles of approach of the jet to the slide the drops were large and appeared uniform in size. As the velocity increased the drop size decreased and the drops still appeared to be uniform. Detailed examination of the deposits indicated that they were not as uniform as they seemed to be on first inspection, particularly at large velocities and large angles of approach. Most of the deposits were, however, much more uniform than would be expected on the basis that under a given set of conditions all the particles above a given size in the jet were being deposited. Since the size distribution of the drops in the jet was found to be independent of the velocity of the jet, it was concluded that for some reason the probability of capturing drops of a given size at first increased with increase in the jet velocity and then decreased. In Fig. 2 the probability of capture of drops of a given size was plotted against the velocity of the jet. All of the data for such plots were obtained in experiments in which the velocity of the sampling slide down the inclined plane was the same. The probability of capture, p, was therefore defined as

$$\mathrm{p} = \frac{nV'}{n'V}, \qquad [1]$$

where n denotes the number of drops of the stated size in a given length of the deposit obtained at a jet velocity V, and n' is the value of this quantity at a jet velocity V', where the maximum in the probability of capture versus velocity curves occurs.

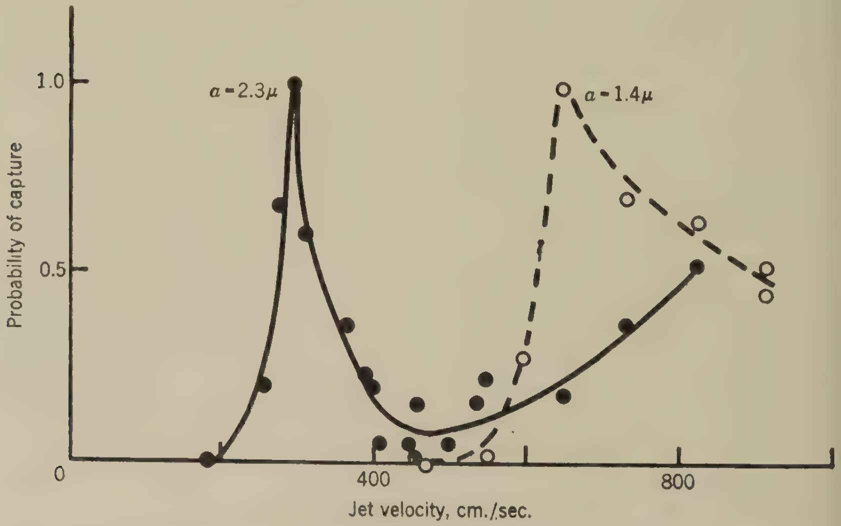

FIG. 2. Variation in the probability of capture of dibutyl phthalate drops on oblique impact with a solid surface.

To determine whether the flow in the jet and particularly whether the viscous boundary layer at the surface of the slide was responsible for the dips in the plots such as those illustrated in Fig. 2 an attempt was made to analyze the flow field by considering the oblique impact of a couple of two-dimensional jets. Although for a number of experimental reasons the jet actually used was round, the solution of the two-dimensional case should be adequate for the present purpose. The flow field was first calculated and hence the velocity along the surface of the slide just outside the viscous boundary layer on the basis of ideal fluid theory. The flow in the boundary layer was then determined. Finally the effect of the moving slide was considered. With the technique of Davies and Aylward (3) the trajectory of a given drop could be calculated and hence the effect of the air flow deduced on the assumption of adherence on contact. Further details are given in the appendix.

The free streamlines and the velocity along the plate just outside the viscous boundary layer in a typical case are illustrated in Fig. 3. The majority of the drops would be expected to take the left-hand path. In this region the viscous drag in the boundary layer increases from zero at the stagnation point, rises to a maximum, and then decreases. At low jet velocities the thickness of the boundary layer would be considerably greater than the diameter of the drops. The effect of the boundary layer is to decrease the chances of a given drop's arriving at the surface of the slide, but the effect is small. As the jet velocity increases the effect becomes relatively smaller owing to the decrease in the boundary layer thickness. The efficiency of collection of drops would always be expected to increase as the jet velocity was increased. Owing to the boundary layer the velocity of the drops near the slide surface would be of the same order as occur near filter fibers in filtration experiments, so there is good reason to believe that the dips in curves such as those in Fig. 2 are fresh examples of the lack

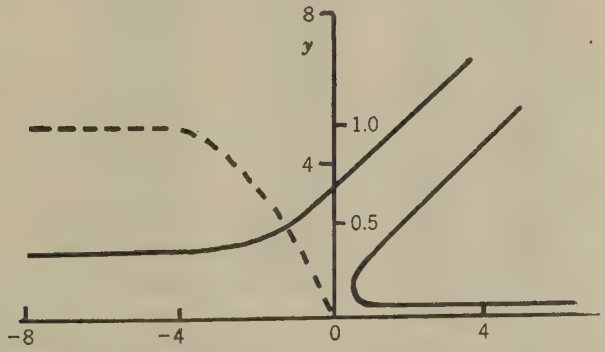

Fig. 3. The free streamlines and the velocity along the microscope slide just outside the viscous boundary layer for a jet impacting at an angle of 45 degrees onto the slide.

of adherence in a restricted velocity range. Since the experimental necessity of using a round jet made any theoretical analysis only qualitatively correct and also since the velocity range over which experiments were possible was strictly limited owing either to instability or spreading out of the jet, this technique was not further exploited.

Aside from providing independent evidence of the lack of adhesion of drops to solid surfaces on impact this group of experiments showed that since the viscous drag decreased at a distance from the strip deposits and no drops were observed outside the strips, the mechanism responsible for the lack of adhesion must be such that the drops left the surface at or near to the point of impact. This is in agreement with the interpretation of previous results for the deposition of particles on cylinders (1). In an attempt to establish the mechanism a high-speed photographic study of the impact of large drops of dibutyl phthalate with the same slides used in the jet impaction studies was initiated.

III. The Oblique Impaction of Large Drops

Except for the work of Ollivier (5), who considered the collision of large drops on a very rough surface, the problem of impaction of large drops onto a solid surface has received little attention. It is well known that many liquid drops bounce readily from smooth solid surfaces provided the contact angle formed by the liquid resting on the solid is large, e.g., mercury drops bounce readily from a glass surface. In our experiments we were more interested in the case where the contact angle is much smaller. Drops of dibutyl phthalate of about 2 mm. diameter were released from an

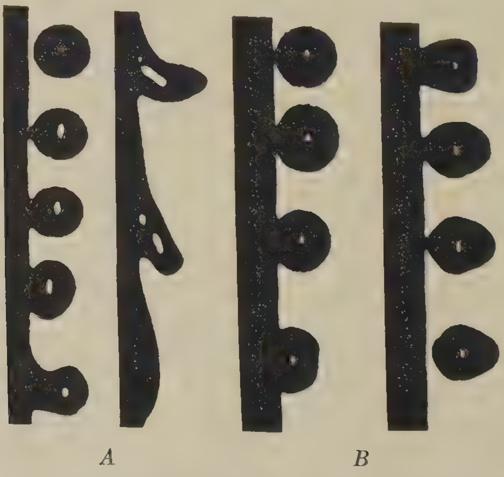

FIG. 4. The oblique impact of large drops of dibutyl phthalate onto a glass slide. Drop diameters were 2.2 mm. and 1.8 mm. in *A* and *B*, respectively. The last picture in the second column illustrates a drop which was on the glass surface for 10 min.

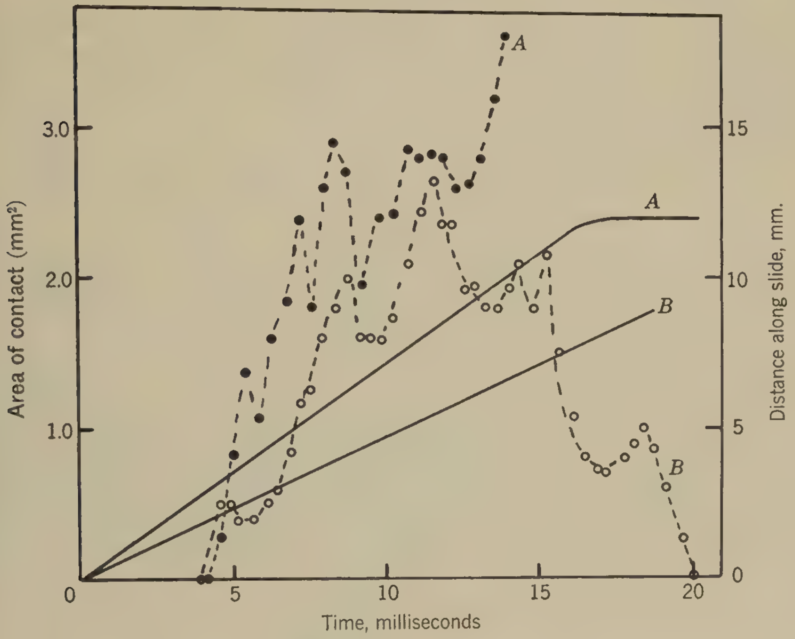

FIG. 5. Variation in the apparent area of contact and the distance along the slide with time for the drops illustrated in Fig. 4.

Agla syringe fixed rigidly at various heights above a microscope slide slightly inclined to the vertical. At a given height some of the drops bounced and some did not. High-speed (about 2000 frames/sec.) photographs were taken in a number of cases. Typical results are indicated in Fig. 4, where individual frames selected from the cine film have been pieced together. It should be noted that the contact angle is less than 90 degrees both for drops which adhere and for those which do not.

In Fig. 5 the apparent area of contact and the distance of the drop along the slide from an arbitrary origin are plotted against time for two typical drops. Knowing the velocity of a given drop along and toward the slide at each stage it was possible to calculate the energy available for removing the drop when the area of contact was a maximum. The work of adhesion was calculated for the drops which did not adhere. The oscillation of the drops prior to impact was so small that this effect could be neglected. On the assumption that the real area of contact was equal to the apparent the work required to remove the drops was of the order of 4 ergs/cm.^{2}, which is surprisingly low. Three things are apparent from these experiments: (1) the area of contact depends upon the velocity of impact and the drop size; (2) when a drop strikes a surface its area of contact might be small for a considerable time; and (3) the real area of contact might be very small presumably owing to air trapped between the liquid and solid surface. This evidence combined with the results of the aerosol experiments suggests a mechanism for the lack of adhesion of aerosol drops and particles in a restricted velocity range.

IV. The Lack of Adhesion of Aerosol Drops and Particles

1. Normal Impact

The normal impact of spherical particles with a flat solid surface is the easiest case to discuss, and it will be treated first because, although even it cannot be treated rigorously, the important factors operative can be described in a fairly satisfactory manner.

When a particle comes in contact with a solid surface in the absence of external forces, it will be deformed and may bounce if the energy stored in the deformation is greater than the energy of adhesion. If the radius of the area of contact of a particle or drop with a smooth flat solid surface is R_c it has been shown (1) that provided R_c is small in comparison with the radius, a, of the drop or particle, the force of adhesion is given by

$$F_A = 6\pi\epsilon_A a\left(1 + \frac{R_c^2}{3ar_0}\right), \qquad [2]$$

where F_A denotes the force of adhesion. ϵ_A is the surface energy of adhesion/cm.^{2} of contact and r_0 is the distance between the molecules of the drop or particle and the solid surface which are in contact. Equation [2] is based on the assumptions that the attraction is entirely due to Van der Waals forces and that the solid surfaces are perfectly smooth. While this second assumption is unlikely to be true in actual practice, Eq. [2] should be qualitatively correct and adequate for the present purpose. The energy of adhesion, E_A , which will determine whether a particle will bounce on impact, is given by

$$E_A = 6\pi\epsilon_A r_0 a + \pi\epsilon_A R_c^2. \qquad [3]$$

If the energy of deformation during the contact process is greater than E_A , the particle may bounce.

For a solid spherical particle impinging normally with velocity V_I on a flat solid surface under conditions in which Hertz's theory of impact applies (6)

$$R_{c_{\max}}^2 = 1.75\rho^{2/5}(K_1 + K_2)^{11/15}a^2V_I^{4/5}, \qquad [4]$$

where ρ is the density of the particle.

$$K_1 = \frac{1 - v_1}{B_1} \quad \text{and} \quad K_2 = \frac{1 - v_2}{B_2} \qquad [5]$$

TABLE I

Normal Impingement of Spherical Quartz Particles on a Flat Quartz Plate

a, (μ)	V_I (*cm./sec*)	$R_{c_{\max}}$ $\times 10^4$ (μ)	Kinetic energy $\times 10^9$ (*ergs*)	Energy of adhesion $\times 10^9$ (*ergs*)
2.0	0	0	0	6.8
2.0	1	1.8	0.045	6.8
2.0	10	4.5	4.5	6.8
2.0	100	11.3	450	6.8
0.5	1	0.45	0.0007	1.7
0.5	10	1.1	0.07	1.7
0.5	100	2.8	7.0	1.7
0.25	1	0.22	8.7×10^{-5}	0.85
0.25	10	0.55	0.0087	0.85
0.25	100	1.4	0.87	0.85

where v_1, v_2, and B_1, B_2, are the Poisson ratios and the moduli of elasticity in tension of the particle and the surface, respectively. $R_{c_{\max}}$ in Eq. [4] denotes the radius of the area of contact at maximum compression. There is a possibility that a particle of mass m will bounce if gravity can be neglected and

$$\tfrac{1}{2}mV_I^2 > E_A, \qquad [6]$$

where E_A is calculated from Eqs. [3] and [4]. For a quartz particle (spherical) impinging on a quartz plate taking $B_1 = B_2 = 6 \times 10^{11}$ dynes/cm.^{2}, $v_2 = v_2 = 0.2$, and $\epsilon_A = 30$ ergs/cm.^{2} (7), the results of calculations are given in Table I.

In filtration experiments it is often the practice to use particles which may not obey Hertz's theory of impact (6). In order to assess the behavior of such particles small spheres of "Q" compound (similar to plasticene) were dropped from various heights onto a horizontal microscope slide. The radius of the apparent maximum area of contact was determined by measuring the diameter of the flattened portion of the sphere or the stain left on the glass surface. A typical result is illustrated in Fig. 6. The straight line was calculated from

$$R_{c_{\max}}^2 = kR^2V^{4/5}, \qquad [7]$$

where $k = 0.007$. Taking $\epsilon_A = 30$ ergs/cm.^{2} as before, the results given in Table II were calculated.

It would seem that bouncing after normal impact may occur for sufficiently large values of the kinetic energy of approach. In practical cases the results obtained would be affected by surface contamination, which may either increase or decrease the energy of adhesion. The irregularity of the surfaces must also play a part by reducing the real area of contact. At maximum compression during impact the real area of contact should be proportional to the apparent area multiplied by the maximum pressure (8). Hence using Hertz's expression for the maximum pressure (6)

$$\text{Real } R^2_{c_{\max}} \propto \rho(K_1 + K_2)^{5/6}R^4V_I^2. \qquad [8]$$

In the event that a particle did not bounce, there would almost certainly be a partial joint fracture by elastic effects (9) which would depend upon V_I^2, so that correcting Eq. [2] for these effects

$$F_A = 6\pi\epsilon_A a(1 + GV_I^2), \qquad [9]$$

where G is independent of the velocity of impact but may depend upon the radius of the particle, etc. This expression for the force of adhesion is similar to that previously derived semiempirically in describing the lack of adhesion of aerosol particles on contact with filter fibers and other cylinders (1).

Whether we consider the effect of surface irregularities or not, it does not seem likely that bouncing alone is responsible for the velocity effects previously described, as there is no apparent reason why there should be a lack of adhesion in a restricted velocity range if this were the only mecha-

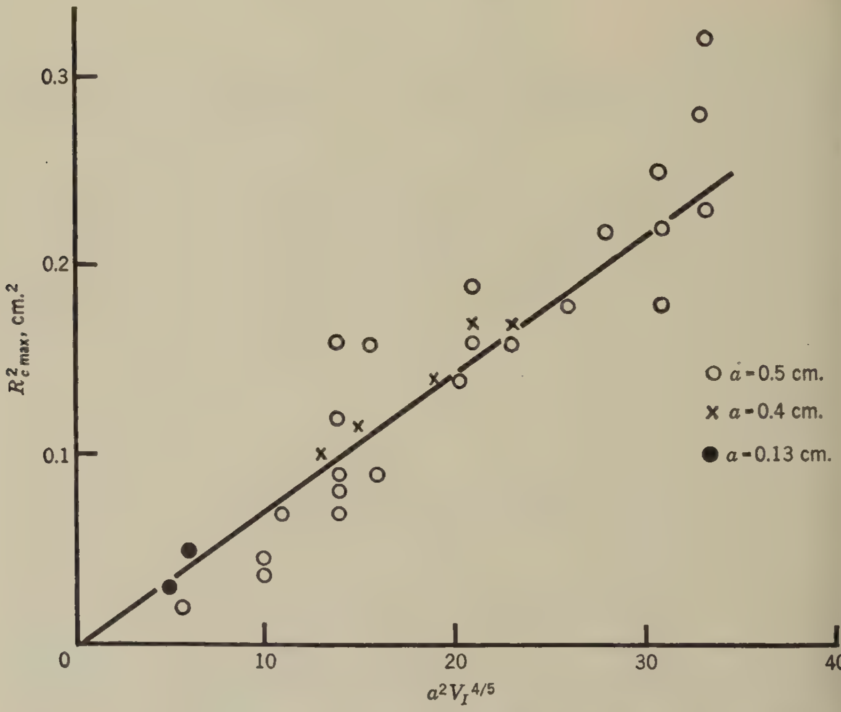

FIG. 6. Illustration of the proportionality between R^2_{cmox} and $a^2V_I^{\frac{4}{5}}$ for particles o "Q" compound.

TABLE II

Normal Impingement of Spherical Particles of "Q" Compound on a Flat Glass Plate

a (μ)	V_I (*cm./sec.*)	$Rc_{\max}$ (μ)	Kinetic energy $\times 10^9$ (*ergs*)	Energy of adhesion $\times 10^9$ (*ergs*)
2.0	1	0.17	0.034	34
2.0	10	0.43	3.4	180
2.0	100	1.08	340	1100
0.5	1	0.042	5.2×10^{-4}	3.4
0.5	10	0.11	0.052	13.3
0.5	100	0.27	5.2	71

nism operating. In the presence of external forces such as viscous aerodynamic drag, however, the tendency to bounce would greatly facilitate the chances of the particles' escaping adhesion. In view of the fact that the area of contact of drops depends upon the velocity of impact and the real area of contact is often less than the apparent, it is not unreasonable to suspect that similar considerations apply to drops as well as particles.

Without suggesting a definite mechanism Gillespie (1) found that the lack of adhesion of drops and particles to filter fibers and other cylinders could be attributed to the viscous drag parallel to the surface of the fibers and the chances of nonadherence were greatest for oblique impact. In the next section the meaning of his semiempirical equations is discussed, and it is shown that the experimental expression which was used to interpret filtration results (1) is in qualitative agreement with aerosol impaction experiments and the ideas expressed above.

2. *The Oblique Impact of Aerosol Drops and Particles in the Presence of a Viscous Drag*

Most of the mechanisms which might be expected to account for the lack of adhesion of aerosol drops and particles on impact at solid surfaces may be neglected. In view of the fact that in the impaction studies of Section II both the velocity along the slide and the viscous drag at the surface decreased as the distance from the strip deposits increased, the absence of drops outside the strip of width equal to that of the jet rules out electric forces and movement of the drops along the slide as major factors. Electric effects may, however, be responsible for some of the scatter illustrated in Fig. 2. The possibility of a complete air film's acting as a cushion can also be disregarded. The breaking of this film would be expected to be a statistical process, and hence some drops would have been observed outside the limit actually determined. This effect is more important in media of higher viscosity than air, and an independent investigation of it is currently in progress. Calculations indicate that it may be partially responsible for the fact that there is a critical velocity in aerosol impaction experiments below which no drops are collected. The vibration of the drops prior to impact as described by Ollivier (5) may contribute to the scatter of data as illustrated in Fig. 2, but in view of our photographic studies it would not be expected to be a major factor.

A common feature of filtration, coagulation, and aerosol impaction studies is that the drops and particles are subjected to a viscous drag continuously throughout the process of impact with a solid surface. Once the base of the drop or particle was arrested, the full force of the air drag aided by distortion and vibration due to impact may detach drops by a "necking" out process or particles by a peeling action.

The equation of motion of a drop or particle parallel to a solid surface at contact is approximately

$$m\frac{du}{dt} = 6\pi\eta a(V_a - u) - \text{friction}, \qquad [10]$$

where u denotes the velocity of the drop or particle along the solid surface and m is its mass. V_a denotes the velocity of the air parallel to the solid surface at distance a. Figure 4 indicates that at the perimeter of the area of contact of a drop there is likely to be real contact between the drop and the surface. The frictional force retarding the base of the drop would be given approximately (10) by

$$\text{Friction} = 2\gamma_{SL}R_c, \qquad [11]$$

where γ_{SL} is equal to or greater than the work of adhesion calculated in the usual manner from the contact angle depending upon the surface roughness. Hence

$$\text{u} = V_a - \frac{2\gamma_{SL}R_c}{6\pi\eta a}\left[1 - \exp\left(-\frac{6\pi\eta at}{m}\right)\right]. \qquad [12]$$

On this basis the bottom of a drop of small mass would be arrested very quickly for small values of V_a.

Once the velocity of the base of a drop or particle was relatively small, a "necking" out process or a peeling action would occur, provided the viscous drag was greater than or equal to a certain fraction, σ, of the force of adhesion. Using Eq. [9] drops or particles would not be expected to adhere to a solid surface on impact if

$$6\pi\eta aV_a \geqslant \sigma[6\pi\epsilon_A a(1 + GV_I^2)]. \qquad [13]$$

This is practically identical with the experimental relationship previously found (1) to be descriptive of the lack of adhesion of aerosol particles and drops to filter fibers in a restricted velocity range, the only difference being that empirically the total velocity of the drop or particle which in

TABLE III

Typical Values of the Coefficient of Adhesion in Shear on Impact

Aerosol	Collecting surface	$\sigma \epsilon_A \times 10^5$ (*ergs/cm.*^{2})	$\sigma^a \times 10^6$	Type of experiment
Dioctyl phthalate	Glass	34	11.1	Filtration
Dioctyl phthalate	Viscose	2.5	0.83	Filtration
Sulfuric acid	Viscose	0.67	0.22	Filtration
Stearic acid	Steel	2.1	27	Deposition on a Cylinder

[a] Calculated assuming $\epsilon_A = 30$ ergs/cm.^{2}

practical cases is nearly equal to V_a should replace V_I, the normal velocity of impact. There may be a number of reasons for this, one of which being that the fibers are curved and another that relative motion of two surfaces in contact might increase their adhesion (11).

With the use of the results of calculations described in the appendix it is possible to derive an inequality similar to Eq. [13] which gives a qualitative explanation of aerosol impaction results, such as illustrated in Fig. 2.

Typical values of σ, which might be termed the "coefficient of adhesion in shear during impact," calculated from filtration data and the results of measuring the position of aerosol particles deposited on a cylinder exposed to an aerosol stream (1) are given in Table III. Even considering the qualitative nature of our arguments the values of σ are small, indicating that when a "necking" out process or a peeling action occurs, the force required to detach a drop or particle from a solid surface is small. To investigate this further we tried to measure the force for dibutyl phthalate drops on glass using a centrifuge.

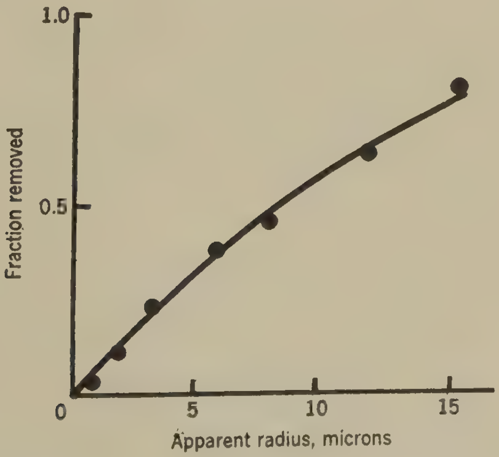

FIG. 7. Detachment of dibutyl phthalate drops from a glass surface using a centrifugal force of 400 g.

V. Measurement of the Force of Adhesion

Dibutyl phthalate drops collected on a small glass slide by sedimentation were placed in an ultracentrifuge and the number removed under various conditions determined. Typical results are illustrated in Fig. 7. The radii of the drops were determined by the technique described above. The results of Fig. 7 were obtained with the centrifugal force acting as nearly as possible normal to the surface of the glass, although owing to the slight vibration of the rotor there was some doubt as to its actual direction. For our present purposes this is not really important.

We may conclude that (*1*) not all the drops of the same mass are removed at the same rate; this was true regardless of the area of the slide chosen for assessment. (*2*) The number of drops of a given size removed from the surface depends upon the time the centrifugal force acts. (*3*) Since the apparent radii of contact were found to be proportional to the radii of the equivalent spheres to which the drops were equal in volume, we would expect plots such as illustrated in Fig. 7 to be linear if Eq. [2] were to apply. The curvature of these plots increased with the length of the interval between collection and testing in the centrifuge. As a microscopic assessment was necessary before testing, this interval was generally greater than 20 min. For this reason and also because the assumptions leading to Eq. [2] are likely to be more valid when $R_c \ll a$, which was not the case in these centrifuge experiments, Eq. [2] is probably qualitatively correct when applied to the problem of detachment on impact as above.

Some idea of the actual force required to detach drops as compared to that calculated from Eq. [2] on the assumption that the real area of contact is equal to the apparent may be obtained on inspection of Table IV. Centrifuge experiments with large drops of the order of 2-mm. diameter indicated that one or a number of very small drops were left behind on detachment of the major part of the drop. Such remnants would have been too minute to detect in the experiments with small drops. This suggests that not all of the bonds at the surface are broken simultaneously and that a "necking" out process occurs, which accounts in part for the small forces required for detachment.

TABLE IV

Comparison of the Force Required to Detach Dibutyl Phthalate Drops from a Glass Surface Experimentally and the Calculated Force of Adhesion

(ϵ_A = 30 ergs/cm.^{2} and $r_0 = 6 \times 10^{-8}$ cm.)

		Force of adhesion (*dynes*)		
a (μ)	R_c (μ)	Calculated	Experimental	Per cent removed
6.8	15	7100	5.2×10^{-4}	80
1.4	3	284	8.9×10^{-6}	25

VI. DISCUSSION

In the present study the role played by the particle or drop velocity has been emphasized, whereas the effect of the size of a particle or drop on its chances of adhering on impact onto a solid surface has received little attention. Any attempt to obtain further information on the effect of particle or drop size using impaction or deposition experiments (1) would be difficult particularly for small particles or drops. There is a good chance that such information could be obtained in carefully planned filtration experiments.

The present article combined with previous work (1, 12) represents an attempt to establish a working theory for the interpretation of such experiments. The attitude adopted has been that whereas the concept of an ideal filter (12, 13) as a basis for the discussion of the filtration process may not lead to numerically correct results, it should be possible to trace the effect of the individual variables, including electric effects and the possibility that aerosol particles or drops do not always adhere to the filter fibers on contact. To describe this last effect we may say (1) the slippage coefficient α is given by

$$\alpha \div (1 - f)\left[\frac{1 - \epsilon_A \sigma R\left(1 + \frac{10^{-5}}{a}\right)}{\psi \eta a}\left(\frac{1}{V_0} + G'V_0\right)\right] \qquad [14]$$

where ψ is a function of the packing density (1), R is the fiber radius, and f is the fraction of the aerosol particles or drops which would adhere on impact regardless of the velocity. V_0, is the mean velocity of the air through the filter. f and G', which is related to the proportionality constant between the real area of contact of a drop or particle on impact onto a solid surface and the square of the velocity of impact (Eqs. [8] and [9]), would be difficult to determine from theory. Provided electrical effects are small and filtration measurements are made under conditions where diffusion effects are negligible, it should be possible to determine G' for various aerosols, since it is equal to $1/V_m^2$, where V_m is the velocity at which slippage is a maximum in any particular case (1). La Mer-Sinclair homogeneous aerosols are particularly suited to such experiments, and if the same care were taken in preparing model filters as has been taken in producing these test aerosols (14), there is good reason to expect interesting results. In such studies the working theory which has been developed should be of considerable help.

VII. SUMMARY

The results of a study of the oblique impaction of aerosol drops onto a solid surface may be interpreted on the hypothesis that there is a range of velocities of impact in which adhesion on contact is not certain and that

the drops leave the surface at or near the point of impact. A high-speed photographic study of the oblique impact of large drops onto a solid surface has revealed that there is an elastic reaction on impact and (*1*) the area of contact depends upon the velocity of impact and the drop size; (*2*) when a drop strikes a surface, the area of contact might be relatively small for a considerable time; and (*3*) the real area of contact might be very small, presumably owing to air trapped between the liquid and solid.

Using Hertz's theory of elastic impact and introducing a qualitative correction for the possibility that the real area of contact may be less than the apparent led to a deeper understanding of the experimental expression previously presented for the lack of adhesion of aerosol drops and particles in filtration and other experiments. The lack of adhesion is attributed to the air drag which acts throughout the contact process and aided by the tendency to bounce removes drops by a necking out process and particles by a peeling action. At low velocities the air drag is not large enough to detach drops and particles on impact, and at large velocities the real area of contact is large enough to ensure adhesion. This accounts for there being a range of velocities in which adhesion on contact is not certain, whereas adhesion occurs above and below this range.

REFERENCES

1. GILLESPIE, T., *J. Colloid Sci.* **10,** 266 (1955).
2. GILLESPIE, T., AND LANGSTROTH, G. O., *Can. J. Chem.* **29,** 201 (1951).
3. DAVIES, O. N., AND AYLWARD, M., *Proc. Phys. Soc. (London)* **64,** 889 (1951).
4. MAY, K. R., *J. Sci. Instr.* **22,** 187 (1945).
5. OLLIVIER, M., *Ann. chim. et phys.* **8,** 289 (1907).
6. HERTZ, H., *J. reine u. angew.*, **92** (1881).
7. BRADLEY, R. S., *Phil. Mag.* **13,** 853, (1932).
8. BOWDEN, F. P., AND TABOR, D., *Proc. Roy. Soc. (London)* **A169,** 391 (1939).
9. CROOK, A. W., *Proc. Roy. Soc. (London)* **A212,** 482 (1952).
10. BIKERMANN, J. J., *J. Colloid Sci.* **5,** 349 (1950).
11. MCFARLANE, J. S., AND TABOR, D., *Proc. Roy. Soc. (London)* **A202,** 244 (1950).
12. GILLESPIE, T., *J. Colloid Sci.* "The Role of Electric Forces in the Filtration of Aerosols by Fiber Filters" (submitted for publication).
13. LANGMUIR, I., O.S.R.D. Report 865, 1942.
14. SINCLAIR, D., AND LA MER, V. K., *Chem. Revs.* **44,** 245 (1949).
15. MILNE-THOMSON, L. M., "Theoretical Hydrodynamics." Macmillan, London, 1949.
16. GOLDSTEIN, S., "Modern Developments in Fluid Dynamics." Oxford Engin. Sci. Series, Oxford University Press, 1943.

APPENDIX

The Oblique Impact of a Two-Dimensional Jet onto a Flat Surface

Milne-Thomson (15) has calculated the complex potential for the oblique impact of a two-dimensional jet onto a solid surface by considering the impact of two such jets as indicated in Fig. 8. If x and y are the cartesian coordinates with origin at the stagnation point, we find in region I where $0 \leqslant \theta \leqslant \pi - \beta$

$$x = \frac{2h}{\pi}\left[\frac{\cos\beta}{2}\left\{\frac{\left(\frac{V}{q}+\frac{q}{V}+2\cos\theta\right)\left(\frac{V}{q}+\frac{q}{V}-2\cos\theta\right)}{\left(\frac{V}{q}+\frac{q}{V}+2\cos(\theta-\beta)\right)\left(\frac{V}{q}+\frac{q}{V}+2\cos(\theta+\beta)\right)}\right\}\right.$$

$$+ \tfrac{1}{2}\log\left\{\frac{\frac{V}{q}+\frac{q}{V}+2\cos\theta}{\frac{V}{q}+\frac{q}{V}-2\cos\theta}\right\} + \beta\sin\beta \qquad [15]$$

$$\left. + \sin\beta\left\{\tan^{-1}\left(\frac{V-q}{V+q}\tan\frac{\theta-\beta}{2}\right) - \tan^{-1}\left(\frac{V-q}{V+q}\tan\frac{\theta+\beta}{2}\right)\right\}\right]$$

$$y = \frac{2h}{\pi}\left[\frac{\sin\beta}{2}\log\left\{\frac{\frac{V}{q}+\frac{q}{V}+2\cos(\theta+\beta)}{\frac{V}{q}+\frac{q}{V}+2\cos(\theta-\beta)}\right\}\right.$$

$$-\cos\beta\left\{\tan^{-1}\left(\frac{V-q}{V+q}\tan\frac{\theta-\beta}{2}\right)\right\} + \tan^{-1}\left\{\frac{V-q}{V+q}\tan\frac{\theta+\beta}{2}\right\}$$

$$+\tan^{-1}\left(\frac{V-q}{V+q}\tan\frac{\theta}{2}\right) + \tan^{-1}\left(\frac{V-q}{V+q}\cot\frac{\theta}{2}\right) \qquad [16]$$

$$+\cos\beta\left\{\tan^{-1}\left(\frac{V-q}{V+q}\tan\frac{\theta}{2}\right) - \tan^{-1}\left(\frac{V-q}{V+q}\cot\frac{\theta}{2}\right)\right\}$$

$$-\frac{\pi}{2}(1-\cos\beta),$$

where V is the mean velocity in the jet and q is the velocity at any point. The other symbols are illustrated in Fig. 8 and θ has its usual significance.

In region II $\pi > \theta \geqslant \pi - \beta$,

$$x = x \text{ of region I minus } 2h\sin\beta; \qquad [17]$$

$$y = y \text{ of region I minus } 2h\cos\beta. \qquad [18]$$

When $\beta = \pi/2$, Eqs. [15] and [16] are equivalent to the values given by Davies and Aylward (3) for the normal impaction of a jet when the distance from the jet orifice to the point of impaction is relatively large. Since $k_1 = h(1 + \cos\beta)$ and $k_2 = h(1 - \cos\beta)$ for small angles of approach, the vast majority of the drops in such a jet would follow the left-hand path.

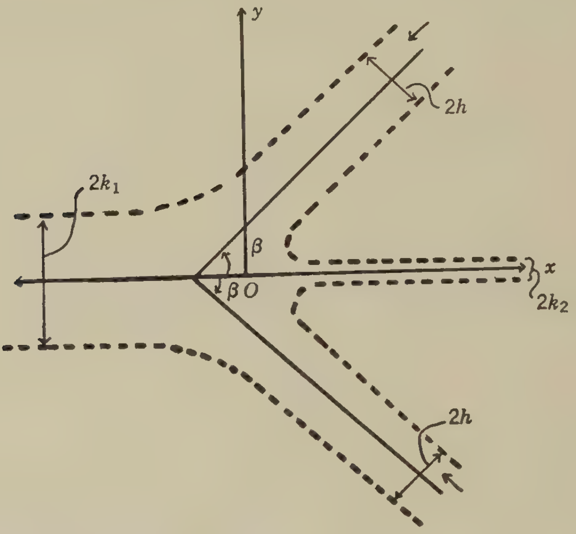

FIG. 8. The oblique impact of a pair of two-dimensional jets.

When the sampling slide in impaction experiments is stationary, as an approximation the velocity along the slide just outside the viscous boundary layer, V_1, would be $V_1 = \beta_1 x$ up to the point where $V_1 = V$. β_1 is a constant which depends upon β, the angle of approach. The thickness of the boundary layer and the flow in it may be calculated using this approximation (16). When the sampling slide is moving with velocity V_S we have $V_1 = \beta_1 x - V_S$ or $V_1 = \beta_1 x'$, where $x' = x - V_S/\beta_1$. The effect of movement of the sampling slide is therefore to move the stagnation point along the slide and increase the drag on one side of the jet and decrease it on the other. The changes in the stagnation point in the experiments described in Section II above would be slight. In any consideration of aerosol impaction data on the basis of the ideas developed in this article it is to be noted that the drag at the surface is proportional to $V^{3/2}$ and that it increases from the stagnation point to a maximum and then decreases.

THE ROLE OF ELECTRIC FORCES IN THE FILTRATION OF AEROSOLS BY FIBER FILTERS

T. Gillespie[1]

Chemical Defence Experimental Establishment, Porton, near Salisbury, Wiltshire, England

Received December 1, 1954; revised April 12, 1955

I. Introduction

A survey of the reported data on the filtration of aerosols by fiber filters (1, 2, 3, 4) reveals large variations in the shape of the per cent penetration versus particle size curves according to the nature of the aerosol, the characteristics of the filter, and the air flow. These variations are considerably greater than those allowed by mechanical theories of filtration (5, 6) which do not take electric forces into account. This investigation was undertaken to obtain a quantitative estimate of the role of electric forces in the filtration process, since they may account for some of the variation in the experimental filtration results (7).

Electric charges may affect the filtration process in two possible ways: (*1*) Particles or drops may be pulled to the fibers from an appreciable distance; and (*2*) the presence of electric charges may help to ensure that particles or drops which have come in contact with the fibers are retained. In this article the first possibility is considered.

Measurements were made of the electric charge distributions of typical test aerosols and the net electric charge per unit length on the fibers of various filters. These data were then applied to corresponding filtration data. In order to do this a theory of filtration was developed which takes into account electrical as well as mechanical effects.

It is believed that the electric charges are responsible for some of the discrepancies in filtration data. In particular the difference in results obtained with the La Mer-Sinclair monodisperse aerosol generator (8) and with the older techniques is attributed to the fact that the carefully prepared monodisperse aerosols are known to have few particles with electric charges (9), whereas the heterogeneous aerosols used in the other techniques may be expected to have an appreciable number of such particles.

---

[1] Present Address: Department of Physical Chemistry, King's College, University of London.

II. Experimental

1. Measurement of the Electric Charge Distributions of the Test Aerosols

Two aerosols were chosen for assessment which are representative of the types of aerosol commonly used in filtration experiments. The first was a homogeneous stearic acid aerosol from a La Mer-Sinclair generator (8). The second consisted of spherical polystyrene particles produced by spraying a solution of polystyrene in carbon tetrachloride.

The electric charge distributions were determined with the aid of an instrument which has been fully described elsewhere (10). A sample of stearic acid aerosol from a La Mer-Sinclair generator was introduced into a 500-ml. flask and was then tested with the instrument. The polystyrene aerosol was formed by spraying a 4% solution of polystyrene in carbon tetrachloride from a Collison atomizer (11) operating at 30 lb./in.^{2} into a 0.2-m.^{3} wooden chamber. The aerosol was fanned during the production, which took 30 sec., and was dilute enough to avoid serious coagulation effects. The electric charge distribution samples were then taken as quickly as possible (time of sampling <5 min.).

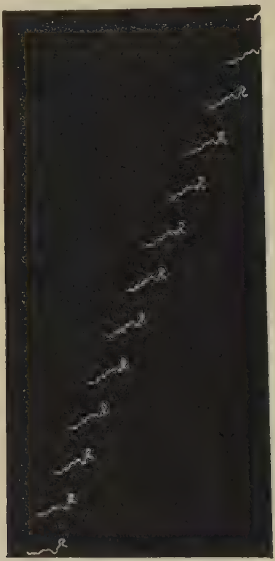

FIG. 1. Photograph of a wool resin fiber falling in a uniform **horizontal electric** field (E equals 0.26 e.s.u.).

2. Measurement of the Electric Charge on Single Filter Fibers

The net electric charge per unit length on the filter fibers was determined by photographing the trajectories of specimen fibers which were dropped between two parallel and vertical electrodes maintained at a high d.-c. potential difference (1–8 kv.). The apparatus consisted of a polystyrene box 30 cm. by 28 cm. by 12.7 cm. The end through which the fibers were photographed consisted of a piece of removable plate glass. The fibers were illuminated by a stroboflash lamp which threw an intermittent beam of light up through the bottom of the box. A ½-in. diameter hole was bored in the top of the box to allow the fibers to be introduced between the electrodes, which consisted of aluminum foil completely covering the two largest sides of the box. One electrode was maintained as much above ground potential as the other was below. The fibers chosen for assessment were generally from 1 cm. to 2 cm. long. Figure 1 illustrates the type of trace obtained.

The equations of motion of a cylindrical fiber which is long enough so that end effects may be neglected falling in a uniform horizontal electric field of strength E are

$$\beta' \frac{dx}{dt} = EQ, \qquad [1]$$

$$\beta' \frac{dy}{dt} = mg, \qquad [2]$$

where m denotes the mass per unit length of the fiber, Q denotes the net electric charge per unit length of the fiber, and g denotes the acceleration due to gravity; x and y are to be taken in the horizontal and vertical directions, respectively, and β' is given by

$$\beta' = \frac{4\pi\eta}{\frac{1}{2} - \psi - \log\left(\frac{1}{2}\phi R\right)}; \qquad \phi = \frac{u}{2\nu} \qquad [3]$$

where R is the fiber radius and η and ν denote the viscosity and kinematic viscosity of air, respectively. ψ denotes Euler's constant (0.577) and u refers to either dx/dt or dy/dt, whichever is applicable. Since for fibers with radii of the order of 10 μ or less, β' is independent of u (12), we should expect from Eqs. [1] and [2] that the trajectory of a fiber would be a straight line of slope mg/EQ. The net electric charge per unit length, Q, was calculated from a measurement of the slope, and a calculation of m was made from a knowledge of the density of the fiber and a microscopic assessment of the radius.

The use of β' in both Eqs. [1] and [2] is based on the assumption that Eq. [3] is applicable not only to broad-on motion but to motion along the axis of the fiber. In view of the fact that the fibers were usually curled up (Fig. 1) and often had rough surfaces, this procedure should lead to values of Q which are sufficiently accurate for the present purpose.

3. *Filtration Experiments*

Penetrations were measured in the La Mer-Sinclair generator experiments optically with a Pulfrich nephelometer, and particle size was determined by measurement of sedimentation velocities or by means of the light-scattering techniques described by Sinclair and La Mer (8). The penetrations were measured at suitable intervals and the initial penetrations obtained by extrapolation of penetration versus time curves.

The polystyrene aerosol filtration results were obtained from Mr. W. J. Harris of this laboratory. Working under the direction of Dr. D. J. Thomas, he used a method similar in principle to that described by Burton (1). The chief difference was the use of electrostatic rather than thermal precipitation for the collection of samples of the test aerosol. The experimental results which are given below are the mean of two experiments in each of which about 1000 particles were counted per sample.

III. Experimental Results

In all cases the electric charge distributions of the aerosols were found to be symmetrical. When the La Mer-Sinclair generator was functioning so as to provide a homogeneous aerosol, less than 5 % of the particles had an electric charge. In what follows such aerosols have been considered as uncharged. It is interesting to note that when the generator was yielding a heterogeneous aerosol, as many as 70 % of the particles were charged.

The theory of filtration given below indicates that it is not always essential to know the complete electric charge distribution of a given test aerosol, although it was determined in the present experiments. All that is really required is (*1*) the fraction of particles of a given size which are charged (f_{aq}) and (*2*) the manner in which the average electric charge ($\bar{q}$) varies with the particle radius. Figures 2*a* and 2*b* illustrate these quantities for the polystyrene aerosols. The average electric charge was calculated in each case with neglect of the neutral particles and with disregard of the sign. With the instrument used in these experiments it was possible to determine these factors only for particles above the limit of visibility of

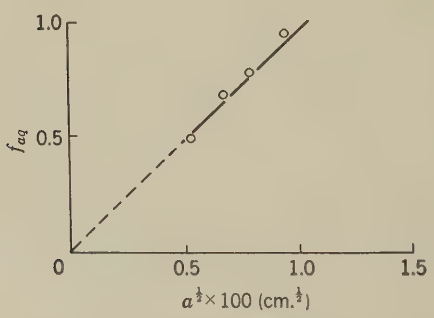

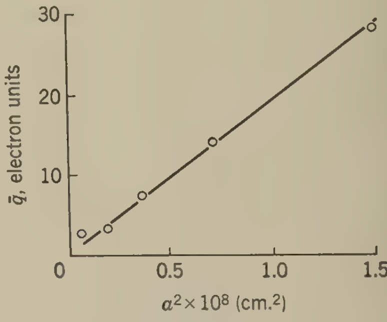

Fig. 2*a*. Relation between the average electric charge of polystyrene aerosol particles of a given radius and the square of the radius.

Fig. 2*b*. Relation between the fraction of the particles of a polystyrene aerosol of a given radius which are charged and the square root of the radius.

the optical microscope. For smaller particles it was necessary to extrapolate, as shown in Fig. 2*a* for the polystyrene aerosols, and to assume that the aerosols of radii less than 0.2μ from our La Mer-Sinclair generator are uncharged. Both the extrapolation and the assumption may lead to difficulties for particles below this limit.

The characteristics of some of the filters examined are listed in Table I. Among the data given is the average net electric charge per unit length of the fibers of each filter. In all cases there seemed to be more negative than positive fibers but the difference was small and it was doubtful if it was real. The tabulated values refer to the average net electric charges per unit length calculated disregarding the sign of the charge. The average positive value was approximately equal to the average negative value. The possible errors given in the table do not take into account errors which might conceivably occur owing to frictional effects involved in removing the fibers from the filters. Such errors are probably greatest in the case of the U.S. Chemical Corps paper No. 5, because of the difficulty encountered in removing the fibers.

Determination of the net electric charge of filter fibers not listed in Table I revealed that a wide range of values was possible. The values obtained for a given material seemed to depend upon the method of production or the conditions of storage. For example, wool fibers taken from one wool asbestos filter had a net electric charge of 0.003 ± 0.001 e.s.u./cm., whereas fibers from a similar filter had a net electric charge of less than 10^{-4} e.s.u./cm.

IV. THEORY OF FILTRATION

At the present stage in our knowledge of the part played by electric forces in the filtration process there is a need for a simple theory of filtration which has two main characteristics. It should be based on first principles so that the effect of the individual variables may be traced, and it should take into account electrical as well as mechanical effects. It is believed that the following analysis leads to a working theory which has these characteristics for particles of radius less than 0.5μ when the mean velocity of the air past the fibers is less than 30 cm./sec.

Following the lead of Langmuir (5) a simple model of a filter is suggested such that the fibers are considered to be uniformly distributed in a series of layers perpendicular to the direction of the air flow. If Δ denotes the fraction of the aerosol taken out by each layer, the penetration through the filter is given by

$$P = (1 - \Delta)^x, \qquad [4]$$

where x is the number of layers and P denotes the penetration expressed as a fraction. Since $\Delta \ll 1$ in the cases of practical interest (5),

$$P = e^{-\Delta x}. \qquad [5]$$

If the chances of a particle's being caught by a fiber by diffusion processes is assumed to be independent of its chances of being caught by direct interception when a quasi stationary state has been reached, we may write

$$\Delta x = \frac{L}{V_0 A}(2R_{\text{eff}} V_0 + I), \qquad [6]$$

where L denotes the total length of the fiber, and A is the cross-sectional area of the filter. R_{eff} is the effective radius of the fibers for collisions by interception. V_0 denotes the mean linear flow rate past the fibers, and I is a measure of the probability of a particle's being intercepted in unit time by unit length of the fibers through diffusion processes. Provided the total length of fiber in the filter, the effective radius of the fibers for collisons by interception, and the probability of capture of particles by diffusion processes were known, it should be possible to calculate the per cent penetration versus particle size curves for a given filter. An attempt to determine these quantities taking electric forces into account is described below.

1. *Filtration by Diffusion Processes*

The diffusion of spherical aerosol particles of radius a and electric charge q toward a cylindrical fiber of radius R and net electric charge Q e.s.u./cm. is described by

$$\frac{1}{r}\frac{dn}{dr} + \frac{d^2n}{dr^2} - \left(\frac{G}{r} - \frac{H}{r^3} - \frac{J}{(r-R)^2}\right)\frac{dn}{dr} = 0, \qquad [7]$$

where n denotes the number of particles per cubic centimeter at distance r from the axis of the fiber.

$$G = \frac{2Qq}{kT}; \qquad [8]$$

$$H = \frac{2}{3}(\epsilon - 1)\frac{Q^2a^3}{kT}; \qquad [9]$$

$$J = \frac{q^2}{4kT}\left(\frac{K-1}{K+1}\right); \qquad [10]$$

where k denotes Boltzmann's constant, T is the temperature, and ϵ and K are the dielectric constants of the particles and the fiber, respectively. Equation [7] was obtained through an argument very similar to Townsend's treatment of the diffusion of ions toward a charged sphere (13). The boundary conditions necessary for the solution of Eq. [7] were taken as $n = 0$ at $r = R + a$ (the particles stick on contact with the fiber) and $n = n_0$ at $r = S$ where n_0 is the number of particles per cubic centimeter at distance

S from the axis of the fiber. S has been taken as half the mean distance between the axes of the fibers given by Albrecht (14) and Kaufmann (15) as

$$S = \frac{R}{2}\left(\frac{\pi\rho}{M}\right)^{\frac{1}{2}}, \qquad [11]$$

where ρ denotes the density of the fiber material and M is the mass of fiber per unit volume of the filter. The number of particles arriving at the fiber per second per unit length denoted by N is given by

$$N = \frac{2\pi D(R + a)^G \exp\left(\frac{H}{2(R + a)^2} + \frac{J}{a}\right)}{\psi(R + a) - \psi(s)}, \qquad [12]$$

where D is the diffusion coefficient of the particles.

$$\psi(R + a) - \psi(s) = \int_s^{R+a} r^{G-1} \exp\left(\frac{H}{2r^2} + \frac{J}{r}\right) dr. \qquad [13]$$

When there are no electric effects

$$N = \frac{kT\left(1 + \frac{C\lambda}{a}\right) n_0}{3\eta a \ln\left(\frac{S}{R + a}\right)}, \qquad [14]$$

as has been shown by Davies (16). k is Boltzmann's constant and C is Cunningham's constant. T, η, and λ refer to the temperature, viscosity, and the mean free path of the air, respectively. If we neglect image and induction effects ($J = H = 0$),

$$N = \frac{2\pi DG(R + a)^G n_0}{(R + a)^G - S^G}. \qquad [15]$$

When induction and image effects are appreciable, the equations cannot be solved exactly.

For small values of H and J Eqs. [12] and [13] may be solved by expanding the exponential terms in series. For large values of H and J this was impracticable. If we substitute

$$\frac{H}{r^3} + \frac{J}{(r - R)^2} = \frac{H}{r(R + a)^2} + \frac{JR}{a^2 r} \qquad [16]$$

in Eq. [7],

$$N = \frac{2\pi D\left(G - \frac{H}{(R + a)^2} - \frac{RJ}{a^2}\right) n_0}{\left(\frac{S}{R + a}\right)^{G-(H/(R+a)^2)-(R/a^2)J} - 1}. \qquad [17]$$

This equation overemphasizes the effect of induction and image forces and is of particular value in determining the conditions under which these effects are negligible. When electric effects are large, Eq. [17] reduces to

$$N = \frac{1}{3\eta a}\left(2\,|\,Qq\,| + \frac{2}{3}\,\frac{(\epsilon - 1)Q^2a^3}{(R + a)^2} + \frac{Rq^2(K - 1)}{4a^2(K + 1)}\right) \qquad [18]$$

for particles having an electric charge of opposite sign to that of the fiber.

The quantity I which is used in Eq. [6] as a measure of the probability of a given particle's being intercepted by unit length of the fiber by diffusion processes per second may be obtained in each case from

$$I = \frac{N}{n_0}. \qquad [19]$$

2. Filtration by Interception

In order to calculate the effective radius of a filter fiber for collisions by direct interception when electric effects are appreciable it was assumed that (*1*) the majority of the fibers were perpendicular to the direction of the air flow, (*2*) the aerosol particles were spherical, (*3*) the particles stick to the fibers on contact, (*4*) the flow was laminar (5), and (*5*) inertia effects were negligible for particles of radius less than 0.5μ and flow rates less than 30 cm./sec. (5).

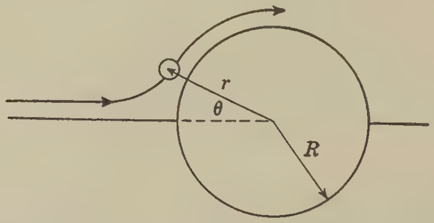

FIG. 3. The approach of an aerosol particle toward a filter fiber.

To solve the equations involved it was necessary to assume a potential air flow. Although this is not as rigorous as the use of viscous flow equations in previous work in which mechanical effects alone were considered (5, 6), it should lead to results that ought to show up the difference in performance of a filter with and without electric forces operating.

The equations of motion of a spherical particle of radius a relative to the axis of a fiber as illustrated in Fig. 3 are

$$-\frac{dr}{dt} = V_0\left(1 - \frac{R^2}{r^2}\right)\cos\theta - \frac{F}{6\pi\eta a}\left(1 + \frac{C\lambda}{a}\right) \qquad [20]$$

$$r\,\frac{d\theta}{dt} = V_0\left(1 + \frac{R^2}{r^2}\right)\sin\theta \qquad [21]$$

here t denotes time, V_0 is the mean linear flow rate past the fiber, and θ as illustrated in Fig. 3; F refers to the radial electric force acting on the article.

$$F = \frac{-2Qq}{r} + \frac{2}{3}Q^2(\epsilon - 1)\frac{a^3}{r^3} + \frac{q^2}{4(r - R)^2}\left(\frac{K - 1}{K + 1}\right). \qquad [22]$$

If $V_0 \neq 0$ and the equation of the most distant path leading to contact taken such that $r = R + a$ when $\theta = \pi/2$,

$$r - \frac{R^2}{r}\Big)\sin\theta = \left(1 + \frac{C\lambda}{a}\right)\left(\frac{1}{6\pi\eta a V_0}\right)\int_\theta^{\pi/2} Fr\,d\theta + R + a - \frac{R^2}{R + a}. \qquad [23]$$

ince $R_{\mathrm{eff}} =$ limit $r \sin\theta$ as $\theta \to 0$,

$$R_{\mathrm{eff}} = R + a - \frac{R^2}{R + a} + \left(1 + \frac{C\lambda}{a}\right)\frac{1}{6\pi\eta a V_0}\int_0^{\pi/2} Fr\,d\theta. \qquad [24]$$

Ience referring to Eq. [22] and Fig. 3

$${}_{\mathrm{eff}} = R + a - \frac{R^2}{R + a} + \left(1 + \frac{C\lambda}{a}\right)\left(\frac{1}{6\eta a V_0}\right) \cdot \left(-Qq + \frac{\alpha Q^2 a^3(\epsilon - 1)}{3(R + a)^2} + \frac{wq^2(R + a)(K - 1)}{8a^2(K + 1)}\right), \qquad [25]$$

vhere $\alpha \leqslant 1$ and $w \leqslant 1$. Using $\alpha = w = 1$ will tend to overemphasize inluction and image effects, but the error will be small when $R_{\mathrm{eff}} \ll R$.

3. *Determination of the Mean Fiber Radius*

In order to calculate the total length of fiber (L) in a given filter Langmuir's quation for the mean fiber radius ($\bar{R}$) was used (5). This formula, which ives the radius in terms of the pressure drop across the filter and the acking density (the fraction of the total volume of the filter occupied by he fibers), partially compensates for clumping of the fibers and the possiility that some of the fibers do not lie in a plane perpendicular to the lirection of the air flow. The equation recently developed by Davies (6) nd supported by direct microscopic examination of a wide variety of

TABLE I

The Characteristics of the Filters

Filter	Mass, g.	A, (cm²)	Thickness, (cm.)	ρ, (g./cm.³)	Pressure drop, (cm. of water at 85 l/min.)	$\bar{R}$, (μ)	$L \times 10^5$, (cm.)	100 Q, (e.s.u./cm.)	S, (μ)
Vool resin	3.2	58	1.27	1.33	0.51	10	7.0	0.9 ± 0.4	52
Vool resin[a]	3.2	58	1.27	1.33	0.51	10	7.0	0.2 ± 0.1	52
.S. C.C. No. 5	0.5	58	0.033	1.33	2.1	3.8	11.1	0.03 ± 0.01	7.7

[a] Exposed to X-ray radiation of 5000 roentgens.

filters is in excellent agreement with Langmuir's formula. The values of L and $\bar{R}$ for the filters discussed below are given in Table I.

4. Calculation of Filter Performance

a. Impregnated Fiber Filters. Filter fibers which have been coated with resin have an appreciable net electric charge per unit length which appears to be uniform. It has been shown above that the fibers have an equal chance of having a negative or positive charge. Since the test aerosols which have been examined have symmetrical electric charge distributions, using Eq. [25] we may write

$$\begin{aligned} R_{\text{eff}} = {} & f_{a0}\Bigg[\bar{R} + a - \frac{\bar{R}^2}{\bar{R}+a} + \frac{Q^2a^2(\epsilon-1)}{18\eta V_0(R+a)^2}\left(1+\frac{C\lambda}{a}\right)\Bigg] \\ & + \frac{f_{aq}}{2}\Bigg[\bar{R} + a - \frac{\bar{R}^2}{\bar{R}+a} + \Bigg(\frac{Q^2a^2(\epsilon-1)}{18\eta V_0(\bar{R}+a)^2} + \frac{|Q\bar{q}|}{6\eta V_0 a} + \left(\frac{K-1}{K+1}\right) \\ & \cdot \frac{q^2(\bar{R}+a)}{48\eta V_0 a^3}\Bigg)\left(1+\frac{C\lambda}{a}\right)\Bigg] + \frac{f_{aq}}{2}\Bigg[\bar{R} + a - \frac{\bar{R}^2}{\bar{R}+a} \\ & + \Bigg(\frac{Q^2a^2(\epsilon-1)}{18\eta V_0(\bar{R}+a)^2} - \frac{|Q\bar{q}|}{6\eta V_0 a} + \left(\frac{K-1}{K+1}\right)\frac{q^2(\bar{R}+a)}{48\eta V_0 a^3}\Bigg)\frac{1+C\lambda}{a}\Bigg], \end{aligned} \tag{26}$$

where f_{aq} and f_{a0} denote the fraction of the aerosol particles of radius a which have an electric charge and are neutral, respectively. $\bar{q}$ is the mean electric charge of the charged particles of radius a calculated disregarding the sign. V_0 refers to the mean velocity of the air past the fibers and is given by

$$V_0 = \frac{\text{Volume of air drawn per second}}{A(1-\beta)}, \tag{27}$$

where β is the packing density.

Referring to Eq. [17] we can obtain an expression for the filtration of aerosol particles by diffusion processes, namely,

$$\begin{aligned} I = {} & \frac{kT}{3\eta a}\left(1+\frac{C\lambda}{a}\right)\Bigg\{\Bigg[f_{a0}\frac{H}{(\bar{R}+a)^2}\Big/ 1 - \left(\frac{\bar{R}+a}{S}\right)^{H/(R+a)^2}\Bigg] \\ & + \Bigg[\frac{f_{aq}}{2}\left(|G| + \frac{H}{(\bar{R}+a)^2} + \frac{J\bar{R}}{a^2}\right)\Big/ 1 - \left(\frac{\bar{R}+a}{S}\right)^{|G|+(H/(\bar{R}+a)^2)+J\bar{R}/a^2}\Bigg] \\ & + \Bigg[\frac{f_{aq}}{2}\left(\frac{H}{(\bar{R}+a)^2} + \frac{J\bar{R}}{a^2} - |G|\right)\Big/ 1 - \left(\frac{\bar{R}+a}{S}\right)^{(H/(\bar{R}+a)^2)+J\bar{R}/a^2-|G|}\Bigg]\Bigg\}. \end{aligned} \tag{28}$$

The third term in both Eqs. [26] and [28] refers to the contact of a charged particle with a fiber having a charge of the same sign. Obviously when these terms are negative they should be neglected. Calculations using complete electric charge distribution data have shown that the use of a mean q in Eqs. [26] and [28] leads to essentially the same result as the use of the actual values of q weighted according to their frequency of occurrence in the test aerosol examined.

b. Unimpregnated Fiber Filters. It can be seen from the above equations that when the electric forces are small

$$P = \exp\left[-\frac{2L}{A}\left(\bar{R} + a - \frac{\bar{R}^2}{\bar{R} + a} + \frac{kT\left(1 + \frac{C\lambda}{a}\right)}{6\eta a\gamma V_0}\right)\right] \qquad [29]$$

where

$$\gamma = \ln\left(\frac{S}{\bar{R} + a}\right). \qquad [30]$$

These equations should apply to "mechanical" filters. When the test aerosol contains an appreciable number of charged particles, electric effects may be important even for quite small values of Q. Since there is some experimental evidence that unimpregnated fibers may have a net electric charge and that charge has an equal chance of being positive or negative, Eqs. [26] and [28] should be applicable.

V. Discussion

By comparing theory with experiment it was hoped to show two things (*1*) that the equations developed above give a reasonable description of the available data when electric effects are small and (*2*) that there is a possibility of electric effects occurring in some cases which would be large enough to alter the shape of the per cent penetration versus particle size curve.

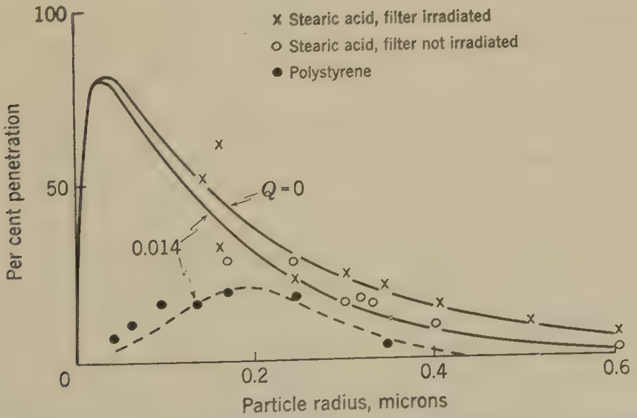

Fig. 4. Penetration curves for the wool resin filters (Table I). The full and dotted lines illustrate the calculated performance using homogeneous and heterogeneous aerosols respectively for the Q values as indicated. V_0 = 11.3 cm./sec.

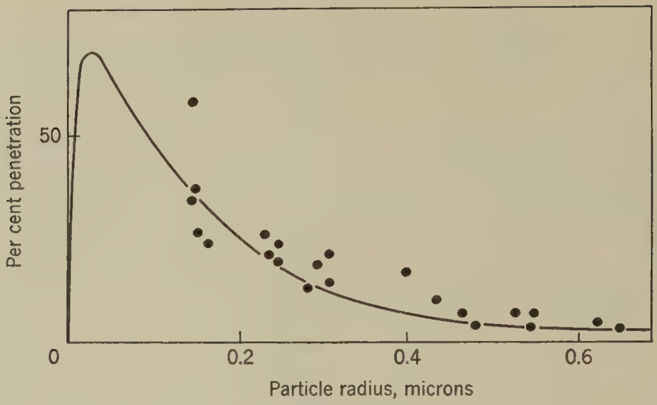

FIG. 5. A comparison of the calculated performance of U.S.C.C. No. 5 filter paper with the experimental results of Lane *et al.* (4) for a homogeneous oleic acid aerosol. (V_0 equals 25 cm./sec.)

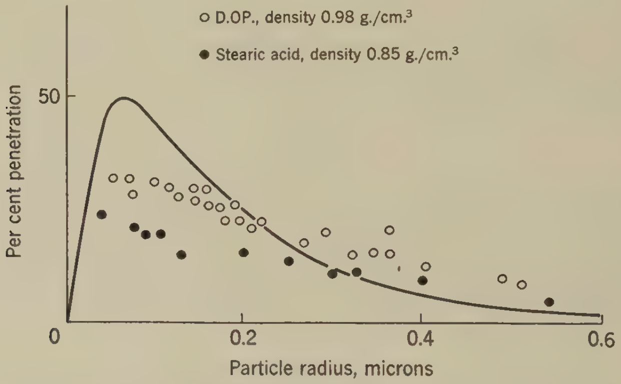

FIG. 6. A comparison of the calculated performance of U.S.C.C. No. 5 paper with the experimental results of La Mer *et al.* (3). V_0 equals 3.3 cm./sec.

When the electric charge on the fibers of a wool resin filter is negligible and the test aerosol is uncharged Eq. [29] may be used. The result is illustrated in Fig. 4 for a 3.2-g. wool resin filter with V_0 equal to 11.3 cm./sec. The experimental filtration results obtained by testing the filter listed in Table I which had been exposed to X-ray radiation with a homogeneous aerosol from a La Mer-Sinclair generator are plotted in Fig. 4 for comparison.

Also in Fig. 4 the effect of an average net electric charge on the fibers of 0.014 e.s.u./cm. is illustrated for an uncharged aerosol. The data obtained using stearic acid homogeneous aerosols from a La Mer-Sinclair generator and wool resin filters which were not exposed to X rays are given in Fig. 4

for comparison. The corresponding case when the test aerosol is a polystyrene aerosol with the electrical characteristics as shown in Figs. 2*a* and 2*b* is also illustrated in Fig. 4. In making the calculations it was assumed as suggested by Figs. 2*a* and 2*b* that

$$f_{aq} = 100a^{\frac{1}{2}} \qquad [31]$$

$$\bar{q} = 19.4a^2 \times 10^8 \text{ (electron units)}, \ \bar{q} \text{ always} \geqslant 1. \qquad [32]$$

It would appear that the effect of using a charged aerosol instead of an uncharged aerosol in filtration experiments is to increase the size of the particle most difficult to filter. All the available data for the filtration of uncharged aerosols from La Mer-Sinclair generators by "mechanical" filters have been compared with the performance predicted for an ideal filter. Figures 5 and 6 illustrate typical results. Both theory and experiment indicate that if there is a peak in the per cent penetration versus particle radius curve it is not in the region of 0.2 μ, as suggested by Langmuir (5), but at much lower values. Using the polystyrene aerosol Dr. D. J. Thomas and Mr. W. J. Harris in this laboratory have found that with "mechanical" type filters the most difficult particle to filter has a radius of the order of 0.1 μ; this would indicate that the fibers of the filters they have examined have a net electric charge per unit length of less than 10^{-3} e.s.u./cm. The greater alteration in the shape of the per cent penetration versus particle radius curve observed previously by Burton (1) may have been due to a greater net electric charge per unit length on the fibers of his filters or the test aerosol may have had a significantly different electric charge distribution from that of the aerosol chosen in this study as typical of heterogeneous test aerosols.

A promising approach to the problem of electric effects in the filtration process has recently been described (9). U.S. C.C. No. 5 filter paper was tested using homogeneous aerosols, all of the particles being charged deliberately to approximately the same extent. On the assumption that the electric charge on the fibers of the paper was such that induction effects may be neglected, the theory above would predict

$$\log P \doteqdot C_1 + C_2\bar{q} + C_3\bar{q}^2, \qquad [33]$$

where C_1, C_2, and C_3 are constants. Figure 7 illustrates plots of log P versus $\bar{q}$ obtained using the data of Goyer, Gruen, and La Mer (9) for V_0 equal to 3.15 cm./sec. The plots are straight lines, indicating that the image effects were not the most important. The slope of these lines should equal C_2. Since

$$C_2 \doteqdot -\frac{2L}{A}\left(\frac{Q}{6\eta a V_0}\right)\left(1 + \frac{C\lambda}{a}\right), \qquad [34]$$

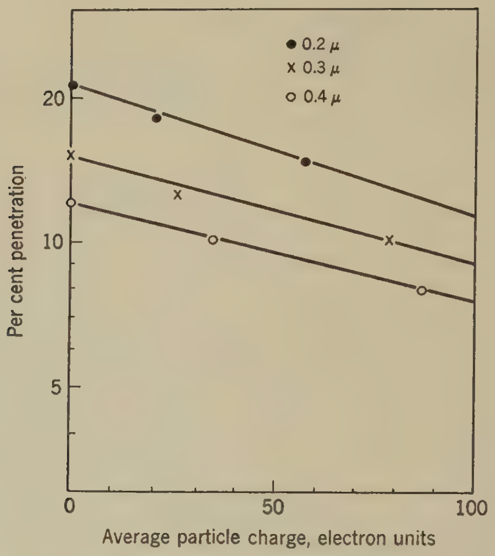

FIG. 7. Illustration of the proportionality between log P and $\bar{q}$ in the experiments of Goyer, Gruen, and La Mer (9). V_0 equals 3.2 cm./sec.

Q may be determined. The value of Q for each case was approximately 2×10^{-5} e.s.u./cm. Further experiments of this type would be well worthwhile particularly at large values of $\bar{q}$, where Eq. [34] is likely to be most valid.

When applied to penetration versus velocity data such as that of Ramskill and Anderson (17) the simple theory presented above is not satisfactory. It is believed that this is not entirely due to the neglect of inertia effects but that the differences in behavior of different homogeneous aerosols is the essential clue to the problem. The observation of La Mer *et al.* (Fig. 6) and Ramskill and Anderson (17) that it is often more difficult to filter a heavy particle than a light particle of the same size was verified in a set of subsidiary experiments. This suggests that the particles may not always adhere to the fibers on contact. All of the available filtration data are in agreement with the hypothesis that there is a restricted range of velocity where adhesion on contact is not a certainty. This complex question has been the subject of a separate investigation by the author. Also the general problem of the lack of adhesion of drops and particles on oblique impact with solid surfaces has been studied by the author in collaboration with Professor Sir Eric Rideal at King's College. It is hoped that the results of these studies will be presented in the near future. As far as the present experiments are concerned, large electric forces would seem to ensure that particles adhere to fibers on contact; just how large the forces must be has not been ascertained.

VI. Summary

The net electric charge on the fibers of various filters and the electric charge distributions of typical test aerosols were measured. A simple theory of filtration which included electric as well as mechanical effects was developed in order to apply these data to appropriate filtration results. Most fibers have an electric charge, even though it may be very small. When the test aerosol in filtration experiments is a homogeneous uncharged aerosol from a La Mer-Sinclair generator, a peak in the per cent penetration versus particle radius curves appears at approximately 0.05 μ, depending on the velocity of the air through the filter. The presence of electric forces of induction decreases the penetration of large particles and tends to decrease the radius at which maximum penetration occurs. When the aerosol used is a heterogeneous aerosol produced by any of the normal means, the peak in the penetration versus particle radius curves appears at larger values of the radius, depending upon the net electric charge per unit length of the fibers and the electric charge distribution of the test aerosol. It is pointed out that some unexplained filtration results may be due to some of the aerosol particles' escaping capture on contact. No attempt was made to assess the part played by electric forces in ensuring adhesion on contact.

Acknowledgments

This paper is published by permission of the Chief Scientist British Ministry of Supply. The author appreciates the interest shown by Mr. H. L. Green, Dr. D. J. Thomas, and Dr. E. A. Perren of the Chemical Defence Experimental Establishment, Porton. He is also indepted to Mr. W. J. Harris and Dr. D. J. Thomas for the use of unpublished experimental data.

References

1. Burton, E. F., III-I-2000 C.E. 42, Univ. of Toronto, November, 1944.
2. Knudson, H. W., and White, L., U. S. Naval Research Lab., Report P-2642, September 14, 1945.
3. La Mer, V. K., Gendron, T., and Gruen, R., *Nuclear Science Abstracts* **5**, No. 775 (1951).
4. Lane, W. R., Edwards, J., and Blyth, D. A., Unpublished Report, 1953.
5. Langmuir, I., O.S.R.D. Report No. 865, Serial No. 335, 1942.
6. Davies, C. N., *Inst. Mech. Engrs. (London) Proc.* (B), **1B**, 185 (1952).
7. D'Agostino, O., *Rend. ist. super sanita* **12**, 398 (1949).
8. Sinclair, D., and La Mer, V. K., *Chem. Revs.* **44**, 245, (1949).
9. Goyer, G. G., Gruen, R., and La Mer, V. K., *J. Phys. Chem.* **58**, 137 (1954).
10. Gillespie, T., and Langstroth, G. O., *Can. J. Chem.* **30**, 1056 (1952).

11. Collison, W. E., "Inhalation Therapy Technique." W. Heinemann (Medical Books) Ltd., London, 1937.
12. Lamb, H., "Hydrodynamics," 4th ed., p. 606. Cambridge University Press, 1916.
13. Townsend, J. S., "Electricity in Gases," Ch. 6. Oxford University Press, 1915.
14. Albrecht, F., *Physik. Z.* **32,** 48, 1931.
15. Kaufmann, A., *Z. Ver. Deut. Ing.* **80,** 593 (1936).
16. Davies, C. N., Reprint from the Ninth International Congress on Industrial Medicine, September, 1948.
17. Ramskill, E. A., and Anderson, W. L., *J. Colloid Sci.* **6,** 416 (1951).

LETTER TO THE EDITOR

ELECTROVISCOUS EFFECT

It has been shown that the K-value of silver iodide sols in water is independent of the electrolyte concentration at zero sol concentration, but that the decrease in the K-value of the sol on addition of electrolyte is larger the higher the concentration of the sol (1) ($K = (\eta_r - 1)/\varphi$; η_r = relative viscosity; φ = parts by volume of dispersed silver iodide). The latter effect was ascribed to an interaction between the diffuse double layers of the particles (second-order effect). It was consequently expected that the influence of the electrolyte on the viscosity of sols of moderate or high concentrations would increase with a decrease in size of the particles. Evidence for this supposition has now been obtained with the aid of emulsions of oils in water.

The emulsions of a medicinal oil in water, stabilized by sodium naphtha sulfonates and prepared by the method of phase inversion, described earlier (2), were fairly homodisperse. To 10% (vol.) emulsions of oil + emulsifier in water, varying concentrations of sodium chloride were added. Owing to the differing emulsifier content of the oils different particle sizes were obtained, as described previously (2). The relative viscosities (η_r) of the emulsions are listed in the table.

10% (vol.) emulsions particle diameter (*A.*)	Sodium chloride conc. in emulsion (*meq./l.*)	η_r of emulsion	Decrease in η_r (%)
2050	0	1.42	
2050	43	1.41	about 1
585	0	1.63	
585	13	1.47	about 10
275	0	2.00	
275	17	1.60	about 20

These results tend to show that the phenomena observed for silver iodide sols (1) and emulsions (2) can be considered from the same point of view. Taking the results as a whole, it appears possible to discern the following distinct features in the phenomenon known as the "electroviscous effect."

I. First-order electroviscous effects, caused by an interaction between particles and medium and to be recognized only by an extrapolation of experimental data to zero concentration. This effect may be of two kinds: *a*. The classical electroviscous effect. *b*. The "apparent volume increase" (2).

II. Higher-order electroviscous effects, which are caused by an interaction between the particles and therefore become more marked with increasing particle concentration (1).

Only the classical electroviscous effect (I, *a*) has been elaborated fundamentally (von Smoluchowski (3), Krasny-Ergen (4), and Booth (5)); no conclusive experimental data have, however, been obtained on this effect, possibly because the effect I, *b* is always involved. The "apparent volume increase" (I, *b*) is derived from the ratio between K and 2.5 (Einstein). It corresponds to an apparent increase in particle radius, the increase being about 20 A. for the silver iodide particle ($K = 3.55$, particle radius about 170 A.) and 30 to 35 A. for the particles of various sizes in oil emulsions. This phenomenon has not yet been explained satisfactorily. However, as both the surface potential of the particles and the apparent increase in radius were constant under varying conditions, it seems justifiable to correlate these quantities and to consider the "apparent volume increase" as an electroviscous effect. Possibly it is related to a decreased mobility of the liquid molecules in the neighborhood of the particle surfaces as a consequence of the highly inhomogeneous electrical field present there.

It may be considered that much experimental work on well-defined systems, under well-defined conditions, coupled with theoretical considerations on the properties of liquids in an electrical double layer is needed in order to gain a deeper insight into the viscous behavior of solutions of lyophobic colloids.

REFERENCES

1. HARMSEN, G. J., SCHOOTEN, J. VAN, AND OVERBEEK, J. TH. G., *J. Colloid Sci.* **8,** 72 (1953).
2. WAARDEN, M. VAN DER, *J. Colloid Sci.* **9,** 215 (1954).
3. SMOLUCHOWSKI, M. VON, *Kolloid-Z.* **18,** 194 (1916).
4. KRASNY-ERGEN, W., *Kolloid-Z.* **74,** 172 (1936).
5. BOOTH, F., *Proc. Roy. Soc.* (*London*) **A203,** 533 (1950).

Koninklijke/Shell-Laboratorium, Amsterdam
(N.V. De Bataafsche Petroleum Maatschappij)
Received May 2, 1455

G. J. HARMSEN
J. VAN SCHOOTEN
M. VAN DER WAARDEN

BOOK REVIEW

Degradation of Vinyl Polymers. By H. H. G. JELLINEK, University of Adelaide, South Australia. Academic Press Inc., New York, 1955. x + 329 pp. Price $8.50.

This handy volume presents a detailed summary of the present state of knowledge of vinyl polymer degradation under the influence of heat, radiation (light, X-ray, and nuclear pile) ultrasonic waves, milling, oxygen, peroxide catalysts, and other reagents. The subjects are treated mainly from the standpoint of reaction kinetics and do not include discussions of the patent literature or industrial problems of preventing degradation.

The first chapter comprising 59 pages presents a mathematical treatment of the various mechanisms of vinyl degradation which has a bearing not only on vinyl polymers but on all polymeric materials. The second chapter of 113 pages discusses in great detail bulk degradation of all common vinyl polymers by heat *in vacuo*.

The third section (48 pages) is concerned with oxidative degradation and degradation in solution. Since the discussion is limited to vinyl polymers, the reader may be disappointed to find that many areas of research on oxidative degradation of other types of polymers have been entirely omitted. The last chapter is extremely interesting and reviews in 61 pages recent publications dealing with the mechanical and ultrasonic degradation of vinyl polymer, as well as several nonvinyl polymers. The volume concludes with an appendix of 22 pages devoted to recent developments including degradation by high-energy radiation.

Research workers in the field of polymer degradation will find the volume informative and a useful source of reference.

R. B. MESROBIAN, Brooklyn, New York

ANNOUNCEMENT

INTERNATIONAL SYMPOSIUM ON POLYMERS, BIOCOLLOIDS AND POLYELECTROLYTES IN SOLUTION

An International Symposium on Macromolecules, sponsored by the Commission on Macromolecules of the International Union of Pure and Applied Chemistry, will be held in Israel, from April 3rd to April 9th, 1956, inclusive. Host to this symposium will be the Weizmann Institute of Science Rehovoth.

The Symposium will be devoted to the behavior of polymers, biocolloids and polyelectrolytes in solution. Papers will be presented in three sections to be held successively: 1) General Behavior of Polymers in Solution; 2) Behavior of Biocolloids and Polyelectrolytes in Aqueous Solutions; and 3) the Behavior of Special Polymeric Systems.

A number of tours have been arranged for delegates and visitors, including visits to biblical sites. A ladies' program has been planned.

For further information write to Prof. A. Katchalsky, Weizmann Institute of Science, Rehovoth, Israel.

ON PHYSICAL ADSORPTION.

VIII. Monolayer Adsorption of Argon and Nitrogen on Graphitized Carbon[1]

Sydney Ross and Werner Winkler

Departments of Chemistry and Chemical Engineering, Rensselaer Polytechnic Institute, Troy, N. Y.

Received May 6, 1955

ABSTRACT

Low-pressure adsorption isotherms of argon and nitrogen at 77.8°K. and 90.1°K. on graphitized carbon black, P-33, are reported. It is found that the adsorbed monolayer behaves like a two-dimensional ideal gas at the lowest pressures measured; and that its behavior at slightly higher pressures can be described by a two-dimensional van der Waals equation. The critical temperature of the adsorbed monolayer is estimated from the van der Waals constants. Above about 50% coverage the adsorption isotherm has the form of the Langmuir equation; which is interpreted as the adsorption of a mobile film on localized sites, where the sites are superposed on the low-energy solid substrate by the packing of the adsorbate. The isosteric heats of adsorption are calculated as a function of the fraction of the surface covered, and are found to follow the same general pattern as that reported by Amberg, Spencer, and Beebe (4) for krypton adsorbed on an identical substrate.

INTRODUCTION

Previous papers in this present series (1) have discussed the similarities in behavior of an insoluble film on water and a layer of adsorbed molecules on a uniform solid surface. In this paper this similarity is further demonstrated by the behavior of argon and of nitrogen, adsorbed as a monomolecular layer on graphitized carbon.

Polley, Schaeffer, and Smith (2), Singleton and Halsey (3), and Amberg, Spencer, and Beebe (4) have recently published multimolecular adsorption isotherms for argon and for nitrogen, and calorimetric heats of adsorption for krypton, on the graphitized carbon black, P-33. The marked step-wise adsorption isotherms and low initial heats of physical adsorption obtained indicate that this adsorbent has a surface that, if not uniform, has at least very small energy contour intervals.

---

[1] Based on a Thesis presented by W. Winkler, in partial fulfillment of the requirements for the degree of Doctor of Philosophy, to the Department of Chemical Engineering, Rensselaer Polytechnic Institute, June, 1955. The experimental observations are reported in full in the original Thesis, copies of which may be obtained from University Microfilms, Ann Arbor, Mich.

Only in the monolayer region, however, i.e., at relative pressures below 0.10, can analogies between liquid and solid substrates be legitimately drawn. This present paper reports investigations in that region, using the graphitized carbon black P-33 as the adsorbent.

Materials, Apparatus, and Methods

A sample of carbon black P-33, which was graphitized at 2700°C., was supplied by the courtesy of Dr. Walter R. Smith of Godfrey L. Cabot, Incorporated. Other samples of the same lot have been used in investigations reported by others (2, 3, 4). The surface area, by "point B" method, is reported as 12.5 m.^{2}/g. Spectroscopically pure grades of argon, nitrogen, and helium were obtained from the Matheson Company.

The low-pressure portion of the adsorption isotherm (2 to 50 μ) was determined by a McLeod gauge and a volumetric system with mercury cut-offs, as designed by Wooten and Brown (5). Corrections for thermal transpiration are sometimes large in this pressure range; they were reduced by constructing the sample holder of 30-mm. tubing to a distance of 4 inches above the level of the low-temperature bath. The corrections to be applied to the measured pressures of argon, nitrogen, and helium were then calculated from a formula given by Liang (6). The higher pressure portions of the isotherms (0.05 to 14 mm.) were determined on a different volumetric apparatus, in which the pressures were read on an oil manometer containing Apiezon B fluid by means of a Gaertner cathetometer. In the range common to the two sets of measurements, values agreed closely. The temperature of the adsorption bath was maintained by liquid nitrogen or liquid oxygen, and measured with an oxygen-vapor thermometer. The initial desorption of the sample was done at 150°C. for 4 hours, followed by 24 hours *in vacuo* at room temperature. The times allowed for adsorption varied from several hours to 30 minutes, depending on whether any further change in the pressure could be detected after several consecutive readings.

Experimental Results

The adsorption isotherms of argon and nitrogen from 2 to 40 μ at 77.8°K. on graphitized carbon black, after correction for thermal transpiration, are reported in Fig. 1. The adsorption isotherms at pressures from 0.05 to 14 mm. at 77.8°K. and at 90.1°K. are reported for argon in Figs. 2 and 3; and for nitrogen in Figs. 4 and 5; corrections for the effects of thermal transpiration are negligible at these pressures. The isotherms are determined chiefly by adsorption, with enough points by desorption to prove that the results reported are true equilibrium values. The equations that are used to describe the experimental findings are listed below, and

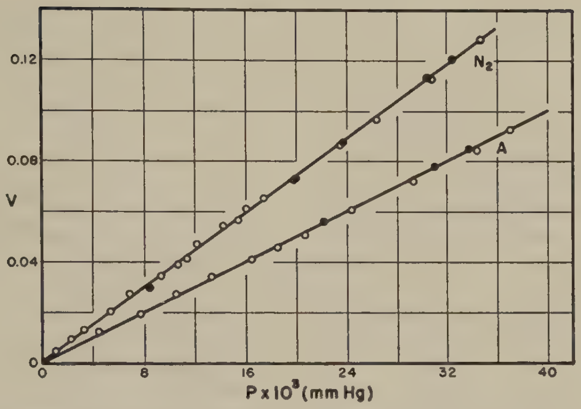

FIG. 1. Adsorption isotherms of argon and nitrogen from 2 to 40 μ at 77.8°K. on graphitized carbon black P-33, after correction for thermal transpiration. Black circles represent desorption points.

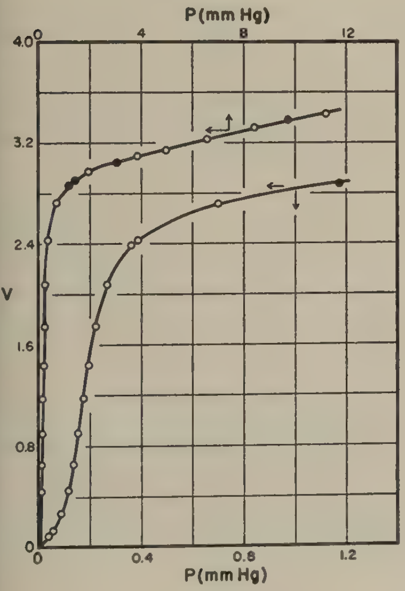

FIG. 2

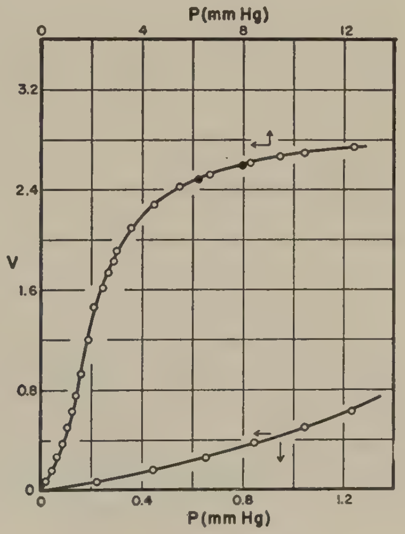

FIG. 3

FIG. 2. Adsorption isotherms of argon on graphitized carbon black P-33 from 0.05 to 14 mm. at 77.8°K. The low-pressure part of the isotherm is shown on an expanded scale by the lower curve. Black circles represent desorption points.

FIG. 3. Adsorption isotherm of argon on graphitized carbon black, P-33, from 0.05 to 14 mm. at 90.1°K. The low-pressure part of the isotherm is shown on an expanded scale by the lower curve. Black circles represent desorption points.

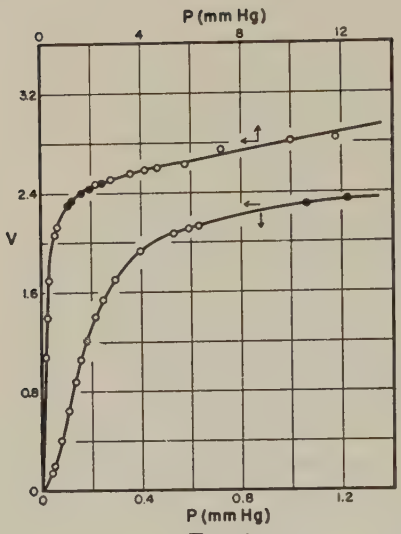

FIG. 4

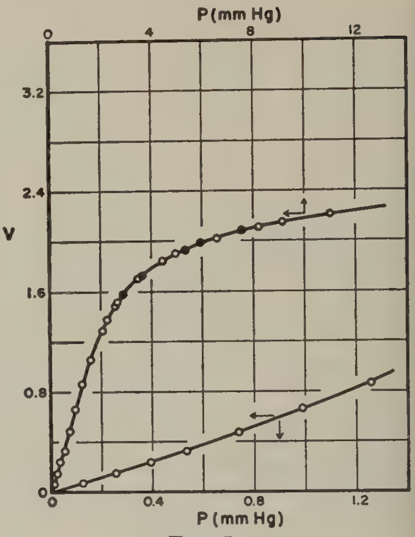

FIG. 5

FIG. 4. Adsorption isotherm of nitrogen on graphitized carbon black, P-33, from 0.05 to 14 mm. at 77.8°K. The low-pressure part of the isotherm is shown on an expanded scale by the lower curve. Black circles represent desorption points.

FIG. 5. Adsorption isotherm of nitrogen on graphitized carbon black, P-33, from 0.05 to 14 mm. at 90.1°K. The low-pressure part of the isotherm is shown on an expanded scale by the lower curve. Black circles represent desorption points.

the equation constants and other physical constants derived from them are reported in Table I.

Isotherm Equations	Approx. Range of θ	
$p = k\theta$	0–0.10	[1]
$p = k_b(\theta/1 - \theta)\ \text{exp.}\left(\dfrac{\theta}{1-\theta} - k_1\theta\right)$	0.10–0.50	[2]
$V = V_m\beta p/(1 + \beta p)$	0.60–0.90	[3]

where θ is the fraction of the surface covered by the adsorbed monolayer, and is defined by the ratio V/V_m of Eq. [3]. The constants k of Eq. [1] and k_b of Eq. [2] are not identical, though close to each other, because the finite range of the ideal-gas behavior defines k, whereas k_b is defined by the limiting form of Eq. [2], θ tending to zero.

DISCUSSION OF RESULTS

1. *Ideal and van der Waals Gas Laws at Low Coverage*

The straight-line isotherms of Fig. 1 offer convincing evidence that the surface of this graphitized carbon black, while not necessarily homotattic, presents (at least, to molecules as large as those of argon and nitrogen) a surface with no significant energy differences. A linear adsorption isotherm

TABLE I

Equation Constants and Estimated Physical Constants of Argon and Nitrogen Adsorbed on Graphitized Carbon at 77.8°K. and 90.1°K.

Constant	Definition by equation no.	Unit	Argon		Nitrogen	
			77.8°K.	90.1°K.	77.8°K.	90.1°K.
k	1	mm.	1.29	—	0.717	—
k_b	2	mm.	1.28	9.5	0.69	4.72
V_m	3	cc. at STP	3.23	3.12	2.65	2.56
k_1	2	ratio	5.57	4.62	4.28	3.48
β	3	mm.$^{-1}$	5.95	0.593	6.87	0.558
T_c	5	°K.	64.2	61.5	49.3	46.4
ΔH (low θ)	12	cal./mole	2270		2190	
ΔH (high θ)	13	cal./mole	2650		2860	
zE	7	cal./mole	380		670	

can be shown to result when the adsorbate behaves as an ideal two-dimensional gas on the surface (7), thus implying constant heat of adsorption throughout the whole surface. It is, of course, possible that an investigation carried to higher powers of precision would disclose a small percentage of adsorption sites more active than the remainder, which would be revealed by a small initial curvature of the isotherm. On the scale of the measurements reported here, however, the linear isotherms pass through the origin. It is important to notice that ideal two-dimensional gas behavior is observed for an appreciable portion of the monolayer coverage, and is not merely a limiting case of a van der Waals or a Langmuir equation.

Figures 2, 3, 4 and 5 show that the linear isotherms pass smoothly and continuously into curves convex to the pressure axis. This feature has already been observed by Jura and Criddle (8) for argon adsorbed on graphite; and also deduced from theory by Hill (9) and de Boer (10), as characteristic of a mobile adsorbed film in which the effects of molecular size and interaction cause deviations from the ideal gas law. Both Hill and de Boer develop the following adsorption isotherm equation, to describe an adsorbed monolayer that obeys a two-dimensional van der Waals equation:

$$p = k_b \frac{\theta}{1-\theta} \exp. \left(\frac{\theta}{1-\theta} - \frac{2a_2}{b_2 RT} \theta \right) \qquad [2b]$$

where p is the equilibrium pressure, θ is the fraction of the surface covered by the adsorbed monolayer, a_2 and b_2 are the two-dimensional van der Waals constants, and k_b is a constant related to the heat of adsorption. To test Eq. [2b] a value of V_m, the complete monolayer coverage, is necessary from which $\theta = V/V_m$ can be derived. Satisfactory values of V_m can be obtained from the monolayer adsorption isotherm at higher pressures where the observations can be described by a Langmuir equation. Using the values of θ thus obtained, Eq. [1] is tested by rearranging it as follows:

$$W = \ln \theta/(1-\theta) + \theta/(1-\theta) - \ln p = -\ln k_b + (2a_2/b_2RT)\theta \quad [4]$$

In Fig. 6 the expression W of Eq. [4] is plotted vs. θ for adsorbed argon at 77.8°K. and 90.1°K.; and in Fig. 7 similar plots are reported for adsorbed nitrogen. The values of the Langmuir V_m used in the calculation are reported in Table I. These diagrams show that Eq. [2] provides a satisfactory description of the adsorption isotherm, beginning where deviations from ideal gas behavior first occur, and holding good to the point where the surface is about half covered with adsorbed molecules. The reason why the van der Waals equation does not extend its description all the way to complete monolayer coverage will be discussed later; meanwhile, the agreement of the experimental observations with Eq. [2*b*] enables us to estimate the two-dimensional critical temperature of condensation of the adsorbate monolayer.

The straight-line portions of Figs. 6 and 7 yield slopes and intercepts

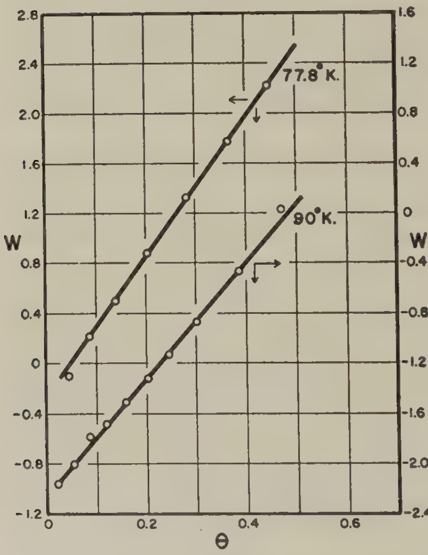

FIG. 6

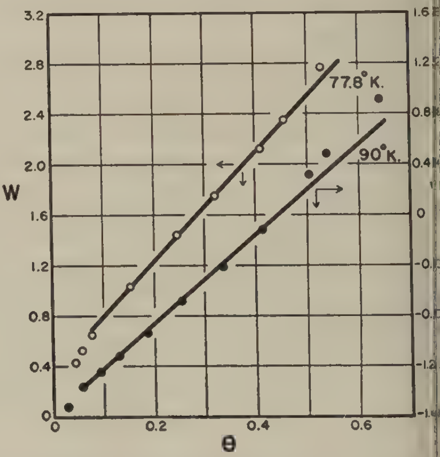

FIG. 7

FIG. 6. Test of the adsorption isotherms of argon on graphitized carbon, P-33, at 77.8°K. and 90.1°K., to show the description of the adsorbed monolayer by a two-dimensional van der Waals equation, at coverage below 50%.

FIG. 7. Test of the adsorption isotherms of nitrogen on graphitized carbon black, P-33, at 77.8°K. and 90.1°K., to show the description of the adsorbed monolayer by a two-dimensional van der Waals equation, at coverage below 50%.

from which can be calculated k_b and $2a_2/Rb_2$, from which, in turn, an estimate of the critical temperature for two-dimensional condensation can be obtained by use of the following equation (10):

$$T_c = 8a_2/27Rb_2. \qquad [5]$$

The values for the critical constants of argon and nitrogen adsorbed on graphite, as estimated from isotherms at 77.8°K. and 90.1°K., are included in Table I. The variation of a_2 and b_2 with temperature accounts for the deviation between the estimated critical constants at 77.8°K. and 90.1°K.; the values derived from the lower temperature isotherm are presumably closer to the correct ones.

2. Langmuir Equation at Higher Values of θ.

We have already referred to the Langmuir V_m, in the testing of Eq. [2]. We find in the present experiments that, at pressures slightly greater than those at which the two-dimensional van der Waals equation successfully describes the data, the latter equation no longer holds and the Langmuir equation provides the better mathematical description. This statement is based on a comparison of Figs. 6 and 7 with Figs. 8 and 9: deviations from Eq. [2] appear at about $\theta = 0.5$, and conformity with the Langmuir equation appears at about $\theta = 0.6$. Evidently the adsorbed monolayer has changed its physical nature.

It is surprising at first glance to find the adsorption isotherm assume the form of the Langmuir equation, which is predicated on no interaction between adsorbed molecules, especially when the van der Waals equation (i.e., interaction) has already been successfully invoked at lower pressures.

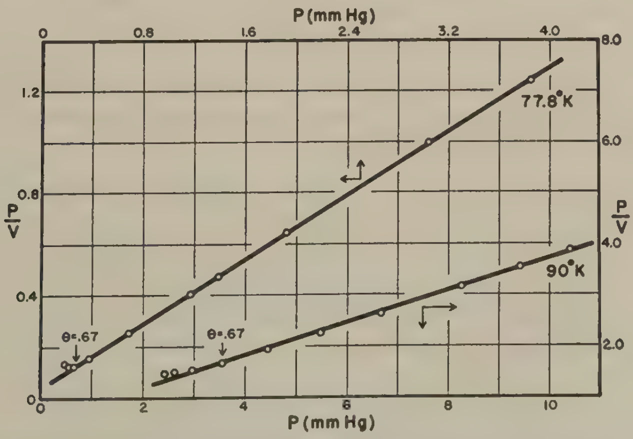

FIG. 8. Test of the adsorption isotherms of argon on graphitized carbon black, P-33, at 77.8°K. and 90.1°K., to show their description by the Langmuir equation, at coverage above 50%.

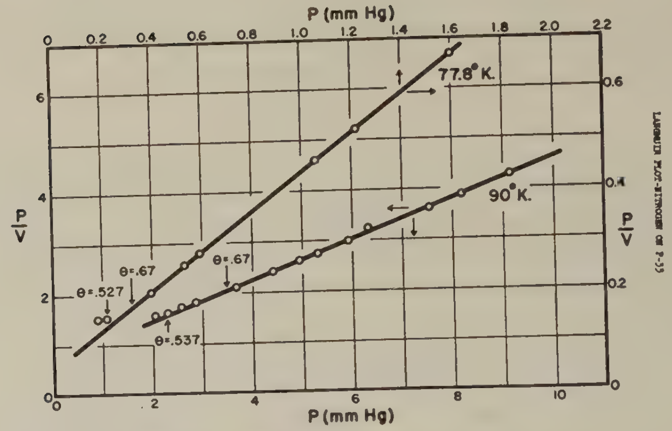

Fig. 9. Test of the adsorption isotherms of nitrogen on graphitized carbon black, P-33, at 77.8°K. and 90.1°K., to show their description by the Langmuir equation, at coverage above 50%.

Since interaction at higher pressures cannot be assumed to have abruptly disappeared, the new situation corresponds to an interaction energy that is constant with increasing coverage; hence a pattern of uniform, localized sites has been established by the adsorbed molecules themselves. The surface now presented to an adsorbate molecule in the vapor phase has changed from the initial level uniformity of the bare surface, to a homotattic pattern of periodically recurring, equivalent sites. Expressed mathematically, adsorption on the bare surface is described by:

$$\theta = \frac{k_0 e^{Q/RT} p}{\sqrt{T}}, \qquad [6]$$

where Q is the energy of adsorption per mole when all neighboring sites are unoccupied. Adsorption at the higher coverage where the Langmuir equation is followed, is described by:

$$\frac{\theta}{1-\theta} = \frac{k_0 e^{Q/RT}}{\sqrt{T}} e^{zE/RT} p \qquad [7]$$

where E is the interaction energy (attractive), and z is the number of occupied sites adjacent to any given site on which adsorption can take place (11). The energies of adsorption per mole in the two cases described by Eq. [6] and [7] are Q and $Q + zE$, respectively, and can be obtained experimentally from the calorimetric or the isosteric heats.

The value of z depends on the nature of the packing of the adsorbate molecules when close together at high monolayer coverage. For cubic packing, each unoccupied site is surrounded by four closest neighboring adsorbed molecules; for hexagonal packing, each unoccupied site has six closest neighbors. In the solid state both argon and nitrogen form cubic crystals, in which the ratio of their respective molecular areas is 14.7/16.0 = 0.92. For every gas on a given surface, $V_m A$ is constant, where A is the limiting area per molecule; hence the ratio of the Langmuir V_m for argon and nitrogen at the same temperature equals the reciprocal ratio of the limiting values of their molecular areas. It may be significant that, when compared with the crystallographic ratio of 0.92, the experimentally observed ratio of V_m would require a smaller value for the molecular area of the adsorbed argon. If then the argon is taken as hexagonally packed, with a molecular area of $0.866 \times 14.7 = 12.8$ A.^{2}, and the nitrogen is still assumed to be cubically packed, the crystallographic ratio becomes $12.8/16.0 = 0.80$; in close agreement with the reciprocal ratio of V_m, 0.82. Another indication that argon may pack hexagonally, and nitrogen cubically is obtained by a comparison of Figs. 8 and 9. Cubic packing should become evident after half-coverage, whereas hexagonal packing cannot be observed until at least two-thirds coverage. The difference between those two points on a sharply rising isotherm is not great; nevertheless, it can be seen (Fig. 8) that the Langmuir equation for nitrogen does hold at values of θ less than 0.67, whereas it does not for argon (Fig. 9).

3. Isosteric Heats of Adsorption

The variation of the isosteric heat of adsorption with coverage of the surface by a monolayer can be calculated for each of the three portions into which the isotherm has been divided. The isosteric heat of adsorption is defined by the expression:

$$\Delta H = RT^2(\partial \ln p/\partial T)_\theta. \qquad [8]$$

Applied to the first, ideal-gas, portion of the isotherm (Eq. [6]), Eq. [8] yields:

$$\Delta H = Q + \tfrac{1}{2}RT \text{ and } (\partial \Delta H/\partial \theta)_T = 0; \qquad [9]$$

for the range of θ in which the adsorbed monolayer behaves like an ideal gas, the isosteric heat is constant. Applied to the second, or van der Waals equation, portion of the isotherm (Eq. [2b]), Eq. [8] yields:

$$\Delta H = RT^2(\partial \ln k_b/\partial T)_\theta + 2a_2\theta/b_2$$

and

$$(\partial \Delta H/\partial \theta)_T = 2a_2/b_2; \qquad [10]$$

for the range of θ in which the adsorbed monolayer obeys the van der Waals equation, the isosteric heat rises linearly with θ. Applied to the third, Langmuir-equation, portion of the isotherm (Eq. [7]), Eq. [8] yields:

$$\Delta H = Q + \tfrac{1}{2}RT + zV, \text{ and } (\partial \Delta H/\partial \theta)_T = 0; \qquad [11]$$

for the range of θ in which the Langmuir equation holds, the isosteric heat is constant.

Equations [9], [10], and [11] predict that the isosteric heat of adsorption is first constant to about $\theta = 0.10$; then rises linearly to about $\theta = 0.50$; and then assumes a new constant value to about $\theta = 0.90$, after which adsorption on top of the monolayer is accompanied by a decrease in the isosteric heat. The initial constant value of ΔH can be estimated from the two isotherms here reported for each gas, using the Clausius-Clapeyron equation applied to Eq. [1]:

$$\Delta H = \frac{RT_2T_1}{T_2 - T_1} \ln \frac{k_2}{k_1}. \qquad [12]$$

The linear part of the isotherms at 90.1°K. is not precisely determined in the present reported measurements, but the ratio k_2/k_1 is given approximately by the ratio, more readily determined, of $(k_b)_2/(k_b)_1$; the distinction between the two constants was mentioned previously. The second constant value of ΔH for the Langmuir-equation portion of the isotherm is given similarly by

$$\Delta H = \frac{RT_2T_1}{T_2 - T_1} \ln \frac{\beta_1}{\beta_2}, \qquad [13]$$

where β_1 and β_2 are the constants defined, for two different temperatures, by Eq. [3]. The values of ΔH, at low θ and at high θ, calculated, respectively, from Eq. [12] and [13], are reported in Table I. The difference between them gives the value of zE, as defined by Eq. [7].

Although two different isotherms have been determined for each gas in the present investigation, they are separated by a large temperature difference, and it is difficult to estimate how accurate are the values of ΔH reported in Table I. A better test of Eqs. [9], [10], and [11] would be afforded either from isotherms at a smaller temperature interval or from the more precisely determined calorimetric heats. At present the calorimetric heats of adsorption of neither argon nor nitrogen on graphitized carbon black P-33 are available; however, the calorimetric heats of adsorption of krypton at 90.1°K. on this adsorbent have been reported by Amberg, Spencer, and Beebe (4), and show general similarities to the predictions of Eqs. [9], [10], and [11] above. For the first monolayer the heat curve can be divided into three distinctive portions. There is first a constant heat of adsorption of 3.94 kcal./mole to about one-eighth coverage; the heat of adsorption then rises linearly to about half-coverage; followed by a second constant heat to about 0.8θ; then declining again as second-layer adsorption takes place. The value of zE is about 600 cal./mole, by Eq. [7]. Each of these features of the calorimetric heat curve corresponds to the description afforded by Eqs. [9], [10], and [11], respectively. Collectively, they provide independent corroboration of the general pattern of the course of the adsorption on this uniform, low-energy surface: a pattern that is probably one of the simplest of those to be encountered experimentally, and which nevertheless cannot be interpreted by a single physical mechanism.

ACKNOWLEDGMENT

The authors gratefully acknowledge grants (G353 and G754) from the National Science Foundation for the support of the present series of researches.

REFERENCES

1. Ross, S. and Boyd, G. E., "New Two-Dimensional Condensation Phenomena," MDDC 864, 1947; Ross, S., *J. Am. Chem. Soc.* **70,** 3830 (1948); Ross, S., and Secoy, C. H., *J. Phys. & Colloid Chem.* **53,** 306 (1949); Ross, S., *ibid.* **53,** 383 (1949); Ross, S., and Winkler, W., *J. Am. Chem. Soc.* **76,** 2637 (1954); Ross, S., and Clark, H., *ibid.* **76,** 4291, 4297 (1954).
2. Polley, M. H., Schaeffer, W. D., and Smith, W. R., *J. Phys. Chem.* **57,** 469 (1953).
3. Singleton, J., and Halsey, G. D., *J. Phys. Chem.* **58,** 330, 1011 (1954).
4. Amberg, C. H., Spencer, W. B., and Beebe, R. A., *Can. J. Chem.* **33,** 305 (1955).
5. Wooten, L. A. and Brown, J. R. C., *J. Am. Chem. Soc.* **65,** 113 (1943).
6. Liang, C. S., *J. Phys. Chem.* **57,** 910 (1953).
7. Innes, W. B., and Rowley, H. H., *J. Phys. Chem.* **45,** 158 (1941).
8. Jura, G., and Criddle, D., *J. Phys. & Colloid Chem.* **55,** 163 (1951).
9. Hill, T. L., *J. Chem. Phys.* **14,** 441 (1946).
10. de Boer, J. H., "The Dynamical Character of Adsorption." Clarendon Press, Oxford, 1953: especially Chapters VI, VII, and VIII.
11. Peierls, R., *Proc. Cambridge Phil. Soc.* **32,** 471 (1936); Wang, J-S., *Proc. Roy. Soc. (London)* **A161,** 127 (1937).

ON PHYSICAL ADSORPTION

IX. Sub-critical and Supracritical Adsorption Isotherms for Krypton Monolayers on Graphitized Carbon Black[1]

Sydney Ross and Werner Winkler

Departments of Chemistry and Chemical Engineering, Rensselaer Polytechnic Institute, Troy, New York

Received May 12, 1955

ABSTRACT

The critical temperature of condensation for an adsorbed monolayer of krypton on graphitized carbon black, P-33, is shown to be approximately 82°K. Adsorption isotherms for temperatures (77.1°K. and 90.1°K.) close to this critical temperature offer experimental evidence that two-dimensional condensation may be described by a two-dimensional analogue of van der Waals' equation.

INTRODUCTION

Hadden Clark (1) reports that krypton adsorbed on graphitized carbon black, P-33, at 70°K. shows evidence of a two-dimensional phase transition. Amberg, Spencer, and Beebe (2) have determined calorimetric heats of adsorption of krypton on the same adsorbent. From data in the latter paper, the two-dimensional critical temperature of condensation for the adsorbed monolayer can be estimated as approximately 85°K.

This paper reports and discusses adsorption isotherms for krypton on graphitized carbon black, P-33, at temperatures (77.8°K. and 90.1°K.) lying slightly above and slightly below the estimated critical temperature of condensation for the adsorbed monolayer.

MATERIALS, APPARATUS, AND METHODS

A sample of carbon black, P-33, which was graphitized at 2700°K., was supplied by the courtesy of Dr. Walter R. Smith of Godfrey L. Cabot, Inc. A spectroscopically pure grade of krypton was obtained from the Matheson Company.

The determinations of the adsorption isotherms were made with the volumetric adsorption system and McLeod gauge previously described (3); and the corrections for thermal transpiration obtained from Liang's formula (4). A few points at high coverage on the 90.1°K. isotherm had to be determined with a higher pressure adsorption apparatus, using an oil manometer. The time required for adsorption equilibrium varied at different portions of the isotherm, and was markedly longer at 77.8°K., and particularly in the range of the isotherm during and following the vertical discontinuity. It was found also that the time required depended on the sample weight and could be greatly reduced with small quantities of adsorbent. In the

---

[1] Based on a Thesis presented by W. Winkler, in partial fulfillment of the requirements for the degree of Doctor of Philosophy, to the Department of Chemical Engineering, Rensselaer Polytechnic Institute, June, 1955. The experimental observations are reported in full in the original Thesis, copies of which may be obtained from University Microfilms, Ann Arbor, Mich.

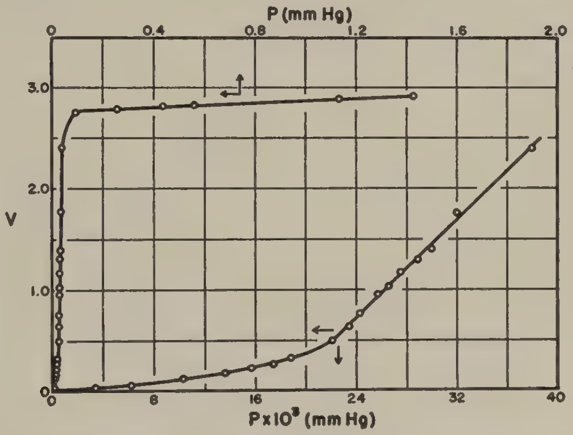

FIG. 1. Adsorption isotherm of krypton at 90.1°K. on graphitized carbon black, P-33, after correction of the values at lower pressures for thermal transpiration. The low-pressure part of the isotherm is shown on an expanded scale by the lower curve.

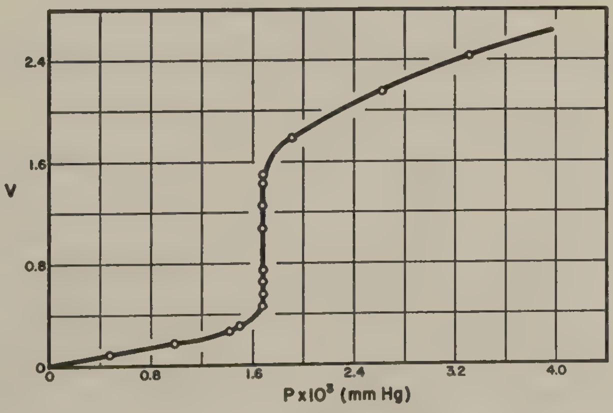

FIG. 2. Adsorption isotherm of krypton at 77.8°K. on graphitized carbon black, P-33, after correction of the values for thermal transpiration.

present experiments the weight of sample was 175 mg., and the time required was from 20 minutes to a few hours.

EXPERIMENTAL RESULTS

The adsorption isotherm of krypton at 90.1°K. on graphitized carbon black, after correction of the values at lower pressures for thermal transpiration, is reported in Fig. 1. The adsorption isotherm of the same system at 77.8°K., after correction for thermal transpiration, is reported in Fig. 2.

The equations that are used to describe the experimental findings are listed below, and the equation constants and other physical constants derived from them are reported in Table I.

Equations	Approx. Range θ	
$p = k\theta$	0–0.10	[1]
$p = k_b \dfrac{\theta}{1-\theta} \exp\left[\dfrac{\theta}{1-\theta} - \dfrac{2a_2}{b_2RT}\theta\right]$	0.10–0.50	[2]
$V = V_m\beta p/(1 + \beta p)$	0.60–0.90	[3]
$T_c = 8a_2/27\,Rb_2$		[4]

Equations

$$\Delta H\ (\text{low }\theta) = \frac{RT_2T_1}{T_2 - T_1}\ln\frac{k_2}{k_1} \qquad [5]$$

$$\Delta H\ (\text{high }\theta) = \frac{RT_2T_1}{T_2 - T_1}\ln\frac{\beta_1}{\beta_2} \qquad [6]$$

$$zE = \Delta H\ (\text{high }\theta) - \Delta H\ (\text{low }\theta) \qquad [7]$$

Equations [5], [6], and [7] are derived and the symbols used are defined in the previous paper of the series (3).

TABLE I

Equation Constants and Estimated Physical Constants of Krypton Adsorbed on Graphitized Carbon

Constant	Definition by eq. no.	Unit	θ-Range to which eq. applies	77.8°K.	90.1°K.
k	1	mm.	0–0.1	0.0162	0.28
k_b	2	mm.	0.1–0.5	—	0.25
$\dfrac{2a_2}{b_2RT}$	2	ratio	0.1–0.5	—	6.16
V_m	3	cc at STP	0.50–0.89	4.85	2.94
V_m	3	cc at STP	0.89–0.95	3.23	
β	3	mm.$^{-1}$	0.89–0.95	1820	68.0
T_c	4	°K.	—	82.1	
ΔH (low θ)	5	cal./mole	—	3240	
ΔH (high θ)	6	cal./mole	—	3740	
zE	7	cal./mole		500	

DISCUSSION

1. The Adsorption Isotherms

The adsorption of krypton on graphitized P-33 at 90.1°K., reported in Fig. 1, follows a similar pattern to that shown by adsorbed argon or nitrogen on the same adsorbent: the adsorbed molecules behave first as an ideal two-dimensional gas, as is evident from the initial linear portion of the adsorption isotherm, conforming to Eq. [1]; at higher pressures the adsorption isotherm can be described by Eq. [2], which is based on a two-dimensional van der Waals equation; and at still higher pressures, when more than half the available surface is covered with adsorbate molecules, the adsorption isotherm has the form of a Langmuir equation, Eq. [3]. The precision of the description of the experimental results by Eq. [2] is shown in Fig. 3, in which the function $W = \ln \frac{\theta}{1-\theta} + \frac{\theta}{1-\theta} - \ln p$ is plotted *vs.* θ, for the range $0.1 < \theta < 0.5$. After half the surface is occupied the description of the isotherm is continued by Eq. [3], and the precision of this description is shown in Fig. 4. The value of V_m derived from the plot of Fig. 4 is the basis for the calculation of θ in Eq. [2], and hence for the construction of the plot given in Fig. 3. An estimate of the two-dimensional critical temperature of condensation of the adsorbed mono-

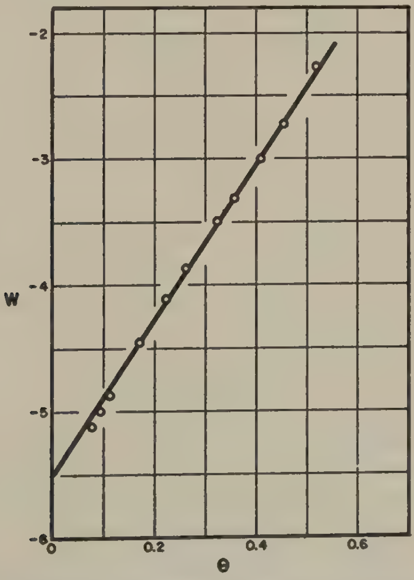

FIG. 3. Test of the adsorption isotherm of krypton on graphitized carbon black, P-33, at 90.1°K., to show the description of the adsorbed monolayer by a two-dimensional van der Waals equation, at coverage below 50%.

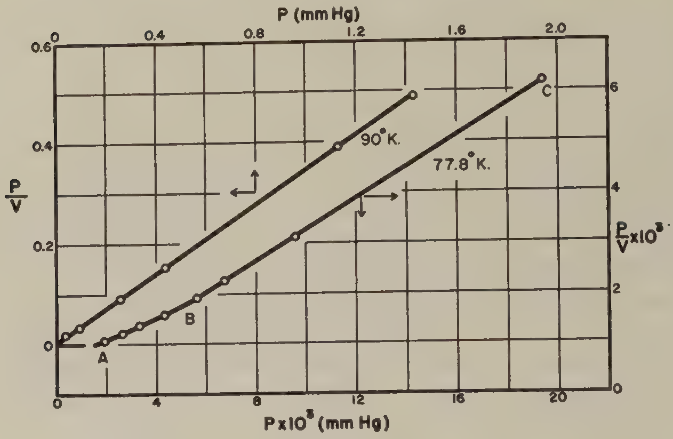

FIG. 4. Test of the adsorption isotherms of krypton on graphitized carbon black, P-33, at 90°K. and 77.8°K., to show their description by the Langmuir equation, at coverage above 50%. The lines *AB* and *BC* represent two Langmuir equations for the description of the 77.8° isotherm.

layer can be obtained from the slope of the straight-line portion of Fig. 3, which equals $2a_2/b_2RT$, yielding (Eq. [4]) $T_c = 82.1$°K.

The adsorption isotherm at 77.8°K. is reported in Fig. 2. At the lowest pressures measured the isotherm is linear; at higher pressures a vertical discontinuity appears in the range of monolayer coverage ($0.1 < \theta < 0.5$), which is the same portion of the isotherm described at 90.1°K. by a two-dimensional van der Waals equation. This finding offers a complete analogy to the behavior of a gas below its critical temperature; it also substantiates the van der Waals equation applied to the description of an adsorbed monolayer. This is the first experimental evidence that the two-dimensional van der Waals constants have an exactly analogous significance with respect to the critical point of an adsorbed monolayer, as their three-dimensional originals have for the critical point of a gas.

Above 50% coverage the isotherm would be expected to have the form of a Langmuir equation, if it were to behave in the same way as the supracritical isotherm at 90.1°K. The Langmuir plot is shown in Fig. 4, from which it can be seen that the experimental data are described by two Langmuir equations, with a transition at $\theta = 0.89$. The determination of this portion of the isotherm was confirmed by duplication of the measurements. The two Langmuir equations give values of V_m that are, respectively, for the *AB* and the *BC* portions of the Fig. 4 plot, 4.85 and 3.23 c.c. at S.T.P. per gram. The monolayer capacity of this sample of graphitized carbon per gram is 2.65 c.c. in terms of nitrogen at S.T.P., which corresponds closely to 3.23 c.c. in terms of krypton, based on normally used molecular areas of nitrogen and krypton. The calculation of θ is based, therefore, on $V_m = 3.23$ c.c./g. The lower pressure Langmuir equation has a value of V_m corresponding to 1.50 θ. A tentative model that describes this phenomenon is suggested in Fig. 5, where the order in which krypton molecules adsorb on an energetically uniform solid substrate is designated by the numbers; equivalent positions being given the same number. The suggested arrangement is cubic, with $\theta = 0.50$ corresponding to the completion of the adsorption of the No. 4 atoms. Second-layer adsorption occurring at that point, on sites indicated by shaded circles, would show, by virtue of the number and nature of these sites, localized adsorption with an available $V_m = 1.50\ \theta$. If the observed transition at higher pressures is caused by a shifting of the second-layer adsorption to the filling in of the No. 5 sites on the first layer, the isotherm would also shift, to display localized adsorption with $V_m = 1.00\ \theta$. The adsorption of nitrogen on *Graphon* has been similarly characterized by Graham (5): "... a delayed equilibration involving the necessity for some shifting of adsorbed molecules to permit occupancy of the last portion of the adsorbent surface."

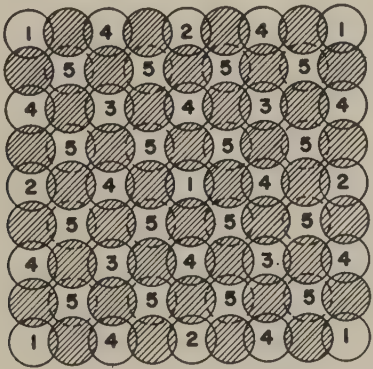

FIG. 5. First and second adsorbed layers of krypton in cubic array. It is suggested that adsorption on the second layer (shaded circles) begins before the sites on the first layer occupied by the No. 5 atoms are occupied.

2. Heats of Adsorption

The initial linear isotherms define a constant isosteric heat of adsorption, which can be calculated from the slopes k_1 and k_2 at temperatures T_1 and T_2 by means of the Clausius-Clapeyron equation; the equation that is developed is Eq. [5]. The value of 3240 cals./mole (Table I) is significantly lower than the heat of adsorption for the same system determined calorimetrically (2), which, for low values of θ, is about 4000 cals./mole. Isosteric heats of adsorption, particularly when based on constant θ rather than constant amount adsorbed, V, have been found to be less than their calorimetrically determined counterparts (6), although the difference does not account fully for the present discrepancy. It is also possible that there are differences in the adsorbent, which is prepared by batch process and so is not necessarily always equally free of high-energy adsorption sites on the surface.

A method of calculating the nonpolar van der Waal's forces (dispersion forces) between an argon atom and the basal-plane surface of graphite, and evaluating the resulting energy of adsorption, has been employed by de Boer (7). A similar calculation can be made for krypton, using the following numerical data:

Operating radius of krypton atom, from equation of state = 2.03 A.
Operating radius of carbon atom in van der Waals interaction, from interlayer spacing of graphite = 1.70 A.

$\alpha_c = 1 \times 10^{-24}$ cm.^{3}
$I_c = 258$ kcal./mole
$r_0 = 3.45$ A.
$\alpha_{Kr} = 2.46 \times 10^{-24}$ cm.^{3}
$I_{Kr} = 321$ kcal./mole
$N_s = 1.13 \times 10^{23}$

The symbols used are defined by de Boer (7). The distance of an adsorbed krypton atom to the 6 nearest carbon atoms of the basal plane of graphite will be 3.73 A.; the distance to the next 6 is 4.52 A.; and the distance to the next 12 is 5.21 A. Summations over the 24 nearest carbon atoms and integration over the rest leads to an adsorption energy of 2.8 kcal./mole; this is as close to our present reported value of 3.2 kcal./mole as a calculation of this type can be expected to come.

A test of the internal consistency of the reported isosteric heats of argon and krypton at low coverage is the ratio of the heat of evaporation to the heat of adsorption of each gas on the same adsorbent: at corresponding temperatures this ratio would be expected to be constant for all the noble gases. The numerical values are:

	Argon	Krypton
ΔH evaporation	1570	2170
ΔH adsorption (78°–90°K.)	2270	3200
Ratio	0.69	0.68

Although the calorimetric heats of adsorption of krypton on graphitized P-33 at 90°K. (2) are higher at all values of θ than the isosteric heats reported here, both methods agree in their determination of the variation of ΔH with θ. On the calorimetric curve the initial constant ΔH at low coverage corresponds to the ideal linear adsorption isotherm; the rising calorimetric heat from $0.2 < \theta < 0.6$ corresponds approximately to the central portion of the isotherm that is described by Eq. 2, for it can be shown that this isotherm equation leads to $\left(\frac{\partial \Delta H}{\partial \theta}\right)_T = 2a_2/b_2$; and the final constant ΔH at high monolayer coverage corresponds to the portion of the adsorption isotherm that has the form of a Langmuir equation. It is indeed possible to find more than this qualitative similarity: the slope of the rising portion of the calorimetric heat curve yields a value of $2a_2/b_2$, from which the critical temperature is estimated (Eq. 4) at about 85°K; the adsorption isotherm in the same range of coverage can be used for the same purpose (Table I), yielding a critical temperature of 82°K.

ACKNOWLEDGMENT

The authors gratefully acknowledge grants (G353 and G754) from the National Science Foundation for the support of the present series of researches.

REFERENCES

1. CLARK, H., *J. Phys. Chem.*, in the press.
2. AMBERG, C. H., SPENCER, W. B., AND BEEBE, R. A., *Can. J. Chem.* **33**, 305 (1955).
3. ROSS, S., AND WINKLER, W., *J. Colloid Sci.* **10**, 319 (1955).
4. LIANG, C. S., *J. Phys. Chem.* **57**, 910 (1953).
5. GRAHAM, D., *J. Phys. Chem.* **58**, 869 (1954).
6. JOYNER, L. G., AND EMMETT, P. H., *J. Am. Chem. Soc.* **70**, 2353 (1948).
7. DE BOER, J. H., "Advances in Colloid Science," Vol. III, p. 26. Interscience Publishers, Inc., New York, 1950.

SORPTION OF MACROMOLECULES TO SOLID SURFACES: SORPTION OF DEXTRAN TO CELLULOSE NITRATE MEMBRANES IN THE PRESENCE OF SERUM ALBUMIN AND SURFACE-ACTIVE AGENTS[1, 2]

S. Rothman, John Mandel, Florence R. McCann, and S. G. Weissberg

National Bureau of Standards, Washington, D. C.

Received March 11, 1955

Abstract

Dynamic measurements of osmotic pressure may be affected by sorption phenomena on the membrane. Likewise the sorption of polymeric plasma expanders to tissue after infusion may have adverse physiological effects.

The sorption of C^{14} carboxy-labeled dextran ($M_n = 35{,}000$) to collodion membranes was studied in several media. The membranes were cast over mercury from a Merck collodion solution under controlled conditions. Aqueous solutions were prepared containing dextran, sodium chloride, serum albumin, and three detergents having different chemical characteristics, in different combinations. Both sides of the membranes were exposed to these solutions for a selected sequence of time intervals up to 52 hours; they were uniformly washed (without scrubbing) and air-dried at 30°C. The radioactivity in each membrane, which is a measure of the amount of dextran present, was determined with a PC-1 Proportional Counter.

The experiment was statistically designed in order to isolate and compensate for possible systematic errors due to differences between membranes and to variations in the counting procedure or fluctuations in the instrument, and in order to evaluate the precision of the data.

The results indicate differences between membranes, despite the precautions taken in their preparation. Aqueous solutions containing only dextran show a continuous increase in sorption with a high initial rate. Addition of sodium chloride increases the amount of sorption, whereas the presence of serum albumin decreases it, whether or not sodium chloride is present. The cationic detergent markedly increases the sorption of dextran to the membrane, whereas the nonionic detergent has the reverse effect.

I. Introduction

The adsorption of high polymers from solution to solid surfaces has been under study for several years. Early interest stemmed from the investigation of the factors involved in adhesion. Recently the approach has been more fundamental and investigators like Simha, Frisch, and

---

[1] This work was sponsored, in part, by the Office of the Surgeon General, Department of the Army.

[2] Presented at the 126th National Meeting of the American Chemical Society in New York City, N. Y., September 12–17, 1954.

Eirich (1, 2) and Sonntag and Jenckel (3) have proposed theories to predict and explain adsorption behavior.

The study undertaken and discussed in this paper follows a slightly different approach. The possible adsorption problems associated with osmotic pressure measurements have been reported in the literature by Robertson, McIntosh, and Grummitt (4) and again by Cleverdon, Laker, and Smith (5). Static measurements are usually made over a period of 2 to 3 days, during which time any polymer coating of the membrane would reach equilibrium and subsequently would not interfere with the determination. On the other hand, dynamic measurements have been made within short periods of time without giving consideration to the transfer of polymer to the membrane surface and its possible consequences. It had been found in this laboratory, while using the Hepp-Scatchard osmometer (6), that if reliable static osmotic pressure measurements of dextran solutions were to be obtained within 4 hours, the membrane had to be "conditioned" to the solution during a 2-day period (7).

Another factor that influenced this study was the possible adverse physiological effect of infused plasma expanders due to the adsorption of the expanders to tissue. It was reported by Furth *et al.* (8) that certain plasma expanders cause an increase in bleeding tendency shortly after infusion. In addition, it has been reported by Hint and Thorsén (9) that the sedimentation rate of red cells and their tendency to agglomerate are greater for higher molecular weight expanders. It was therefore considered that a similar phenomenon might be taking place with the blood platelets, which play a primary role in bleeding stoppage; that is, the expander is adsorbed to the platelet, forming a film which interferes with the normal processes. The final proof of the suppositions can be obtained only by a critical study of the degree of adsorption of the expander to the platelet and the physiological processes involved.

Prior to the direct approach, it is necessary to learn more about the behavior of an expander on adsorption to solid surfaces, as well as techniques whereby this phenomenon can be affected. Dextran was chosen because it is the principal blood plasma expander in use in this country, is readily available, and is known to require membrane conditioning for osmotic pressure measurements. Collodion membranes are used because they can be fairly uniformly cast. The rate of adsorption of radioactively labeled dextran alone and in the presence of sodium chloride, serum albumin, and three surface-active agents was determined during a 52-hour period.

II. MATERIALS

Films were cast from Merck collodion solutions over mercury using 47 ml. of the 5% solution and confining the film within a metal ring 12 cm. in diameter. The solvents were permitted to evaporate while in an uncovered petri dish. The membranes were stored in a cabinet with slight leakage for 1½ hours, and then immersed in distilled water to displace the residual solvents. Ten discs, approximately 2.8 cm. in diameter, were cut from each of the films. Each disc was suspended in distilled water by an S-shaped nichrome hook for 4 days to achieve equilibrium swelling conditions.

The dextran fraction, number average molecular weight 35,000 and activity 60 μc./g., was radioactively carboxy-labeled at the National Bureau of Standards by means of C^{14} cyanide, using the method of Isbell (10). The activities were measured with a PC-1 Proportional Counter.[3]

The serum albumin was human fraction V, and of the three detergents the first had a positive surface-active group (Hyamine 1622),[4] the second a negative group (sodium dodecyl sulfate),[5] and the third was neutral (Triton X100).[4]

III. STATISTICAL CONTROL

In designing an experiment of the nature discussed here, it is essential to take a number of precautions aimed at the elimination of factors that may impair the reliability of the results. In the present case an important potential source of error is possible variability between different collodion castings. Another factor of variability is the possibility of drift in the instrument. Unless proper attention is given to both of these factors, spurious differences in the data may appear that are due neither to the nature of the solution nor to the time of exposure. The entire study was therefore divided into two series with overlapping experiments, which were carried out and analyzed separately.

1. First Series

In view of the large number of combinations that are of interest—6 solutions at each of 10 exposure times—it was decided to run only duplicate specimens for each of these 60 combinations. Since each sheet of collodion provided only 10 specimens, this required the casting of 12 sheets, and an unavoidable subdivision of the measurements into groups of 10. The design of the experiment must allow for the evaluation of differences among sheets so that all 60 combinations can be compared without the interference of sheet-to-sheet variability. Furthermore, in order to counteract possible effects of drift in the measuring instrument, the measurements were also subdivided in a different manner, into 10 groups of 12, in such a way that all measurements within a group (a "run") were made consecutively without substantial interruptions. The complete design is shown in Table I,

---

[3] Manufactured by Nuclear Measurements Corporation.

[4] Obtained from Rohm and Haas Company.

[5] Prepared at the National Bureau of Standards.

TABLE I

Design of First Series

Activity counting set[a]	Exposure time (code)[b]	Sheet						Exposure time (code)[b]	Sheet					
		20	31	25	24	30	21		27	22	26	29	28	23
7	8	A[c]	E	F	D	B	C	2	C	F	A	B	E	D
2	1	B	A	C	F	E	D	10	F	C	D	E	B	A
9	7	F	D	A	E	C	B	9	B	E	C	A	D	F
4	5	E	B	D	C	A	F	3	E	B	F	D	A	C
1	6	C	F	B	A	D	E	4	D	A	E	F	C	B
3	10	F	C	D	E	B	A	8	E	F	D	B	C	A
6	9	B	E	C	A	D	F	1	A	C	F	E	D	B
10	3	E	B	F	D	A	C	7	D	A	E	C	B	F
5	4	D	A	E	F	C	B	5	B	D	C	A	F	E
8	2	C	F	A	B	E	D	6	F	B	A	D	E	C

[a] Numbers refer to the order in which experiments were done.

[b] See Tables III–VI for exposure times corresponding to code numbers.

[c] The letter entries refer to solutions listed in Table II.

in which the letters represent the 6 solutions, the rows correspond to runs of measurements, and the columns represent sheets of collodion. This design, together with the appropriate method of analysis, is described in reference (11).

2. *Second Series*

A similar design was used in the second series of experiments, except that 80 combinations rather than 60 were examined. This required the use of 16 sheets of 10 specimens each.

IV. EXPERIMENTAL

The solutions used in the series appear in Table II. The discs were immersed in the solutions by means of metal hooks; eight stainless steel vessels were used. In this manner both sides of the discs were exposed to the solution. The solutions were stored during the exposure periods at 5°C.

After each predetermined exposure time, the discs were removed from the containers and gently washed for ½ hour by immersion in a distilled water bath in which the water was constantly changed at the rate of 40 ml./min. This was done in order to remove any dextran not actually adsorbed to the disc. It is realized that some of the adsorbed dextran may have been removed from the membrane in the washing procedure, but by means of duplicate discs and overlapping experiments, the technique was shown to be reproducible and therefore the data are comparable.

After washing, each of the discs was placed between two glass plates

TABLE II

Solutions[a]

Code	Solution	Series
A	0.1% Dextran in water	I
A′	0.1% Dextran in water	II
B	0.1% Dextran + 0.35% human serum albumin in water	I
C	0.1% Dextran + 0.1% cationic detergent in water	I
C′	0.1% Dextran + 0.1% cationic detergent in water	II
D	0.1% Dextran + 0.15*M* sodium chloride in water	I
D′	0.1% Dextran + 0.15*M* sodium chloride in water	II
E	0.1% Dextran + 0.15*M* sodium chloride in water 0.1% Dextran + 0.35% human serum albumin in water	I
F	0.1% Dextran + 0.15*M* sodium chloride in water 0.1% Dextran + 0.1% cationic detergent in water	I
F′	0.1% Dextran + 0.15*M* sodium chloride in water 0.1% Dextran + 0.1% cationic detergent in water	II
G	0.1% Dextran + 0.1% anionic detergent in water	II
H	0.1% Dextran + 0.1% nonionic detergent in water	II
I	0.1% Dextran + 0.15*M* sodium chloride in water 0.1% Dextran + 0.1% anionic detergent in water	II
J	0.1% Dextran + 0.15*M* sodium chloride in water 0.1% Dextran + 0.1% nonionic detergent in water	II

[a] The code letters are referred to in later tables, and the numbers in the right column indicate the experimental series in which they were used.

held firmly in place with strips of cellulose tape. While being held between the plates, the discs were air-dried for 3 days, followed by infrared exposure for 8 hours. This procedure was followed to minimize deformity of the discs due to shrinkage.

The procedure for counting, as recommended by the manufacturer of the Counter, was kept uniform throughout the series. Each disc was discharged by touching it with a brass rod before closing the chamber. The chamber was flushed with P-10 gas (90% argon, 10% methane) prior to each measurement and the time setting for the counting period was adjusted to the activity (counts per minute) of the disc.

V. RESULTS AND CONCLUSIONS

1. *First Series*

The statistically corrected[6] data for aqueous solutions of dextran, dextran and serum albumin, and dextran and the cationic detergent are shown in Table III and plotted in Fig. 1 as the log activity versus exposure time. It can be seen that the changes in slope of all the systems are practically identical. The amount of dextran sorbed to the disc when in solution with the cationic detergent is much greater than without it. The detergent could conceivably cause greater adsorption either because of the charge deposited on the dextran or membrane surface or because it is changing the character of the solvent environment, thereby affecting the configuration of the polymer molecule. The latter supposition is less likely than the former one. Serum albumin, on the other hand, decreases the amount of dextran adsorption, indicating that it is preferentially adsorbed to the surface, thereby occupying sites otherwise available to the dextran. In addition, the albumin molecules present in the solution close to the surface probably inhibit the transfer of dextran from solution to surface. It can be seen on the curves that there is a rapid initial rise during the first

---

[6] See Section VI of this paper.

TABLE III

Sorption of Dextran to Collodion Membranes in the Presence of Human Serum Albumin and a Cationic Detergent

Solution (code)	Exposure time (code)	Exposure time (*hours*)	Log activity (average of 2 determinations)
A	1	1.50	2.145
	2	2.50	2.290
	3	3.50	2.475
	4	4.50	2.485
	5	6.50	2.710
	6	8.50	2.615
	7	22.50	3.150
	8	29.50	3.140
	9	46.50	3.310
	10	52.50	3.315
B	1	1.42	1.920
	2	2.42	2.150
	3	3.42	2.330
	4	4.42	2.270
	5	6.42	2.385
	6	8.42	2.455
	7	22.42	2.720
	8	29.42	2.905
	9	46.42	2.980
	10	52.42	3.050
C	1	1.25	3.145
	2	2.25	3.245
	3	3.25	3.395
	4	4.25	3.485
	5	6.25	3.535
	6	8.25	3.610
	7	22.25	3.870
	8	29.25	3.945
	9	46.25	3.965
	10	52.25	3.975

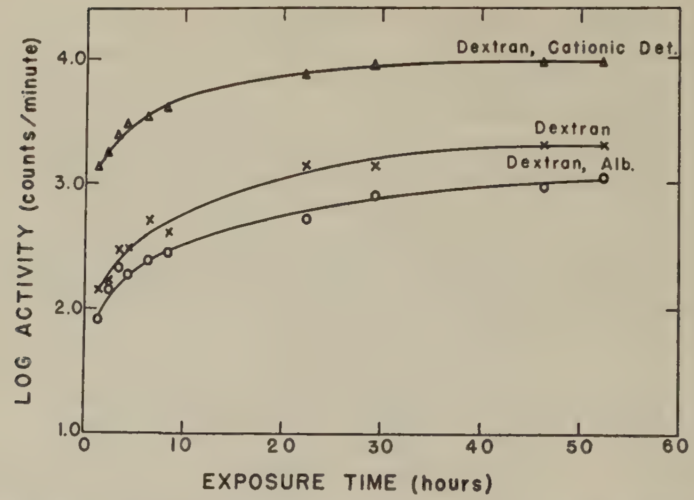

Fig. 1. Log activity versus exposure time: sorption of C^{14} dextran to collodion in presence of cationic detergent or human serum albumin.

10 hours, followed by a leveling off. This would seem to indicate that during the early exposure periods the dextran was being adsorbed to the disc surface rather rapidly. Diffusion of the dextran into the pores of the collodion membrane probably begins to be appreciable soon after the initial adsorption period. In the later periods both adsorption and diffusion occur, with adsorption probably being near equilibrium and diffusion the major element.

Data for the solutions appearing in Fig. 1 with 0.15 *M* sodium chloride added are shown in Table IV and Fig. 2. The curve for the solution of dextran in water is repeated from Fig. 1. The addition of chloride ion has probably given the dextran molecule sufficient charge, most likely by adsorption, to increase its affinity for the collodion surface. Dextran approaches equilibrium with the surface more rapidly in the presence of the cationic detergent plus sodium chloride than without the salt. This effect also occurs if, instead of detergent, serum albumin is used. It should be noted that the presence of serum albumin in 0.15 *M* saline decreases the amount adsorbed by a factor of 10. In the last two sets of data the rate of adsorption decreased markedly after 5 hours.

2. Second Series

In this section the effects of two additional detergents on the sorption of dextran were investigated: an anionic detergent and a nonionic one. Here again both aqueous and saline solutions were used. The study, using aqueous and saline solutions of dextran and aqueous and saline solutions

TABLE IV

Sorption of Dextran to Collodion Membranes in the Presence of Sodium Chloride with Human Serum Albumin and a Cationic Detergent

Solution (code)	Exposure time (code)	Exposure time (*hours*)	Log activity (average of 2 determinations)
D	1	1.08	2.360
	2	2.08	2.585
	3	3.08	2.715
	4	4.08	2.715
	5	6.08	2.870
	6	8.08	3.025
	7	22.08	3.380
	8	29.08	3.415
	9	46.08	3.665
	10	52.08	3.635
E	1	1.00	2.085
	2	2.00	2.330
	3	3.00	2.320
	4	4.00	2.485
	5	6.00	2.455
	6	8.00	2.600
	7	22.00	2.455
	8	29.00	2.505
	9	46.00	2.545
	10	52.00	2.520
F	1	0.83	2.575
	2	1.83	2.685
	3	2.83	2.820
	4	3.83	2.850
	5	5.83	2.970
	6	7.83	2.995
	7	21.83	3.105
	8	28.83	3.175
	9	45.83	3.220
	10	51.83	3.225

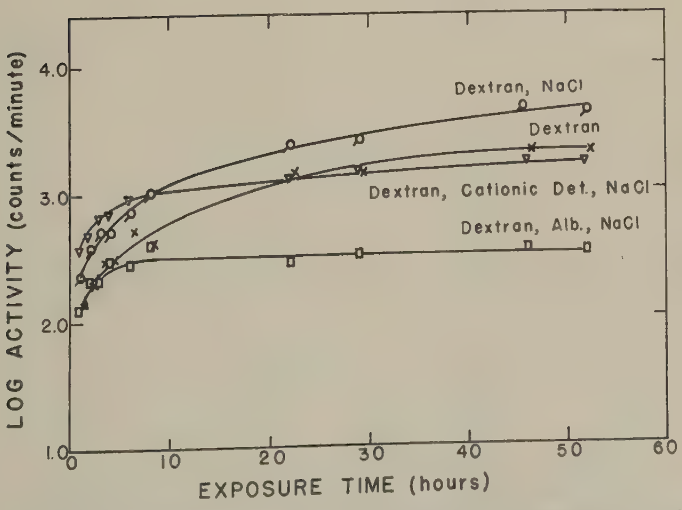

FIG. 2. Log activity versus exposure time: sorption of C^{14} dextran to collodion in the presence of sodium chloride, cationic detergent, or human serum albumin.

TABLE V

Sorption of Dextran to Collodion Membranes in the Presence of Cationic, Anionic, and Nonionic Detergents

Solution (code)	Exposure time (code)	Exposure time (*hours*)	Log activity (average of 2 determinations)
A′	1	1.33	2.039
	2	2.33	2.349
	3	3.33	2.382
	4	4.33	2.437
	5	5.33	2.566
	6	6.33	2.589
	7	24.33	2.996
	8	29.33	3.129
	9	49.33	3.179
	10	53.33	3.248
C′	1	1.25	3.026
	2	2.25	3.229
	3	3.25	3.287
	4	4.25	3.379
	5	5.25	3.358
	6	6.25	3.448
	7	24.95	3.807
	8	29.25	3.755
	9	49.25	3.912
	10	53.25	3.897
G	1	1.17	1.699
	2	2.17	1.982
	3	3.17	2.117
	4	4.17	2.152
	5	5.17	2.271
	6	6.17	2.189
	7	24.17	2.699
	8	29.17	2.563
	9	49.17	2.756
	10	53.17	2.700
H	1	1.08	1.660
	2	2.08	1.799
	3	3.08	1.667
	4	4.08	1.796
	5	5.08	1.817
	6	6.08	1.638
	7	24.08	1.957
	8	29.08	1.894
	9	49.08	2.001
	10	53.08	1.879

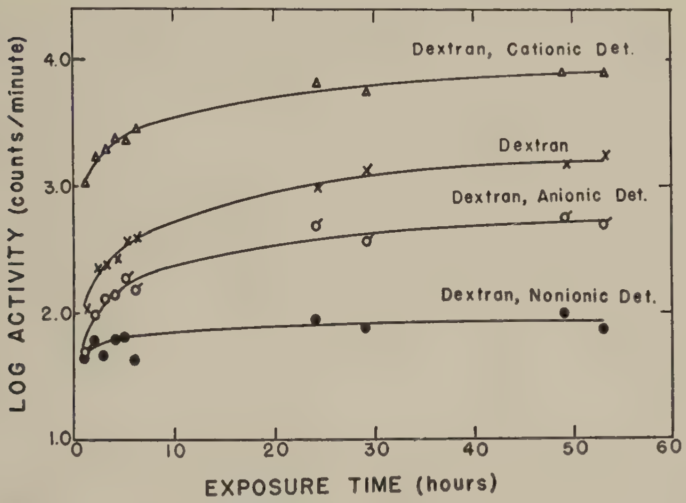

FIG. 3. Log activity versus exposure time: sorption of C^{14} dextran to collodion in the presence of cationic, anionic, or nonionic detergents.

of the cationic detergent and dextran, were repeated in this series to be certain that the procedures and techniques were reproducible within experimental error; this was found to be true.

In Table V and Fig. 3 are shown the rates of sorption of dextran from aqueous solutions of dextran, dextran and cationic detergent, dextran and anionic detergent, and dextran and nonionic detergent. Here again is evidence that the slopes of all the curves are very similar. The amount of dextran adsorbed is less in the presence of the anionic detergent and still less in the presence of the nonionic detergent. It can be seen that the dextran adsorption differs by a factor of 100, depending on whether the cationic or nonionic detergent is present.

Data for the solutions appearing in Table V with 0.15 *M* sodium chloride added are shown in Table VI and plotted in Fig. 4. The amount of dextran sorbed in the presence of the anionic detergent and sodium chloride is little different from the amount sorbed without the detergent. The nonionic detergent, on the other hand, causes a more than tenfold decrease in the amount sorbed. It has been shown (12) that the nonionic detergent molecule can lie flat on the surface due to hydrogen bridges; if this were the case, it would account for the large decrease in dextran adsorption.

VI. STATISTICAL ANALYSIS OF THE DATA

1. *First Series*

Because of the wide range covered by the data (the largest count was approximately 100 times greater than the lowest), a logarithmic trans-

TABLE VI

Sorption of Dextran to Collodion Membranes in the Presence of Sodium Chloride with Cationic, Anionic, and Nonionic Detergents

Solution (code)	Exposure time (code)	Exposure time (*hours*)	Log activity (average of 2 determinations)
D′	1	1.00	2.300
	2	2.00	2.604
	3	3.00	2.705
	4	4.00	2.859
	5	5.00	2.890
	6	6.00	2.963
	7	24.00	3.425
	8	29.00	3.440
	9	49.00	3.545
	10	53.00	3.493
F′	1	0.92	2.550
	2	1.92	2.761
	3	2.92	2.849
	4	3.92	2.849
	5	4.92	2.839
	6	5.92	2.900
	7	23.92	3.001
	8	28.92	3.032
	9	48.92	3.082
	10	52.92	3.022
I	1	0.83	2.054
	2	1.83	2.362
	3	2.83	2.536
	4	3.83	2.577
	5	4.83	2.785
	6	5.83	2.753
	7	23.83	3.304
	8	28.83	3.385
	9	48.83	3.461
	10	52.83	3.539
J	1	0.75	1.941
	2	1.75	2.128
	3	2.75	2.127
	4	3.75	2.079
	5	4.75	2.139
	6	5.75	2.198
	7	23.75	2.230
	8	28.75	2.328
	9	48.75	2.489
	10	52.75	2.477

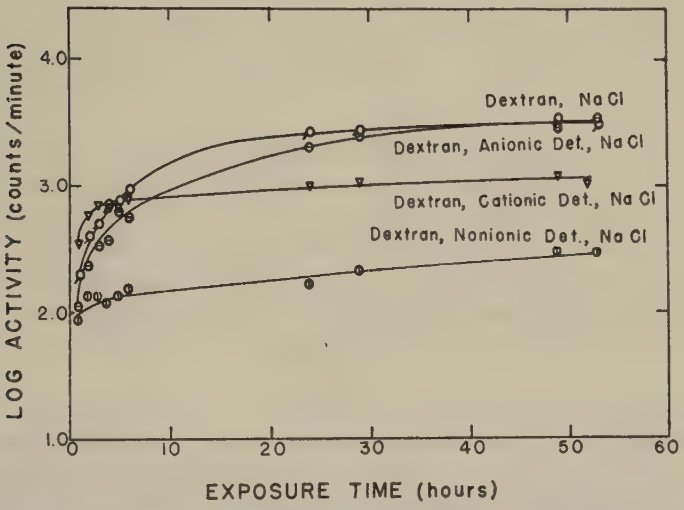

FIG. 4. Log activity versus exposure time: sorption of C^{14} dextran to collodion in the presence of sodium chloride and cationic, anionic, or nonionic detergents.

TABLE VII

Breakdown of Error in First Series (Logarithms of Counts)

Source of variation	Degrees of freedom	Mean square	
Duplicates (not corrected)	60	0.0069	
Sheet-to-sheet variation	11	0.0185	
Activity counting sets	9	0.0036	0.0043
Duplicates (corrected)	40	0.0045	

TABLE VIII

Breakdown of Error in Second Series (Logarithms of Counts)

Source of variation	Degrees of freedom	Mean square	
Duplicates (not corrected)	80	0.0056	
Sheet-to-sheet variation	15	0.0158	
Activity counting sets	9	0.0026	0.0033
Duplicates (corrected)	56	0.0034	

formation was made prior to analysis. The method of analysis described in reference (11) was applied to the logarithms of the counts. The breakdown of the error, in terms of mean squares, is given in Table VII. This table leads to the conclusion that there was no drift in the instrument. It also shows conclusively that part of the variability between duplicate discs is due to differences between sheets. By correcting the data for this effect, the error mean square for logarithms of counts is reduced from 0.0069 to 0.0043. In terms of the precision of counts, this represents a reduction in the coefficient of variation of a single count from 19% to 15%. The corrected average of duplicate measurements has a coefficient of variation of about 11%.

2. Second Series

The breakdown of error is given in Table VIII. The conclusions are similar to those drawn from the results of the first series. The estimated over-all precision is comparable to that found in the first series.

Combining the information from both series, it can be stated with 95% confidence that the position of any point in Figs. 1 to 4 is not likely to be in error by more than 0.08 on the logarithmic scale.

VII. SUMMARY

The sorption of radioactively labeled dextran to collodion membranes was studied in the presence of 0.15 *M* sodium chloride, serum albumin, and three specific detergents. It was shown that dextran is adsorbed to collodion and that this process is time dependent and may take up to 50 hours to reach a stable state. It can be seen that, in order to obtain reliable osmotic pressure measurements with this system, it is necessary to "condition" the membrane to the solution for a sufficient time to achieve adsorption equilibrium.

Evidence is given that the amounts of dextran adsorbed to the surface can be varied depending upon the presence of an additional solute component. In terms of the physiological applications of dextran, it is interesting to note that serum albumin decreases the amount of dextran adsorbed.

REFERENCES

1. SIMHA, R., FRISCH, H. L., AND EIRICH, F. R., *J. Phys. Chem.* **57,** 584 (1953).
2. FRISCH, H. L., AND SIMHA, R., *J. Phys. Chem.* **58,** 507 (1954).
3. SONNTAG, F., AND JENCKEL, E., *Kolloid-Z.*, **135,** 1 (1954); *ibid.* **135,** 81 (1954).
4. ROBERTSON, R. E., MCINTOSH, R., AND GRUMMITT, W. E., *Can. J. Research* **B24,** 150 (1946).
5. CLEVERDON, D., LAKER, D., AND SMITH, P. G., *J. Polymer Sci.* **11,** 225 (1953).
6. SCATCHARD, G., *Am. Scientist* **40,** 61 (1952).
7. WALES, M., ROTHMAN, S., STASNY, R. J., AND WEISSBERG, S. G. (National Bureau of Standards), unpublished data.
8. FURTH, F. W., CARBONE, J. V., FOX, A. C., AND JABLON, S. (Walter Reed Army Medical Center), private communication.
9. HINT, H. C., AND THORSÉN, G., *Acta Chem. Scand.* **1,** 808 (1947).
10. ISBELL, H. S., U. S. Patent 2,653,931, September 29, 1953.
11. MANDEL, J., *Biometrics* **10,** 251 (1954).
12. HARRIS, J. C., *Textile Research J.* **18,** 669 (1948).

THE MOLECULAR WEIGHT OF INSULIN, DETERMINED BY THE SURFACE BALANCE TECHNIQUE

B. S. Harrap

Biochemistry Unit, Wool Textile Research Laboratory, C.S.I.R.O., Melbourne, Australia

Received March 24, 1955

Abstract

The influence of pH and ionic strength on the molecular weight of insulin, measured by the surface balance technique, has been studied. The balance employed was considerably more sensitive than that used by Fredericq in a previous study, and it enabled measurements to be made at much lower surface concentrations. The value of ~ 6000 for the molecular weight of insulin spread on $0.01N$ hydrochloric acid found by Fredericq has been confirmed. However, at higher pH values, where Fredericq observed increased molecular weights, it is shown that at very low surface concentrations the molecular weight tends towards ~ 6000, association being favored as the surface concentration is increased. An increase in ionic strength is shown to have different effects at the isoelectric point and at pH values removed from this point; in the former case it has a dissociating effect and in the latter, an associating effect, although at infinite dilution the molecular weight tends to ~ 6000. These effects and that of pH are discussed in terms of the Coulombic and non-Coulombic forces operating in the system.

Introduction

For several years there has been considerable controversy regarding the "minimum" molecular weight of insulin and the association-dissociation phenomena which this protein undergoes on change of pH and ionic strength. Until recently most of the data available from such different experimental methods as osmotic pressure (1), ultracentrifuge (2, 3), and light scattering (4) pointed to a value in the vicinity of 12,000 for the molecular weight of the minimum subunit. In 1950 some ultracentrifuge measurements by Fredericq and Neurath (5) suggested a value of the order of 6000, but a subsequent re-examination of these measurements by Tietze and Neurath (6) led to a molecular weight of approximately 12,000, in conformity with the values of most previous workers.

The question of the minimum molecular weight assumed considerably greater proportions with the publication by Sanger and co-workers (7, 8) of the complete amino acid sequences of the A and B chains of oxidized insulin. The minimum molecular weight calculated from their data is approximately 5700, but a value of twice this figure was possible, depending upon whether the four disulfide bonds in the intact insulin molecule interlinked four chains or whether only two chains were linked, the remaining two disulfide bonds being of an intra-chain nature. Support for the latter alternative has recently been given in a study by Sanger, Smith, and Kitai (9) of the cystine peptides in degradation products of unoxidized insulin.

Further evidence for the lower value has come from the results of Harfenfist and Craig (10) using the method of partial substitution by 1-fluoro-2,4-dinitrobenzene followed by solvent partition. Similar values have also been found under conditions favorable to dissociation by Kupke and Linderstrøm-Lang (11) from osmotic pressure measurements using concentrated guanidinium hydrochloride solutions as solvent; also by Fredericq (12) from ultracentrifuge data using alkaline dioxan solutions as solvent. Fredericq (13), using Guastalla's technique (14), has also obtained a value of approximately 6000 from a study of monolayers of insulin spread on subsolutions of 0.01 *N* hydrochloric acid. Fredericq used this technique to investigate the variation of the molecular weight of insulin with pH—a particularly suitable method since it has the advantage of enabling protein films to be studied under conditions in which they are insoluble in bulk solution. However, closer examination of Fredericq's data reveals that, owing to the limited sensitivity of the apparatus used, some measurements were made at relatively high surface concentrations of protein where considerable interaction might be expected. This introduces serious uncertainties into the extrapolation of the *FA*-*F* curve to zero pressure, particularly in the vicinity of the isoelectric point. Previous work by the present author (15) had indicated interesting effects of ionic strength on the *F*-*A* curves in this region for insulin monolayers at higher surface concentrations. This paper reports the results of an investigation of the effect of pH and also of ionic strength on insulin monolayers at lower surface concentrations with the use of a considerably more sensitive surface balance than that described by Fredericq.

Experimental

The surface balance used was of the horizontal-float type previously described (15). The only modification was the construction of the trough and barriers from polytetrafluoroethylene ("Teflon") in place of paraffined glass. This gave freedom from contamination and ease of cleaning. The sensitivity of the balance was such that changes in surface pressure of approximately 0.3 millidyne/cm. could be measured.

The sample of crystalline insulin used was supplied by Boots Pure Drug Co., sample number 9095/193. A 1% (w/v) solution in 0.03 *N* hydrochloric acid was dialyzed through cellophane against several changes of the same solvent in order to free the insulin from zinc (Oncley *et al.* (3)). The

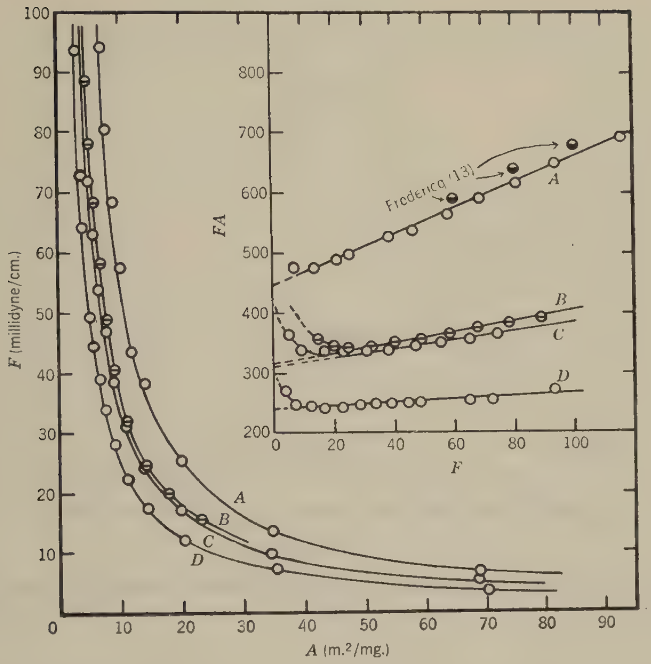

FIG. 1. *F-A* and *FA-F* curves for insulin films spread on subsolutions of pH 2.05 and differing ionic strength. Curve A: $\Gamma/2 = 0.01$; B: $\Gamma/2 = 0.1$; C: $\Gamma/2 = 0.2$; D: $\Gamma/2 = 0.5$. Some values given by Fredericq (13) are also shown for the range in which the two sets of data overlap.

concentration of the protein solution was determined by the micro-Kjeldahl procedure, assuming the nitrogen content of the protein to be 15.5% (16). The spreading solution was prepared by quantitative dilution of the stock solution to approximately 0.01% (w/v) with 0.01 *N* hydrochloric acid and was made 0.1% (v/v) with respect to isoamyl alcohol to facilitate spreading on subsolutions of low ionic strength.[1] The surface concentration was increased and the *F-A* curve built up by successive additions of the spreading solution; drops of the latter were gently touched against the surface of the subsolution.

All water used was doubly distilled, the second time from alkaline permanganate in a well-steamed Pyrex glass still. Buffer salts and potassium chloride were of analytical reagent quality, and the buffer solutions were allowed to stand overnight before use. This allowed surface-active impurities to accumulate at the surface, the solution to be used being drawn off from below the surface. The buffers used in the pH range 1–8 were hydrochloric acid, sodium acetate-hydrochloric acid, and borax-

---

[1] It was shown that identical results were obtained whether or not the alcohol was present, only the rate at which equilibrium was attained being affected.

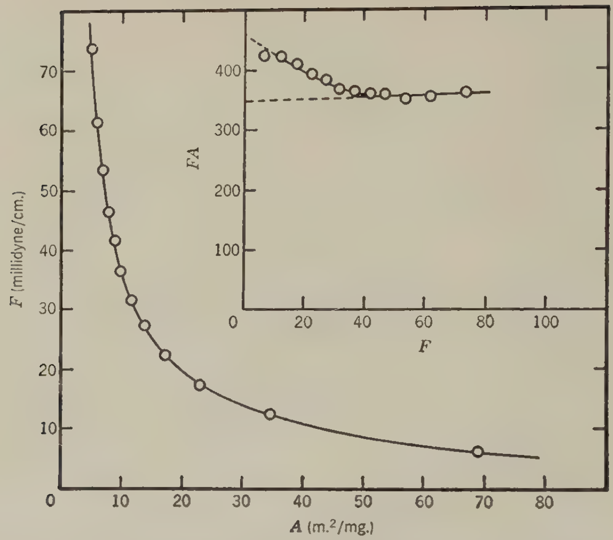

FIG. 2. *F-A* and *FA-F* curves for insulin films spread on 0.1*N* hydrochloric acid subsolution, pH 1.20.

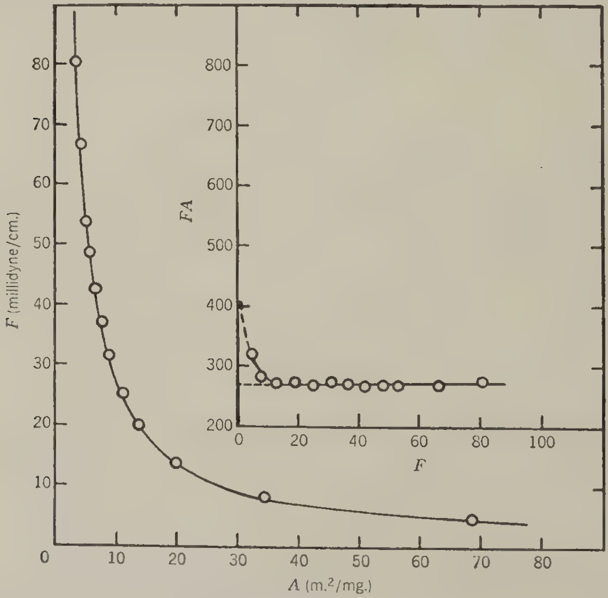

FIG. 3. *F-A* and *FA-F* curves for insulin films spread on subsolution of pH 2.81 and ionic strength 0.5.

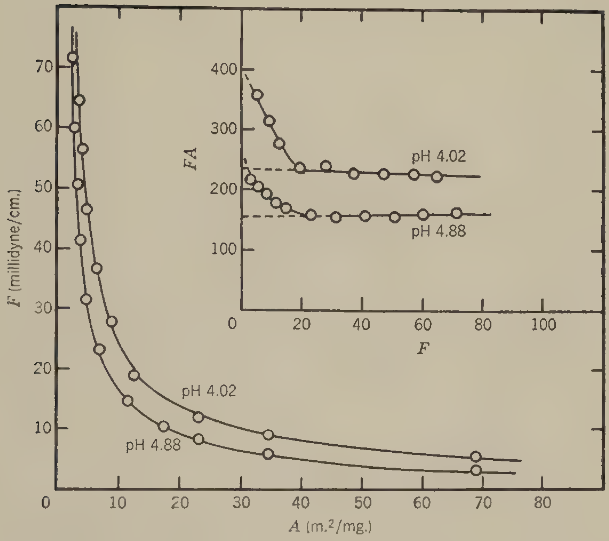

FIG. 4. *F-A* and *FA-F* curves for insulin films spread on 0.5 ionic strength subsolutions of pH 4.02 and 4.88.

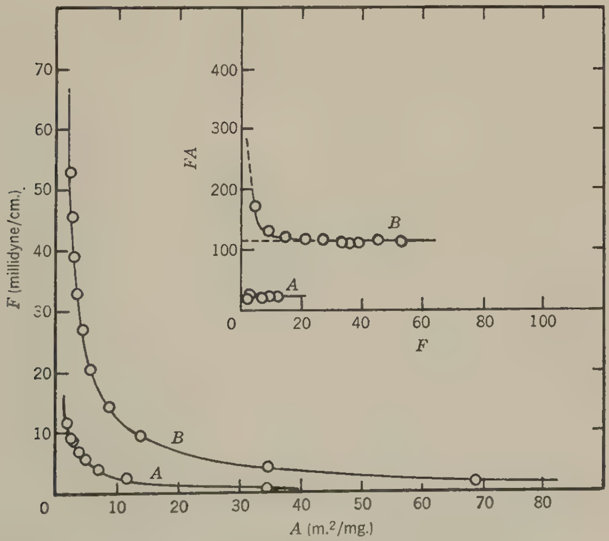

FIG. 5. *F-A* and *FA-F* curves for insulin films spread on the following subsolutions: Curve *A*: pH 5.47 and ionic strength 0.01; *B*: pH 5.49 and ionic strength 0.5.

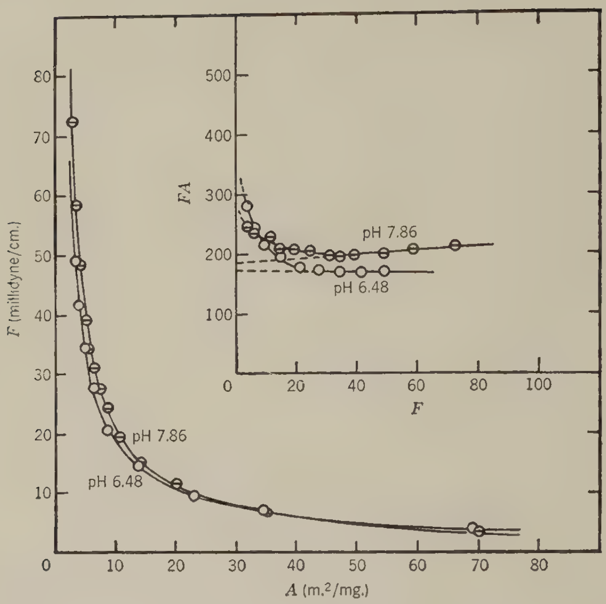

FIG. 6. F-A and FA-F curves for insulin films spread on 0.5 ionic strength subsolutions of pH 6.48 and 7.86.

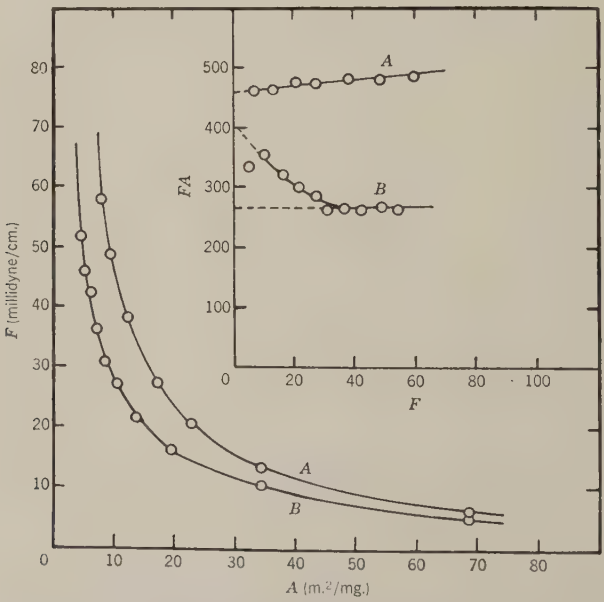

FIG. 7. F-A and FA-F curves for insulin films spread on the following subsolutions: Curve A: pH 8.48 and ionic strength 0.01; B: pH 8.53 and ionic strength 0.5.

hydrochloric acid, all of ionic strength $\Gamma/2 = 0.01$. All measurements were made at room temperature (18°–22°C.).

RESULTS

The surface pressure-area (F, millidyne/cm.; A, m.^{2}/mg.) curves for insulin spread on a number of subsolutions ranging in pH from 1.1 to 8.6 are shown in Figs. 1–7. In general the total ionic strength of the subsolution was 0.5, prepared by adding sufficient potassium chloride to the $\Gamma/2 = 0.01$ buffer solution. In certain cases, as noted in the figure legends, the concentration of potassium chloride was varied to permit the effect of ionic strength to be studied. In the insets to each figure the results are plotted in the form FA-F (Bull (17)). The inset to Fig. 1 also shows the values of Fredericq (13) over the range in which the two sets of data overlap.

DISCUSSION

Results at pH 2.05

It is initially of interest to consider the results shown in Fig. 1, Curve A, for insulin spread on a subsolution of 0.01 N hydrochloric acid, that is, under the conditions where Fredericq's results (13) led to a molecular weight of approximately 6000. The present results extend to much lower surface pressures and higher areas than Fredericq's values; nevertheless, on this subsolution agreement between the two sets of data is satisfactory in the range in which they overlap and they both extrapolate to a value of $(FA)_{F=0}$ of approximately 430. On the assumption that at infinite surface dilution ideal conditions prevail, substitution in the equation $FA = (1/M)RT$, where M is the number-average molecular weight and R and T the gas constant and absolute temperature, respectively, gives a molecular weight of approximately 5500.

In deriving an equation of state for monolayers at low surface concentration, Bull (17) has pointed out the analogy between surface pressure and osmotic pressure. It is clear that the floating boom which separates the film-covered surface from the free surface may be regarded as a semipermeable membrane and thus the surface pressure may be related more closely to a two-dimensional osmotic pressure than to a two-dimensional gas pressure, as was done by Guastalla (14). In this case, it might be argued that, under the conditions of acid pH and low ionic strength in which this film was studied, there would be a considerable Donnan effect which would make difficult the extrapolation of the FA-F curve. However, curves obtained under conditions of higher ionic strength, where the Donnan effect would be eliminated, also tend to the same value of $(FA)_{F=0}$ (see below), suggesting that the extrapolation is valid. It is therefore established that, at least under the conditions of Fig. 1, curve A, we are dealing with the minimum subunit of insulin.

TABLE I

Insulin Spread on Subsolutions of pH 2.05 and Differing Ionic Strength

Ionic strength	"Apparent" molecular weight
0.01	5.5×10^3
0.1	7.5×10^3
0.2	7.7×10^3
0.5	10.0×10^3

In view of the effects of ionic strength on the F-A curves for insulin at higher surface concentrations, previously reported by the author (15), Fig. 1 shows also the effect of ionic strength on the present F-A curves at pH 2.05. Increase in ionic strength has a marked effect in that the FA-F curve is no longer linear over the whole range investigated, but shows a sharp upward turn in the region of low pressures and surface concentrations. Although the experimental accuracy is not sufficient to allow an effective extrapolation of the curves to the FA ordinate[2], all curves in Fig. 1 tend towards a value of $(FA)_{F=0} \sim 400$, corresponding to a molecular weight of ~6000. By analogy with osmotic pressure the negative deviations from linearity observed in the FA-F curves B, C, and D indicate association of the monomer units as the surface concentration is increased. As the ionic strength increases, the surface pressure at which deviations from linearity occur decreases, so that at the highest ionic strength investigated the deviation is barely perceptible. Thus, unless the system is investigated with the use of a surface balance at least as sensitive as that used in the present study, these phenomena will not be observed.

From these results it appears that at very low surface concentrations the insulin exists as a "monomer" of molecular weight ~6000, irrespective of ionic strength. Since the insulin molecule carries its maximum positive charge at pH 2, it might be expected that at low ionic strength the repulsive Coulombic forces outweigh the attractive van der Waals and hydrogen-bonding forces at all surface concentrations studied. Thus the insulin remains in the monomeric form and the FA-F curve is linear. However, as the ionic strength is increased, the Coulombic interaction is reduced to such an extent that a certain amount of association can occur at higher surface concentrations (where the distance between molecular centers decreases). Oncley *et al.* (3), Steiner (18), and Gutfreund (1) have already observed that increased ionic strength favors association in acid solutions of insulin in the bulk phase. This association is probably an equilibrium process so that, by extrapolating the linear portions of the curves, the "apparent" molecular weights obtained might be expected to reflect the equilibrium between monomer and polymer units. These values are shown in the second column of Table I and suggest that at pH 2.05 the highest polymer formed in the range of ionic strengths investigated is the dimer, of molecular weight ~11,000.

---

[2] To extrapolate with any certainty the sensitivity of the apparatus would have to be increased tenfold. Even if this could be done, the contribution of surface-active impurities would probably be sufficient to prevent accurate values being obtained.

Results at pH 1.1

Fredericq (13) found that the molecular weight of insulin spread on 0.1 *N* hydrochloric acid was "about 12,000." However, the results given in his paper show that the lowest surface pressure recorded was approximately 200 millidyne/cm., corresponding to an area of ~2 m.^{2}/mg. Figure 2 shows, on the other hand, that in the region of much lower surface pressures the *FA-F* curve again bends upward and tends to a value of $(FA)_{F=0}$, corresponding to a molecular weight of ~6000. Comparison with curve *B* in Fig. 1 giving the results at ionic strength $\Gamma/2 = 0.1$ shows that the two curves are very similar. This is to be expected since the main effect of passing from a subsolution of 0.01 *N* hydrochloric acid to one of 0.1 *N* hydrochloric acid is to increase the ionic strength.

Results from pH 2.05 to the Isoelectric Point

As the pH is increased above 2.05 (Figs. 3–5), the effect (at constant ionic strength, 0.5) on the *F-A* and *FA-F* curves is similar to that of increasing ionic strength at pH 2.05 in that association is favored. The Coulombic interaction is reduced in this case because of the decreased net charge on the molecule rather than from an electrostatic screening effect due to increased ionic strength. With the exception of the results in Fig. 5, curve *A*, where the surface pressures involved are too low to allow any valid deduction, it is not inconsistent with the results to suggest that all *FA-F* curves in Figs. 3–5 extrapolate to a value of $(FA)_{F=0}$, corresponding to a molecular weight of ~6000. Extrapolation of the linear portions of the curves yields the apparent molecular weight values shown in Table II, suggesting that polymers considerably greater than the dimer are formed. When these higher polymers are formed, the experimental accuracy is lowered by the fact that aggregation seems to occur at a finite velocity and equilibrium is attained only very slowly. With each successive addition of spreading solution there is a sharp rise in surface pressure, comparable with that observed at pH 2.05 (i.e., with only monomer or dimer present), followed by a slow decrease. Readings were taken when the surface pressure was constant for 5 min., but additional slow changes almost certainly occurred in some cases, indicating even further aggregation. This effect does not seem to have been observed directly before, probably because of the longer time interval necessary in most methods between preparation of the solution and the taking of the first reading. However, it is interesting that Oncley *et al.* (3) state that their ultracentrifuge results on boundary spreading could be better explained if equilibrium took a finite time to be reached.

In a previous investigation of insulin monolayers at higher surface concentrations it was found (15) that an increase in ionic strength resulted in an increase in surface pressure in the vicinity of the isoelectric point, in contrast to the decrease observed at acid and alkaline pH values. Figure 5 shows the effect of ionic strength in the range of surface concentrations investigated in the present study. Assuming that both FA-F curves extrapolate to the same $(FA)_{F=0}$ value at infinite surface dilution, it is evident from Fig. 5 and from the apparent molecular weight values in Table II that aggregation is considerably greater at low ionic strength than at high ionic strength. Moreover, the time effect of aggregation is much more pronounced at low ionic strength. Since the net charge on the molecule is very low in this region, it seems likely that change in ionic strength affects not only the Coulombic repulsive forces but also the non-Coulombic attractive forces. Thus, at any particular pH the net effect of changing ionic strength is a balance between its opposite effects on Coulombic and non-Coulombic interactions. The disassociating effect of increased ionic strength in the vicinity of the isoelectric point probably explains the low value of 10,000 obtained for the molecular weight at pH 4.5 by Allen and Alexander (19), even though their lowest recorded pressure was ~20 millidyne/cm. They used a 25% ammonium sulfate solution, $\Gamma/2 \sim 6$, as subsolution.

Results on the Alkaline Side of the Isoelectric Point

Figures 6–7 show that as the pH is increased beyond the isoelectric point the effects are similar to those on the acid side. As the pH increases the extrapolation of the linear parts of the FA-F curves (Table II) provides evidence for decreasing aggregation. Furthermore, measurements at the highest pH investigated show that an increase in ionic strength again causes aggregation, parallel with the observations at pH 2.05. Measure-

TABLE II

Insulin Spread on Subsolutions of Differing pH and Ionic Strength

pH	Ionic strength	"Apparent" molecular weight
1.20	0.5	7.0×10^3
2.81	0.5	9.8×10^3
4.02	0.5	10.0×10^3
4.88	0.5	15.0×10^3
5.47	0.01	$\sim 100 \times 10^3$
5.49	0.5	20.9×10^3
6.48	0.5	13.7×10^3
7.86	0.5	12.9×10^3
8.48	0.01	5.3×10^3
8.53	0.5	9.2×10^3

ments could not be made at pH values greater than 8.6, partly because of the difficulty of maintaining the pH constant with such a large surface exposed to an atmosphere containing CO_2, and also because of the difficulty of obtaining a clean surface at the solution-air interface. Despite the most rigorous cleaning procedures, surface-active material continually appeared at the interface at high pH values.

The author wishes to thank Mr. I. J. O'Donnell and Mr. E. F. Woods for helpful discussions.

References

1. Gutfreund, H., *Biochem. J.* **50,** 564 (1952).
2. Gutfreund, H., and Ogston, A. G., *Biochem. J.* **40,** 432 (1946).
3. Oncley, J. L., Ellenbogen, E., Gitlin, D., and Gurd, F. R. N., *J. Phys. Chem.* **56,** 85 (1952).
4. Doty, P., Gellert, M., and Rabinovitch, B., *J. Am. Chem. Soc.* **74,** 2065 (1952).
5. Fredericq, E., and Neurath, H., *J. Am. Chem. Soc.* **72,** 2684 (1950).
6. Tietze, F., and Neurath, H., *J. Am. Chem. Soc.* **75,** 1758 (1953).
7. Sanger, F., and Tuppy, H., *Biochem. J.* **49,** 463, 481 (1951).
8. Sanger, F., and Thompson, E. O. P., *Biochem. J.* **53,** 353, 366 (1953).
9. Sanger, F., Smith, L. F., and Kitai, R., *Biochem. J.* **58,** vi (1954).
10. Harfenfist, E. J., and Craig, L. C., *J. Am. Chem. Soc.* **74,** 3087 (1952).
11. Kupke, W., and Linderstrøm-Lang, K., *Biochim. et Biophys. Acta* **13,** 153 (1954).
12. Fredericq, E., *Nature* **171,** 570 (1953).
13. Fredericq, E., *Biochim. et Biophys. Acta* **9,** 601 (1952).
14. Guastalla, J., *Compt. rend.* **208,** 1078 (1939).
15. Harrap, B. S., *J. Colloid Sci.* **9,** 522 (1955).
16. Harfenfist, E. J., *J. Am. Chem. Soc.* **75,** 5528 (1953).
17. Bull, H. B., *Advances in Protein Chem.* **3,** 95 (1947).
18. Steiner, R. F., *Arch. Biochem. and Biophys.* **39,** 332 (1952).
19. Allen, A. J. G., and Alexander, A. E., *Trans. Faraday Soc.* **8,** 863 (1954).

MEASUREMENT OF THE MOLECULAR WEIGHT OF A POLYESTER AND EVALUATION OF ITS MOLECULAR VOLUME

Henri L. Rosano

Department of Chemistry, Columbia University, New York, New York

Received May 5, 1955

Abstract

The micro- and macromanometer technique for the determination of molecular weight has been applied to a polyester (m.w. = 4000). The polymer was studied in several solvents; the values obtained for the molecular weight are practically the same. However, the surface area occupied by one molecule is a function of the solvent. This result leads to the hypothesis that a molecule deposited on the surface is more or less spread out depending on the degree of solvation.

I. Introduction

Surface monolayers at great dilutions can be considered as *surface gases.* These gases obey the Mariotte Law (in two dimensions) $PS = RT$ either for a fairly extended region (tricapryline) or as a limiting law at great dilutions (myristic acid) (1). Putting nonvolatile substances in the gaseous state (as in osmometry) permits the determination of molecular weights. The first attempt at such determination was made on protein films in 1939 (2). Since then, this technique has hardly been used for reasons essentially practical. The problem to be solved is the measurement of the extremely small pressures.

Recently, G. C. Benson and R. L. MacIntosh (3) deduced from their experiments in spreading polymers of polyvinyl acetate on water the impossibility of extrapolating surface pressure vs. surface area curves for calculating molecular weights.

In 1946, J. Guastalla tried to determine the molecular weight of several samples of polyvinyl chloride with the help of this technique; the study was discontinued because of poor results. Nevertheless, we have kept an important hypothesis, namely, that a molecule will probably keep the same shape in the gaseous monolayer state that it has in solution. M. Abribat and J. Pouradier (4) have confirmed this idea in the case of cellulose acetate.

Except for the above-mentioned references, no workers seem to be interested in this technique for studying polymers; we felt that by using it we could get more information for determining molecular dimensions as well as molecular weights than by other methods. To verify our method, we reproduced the molecular weight of myristic acid; before each experiment we repeated this measurement as a check on the technique.

We measured the molecular weight of a sample of polyester in solutions of different solvents (benzene, acetone, methylethylketone, chloroform, and also mixtures of benzene and methanol) and determined the compression isotherm in each case with the aid of another apparatus.

The results obtained with our method checked with the molecular weight of the polyester which has been previously determined. This study of the behavior of the polymer with different solvents showed us that the molecular weight obtained was constant and that only the cosurface, defined below, was a function of the solvent.

II. Apparatus

The apparatus could be used with either of two measuring devices developed by J. Guastalla (1).

1. Pendulum Surface Manometer (*Fig. 1*)

The pendulum surface manometer consists of a metallic piece P hung from the roof of the apparatus by two wires of equal length, each of which forms a V. The branches of the V are parallel and constrain the piece P to move only by translation. All the points of the piece describe arcs of

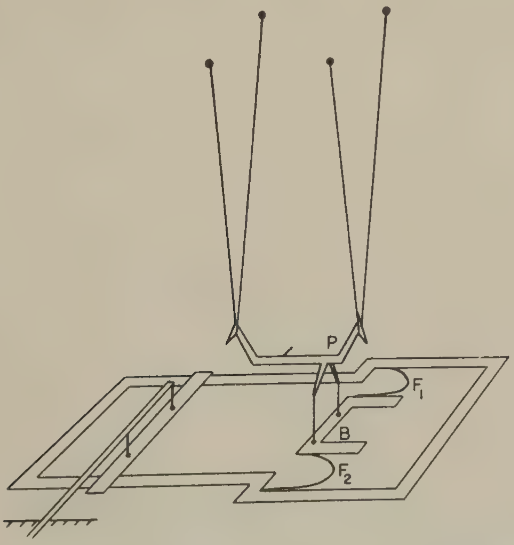

FIG. 1. Pendulum surface manometer. P: metallic piece hung from roof of apparatus by two wires of equal length, each of which forms a V. B: movable mica barrier coated with paraffin. F_1, F_2: vaselinated silk thread.

identical circles when one displaces the pendulum from its equilibrium position, and the force necessary to maintain it in any position has the same value no matter where the point of application is. This force is the force directed toward the point of equilibrium and is equivalent to a pendulum of the same mass as the piece concentrated at a point attached to a weightless suspension of the same length.

The piece *P* has two vertical needles which penetrate a movable paraffined mica barrier *B* through two holes. The mica is a rectangle with one of its longer sides missing and separates the surface, which is confined in a floating frame, into two compartments. The separation is assured by two vaselinated silk threads F_1 and F_2, each attached to one of the sides of the barrier and the frame, which become U-shaped under the action of surface pressure. The liquid surface is cleaned in the two compartments by dropping calcinated talcum powder on it to detect impurities, which can then be removed by blowing the film into one corner of the mica frame with compressed air and removing them by suction. A film is spread in one compartment where a movable barrier can compress it. The pressure exerted by the film on the barrier is determined by the displacement of the pendulum piece multiplied ten times by an optical system and projected onto a vertical scale. The sensitivity of this apparatus is 0.1 dyne/cm.

2. Surface Micromanometer Using a Stretched Thread (Fig. 2)

In the stretched thread micromanometer, a floating rectangular frame of paraffined mica is separated into two compartments by a long thread of vaselinated silk. A horizontal rod *B* suspended freely from a vertical

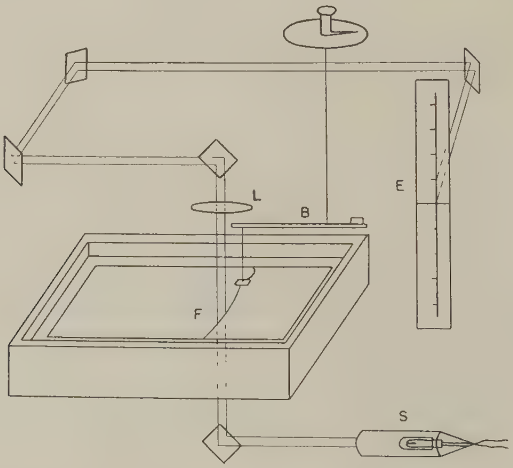

FIG. 2. Surface micromanometer. *B:* horizontal rod hung from the torsion wire. *L:* lens which projects image of the stretched thread on the scale. *E:* graduated scale. *S:* light source.

torsion wire has a vertical needle at one end; the needle passes through a hole in the center of a small piece of paraffined mica floating on the surface. The mica is joined to the frame by two silk threads; that on one side is a short thread used only to contain the film, that on the other is a long thread whose displacement determines the pressure of the film. When a film is spread on one side of the surface, the longer silk thread becomes curved because of the pressure of the film. The displacement of the center of this thread is measured by an optical system; a glass trough allows the transmission of light to project an image of the thread on a scale. One millimeter deflection on the scale is equivalent to 1/1000 dynes/cm. of surface pressure.

The spreading of a polymer on the water surface, starting with a known weight of polymer in solution in several solvents, is done with the aid of a very fine pipet previously calibrated. One deposits a certain number of drops.

III. Film of the Polymer

The curve of compression of a polymer film represented in the coordinate surface pressure vs. area is composed of three distinct parts analogous to those obtained with films of proteins.

1. *AB*, which does not have any change in direction from extremely dilute concentration, represents very low surface pressure, and corresponds to the gaseous state of the film.

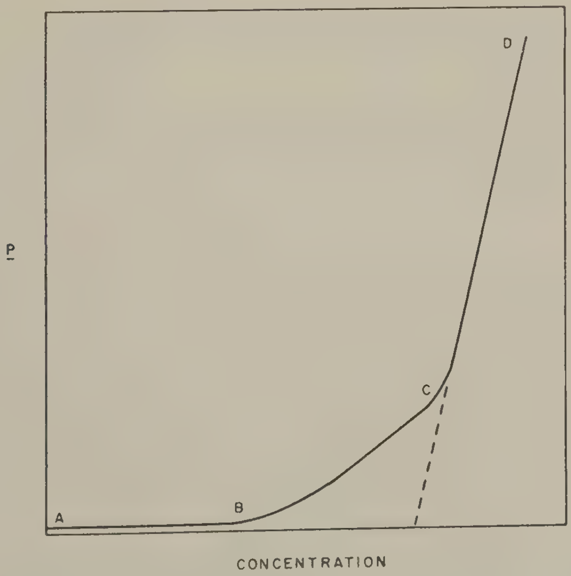

Fig. 3. Schematic curve of compression isotherm of a macromolecule.

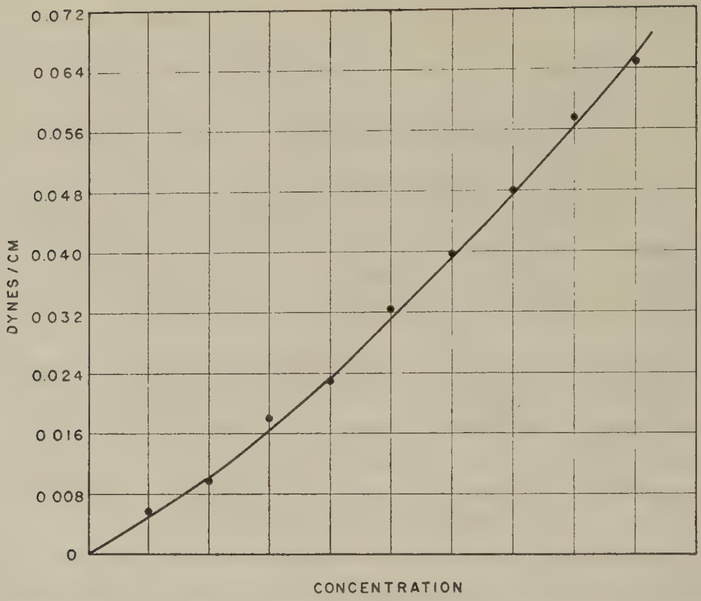

FIG. 4. Surface isotherm of the polyester dissolved in benzene in the gaseous region.

2. *BC* represents the transition between the gaseous state and the high-pressure curve.
3. *CD* corresponds to the curve at high pressure.

Study of the compression isotherm of the polymer shows a variation in the thickness of the molecular layer depending on the nature of the solvent; this fact proves that the polymer molecule is more or less spread according to the solvent used. Figure 3 represents the compression isotherm of the polyester; a similar curve is obtained with the proteins.

IV. STUDY OF THE GASEOUS FILM

As a first approximation, the law of the gaseous film in the limit of dilution is $PS = RT$ for 1 mole. The pressure vs. concentration curve in the gaseous region of the polyester studied, which would be a straight line if the gas were perfect, is concave at higher concentrations. Figure 4 represents an isotherm in the gaseous region of a polyester in dissolved benzene. In the same way that the introduction of *covolume* changes the equation of perfect gases to an equation better adapted to real gases, we have introduced the concept of *cosurface* (b) which appears to represent the facts better.

$$P\,(S_{\text{mole}} - b_{\text{mole}}) = RT \quad \text{for 1 mole,}$$

$$P\,(S - b) = RT/M \qquad \text{for 1 g., } M \text{ being the molecular weight,}$$

or

$P\ (1/C - b) = RT/M,$ C being the surface concentration in g./cm.^{2}, from which one deduces

$$P\ (1 - bC) = (RT/M)C$$

$$1 - bC = (RT/M)C/P.$$

Thus, using the idea of a cosurface, the ratio C/P vs. C is a straight line. The data bear out this assumption. Figure 5 is a curve C/P vs. C deduced from the isotherm of Fig. 4. Extrapolating the line to the x-axis gives the value of C/P at infinite dilution, from which the molecular weight, which is equal to RT (limit C/P), can be calculated.

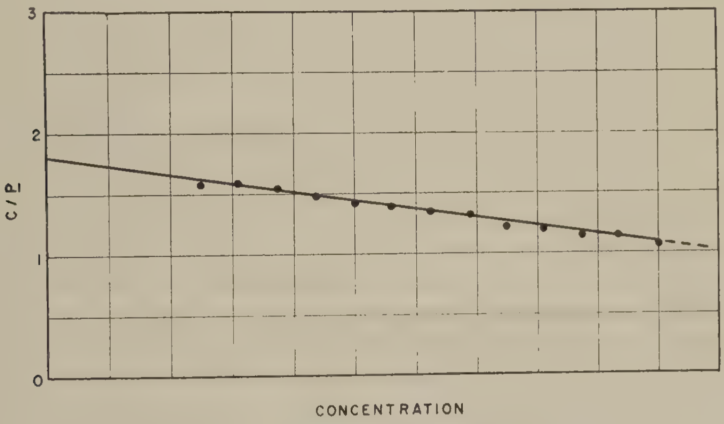

FIG. 5. Curve C/P vs. C deduced from the isotherm of Fig. 4.

If the line is extrapolated to the x-axis at the intersection $C/P = 0$, $bC = 1$, and $C = 1/b$. The concentration obtained is therefore the inverse of the cosurface. From the found value of the cosurface, the space occupied by a molecule at zero surface pressure can be easily deduced.

V. EXPERIMENTAL RESULTS

The polymer chosen was that obtained from the condensation of sebacic acid and dioxyethylene glycol which has a formula

$HO—(CH_2)_2—O—(CH_2)_2—[—OOC—(CH_2)_8—COO—(CH_2)_2—O—(CH_2)_2—]_n—OH$

The molecular weight, determined by the number of free hydroxyl groups, was close to 4000; the density was determined as 1.1. The polymer was insoluble in water, and distilled water was used as the subphase.

According to the molecular weight of the polymer, n had a value of about 15. The chain length of the polymer was about 250 Å.

With the aid of the pendulum surface manometer, the compression isotherm of the polyester described above was determined using different

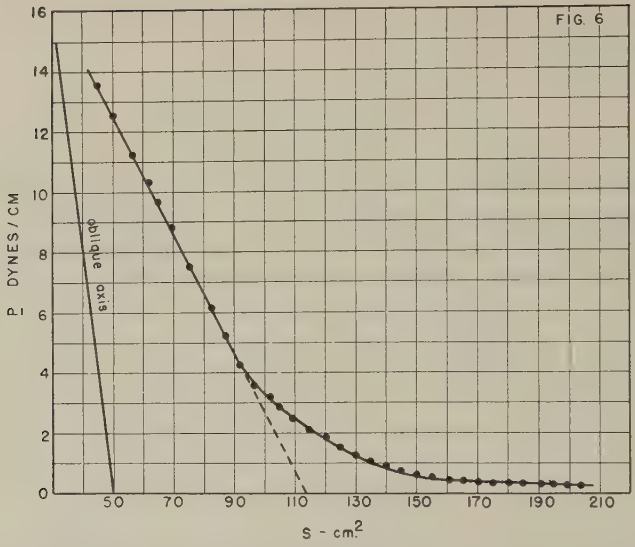

Fig. 6. Compression surface isotherm obtained with benzene as the spreading solvent.

spreading solvents. Figure 6 is the compression surface isotherm obtained with benzene as the spreading solvent. With the aid of the surface micromanometer, a value of the molecular weight was determined, and the molecular area occupied at zero pressure (Ω) was deduced.

The results are given for different solvents in Table I. The first column represents the molecular weight, the second the molecular area Ω, the third the calculated molecular area at the point corresponding to the end of the gaseous state (point *B*), the fourth the area at high pressure (point *C*), and the fifth the film thickness at point *C* (5).

The thickness of the films from different solvents appears to vary inversely with the molecular area.

From the values of the area obtained at different points, the diameters of circles of equal area were calculated. In each of these cases (Table II), from the values given together with the length of the molecule (which is

TABLE I

Results Obtained for Different Solvents

Solvents	*M*	Ω (*A.*²)	Area in *B* (*A.*²)	Area in *C* (*A.*²)	Thickness in *C* (*A.*)
C_6H_6	4370	4619	3815	2501	3.19
C_6H_6 + 10% CH_3OH	4370	4691	2670	2202	2.97
C_6H_6 + 22% CH_3OH	4130	5112	2712	2280	2.7
C_6H_6 + 36% CH_3OH	4370	5269	2884	2402	2.6
CH_3—CO—C_2H_5	3900	3862	2300	1683	4.18
$CHCl_3$	4130	2863	2000	1482	4.95
CH_3—CO—CH_3	3900	2316	1615	964	7.37

TABLE II

Calculated Diameters of Circles of Equal Area

Solvents	Diameter deduced from Ω (*A.*)	Diameter in *B* (*A.*)	Diameter in *C* (*A.*)
C_6H_6	76.4	72	56.4
C_6H_6 + 10% CH_3OH	77.4	58.4	52.8
C_6H_6 + 22% CH_3OH	81.4	58.8	53.9
C_6H_6 + 36% CH_3OH	81.6	63.4	55.4
CH_3—CO—C_2H_5	71	54.1	46.3
$CHCl_3$	62	52	43.3
CH_3—CO—CH_3	54.4	45.4	36.6

about 250 Å.), one can deduce that the spread molecule is always curled up even in the best solvent. *It can be deduced from these tables that the molecular weight is constant and is practically independent of the solvent used; the molecular area is a function of the solvent and depends directly on the extent of solvation.*

Tests made using benzene as solvent with successive additions of from 10% to 36% methanol seem to show that mixtures of methanol and benzene are better solvents for the polymer than pure benzene. Tests were also made with higher percentages of methanol, but the instability of the films led us to believe that the polymer becomes slightly soluble in water.

That the addition of methyl alcohol (in which the polymer is insoluble) to benzene makes it a better solvent can be seen from the solubility of propylene glycol in benzene only in the presence of sodium stearate (6). We imagine that hydrocarbon chains are easily solvated by the benzene and that the terminal hydroxyl groups of the polymer are associated with the methanol.

This technique has been used to determine the molecular weight of several substances. In the case of slightly soluble substances, it was possible to determine the surface pressure as if the substance were insoluble. Saraga (7) has shown that in the case of lauric acid films (slightly soluble in water) the surface pressure is a linear function of the square root of time a short time after spreading. It is therefore possible to obtain the surface pressure of the substance by extrapolating surface pressure vs. square root of time to zero time.

References

1. Guastalla, J., Thesis Montpellier, pp. 44–48 (1948).
2. Guastalla, J., *J. chim. phys.* **13,** 71 (1945).
3. Benson, G. C., and MacIntosh, R. L., *J. Colloid Sci.* **3,** 323–331 (1948).
4. Abribat, M., and Pouradier, J., *Compt. rend.* **233,** 1006–1008 (1951); *J. chim. phys.* **49,** No. 5, 248–249 (1952).
5. Rosano, H. L., and Vaillet, G., *Peintures, pigments, vernis* **29,** No. 9, 719–724 (1953).
6. Petit, S. R., and McBain, J. W., *Ind. Eng. Chem.* **38,** 741 (1946).
7. Saraga, L., *Mém. services. chim. état* (*Paris*) **37,** 28–43 (1952).

PHENYLSULFONIC ACID AS A MEDIATING AGENT IN HISTAMINE-HUMAN GAMMA GLOBULIN INTERACTIONS

T. D. Lyons[1] and A. C. Andrews

Chemistry Department, Kansas State College, Manhattan, Kansas

Received May 6, 1955

Abstract

By the method of equilibrium dialysis it was found that histamine does not bind *in vitro* to representative human and bovine proteins at 0°C. A modified protein formed by coupling the diazonium salt of *p*-sulfanilic acid was found to form a stable complex with histamine. The energy of binding of the first mole of histamine to this modified protein has been determined to be −1391 cal.

Introduction

Many experiments have been directed toward proving that 4 (or 5) ethylamineimidazole (histamine) is the toxic substance involved in the anaphylactic shock. That histamine is liberated, *in vivo*, during anaphylactic shock was first demonstrated by Best *et al.* (1), who were able to show the presence of histamine in sufficient quantity to account for the anaphylactic shock suffered by the ox. Recently Parrot and coworkers (2, 3) reported success in attempts to bind histamine to animal proteins *in vitro* and thus provide a mechanism for histamine action in anaphylaxis. Conversely, however, Kaplan and Davis (4), using a radioactive tracer technique to follow histamine, could find no evidence of binding *in vitro* to the human plasma proteins.

This work was undertaken to resolve the above-mentioned discrepancy and investigate the possibility of histamine binding through a mediating agent to the protein.

The equilibrium dialysis method was used to study the interaction of histamine with five different animal proteins. These included gelatin, bovine gamma globulin fraction II, milk whey, human gamma globulin, and whole blood serum.

Experimental

The concentration of histamine was determined spectrophotometrically using a method developed in this laboratory (5). All solutions were prepared in a phosphate buffer, the ionic strength of which was 0.2 at a pH 6.9. The bovine proteins and the human gamma globulin were obtained from Armour and Company, and the whole human blood serum was collected at Ft. Riley, Kansas, and represented a composite mixture of many types. The whey protein was prepared from a casein-free solution by precipitation at a pH of 2.0 with hydrochloric acid (1/10). The precipitate was outdialyzed against distilled water until free of chloride ion. The proteins were purified by outdialysis against phosphate buffer. The final protein concentrations were adjusted to 0.2% as determined by gravity oven at 90°C. Histamine diphosphate was obtained from Nutritional Biochemicals Corporation.

---

[1] Abstracted from Master of Science Thesis, Kansas State College, Manhattan, Kansas, 1955.

A volume of 10 ml. which contained 20 mg. of protein was introduced into Visking 18/32 cellulose casing which then was equilibrated with varying concentrations of histamine for 24 hours. Blank cells were prepared with the same volume of buffer and equilibrated with corresponding histamine solutions 24 hours. After equilibration, comparison was made of the histamine concentration in the blank and protein cells to find the magnitude of binding by the protein as influenced by histamine concentrations.

Results and Discussion

Typical data for histamine binding to each animal protein are presented in Table I. The absence of binding is observed over wide concentration ranges of histamine in all cases. The absence of binding in the case of human gamma globulin might be explained by the amino acid composition. Haurowitz (6) reports 100 basic groups compared with 67 acid groups per 10^5 grams of protein. Since histamine exists in solution as a cation, the excess of basic amino acids in the protein should repel rather than attract the histamine.

To provide a site for histamine binding, the following functional groups were linked to human gamma globulin: arsonic, carboxylic, and sulfonic acid. This was accomplished by the diazotization of the *p*-arsanilic, *p*-aminobenzoic, and *p*-sulfanilic acids and subsequent coupling to the protein in alkaline solution. In this manner these functional groups (*para* to the azo linkage) were irreversibly bound to the protein. Attempts to bind histamine to those azo proteins containing either the carboxylic or arsonic acid groups met with no success. In the case of the azo protein containing the sulfonic acid group, however, binding did occur. The effect of concentration of histamine on the amount bound per mole of protein is shown in Table II. The effect of temperature on the stability of the complex is also shown in Table II, which indicates a decrease in stability with an increase in temperature.

The maximum number of bound molecules of histamine per azo protein molecule and the free energy of formation of this complex were calculated

TABLE I

Histamine Binding to Various Animal Proteins at 0°C.

Histamine concentration (Moles per liter × 10^{-5})		
Blank cell	Protein cell	Moles bound
	Gelatin	
1.56	1.31	0
3.04	3.12	0
6.76	6.74	0
	Bovine Gamma Globulin	
2.21	2.29	0
5.69	5.50	0
8.38	8.45	0
	Milk Whey	
0.90	0.90	0
1.76	1.76	0
2.88	2.88	0
	Human Gamma Globulin	
2.43	2.43	0
1.20	1.20	0
4.28	4.27	0
	Whole Human Blood Serum	
2.94	3.10	0
3.65	3.65	0
6.66	6.70	0

TABLE II

Binding of Histamine to Human Gamma Globulin Azo-Phenylsulfonic Acid

Temperature (°C.)	Histamine concentration (*moles × 10^{-6}*)	Moles histamine bound (*per mole protein*)
0.0	0.23	0.79
	0.26	0.53
	0.29	0.87
	0.35	0.88
	0.43	0.95
	0.62	1.15
	0.61	1.28
	0.86	1.60
	0.90	1.46
	1.18	1.31
	2.78	1.88
12.5	0.28	0.30
	0.43	0.36
	0.49	0.39
	0.53	0.39
	0.95	0.45
	1.66	0.36
	3.29	0.45
	4.90	0.48

by the method of Klotz (7). Assuming a stepwise formation of the complex, in which the first bound molecule is held more firmly than the second, etc., the following expression is valid:

$$1/r = \frac{K}{m}\frac{1}{(A)} + \frac{1}{m} \qquad [1]$$

in which r is the number of bound molecules per protein molecule, m is the maximum number of bound molecules per protein molecule, (A) is the concentration of unbound histamine in moles per liter, and K is the intrinsic binding constant for the system. Since (A) and r may be determined experimentally, evaluation of K and m is carried out by plotting $1/r$ against $1/(A)$ and extrapolating to infinite (A). This is shown in Fig. 1, which was constructed by the method of least squares. It is seen from Eq. [1] that K/m is the slope of the line and $1/m$ the intercept on the $1/(A)$ axis. The binding was carried out at 0.0° and 12.5°C. The free energy of formation of the first bound molecule was evaluated by:

$$\Delta F = -RT \ln K_{eq} \qquad [2]$$

where K_{eq} is obtained by applying experimental data to

$$K_{eq} = \frac{m - (i - l)}{iK} \qquad [3]$$

in which i is the order of binding, $i = 1$ for the first mole bound and 2, 3, 4, 5, . . . i for successive binding.

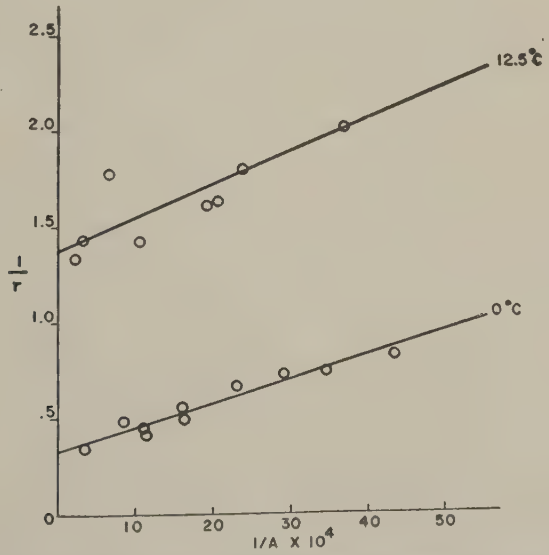

FIG. 1. The binding of histamine to human gamma globulin azophenylsulfonic acid.

The value of the free energy of formation at 0.0°C. was −1391 cal. per mole and decreased with an increase in temperature.

Even though this histamine-azo protein bond is relatively weak, a site for histamine binding has been provided by mediation of the original protein. Although this particular type of mediation is not assumed to be present *in vivo* other functional groups capable of attracting histamine might be present. Such groups as sulfhydryl might act as mediating agents or perhaps metal ions, which are known to form complexes with histamine (8, 9), might form sites for binding *in vivo*.

The authors wish to thank the Public Health Service for Grant No. G. 3920, which made this investigation possible, and Maj. Alex Gerber and Dr. B. W. Lafene for assistance in procuring human gamma globulin for this research. They also wish to thank Dr. B. L. Mickel for valuable suggestions offered and Mr. E. B. Beetch for the preparation of the whey protein.

REFERENCES

1. BEST, C. H., DALE, H. H., DUDLEY, H. W., AND THORPE, W. V., *J. Physiol. (London)* **62,** 397 (1927).
2. PARROT, J. L., URGUIA, D. A., AND LABORDE, C., *Compt. rend. soc. biol.* **145,** 885 (1951).
3. PARROT, J. L. AND LABORDE, C., *Compt. rend soc. biol.* **147,** 1203 (1953).
4. KAPLAN, E. H. AND DAVIS, JANE, *Proc. Soc. Exptl. Biol. Med.* **84,** 218 (1953).
5. LYONS, T. D., Masters Thesis, Kansas State College, Manhattan, Kansas, 1955.
6. HAUROWITZ, F., "Chemistry and Biology of Proteins." Academic Press Inc., New York, 1950.
7. KLOTZ, IRVING M., *Arch. Biochem.* **9,** 109 (1946).
8. MICKEL, B. L., AND ANDREWS, A. C., *J. Am. Chem. Soc.* **77,** 323 (1955).
9. MICKEL, B. L., PH.D. Dissertation, Kansas State College, Manhattan, Kansas, 1955.

STRESS-RELAXATION OF POLYISOBUTYLENE IN THE TRANSITION REGION (1, 2)

E. Catsiff and A. V. Tobolsky

Frick Chemical Laboratory, Princeton University, Princeton, New Jersey

Received April 18, 1955

ABSTRACT

New data are reported on the stress-relaxation of the National Bureau of Standards sample of polyisobutylene at temperatures from −40°C. to −83°C. When properly adjusted, the data agree very well with dynamic-property data at temperatures above −45°C. The data do not agree with the reduced equation for viscoelastic behavior applicable for butadiene-styrene copolymers. A new approach to this problem appears to be fruitful.

INTRODUCTION

In a previous article (1) the theoretical relationships between stress-relaxation properties and dynamic properties of linearly viscoelastic materials were presented. The best experimental dynamic data (3, 4) were compared with the best stress-relaxation data (5, 6, 7) then available. Good agreement was found in the rubbery region (reduced frequency less than 10^4/hr.), and qualitative agreement was found in the transition region. A marked discrepancy appeared in the low-modulus portion of the transition region, and there was doubt as to the correct slope of the log $E_r(t)$ versus log t curve in this region. The data were insufficient to distinguish between experimental error and partial failure of the time-temperature superposition principle as possible causes of the discrepancy. The dynamic data were highly self-consistent, so that attention was focused on the stress-relaxation data as the more likely to require improvement. Furthermore, these measurements did not extend into the high-modulus portion of the transition region.

It was decided to repeat and extend the stress-relaxation measurements below −40°C., using the glassy-state relaxometer developed by McLoughlin (8) in this Laboratory. After some reconstruction, temperatures as low as −83°C. were obtained with this instrument. This permitted the extension of the stress relaxation master curve to as high reduced frequencies (short times) as had been reached by dynamic measurements, so that comparison of the two approaches is now possible for the entire transition region.

Experimental Results

The glassy-state relaxometer has been partially described elsewhere (8). It consists of a copper-lined, insulated inner chamber supported within a well-insulated thermostated outer chamber, to which is attached a Tenney "Packaged Air" circulator containing dry ice. The outer chamber is mounted on a sturdy framework which also supports the stress gauge and sample-stretching apparatus.

For this work, in addition to the changes previously made in the stress-measuring system (9), it was found necessary to rebuild the inner chamber, providing it with a baffle and air fan so that adequate air circulation could be maintained. The heat capacity of the system was quite large, so that for temperatures below −55°C. it was advantageous to place enough dry ice in the outer chamber to cool the entire system. This was in addition to the dry ice in the cooling chamber of the Tenney "Packaged Air" box which served as a cold sink during the course of the run. For temperatures below −75°C., dry ice was also packed into the inner chamber, behind the baffle, so that the circulating air passed over the dry ice, around the baffle, and then over the sample. In this way, the sample was kept cold without permitting large temperature gradients within the inner chamber. It was necessary to replenish the dry ice in the inner chamber shortly before stretching the sample; for the very lowest temperatures reached, two such replenishments were necessary prior to stretching. (It was impossible to add dry ice after stretching, since the air temperature rose sharply when the door was opened, and returned less rapidly to its former value after the door was reclosed.) It proved virtually impossible to thermostat the system with dry ice in the inner chamber. Fortunately, experience with the cooling characteristics of the system showed a long, nearly flat, minimum in the temperature-time curve during which the sample could be stretched, and its relaxation followed for 30 minutes to an hour. A thermistor-actuated temperature-recording system sensitive to 0.01°C. greatly facilitated detection of this minimum early enough to permit full use of the available time, while two nonrecording copper-constantan thermocouples were used to calibrate and check the recording system. The exact value of the minimum temperature reached depended largely on the temperature reached just before opening the door to replenish the inner-chamber dry ice, on the amount of dry ice then added, and on the speed with which this could be done. It was also noted that the room temperature affected the temperature which could be reached. Thus some predictive control was possible over the temperature at which a run was to be made.

Because of the large forces required to stretch the sample a measurable amount at the lowest temperatures, a small amount of slippage sometimes occurred. An arbitrary strain correction was applied to those runs in which

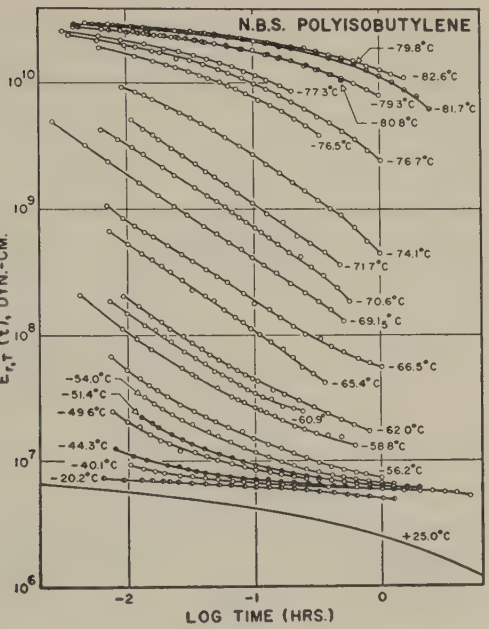

FIG. 1. Stress-relaxation of N.B.S. (National Bureau of Standards) polyisobutylene.

slippage was suspected, to make them superpose satisfactorily. Hence, there is some uncertainty as to the absolute value of the limiting glassy modulus. However, as will be shown in the discussion, good agreement with the dynamic measurements was obtained. The experimental data are plotted in Fig. 1, which includes a curve at 25°C. from earlier work (10).

DISCUSSION

Before comparing the new stress-relaxation data with the best dynamic data, it is necessary to reduce all data to the same reference temperature. This is a two-step process: a small correction for the kinetic-theory temperature dependence of the stress in a rubber followed by a horizontal shift in log time to allow for the effect of temperature on relaxation times.

Step 1. Modulus-Reduction. Ferry (11) has proposed a formula which allows that part of the compliance which is ascribed to distortion of bond angles and bond distances (and which we shall call the glasslike compliance) to be independent of temperature *and of density.* This latter provision, it seems to us, is in error, since the glasslike compliance should still depend on the number of chains threading unit cross section, and hence on the density.

Following Ferry's treatment, the total stress-relaxation compliance, $J_{r,T}$ is considered to have two additive components, $J_{g,T}$ (glasslike compliance) and $J_{k,T}$ (rubber-like compliance). We assume that the density dependence of the former is given by $J_{g,T} \propto d^{-x}$. A case can be made for $x = \frac{1}{3}, \frac{2}{3}$, or 1, but since experimental data are inconclusive, we shall derive the general case. Then

$$J_{r,T_0} = J_{g,T}(d/d_0)^x + (J_{r,T} - J_{g,T})(Td/T_0d_0), \qquad [1]$$

where $J_{r,T}$ = strain/stress in stress-relaxation at temperature T;

J_{r,T_0} = total compliance corrected to reference temperature T_0.

On rearrangement,

$$J_{r,T_0} = J_{r,T}\{(Td/T_0d_0) + (J_{g,T}/J_{r,T})(d/d_0)^x[1 - (Td^{1-x}/T_0d_0^{1-x})]\} \qquad [2]$$

or

$$\begin{aligned} E_{r,T_0} &= 1/J_{r,T_0} \\ &= E_{r,T}/\{(Td/T_0d_0) + (E_{r,T}/E_{g,T_0})[1 - (Td^{1-x}/T_0d_0^{1-x})]\}. \end{aligned} \qquad [3]$$

In our work, we measured total force, without correcting the cross-sectional area of the sample for the change due to thermal contraction. If we designate this uncorrected modulus by $M_{r,T}$, we may write

$$E_{r,T} = M_{r,T}(d/d_1)^y \qquad [4]$$

where d_1 = density at T_1, the temperature at which cross-sectional area was measured. If the sample was brought to the working temperature free from restraints, $y = \frac{2}{3}$, whereas if it was held at constant length instead, $y = 1$. Since we do not know the exact situation, it is again preferable to derive the general case. Equation [3] becomes

$$E_{r,T_0} = M_{r,T}/\{(Td^{1-y}d_1^y/T_0d_0) + (M_{r,T}/E_{g,T_0})[1 - (Td^{1-x}/T_0d_0^{1-x})]\}. \qquad [5]$$

For convenience in computation, this may be rearranged to

$$\log E_{r,T_0} = \log M_{r,T} - \log [(Td^{1-y}d_1^y/T_0d_0) + W] \qquad [6]$$

where

$$\log W = \log M_{r,T} - \log E_{g,T_0} + \log [1 - (Td^{1-x}/T_0d_0^{1-x})]. \qquad [7]$$

For the real component of dynamic modulus, the corresponding equations are (in Ferry's notation)

$$\log J_p' = \log J' + \log [(T\rho/T_0\rho_0) + W'], \qquad [8]$$

where

$$\log W' = \log J_{\infty,T_0} - \log J' + \log [1 - (T\rho^{1-x}/T_0\rho_0^{1-x})]. \qquad [9]$$

The best dynamic measurements are those of Fitzgerald, Grandine, and Ferry (3) (hereafter called FGF), which have been corrected to 25°C.

(4). We may use these data to select an appropriate value of $E_{g,298}$ to use in correcting our own data. FGF took the glasslike compliance in shear to be $J_\infty = 1.1 \times 10^{-10}$ cm.^{2}/dyne, apparently because this is the reciprocal of the highest value of G' which they measured. However, the value of J' corresponding to this G' is less than this, viz., 0.995×10^{-10} cm.^{2}/dyne, and J_∞ should be even smaller. Extrapolation of log G' and $-\log J'$ on the same graph (not shown) to infinite frequency indicates that a better value would be $\log J_\infty = -10.05$. Only FGF's data at −44.6°C. were used in this extrapolation; hence $\log 3G_{g,229} = 10.53$. This is in good agreement with the value of $\log E_1 = 10.52$ which was used in a previous paper (1) based on FGF's data.

Data are now available on the bulk modulus (B) of N.B.S. polyisobutylene at 25°C. (12). Since, by the classical theory of elasticity,

$$\log E_g = \log 3G_g - \log [1 + (G_g/3B_g)], \qquad [10]$$

we may use these data to compute $\log E_{g,229}$ if we assume that $G_{g,T}$ and $B_{g,T}$ depend on density in the same way. We shall use the same value for the coefficient of thermal expansion of polyisobutylene as did FGF, viz., 0.585×10^{-3}/°C. The apparent maximum of B_{298} is 4.8×10^{10} dynes/cm.^{2},

TABLE I

Values of log a_{298} and of log K for N.B.S. Polyisobutylene

T, °C.	$\log a_{298}$	$\log K$
−82.6	12.05	2.73
−81.7	11.89	2.57
−80.8	11.53	2.21
−79.8	11.95	2.63
−79.3	11.51	2.19
−77.3	10.89	1.57
−76.7	10.70	1.38
−76.5	10.47	1.15
−74.1	9.70	0.38
−71.7	9.13	−0.19
−70.6	8.85	−0.47
-69.1_5	8.46	−0.86
−66.5	7.93	−1.39
−65.4	7.62	−1.70
−62.0	7.06	−2.26
−60.9	6.79	−2.53
−58.8	6.55	−2.77
−56.2	6.04	−3.28
−54.0	5.77	−3.55
−51.4	5.47	−3.85
−49.6	5.31	−4.01
−44.3	4.72	−4.60
−40.1	4.20	−5.12
−20.2	2.34	−6.98

TABLE II

Master Stress-Relaxation Curve of Polyisobutylene

log t/a_{298} (*hours*)	log $E_{r,298}(t)$ (*dyne cm.*$^{-2}$)	
	Observed	From Eq. [22]
−14.32	10.48_5	10.46
−14.07	10.47	10.45_5
−13.82	10.45_5	10.44
−13.57	10.44	10.43
−13.32	10.42_5	10.41
−13.07	10.40_5	10.38
−12.82	10.37	10.35_5
−12.57	10.33	10.31
−12.32	10.28_5	10.26
−12.07	10.22_5	10.20
−11.82	10.15_5	10.13
−11.57	10.06	10.04
−11.32	9.94_5	9.94
−11.07	9.81	9.82_5
−10.82	9.67	9.69
−10.57	9.50_5	9.55
−10.32	9.43	9.39
−10.07	9.17	9.22
−9.82	9.00_5	9.05
−9.57	8.84	8.86
−9.32	8.68	8.68
−9.07	8.51	8.49
−8.82	8.35	8.31
−8.57	8.17	8.13
−8.32	7.99_5	7.96_5
−8.07	7.85	7.81
−7.82	7.70_5	7.66_5
−7.57	7.57	7.53
−7.32	7.44_5	7.42
−7.07	7.32_5	7.32
−6.82	7.22_5	7.23
−6.57	7.13	7.15_5
−6.32	7.06_5	7.09
−6.07	7.01_5	7.04_5
−5.82	6.98_5	7.00
−5.57	6.95_5	6.97
−5.32	6.93_5	6.95
−5.07	6.92	6.93
−4.82	6.90_5	6.91
−4.57	6.90	6.90
−4.32	6.89_5	6.89_5
−4.07	6.89	6.89
−3.82	6.88_5	6.89
−3.57	6.87_5	6.88
−3.32	6.86_5	6.88
−3.12	6.85_5	
−2.92	6.83_5	
−2.72	6.82	
−2.52	6.80	

TABLE II—*Continued*

$\log t/a_{298}$ *(hours)*	$\log E_{r,298}(t)$ *(dyne cm.$^{-2}$)*
	Observed
−2.32	6.78_5
−2.12	6.77
−1.92	6.75
−1.72	6.72_5
−1.52	6.70
−1.32	6.67
−1.12	6.64_5
−0.92	6.61
−0.72	6.57
−0.52	6.53_5
−0.32	6.49
−0.12	6.43_5
0.08	6.37
0.28	6.30
0.48	6.22_5
0.68	6.14
0.88	6.04_5
1.00	5.97
1.20	5.85
1.40	5.70
1.60	5.54
1.80	5.34
2.00	5.18
2.20	4.9
2.40	4.5
2.60	4.0
2.80	$-\infty$

so that $B_{g,229}$ lies between 4.9 and 5.0 × 10^{10} dynes/cm.^{2}, depending on the value chosen for x in the expression $B_{g,T} \propto d^x$. $G_{g,229} = 1.12 \times 10^{10}$ dynes/cm.^{2}, so $\log E_{g,229} = 10.53 - 0.03 = 10.50$. Again depending on the value chosen for x, $\log E_{g,298}$ will be 10.48–10.49. We have chosen the former value, corresponding to $x = 1$, for our computations.

By way of comparison with our data, the above assumptions lead to $\log E_{g,190} = 10.51$. The maximum value of $\log M_{r,190}$ which we found was 10.49, corresponding to $\log E_{r,190} =$ 10.51–10.52, depending on the value chosen for y. The agreement is highly satisfactory.

Step 2. Time Scale Reduction. Our stress-relaxation data have been corrected to 25°C. in accordance with Eqs. [6] and [7], using $d_1 = d_0$, $y = 1$, Log $E_{g,298} = 10.48$, and $x = 1$, and the resulting curves superposed in the usual manner. The relative flatness of the relaxation curves between −45°C. and 25°C. makes superposition difficult in this region. To avoid this, we assigned the value of the shift factor at −44.3°C. to fit that found by FGF, viz. $\log a_{298}$ (229) = 4.72.[1] The resulting set of a_{298} factors

---

[1] The symbols a and κ may be used interchangeably.

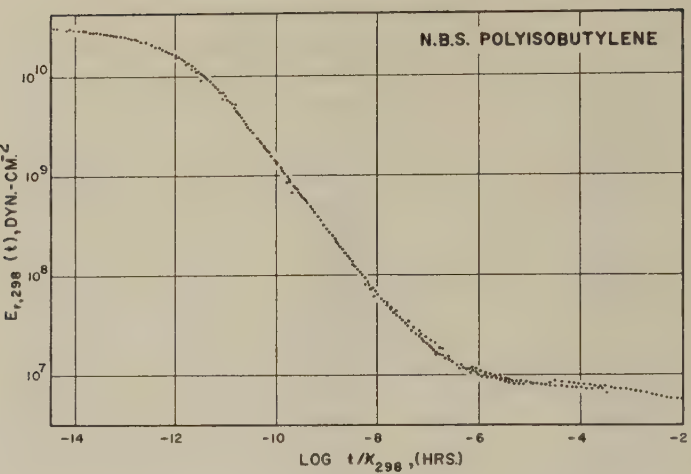

FIG. 2. Stress-relaxation master curve of N.B.S. polyisobutylene, showing experimental points after modulus-reduction and time scale shift to 25°C.

is listed in Table I, while the superposed reduced-modulus data are shown in Table II and Fig. 2.

Prediction of Complex Dynamic Shear Modulus

Step 1. Prediction of Dynamic Young's Modulus. In an unpublished study (13, 14) it was shown that the most convenient and accurate method for computing the real component of the dynamic modulus (E') from the stress-relaxation modulus (and vice versa) was by means of an approximation to Marvin's difference function (15). This approximation is:

$$E'(\omega) - E_r(t)\,\big|_{t=1/\omega} = \Delta E(\omega) \approx \Upsilon(m)H_{2b}(\log \tau)\,\big|_{\tau=1/\omega} \qquad [11]$$

where

$$H_{2b}(\log \tau) = -\left.\frac{dE_r(t)}{d \log t}\right|_{t=\tau} \Big/ \; \Gamma(1 + m) \qquad [12]$$

and

$$m = -\frac{d}{d \log t} \log\left(-\frac{dE_r(t)}{d \log t}\right). \qquad [13]$$

$\Gamma(1 + m)$ is the well-known Γ-function, the use of which is due to Ferry (16, 17, 18), while $\Upsilon(m)$ is a new function (1, 14) defined by

$$\Upsilon(m) = 0.4343[(\pi/2) \csc (m\pi/2) - \Gamma(m)]. \qquad [14]$$

A table of $\Upsilon(m)$ is given in Table III.

The master curve of $E_{r,298}$ was numerically differentiated to yield H_{2b} ($\log \tau$), the relaxation spectrum. This is shown in Fig. 3. From H_{2b} and

TABLE III

The Function $\Upsilon_{(m)}$

−m			0	1	2	3	4	5	6	7	8	9
0.	0	0.2	51	53	56	58	61	64	67	70	74	77
	1		80	84	88	91	95	99	*03	*07	*12	*16
	2	0.3	20	25	30	35	40	46	52	58	64	70
	3		77	83	90	98	*05	*13	*20	*29	*38	*47
	4	0.4	57	67	77	87	98	*10	*22	*35	*48	*61
	5	0.	575	590	606	622	640	658	676	696	718	740
	6		763	788	814	841	872	902	935	970	*008	*048
	7	1.	090									

+m			0	1	2	3	4	5	6	7	8	9
0.	0	0.2	51	48	46	44	42	40	38	35	33	31
	1		29	28	26	24	22	21	20	18	17	15
	2		14	13	12	11	10	08	07	06	05	05
	3		04	03	02	01	01	00	*99	*99	*98	*98
	4	0.1	97	97	97	97	96	96	96	96	95	95
	5		95	95	95	95	95	96	96	96	96	96
	6		97	97	97	98	98	99	99	*00	*01	*01
	7	0.2	02	03	04	04	05	06	07	08	09	10
	8		12	13	14	16	17	18	20	21	23	25
	9		27	28	30	32	35	37	39	41	44	46
1.	0		48	51	53	56	59	62	65	68	71	74
	1		78	81	85	88	92	96	*01	*05	*10	*14
	2	0.3	18	23	28	34	39	45	51	57	63	69
	3		76	83	90	98	*05	*13	*22	*31	*40	*49
	4	0.4	59	69	79	90	*02	*13	*25	*38	*51	*65
	5	0.	580	595	612	628	646	665	685	706	727	750
	6		774	798	825	855	885	917	950	986	*023	*064
	7	1.	108									

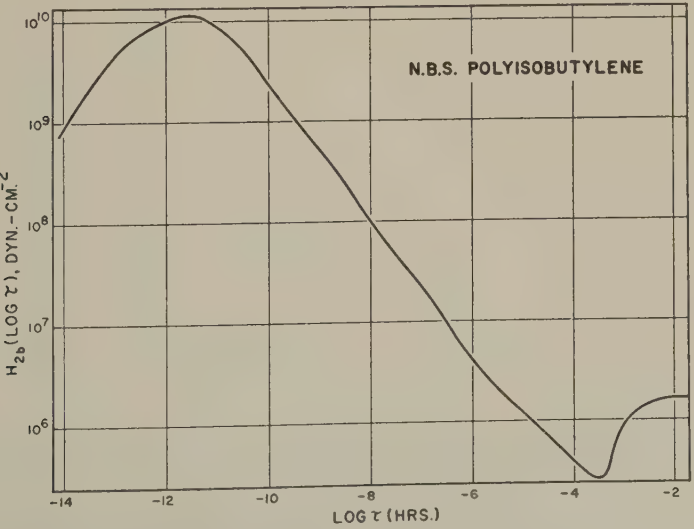

FIG. 3. Distribution of relaxation times (relaxation spectrum) for N.B.S. polyisobutylene adjusted as in Fig. 2. Second approximation.

Eq. [11], $E'_{2b}(\omega)$ was computed, while from H_{2b}, E''_{2bq} was computed by numerical integration of the following equation:

$$E''_{2bq} = \int_{-\infty}^{\infty} H_{2b}(\log \tau) \frac{\omega\tau}{1 + \omega^2\tau^2} \, d \log \tau. \qquad [15]$$

Step 2. Conversion from Young's Modulus to Shear Modulus. The relationship between the complex dynamic Young's modulus, the complex dynamic shear modulus, and the complex dynamic bulk modulus is:

$$G^* = 3B^*E^*/(9B^* - E^*). \qquad [16]$$

This may be solved for its components, yielding

$$G' = E'/3[1 - (E'/9B')(1 - u)] \qquad [17]$$

$$G'' = E''/3[1 - (2E'/9B')(1 - v/z)] \qquad [18]$$

where

$$u = (\tan \delta_E - \tan \delta_B)^2/[(1 + \tan^2 \delta_B) - (E'/9B')(1 + \tan^2 \delta_E)]; \qquad [19]$$

$$\begin{aligned} v = {} & [(E'/9B') + (\tan \delta_B/\tan \delta_E)](1 + \tan^2 \delta_E)/2 \\ & -[(E'/9B')(1 + \tan^2 \delta_E)/\tan \delta_E + (\tan \delta_E - \tan \delta_B)] \tan \delta_B; \end{aligned} \qquad [20]$$

$$z = (1 + \tan^2 \delta_B) - (E'/9B')(\tan \delta_B/\tan \delta_E)(1 + \tan^2 \delta_E); \qquad [21]$$

and

$$\tan \delta_E = E''/E'; \tan \delta_B = B''/B'.$$

Equations [17] and [18] differ from the approximate relationships which apply in the rubbery region by the correction factors in brackets. The quantity $(E'/9B')$ is significant only when $E' > 2 \times 10^9$ dynes/cm.^{2}. The second-order correction to G' given by the term u tends to reduce the primary correction term so that $G' \approx E'/3$ even when $E' \approx 5 \times 10^9$ dynes/cm.^{2}. At sufficiently high frequencies, u, which depends largely on $\tan \delta_E$, vanishes, and Eq. [17] becomes equivalent to Eq. [10], as it should.

The term z never differs from unity by more than 2%, so that the second-order correction to G'' is chiefly dependent on v, which in turn is largely dependent on $\tan \delta_B$. Consequently, v/z passes through a fairly sharp maximum near $\omega a_{298} = 10^{11.5}$/hr. Even here, it reduces the primary correction term by but 20%, so that the effect of v/z on G'' is quite small.

The values of G', G'', and $\tan \delta_G$ $(=G''/G')$ predicted from stress-relaxation data are shown in Figs. 4–6, where they are compared with FGF's experimental data. Also shown are dynamic data found by Philipoff (19). The over-all agreement is remarkably good, and serves to demonstrate the validity of the theory of linear viscoelasticity in the transition region. The discrepancy at the peak of the imaginary component is no greater

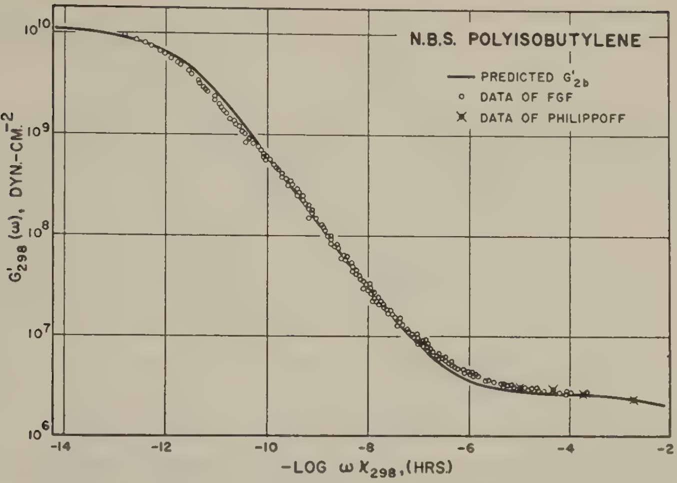

FIG. 4. Predicted and observed real component of complex dynamic shear modulus of N.B.S. polyisobutylene.

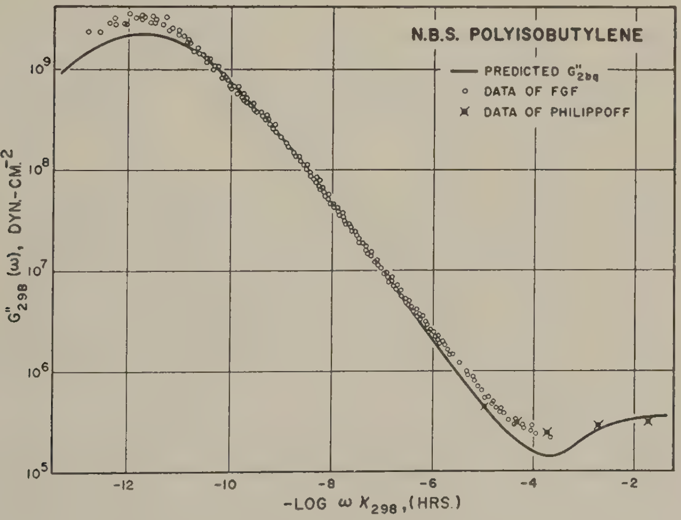

FIG. 5. Predicted and observed imaginary component of complex dynamic shear modulus of N.B.S. polyisobutylene.

than that previously shown (1) to exist between the real and imaginary components themselves. This discrepancy is considerably magnified in computing the loss tangent. The experimental scatter of the loss tangent in the vicinity of its peak greatly confuses any attempt to understand the peculiar shape of that peak.

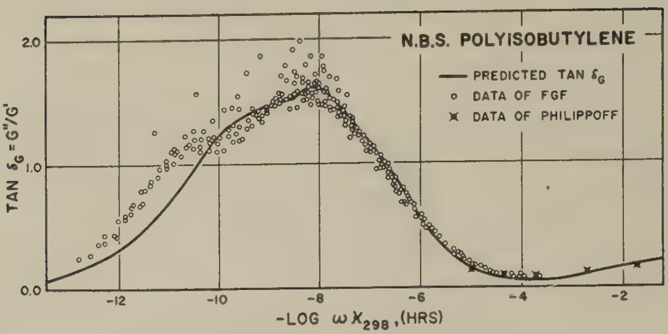

FIG. 6. Predicted and observed loss tangent in shear of N.B.S. polyisobutylene.

Another discrepancy between predicted and observed dynamic properties is connected with the time-temperature superposition principle. It is quite clear that this useful principle can be applied in the transition region as well as in the rubbery region. In so doing, it was in effect necessary to choose as reference a temperature (−44.3°C.) at which data were available in the transition region from both dynamic and stress-relaxation measurements. These data then agree well. A direct attempt to determine log a_{298} (2, 29) by superposition of stress-relaxation data led to a value of about 3.8 instead of 4.72. This large discrepancy in a_{298} is directly responsible for the apparent anomaly in the region in which $E_r(t)$ has been reported to be larger than $E'(\omega)$ (1, 20, 21, 22).

The discrepancy in a_{298} is considerably greater than that demonstrated by FGF, and ascribed by them to a higher activation energy associated with short-time relaxation processes. The latter effect, however, would tend to make the predicted G' (based on low-temperature studies) smaller than the observed value (obtained by high-temperature studies) at the long-time end of the transition region, and larger at the short-time end. This is the trend noted in Fig. 4.

The approximations used to find the relaxation spectrum are most reliable where the slope of the latter is fairly constant. In the vicinity of the peak in $H(\log \tau)$, the approximation $H_{2b}(\log \tau)$ is too small (13, 14), so that the peak is not sharp enough. Similarly, the trough in $H(\log \tau)$ which lies between the transition and rubbery flow regions is deepened by the approximation $H_{2b}(\log \tau)$. Both these defects occur in regions where the experimental difficulties are relatively acute. Dynamic measurements are rather difficult in regions of high modulus and high dispersion (3). The trough in $H(\log \tau)$ coincides with the region where relaxation measurements with the glassy-state relaxometer became inaccurate because of the very small forces involved. It is, therefore, not surprising that the predicted G'' differs most noticeably from observed values in these regions. The location of the peak and trough on the time scale are quite accurately predicted, however.

Analytical Representation of Stress-Relaxation Data

In previous papers (1, 9, 23), we have fitted experimental data on several polymers by an equation of the Gauss Error Integral form. Our stress-relaxation data on polyisobutylene in the transition region are moderately well fitted by:

$$\log E_{r,298}(t/a_{298}) = 8.68 - 1.80 \text{ erf } 0.367 (\log t/a_{298} + 9.32) \qquad [22]$$

where

$$\text{erf } x = 2\pi^{-1/2} \int_0^x \exp(-u^2)\, du. \qquad [23]$$

This is shown in Fig. 7, where we have plotted on probability paper

$$100 \times \frac{\log E_{r,298}(t/a_{298}) - 6.88}{3.60} \text{ versus } \log t/a_{298}. \qquad [24]$$

Equation [22] is the straight line shown in the figure. By comparison, FGF's data were fitted by

$$\log G'_{298}(\omega a_{298}) = 8.22 + 1.82 \text{ erf } 0.352 (\log \omega a_{298} - 9.08). \qquad [25]$$

For a linearly viscoelastic material, $\log E' - \log G' \approx 0.48$, while for polyisobutylene, $E_r(t) \approx E'(\omega)$ when $\log t + \log \omega \approx -0.21$. Thus, the

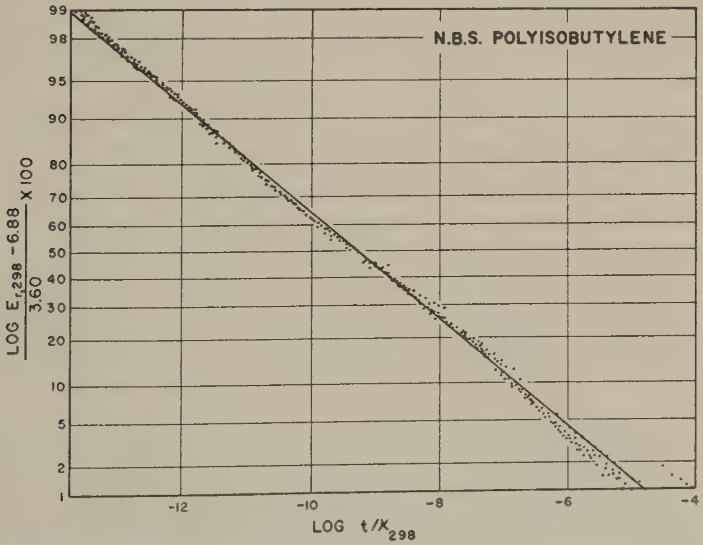

FIG. 7. Master stress-relaxation curve of N.B.S. polyisobutylene on normal probability graph paper.

two sets of parameters agree quite well, bearing out our previous conclusions (1).

Reduced Time-Temperature Scales

Ferry's modulus-reduction scheme, the time-temperature superposition principle, and the Gauss Error Integral representation together appear to constitute a general method for condensed representation of mechanical-properties data in the transition region. To complete the generalization, it is necessary to find a method for representing the time-temperature superposition principle in terms of a reduced time-temperature scale valid for all amorphous polymers.

We have proposed an extension of the Gauss Error Integral representation, leading to a five-parameter equation (9, 23), which was later simplified to a three-parameter equation (2). More recently, Williams (24) has proposed a different method of temperature reduction. The new data on polyisobutylene have been treated according to each of these schemes.

A. The Three-Parameter Reduced Equation. In order to use this equation, it is necessary to find T_d, the temperature of maximum apparent activation energy. This determination is shown in Fig. 8, where T_d is found to be about 197°K. The corresponding mean relaxation time, K_d, is about 11 hours ($\log K_d = 1.04$). It is immediately obvious that the three-parameter equation cannot apply, for not only is $\log K_d$ about 2.5 decades too large, but also the product $hT_d = 72.5$, which is considerably less than 100, the value which was found to hold for a group of butadiene copolymers. (For polymethyl methacrylate, $hT_d = 119$, which is almost equally far from 100.) Although it would be possible to redefine T_d as the temperature at

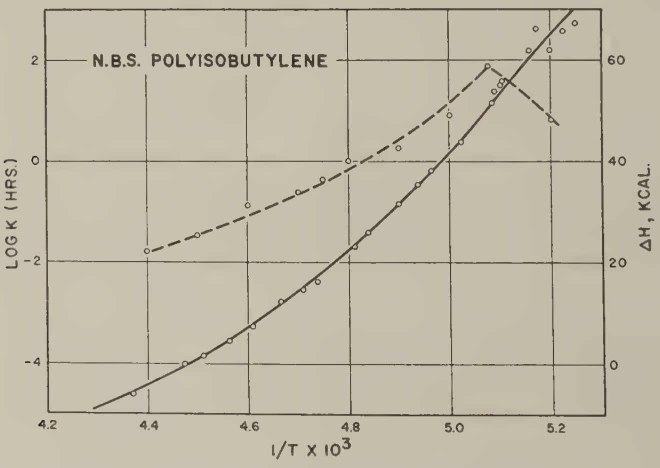

FIG. 8. Temperature dependence of mean relaxation time and of apparent activation energy of N.B.S. polyisobutylene.

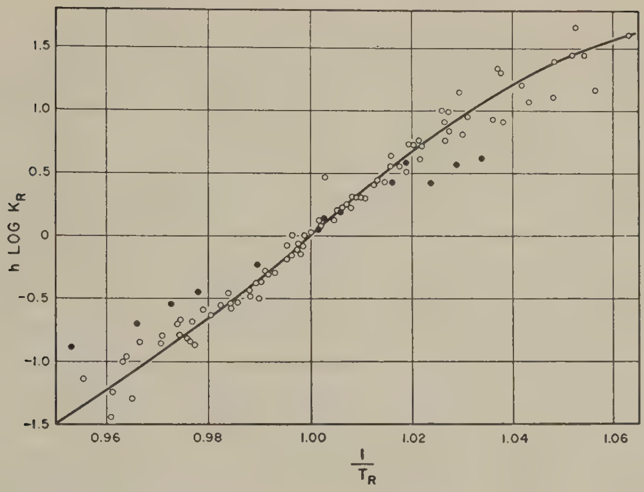

FIG. 9. Reduced-temperature dependence of reduced mean relaxation time. Comparison of polyisobutylene (black circles) with other polymers.

which log $K = -1.45$, this would not raise the product hT_d sufficiently close to 100.

It should also be pointed out here that in our treatment of the other polymers mentioned, we did not apply the modulus-temperature reduction to our data. This probably effects a small change in the value of h; more important, the time-temperature shift factors are increased by application of this reduction. This would increase the disagreement between the polyisobutylene data and the older stress-relaxation data on which the reduced equation was based.

B. The Five-Parameter Reduced Equation. The three-parameter reduced equation is essentially a special case of the five-parameter reduced equation, the parameters h and K_d having been eliminated on the basis of empirical observation. When these parameters are included, the goodness of fit of the equation is tested by plotting $h \log K/K_d$ versus T_d/T, as shown in Fig. 9. The points for polyisobutylene do not fit the equation satisfactorily. Furthermore, it appears that the redefinition of T_d (as the temperature at which log $K = -1.45$) would worsen the fit. Application of the modulus-temperature reduction to the older data would increase the slope of that data and also worsen the fit.

C. Williams' Temperature-Reduction Method. In the aforementioned temperature-reduction schemes, reduced temperature was defined as T/T_d, in analogy to the definition of reduced temperature with reference to the critical point of a gas. Williams proposed instead to *subtract* the reference temperature to obtain a suitable reduced temperature, and was able to construct a composite curve of a_{T_s} as a function of $T - T_s$.

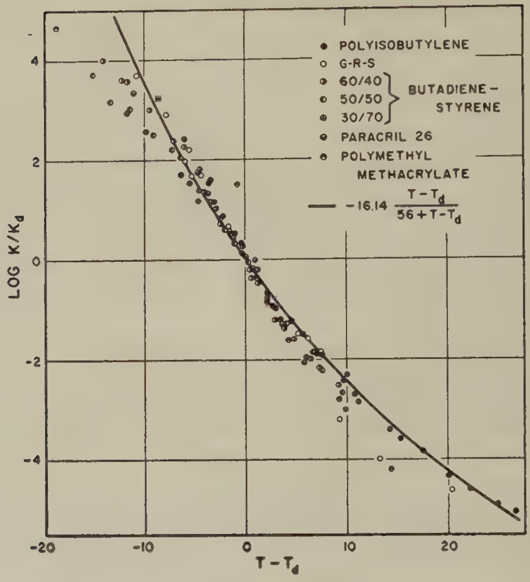

FIG. 10. Log K/K_d plotted against $T - T_d$. Comparison of polyisobutylene (black circles) with other polymers and with WLF's analytical expression, taking $T_s - T_d = 46°$.

The low-temperature portion of Williams' curve was constructed from our published stress-relaxation data on several polymers, none of which were studied at temperatures close to the values of T_s chosen by Williams. Consequently, there is enough uncertainty as to the correct value to choose for (log a_{T_s} − log K) for each polymer to obscure any disagreement among the data, particularly since the slope of the composite curve is so steep in this region.

As Williams has pointed out also, the various empirical interrelationships of our three-parameter reduced equation result in essentially the same temperature-dependence in the stress-relaxation transition region as does his method. We therefore plotted log K/K_d versus $T - T_d$ in Fig. 10, as an alternate representation of our data in accordance with Williams' suggestion. The polyisobutylene data agree rather well with the older data, although not quite perfectly. Again, redefinition of T_d would worsen the fit.

Also shown in Fig. 10 is the analytical function shown by Williams, Landel, and Ferry (25) (hereafter referred to as WLF) to fit Williams' curve. We have converted it to use T_d as the reference temperature thus:

$$\log K/K_d = -16.14(T - T_d)/(56 + T - T_d). \qquad [26]$$

Maximum Apparent Activation Energy

Both theoretical and practical considerations indicate that the time-temperature superposition principle must fail at temperatures well below the glass transition, T_g. For example, it has been shown that the stress-relaxation of glassy polymethyl methacrylate is strongly dependent on previous thermal history (26, 27), while the ratio of stress to (temperature × birefringence) does not remain constant in the transition region (28), indicating a change in the mechanism of deformation, as has also been deduced for lactoprene rubbers (29). In all likelihood, the time-temperature superposition principle is of but partial applicability at temperatures just below T_g, so that the shift factors obtained in this region are somewhat fictitious. In consequence, the existence of an apparent maximum for the apparent activation energy for viscoelastic behavior may be an artefact. Nevertheless, this apparent maximum has been noted for several polymers, and can be useful in defining T_d without obvious reliance on an arbitrary time scale.

In connection with the three-parameter reduced equation, we showed that this maximum heat of activation was roughly proportional to T_d^2. Although the data on polyisobutylene do not fit this reduced equation, the more generally applicable relationship of Fig. 10 can also be used to derive this proportionality, as follows:

$$\Delta H_{Act} = 2.303R\,\frac{d \log K}{d(1/T)} = -2.303RT^2\,\frac{d \log K}{dT} \qquad [26]$$

$$= -2.303RT^2\,\frac{d \log K/K_d}{d(T - T_d)}. \qquad [27]$$

Figure 10 and Williams' curve show that the slope of this plot is the same for many polymers, so that, at T_d,

$$(\Delta H_{Act})_{Max.} = -2.303R\,\frac{d \log K/K_d}{d(T - T_d)} \cdot T_d^2. \qquad [28]$$

For the other six polymers, the proportionality factor ranged from 1.57 to 2.03. For polyisobutylene it is 1.51. From a measurement of the slope of Fig. 10, it is 1.58.

REFERENCES

1. Part VIII of a series, "Elastoviscous Properties of Polyisobutylene." Part VII appeared in *J. Appl. Phys.* **25**, 145 (1954).
2. Part IV of a series, "Elastoviscous Properties of Amorphous Polymers in the Transition Region." Part III appeared in *J. Am. Chem. Soc.* **76**, 4204 (1954).
3. FITZGERALD, E. R., GRANDINE, L. D., JR., AND FERRY, J. D., *J. Appl. Phys.* **24**, 650 (1953).

4. Ferry, J. D., Grandine, L. D., Jr., and Fitzgerald, E. R., *J. Appl. Phys.* **24,** 911 (1953).
5. Brown, G. M., and Tobolsky, A. V., *J. Polymer Sci.* **6,** 165 (1950).
6. Tobolsky, A. V., and McLoughlin, J. R., *J. Polymer Sci.* **8,** 543 (1952).
7. Tobolsky, A. V., *J. Am. Chem. Soc.* **74,** 3786 (1952).
8. McLoughlin, J. R., *Rev. Sci. Instr.* **23,** 459 (1952).
9. Catsiff, E., and Tobolsky, A. V., *J. Appl. Phys.* **25,** 1092 (1954).
10. Andrews, R. D., and Tobolsky, A. V., unpublished results.
11. Ferry, J. D., and Fitzgerald, E. R., *J. Colloid Sci.* **8,** 224 (1953).
12. Marvin, R. S., Aldrich, R., and Sack, H. S., *J. Appl. Phys.* **25,** 1213 (1954), hereafter called MAS.
13. Catsiff, E., and Tobolsky, A. V., report RLT-5 to U. S. Office of Naval Research, Contract No. N6onr-27021, project NR 330-023.
14. Catsiff, E., report RLT-6 to U. S. Office of Naval Research, Contract No. N6onr-27021, project NR 330-023.
15. Marvin, R. S., *Phys. Rev.* **86,** 644 (1952).
16. Ferry, J. D., Fitzgerald, E. R., Grandine, L. D., Jr., and Williams, M. L., *Ind. Eng. Chem.* **44,** 703 (1952).
17. Ferry, J. D., and Williams, M. L., *J. Colloid Sci.* **7,** 347 (1952).
18. Williams, M. L., and Ferry, J. D., *J. Polymer Sci.* **11,** 169 (1953).
19. Philipoff, W., 312th Meeting, American Physical Society, Columbus, Ohio, March 22, 1952.
20. Tobolsky, A. V., Dunell, B. A., and Andrews, R. D., *Textile Research J.* **21,** 404 (1951).
21. Andrews, R. D., *Ind. Eng. Chem.* **44,** 707 (1952).
22. Marvin, R. S., private communication.
23. Bischoff, J., Catsiff, E., and Tobolsky, A. V., *J. Am. Chem. Soc.* **74,** 3378 (1952).
24. Williams, M. L., *J. Phys. Chem.* **59,** 95 (1955).
25. Williams, M. L., Landel, R. F., and Ferry, J. D., *J. Am. Chem. Soc.*, in press.
26. McLoughlin, J. R., and Tobolsky, A. V., *J. Polymer Sci.* **7,** 658 (1951).
27. McLoughlin, J. R., and Tobolsky, A. V., *J. Colloid Sci.* **7,** 555 (1952).
28. McLoughlin, J. R., "Physical Studies of Some High Polymers." Ph.D. Dissertation, Princeton University, Princeton, New Jersey, 1951.
29. Stein, R. S., Krimm, S., and Tobolsky, A. V., *Textile Research J.* **19,** 8 (1949).

THE ROLE OF COLLOIDAL ELECTROLYTES IN DECONTAMINATION STUDIES

Ray C. Chandler and Wesley E. Shelberg

U. S. Naval Radiological Defense Laboratory, San Francisco, California

Received August 20, 1954

Abstract

The relation of the physical properties of two soap solutions to their capacities to remove a typical radioactive contaminant from a surface were studied over a wide range of surface tension up to the critical micelle concentration (CMC) and thence through a range of micelle concentrations in which surface tension remained constant. The CMC of the two soaps differed about 10-fold.

Decontamination began at or near the CMC for each colloidal electrolyte and was a function of micelle concentration but not of surface tension. The significance of anomalous phenomena at concentrations less than the CMC is discussed.

Introduction

The removal of radioactive contaminants from surfaces, termed decontamination, is of great concern in the laboratory, industry, and warfare. Where solutions are employed the decontamination may be considered as a special case of detergency. Since colloidal solutions have been used in decontamination procedures (1), the fundamental principles involved in their use merit investigation.

The properties of a solution responsible for detergency is a controversial subject, workers variously attributing dominance to surface tension, solubilization, ion exchange, adsorption, and protective colloids. In this paper emphasis is placed upon a study of the relation of surface tension, colloidality of the solution, and the concentration of micelles as factors in decontamination. The use of radionuclides affords an approach of especial interest to students of detergency since (*a*) the contaminant may be simplified, as in the present study, to a single chemical species in contrast to the complex "soil" ordinarily encountered or (*b*) a single component of a complex soil may be radioactively traced.

Soaps were selected for this study chiefly because they could be prepared easily in pure form. Soaps per se are not exceptional decontaminants but by selecting appropriate members of a homologous series having a distinctive difference between their critical micelle concentrations (CMC) the relative merits of surface tension, colloidality, and micelle concentration in the decontamination process may be assessed. In general, soaps reflect the properties of colloidal electrolytes.

Certain undesirable characteristics of soaps as research tools are due to their tendency to hydrolyze. A highly controversial field of literature has been written about the extent of their hydrolysis, saturation with organic acids, acid soaps, and critical micelle concentrations (2–6). In the course of this study certain anomalies appeared in concentrations near the CMC which were of minor interest in decontamination but of sufficient scientific interest to merit their discussion.

A colloidal electrolyte may be defined as any ionizable compound composed of ions differing so greatly in hydrophilicity that either the cation or anion tends to aggregate and thus form a two-phase system at a concentration less than that required for precipitation of the electrolyte. An ideal colloidal electrolyte is defined here as one in which no physical or chemical reactions other than aggregation are involved. Figure 1 illustrates schematically the relationship between the concentration of species and the electrolyte concentration. The line *AB* represents the ideal behavior of ions of a completely ionized uni-univalent electrolyte. The ions of the ideal colloidal electrolyte MP obey this relationship up to the point *C* (CMC). Beyond *C* (P^-) remains constant (7) and (M^+) as shown by the line *CD* departs from *AB* as electrostatic forces bind M^+ to the micelles (8). The line *C′E* represents the concentration of micelles of variable composition (9). At the points *D* and *F* the concentrations of M^+ and P^-, respectively, satisfy the solubility product of the electrolyte, and beyond the line *DEF* the activities of M^+ and of micelles are assumed to remain constant. Where hydrolysis or other side reactions occur the simple behavior outlined is modified near the CMC. The soap solutions investigated provide some illustrations of departures from ideal behavior.

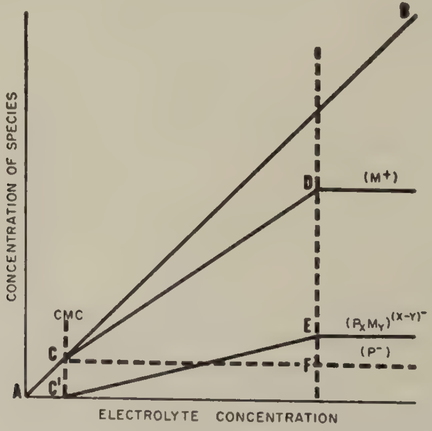

FIG. 1. Relations between species in an ideal colloidal electrolyte.

STATEMENT OF PROBLEM

The major variables in liquid decontamination are surface, contaminant, decontaminant, and decontaminating method. In the present study surface, contaminant, and decontaminating method were held constant while the decontaminant varied with respect to chain length and concentration. The specific objectives were (*a*) to disclose what major physical properties of the solution contribute to the removal of the contaminant, (*b*) to gain an insight into the mechanism of decontamination, and (*c*) to investigate the properties of the solutions near the critical micelle concentration. Observations were made by means of surface tension, conductance, and pH measurements. Decontamination was followed by a tracer technique.

MATERIALS

The experimental surface was Navy gray paint placed on aluminum blanks 1¼ inch square by 1⁄32 inch thick, aged a minimum of 60 days. This paint surface is typical for naval craft and equipment.

The contaminant stock solution was acidic YCl_3 traced with Y^{91}. Yttrium is of interest in the problem of contamination by the mixture of products formed by uranium-235 fission, since strong gamma emitting yttrium isotopes exist in significant quantities within 2 days following fission (10). Yttrium contamination is also important since its isotopes are used as beta tracers.

The decontaminants were the potassium salts of lauric and palmitic acids composed of 12 and 16 carbon atom chains, respectively. These two organic salts reduce the surface tension of their aqueous solutions to about the same minimal value and both become colloidal but at quite different concentrations. These colloidal electrolytes were prepared in the laboratory from the best obtainable acids which were subsequently recrystallized from ethyl alcohol. Their melting points and chemical analysis indicated a very high degree of purity.

Equivalent amounts of the acid and alcoholic KOH were allowed to react at 50°C., the excess alcohol was removed, and the soap brought into solution when needed. Stock solutions of 0.1 *M* potassium laurate (KL) and 0.01 *M* potassium palmitate (KP) were prepared using deionized water having a conductance of approximately 2×10^{-6} ohms^{-1} at 57°C. Since 0.01 *M* KP requires a temperature of 55°C. to maintain a clear solution, both solutions were held constantly at 57°C. The two stock solutions had pH's of 8.94 and 9.28 for the laurate and palmitate, respectively. Concentrations of lower order were prepared with deionized water adjusted to the pH of the stock solution so that the diluted solutions progressively had more hydroxide ion to suppress hydrolysis and maintain constancy of pH. A range of concentrations from zero to the approximate maximal decontamination was studied, the entire range being run during the same day.

EXPERIMENTAL

The working solution of the contaminant, 10^{-6} *M* YCl_3, was prepared for each daily run by dilution from the acidic stock solution (pH 3.5) and subsequent adjustment to pH 7. Aliquots of 300 microliters were pipetted onto the array of surfaces. The liquid contaminant was then dried overnight at 25°–30°C.

The contaminating solution when applied was near the point for precipitation of the hydroxide. It is believed that on drying a particulate hydrous oxide was formed on the surface and persisted in the alkaline decontaminant.

The dried contaminated samples were counted conventionally with a Geiger counter and placed on specially designed plastic cup-type holders which each held triplicate samples. Each holder was immersed in an 800 cc. beaker containing 250 ml. of the appropriate decontaminating solution held at 57°C. ± 1°. Six beakers were held simultaneously in the bath. The samples were exposed 20 minutes to the action of the solution as it was gently stirred. The samples were then removed, dried by a heat lamp, and again counted. Results were expressed as percentage of counts removed.

Decontamination of the samples by simple immersion free from mechanical force such as often is involved in practical decontamination permits the interaction alone between the solution, contaminant, and surface to be measured.

Surface tension measurements were made on each of the concentrations at 57°C. ± 1° with a du Nouy Tensiometer.

Conductance was measured for all principal concentrations with a Jones-Dyke Conductivity Bridge (L and N) equipped with General Radio Oscillator Type 1301-A and a Cathode-Ray Null Detector Type 707-A. The conductivity cells were in a constant temperature oil bath at 57°C. with a variation less than 0.01°C. Readings were checked frequently at both 1000 and 2000 cps.

The data on pH were determined with a glass electrode pH meter (Beckman, Model G) at 57°C.

RESULTS AND DISCUSSION

The data on decontamination, surface tension, and conductance vs. $C^{\frac{1}{2}}$ for KL are illustrated in Fig. 2, and similar data on KP are found in Fig. 3. The pH data are shown graphically in Fig. 4.

The anomalous behavior of a very dilute soap silution is illustrated in Fig. 5.

Inspection of Figs. 2 and 3 shows that surface tension of both experimental solutions decreased rapidly at very low concentrations and reached the minimal value before any important degree of decontamination occurred, thereby indicating that decontamination under these conditions

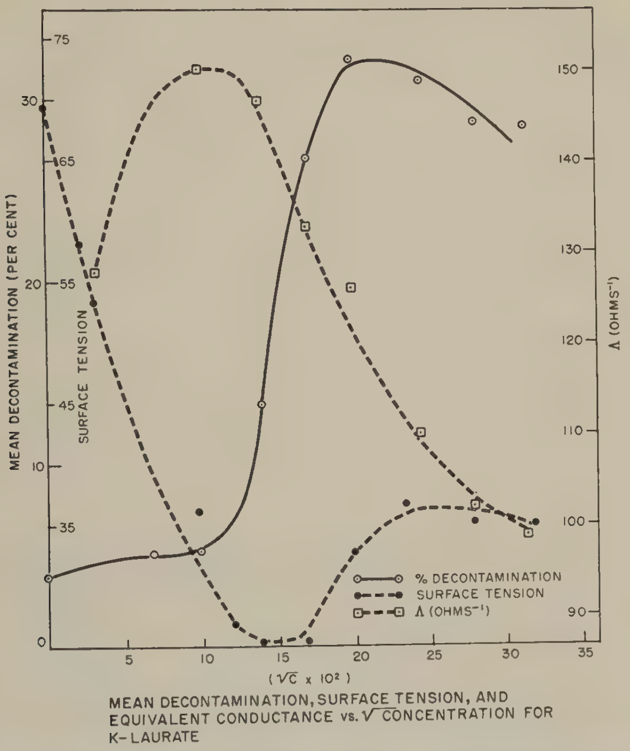

FIG. 2. Mean decontamination, surface tension, and equivalent conductance vs. square root of concentration for K-laurate.

was independent of surface tension. However, decontamination began a rapid increase at a concentration closely agreeing with the beginning rapid decline in equivalent conductance. This concentration is commonly assumed to be the critical concentration for micelle formation (CMC). Decontamination then improved sharply over a range of 2- to 3-fold the CMC. Clearly decontamination was closely related to the electrolyte concentration but in no simple manner. The two electrolyte solutions show a close similarity in their surface tension, conductance, and decontamination curves, but their concentration ranges for these similar effects differ widely, with an approximate 10-fold difference in CMC. The fact that effective decontamination began with soap micelle formation (CMC) even when the concentrations differed widely supports the view that soap micelles are essential to decontamination under the conditions of this study. In practical decontamination the application of various mechanical forces may overshadow the importance of micelles in removing radioactive materials from surfaces.

Inspection of the decontamination curves in Figs. 2 and 3 suggests ad-

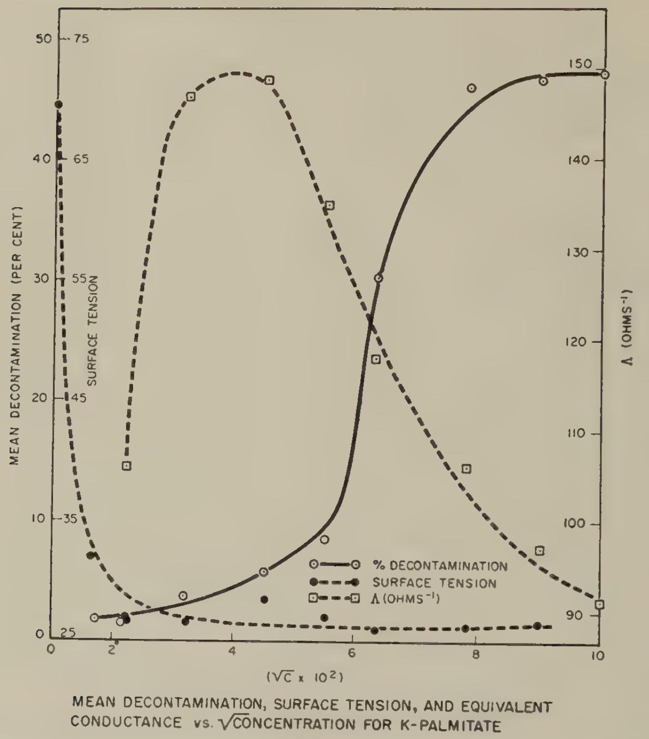

FIG. 3. Mean decontamination, surface tension, and equivalent conductance vs. square root of concentration for K-palmitate.

sorption isotherms such as might represent an equilibrium between micellar and contaminated surfaces over the range of micellar concentrations. The indication of a maximum for decontamination in the KL curve arouses interesting speculations. Such factors as variation in particle size of contaminant, relative retentive power over various areas of the original surface, and qualitative changes in the micellar surface with concentration may affect the shape of the curve. Further investigation is warranted.

Both electrolytes showed some very slight increase in decontamination before the CMC was reached. This focuses attention upon this controversial range of soap solutions. The behavior of potassium and sodium soaps in this region is generally attributed to hydrolysis. There is general agreement that fatty acids and soap ions form acid soaps before the CMC is attained, but there is considerable disagreement as to the first products of hydrolysis and attending phenomena (2, 3, 4, 11, 12). Other workers have contributed important discussions on phenomena attending hydrolysis and the suppression of hydrolysis (5, 14, 17, 18).

The causes of departure of dilute soap solutions from the behavior of

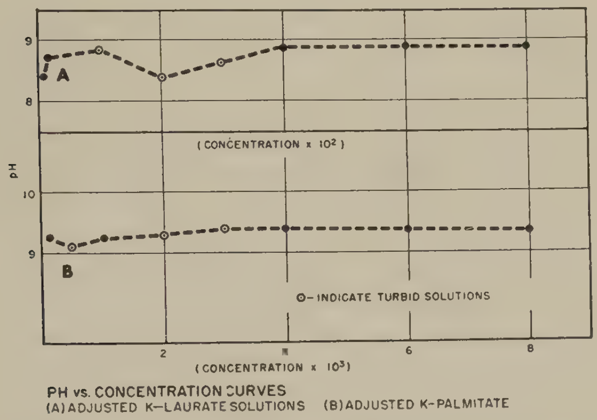

FIG. 4. pH vs. concentration curves: (*A*) Adjusted K-laurate solutions; (*B*) adjusted K-palmitate.

ideal colloidal electrolytes thus remains controversial. Figure 5 presents two theoretical and two experimental equivalent conductance curves for palmitate soaps at 57°C. All curves have been adjusted to a common CMC for sake of comparison. Our experimental net value for the equivalent conductance of KP at 2×10^{-3} M was 150. The calculated equivalent conductance of K^+ at this concentration and temperature is 116.6, and the contribution of OH^- due to hydrolysis is 3.5, leaving 29.9 as the value for the palmitate ion. Curve I represents the conductance throughout the dilute area if the ions acted as a fully ionized and nonhydrolyzable electrolyte in accordance with the Onsager equation (15). Curve II represents the conductance if hydrolysis characteristic of the palmitate ion were the only additional influence.[1] Curve III is the experimental curve obtained by Ekwall (14) for pure NaP at concentrations less than the CMC, and Curve IV is the net conductance for our *adjusted* KP solutions in the present investigation.

The striking deviations of the experimental curves in Fig. 5 from the theoretical curves emphasize the complexity of the physical and chemical system in this region. Ekwall has discussed these anomalies as shown by conductance (14), turbidity (12), and pH (16), and on the basis of his observations he offered the theory (3) that at very low concentrations fatty acid ions progressively aggregate into polyvalent ions having 2 to 8 charges which likewise progressively increase in their degree of hydrolysis. Aggregation tends to reduce conductance leading to a minimum, the increase in hydrolysis tends to reverse the trend, the progressive formation of acid soap

[1] Curve II is calculated by Stainsby and Alexander's $K_a = 2.9 \times 10^{-7}$, and K_w at 57°C. was calculated from H. S. Harned and W. J. Hamer, *J. Am. Chem. Soc.* **55**, 2194 (1933).

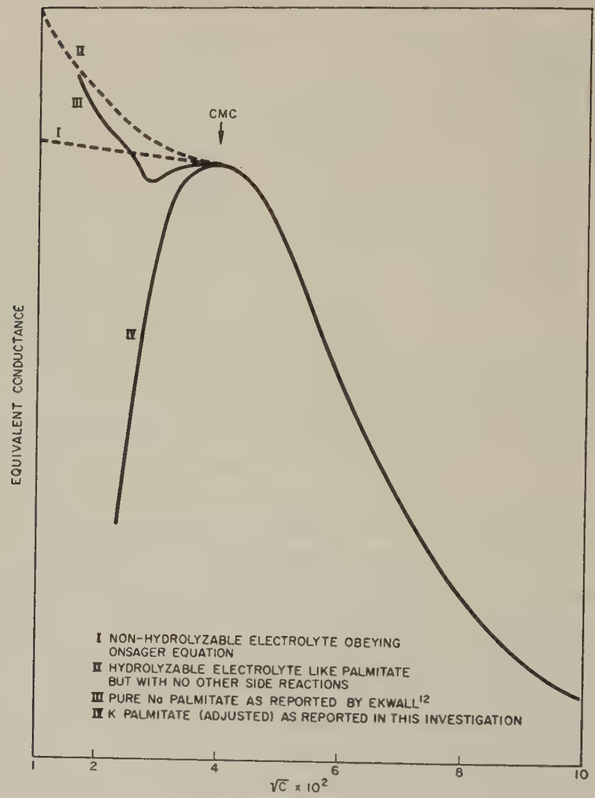

FIG. 5. The non-ideal behavior of a hydrolyzable colloidal electrolyte.

from accumulating products of hydrolysis reduces conductance due to hydrolysis, and then the incipient formation of typical soap micelles (CMC) rapidly reduces conductance. Ekwall thus accounts for the observed minimum, maximum, and CMC.

The concept of very highly charged long-chain ions does not agree with the evidence found by Chandler and McBain (8, 9) that cationic micelles held charges of the same order as inorganic ions; hence an alternative explanation for maxima and minima in equivalent conductance is desirable. Powney and Jordan (4) offered experimental evidence for maximal and minimal degrees of hydrolysis. Stainsby and Alexander (6) reinterpreted Powney and Jordan's data postulating that micelles of fatty acid begin formation at one half the generally accepted CMC. The concept that micelles may arise from hydrolytic products before typical soap micelles form agrees well with the experimental evidence in this study where the pH was held approximately constant, permanent turbidity occurred in certain very dilute solutions, and net equivalent conductance declined as much as 30%

in an area considered to be below the CMC. Obviously the interfacial surface area for adsorption (or ion exchange) would be extremely small. The small but persistent degree of decontamination observed suggests that micelles exist there even at lower concentrations than postulated by Stainsby and Alexander (6). Similar unpublished data were obtained in our studies with strontium contaminant. Possibly decontamination as carried out in this investigation is a very sensitive method for the determination of the origin and extent of micellization.

All previous quantitative data on hydrolysis have been calculated from pH measurements assuming that the OH^- activity behaved in a normal manner, but some doubt has been expressed about this (3, 19). Any unusual behavior of OH^- that changes its conductance would invalidate conclusions drawn on hydrolysis data, and net equivalent conductance.

The authors favor the view that the products of hydrolysis in colloidal salts of very weak acids may contribute to small concentrations of secondary colloids at concentrations well below the point of primary colloidal formation commonly called the critical micelle concentration and, under such conditions, lead to a significant reduction in the net equivalent conductance.

Conclusions

The removal of radioactive particulate matter from surfaces by immersion in colloidal electrolytes began with the formation of micelles and increased rapidly with micellar concentration up to 2- to 3-fold the CMC.

Decontamination was independent of surface tension.

The relation between micellar concentration and decontamination suggested that adsorption of the particulate matter occurred on the micellar interface competing with the original surface.

In very dilute solutions at concentrations below the CMC the surface tension, conductance, and turbidity data suggested that small concentrations of secondary colloids were formed in that region.

References

1. Los Alamos Scientific Laboratory, "The Effects of Atomic Weapons," Chapter X. U. S. Government Printing Office, Washington, D. C., June, 1950.
2. McBain, J. W., Laurent, P., and John, L. M., *J. Am. Oil Chemists' Soc.* **25,** 77 (1948).
3. Ekwall, P., *Kolloid-Z.* **92,** 141 (1940).
4. Powney, J., and Jordan, D. O., *Trans. Faraday Soc.* **34,** 363 (1938).
5. Powney, J., and Addison, C. C., *Trans. Faraday Soc.* **34,** 372 (1938).
6. Stainsby, G., and Alexander, A. E., *Trans. Faraday Soc.* **45,** 585 (1949).
7. Kolthoff, I. M., and Johnson, W. F., *J. Phys. & Colloid Chem.* **52,** 22 (1948).
8. Chandler, R. C., and McBain, J. W., Paper presented at 21st National Colloid Symposium, Stanford University, June, 1947.
9. Chandler, R. C., and McBain, J. W., *J. Phys. & Colloid Chem.* **53,** 930 (1949).

10. HUNTER, H. F., AND BALLOU, N. E., *Nucleonics* **9**, No. 5, C-1 to C-7 (1951).
11. HARTLEY, G. S., "Aqueous Solutions of Paraffin Salts." Hermann et Cie, Paris, 1936.
12. EKWALL, P., *Kolloid-Z.* **77**, 320 (1936).
13. KLEVENS, H. B., *J. Phys. & Colloid Chem.* **52**, 130 (1948).
14. EKWALL, P., *Kolloid-Z.* **101**, 135 (1942).
15. ONSAGER, L., *Physik. Z.* **27**, 388 (1926); *ibid.* **28**, 277 (1928).
16. EKWALL, P., AND LINDBLAD, L. G., *Kolloid-Z.* **94**, 42 (1941).
17. FLOCKHART, B. D., AND GRAHAM, H., *J. Colloid Sci.* **8**, 105 (1953).
18. FLOCKHART, B. D., AND UBBELOHDE, A. R., *J. Colloid Sci.* **8**, 428 (1953).
19. TYUTYUNNIKOV, B., AND KAS'YANOVA, N., *Allgem. Oel- u. Fett-Ztg.* **31**, 276 (1934).

THE OSMOTIC PROPERTIES OF TETRADECYLSULFONIC ACID

George W. Fuller

(communicated by M. E. L. McBain)

Stanford University, Palo Alto, California

Received March 25, 1955; revised May 23, 1955

Abstract

The osmotic coefficient "g" of a series of aqueous solutions of tetradecylsulfonic acid have been measured, with the use of precision methods of freezing point and vapor pressure lowerings.

The results conform to the pattern of similar long-chain acids and confirm the fact that they belong to the class of colloidal electrolytes.

The higher aliphatic sulfonic acids, RSO_3H, are typical colloidal electrolytes and yet are simpler than ordinary soaps in that they do not show the disturbing effects of hydrolysis in dilute solution. The following report summarizes experimental measurements of the osmotic properties of the tetradecylsulfonic acid. For dilute solutions, the freezing point method of Scatchard (1) was employed and for higher concentrations the isopiestic method of Sinclair (2), as developed by Robinson (3).

Following these authors, solutions of potassium chloride were used as standards of comparison with the long-chain acid. When the two sets of solutions, the known and the unknown, are rocked in an evacuated desiccator in a thermostat until equilibrium is attained, then both solutions have the same vapor pressure. In Robinson's work with alkali halides he was able to start with solutions close to the equilibrium point, whereas it took many experiments to find that it required almost ten times the concentration of the sulfonic acid to give the same vapor pressure as the potassium chloride standard. When this was ascertained the time of reaching equilibrium was reduced to 24 hours. Thus, working with concentrations of tetradecyl of 0.1 to 0.5 N_w the corresponding concentrations of potassium chloride varied from 0.01 to 0.06 N_w. The tetradecylsulfonic acid was made by the method of Noller and Gordon (4). Its molecular weight was 278.0 (theory 278.3).

The results for both sets of experiments are recorded in terms of the osmotic coefficient "g", which is the ratio of experimental freezing point

TABLE I

Osmotic Coefficients "g" of Tetradecylsulfonic Acid Solutions

From freezing point (Andresen)		From vapor pressure lowering (Fuller)			
Conc. N_w	"g"	C_{14} conc. N_w	KCl conc. in equilm.	$-\Delta P_{25}$ C_{14}	"g"
0.0016	0.980	0.096	0.0104	0.0086	0.106
0.0025	0.980	0.115	0.0140	0.0115	0.117
0.0036	0.979	0.125	0.0140	0.0115	0.110
0.0049	0.977	0.130	0.0147	0.0121	0.109
0.0064	0.970	0.155	0.0185	0.0154	0.117
0.01	0.955	0.232	0.0307	0.0248	0.126
0.0156	0.922	0.259	0.0337	0.0271	0.123
0.02	0.881	0.260	0.0350	0.0283	0.128
0.0225	0.848	0.265	0.0350	0.0284	0.126
0.0296	0.740	0.275	0.0367	0.0298	0.128
0.0310	0.695	0.318	0.0440	0.0329	0.122
0.0324	0.685	0.313	0.0414	0.0332	0.125
0.0361	0.620	0.355	0.0461	0.0372	0.124
0.040	0.516	0.373	0.0467	0.0378	0.120
0.0414	0.428	0.435	0.0550	0.0443	0.120
0.0506	0.352				
0.0529	0.315				

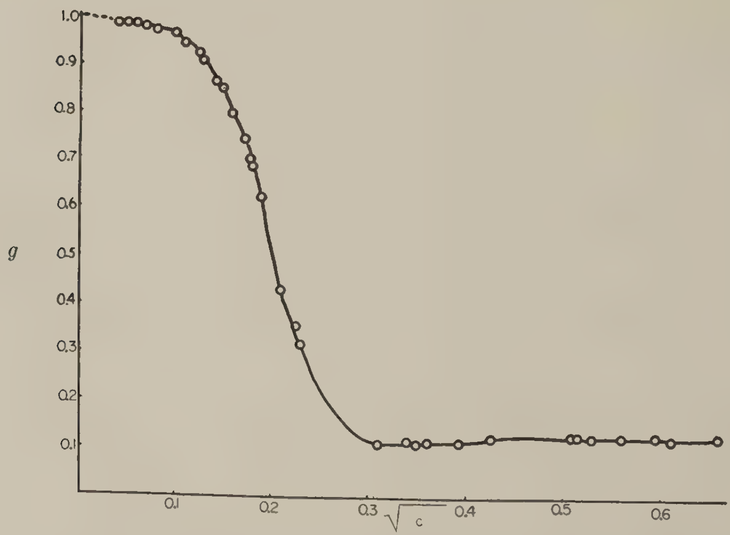

FIG. 1. The osmotic coefficient g of tetradecylsulfonic acid throughout the concentration range 0.0016 N_w to 0.435 N_w.

or vapor pressure lowering to that for a completely dissociated ideal electrolyte. It was found that the lowering of vapor pressure calculated on the assumption that g (0°C.) = g (25°C.) did not vary more than 0.08% from those calculated using the necessary temperature correction.[1] Since the accuracy of the work done did not warrant this small correction, the values are left unchanged in Table I. The results are also presented graphically in Fig. 1.

REFERENCES

1. SCATCHARD, G., JONES, P. T., AND PRENTISS, S. S., *J. Am. Chem. Soc.* **54,** 2676 (1932).
2. SINCLAIR, D. A., *J. Phys. Chem.* **37,** 495 (1933).
3. ROBINSON, R. A., AND SINCLAIR, D. A., *J. Am. Chem. Soc.* **56,** 1820 (1934).
4. NOLLER, C., AND GORDON, J. J., *J. Am. Chem. Soc.* **55,** 1090 (1933).

---

[1] $$(\ln P_{25^\circ} - \ln P_0) = \int_0^{25} \frac{R\bar{L}}{T^2} \cdot dT = \frac{\bar{L}}{R} \cdot \frac{T_{25} - T_0}{T_{25}T_0},$$

where $\bar{L}$ is the average heat of vaporization between the two temperatures.

Book Reviews

Dynamics of Growth Processes. Edited by EDGAR J. BOELL. Princeton University Press, 1954. Price $7.50.

This volume contains 13 papers contributed to the Eleventh Growth Symposium held during June, 1952, under the auspices of the Society for the Study of Development and Growth and of the Committee on Developmental Biology of the National Research Council. The list of contributions is an impressive and representative one, and the scope of the volume ranges from cytochemistry, and amino acid synthesis in bacteria, through physical and chemical growth factors in plants and in animals, to the mathematics of population growth. Although chemical aspects of growth are referred to in every paper, only four of the papers (Novick and Sziland on amino acid synthesis in bacteria; Pollister on cytochemical aspects of protein synthesis; Skoog on chemical regulation on growth in plants; and Gaunt on chemical control of growth in animals) deal explicitly with chemistry. Three of these papers are biochemical in the usual sense, and only one (Novick and Sziland) leans heavily toward physical chemistry.

The colloid chemist will find no applications of his own specialty among these studies. However, like all other scientists, he may find much that is stimulating and thought-provoking if he takes advantage of the unusual opportunity presented in these pages to learn easily and quickly of the rapid increase of our knowledge of growth processes (in plants, animals, and most interesting of all, viruses and bacteria) that has occurred in recent years.

JACINTO STEINHARDT, Cambridge, Massachusetts

Fluorine Chemistry, Volume II. Edited by J. H. SIMONS (Fluorine Research Center, The University of Florida, Gainesville, Florida), Academic Press Inc., New York, 1954. x + 565 pp. Price $13.50.

This second volume in the series on Fluorine Chemistry continues the high standard of reference works in this field. The inorganic and organic chemists working in this field will find this book an invaluable summary reference by some of the outstanding men in the field. The chapters with contributors are as follows:

"Fluorine Containing Complex Salts and Acids" by Alan G. Sharpe.

"Halogen Fluorides—Recent Advances" by H. J. Emeleus.

"Analytical Chemistry of Fluorine and Fluorine-Containing Compounds" by Philip J. Elving, Charles A. Horton, and Hobart H. Willard.

"Organic Compounds Containing Fluorine" by Paul Tarrant.

"Metallic Compounds Containing Fluorocarbon Radicals and Organometallic Compounds Containing Fluorine" by H. J. Emeleus.

"Fluorocarbon Chemistry" by J. H. Simons and T. J. Brice.

"The Infrared Spectra of Fluorocarbons and Related Compounds" by D. G. Weiblen.

The analytical chemistry of fluorine presents a long-needed complete survey of the field. The chapter devoted to the fluorocarbon derivatives of the metals and nonmetals presents a review and introduction to an increasingly active field of research. The almost encyclopedic chapters on the fluorocarbons and organic compounds containing fluorine are an invaluable critical survey of work in these fields from the time Volume I was complete to early 1952. The new chapter in this series devoted to the infrared spectra of fluorine-containing organic compounds is of inestimable value to workers in the field and will stand for many years as a standard reference work. Collected here are the important spectra, interpretations, and a critical summary of the published data.

The reviewer would like to draw particular attention to the chapters by Tarrant and Simons. There appears to be a lack of consistency in the nomenclature of fluorine-containing organic molecules. This results in some difficulty in the immediate understanding of the compounds mentioned. There is a definite need for the standardization of this aspect of nomenclature.

The use of symbols, such as ⦵, which have been modified or changed from their accepted representation, gives rise to considerable confusion and sometimes to misunderstanding. The inconsistent use of methforyl and trifluoromethyl to mean the same thing, CF_3–, appears to be unnecessary. This hybridization of nomenclature is unworthy of the subject matter presented. The average reader will have difficulty in justifying Simons' statement concerning the preparation of fluorine-containing organic compounds that "the reaction employed for the syntheses will not be those of organic chemistry, but will be either entirely new methods or drastic modifications of known organic or inorganic reactions," with the facts presented in the chapter. The vast number of organic compounds possessing functional groups and perfluorocarbon radicals is attested to by the complete bibliographies of the chapters in this book, and it is obvious that, though the functional reactivity is modified from the standard hydrocarbon chemistry, it is more a matter of degree than an absolute difference.

In the reviewer's opinion this volume deserves the attention of every chemist in the field of fluorine chemistry and will be of use also to chemists not actively engaged in the field.

C. W. ROBERTS, Lafayette, Indiana

The Proteins. Chemistry, Biological Activity, and Methods. Edited by HANS NEURATH and KENNETH BAILEY. Academic Press Inc., New York 10, N. Y., 1954. Volume II, Part B, 1418 pp. Price $16.50.

The final volume (the fourth) of this important detailed treatise on the subject contains authoritative chapters on Interstitial Proteins (W. L. Hughes); Proteins of Immune Reactions (W. C. Boyd); two chapters on Structure Proteins (J. C. Kendrew and K. Bailey, respectively); Proteolytic Enzymes (N. M. Green and H. Neurath); and Peptide and Protein Synthesis (H. Tarver). It also contains author and subject indices for the third and fourth volumes (Vol. II, Parts A and B).

The articles in the final volume are up to the general high standard set by the three previously published. All are characterized by a high degree of inclusiveness and by a good measure of critical discernment in fields in which new observations have multiplied with great rapidity in recent years. Some of the reviews of the present volume are thus of particular value.

It is unfair to single out particular papers; however, the reviewer was especially interested in the following:

The paper of Hughes on plasma proteins, which not only summarizes clearly much new information but also removes many of the earlier misstatements in the literature (the alleged existence of solubilities independent of amount of saturating body is one example). Boyd's paper on immune proteins starts with a careful enumeration of empirical phenomena before discussing current theories. Bailey's paper on the proteins of muscle covers not only chemical and enzymological aspects but also the evidence from X-ray and electron microscope examination of muscle fibers. The paper on proteolytic enzymes by Green and Neurath not only discusses the wide domain of the enzymes themselves, their activators, and specificities, but also illuminates the unsettled questions and hypotheses of the mechanism of hydrolysis and its relation to denaturation.

Now that this very impressive work is completed, its full stature becomes quite evident. It will undoubtedly remain the standard authority and reference on proteins and protein phenomena for many years to come. In few fields of modern science are workers fortunate enough to have available one as good.

JACINTO STEINHARDT, Cambridge, Massachusetts

LIESEGANG RINGS IN INHOMOGENEOUS MEDIA. POWDERED GLASS

Don R. Manley and Kurt H. Stern

Department of Chemistry, University of Arkansas, Fayetteville, Arkansas

Received July 6, 1955

Abstract

The formation of Liesegang rings has been studied in powdered glass suspended in gelatin. The diffusion velocity is shown to decrease with increasing glass concentration.

Introduction

In a previous study by one of us (1) it was shown that the diffusion velocity of silver nitrate into gelatin partially coagulated by the addition of methanol is inversely related to the methanol concentration. It was assumed there that the effect of inhomogeneities on the diffusion velocity is mechanical, i.e., that any inert material dispersed in gelatin would produce the same effect as coagulated gelatin. The present work is a proof of that assumption.

Experimental Part

Procedure

Measurements were carried out in the tubes described previously. Each tube contained 10 ml. of a solution made by dissolving 6 g. gelatin and 0.5 g. K_2CrO_4 in 100 g. water and the indicated amount of powdered glass. Tube I contained no glass, Tube II, 0.5 g. of glass, with an increment of 0.5 g. of glass for each succeeding tube ending with 3.0 g. in Tube VII.

The gelatin was Baker's U.S.P. grade. The powdered glass, 200 mesh, was carefully mixed with the gelatin before filling the tubes. When the gelatin solidified the glass was homogeneously dispersed in it. The remainder of the experimental procedure is as previously described.

In order to determine whether either silver or chromate ions are adsorbed on powdered glass a chromatographic tube was packed with powdered glass and wetted successively with solutions of $AgNO_3$ and K_2CrO_4. Since the second solution added displaced the first, independently of which was added initially, it seems safe to conclude that neither silver nor chromate ions are adsorbed on glass.

If a silver nitrate solution diffuses into a tube closed at the bottom and packed with powdered glass wet with chromate solution Liesegang rings form in the usual manner. Diffusion is extremely slow, since the $AgNO_3$ must diffuse through the small interstices between the glass particles. Since the amount of K_2CrO_4 wetting the glass is very small it is completely exhausted by counter diffusion and precipitation before ring formation has proceeded half-way down the tube. No quantitative data on this experiment are presented.

RESULTS

Measurements of distance x traveled by the diffusing solution in time t were made on the tubes referred to. A plot of these is shown in Fig. 1. Since the diffusion velocity is constant for $800 \leq t \leq 1300$ hours, average

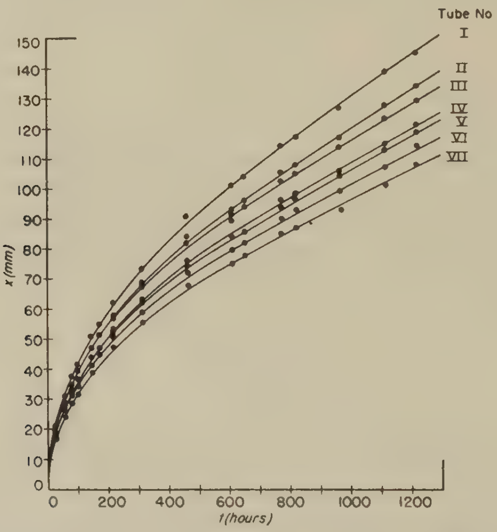

FIG. 1. Diffusion velocity for systems of different glass concentrations.

TABLE I

Diffusion Velocity as a Function of the Composition of the Medium

Tube No.	Wt. % Glass	x/t (*mm./hr.*)
I	0	0.070
II	4.8	0.066
III	9.1	0.062
IV	13.0	0.058
V	16.7	0.058
VI	20.0	0.054
VII	23.0	0.052

TABLE II

"Steady-State" Values of $x/\sqrt{t}$ *for Various Systems*

Tube No.	$x/\sqrt{t}$ ($mm.\ hr^{-\frac{1}{2}}$)
I	4.10
II	3.78
III	3.70
IV	3.45
V	3.38
VI	3.24
VII	3.06

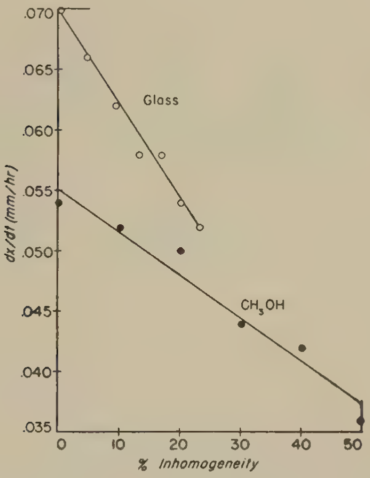

FIG. 2. Diffusion velocity as a function of per cent inhomogeneity.

velocities were calculated from the slope of the plot. Data are shown in Table I.

The diffusion velocity decreases with increasing glass concentration in a manner exactly analogous to gelatin partially coagulated with methanol.

Similarly, values of $x/\sqrt{t}$ decrease for each of the tubes with time, reaching a steady value over that portion of the curve for which the x *versus* t plot is a straight line, and also decrease with increasing glass concentration. This latter dependence is shown in Table II.

A plot of $x/\sqrt{t}$ *versus* weight per cent glass is approximately linear as is a similar plot for the gelatin-methanol system, although the slope in the latter case is somewhat smaller.

DISCUSSION

As is shown by the results in the preceding section the variation of diffusion and Liesegang ring formation in gelatin made increasingly inhomogeneous by powdered glass and methanol is qualitatively analogous and quantitatively similar. This confirms the assumption made in the earlier paper, that the effect of inhomogeneities on the diffusion velocity is mechanical, and that in fact an inert material dispersed in gelatin produces the same effect as coagulated gelatin. This implies that coagulated gelatin has no specific adsorptive affinity for either chromate or silver ions.

One more relation remains to be pointed out. If the steady-state diffusion velocity is plotted against per cent inhomogeneity (Fig. 2) it is seen that, though the plot is linear in both cases, the slope is distinctly less for the methanol system. If it is assumed that the relation between the methanol added is proportional to the inhomogeneity produced, as the linearity of the plot strongly suggests, then the difference in the slopes implies that coagulated gelatin offers less impedance to diffusion than does glass. Since it may be safely assumed that no diffusion occurs through the glass particles, this suggests that coagulated gelatin may be somewhat permeable to diffusing ions.

REFERENCE

1. STERN, K. H., *J. Colloid Sci.* **9**, 329 (1954).

MAXIMUM PARTICLE SIZES IN POLYDISPERSED AEROSOLS[1]

Milton Kerker, A. Lucile Cox, and Melvin D. Shoenberg

Department of Chemistry, Clarkson College of Technology, Potsdam, New York

Received October 25, 1954; revised March 24, 1955.

Abstract

The size distributions of mercury and sulfur aerosols have been investigated by a light scattering–settling technique and the results compared with direct electron microscope observations. For the larger size aerosols the maximum size obtained by light scattering agrees with the electron microscope maximum but the distribution curves differ. For smaller aerosols (maximum by electron microscope less than 0.1 μ) the light scattering shows no maximum size. These discrepancies are attributed to convection and coagulation. The liquid nature of sulfur aerosols is demonstrated by photomicrography and a new technique of preparing them for the electron microscope is described.

I. Introduction

Methods involving (*1*) the scattering of light as a function of angle (Higher Order Tyndall Spectra) and (*2*) the transmission of light as a function of wavelength, have been developed in the Columbia University Laboratories over the past 13 years by V. K. La Mer and co-workers, notably David Sinclair, for the determination of particle size of monodispersed aerosols (1, 1*a*) and hydrosols (2–4) for the micron and submicron (5) size ranges.

By combining these methods with differential settling (6) under gravity, they found (1941) it was possible to make an estimate of the distribution of particle size of polydispersed aerosols in the micron range. These early studies have recently (1950–1951) been refined and extended (7) in a series of reports where the importance of taking precautions to eliminate convection currents is stressed. In all cases, the Mie theory of light scattering and Stokes law of settling are involved; hence the methods are restricted to particles closely approximating spheres and to conditions permitting tranquil settling.

More recently, Gumprecht and Sliepcevich (8) have extended Lowan's tables of the Mie functions to larger values of the argument (r/λ), thus enabling them to investigate the much larger sized polydispersed aerosols

---

[1] Supported in part by Office of Ordnance Research, Contract No. DA-30-115-ORD-309.

produced by spraying. In this paper, we report on investigation of the size distribution of polydispersed mercury and sulfur aerosols by light scattering–settling techniques. The distribution curves thus obtained are compared with direct electron microscope counts. Furthermore, the very high density and the metallic character of mercury, requiring the use of the complex index of refraction, make this aerosol an interesting and unique material for this type of investigation.

II. EXPERIMENTAL

The aerosol generator was similar to that of Sinclair and La Mer (1). The temperature was not controlled as carefully, probably accounting for the greater polydispersity of our aerosols. For our purposes this was not an undesirable feature.

Nuclei for the mercury aerosols were provided, at first, by a high-voltage discharge through a carrier gas mixture of nitrogen and oxygen, the latter being in excess. This suggested that the nucleating agent was an oxide of nitrogen. Indeed, it was possible to nucleate the mercury vapor with either NO or NO reacted with O_2 to form NO_2. NO_2 was the more effective nucleating agent, and it is even possible that small amounts, present as impurities, may have been responsible for the nucleating activity of the tank NO. No differences were observed among the aerosols produced by these various nuclei. Mercury aerosols could not be produced in the absence of nuclei and such a common nucleating agent as NaCl failed to produce an aerosol.

Sulfur aerosols were nucleated with H_2SO_4 vapor (9) to produce the smaller particles, whereas the large-particle sulfur aerosols were prepared by self nucleation.

The nuclei laden carrier gas passed into the boiler and the reheater at a rate of about 2 l. per minute. The boiler temperature was maintained at 190° to 230°C. for mercury aerosols and 100° to 150°C. for sulfur. The temperature of the reheater was about 20° higher than the boiler. Both boiler and reheater were heated by electric mantles, and the entire unit was enclosed in an asbestos box. The vapors condensed to an aerosol which could be led to a visual viewing chamber, the light-scattering apparatus, or the electron microscope sample-collecting chamber.

Because of its toxicity, the mercury was removed from the gas stream before flowing to the outside by heating the aerosol to over the boiling point of mercury and then condensing the vapors in a dry ice-acetone cold trap. The laboratory air was monitored by a G. E. mercury vapor detector. The apparatus was constructed entirely of glass with vacuum-tight joints except for a short rubber tubing connection to the light-scattering cell.

The Aminco light-scattering photometer was modified by replacing the rigid platform with an elevator platform which could be raised or lowered during the course of an experiment to permit observations at different levels in the light-scattering cell. This elevator was controlled by a knob on the outside of the instrument so that the level could be rapidly changed without opening the instrument lid. The cylindrical scattering cell which had flat entrance and exit windows had an inside diameter of 3.7 cm. and an inside height of 4.1 cm. Aerosol entered and left the cell through two side arms.

In order to minimize convection the scattering chamber of the photometer and the scattering cell were completely coated with asbestos paper except for holes for the light beams. Furthermore, a heat filter was placed in the incident beam and the path of the aerosol from the generator to the light-scattering cell was sufficiently long so that the aerosol had cooled to room temperature before entering the cell.

When a preliminary examination in the visual viewing chamber indicated a satisfactory aerosol, it was passed through the light-scattering cell until the intensity of scattered light remained constant, indicating a minimum of turbulence. A steady reading was usually obtained after a few minutes of flowing. At this point the scattering cell was closed off from the system and the intensity of light scattered by the aerosol at a known distance from the top of the cell was measured until that intensity had been reduced to at least 10% of its initial value. The angle of observation was 130° from the backward direction of the incident beam. The 5461 A. line of the mercury vapor light source, isolated by Corning filters, was used.

Random fluctuations of the readings were usually less than 2% or 3% of the signal. This was due to convection in the aerosol, since the light source and phototube were quite stable, as shown by the steady readings obtained with the incident beam in the absence of aerosol. The beam width was 3 mm. and the height 0.3 mm. The analysis of the data requires that the height be kept small compared to the distance from the top of the cell. The beam height we chose was large enough to give an appreciable scattering signal and yet sufficiently small for the analysis. We did not investigate the effect of slit width upon the observed results.

Immediately after closing off the scattering cell, the electron microscope sample-collecting chamber was filled with aerosol and then closed off from the system. Collodion-coated grids had been previously placed at levels corresponding to those at which scattering observations were to be made, and the aerosol particles were permitted to settle upon these.

The size distribution of particles observed in the electron microscope was obtained by counting directly from the microscope screen rather than from photographs. The telescope through which the screen was observed was fitted with a reticle.

No preparative procedures were necessary prior to observation of the mercury particles in the electron microscope. Hall (10) reports that sandwiching between two layers of silicon monoxide was necessary to prevent evaporation, in the electron beam, of mercury particles from a water emulsion. However, we found that our droplets were stable in the electron microscope without any preparative treatment. In order to confirm that a mercury particle could be stable in the electron microscope, some grids were provided with droplets formed by shearing mercury between two glass microscope slides. These were examined and rather than evaporate, they would increase in size slightly over a period of 20 minutes exposure to the high-intensity beam, presumably owing to accretion of pump oil or other contaminating material. Plate 1 is an electron micrograph of particles from a mercury aerosol. Plate 2 represents a particle formed by shearing mercury between two glass microscope slides.

In view of our success in observing mercury particles in the electron microscope without any fixative procedures, we had hoped to be able to do the same with sulfur, which has a lower vapor pressure than mercury. It was possible to see sulfur particles in the microscope, but upon continued exposure to the electron beam, they would evaporate, the small ones disappearing much more rapidly than the large ones.

Attempts to sandwich the particles between layers of silicon monoxide were not always successful. The smaller particles apparently evaporated in the shadow caster, probably owing to the combined effect of the vacuum

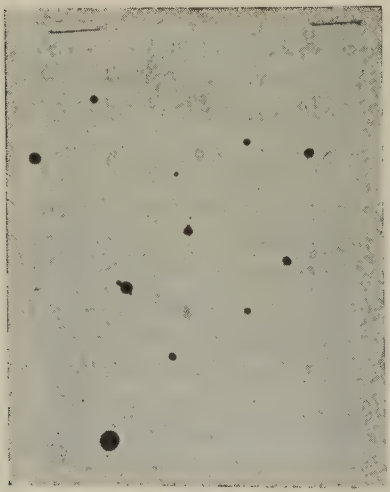

PLATE 1

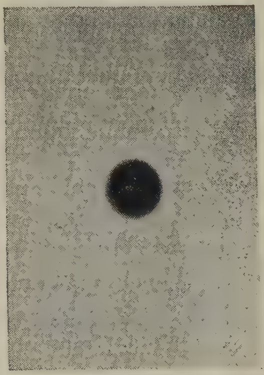

PLATE 2

PLATE 1. Electron micrograph of mercury particles in aerosol #15. Magnification 3550.

PLATE 2. Electron micrograph of mercury droplet ($r = 0.6\ \mu$) formed by shearing mercury between two glass slides. Magnification 5500.

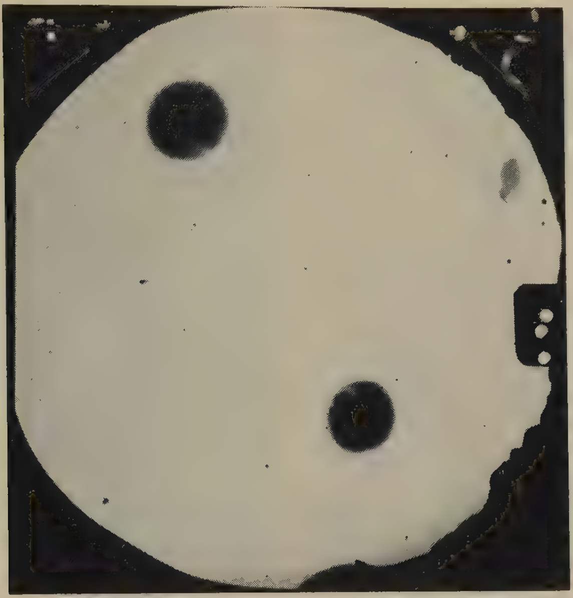

PLATE 3. Electron micrograph of sulfur aerosol particles. Magnification 4125.

and radiation from the filament, and there was no assurance that even those particles that were observed had not partially evaporated. A replica technique did not seem feasible, since sulfur is soluble in the organic solvents used.

A new procedure was finally developed that appears satisfactory for this system. The particles were collected on collodion-coated grids supported on a glass microscope slide. A second collodion film cast on water was then picked up by this slide, so that the particles were sandwiched between two films of collodion. These afforded the particles sufficient protection to stabilize them in the electron microscope. Plate 3 is an electron micrograph of sulfur aerosol particles prepared in the above manner.

As is well known, the particles which make up this aerosol consist of spheres of supercooled liquid sulfur. Their liquid nature is apparent from the photomicrographs depicted in Plates 4 and 5. Plate 4 is a view of some aerosol particles 3 hours after collection on a glass microscope slide in which the particles show diffraction patterns characteristic of liquid droplets. There is also present a crystalline mass. Upon standing the liquid droplets evaporate while the crystal grows. Plate 5 shows the same field of view 45 hours after collection. By this time, the supercooled liquid sulfur droplets have completely evaporated and condensed upon the crystal. Intermediate stages of this process were observed during the intervening time. The glass slide was held in a vertical position and without a cover glass; yet the sulfur diffused from the supercooled liquid to the crystal without excessive loss

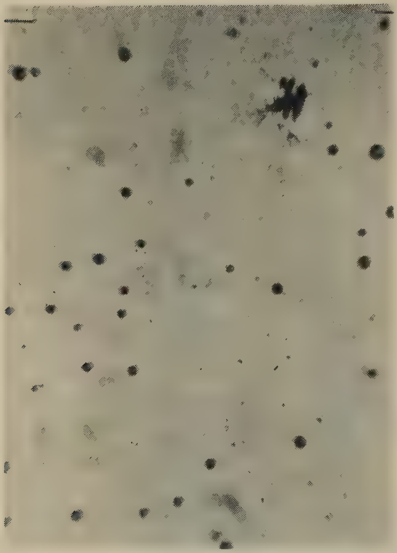

Plate 4

Plate 5

Plate 4. Photomicrograph of sulfur aerosol particles 3 hours after preparation. Magnification 5950.

Plate 5. Photomicrograph of sulfur aerosol particles 45 hours after preparation. Magnification 5950.

of vapor into the atmosphere. This suggests that the diffusion may be along the surface. The question of whether condensation upon a crystal from the vapor phase takes place directly, or via a surface adsorption mechanism, has received considerable attention recently (12).

The crystals are plainly apparent to the naked eye. A glass slide with freshly collected samples appears coated with a uniform film which is replaced after a time by scintillating crystal centers. The crystallization is inhibited by sandwiching the freshly collected aerosol between the two collodion films as described above.

III. Analysis of Light-Scattering Data

Our analysis is an extension of that of Sinclair (1*a*) and of Gumprecht and Sliepcevich (8). Let the aerosol be characterized by the size distribution $n_r dr$ which gives the fraction of particles with radii between r and $r + dr$. The intensity of light scattered by this aerosol at angle of observation, γ, is

$$I_\gamma = \int_0^\infty i_{\gamma,r}\, n_r\, dr, \qquad [1]$$

where $i_{\gamma,r}$ is the scattering function of a single particle of radius, r, at angle of observation, γ. The integral above should be multiplied by a constant determined by the aerosol concentration and the optical system.

However, we are not concerned with the absolute concentration of the aerosol and will continue with the intensity in arbitrary units.

If uniformly mixed aerosol undergoes tranquil settling, the intensity of scattered light observed h centimeters from the top of the cell will remain constant until the largest particles have had time to fall from the top of the cell through the light beam. The intensity of scattered light will then continue to decrease as each successively larger range of particles falls through the beam. Figure 1 is a schematic representation of the model for a system consisting of three discrete size groups.

The radius, R, of particles that have fallen from the top of the cell to the light beam at any given time is determined by the Stokes-Cunningham law

$$R = \frac{-Al + \sqrt{A^2l^2 + 18\,\frac{\eta h}{\rho g t}}}{2}, \qquad [2]$$

where

t = time.
h = distance from top of cell to the light beam.
ρ = density of the particle.
g = acceleration of gravity.
η = viscosity of the carrier gas.
l = molecular mean free path of the carrier gas.
A = empirical constant which varies slightly with R/l. For our conditions the value 0.43 is applicable.

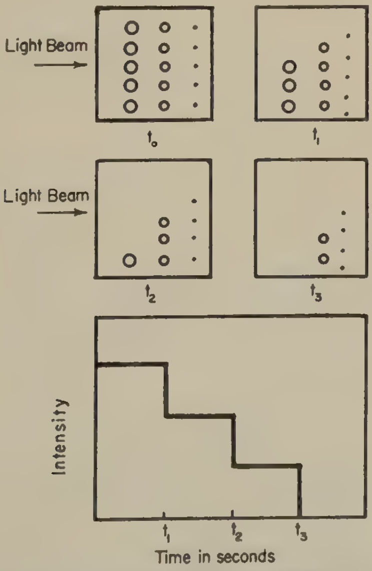

FIG. 1. The four squares at top schematically illustrate tranquil settling and the curve below shows how the intensity of scattered light would decay with time.

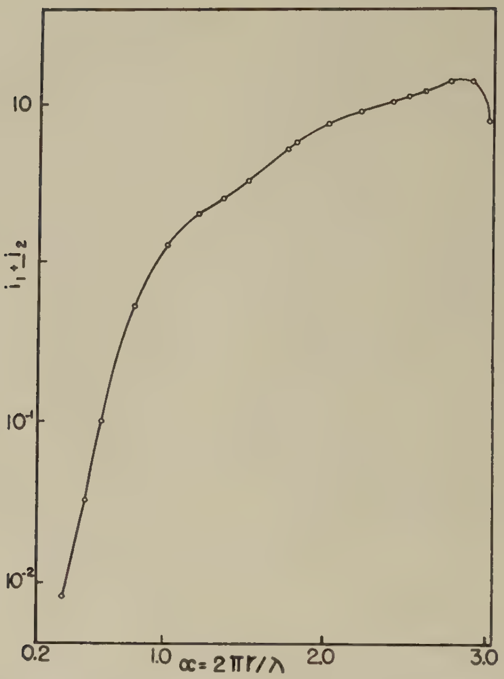

FIG. 2. Light-scattering functions, $i_1 + i_2$, for index of refraction $m = 1.46 - 4.30i$ at angle of observation $\gamma = 130°$.

At any given time the decrease of the intensity of scattered light due to the fall out is

$$-dI_\gamma = i_{\gamma,R}\, n_R\, dR, \qquad [3]$$

and the rate of decrease of intensity is

$$-\frac{dI_\gamma}{dt} = i_{\gamma,R}\, n_R \frac{dR}{dt}. \qquad [4]$$

The value of dI_γ/dt in the above equation is obtained from the decay of the intensity of scattered light as a function of time. The scattering functions, $i_{\gamma,R}$, are computed from the Mie theory. The value of dR/dt is calculated with the aid of Eq. [2]. Equation [4] is then solved for n_R, which is obtained in arbitrary units.[2]

IV. LIGHT-SCATTERING FUNCTIONS

Scattering functions were computed for the appropriate indexes of refraction. These functions, i_1 and i_2, are proportional to the light intensity scattered for incident light respectively polarized vertically and horizontally to the scattering plane. In our work, unpolarized incident light was used so that the appropriate scattering function is $i_1 + i_2$.

---

[2] The Stokes-Cunningham law must be further refined when $l/R < 1$. [See C. N. Davis, *Proc. Phys. Soc.* **57**, 259 (1945).] We have found by such calculations that the Stokes-Cunningham law does not involve appreciable errors for the aerosols reported.

The index of refraction (13–15) of mercury for light of wavelength 5461. A is $m = 1.46 - 4.30i$. The value of $i_1 + i_2$ for this index is plotted in Fig. 2 as a function of α at angle of observation $\gamma = 130°$; $\alpha = 2\pi r/\lambda$ where r is the particle radius and λ is the wavelength of the light in the medium.

The index of refraction of sulfur for light of wavelength 5461 A. is $m = 2$. Functions were available at this index of refraction (16–18) for a number of α values and these were supplemented by additional calculations at $\alpha = 3.3, 3.8, 4.2, 4.4, 4.6, 5.5, 6.5, 7, 8, 10$, and 12.5 for angle of observation $\gamma = 130°$. The value of $i_1 + i_2$, at $\gamma = 130°$ and $m = 2$, is plotted versus α in Fig. 3.

The detailed results of these calculations will be reported elsewhere (18). The values for mercury include 23 values of α between 0.2 and 5.0 at every 10° of angle of observation from $\gamma = 30°$ to $\gamma = 150°$.

V. RESULTS

A typical curve showing the decay of the intensity of scattered light is given in Fig. 4. The light beam is 2.74 cm. from the top of the cell in this

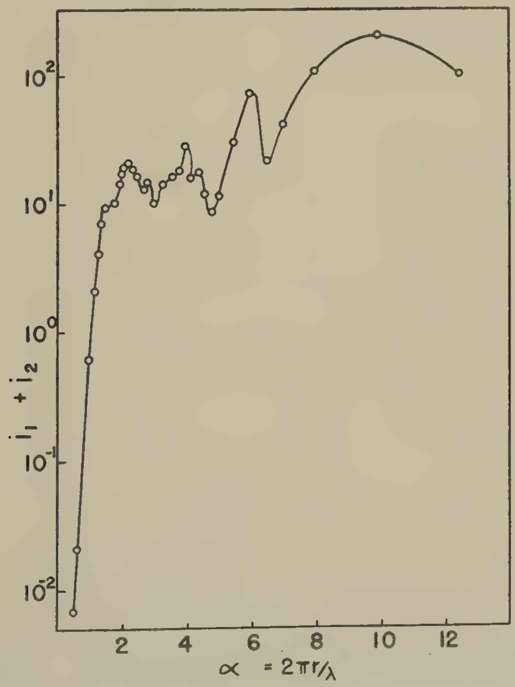

FIG. 3. Light scattering functions, $i_1 + i_2$, for index of refraction $m = 2$ at angle of observation $\gamma = 130°$ as a function of α.

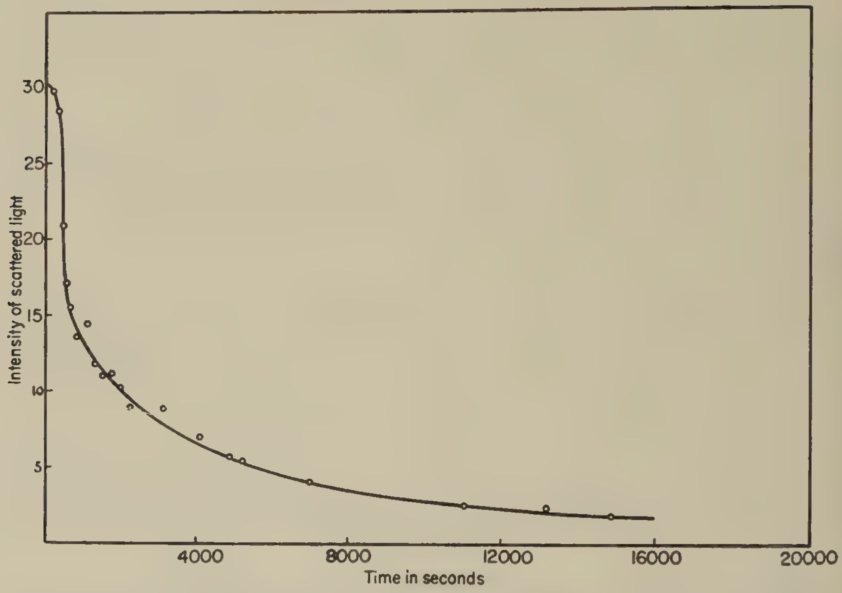

FIG. 4. Decay of intensity of scattered light for mercury aerosol #15 at angle of observation $\gamma = 130°$, 2.74 cm. from top of light scattering cell.

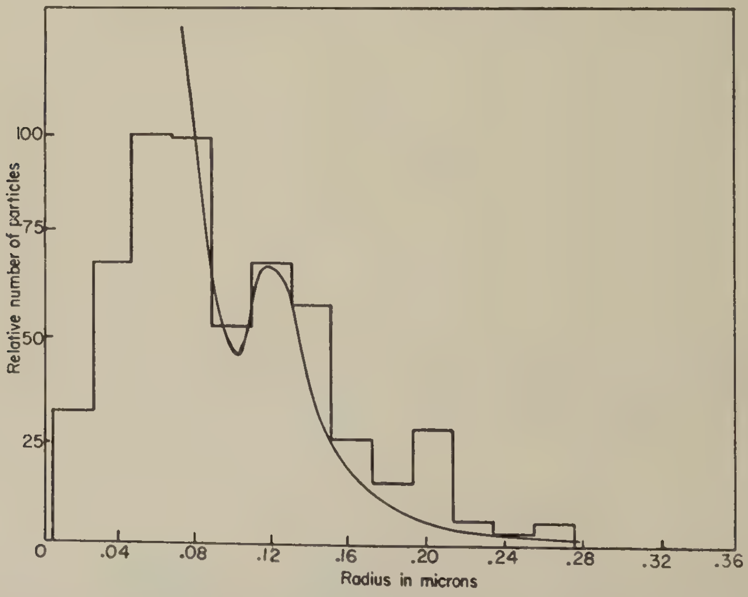

FIG. 5. Size distribution curves of mercury aerosol #15. Smooth curve by light scattering. Step curve by electron microscopy (2000 particles counted). Light scattering 2.74 cm. from top of cell.

case. In Fig. 5, the size distribution obtained with these data (smooth curve) is compared with that obtained by direct electron microscope count (step curve). The ordinates have been so chosen that the curves are in good coincidence in the larger size range. However, below 0.07 μ the distribution curve obtained by light scattering continues to increase while the electron microscope distribution goes through a maximum. This behavior was typical of all our work with mercury aerosols.

This discrepancy in the region of small sizes is undoubtedly due to convection in the aerosol. If, instead of tranquil settling, there is a holdup of just a small fraction of the larger sized material, this will influence the calculated number of small particles markedly. At the time that particles of a small size are presumably settling out, the decrease of intensity of scattered light will actually be due, in part, to the delayed settling of larger material. Because of their greater scattering power, a small number of large particles can introduce considerable error.

To illustrate this, consider an aerosol with a size distribution given by the step curve in Fig. 5. Suppose that 1% of the particles larger than 0.07 μ are held up by convection so that they fall out during the interval that particles of size 0.05 to 0.07 μ have their normal fall out (3000 to 5000 seconds). The decay in intensity of scattered light during this interval would be increased fourfold by the holdup, and the calculated number of particles would be larger by this factor. Furthermore, if only 0.1% of particles larger than 0.05 μ fall out during the interval that 0.035 to 0.05 μ particles normally fall out (5000 to 9000 seconds), the number calculated for this interval would be too large by a factor of nine.

Another possible source of error might be coagulation. It would give rise to slight differences in size distribution obtained by observations at different levels in the scattering cell. Since at a lower level the observations extend over a greater period of time, the coagulation will proceed to a greater extent, and the drop out will be relatively faster, resulting in a distribution curve less heavily weighted in the region of smaller sizes. This is illustrated by the two size distribution curves in Fig. 6, which are obtained from observations on the same aerosol but at different distances from the top of the scattering cell. The curves have been plotted so that they meet at $r = 0.174\ \mu$.

Coagulation produces a similar effect on the size distribution obtained by electron microscope count. Microscope grids placed at a lower level in the collection chamber will collect aerosol over a longer period of time, during which a greater degree of coagulation can take place than in the portion of the aerosol which is settling out over a grid placed at a higher level. Because of this, care was taken to position grids at the same distance from the top of the collection chamber as the intensity observations were taken from the top of the light-scattering cell. Figure 7 represents size

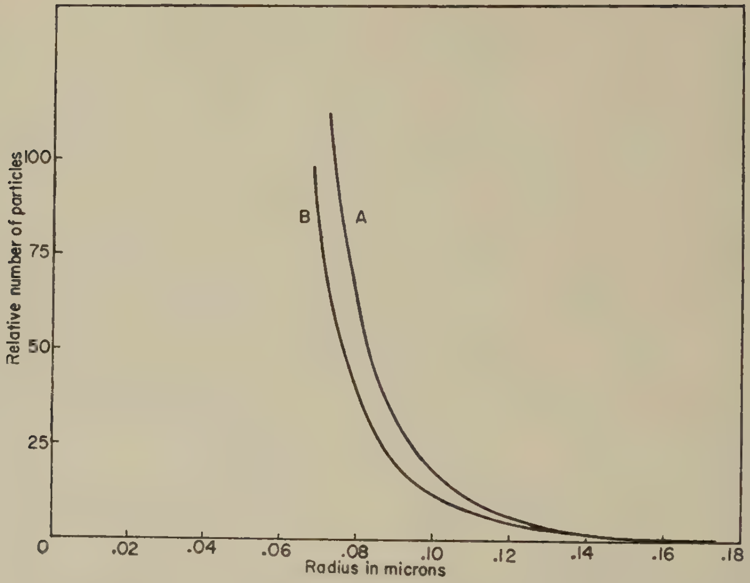

FIG. 6. Size distribution curves for mercury aerosol #7 from light scattering. *A*, light scattering 0.95 cm. from top of cell. *B*, light scattering 2.63 cm. from top of cell.

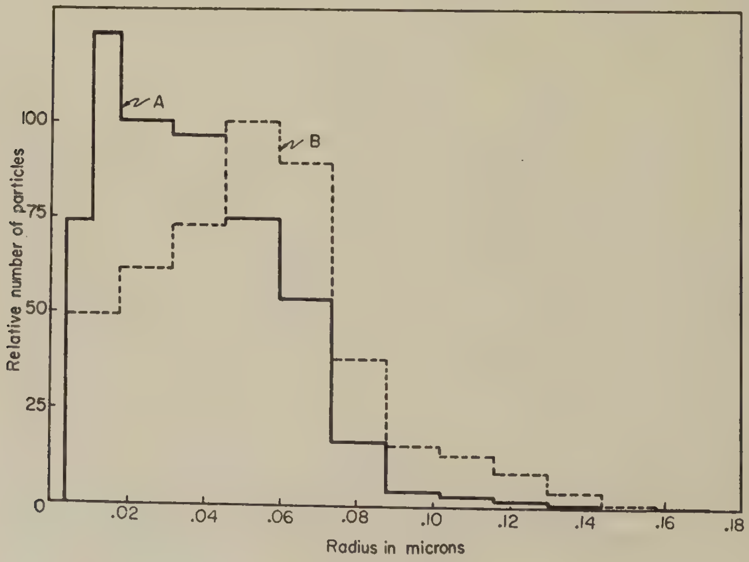

FIG. 7. Size distribution curves for mercury aerosol #7 from electron microscope count. *A*, 1 cm. from top of collection chamber; 3600 particles counted. *B*, 3 cm. from top of collection chamber; 5000 particles counted.

distributions at two levels obtained by electron microscope count. The aerosol is the same as that depicted in Fig. 6. For both methods, the distribution obtained at the lower level has a smaller proportion of the smaller particles.

It should be noted that some discrepancy between the electron microscope count and the light-scattering distribution may result from coagulation. Some particles observed in the microscope are coagulates whose drop-out times will be greater than their final size would indicate. This means that they would turn up in the light-scattering distribution as smaller particles. This, as well as convection, would contribute to the greater number of small particles obtained in the light-scattering distribution.

The effect of convection should be less important for aerosols with larger particles. However, the aerosol chosen for illustration in Figs. 4 and 5 represents the largest size mercury aerosol that we were able to prepare. Sulfur aerosols were prepared over a wider range of size distributions. Although convection again interferes for small-particle aerosols, its effect is mitigated somewhat when the sulfur aerosol particles are sufficiently large.

The size distribution curves obtained by the light scattering–differential

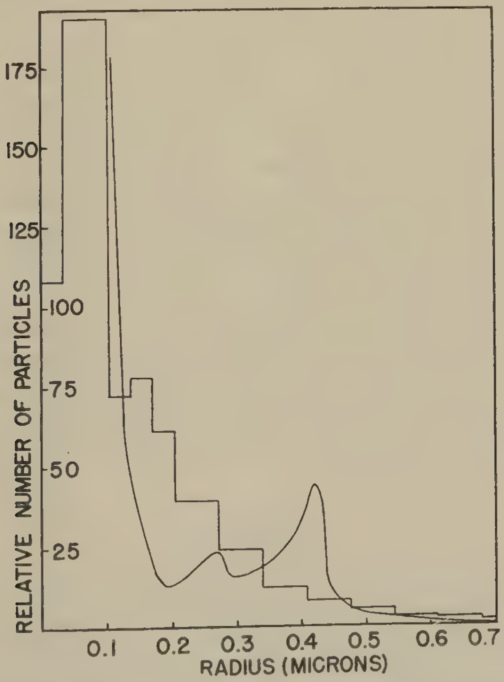

FIG. 8. Size distribution of sulfur aerosol #10. Smooth curve by light scattering. Step curve by electron microscopy (800 particles counted).

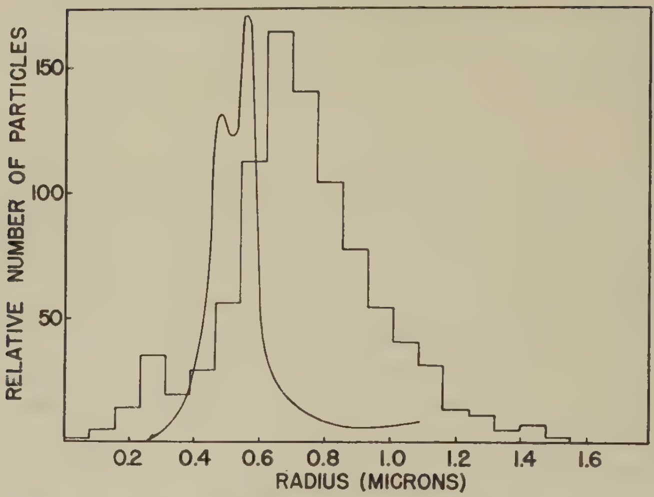

Fig. 9. Size distribution of sulfur aerosol #1. Smooth curve by light scattering. Step curve by electron microscopy (1800 particles counted).

settling technique and by electron microscope count for a sulfur aerosol of small particles are presented in Fig. 8. Just as for mercury aerosols, the distribution curves diverge in the region of small sizes ($\tau < 0.1\mu$). The maxima in the light-scattering curve are due to the characteristics of the light-scattering functions and are related to the failure of our instrument to resolve sharply the angular pattern of the scattering.

Figure 9 represents a sulfur aerosol consisting of larger particles. The two curves have been plotted so that the ordinate of the maxima correspond. It is obvious that, although the maximum sizes obtained by the two methods are in agreement, 0.55 μ by light scattering and 0.66 μ by electron microscopy, the distribution curves are not in agreement, the electron microscope giving a broader distribution. The extent to which convection and coagulation influence this discrepancy will bear further investigation. The possibility of accretion of particles to the walls of the settling chamber and the identity of the electron microscope sample with that in the settling chamber are additional matters that we hope will be looked into in the future.

References

1. Series of N.D.R.C.-O.S.R.D. reports (1941–1945) summarized by Sinclair, D., and La Mer, V. K., *Chem. Revs.* **44**, 245 (1949).

1*a*. Atomic Energy Commission, "Handbook on Aerosols," Washington, D. C., 1950.

2. La Mer, V. K., and Barnes, M., *J. Colloid Sci.* **1**, 71, 79 (1946).

3. Johnson, I., and La Mer, V. K., *J. Am. Chem. Soc.* **69**, 1184 (1947).

4. Kerker, M., and La Mer, V. K., *J. Am. Chem. Soc.* **72**, 3516 (1950).

5. La Mer, V. K., Inn, E., and Wilson, I., *J. Colloid Sci.* **5,** 471 (1950).
6. See reference 1*a*.
7. Series of Columbia University Reports by La Mer, V. K., Goyer, G., and Benedict, J., to U. S. Air Force Geophysical Base Directorate, Cambridge, Mass. (1950–51). Contract AF-19 (122)-164, Progress Reports No. 3, 4, 5, 6, Scientific Report No. 1, and Final Report of 31 March 1952.
8. Gumprecht, R. O., and Sliepcevich, C. M., *J. Phys. Chem.* **57,** 95 (1953).
9. La Mer, V. K., and Gordieyeff, V. A., *Science* **112,** 447 (1950).
10. Hall, C. E., "Introduction to Electron Microscopy," p. 380. McGraw-Hill, New York, 1953.
11. Ford, G. P., and La Mer, V. K., *J. Am. Chem. Soc.* **72,** 1959 (1950).
12. Pound, G. M., Siminad, M. T., and Yang, L., *J. Chem. Phys.* **22,** 1215 (1954).
13. Meir, *Ann. Physik* **31,** 1016 (1910).
14. O'Brien, B., and Wheeler, L., *Phys. Rev.* **21,** 376 (1923).
15. O'Brien, B., *Phys. Rev.* **27,** 93 (1926).
16. Lowan, A. N., "Tables of Scattering Functions for Spherical Particles." Department of Commerce, National Bureau of Standards, Applied Mathematics Series 4. Washington, D. C., 1949.
17. Kerker, M., and Perlee, H., *J. Opt. Soc. Amer.* **43,** 49 (1953).
18. Kerker, M., and Cox, A. L., accepted by the *J. Opt. Soc. Amer.*

LIGHT SCATTERING AND MICELLE STRUCTURE IN THE SYSTEM SODIUM DODECYL SULFATE–SODIUM CHLORIDE–WATER

Lawrence M. Kushner and Willard D. Hubbard

Surface Chemistry Section, National Bureau of Standards, Washington 25, D. C.

Received January 14, 1955

Abstract

Light-scattering measurements have been made on solutions of the detergent, sodium dodecyl sulfate, in water and in sodium chloride solutions up to 0.20 *M*. The micelle weights calculated from the data increase from 11,400 in water to 24,000 to 27,000 in the presence of 0.06 to 0.20 *M* sodium chloride. A discussion of the dependence of the micelle weight on sodium chloride concentration is presented.

Introduction

Light-scattering measurements on solutions of detergent micelles have been interpreted (1, 10, 13) as indicating that the micelles of these detergents increase in size (i.e., molecular weight) as low molecular weight, inorganic electrolyte is added to their solutions. On the other hand, the intrinsic viscosity of sodium dodecyl sulfate micelles in sodium chloride solutions (2) does not reflect such growth.

To provide additional information concerning the effect of electrolyte concentration on micelle size, light-scattering measurements have been made on a number of aqueous solutions of sodium dodecyl sulfate. Concentrations of detergent up to about 1% and concentrations of sodium chloride up to 0.20 *M* have been used.

Experimental

Materials

Two batches of sodium dodecyl sulfate, synthesized by the method described by Shedlovsky (3), were used in these measurements. For one batch the starting dodecyl alcohol was purified by a vacuum fractional distillation; only the center fraction was used. For the other, the alcohol was purified by repeated crystallizations from its melt. No difference was observed between the sodium dodecyl sulfate synthesized from the distilled and from the recrystallized dodecyl alcohol.

The chlorosulfonic acid used to sulfate the alcohol was distilled immediately before use. All other reagents and solvents used in the preparation of the final product conformed to ACS specifications.

Light Scattering

All turbidity measurements were made at 436 mμ with a light-scattering photometer which has been previously described (4). Solutions were prepared by a concentration technique (5).

Refractive index increments at 436 mμ were determined in the usual manner with a differential refractometer (6). The results are represented by the equation

$$\frac{\Delta n}{\Delta c} = 0.120 - 0.020m,$$

where Δn is the refractive index change accompanying a change in the concentration of detergent, Δc, for fixed values of m, the molarity of sodium chloride. The units of $\Delta n/\Delta c$ are milliliters per gram.

RESULTS

Dissymmetry

As has been discussed in an earlier publication (5), a general feature of our light-scattering measurements on detergent solutions is the presence of a measurable dissymmetry, at least at detergent concentrations up to 2.5 g./dl. With sodium dodecyl sulfate solutions, in an average run, the dissymmetry of the solvent is about 1.02. On the addition of detergent the dissymmetry increases to about 1.35 at the critical micelle concentration (CMC). As the detergent concentration is increased beyond the critical micelle concentration, the dissymmetry decreases rapidly to a value of about 1.12 or lower and is then virtually independent of detergent concentration. The effect of addition of electrolyte is merely to shift the region of maximum dissymmetry to lower detergent concentrations by an amount corresponding to the decrease in the critical micelle concentration.

Measurements made on commercial-grade sodium dodecyl sulfate (8) and on pure sodium dodecyl sulfate purposely contaminated with dodecyl alcohol (10) show a peak in the turbidity at the critical micelle concentration corresponding to the peak in dissymmetry as discussed here. However, in none of the runs reported here was any such effect evident (see Fig. 1).

On the basis that micelles of molecular weight about 27,000 are too small to exhibit internal interference with visible light and that the effect of the addition of electrolyte is not what is expected if external interference (7) is important, the observed dissymmetry must be associated with the presence of foreign matter in the solutions which can be solubilized within the detergent micelles above the CMC.

It has been noticed that in the regions of highest dissymmetry, the radiation scattered at 45° fluctuates considerably, whereas this is not the case at either 90° or 135°. This suggests that the foreign particles are quite large but relatively few in number and that the correction to be ap-

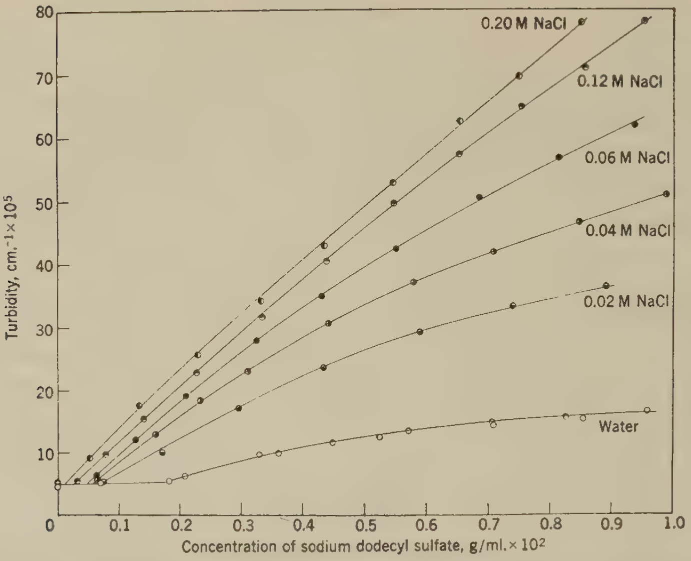

FIG. 1. The dependence of turbidity on the concentration of sodium dodecyl sulfate and on the concentration of sodium chloride.

plied to the light scattered at 90° is considerably less than would be the case if the dissymmetry was due to the micelles. Hence no corrections have been applied to the 90° scattered flux. Although the calculated molecular weights are thus somewhat in error, this error is small and can probably be safely included in the estimated accuracy of ±5% for each of the calculated molecular weights. Further, since the error arising from not

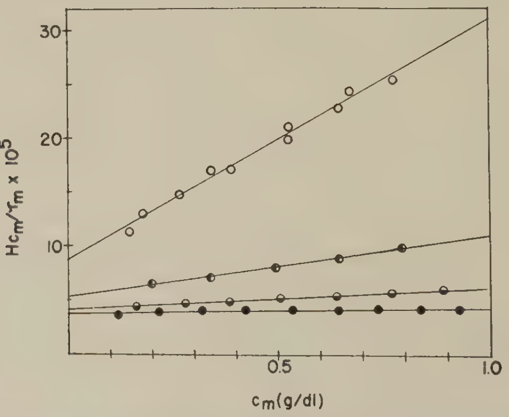

FIG. 2. The dependence of Hc_M/τ_M on c_M for sodium dodecyl sulfate micelles in water and in sodium chloride solutions. ○, in water; ◐, in 0.02 *M* NaCl; ◒ in 0.06 NaCl; ●, in 0.20 *M* NaCl.

TABLE I

The Molecular Weight of Sodium Dodecyl Sulfate Micelles

Solvent	Molecular weight
Water	11,400
0.02 *M* NaCl	19,000
0.03 *M* NaCl	21,700
0.04 *M* NaCl	23,100
0.06 *M* NaCl	24,400
0.08 *M* NaCl	24,400
0.12 *M* NaCl	24,800
0.20 *M* NaCl	26,800

making a dissymmetry correction is in the same direction and of about the same magnitude for each molecular weight calculated, the nature of the dependence of molecular weight on electrolyte concentration cannot be questioned on these grounds.

Turbidity and Calculation of Micelle Weight

Each of the micelle weights was evaluated by the method of Debye (1) in which Hc_M/τ_M is plotted as a linear function of c_M. The quantity c_M is the concentration of micelles in g./ml. and τ_M (cm.$^{-1}$) is that portion of the total turbidity that is due to the micelles. It is assumed that $c_M = c -$ CMC and $\tau_M = \tau - \tau_0$, where c and τ are the total concentration of detergent and the observed turbidity, respectively, CMC is the critical micelle concentration, and τ_0 is the turbidity at the CMC. Since unassociated detergent contributes a negligible amount to the total turbidity of a micellar solution, τ_0 is assumed to be equal to the turbidity of the solvent alone.

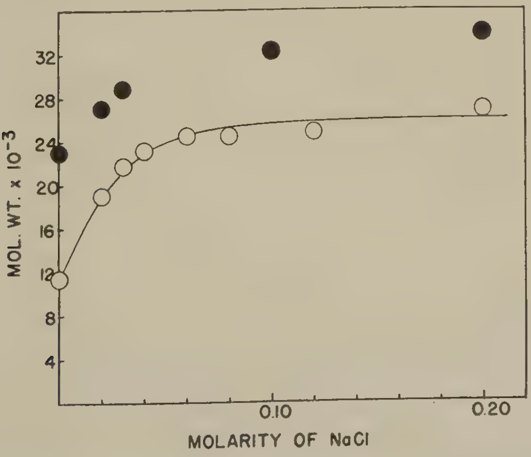

FIG. 3. The dependence of the molecular weight of sodium dodecyl sulfate micelles on the concentration of sodium chloride. ○, this research; ●, Phillips and Mysels (10).

H is the usual light-scattering constant as defined by Debye (1). The value of Hc_M/τ_M at $c_M = 0$ is the reciprocal of the weight-average molecular weight of the micelles.

In each solvent, the critical micelle concentration of the detergent was obtained by extrapolating turbidity data obtained above the CMC back to the turbidity of the solvent. The values obtained in this manner generally fell between those of Corrin and Harkins (9) and those of Phillips and Mysels (10).

Figure 1 presents a number of curves which show the dependence of turbidity on the concentration of sodium dodecyl sulfate and on the concentration of sodium chloride.

In Fig. 2 are shown typical plots of Hc_M/τ_M as a function of c_M in water and in various strengths of sodium chloride. The dependence of the micelle weight on the concentration of sodium chloride is given in Table I and is shown graphically in Fig. 3. Also shown in Fig. 3 are the results of Phillips and Mysels (10) using the green line of mercury (546 mμ). Other values for the molecular weight of sodium dodecyl sulfate micelles are 22,000 in 0.05 to 0.20 M sodium chloride (11) and 23,600 in water (12).

Discussion

In agreement with other light-scattering studies on detergents (1, 10, 13), the data presented here indicate a dependence of the micelle weight on the concentration of simple electrolyte present in the solutions. In water, a micelle weight of 11,400 is obtained. At low concentrations of sodium chloride, the calculated micelle weight increases rapidly with concentration of electrolyte. At electrolyte concentrations above approximately 0.05 M sodium chloride the micelle weight appears to be nearly independent of electrolyte concentration and has a value of about 24,000 to 28,000.

Such data have been interpreted (1, 10) as reflecting an increase in the size of the micelles on the addition of electrolyte. There are, however, some factors which tend to make such an interpretation less certain.

The equation of Debye,

$$\frac{Hc}{\tau} = \frac{1}{M} + 2Bc$$

for the calculation of molecular weights by light scattering is applicable only to uncharged colloidal particles. Doty and Steiner (7), Mysels (14), and Hermans (17) have treated light scattering from solutions of colloidal ions. Their considerations lead one to expect a nonlinear dependence of Hc/τ on c, the nature of the curvature depending on the magnitude of the charge on the colloidal ions and on the amount of simple electrolyte present in the systems. For a system containing colloidal ions of fixed charge and their gegen-ions (i.e., no added simple electrolyte) Hc/τ initially increases rapidly with c. At higher values of c the slope approaches zero. As simple electrolyte is added to the systems the initial slope of the curve becomes smaller and the decrease in slope as c is increased becomes less marked. In the presence of sufficiently high concentrations of electrolyte, the curvature is virtually eliminated and Hc/τ is, to all intents and purposes, a linear function of c. For lower values of the charge on the colloidal ion, the degree of curvature, even in the absence of electrolytes, is less. Of course, as the charge becomes zero, the simple Debye equation is applicable regardless of the quantity of electrolyte present. The experimental data of Doty and Steiner (7) for bovine serum albumen at various pH values show these effects quite clearly. In the light of this experimental verification of the characteristics of light scattering from solutions of charged colloidal particles, one must examine quite closely the molecular weights of detergent micelles obtained by a simple linear extrapolation of Hc_M/τ_M to $c_M = 0$ (i.e., the CMC).

Mysels' equation III (14), giving the dependence of Hc_M/τ_M on c_M for various values of p, the micellar charge, and x, the concentration of simple electrolyte, is:

$$\frac{Hc_M}{\tau_M} = \frac{1}{M}\left\{1 + \frac{p}{[1 + (2xM/c_M p)]}\right\}.$$

M is the molecular weight of the micelle. If one considers hypothetical detergent micelles of $M = 25{,}000$ and $p = 20$, it is possible to calculate, by means of this equation, the expected dependence of Hc_M/τ_M on c_M. In the absence of added electrolyte (x is taken as equal to the CMC expressed in appropriate units), a curve of large initial slope is obtained. The slope decreases as c_M increases and it becomes apparent that, from an experimental point of view, Hc_M/τ_M must be precisely evaluated at low values of c_M (below about 0.2 g./dl.) in order to obtain the correct value of the intercept at $c_M = 0$. Unfortunately, it is precisely in this region that errors in Hc_M/τ_M are the largest, owing to uncertainties in the correct value of the CMC and to the very low turbidities involved. If one were to make a linear extrapolation using the more precise, higher concentration data, as is usually done, a micelle weight would be calculated which would be appreciably lower than the correct value. If, on the other hand, one increases x to between 0.06 and 0.1 equiv./l. by adding simple electrolyte to the system, the curves become practically linear and of small slope. It is clear that by adding electrolyte to the systems, the need for data at low c_M is eliminated and a linear extrapolation of the higher concentration data is justified and will provide the correct value of M.

Mention must be made of the fact that notwithstanding the uncertainties in Hc_M/τ_M at low c_M, the data at c_M up to about 0.8 g./dl. in the absence of added electrolyte do not show the anticipated curvature. This strongly suggests that some effect, unaccounted for by theory, is operative and the significance of the intercept at $c_M = 0$ is still more uncertain. Most likely the difficulty arises from the assumption that the charge on the micelles is independent of their concentration. Such an assumption is probably least valid in the absence of added simple electrolyte. The electrophoretic mobility of sodium dodecyl sulfate micelles (15) is indeed dependent both on the concentration of micelles and on the concentration of simple electrolyte.

On the basis of the preceding discussion one cannot unhesitatingly ascribe the rapid increase of the calculated micelle weight at low electrolyte concentration to a real growth in the size of the micelle. The micelle weights evaluated in the presence of 0.06 M to 0.20 M sodium chloride are probably reliable and indicate relatively little, if any, increase in the size of the micelles. This is in agreement with the results of viscosity measurements (2), and one wonders whether or not at lower electrolyte concentrations, the primary effect of the addition of electrolyte is to increase the micelle size, or merely to increase the possibility of independent fluctuations of the micelles, thus increasing the turbidity of the solutions.

A micelle weight of 26,000, which is approximately the value obtained in the presence of swamping amounts of electrolyte, corresponds to 90 molecules of sodium dodecyl sulfate per micelle. The total volume of this number of detergent molecules is consistent with that of a sphere of diameter twice the length of a sodium dodecyl sulfate molecule, as proposed by Hartley (16). Whether a stable micelle, having as an important dimension twice the length of the detergent molecule, can be formed from significantly less than this number of sodium dodecyl sulfate molecules is problematical.

The experiments of Debye and Anacker (13) with hexadecyl trimethyl ammonium bromide in the presence of large amounts of simple electrolyte do no doubt reflect a real increase in the size of the scattering units with increasing electrolyte concentration. However, their measurements were made so close to the salting out region of their detergent that there is a possibility they were determining the particle weight of crystallites of detergent rather than micelles.

REFERENCES

1. DEBYE, P., *Ann. N. Y. Acad. Sci.* **51**, (Art. 4), 575 (1949).
2. KUSHNER, L. M., DUNCAN, B. C., AND HOFFMAN, J. I., *J. Research Natl. Bur. Standards* **49**, 85 (1952) RP2346.
3. SHEDLOVSKY, L., *Ann. N. Y. Acad. Sci.* **46**, (Art. 6), 427 (1946).
4. KUSHNER, L. M., *J. Opt. Soc. Amer.* **44**, 155 (1954).
5. KUSHNER, L. M., AND HUBBARD, W. D., *J. Phys. Chem.* **58**, 1163 (1954).
6. BRICE, B. A., AND HALWER, M., *J. Opt. Soc. Amer.* **41**, 1033 (1951).
7. DOTY, P., AND STEINER, R. F., *J. Chem. Phys.* **20**, 85 (1952).

8. Kushner, L. M., *Soap and Chemical Specialties* **30** (No. 5), 50 (1954).
9. Corrin, M. L., and Harkins, W. D., *J. Am. Chem. Soc.* **69,** 683 (1947).
10. Phillips, J. N., and Mysels, K. J., *J. Phys. Chem.* **59,** 325 (1955).
11. Hakala, N. V., Ph.D. Thesis, University of Wisconsin, Madison, 1943.
12. Philippoff, W., *Discussions Faraday Soc.* No. **11,** 96 (1951).
13. Debye, P., and Anacker, E. W., *J. Phys. & Colloid. Chem.* **55,** 644 (1951).
14. Mysels, K. J., *J. Phys. Chem.* **58,** 303 (1954).
15. Stigter, D., and Mysels, K. J., *J. Phys. Chem.* **59,** 45 (1955).
16. Hartley, G. S., "Aqueous Solutions of Paraffin Chain Salts." Hermann et Cie, Paris, 1936.
17. Hermans, J. J., *Proc. Intern. Colloq. Macromolecules, Amsterdam, 1949,* p. 238, 1950.

SOME STUDIES OF SPONTANEOUS EMULSIFICATION[1]

Homer A. Hartung[2] **and O. K. Rice**

Department of Chemistry, University of North Carolina, Chapel Hill, North Carolina

Received March 31, 1955; revised July 18, 1955

ABSTRACT

Kaminski and McBain have reported that spontaneous emulsification takes place when *p*-xylene is carefully placed on aqueous solutions of dodecylamine hydrochloride. In the present work it has been found that spontaneous emulsification does not occur if the dodecylamine hydrochloride is carefully purified, although apparently stable emulsions can be formed by shaking. These emulsions do not seem to be in thermodynamic equilibrium. A solution of unsaturated amine hydrochlorides will not produce emulsification even on shaking, but when mixed with the solution of purified dodecylamine hydrochloride the resulting solution is capable of spontaneously emulsifying *p*-xylene. Solutions of the purified dodecylamine hydrochloride were tested with a number of organic liquids and in no case did spontaneous emulsification occur. Some impurity, presumably an unsaturated one, thus seems to be essential in order to induce spontaneous emulsification of hydrocarbons by aqueous dodecylamine hydrochloride.

Kaminski and McBain (1) reported that emulsification proceeds spontaneously when *p*-xylene is carefully placed on top of aqueous solutions of dodecylamine hydrochloride at room temperature, if the concentration of detergent solution is 0.1 N or greater, and some further observations were made by Brady and Huff (2). M. H. Peterson, in this laboratory, verified the observations of Kaminski and McBain, using solutions made from a commercial sample of amine without exacting purification. A clear solution of the detergent remained on the bottom, an opaque emulsion in the middle, and a clear layer of hydrocarbon on top, and the resulting system looked like a three-phase system in equilibrium. It was the original purpose of this work to investigate this point, and it was thought that there might be some interesting connections with the behavior of a binary liquid system containing small amounts of a third component near its critical point.

However, when the experiments were repeated with dodecylamine hydrochloride and *p*-xylene that were purified with some care, we found that spontaneous emulsification did not occur even after long standing.

---

[1] Work supported by the U. S. Office of Naval Research.

[2] Present address, Research Laboratory, Linde Air Products Company, Tonawanda, New York.

Stable emulsions of a different character were formed when the mixture was well shaken, if the concentration of detergent solution was greater than about 0.01 *N*. With concentrations between 0.01 and 0.05 *N* it was easy to get what looked like three phases. With greater concentrations very large amounts of the hydrocarbon were emulsified, and it was difficult to get a clear upper layer. In all cases these emulsions were thick and viscous, some seeming almost solid. After standing for a day or so, the emulsions appeared inhomogeneous to the eye upon careful examination, but after this no visible change took place. The boundary between the aqueous solution and the emulsion was always sharp and flat, but that between the emulsion and the hydrocarbon usually was uneven and billowy. In some cases, for no apparent reason, the aqueous solution remained cloudy after the emulsion was formed. In other cases it became quite clear after settling. The top layer of hydrocarbon was clear if formed.

Emulsions formed by shaking at room temperature invariably decreased in volume when kept at 40° or 50° C. for a day or more, often seeming to collapse away from the walls of the container very slowly for awhile and then remaining stable for a long time thereafter. Emulsions formed at room temperature with detergent solution just slightly stronger than 0.01 *N* disappeared completely at 40° C. When returned to room temperature the volume of an emulsion did not seem to change so long as the mixture was not agitated.

ANALYSES

Two aqueous solutions with purified detergent were analyzed for chloride ion after the emulsion systems had been kept at 25°C. and atmospheric pressure for some time. The results were:

Run	*No. 1*	*No. 2*
Normality of Cl^- in aqueous solution before emulsification	0.0108	0.0142
Normality of Cl^- in final solution below emulsion	0.0108	0.0137

The analysis of Kaminski and McBain (1) in the case of the spontaneous emulsion at a somewhat higher concentration of detergent indicates a change in the normality of Cl^- comparable to that shown in our Run No. 2.

If the emulsion were truly a three-phase system in equilibrium, with only three components (water, hydrocarbon, and amine hydrochloride), then according to the phase rule the final concentration of Cl^- should have been the same in the two cases. Since it instead remained close to the original concentration, we might conclude that these systems had not reached an equilibrium state. This conclusion could be upset if the amine itself were appreciably more soluble in the xylene than the hydrochloride.

We believe, in any event, that no true thermodynamic equilibrium is established, and that this system is similar in this respect to other simple emulsions (3).

Emulsions with Other Organic Liquids

The best available organic liquids used without further purification gave the following results with 0.012 and 0.076 *N* solutions of the purified dodecylamine hydrochloride: benzene and toluene behaved almost exactly like *p*-xylene; ethyl ether, dibutyl phthalate, phenol and carbon tetrachloride gave no stable emulsions on shaking; benzaldehyde formed a thick and very viscous emulsion; and cyclohexane seemed to give less viscous emulsions than *p*-xylene, but still did not appear to be in thermodynamic equilibrium, the emulsion setting noticeably in the course of a few weeks. As with the *p*-xylene emulsions, an increase in temperature seemed to make the volume of an emulsion if formed, decrease slowly for a while and to make the emulsions slightly less viscous. No spontaneous emulsification occurred.

Spontaneous Emulsification

Since spontaneous emulsification apparently occurred only if the dodecylamine hydrochloride was impure, we investigated this point further. To this end we obtained a sample of "Armeen 12D," a mixture of amines, which is manufactured by Armour and Company and is stated to be 90% dodecylamine, 9% tetradecylamine, and 1% octadec-9-eneamine, from which we prepared a hydrochloride (called 12D-HCl). Some *p*-xylene was pipetted onto a 0.3 *N* solution of 12D-HCl, with as little mixing as possible. Almost immediately a faint but definite emulsion layer became visible. A 0.5 *N* solution of 12D-HCl caused much more pronounced spontaneous emulsification. There is little reason to believe that these effects are due to tetradecylamine hydrochloride; however, it seems reasonable to think that the unsaturated material might cause the spontaneous emulsification, even though it was present in such small amounts that organic unsaturation could not be detected in the solutions of 12D-HCl by the usual tests.

There is no commercial source of reasonbly pure unsaturated amine or amine hydrochloride. However, Armour and Company, through the courtesy of Dr. H. J. Harwood, kindly supplied us with a sample of "Armeen S," a commercial quality amine containing a large proportion of unsaturated C_{18} amines. The hydrochloride (S-HCl) prepared from it was not very soluble in water. When either xylene or benzene was placed on top of a saturated S-HCl solution nothing happened. Even vigorous shaking caused no stable emulsification. However, solutions made up by mixing more concentrated solutions of the highly purified dodecylamine hydrochloride with water saturated with S-HCl did cause spontaneous emulsification of benzene and xylene. It is clear, therefore, that some impurity, probably an unsaturated amine hydrochloride, is required. It is interesting that spontaneous emulsification can be brought about by a mixture of two solutions, neither of which alone is capable of causing it. It is almost certain that the effect studied by Kaminski and McBain and by Brady and Huff was caused by impurities in their dodecylamine hydrochloride.

All of the systems which emulsified spontaneously gave much more opaque and viscous emulsions of far greater volume when agitated.

Experimental Details

a. Preparation of Pure Dodecylamine Hydrochloride. As starting material we used Matheson dodecylamine with a melting range of about 24°–28°C. Distillation in a spinning band column under vacuum gave several middle fractions with a narrow boiling range and a total freezing range of 27.6° to 28.1°C. These fractions from two distillations were combined. An excess of concentrated HCl solution was added and amine hydrochloride was precipitated by partial evaporation on a steam plate. The product was recrystallized several times from water-alcohol and several times from alcohol-acetone mixtures. Very nice white needle-like crystals were obtained. Well over half of the amine collected from the vacuum distillation was purposely discarded in the recrystallizations to enhance the purity of the product.

b. P-Xylene. Matheson white label *p*-xylene was used. After five fractional crystallizations it had no detectable melting range on a thermometer graduated to 0.1°C.

c. Preparation of "12D-HCl." Excess HCl solution was added to Armeen 12D and the mixture was heated, stirred, and then cooled in ice. The precipitate was recrystallized once from water. It was crystalline to some extent, but was quite different from the purified dodecylamine hydrochloride described in part (*a*), was not so easy to handle, and did not form any large or needle-like crystals.

d. Preparation of "S-HCl." Concentrated HCl solution was added to "Armeen S" in excess, giving a product with the consistency of soft soap. However, hydrochloride precipitated from a benzene solution of Armeen S with dry HCl was not much better. Both products were used.

e. Analyses. The chloride ion in the aqueous layers was determined by a potentiometric titration with dilute silver nitrate solutions. A pH meter with glass electrode (Beckman model G) was used, the calomel electrode being replaced by a silver electrode made from thermal decomposition of silver oxide paste on platinum wire. The solutions were made strongly acid with HNO_3 to keep changes of pH to a minimum. The e.m.f. then depended principally on the silver ion concentration, which in turn depended on the chloride concentration, and gave a sharp end-point. It was necessary to allow about 5 minutes between addition of solution and reading of the pH meter near the end-point. Successive trial determinations on a dodecylamine hydrochloride solution gave concentrations of 0.0444, 0.0443, and 0.0444 *N*.

References

1. Kaminski, A., and McBain, J. W., *Proc. Roy. Soc. (London)* **A198**, 447 (1949).
2. Brady, A. P., and Huff, H., Abstract No. 41, Div. Colloid Chem., 124th Meeting, American Chemical Society, September, 1953.
3. See, e.g., Cockbain, E. G., *Trans. Faraday Soc.* **48**, 185 (1952).

SEDIMENTATION OF NATURALLY OCCURRING POLYELECTROLYTES

D. A. I. Goring and Carol Chepeswick

Maritime Regional Laboratory, National Research Council, Halifax, Nova Scotia

Received May 2, 1955

ABSTRACT

An invariance of sedimentation rate with molecular weight was observed between certain concentrations for the polyelectrolytes sodium carrageenate and sodium alginate. This result was explained by assuming a network model which, at low concentrations, breaks up to permit sedimentation of the molecules individually. By applying the Kozeny equation to the flow through the network the effective specific volume and surface of the molecules were determined.

INTRODUCTION

It is known that the sedimentation constant is insensitive to the chain length of high molecular weight polymers (1, 2). Results obtained recently with polysaccharides from seaweeds have clearly demonstrated this point for naturally occurring polyelectrolytes (3, 4). The substances studied were sodium carrageenate, a sulfated polygalactose prepared from *Chondrus crispus*, and sodium alginate from a variety of brown algae. For wide changes in molecular weight, the graphs of the sedimentation constant, s, vs. the concentration, c, were concurrent above a certain concentration. Below this concentration the curves separated to give appropriately different values of $(s)_{c\to 0}$. Similar behavior has been reported for two samples of deoxypentose nucleic acid of different molecular weights (2).

In this paper an attempt will be made to explain these results on the basis of an analogy proposed by Signer and Egli (5) and later by Fessler and Ogston (6). Above the critical concentration, the sedimenting system is assumed to be an interconnecting fibrous network moving through the solvent. It may then be treated as a permeable bed of fibrous material by the semiempirical Kozeny equation as modified by Sullivan (7) and Robertson and Mason (8). If the pore size is smaller than the length of a molecule, changes in molecular weight, M, will have little effect on the flow characteristics of the network. This would produce the observed invariance of s with molecular weight. Below the critical concentration the network breaks up. The molecules sediment singly and variations of s with M are observed. The present work will be concerned only with the region of concentration in which the network may be assumed to be intact.

THEORETICAL

The model assumed is a random network of long cylindrical fibers of constant radius. The charge and associated counter ions are assumed to have no direct effect on the flow. However, the double layer will make the network rigid as well as binding a layer of solvent. This model is now considered a bed of fibrous material for which the permeability, K, may be written (7),

$$K = \frac{Q\eta L}{AP}, \tag{1}$$

where Q is the volume of solvent flow per unit time, η the viscosity of the solvent, L the length of the bed, A the area of cross section of the bed, and P the fall in pressure across the bed. For sedimentation, K is replaced by a function of s, $f(s)$. To obtain $f(s)$ we consider a boundary at a distance x from the center of the rotor. Let the bottom of the cell be r from the center of the rotor. In Eq. [1], η remains the viscosity of the solvent; L and A become the length of the sedimenting column $(r - x)$ and the area of cross section of the cell. The pressure, P, may be replaced by the total sedimenting force on the molecules per unit area of cross section. Thus, if ρ is the density of the solvent and $\bar{v}$ the partial specific volume of the unhydrated solute,

$$P = \omega^2 xc(r - x)(1 - \rho\bar{v}), \tag{2}$$

where c is the concentration of the solute and ω the angular velocity. The rate of flow will be given by

$$Q = \frac{dx'}{dt}\epsilon A, \tag{3}$$

where dx'/dt is the true velocity of the boundary with respect to the solvent and ϵ is the void fraction or the porosity. The void fraction is the fraction available for flow of any given plane perpendicular to the direction of flow. It is also the fraction of any given volume available for fluid flow. Enoksson's correction will be necessary to allow for the back flow of solvent owing to the piling up of material at the bottom of the cell (9). If the hydrated solute is assumed incompressible,

$$\frac{dx'}{dt} = \frac{1}{\epsilon}\frac{dx}{dt}, \tag{4}$$

where dx/dt is the observed velocity of the boundary.

From Eqs. [3] and [4]

$$Q = \frac{dx}{dt}A. \tag{5}$$

Substituting in Eq. [1]

$$K = \frac{\eta}{c(1-\rho\bar{v})}\frac{dx/dt}{\omega^2 x} = \frac{\eta s}{c(1-\rho\bar{v})} = f(s), \qquad [6]$$

which is identical with the relationship proposed by Signer and Egli (5).

The Kozeny equation can be written (7, 8),

$$K = \frac{\varphi}{k_0 S_0^2}\frac{\epsilon^3}{(1-\epsilon)^2}, \qquad [7]$$

where φ and k_0 are factors determined, respectively, by the orientation and shape of the channels and S_0 is the surface area per effective unit volume of the solid. If α is the effective volume of the hydrated molecules for unit weight of solute, then

$$\epsilon = 1 - \alpha c. \qquad [8]$$

Also, the surface area, σ, per unit weight of solute will be given by

$$\sigma = \alpha S_0. \qquad [9]$$

Substituting for ϵ and S_0 in Eq. [7] we have

$$K = \frac{\varphi}{k_0 \sigma^2}\frac{(1-\alpha c)^3}{c^2}. \qquad [10]$$

If $f(s)$ from Eq. [6] is now substituted for K in Eq. [10], we obtain

$$s = \frac{\varphi(1-\rho\bar{v})}{\eta\sigma^2}\left\{\frac{(1-\alpha c)^3}{k_0 c}\right\}. \qquad [11]$$

Equation [11] is the same as that proposed by Fessler and Ogston (6), except that the term $(1 - \alpha c)^3$, which is ϵ^3, becomes ϵ^2 in their relationship. The difference arises because Fessler and Ogston apply the Enoksson factor directly to the Kozeny equation. In the present derivation it is shown that the Enoksson factor is canceled by the factor ϵ necessary to relate the rate of flow through a plug to the true velocity of the boundary (see Eqs. [3], [4], and [5]).

Before Eq. [11] can be used it is necessary to evaluate the shape factor, k_0. The results of Robertson and Mason (8) show that at porosities lower than 0.8, k_0 is constant. Fessler and Ogston (6) assumed k_0 constant in their treatment. However, in the case of a sedimenting solute at a concentration of less than 1% it is likely that the effective void fraction is greater than 0.8. For such high porosities (0.8 → 0.98) Sullivan (7) has shown that k_0 changes with ϵ in a manner similar to that predicted theoretically by Emersleben (10) for cylinders with axes parallel to flow. The transition to random orientation is achieved by the orientation factor

$\varphi = \overline{\cos^2 \theta}$, where θ is the angle between the direction of flow in a pore and the axis of the bed. The value of φ will be taken as 0.5 (11, 12).

The experimental use of Eq. [11] involves the arbitrary choice of a value of the effective specific volume, α. The quantity $(1 - \alpha c)^3/k_0 c$ is then evaluated for a series of concentrations, k_0 values being obtained from the data of Sullivan (7). The concentration is assumed constant during a run. The graph of s vs. $(1 - \alpha c)^3/k_0 c$ is drawn. Several such curves are constructed for various values of α. The graph giving the best straight line through the origin is then assumed to correspond to the correct value of α. From its slope the effective specific surface, σ, can be calculated. The equivalent pore radius, $\bar{r}$, can be computed for any value of the concentration (13) from

$$\bar{r} = \frac{2(1 - \alpha c)}{\sigma c}. \qquad [12]$$

If the total drag is assumed to arise from a cylindrical fiber, the diameter, D, and length per gram of solid, L_s, of the fiber may readily be computed from

$$\alpha = \frac{\pi D^2 L_s}{4}$$

and

$$\sigma = \pi D L_s. \qquad [13]$$

From L_s it would be possible to calculate the length of the individual molecules making up the network if the molecular weight were known. Clearly, molecular weights derived from the Mandelkern-Flory equation (14) cannot be used for this purpose since they are based on a random coil model. However, by a treatment similar to that of Scheraga and Mandelkern (15), a molecular weight value, M_s, can be obtained by assuming a prolate ellipsoid of large axial ratio, p. The intrinsic viscosity is given by

$$[\eta] = \frac{N \nu V_e}{100 M_s}, \qquad [14]$$

where N is the Avogadro number, ν is a shape factor which depends on the axial ratio, and V_e is the volume of the effective hydrodynamic ellipsoid. If there is no change in α when the network breaks up

$$V_e = \frac{M_s \alpha}{N}, \qquad [15]$$

whence from Eq. [14]

$$[\eta] = \frac{\nu \alpha}{100}. \qquad [16]$$

Thus ν can be found, and a corresponding value of p for the prolate ellipsoid can be obtained from the tables of Mehl, Oncley, and Simha (16).

The Svedberg equation is

$$s = \frac{M_s(1 - \bar{v}\rho)}{Nf}, \tag{17}$$

where f is the frictional coefficient at infinite dilution. The frictional coefficient, f_0, of a sphere having the same effective volume as the molecule is given by

$$f_0 = (162\,\pi^2 V_e)^{1/3}\eta, \tag{18}$$

which from Eq. [15] may be written

$$f = \left(\frac{162\pi^2 M_s}{N}\right)^{1/3} \eta \left(\frac{f}{f_0}\right). \tag{19}$$

Substituting for f in Eq. [17]

$$M_s^{2/3} = \frac{(162\pi^2 N^2 \alpha)^{1/3} \eta s (f/f_0)}{(1 - \bar{v}\rho)}. \tag{20}$$

Svedberg and Pedersen (17) have compiled tables giving f/f_0 in terms of the axial ratio p. Thus M_s may be evaluated and the length of the molecule, l, is given by

$$l = \frac{M_s L_s}{N}. \tag{21}$$

RESULTS

The sedimentation rate was measured with a Spinco ultracentrifuge at 40° C. by the method outlined previously (3). The preparation and fractionation of the polysaccharides have also been described (3, 4). An acetate buffer of pH 5.5 was used throughout at an ionic strength of 0.2 for sodium carrageenate and 0.05 for sodium alginate. The values of $(s_{40}^0)_{c\to 0}$ and the intrinsic viscosity of the various fractions are given in Table I.

TABLE I

Physical Constants of the Fractions of Sodium Carrageenate and Alginate

Polyelectrolyte	Fraction	$[\eta]$ ($g.^{-1}\,dl.$)	$(s_{40}^0)_{c\to 0}$ S
Sodium carrageenate	F60	13.1	13.2
	FC100	11.7	11.8
	FC120-A	7.0	8.0
Sodium alginate	Protonal H	14.1	7.4
	23 B	3.6	4.3

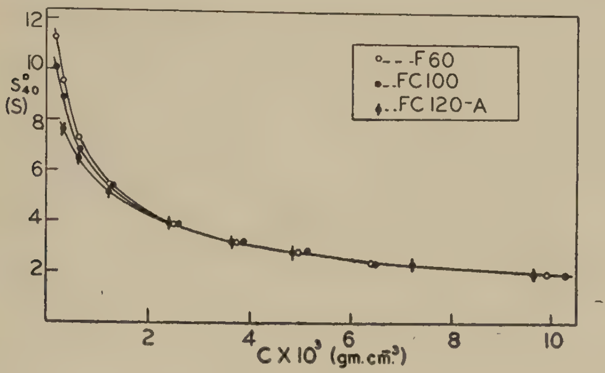

FIG. 1. s^0_{40} vs. c for fractions of sodium carrageenate shown in Table I.

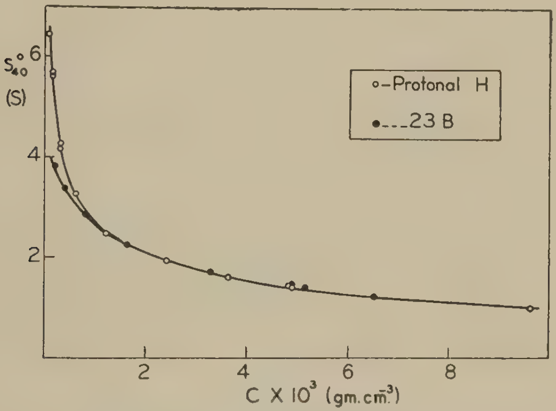

FIG. 2. s^0_{40} vs. c for fractions of sodium alginate shown in Table I.

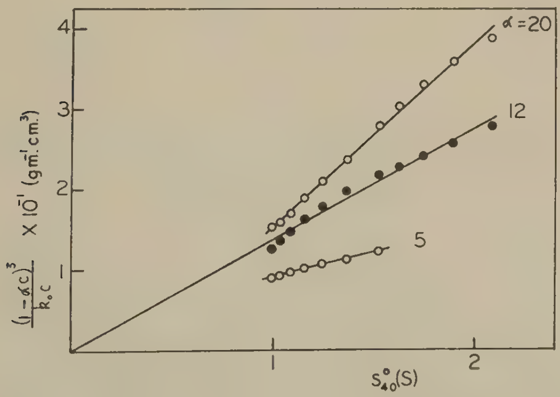

FIG. 3. $(1 - \alpha c)^3/k_0c$ vs. s^0_{40} for carrageenate network.

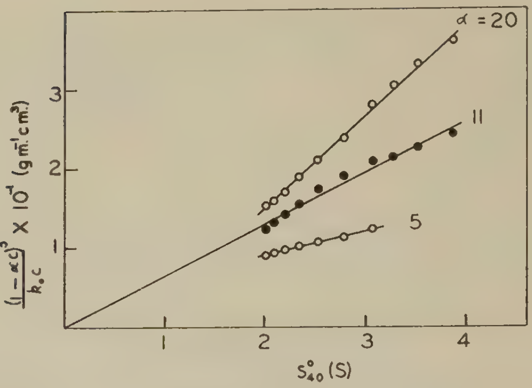

FIG. 4. $(1 - \alpha c)^3/k_0 c$ vs. s^0_{40} for alginate network.

The graphs of s^0_{40} vs. c are given in Figs. 1 and 2. For sodium carrageenate (Fig. 1) s^0_{40} was independent of molecular weight from concentrations of 0.01 g. cm.$^{-3}$ down to 0.0025 g. cm.$^{-3}$; below this concentration the graphs of s^0_{40} vs. c separated, and it was assumed that the network model no longer applied. As shown in Fig. 2 this range of concentration for sodium alginate was 0.01 g. cm.$^{-3}$ to 0.002 g. cm.$^{-3}$.

The graphs for $(1 - \alpha c)^3/k_0\, c$ vs. s^0_{40} for α values from 5 to 20 are shown in Figs. 3 and 4. The best straight line through each set of points was established by the method of least squares. By trial and error the value corresponding to a line through the origin was obtained. For α below and above this critical value, the lines passed, respectively, above and below

TABLE II

Dimensions of the Network for Sodium Carrageenate and Alginate

Polyelectrolyte	α (cm.^{3} g.$^{-1}$)	$\sigma \times 10^{-6}$ (cm.^{2} g.$^{-1}$)	D (A.)	$L_s \times 10^{-12}$ (cm. g.$^{-1}$)	$L_z \times 10^{-12}$ (cm. g.$^{-1}$)
Sodium carrageenate	11	49	89	18	99
Sodium alginate	12	77	62	39	153

TABLE III

Molecular Weights, Lengths, and Equivalent Pore Radii for Fractions of Sodium Carrageenate and Alginate

				$\bar{r}$ (A.)	
Polyelectrolyte	Fraction	M_s	l (A.)	$c = 0.01$ g. cm.$^{-3}$	$c = 0.0025$ g. cm.$^{-3}$
Sodium carrageenate	F60	790,000	2400	360	1580
	FC100	630,000	1900		
	FC120-A	290,000	900		
Sodium alginate	Protonal H	290,000	1900	230	1270 (c = 0.002 g. cm.$^{-3}$)
	23 B	74,000	500		

the origin. The line through the origin represented a value of α which satisfied Eq. [11]. From the slope of the line, $(1 - \rho\bar{v})/\eta\sigma^2$ was determined, from which σ was computed. Values obtained for α, σ, D, and L_s are given in Table II. Also included is the chain length per gram, L_x, of the extended molecule based for carrageenate on the dimensions derived by Bayley (18) and for alginate on a Fisher-Taylor-Hirschfelder model. In Table III values of M_s and l are given for each of the fractions. Also included are values of the equivalent pore radius for the highest and lowest concentrations in the range for which the network model was applied.

DISCUSSION

The invariance of s with molecular weight makes ultracentrifugation unsuitable for studying polydispersity of such molecules. For if the concentration is low enough to be in the region where molecules sediment separately, the resolution is poor. At higher concentrations the rate of sedimentation is independent of M. In addition, the shape of the peak is governed largely by the concentration dependence. This lack of sensitivity to polydispersity is advantageous when studying the naturally occurring polyelectrolytes. For although a given component may be polydisperse a sharp peak will be obtained; another component may then give rise to another peak, thereby permitting a differentiation of components in spite of each component's being present in a range of molecular weights.

The values obtained for α are an order of magnitude higher than the specific volume measured pycnometrically. However, α represents an effective partial specific volume and therefore includes water of solvation around the chain as well as closed pores or occluded liquid within the network. Robertson and Mason (8) and Goring and Mason (13) have found values of α from 1.5 to 5 from the permeability of cellulose pads. Fessler and Ogston (6) have reported values of 4.2 and 18 for polysarcosine and nucleic acid, respectively. It seems likely, therefore, that a relatively large volume of solvent is immobilized by the network.

At the concentrations at which the network begins to disintegrate, the pore radius and the molecular length should be similar. This is the case as shown in Table III. However, the values of $\bar{r}$ at the low concentrations are greater than the lengths of the shorter molecules. This might be expected since molecular interaction would tend to retain the structure for pore sizes which were somewhat greater than the molecular length.

The length per gram, L_s, of the fibers in the network is considerably shorter than L_x for the fully extended chain (Table II). This implies some coiling. A possible model is shown in Fig. 5, based on a helical configuration of the molecule. Each fiber is made up of a long regular coil. Water is bound in and around the coil to give the effective diameters shown in Table II. Watson and Crick (19) and others (20, 21) have proposed helical struc-

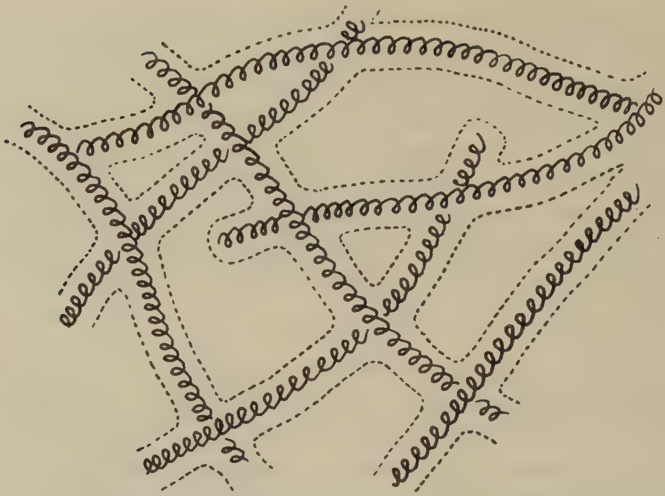

FIG. 5. A possible model of the polyelectrolyte network. The dotted lines are the effective hydrodynamic boundaries of the fibers. The full lines are the coiled polyelectrolyte chains.

tures for nucleic acid. It is realized that the present analysis presents no direct evidence for a helix. However, such a configuration would fit previous viscometric (22, 23) and light-scattering (24) observations on sodium carrageenate which indicated a rodlike shape in buffers of relatively high ionic strength. When the effective charge on the molecule increased at low ionic strength, the helix would be capable of considerable expansion, giving the observed large increase in viscosity (23).

The treatment lacks a rigorous theoretical background. A more detailed derivation of the flow characteristics for random networks of low porosity might profitably be used in the above manner.

ACKNOWLEDGMENT

The authors wish to thank Dr. E. Gordon Young for his interest and advice throughout the work.

REFERENCES

1. MOSIMANN, H., *Helv. Chim. Acta* **26,** 61 (1943).
2. PEACOCKE, A. R., AND SCHACHMAN, H. K., *Biochim. et Biophys. Acta* **15,** 198 (1954).
3. GORING, D. A. I., AND YOUNG, E. G., *Can. J. Chem.* **33,** 480 (1955).
4. VINCENT, D. L., GORING, D. A. I., AND YOUNG, E. G., in press, *J. Appl. Chem.* **5,** (1955).
5. SIGNER, R., AND EGLI, H., *Proc. Intern. Colloq. Macromolecules, Amsterdam, 1949,* pp. 179–192.
6. FESSLER, J. H., AND OGSTON, A. G., *Trans. Faraday Soc.* **47,** 667 (1951).
7. SULLIVAN, R. R., *J. Appl. Phys.* **12,** 503 (1941).

8. ROBERTSON, A. A., AND MASON, S. G., *Pulp & Paper Mag. Can.* **50,** 1 (1949).
9. ENOKSSON, B., *Nature* **161,** 934 (1948).
10. EMERSLEBEN, O., *Physik. Z.* **26,** 601 (1925).
11. GORING, D. A. I., AND MASON, S. G., *Can. J. Research* **B28,** 307 (1950).
12. SULLIVAN, R. R., AND HERTEL, K. L., *Advances in Colloid Sci.* **1,** 37 (1942).
13. GORING, D. A. I., AND MASON, S. G., *Can. J. Research* **B28,** 323 (1950).
14. MANDELKERN, L., AND FLORY, P. J., *J. Chem. Phys.* **20,** 212 (1952).
15. SCHERAGA, H. A., AND MANDELKERN, L., *J. Am. Chem. Soc.* **75,** 179 (1953).
16. MEHL, J. W., ONCLEY, J. L., AND SIMHA, R., *Science* **92,** 132 (1940).
17. SVEDBERG, T., AND PEDERSEN, K. O., "The Ultracentrifuge." Clarendon Press, Oxford, 1940.
18. BAYLEY, S. T., *Biochem. et Biophys. Acta* **17,** 194 (1955).
19. WATSON, J. D., AND CRICK, F. H. C., *Nature* **171,** 737 (1953).
20. WILKINS, M. H. F., STOKES, A. R., AND WILSON, H. R., *Nature* **171,** 738 (1953).
21. FRANKLIN, R. E., AND GOSLING, R. G., *Nature* **171,** 740 (1953).
22. MASSON, C. R., AND CAINES, G. W., *Can. J. Chem.* **32,** 51 (1954).
23. MASSON, C. R., AND GORING, D. A. I., *Can. J. Chem.* **33,** 895 (1955).
24. GORING, D. A. I., *Can. J. Chem.* **31,** 1078 (1953).

ELECTROOSMOTIC FLOW IN HOMOIONIC KAOLINITE

E. Vernon Ballou[1]

Soil Mechanics Laboratory, Division of Applied Science, Harvard University,
Cambridge, Massachusetts

Received May 9, 1955

Abstract

The electroosmotic flow of water was investigated in homogeneous systems of kaolinite clay, as a function of the adsorbed counter-ion and the water content of the systems. The results were compared with the predictions of various theories of electroosmotic flow. Although the nature of the counter-ion affected the rate and the direction of flow, no simple interpretation in terms of ion hydration was warranted. The relation of electroosmotic flow to hydraulic permeability at various water contents was compatible with the Helmholtz-Smoluchowski electrokinetic equations. The equations of Schmid for fine-pored systems were not applicable.

List of Symbols

a = cross-sectional area of pores.
A = counter-ion concentration per unit volume of pore water.
C = constant including factors independent of water content.
D = dielectric constant.
E = applied voltage gradient (volts/cm.).
F_0 = the Faraday electrochemical constant.
I = the electric current through the sample.
k_e = coefficient of electroosmotic permeability per unit potential drop (cm.^{3} volume flow/cm.^{2}/volt/cm./sec.).
k_i = coefficient of electroosmotic permeability per unit current (cm.^{3} volume flow/coulomb).
k_h = coefficient of hydraulic permeability (cm.^{3} volume flow/cm.^{2}/cm. water pressure/sec. for 1 cm. length).
q = effective cross-sectional area available to electroosmotic flow.
r = radius of uniform pores.
V = volume of liquid flow per second.
ζ = the electrokinetic potential.
η = the viscosity of the pore liquid.
κ_0 = specific conductance of bulk solution.

---

[1] Present address: Mellon Institute of Industrial Research, 4400 Fifth Avenue, Pittsburgh 13, Pennsylvania.

κ_s = specific conductance of clay-water sample.
κ_p = specific conductance of pore water.
χ = specific surface conductance.
Ω = perimeter of pores.

INTRODUCTION

As a means of investigating electrokinetic effects at the solid-liquid interface, the study of electroosmosis in a clay system offers several advantages. The ionic constitution of the bulk system can be fixed for the duration of the experiment, the electrical quantities can be readily measured for the bulk system, and the ion-exchange capacity of the solid phase is a constant and determinable quantity. Thus a clay-water system can be used to test theoretical treatments of electroosmotic flow and to determine if a prediction of electroosmotic flow rate can be made from other physicochemical properties. The movement and drainage of water in clay systems is also of interest in the engineering applications of electroosmosis to soil stabilization.

EXPERIMENTAL METHODS

Materials

Peerless #2 kaolinite supplied by the R. T. Vanderbilt Co. was chosen as a simple and homogeneous clay material, which could be made into homoionic systems by chemical treatment. This grade of kaolinite has been used in previous studies (1, 2, 3) of gaseous and liquid phase absorption. The homoionic kaolinite has been the subject of considerable investigation with regard to physicochemical and engineering properties (2). Hydrogen kaolinite was prepared by washing batches of the natural Peerless #2 with 0.05 *N* HCl, as recommended by Puri (4), until the supernatant liquid was Ca^{++} free. This was followed by washing with deionized water until the supernatant liquid was Cl^- free. Portions of this clay were also electrodialyzed until further treatment brought about no decrease in sample conductance. The base-exchange capacity of the hydrogen clay was determined by potentiometric and conductometric titration with standard NaOH solution. The value of the exchange capacity was 3.12 meq./100 g. Homoionic clays with alkali cations, as well as calcium, were prepared by adding the equivalent amount of hydroxide solution to the clay. The thorium clay was prepared by addition of thorium chloride in excess of the base-exchange capacity, followed by limited washing. This method has previously been described (2).

Apparatus

The measurement of electroosmotic flow in a homoionic clay should be a reasonably rapid process, or the current flow will change the nature of the ions in the bulk system, i.e., electrodialysis creates a hydrogen clay at the anode end of the sample. Therefore the apparatus shown in Fig. 1 was used for tests comparing kaolinite samples with different counter-ions. "Instantaneous" flow rates were measured by timing the movement of menisci in "Trubore" capillary tubes of 1.50-mm. diameter. With open end capillary tubes, the inward and outward flow of water could be checked independently, there was no question of flow impedance by a bubble as found by Biefer and Mason (5), and there was only one electrical current path in the apparatus. Ruled mirrors, calibrated in millimeters, were sealed to the capillaries, to aid in reading the menisci positions. By turning the tube in a vertical direction it was possible to record the hydraulic permeability of samples. The sample chamber consisted of a cylindrical lucite tube of 10.9 cm.^{2} cross section, ground to fit over 50/50 standard taper male Pyrex joints. The sample was confined between thin porous carbon plates about 8.0 cm. apart. To avoid the interference of bubble formation at the electrodes with flow rate, the electric potential was applied at silver–silver chloride electrodes in contact with dilute KCl solutions. The potential drop across the sample was measured with an Eico Model 214 electronic voltmeter, and the current was measured with a Rawson Type 501 Multimeter. Both instruments were calibrated with standard resistances and potentials and found to be sufficiently accurate for the measurements involved. The apparatus was thermostated in an air bath at 28.0°C.

A simplified apparatus (Fig. 2) was also used to record the electroosmotic flow of sodium kaolin samples of varying water content. In this apparatus the sample was packed between porous alundum discs, in a lucite tube with the ends ground flat. Interchangeable lucite fittings were bolted to the ends of the tube for measurement of either hydraulic permeability or electroosmotic flow. The voltage was applied to platinum gauze screens in the end compartments, and measured between platinum gauze screens cemented to the alundum discs. Water flow was measured by weighing the

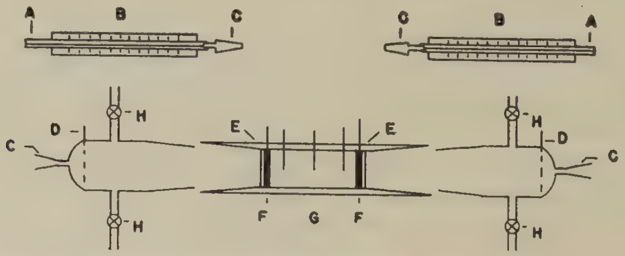

FIG. 1. Apparatus for rapid measurement of electroosmotic flow rate in homoionic kaolinite. *A:* "Trubore" capillary tubes; *B:* scales in mm. on mirror; *C:* standard taper joints; *D:* silver–silver chloride electrodes; *E:* porous stones; *F:* porous carbon discs; *G:* lucite tube; *H:* stopcocks.

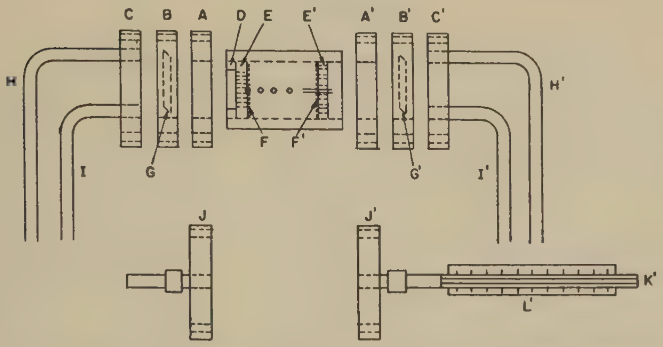

FIG. 2. Apparatus for measurements of electroosmotic flow rate and hydraulic permeability of kaolinite at various water contents. *A*, *B*, *C* and *A′*, *B′*, *C′*: lucite blocks; *D*: lucite ring; *E* and *E′*: porous alundum discs; *F* and *F′*: platinum screens (measured potential drop); *G* and *G′*: platinum screen electrodes (applied potential drop); *H* and *H′*: overflow tubes; *I* and *I′*: drainage tubes; *J* and *J′*: lucite end blocks for permeability tests; *K′*: "Trubore" capillary tube; *L′*: scale.

overflowing liquid. Both the alundum discs and the porous carbon discs chosen for the experiments were found to have very high hydraulic permeability compared to the kaolinite samples. Therefore the influence of these materials on flow through the samples was assumed to be negligible.

Conductance measurements on samples outside the electroosmosis apparatus were carried out in a shortened U.S.D.A. conductance cell, with an Industrial Instrument RC-16B bridge.

RESULTS

Calculation of the Electrokinetic Potential from Experimental Data

The electrokinetic, or zeta, potential of a porous system is obtained from the Helmholtz-Smoluchowski equations (6):

$$\zeta = \frac{4\pi\eta V}{qDE} \qquad [1]$$

or

$$\zeta = \frac{4\pi\eta\kappa_p V}{DI}, \qquad [2]$$

where η is the viscosity of the liquid, D is the dielectric constant of the liquid, V is the volume of liquid transported in unit time, q is the total cross-sectional area available to electroosmotic flow, E is the voltage gradient (presumably within capillaries), I is the total current, and κ_p is the specific conductance of the pore water. In the derivation of Eq. [2] from [1], the assumption is made that the effective cross section for electroosmotic flow is numerically the same as the effective cross section for ionic

TABLE I

Conductance of Kaolinite Impregnated with 0.100 N KCl

Solution content[a] (%)	Volume fraction of solution	Specific conductance (ohm^{-1} $cm.^{-1}$ × 10^3)		Effective cross-section for conductance "q"
		As measured	Corrected for clay	
39.5	0.46	3.26	3.13	0.23
43.5	0.53	4.07	3.94	0.29
45.5	0.54	4.27	4.14	0.30
54.0	0.59	4.85	4.71	0.35
69.5	0.64	5.73	5.59	0.41
114	0.74	7.03	6.89	0.51

[a] Weight solution/clay × 100.

conductance. In the case of homoionic alkali or alkaline-earth clays, the value of κ_p is obviously not that of the bulk deionized water added to the clay, and therefore the problem is that of evaluating either κ_p or q for the system. This was done by a method similar to that proposed by Briggs (7), in which the dry clay was mixed with a salt solution and the conductance measured. In these tests, natural Peerless #2 kaolinite was mixed with various amounts of 0.10 N KCl. The conductance of the natural clay, mixed with deionized water, was also measured and found to account for a small portion of the total conductance. The effective cross-sectional area, q, was evaluated from the corrected conductance values, as given in Table I. The same results allow the evaluation of κ_p, assuming that the pore water conductance involves similar steric factors whether the counter-ion or added salt ions carry the current.

Effect of the Counter-Ion on Electroosmotic Flow

When various counter-ions were associated with kaolinite, the electroosmotic flow per coulomb, k_i, and the zeta potential showed considerable variation. These quantities, as well as the per cent water (weight water/weight clay × 100), the specific conductance of the sample, and the calculated specific conductance of the pore water, are given in Table II. Most samples were originally mixed on the basis of 53 % water. Valid comparisons can be made directly between samples in the 50 %–55 % range.

It can be seen that the lithium and cesium kaolinites had specific conductance and k_i values qualitatively related to the differences in hydration of the ions. These two factors tend to act counter to each other, with the result that the calculated zeta potentials are almost the same for both types of clay. Sodium kaolinite differed from lithium and cesium kaolinite, as it had a considerably higher specific conductance and a higher zeta potential. The experimental specific conductance of the sodium kaolinite was about half that which could be calculated on the basis of the known added concentration of sodium counter-ions and of the steric factor ob-

TABLE II

Electroosmotic Flow in Homoionic Kaolinite

Ionic Type	Water Content[a] (%)	Electro-osmotic Flow (*cc./coulomb*)	Specific conductance of sample (*ohm*$^{-1}$ *cm.*$^{-1}$ × 10^5)	Calculated specific conductance of pore water (κ_p) (*ohm*$^{-1}$ *cm.*$^{-1}$ × 10^5)	Calculated zeta potential (ζ) (*millivolts*)
Hydrogen	52.9	.252	5.8	17.5	−5.2
Hydrogen[b]	70	2.1	1.3	2.0	−5.1
10% Hydrogen, 90% Sodium	53	.19	47.3	139	−32
Sodium	52.1	.24	52.3	157	−45
Sodium + 10% excess NaOH	53	.18	60	178	−38
Lithium	50.4	.46	16	50	−28
Cesium	54.8	.23	25	74	−26
Calcium	66	.25	15	39	−12
Thorium	51.2	.72	5.5	17	+15
Sodium chloride	53	0	136	400	0

[a] Weight water/weight clay × 100.

[b] Drainage of electrodialyzed sample.

tained from conductance tests with clay and potassium chloride. The experimental specific conductance values of cesium, lithium, and calcium clay were nearer one-fifth of the calculated conductance. When sodium kaolinite samples were made up with either a deficiency or an excess of the amount of sodium hydroxide equivalent to the base-exchange capacity, the values of k_i and the zeta potential were lower.

The experimental results for calcium kaolinite, at a water content of 66%, showed a zeta potential less than that of the alkali clays. The water flow value per ion was high, as it was proportional to double the k_i value. It is of interest that the tension needed to prevent electroosmotic flow (the negative of the electroosmotic pressure) was also measured on this sample and compared with the value calculated from electroosmotic flow and hydraulic permeability. Using 1.00 ma. current, the measured electroosmotic tension was 78 to 79 cm. of water, while the calculated value was 76 cm. of water. The condition of null flow was determined by a bellows and mirror device described by Miller (8) and kindly loaned by Dr. Miller. The agreement was close enough to verify the capillary flow method used in evaluating the electroosmotic permeability.

The first sample of hydrogen kaolinite listed in Table II was prepared by washing with acid and water, and has a specific conductance higher than that of an electrodialyzed sample but lower than that of metallic counter-ion samples. The zeta potential of the hydrogen clay was low. It was found difficult to obtain consistent capillary flow rates on electrodialyzed clay, the rate being erratic and, in one case, to the direction of the anode. However, the drainage to the cathode of a sample of hydrogen kaolinite being electrodialyzed was observed over a period of days, and an average flow rate of 2.1 cm.^{3}/coulomb found. The calculated zeta potential from this sample agreed with that of the above-mentioned hydrogen clay with a higher conductance and lower flow rate per coulomb.

In accord with the effect of thorium chloride on electrophoresis measurements (2), this salt reversed the zeta potential, providing water flow to the anode. Addition of sodium chloride in an amount equivalent to the base-exchange capacity nullified electroosmosis.

Any attempt to correlate water flow during electroosmosis with hydration of ions encounters the fact that the magnitude of flow involved is one to three thousand water molecules per ion. Therefore the amount of water moved per ion has little relation to the hydration numbers determined by other means. The views on ion hydration put forward by Darmois (9, 10), Swyngedauw (11, 12), Collet (10, 13), and Sernesse (13) do not appear fruitful in the clay-water system. Considerations of the magnitude of ion-dipole interactions between counter-cation and water would also lead to a very small interaction effect at the distances involved in high degrees of hydration.

The Relation of Hydraulic Permeability and Electroosmotic Flow

Sodium kaolinite at various water contents was packed into the apparatus shown in Fig. 2, which could be used to measure either hydraulic permeability or continuous electroosmotic flow. The values of the electroosmotic permeability per volt per centimeter, k_e, the flow per coulomb, k_i, and the hydraulic permeability, k_h, are listed in Table III. All coefficients of flow increase with increasing water content of the sample. At appreciably more than 92% water content, the clay would not form a stable continuous solid phase, and true electroosmotic flow could not be measured. It can be noted that the hydraulic permeability increases over tenfold, while the flow per coulomb almost doubles and the flow per volt per centimeter has increased about 40%. The hydraulic permeability, then, does not appear to be directly involved in the electroosmotic flow rate. These results are considered further in the next section.

TABLE III

Comparison of Electroosmotic and Hydraulic Flow in Sodium Kaolinite

Water content[a]	Porosity[b]	Calculated[c] q	k_i[d]	$k_e \times 10^4$[e]	$k_h \times 10^7$[f]
41	0.51	0.27	0.19	0.82	1.21
57	0.59	0.35	0.26	0.94	3.5
92	0.705	0.465	0.38	1.14	14.1

[a] Weight water/weight clay × 100.

[b] Volume voids/total volume.

[c] Effective porosity.

[d] Flow in cm.^{3}/coulomb.

[e] Flow in cm.^{3}/volt/cm./cm.^{2} area/sec.

[f] Flow in cm.^{3}/cm. of water hydraulic head for 1-cm. sample length /cm.^{2} area/sec.

DISCUSSION

The Relation of Pore Size, Permeability, and Porosity in the Equations of Helmholtz and von Smoluchowski and of Schmid

The Helmholtz-Smoluchowski relationships for electroosmotic flow, given in Eqs. [1] and [2], predict that k_e varies with the zeta potential and with the cross-sectional area available to electroosmotic flow; and k_i varies with the zeta potential and the specific conductance of the pore water. As the solid-liquid ratio of an electroosmosis sample is changed, the average pore size, the porosity, and the hydraulic permeability also change. The zeta potential, a property of the solid-liquid interface, should be affected only by the small changes in the pore water ion concentration due to dilution. In the case of a porous system impregnated by a solution whose specific conductance is the same as bulk solution, the value of k_e should depend directly on the effective porosity, while k_i should be independent of porosity. However, when a homoionic clay is mixed with deionized water, the pore water conductance is contributed largely by counterions. This conductance is then surface-dependent and κ_p for the pore water can be expressed, using an equation of the form given by Bikerman (14) for surface conductance, as

$$\kappa_p = \kappa_0 + \frac{\Omega}{a}\chi, \qquad [3]$$

where κ_0 is the conductance contribution of the bulk pore water, Ω is the perimeter of the pores, a the cross section of the pores, and χ the specific surface conductance. The equation for k_i then becomes

$$k_i = \frac{\zeta D}{4\pi\eta[\kappa_0 + (\Omega/q)\chi]}. \qquad [4]$$

In a system of uniform capillaries $\Omega/q = 2/r$, where r is the pore radius, so that:

$$k_i = \frac{\zeta D}{4\pi\eta[\kappa_0 + (2/r)\chi]}. \qquad [5]$$

Finally, in an ideal homoionic clay system, κ_0 can be neglected and

$$k_i = \frac{\zeta D r}{8\pi\eta\chi}. \qquad [6]$$

In order to relate pore radius and measurable quantities such as permeability and porosity, assumptions concerning pore structure must be introduced. To facilitate comparison with Schmid's equations (15), it is assumed here that the system consists of uniform pores of circular cross section, with hydrostatic flow following Poiseuille's law. Then:

$$k_h = \frac{qr^2}{8}, \tag{7}$$

where q is the effective porosity of the system. Equations [6] and [7] can be combined to obtain the ratio:

$$\frac{k_i}{k_h} = \frac{\zeta D}{qr\chi} \quad \text{or} \quad \frac{\zeta C_1}{qr}, \tag{8}$$

in which ζ and χ are specific surface properties, and D a bulk property assumed to be independent of the pore diameter of the system. Likewise, k_e and k_h can be related from Eqs. [1] and [7] to yield

$$\frac{k_e}{k_h} = \frac{2\zeta D}{\pi r^2} \quad \text{or} \quad \frac{C_2\zeta}{a}, \tag{9}$$

where a is the pore cross section.[2]

The fundamental equations of Schmid for k_i and k_e are

$$k_i = \frac{F_0 A}{\kappa_s} k_h \tag{10}$$

and

$$k_e = F_0 A k_h, \tag{11}$$

where F_0 represents the Faraday constant, A the counter-ion concentration per unit volume of pore water, κ_s the conductance of 1 cm.^{3} of the sample. Both k_i and k_e are then directly dependent on the hydraulic permeability of the sample, as well as the counter-ion concentration. When the Schmid equations are applied to ideal homoionic clay-water systems, the values of A and κ_s vary with the water content. In a geometrical relation, similar to conductance in Eq. [6], A then varies as $2/r$. The sample conductance κ_s is equal to $\kappa_p \times q$ and κ_p also changes as $2/r$. Therefore

$$\frac{k_i}{k_h} = \frac{C_3}{q} \tag{12}$$

and

$$\frac{k_e}{k_h} = \frac{C_4}{r}, \tag{13}$$

C_3 and C_4 being constants. With the aid of Eq. [7], the values of C_1 and C_2, derived according to the Helmholtz-Smoluchowski equations, and C_3 and C_4, derived according to the Schmid equations, may be compared. When this is done for the data in Table III, the values of C_1 are 6.3, 6.6, and 6.0×10^1 for r in centimeters and in volts. The values of C_2 are necessarily constant if r is evaluated from Eq. [7]. On the other hand, the values of C_3 are 4.2, 2.6, and 1.3×10^5, and those of C_4 are 3.7, 2.2, and 1.2×10^3.

---

[2] This ratio can also be obtained from Eqs. [4] and [5] of L. Casagrande (16).

It is not necessary, however, to make assumptions of pore structure in order to qualitatively compare the data with the Helmholtz-Smoluchowski and Schmid equations. As shown in Table III, a change of tenfold in the hydraulic permeability was accompanied by a doubling of k_i and a 40% increase in k_e. Neither k_i nor k_e increased as rapidly as obligated by a direct relationship with k_h, unless A or κ_s changed much more radically than anticipated. On the other hand, k_e appeared to change as the ideal porosity calculated from water content, rather than q calculated from conductance capacity. As some variation in the zeta potential with counter-ion concentration is to be expected, the results are still compatible with the Helmholtz-Smoluchowski equations.

A further test of the applicability of the Schmid equations was made by calculating k_e and k_i for various homoionic clays. In order to carry out this calculation, A was determined from the base-exchange capacity of the clay, and the hydrostatic force in dynes/cm.^{2} was equated to the total electrical force in Newtons on the pore water in the sample. These values are about ten to several hundred times greater than the experimental values. Thus electroosmotic flow in these systems cannot be calculated from these equations with data independent of electrokinetic measurements. As Schmid has expressly formulated his equations for systems of pore diameter <1000 A. (17), it is no reflection on his basic assumptions that they do not apply to the kaolinite-water system. The calculated pore diameters from Eq. [7] are from 1100 to 2800 A. Michaels and Lin (18) also calculated pore diameters of greater than 1000 A. from their permeability study of the kaolinite-water system. The criterion of applicability of the Helmholtz-Smoluchowski or Schmid relationships is, of course, whether the effective double layer thickness is negligible compared with capillary diameter or is distributed throughout the capillary.

ACKNOWLEDGMENTS

This work was carried out as a portion of a program sponsored by the Bureau of Yards and Docks, United States Navy, under Contract NOy-76303. The author wishes to thank Professor Arthur Casagrande and Dr. Leo Casagrande, Soil Mechanics Laboratory, Harvard University, for their guidance and suggestions. The author also expresses thanks to Dr. Gerard Bolt and Dr. Robert Miller of Cornell University and Messrs. Stanley Wilson, Stuart Avery, Alan Richardson, Gdalyah Wiseman, and Ronald Hirschfield of the Harvard Soil Mechanics Laboratory for discussions of the work, and to Messrs. Curtiss Allin and Troy Sitter for assistance with the experiments.

SUMMARY

1. Electroosmotic flow in homoionic kaolinite and water mixtures is affected both in rate and direction by the nature of the counter-ion, especially by its conductance.

2. The amount of water moved per ion discharged is very large compared with hydration numbers determined by other techniques. The interpretation of electroosmotic flow in terms of ion hydration is unsatisfactory.

3. The zeta potential of homoionic kaolinites was calculated by means of the Helmholtz-Smoluchowski equations, with conductance capacity experiments to determine the effective porosity. The zeta potential and electroosmotic permeability was at a maximum when the amount of counterion was equivalent to the base-exchange capacity.

4. The relation of electroosmotic permeability to hydraulic permeability was derived in terms of pore radius and porosity for homoionic clay systems. Both the Helmholtz-Smoluchowski and the Schmid equations were considered. The former were found applicable to the kaolinite-water system, but the latter were not applicable.

REFERENCES

1. KEENAN, A. G., MOONEY, R. W., AND WOOD, L. A., *J. Am. Chem. Soc.* **55**, 1462 (1951).
2. Final Report, Soil Solidification Research, Cornell University, 1946–51. Volume II, "Fundamental Properties, Clay-Water Systems."
3. McLAREN, A. D., *J. Phys. Chem.* **58**, 129 (1954).
4. PURI, A. N., "Soils, Their Physics and Chemistry," p. 6. Reinhold, New York, 1949.
5. BIEFER, G. J., AND MASON, S. G., *J. Colloid Sci.* **9**, 20 (1954).
6. GLASSTONE, S., "Textbook of Physical Chemistry," p. 1223. D. Van Nostrand, New York, 1946.
7. BRIGGS, D. R., *J. Phys. Chem.* **32**, 641 (1928).
8. MILLER, R. D., *Soil Sci.* **72**, 291 (1951).
9. DARMOIS, E., *Compt. rend.* **227**, 339 (1938).
10. COLLET, L. H., AND DARMOIS, E., *Publ. sci. et tech. ministère air* (*France*) No. N.T. **34**, (1950).
11. SWYNGEDAUW, J., Thesis, Paris, 1939.
12. SWYNGEDAUW, J., *Bull. soc. franç. élec.* [5] **9**, 901 (1939).
13. SERNESSE, S., AND COLLET, L. H., *Compt. rend.* **234**, 2281 (1952).
14. BIKERMAN, J. J., "Surface Chemistry," p. 387. Academic Press, New York, 1948.
15. SCHMID, G., *Z. Electrochem.* **55**, 229 (1951).
16. CASAGRANDE, L., *J. Boston Soc. Civil Engrs.* **39**, 55 (1952).
17. SCHMID, G., *Z. Electrochem.* **54**, 424 (1950).
18. MICHAELS, A. S., AND LIN, C. S., *Ind. Eng. Chem.* **46**, 1239 (1954).

TRACER ELECTROPHORESIS.

III. The Mobility of the Na^+ Constituent in Sodium Lauryl Sulfate Solutions

Karol J. Mysels and Cyril I. Dulin[1]

Department of Chemistry, University of Southern California

Received May 23, 1955; revised July 6, 1955

INTRODUCTION

Measurements of electric transport and mobility can often throw considerable light on the constitution of solutions of electrolytes. Their interpretation, although sometimes difficult, has the inherent advantage that it requires no information about activity coefficients and operates entirely in terms of concentrations. It is therefore a valuable supplement to thermodynamic measurements, particularly in nonideal solutions. In the preceding paper (1) of this series the heretofore unobtainable mobility of micelles of sodium lauryl sulfate (NaLS) was reported and interpreted. We have not applied the same method, but using radio tracers, to measure the average mobility of the Na^+ ion in order to obtain a more complete picture of these solutions. The results provide an essentially independent confirmation of certain results previously reported by other workers and by our laboratory about the concentration of unmicellized ions and the ionization of micelles.

EXPERIMENTAL

Materials

The NaLS was prepared from the purified lauryl alcohol, described previously (2), by the same method and was undistinguishable from the one used in previous studies of this laboratory (1–5).

Na^{22} was obtained from the Atomic Energy Commission as carrier-free HCl solution. This was evaporated to dryness and dissolved in water for use. I^{131} obtained from the same source as carrier-free bisulfite solution was used as received for experiments involving I^-. Conversion to IO_3^- was obtained by passing gaseous chlorine through this solution.

---

[1] Present address: E. I. du Pont Co., Pigments Department, Newport, Delaware.

Radioactivity Determination

Known volumes of solutions were placed in test tubes and the activity determined using a Model DS-1 scintillation counter and a model 162 scaler (both manufactured by the Nuclear Instrument and Chemical Corp., Chicago). Counts were corrected for background and volume of liquid and geometry of the tubes.

Conductivity Measurements

Solutions were prepared and diluted by weight in distilled water equilibrated with the laboratory atmosphere. A Jones-Dyke (6) bridge and cells designed according to Jones and Bollinger (7) were used. The oil thermostat was kept at 25.00°C. and Joule heating was carefully avoided by applying a sufficiently low potential to the bridge. The cells were calibrated according to Jones and Bradshaw (8) as well as by intercomparison.

Mobility Measurements

The apparatus and procedure described in the first paper (9) of this series were used with only one major modification. The specificity of radioactive determinations permitted the analysis of the cathode and anode compartments as well as of the middle tube, whereas previously only this last one was possible colorimetrically. The analysis of the end compartments was necessary in several experiments because we found that electroosmotic flow can be sufficiently large at low mobilities to overcome partially the electrophoresis so that tracer is found in *both* end compartments. This situation corresponds to Fig. 2*e* of the first paper (9) and was handled as suggested there in footnote 9. Analysis of the end compartments introduces always a certain complication into the calculation of results. As shown previously (9)

$$u = \frac{\kappa v}{it}$$

where u is the mobility, it the amount of electricity which has passed in time t through the solution of conductivity κ, and v is the volume swept by the tracer with respect to the liquid. Experimentally, the volume V of the central tube is known and the amount of tracer found in the anode compartment, A, in the cathode C, and in the middle tube, M, are determined at the end of the experiment while the specific activity, s, (per cc.) of the tracer solution placed in the middle tube at the start is also measured. The material balance gives of course,

$$\delta + V = \frac{A + C + M}{s}$$

where δ includes all the analytical and manipulative errors. One can express v in terms of any three of the four analytical quantities A, C, M, s, which gives normally four different values

$$v_1 = \frac{C - A}{s}$$

$$v_2 = \frac{M + 2C - Vs}{s}$$

$$v_3 = \frac{Vs - M - 2A}{s}$$

$$v_4 = \frac{(C - A)V}{A + C + M}$$

Since each of these omits one of the analytical determinations they should be accorded equal weight. It can be shown also that v, always lies between v_2 and v_3 and differs from each by δ, while it exceeds v_4 by $v_1\delta/V$. Hence the average of the four values is always $v_1(1 - \delta/4V)$. It may be also noted that v_2 and v_3 are differences between large quantities and correspondingly susceptible to experimental errors. Their variation being opposite, the effects neutralize each other, however, when thus averaged.

ELECTROCHEMICAL DEFINITION AND RELATIONS

Our solutions are formed by two components: H_2O and NaLS, so that specifying the concentration c of one (NaLS) defines the solution. They are formed by three analytically determinable *constituents* H_2O, Na, and LS. By using the first as the point of reference in all transport phenomena we need to consider only the latter two and shall denote these constituents by letter subscripts a and b, respectively.

We are primarily interested in the actual *species*, molecular and ionic, which are present in our solution. We can again neglect the water and shall assume the simplest possible model composed of three species: simple Na^+ ions, simple LS^- ions, and micelles composed of n LS^- and θn Na^+ ions. Hence n is the degree of aggregation of the micelle and $\alpha = 1 - \theta$, its degree of dissociation, while its (empirical) formula is $Na_\theta LS$. These three species will be denoted by numerical subscripts *1*, *2*, and *3*, respectively. These definitions give us a series of material balance relations

$$c = c_a = c_b = c_2 + c_3 = c_1 + \theta c_3 \qquad [1]$$

where c is expressed in moles (gram formula weights) per milliliter.

It is advantageous to define three kinds of charge: (i) z_i the real charge per particle of an ionic species present in solution; (ii) y_i the real charge per mole of a species; (iii) q_i a formal or intrinsic charge of the constituents from which the other charges can be derived if the composition is known. We take naturally $q_a = 1$ for Na and $q_b = -1$ for LS.

For micelles where the degree of aggregation n may be unknown the charge per mole

$$y_3 = \frac{z_3}{n} = \theta - 1 \qquad [2]$$

is not trivial.

The electrokinetic properties of interest (10, 11) are: (i) the mobility, u_i, measured in the direction of the positive current in cm.^{2}/volt sec.; (ii) t_i, the material transport number, sometimes called the transference number, or Hittorf number, measured along the same direction in moles/Faraday; and (iii) T_i, the electric transport number, sometimes called simply transport number, which is the fraction of current carried by species i. These quantities are quite generally related as follows:

$$t_i = u_i c_i F \text{ for any species or constituent.} \qquad [3]$$

$$t_i y_i = T_i \text{ for a species and } t_i q_i = T_i \text{ for a constituent.} \qquad [4a, b]$$

$$\sum T_i = 1 \text{ if all parts of the solution are included but once.} \qquad [5]$$

$$\sum u_i c_i = \sum u_j c_j, \text{ provided } \sum c_i \equiv \sum c_j. \qquad [6]$$

In this last equation the summations may be extended indiscriminately over species or constituents.

RESULTS AND DISCUSSION

Measurements with the Na^{22} tracer are translated as indicated above into the mobility u_a of the sodium constituent and then by Eqs. [3] and [5] into its material transport number t_a and the corresponding quantity t_b for the LS constituent. These are shown in Table I and Figs. 1 and 2. In these figures, as well as further ones, the points and the lines each form a consistent set based on a number of assumptions which will be presented in turn.

The mobility of the simple ions. In our interpretation we shall need the mobilities of the simple Na$^+$ and LS$^-$ ions in the micellar solution. For the sake of simplicity and consistency we shall assume that these mobilities

TABLE I

The Mobility of the Sodium Constituent in Sodium Lauryl Sulfate Solutions at 25°C.

Conc. (*wt. %*)	Mobility (*cm.²/volt sec. × 10⁵*)
0.2993	32.9 ± 0.9
0.3790	25.1 ± 0.5
0.5851	8.9 ± 0.4
0.8418	1.8 ± 0.8
1.204	−3.5 ± 0.7
2.193	−4.88 ± 0.03
3.316	−5.92 ± 0.01

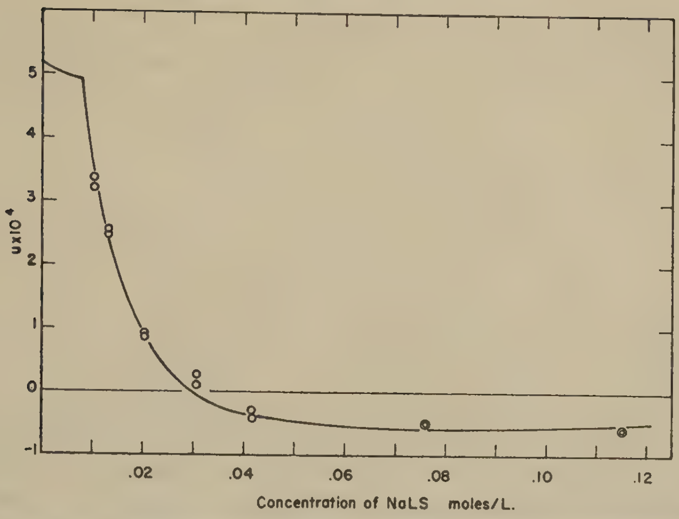

FIG. 1. The electrophoretic mobility of the sodium constituent in sodium lauryl sulfate solutions at 25°C.

vary with the total molar concentration of the solution in the ratio in which the equivalent conductivity of KCl varies with the molar concentration of that salt. This assumes essentially that the detergent solution may, in some respects, be treated as a one-one electrolyte, as has been frequently advocated by McBain (10) and as has recently received direct confirmation from salt effects measurements by Erickson and Lingafelter (12) and a rationalization by Mukerjee (13). The assumed mobilities should represent maximum values.

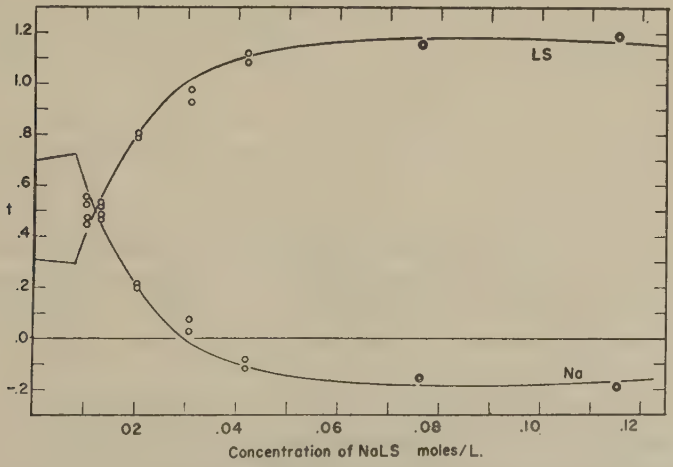

FIG. 2. The material transport numbers of the sodium and of the lauryl sulfate constituents in NaLS.

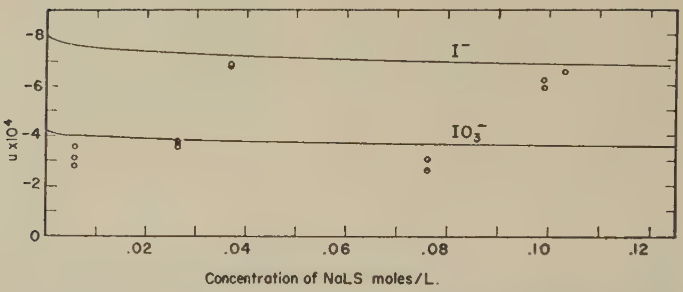

FIG. 3. The mobility of tracer I^- and IO_3^- ions in NaLS solutions. IO_3^- carrier-free. I^- in presence of *ca.* 10^{-3} *M* carrier.

With respect to the LS^- ion this assumption is in principle susceptible to experimental verification because *any* monovalent unmicellized ion should have its mobility reduced to about the same extent as the unmicellized LS^- ion. Variation in size and shape should produce only second- and third-order effects. Tracer electrophoresis permits, in principle, the measurement of the mobility of an ion added in tracer amounts so that the properties of the solution remain unchanged. In practice, difficulties are encountered. When I^- was added in trace amounts the material balance was off by as much as 50% owing to tenacious sorption on the apparatus. With IO_3^- the results shown in Fig. 3 were obtained. When compared with calculated values based on the infinite dilution value of Krieger and Kilpatrick (14), they are obviously low, even below the critical micelle concentration, and scatter considerably as would be expected if some adsorption still interfered. An attempt to improve the I^- results by making the solutions about $10^{-3}M$ in carrier I^- (which has no significant effect on the properties of the solution) gave much improved material balances for tracer I^- but the results are of the same order as with IO_3^-. This is shown also in Fig. 3. Although somewhat disappointing, these results are believed to prove that our assumption is not radically wrong.

With respect to the Na^+ ion no direct experimental verification seems possible until some ion which is not incorporated into the oppositely charged micelle is discovered.

There is one complication: in dilute solutions, below the critical micelle concentration (cmc) the equivalent conductivity of NaLS decreases much less rapidly than expected. We assign arbitrarily all this anomalous behavior to the LS^- ion and base our computation on a mobility at the cmc calculated from the conductivity and the mobility of the Na^+ ion.

THE DISTRIBUTION OF THE LS CONSTITUENT

The mobility u_b of the LS constituent is, by Eq. [6], the weighted average of the mobilities u_2 of free LS^- ions and u_3 of micelles:

$$cu_b = c_2u_2 + c_3u_3 \qquad [7]$$

Since u_2 is given by our assumption and u_3 has been measured by Stigter (1) in the same system and over the same range of concentrations we can calculate c_2 and c_3 with the help of the material balance (Eq. [1]):

$$c_2 = c\,\frac{u_b - u_3}{u_2 - u_3} = c\,\frac{u_a - u_3 - \kappa/Fc}{u_2 - u_3} \qquad [8]$$

and

$$c_3 = c - c_2$$

The resulting points are plotted in Fig. 4. We feel that the best present interpretation of these points is by the straight lines shown. On this basis we have drawn also the lines of the other figures. Several aspects of this procedure may be noted: (*1*) the scatter of experimental points is greatly multiplied in some figures but at the level of direct measurements of mobility (Fig. 1) the average deviation of the line from the average of the points is only 10^{-5} cm.^{2}/v. sec., which is about equal to the average spread of the points. (*2*) If our assumption about the mobility u_2 of the free LS^- ion is in error by 5%, its concentration, c_2, is vitiated by about 7% at low concentrations and 10% at high ones, while the effect on the concentration of micelles c_3 decreases from infinity to less than 0.3%. (*3*) The constancy of concentration of free LS^-, c_2, means that any LS^- added above the cmc goes entirely into the formation of micelles. This is the assumption underlying Debye's (15) treatment of light scattering and made frequently in connection with solubilization and other properties of these solutions. (*4*) Our results have no direct bearing on the activity of the LS^- ions but only on their concentration. The activity coefficient will be subject to two main and opposing influences: a reduction due to the increased concentration of Na^+ ions and an increase due to the expulsion of the LS^- ions from

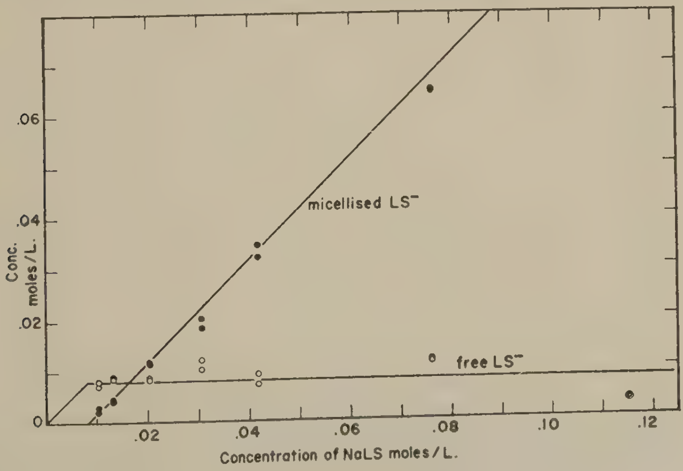

FIG. 4. The concentrations of free and of micellized LS^- in NaLS solutions.

the double layer of micelles and their concentration in the intermicellar liquid (16). Kolthoff and Johnson (17) concluded from their study of cells with liquid junctions in the potassium laurate system that the activity of the corresponding ion (K^+) is constant. On the other hand, consideration of equilibrium between charged micelles and simple ions leads to the expectation of a maximum very close to the cmc (18).

The distribution of the sodium constituent. The mobility, u_a, of the sodium constituent is by Eq. [6] the weighted average of the mobilities u_1 of free and u_3 of the micellized Na^+ ions.

$$cu_a = c_1u_1 + \theta c_3u_3. \qquad [9]$$

Since u_1 is given by our assumption and u_3 by Stigter's (1) measurements, the concentrations follow from the material balance (Eq. [1]):

$$c_1 = c\frac{u_a - u_3}{u_1 - u_3} \quad \text{and} \quad \theta c_3 = c - c_1. \qquad [10]$$

Figure 5 shows the calculated points as well as the lines based on the assumption that c_2 is constant above the cmc. A 10% error in evaluating u_1 vitiates c_1 by less than 5.5% and gives an error in θc_3 which decreases to 3.5% at high concentration.

The degree of ionization of micelles. The value of θ is given directly from Eqs. [8] and [10] by

$$\theta = \frac{\theta c_3}{c_3} = \frac{(u_1 - u_a)(u_2 - u_3)}{(u_1 - u_3)(u_2 - u_a - \kappa/Fc)} \qquad [11]$$

and the degree of ionization of the micelle α is of course $1 - \theta$. Figure 6 shows the calculated points and line. It may be noted that at low concen-

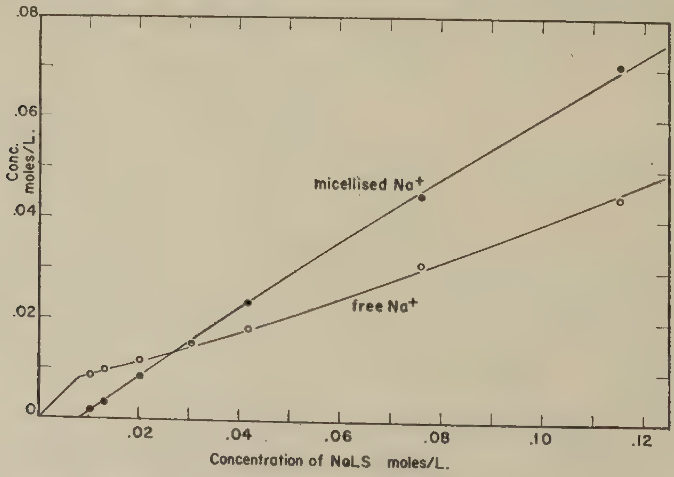

FIG. 5. The concentrations of free and of micellized Na^+ in NaLS solutions.

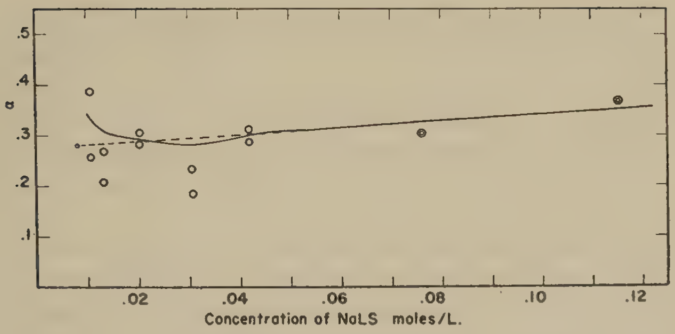

FIG. 6. The degree of ionization of micelles in NaLS solutions.

trations the results are extremely sensitive to any error in either the experiment or the calculation, whereas at high concentrations they become quite insensitive. This is shown by the scatter of points in Fig. 6 and also in Fig. 7, which gives the variation of α with u_1 at the assumed value of c_2 and at a 25% higher value of c_2 for the highest concentration studied (0.115 M NaLS) and for 65% above the cmc (0.0131 M NaLS).

We are therefore inclined to disregard the meandering of the line at lower concentrations and to use a straight-line extrapolation to the cmc. This procedure is further justified below on the basis of conductivity measurements.

This gives a degree of ionization of 0.280 in excellent agreement with Stigter's (1) value of 0.287. Whereas the experimental data are in part common and the same model is used in both studies, the interpretations are completely different, Stigter's (1) result being based on micellar size and

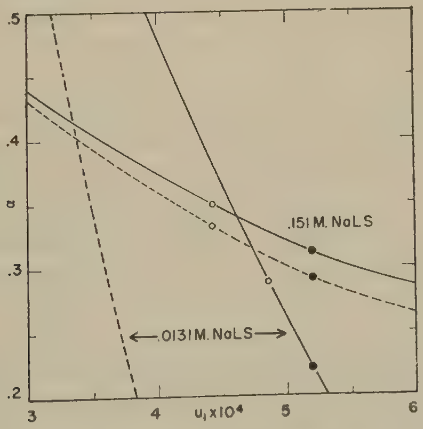

FIG. 7. The effect of some variables on the calculated degree of ionization of micelles. Solid lines: assumed concentration of free LS^-. Dashed lines: 25% higher value. ○: assumed mobility of free Na^- ions; ●: value at infinite dilution.

his modification of Booth's (19) theory of electrophoretic mobility. It may be also noted that if Smoluchowski's or Henry's theories are used instead of Booth's, definitely lower results (*ca.* 0.15 and 0.20) are obtained (1).

Our work therefore provides an experimental confirmation, which we believe to be the first one, of the importance of relaxation effects in colloids, and of the correctness of Booth's theory and the related calculations of Overbeek (20) and of Stigter (1).

It may be also noted that the values of α increase with concentration. The increase is not large, from about 0.288 (average of Stigter's value and our extrapolation) at the cmc to 0.350 at 3.3 % NaLS, but seems to be real. This effect is not due to our assumptions about mobilities of the simple ions for two reasons: (*1*) our mobilities are likely to be too high rather than too low; this would tend to make α low at high concentrations. (*2*) Even if we were to assume that the mobilities have the highest conceivable values, those of infinite dilution, the value of θ would decrease to only 0.33 at 3.3 % NaLS, still considerably above the value at the cmc.

This "retrograde ionization" of micelles is not an isolated finding. Hartley (21) found the same effect in his studies of transference and Bolam and Trivedi (22) found it for Oden sulfur sols. Of special interest is the fact that an increase of α of the same order from 0.287 to 0.324 is obtained for NaLS at the cmc from the electrophoretic mobility alone (1) as NaCl concentration increases to 0.1 *N*. If these findings are all taken at their face value, there seems to be no satisfactory interpretation. As pointed out by Hartley (23), any explanation based on changing kinds of micelles can not apply to the behavior of the sulfur sols. On the other hand, the explanations preferred by him of an artefact produced by an inhomogeneity of the solution or a compensating change of activity coefficients when the ionic strength increases rapidly, seem to fail for the salt effect at the cmc (1), where Booth's treatment guards against the artefact and the ionic strength increases but slowly.

It may be noted that the increased ionization goes parallel with increasing size of the micelle at the cmc, and presumably also in our case. Hence total charge of the micelle increases faster than its size while the surface increases less rapidly. Therefore the surface charge density increases even faster than the degree of ionization. Because of the simultaneous reduction of the thickness of the double layer the zeta potential decreases, but less rapidly than it would at constant α.

Thus the Na^+ gegenions seem to leave the surface while their concentration increases greatly both in the bulk solution and in the immediate neighborhood of the surface! Apparently some new approach to the interpretation is badly needed.

Conductivity. Below the cmc the conductivity of NaLS solutions is definitely higher than predicted by the Onsager theory from the limiting value. This phenomenon is being investigated further and we present now

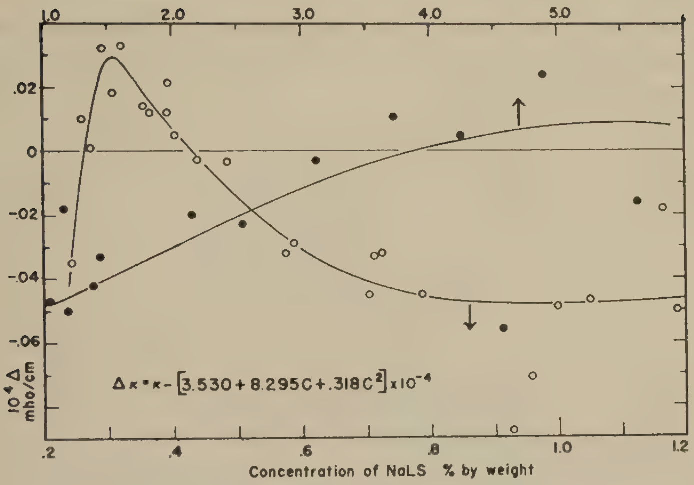

FIG. 8. Deviation graph of conductivity of solutions of NaLS at 25°C.

only the results above the cmc, for concentrations C from 0.25% to 5.6% by weight. Our results can be represented as a first approximation by the equation

$$10^4\kappa = 3.53 + 8.295C + 0.318C^2. \qquad [12]$$

The deviations from this line are plotted in Fig. [8] and are highly methodical. They can be represented by the smooth line shown with an average deviation of 0.08% or 0.01×10^{-4} in κ. The line deviates from the equation by a maximum of 0.44% or 0.046×10^{-4} in κ. Measurements in this range by Lottermoser and Puschel (24) and by Goddard (25) agree with ours within their respective precisions.

The interpretation of conductivity. It is customary to report conductivity measurements in terms of equivalent conductivity Λ. This is perfectly rational for strong electrolytes where Λ corresponds to the average mobility of the ions. In case of association colloidal electrolytes however Λ corresponds to a weighted average of the mobilities of all the species present and the weighting factors change rapidly. As a result the interpretation of Λ is far from simple and may be misleading. Thus for NaLS and many other compounds Λ is characterized by a minimum as shown schematically in Fig. 9*a* at about 4% concentration. This could be taken as an indication that the nature of the solution changes in this region. If one considers, however, the plot of the conductivity κ as shown in Fig. 9*b*, it becomes apparent that the minimum in Λ corresponds simply to the point where the line connecting κ to the origin becomes tangent to the curve. Its existence is conditioned by the fact that the κ plot shows a continuous upward curvature above the cmc. This curvature is almost constant but increases slightly and regularly with concentration as shown by the plot of $d\kappa/dc$ in Fig. 9*c*. Thus the process responsible for the minimum is one which starts at the cmc and continues regularly as the concentration increases. It must therefore be related to the normal process of micellization.

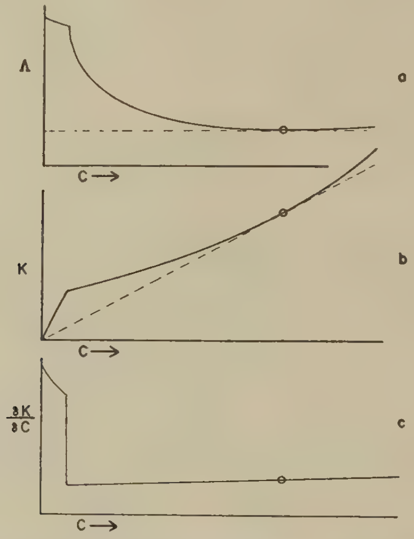

Fig. 9. Schematic variation of equivalent conductivity Λ, conductivity κ, and differential conductivity $\partial\kappa/\partial x$ in NaLS solutions. ○ indicates the position of the minimum in Λ^-.

Since the total conductivity of the solution is related to the mobilities, charges, and concentrations of the species according to Eqs. [3], [4], and [5], by

$$F\sum u_i y_i c_i = \kappa \qquad [13]$$

the value of $d\kappa/dc$ is given by

$$F\sum \frac{du_i}{dc_i} y_i c_i + u_i \frac{dy_i}{dc} c_i + u_i y_i \frac{dc_i}{dc} = \frac{d\kappa}{dc}. \qquad [14]$$

On the basis of our assumptions all the quantities involved can be calculated numerically and show that the main factors responsible for the upward slope of the κ plot are, as would be expected, the increasing concentration of free Na^+ and of micelles while the increasing charge on the micelles makes a minor contribution which is about counterbalanced by the reduction in the mobility of micelles.

When a similar calculation is extended to the second derivative of $\sum u_i y_i c_i$ it is found that the curvature of κ and the upward slope of $d\kappa/dc$ are entirely due to retrograde ionization with its increase in charge of the micelle and more than linear concentration increase of Na^+ ions. The decreasing mobilities of these species are the main opposing factors but are much smaller.

The smooth course of the conductivity curve and its derivatives is an independent argument for the linear extrapolation of α which we used previously.

ACKNOWLEDGMENT

This work was made possible by the support of the Office of Naval Research through Project NR-356-254 for which this forms the Fifth Technical Report. Reproduction in whole or in part is permitted for any purpose of the United States Government.

SUMMARY

The concentration of free LS^- ions appears to be approximately constant and the degree of ionization of micelles seems to increase slowly with concentration. These results of mobility measurements using radio Na^+ tracer and a model of a single type of micelle are in agreement with much previous work and thus provide a confirmation of theories of relaxation effects in electrophoresis of large particles. On the other hand, the retrograde ionization of micelles remains very puzzling.

REFERENCES

1. STIGTER, D., AND MYSELS, K. J., *J. Phys. Chem.* **59,** 45 (1955).
2. WILLIAMS, R. J., PHILLIPS, J. N., AND MYSELS, K. J., *Trans. Farad. Soc.* **51,** 728 (1955).
3. PHILLIPS, J. N., AND MYSELS, K. J., *J. Phys. Chem.* **59,** 225 (1955).
4. STIGTER, D., WILLIAMS, R. J., AND MYSELS, K. J., *J. Phys. Chem.* **59,** 330 (1955).
5. MUKERJEE, P., AND MYSELS, K. J., *J. Am. Chem. Soc.* **77,** 2937 (1955).
6. DYKE, P. H., *Rev. Sci. Instr.* **2,** 379 (1931).
7. JONES, G., AND BOLLINGER, G. M., *J. Am. Chem. Soc.* **53,** 411 (1931).
8. JONES, G., AND BRADSHAW, B. C., *J. Am. Chem. Soc.* **55,** 1780 (1933).
9. HOYER, H. W., MYSELS, K. J., AND STIGTER, D., *J. Phys. Chem.* **58,** 385 (1954).
10. McBAIN, J. W., "Colloid Science," pp. 254–255. D. C. Heath and Co., Boston, 1950.
11. SCATCHARD, G., *J. Am. Chem. Soc.* **75,** 2883 (1953); and *in* Cohn and Edsall "Proteins, Amino Acids and Peptides," p. 39. Reinhold, New York City, 1943.
12. ERICKSON, J. A., AND LINGAFELTER, E. C., *J. Colloid Sci.* **10,** 71 (1955).
13. MUKERJEE, P., Ph.D. Proposition, Chemistry Department, University of Southern California, 1955.
14. KRIEGER, K. A., AND KILPATRICK, M., *J. Am. Chem. Soc.* **64,** 7 (1942).
15. DEBYE, P., *J. Phys. & Colloid Chem.* **53,** 1 (1949).
16. STIGTER, D., *Rec. trav. chim.* **73,** 593 (1954).
17. KOLTHOFF, I. M., AND JOHNSON, W. F., *J. Phys. & Colloid Chem.* **52,** 22 (1948).
18. MURRAY, R. C., AND HARTLEY, G. S., *Trans. Faraday Soc.* **31,** 183 (1935); VOLD, M. J., *J. Colloid Sci.* **5,** 506 (1950).
19. BOOTH, F., *Proc. Roy. Soc. (London)* **A203,** 514 (1950).
20. OVERBEEK, J. TH. G., *Kolloid-Beih.* **54,** 316 (1943); Thesis, Utrecht, 1941.
21. HARTLEY, G. S., COLLIE, B., AND SAMIS, C. S., *Trans. Faraday Soc.* **32,** 795 (1936).
22. BOLAM, T. R., AND TRIVEDI, A. K. M., *Trans. Faraday Soc.* **39,** 247 (1943).
23. HARTLEY, G. S., *Quart. Revs.* (London) **2,** 152 (1948); *Kolloid-Z.* **88,** 33 (1939).
24. LOTTERMOSER, A., AND PUSCHEL, F., *Kolloid-Z.* **63,** 175 (1933).
25. GODDARD, E. D., HIGHAM, E. H., AND STEWART, J. C., *Research (London)* **7,** S8 (1954); and private communication.

DYNAMIC MECHANICAL PROPERTIES OF POLYMETHYL ACRYLATE[1]

Malcolm L. Williams[2] and John D. Ferry

Department of Chemistry, University of Wisconsin, Madison, Wisconsin

Received June 6, 1955

INTRODUCTION

Following previous work on polyisobutylene (1), polystyrene (2), and polyvinyl acetate (3), dynamic mechanical properties are now reported for polymethyl acrylate, measured in the audiofrequency range at temperatures encompassing the transition from rubberlike to glasslike consistency.

MATERIAL AND METHOD

The polymer was furnished by Picatinny Arsenal for this investigation. It was prepared (4) by emulsion polymerization with potassium persulfate as initiator and thiophenol as modifier, and fractionated from mixtures of benzene and ethanol. The sample chosen was refractionated twice and dried from frozen benzene solution. Its weight-average molecular weight was 2.2×10^6. It was probably highly branched, but it is believed that branching has little effect on the mechanical properties in the transition region. Further details of the characterization of the sample will be reported elsewhere (4).

Measurements of the complex shear compliance ($J^* = J' - iJ''$) were made with the double transducer of Fitzgerald and Ferry (5). Recent modifications in the apparatus have been described previously (3). Three pairs of disc-shaped samples were employed, molded at 100°C. at pressures of about 5000 lb./sq. in. for at least 8 hr. Prior to molding, the polymer was dried *in vacuo* at 40°C.; and a porous bag of silica gel was suspended in the transducer apparatus to maintain a moisture-free atmosphere during measurements. There was no change in weight of any of the samples while in the transducer.

Samples 45 had dimensions of $^{11}\!/_{16}$ in. (diameter) by $^{3}\!/_{32}$ in. (thickness) and, after compression, a sample coefficient (5) of 20.2 cm. at 25°C. Samples 46 had dimensions of $^{11}\!/_{32}$ in. by $^{3}\!/_{16}$ in. and a sample coefficient after compression of 2.75 cm. Samples 48 had dimensions of $1\frac{1}{16}$ in. by $\frac{1}{32}$ in. and a nominal sample coefficient of 53.3 cm.

---

[1] Part XX of a series on Mechanical Properties of Substances of High Molecular Weight.

[2] Present address: The Chemstrand Corporation, Decatur, Alabama.

Where the data overlapped at the same temperatures and frequencies, those for samples 45 and 46 agreed very well, but values of J' and J'' for samples 48 were smaller by about 32%. The ratios J''/J' were in agreement in all cases, indicating that the latter discrepancy was due to an error in the sample coefficient, not unexpected in view of the extremely small thickness of samples 48 and the difficulty of measuring this dimension accurately. Accordingly, all the data from samples 48 were corrected by a constant empirical factor.

Sample coefficients at temperatures other than 25°C. were calculated, as usual, on the assumption that the sample thickness remained constant. The change in volume with temperature was calculated taking the thermal expansion coefficient as 6.6×10^{-4} deg.$^{-1}$ (6, 7).

RESULTS

The original data for J' and J'', measured at 12 temperatures from 25.00 to 89.15°C. and at 8 to 12 frequencies at each temperature, from 30 to

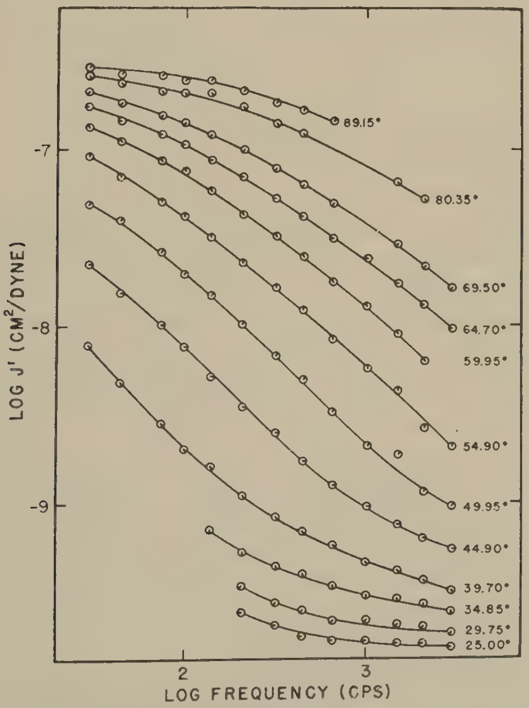

FIG. 1. Real part of the complex compliance, plotted logarithmically against frequency at 12 temperatures as indicated.

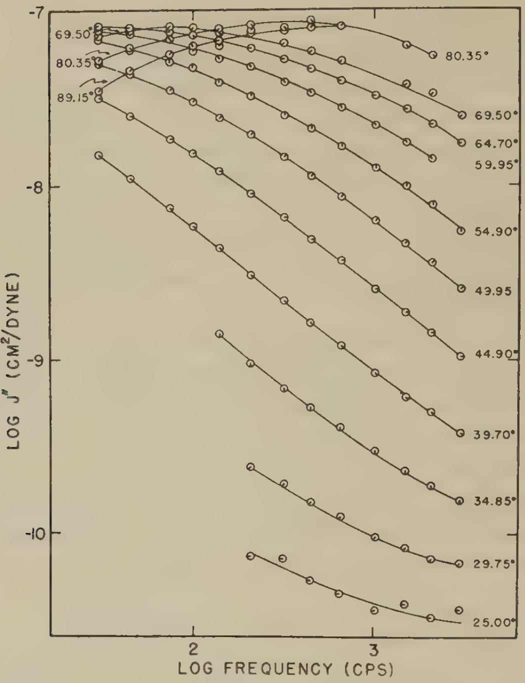

FIG. 2. Imaginary part of the complex compliance, plotted logarithmically against frequency at 12 temperatures as indicated.

3000 cycles/sec., are shown in Figs. 1 and 2. Where data on different samples were taken at the same frequencies and temperatures, the values have been averaged. The results are also presented as plots of the reduced variables J'_p and J''_p, calculated in the usual manner (1–3, 8) with 25°C. chosen as the reference temperature, in Figs. 3 and 4. For the reduction, J_∞ (the limiting high frequency value of J') was estimated to be 1.0×10^{-10} cm.^{2}/dyne. The shift factors a_T used to reduce the frequency scale will be discussed below. The superposition at all temperatures and frequencies is excellent.

The value of J'_p varies from $10^{-9.82}$ to $10^{-6.47}$ within the range of reduced frequency covered, while J''_p passes through a maximum value of $10^{-7.05}$. The maximum value of the loss tangent J''_p/J'_p is 2.85, representing a sharpness of dispersion rather similar to that of polystyrene (maximum of 2.75) and intermediate between those of polyvinyl acetate (maximum of 3.55) and polystyrene (maximum of 1.65).

The data were also calculated as the real and imaginary parts of the complex rigidity, $G' + iG''$. The value of G' ranged from $10^{6.47}$ to $10^{9.79}$, and G'' passed through a maximum value of $10^{9.25}$.

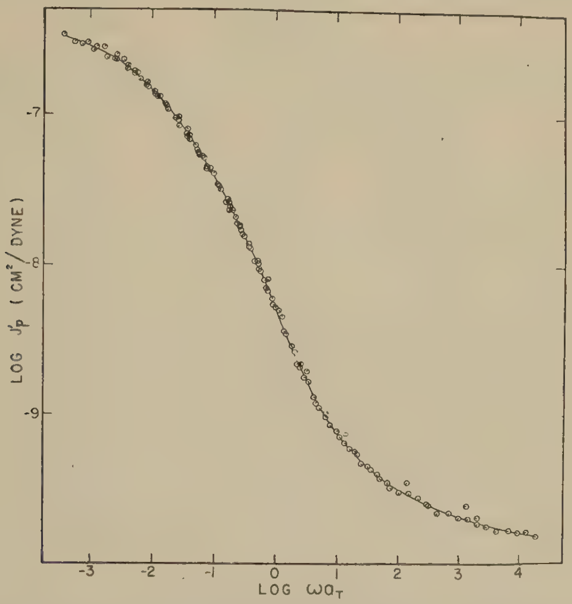

FIG. 3. Real part of the complex compliance reduced to 25°C., plotted logarithmically against reduced frequency. Pip lift at highest reduced frequency, 25.0°C.; successive 45° rotations counterclockwise, successive temperatures as listed in Table II.

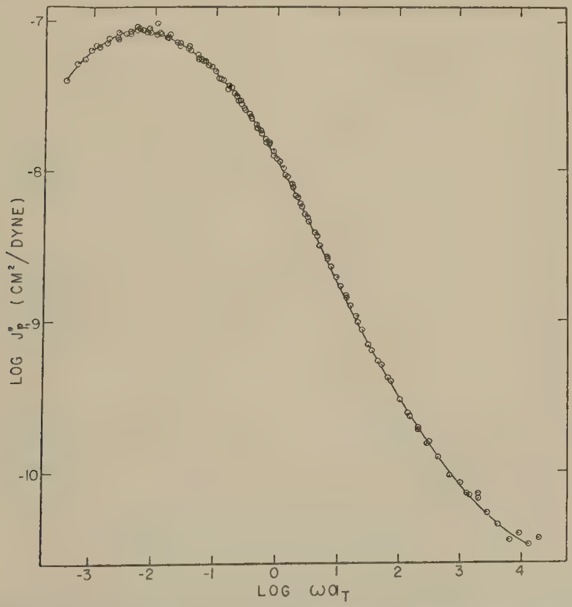

FIG. 4. Imaginary part of the complex compliance reduced to 25°C., plotted logarithmically against reduced frequency. Temperature key same as in Fig. 1.

TABLE I

Relaxation and Retardation Distribution Functions Reduced to 25°C.

Log τ (*sec.*)	Log Φ (*dyne/cm.*^{2})		Log L (*cm.*^{2}*/dyne*)	
	From G'	From G''	From J'	From J''
3.0	5.58	5.50	−7.34	−7.37
2.5	5.77	5.74	−7.22	−7.23
2.0	6.08	6.04	−7.22	−7.24
1.5	6.31	6.32	−7.36	−7.35
1.0	6.56	6.64	−7.62	−7.52
0.5	6.87	6.86	−7.97	−8.00
0.0	7.03	7.16	−8.47	−8.54
−0.5	7.48	7.50	−9.05	−9.32
−1.0	8.11	7.91	−9.59	−9.55
−1.5	8.62	8.67	−9.87	−9.78
−2.0	9.00	9.08	−10.12	−10.04
−2.5	9.06	9.07	−10.36	−10.28
−3.0	8.98	9.04	−10.52	−10.48
−3.5	8.98	9.00	−10.73	−10.64
−4.0	8.50	8.95	−10.92	−10.72

DISTRIBUTION FUNCTIONS

The relaxation and retardation distribution functions, Φ and L, reduced to 25°C., have been calculated from the data of Figs. 3 and 4 and corresponding plots of G' and G'' by our second approximation formulas (9),

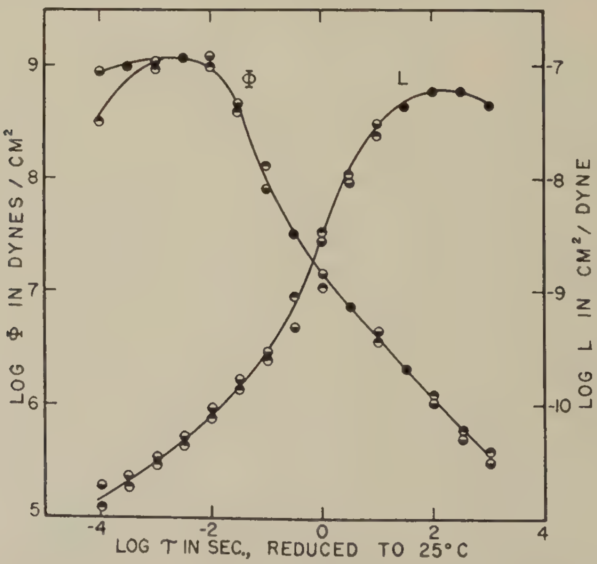

FIG. 5. Distribution functions of relaxation times (Φ) and retardation times (L), plotted logarithmically, reduced to 25°C. Key to points: top black, calculated from G'_p or J'_p; bottom black, from G''_p or J''_p.

TABLE II

Reduction Factors

Temp. (°C.)	Log a_T	Temp. (°C.)	Log a_T
25.00	0.00	54.90	−3.88
29.75	−0.98	59.95	−4.26
34.85	−1.80	64.70	−4.58
39.70	−2.42	69.50	−4.88
44.90	−3.00	80.35	−5.42
49.95	−3.47	89.15	−5.72

and are listed in Table I. The agreement between real and imaginary sources is quite good and provides, as usual, a check on the precision and consistency of the measurements. The shapes of the distribution functions (Fig. 5) are similar to those found for other polymers in the transition zones between rubberlike and glasslike consistency.

At its right end, the double logarithmic plot of Φ has the slope of $-\frac{1}{2}$ required by the Rouse theory (10); from the intercept of a line drawn with this slope through the data, the friction coefficient per monomer unit, ζ_0, can be calculated (11, 12).[3] Taking for a, the root-mean-square end-to-end distance per monomer unit, a value of 6.8 A., we find log ζ_0 at 25°C. (in dyne sec./cm.) to be 0.32.

TEMPERATURE DEPENDENCE

The applicability of the method of reduced variables as illustrated in Figs. 3 and 4 shows that the temperature dependence of mechanical properties can be fully described by that of the shift factor a_T, which in turn is practically identical with the temperature dependence of the friction coefficient ζ_0. Values of a_T, obtained from the reduction process, are listed in Table II, referred to 25°C. as a reference temperature.

It is of interest to compare the factor a_T with the corresponding factor b_T, which describes the temperature dependence of dielectric relaxation, as obtained from a recent analysis (13) of the dielectric dispersion data on this polymer reported by Mead and Fuoss (14). The values are compared in Fig. 6, and show excellent agreement, showing that the rates of molecular response to mechanical and electrical stress have the same temperature dependence.

The reference temperature for the factors plotted in Fig. 6 is not 298°K. as in Table II but 324°K., chosen to compare the temperature dependence with that prescribed by a recently proposed equation (15)

$$\log a_T = -8.86 \frac{T - T_s}{101.6 + T - T_s}, \quad [1]$$

---

[3] Log ζ_0 for polyvinyl acetate and a 5%0 solution thereof (at 40°C.) as given in a previous paper (12) should be corrected to 1.75 and −5.25, respectively. The value used for a in their calculation should have been 6.9 A. rather than 2.8 A.

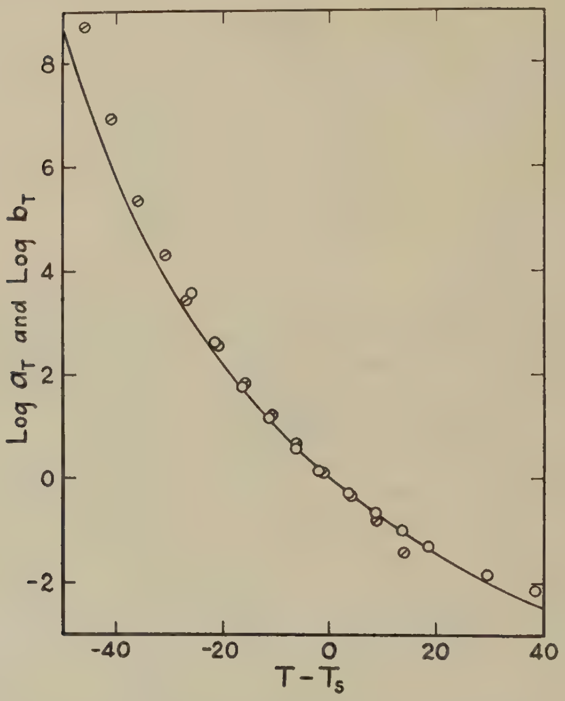

FIG. 6. Log a_T (open circles) and log b_T (slotted circles), reduced to T_s (= 324°K.) and plotted against $T - T_s$. The curve is given by Eq. [1].

which with suitable choices of T_s reproduces approximately data for many polymer systems in the range $-50° < T - T_s < 50°C$. This equation follows the experimental values quite closely except at the lowest temperatures. A closer fit can be obtained by some alteration of the empirical constants in the equation; in terms of the interpretation which has been given (15, 16) this is equivalent to assuming that the fractional free volume at the glass transition temperature (f_g) and its thermal expansion coefficient (α_2) are not exactly the same for all polymers, but vary somewhat from one polymer system to another. For example, the data in Fig. 6 can be fitted by taking $f_g = 0.024$ and $\alpha_2 = 5.3 \times 10^{-4}$ instead of the "universal" values of 0.025 and 4.8×10^{-4} which were derived from Eq. [1]. This modification will be examined further in a later communication.

Earlier conclusions that the apparent activation energies for mechanical and electrical relaxations in polymethyl acrylate are different (17, 18) were evidently based on an erroneous comparison of values calculated in different temperature ranges. The apparent activation energy is of course strongly temperature-dependent (13, 15), but from Fig. 6 it is clear that values for mechanical and electrical relaxations calculated at the same temperature will be practically identical.

ACKNOWLEDGMENTS

The work was supported by Picatinny Arsenal, Ordnance Corps, Department of the Army. We are much indebted to Mrs. J. C. Alexander for assistance in calculations.

SUMMARY

The real and imaginary components of the complex compliance have been measured between 30 and 3000 cycles/sec. in the temperature range 25° to 89°C. for a sample of polymethyl acrylate of weight-average molecular weight 2.2×10^6. Results at all temperatures and frequencies superpose by the method of reduced variables to give the components at 25°C. over 7.5 decades of frequency, corresponding to the transition from rubberlike to glasslike consistency as a function of frequency at this temperature. Relaxation and retardation distribution functions have been calculated, and the friction coefficient per monomer unit has been estimated from an extension of the Rouse theory. The temperature dependence of the relaxation processes agrees with that derived from dielectric measurements, and it has been analyzed in terms of the free volume and its thermal expansion coefficient.

REFERENCES

1. FITZGERALD, E. R., GRANDINE, L. D., JR., AND FERRY, J. D., *J. Appl. Phys.* **24,** 650 (1953).
2. GRANDINE, L. D., JR., AND FERRY, J. D., *J. Appl. Phys.* **24,** 679 (1953).
3. WILLIAMS, M. L., AND FERRY, J. D., *J. Colloid Sci.* **9,** 479 (1954).
4. AXELROD, S., MATLACK, J. D., CHINAI, S. N., AND RESNICK, A. L., to be published.
5. FITZGERALD, E. R., AND FERRY, J. D., *J. Colloid Sci.* **8,** 1 (1953).
6. MATHESON, M. S., AUER, E. E., BEVILACQUA, E. B., AND HART, E. J., *J. Am. Chem. Soc.* **73,** 5395 (1951).
7. FOX, T. G., Private communication.
8. FERRY, J. D., AND FITZGERALD, E. R., *J. Colloid Sci.* **8,** 223 (1953).
9. WILLIAMS, M. L., AND FERRY, J. D., *J. Polymer Sci.* **11,** 169 (1953).
10. ROUSE, P. E., JR., *J. Chem. Phys.* **21,** 1272 (1953).
11. FERRY, J. D., LANDEL, R. F., AND WILLIAMS, M. L., *J. Appl. Phys.* **26,** 359 (1955).
12. WILLIAMS, M. L., AND FERRY, J. D., *J. Colloid Sci.* **10,** 1 (1955).
13. FERRY, J. D., WILLIAMS, M. L., AND FITZGERALD, E. R., *J. Phys. Chem.* **59,** 403 (1955).
14. MEAD, D. J., AND FUOSS, R. M., *J. Am. Chem. Soc.* **64,** 2389 (1942).
15. WILLIAMS, M. L., LANDEL, R. F., AND FERRY, J. D., *J. Am. Chem. Soc.* **77.** 3701 (1955).
16. BUECHE, F., *J. Chem. Phys.*, in press.
17. BROENS, O., AND MÜLLER, F. H., *Kolloid-Z.* **119,** 45 (1950).
18. IWAYANAGI, S., *J. Sci. Research Inst. (Tokyo)* **49,** 13 (1955).

RHEOLOGY OF SYNTHETIC LATEX

V. Flow Behavior of Low-Temperature GR-S Latex

Samuel H. Maron and Shiu Ming Fok

Physical Chemistry Laboratory, Department of Chemistry and Chemical Engineering,
Case Institute of Technology, Cleveland, Ohio

Received June 27, 1955

Introduction

Preceding papers (1–3) from this laboratory have described rheologic studies made on 70:30 and 50:50 butadiene-styrene latices prepared at higher temperatures. The present report describes similar investigations made on X-667 latex, which was prepared at low temperature. The aim was to see whether the rheologic behavior of the two types was similar, and, if not, in what respects they differed. The variables investigated were rate of shear, concentration, and temperature.

Experimental

The GR-S X-667 latex investigated was prepared by low-temperature technique and was supplied by the Copolymer Corp., Baton Rouge, Louisiana. It consisted of an aqueous dispersion of 84:16 butadiene-styrene copolymer emulsified with potassium oleate soap. The original concentration of the latex was 62.2% solids and 58.6% rubber by weight. With the use of the conductometric titration techniques of Maron, Ulevitch, and Elder (4, 5), this latex was found to have the following analysis:

Soap content	0.1354 meq./g. sample
Free acid content	0.0024 meq./g. sample
pH at 25°C.	9.78
Volume to surface average diameter (D_s)	1388 A.

This concentrate was diluted with boiled, distilled water to obtain lower concentrations. Solids contents of the diluted latices were determined by drying weighed samples in a vacuum oven to constant weight.

All flow measurements were made with the continuously variable pressure head viscometer of Maron, Krieger, and Sisko (6). Several different-size capillaries were used to cover the desired range. Calibration and operation of the viscometer have been described in detail by the above authors.

TABLE I

Density of Polymer Calculated by Means of Equation [1] at 30°C.

Total solids (%)	Dry rubber content C_r (%)	Density of latex d (g./cc.)	Density of rubber, d_r (g./cc.)
19.92	18.77	0.9812	0.923
15.08	14.21	0.9848	0.924
10.03	9.45	0.9884	0.924
7.79	7.34	0.9899	0.923
6.02	5.67	0.9912	0.923
4.02	3.79	0.9925	0.920
3.01	2.83	0.9935	0.926
2.16	2.03	0.9941	0.927
2.04	1.92	0.9943	0.932
1.46	1.38	0.9945	0.922
0.997	0.939	0.9950	0.935
		Average	0.925 ± 0.003 ± 0.32%

The four temperatures employed for the present study were 20.13° ± 0.04°C., 29.94° ± 0.04°C., 39.74° ± 0.03°C., and 50.00° ± 0.02°C.

RESULTS AND DISCUSSION

Determination of the Volume Fraction of the Polymer

For calculation of the volume fraction of polymer present in the latex samples, it is necessary to know the density of the contained polymer. It was found possible to obtain this quantity from the densities of the latex solutions by assuming (*1*) that the volumes of rubber and serum were additive, and (*2*) that the density of the serum was the same as that of pure water. On the basis of these assumptions the density of the polymer, d_r, follows as

$$d_r = \frac{C_r}{(100/d) - [(100 - C_r)/d_w]}, \qquad [1]$$

where d is the density of the latex solution, d_w is the density of the water at the temperature in question, and C_r is the dry rubber content of the latex in per cent. Results obtained in this manner are summarized in Table I. Over about a 20-fold concentration range, an average value of $d_r = 0.925 \pm 0.3\,\%$ was obtained.

The volume fraction of rubber in the latex solution is given by

$$v = \frac{V_r}{V} = \frac{C_r/d_r}{100/d}, \qquad [2]$$

where V_r is the volume of the rubber and V the volume of the latex solution.

TABLE II

Relative Viscosity of GR-S X-667 Latex in the Newtonian Range

Total solids (%)	Volume fraction v	Relative viscosity η_r			
		20.13°C.	29.94°C.	39.74°C.	50.00°C.
0.00	0.0000	1.000	1.000	1.000	1.000
3.03	0.0306	1.085	1.088	1.092	1.101
5.09	0.0515	1.157	1.164	1.172	1.183
10.02	0.1010	1.363	1.361	1.366	1.375
17.92	0.1795	1.819	1.845	1.841	1.854
24.89	0.2481	2.479	2.491	2.532	2.528

By combination of Eqs. [1] and [2] to eliminate d, the volume fraction v can be calculated from the equation

$$v = \frac{1}{1 + (d_r/d_w)[(100/C_r) - 1]}. \qquad [3]$$

Since for this latex $C_r = 0.942$ (total solids), and the ratio (d_r/d_w) can be assumed to be temperature-independent, then any concentration of the latex is easily converted into volume fraction by means of Eq. [3].

Flow Behavior of the Latex

The latex studied showed Newtonian behavior up to approximately 25% solids content between 20° and 50°C. The viscosities relative to water, η_r,

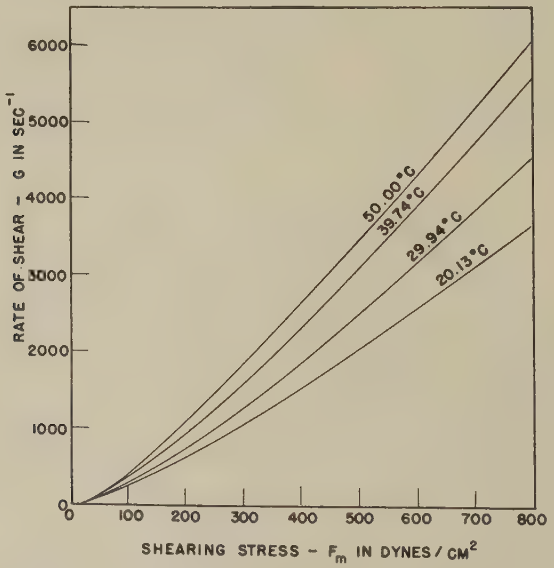

FIG. 1. G vs. F_m plots for 55.25% solids X-667 latex.

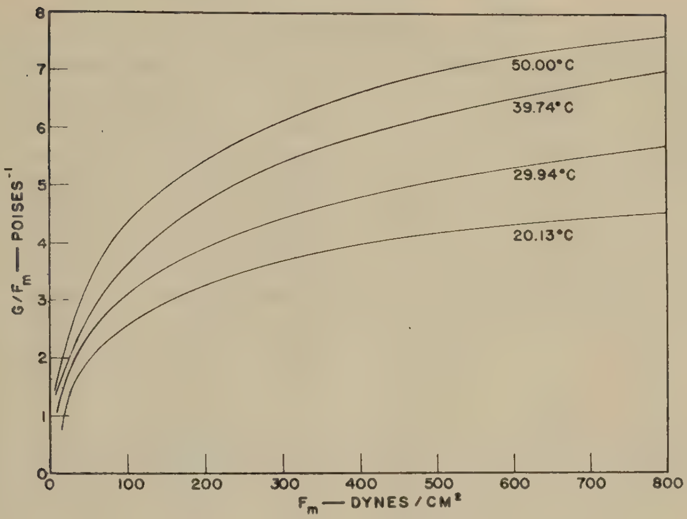

FIG. 2. G/F_m vs. F_m plots for 55.25% solids X-667 latex.

observed in this range of temperatures and concentrations are given in Table II.

Above 25% solids the latex gave non-Newtonian behavior, and here the standard treatment of Krieger and Maron (7) was used to obtain the flow curves for each concentration at the four temperatures. Typical rate of shear (G)-shear stress (F_m) curves observed are shown in Fig. 1. In Fig. 2, in turn, are shown plots of G/F_m vs. F_m. Plots of this type bring out more clearly the non-Newtonian character of the latex, particularly when it is realized that a Newtonian fluid would yield a straight line parallel to the abscissa.

Let us now define the relative viscosity of the latex in the non-Newtonian region to be

$$\eta_r = \frac{(F_m/G)}{\eta_w} = \frac{F_m}{G\eta_w}, \qquad [4]$$

where η_w is the viscosity of water at temperature of measurement. Values of relative viscosity thus calculated from the G/F_m vs. F_m curves at selected constant shear stresses are given in Table III for various concentrations of the latex at the different temperatures.

An attempt was made to represent the above flow data at any given concentration by means of the exponential flow equation (8, 9)

$$F_m^N = \eta' G \qquad [5]$$

which may be rewritten to

$$\log \eta_r = (1 - N) \log F_m + \log \eta_r'. \qquad [6]$$

TABLE III

Relative Viscosities of GR-S X-667 Latex in the Non-Newtonian Range

Total solids (%)	Volume fraction v	F_m (*dynes/cm.*^{2})	Relative viscosity η_r			
			20.13°C.	29.94°C.	39.74°C.	50.00°C.
30.11	0.2990	50	3.249	3.293	3.314	3.328
		100	3.186	3.218	3.240	3.249
		200	3.131	3.157	3.183	3.192
		300	3.107	3.132	3.157	3.175
		500	3.085	3.110	3.130	3.167
40.27	0.3970	50	6.365	6.424	6.519	6.546
		100	6.028	6.081	6.145	6.175
		200	5.761	5.802	5.832	5.890
		300	5.641	5.689	5.695	5.756
		500	5.519	5.607	5.576	5.632
44.74	0.4398	50	9.730	9.879	10.011	10.143
		100	8.821	8.993	9.216	9.254
		200	8.220	8.363	8.472	8.604
		300	7.984	8.082	8.124	8.307
		500	7.737	7.790	7.876	8.008
		800	7.591	7.597	7.791	7.839
49.78	0.4876	50	17.00	17.18	17.90	18.08
		100	14.99	15.17	15.42	15.62
		200	13.24	13.44	13.77	13.81
		300	12.52	12.70	13.02	13.06
		500	11.88	12.03	12.34	12.27
		800	11.36	11.66	12.07	11.61
55.25	0.5390	50	49.32	52.20	55.13	55.33
		100	38.51	40.02	41.80	41.97
		200	31.09	31.55	32.58	33.56
		300	27.36	27.96	28.44	29.74
		500	24.07	24.51	24.38	26.08
		800	21.81	21.98	21.71	24.06
57.53	0.5603	50	99.13	107.07	109.47	117.79
		100	68.58	71.18	74.22	78.03
		200	50.06	52.20	55.13	56.01
		300	43.53	45.39	47.11	48.30
		500	37.22	39.15	39.83	40.85
		800	33.15	34.80	34.58	35.11
60.34	0.5866	50	385.08	404.10	422.67	450.81
		100	196.31	208.78	219.88	237.12
		200	116.42	122.21	128.73	137.28
		300	91.02	96.58	100.17	105.42
		500	72.55	79.28	79.75	82.99
		800	62.58	68.01	67.39	67.62
61.97	0.6017	50	1112.4	1089.3	1289.5	1304.1
		100	455.1	464.0	507.2	545.0
		200	222.5	241.8	258.8	278.7
		300	164.1	176.9	190.2	200.6
		500	125.5	131.2	136.0	142.6
		800	100.6	105.3	108.3	114.1

Here N is an index of non-Newtonian behavior ($N = 1$ in the Newtonian limit), F_m is the shear stress at the wall of the capillary, G is the rate of shear at the wall of the capillary, η_r is the relative viscosity of the latex, and η_r' is the relative viscosity of the latex at unit shear stress. However, the plots of log η_r vs. log F_m made of the data for various concentrations in the non-Newtonian region were found to be nonlinear, and hence, Eq. [6] was inapplicable with constant N. Similar attempts made with other types of equations for representation of G as a function of F_m also failed. Hence, attention was turned to expression of η_r as a function of v.

Maron, Madow, and Krieger (2) employed for this purpose the equation

$$\log \eta_r = \frac{\alpha\beta v}{1 - \alpha v}, \qquad [7]$$

where α and β are constants. However, this equation was also found to be inapplicable. Consequently, the Eilers equation (10), modified to the form

$$\eta_r = \left[1 + \frac{\alpha v}{1 - \beta v}\right]^2, \qquad [8]$$

where α and β are constants, was tried at any given shear stress and temperature, and was found to be satisfactory. This equation can be rearranged to the form

$$\frac{(\eta_r^{1/2} - 1)}{v} = \alpha + \beta(\eta_r^{1/2} - 1) \qquad [9]$$

and hence by plotting $(\eta_r^{1/2} - 1)/v$ vs. $(\eta_r^{1/2} - 1)$ the constants α and β can be obtained from the resulting straight lines at given shear stress,

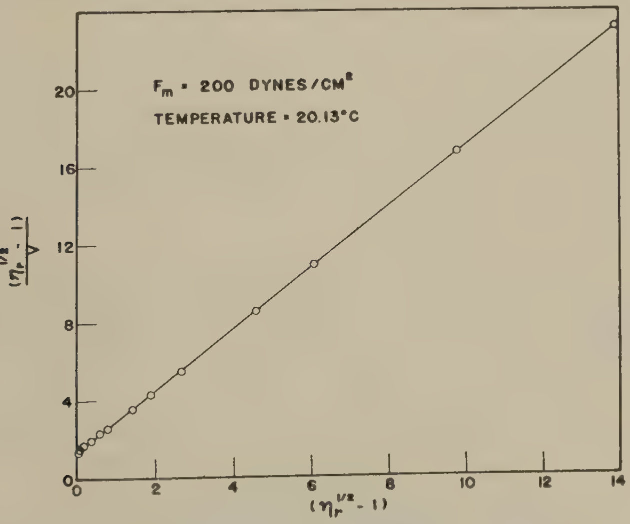

FIG. 3. Modified Eilers equation plot for X-667 latex.

TABLE IV

Flow Constants for X-667 Latex

Temperature (°C.)	F_m (dynes/cm.²)	α	β	$\frac{2\alpha}{1.119}$	$1/\beta$	$1.119\,\frac{1}{\beta}$
20.13	50	1.377	1.623	2.46	0.616	0.689
	100	1.356	1.598	2.42	0.626	0.700
	200	1.353	1.564	2.42	0.639	0.715
	300	1.355	1.545	2.42	0.647	0.724
	500	1.358	1.524	2.43	0.656	0.734
	800	1.360	1.506	2.43	0.664	0.743
29.94	50	1.405	1.622	2.51	0.616	0.689
	100	1.379	1.597	2.46	0.626	0.700
	200	1.371	1.566	2.45	0.638	0.714
	300	1.373	1.548	2.45	0.646	0.723
	500	1.377	1.527	2.46	0.655	0.733
	800	1.382	1.508	2.47	0.663	0.742
39.74	50	1.430	1.624	2.56	0.616	0.689
	100	1.404	1.598	2.51	0.626	0.700
	200	1.396	1.568	2.50	0.638	0.714
	300	1.395	1.549	2.49	0.646	0.723
	500	1.400	1.525	2.50	0.656	0.734
	800	1.414	1.505	2.53	0.665	0.744
50.00	50	1.464	1.624	2.62	0.616	0.689
	100	1.435	1.599	2.57	9.625	0.699
	200	1.428	1.569	2.55	0.638	0.714
	300	1.431	1.549	2.56	0.646	0.723
	500	1.439	1.524	2.57	0.656	0.734
	800	1.457	1.502	2.60	0.666	0.745

F_m, and temperature. A typical such plot is shown in Fig. 3. The values of α and β obtained by least squares from such plots at various F_m and temperatures are summarized in Table IV.

The validity of Eq. [9] can be tested further by using it to calculate v's corresponding to given values of η_r, and comparing these with the observed v values. Such calculations at constant F_m's ranging from 50 to 800 dynes/cm.² and at all four temperatures show the agreement between the equation and experiment to be within better than 2%.

The values of α in the third column may be seen to be independent of F_m but dependent on temperature, while the values of β (fourth column) vary with F_m, but are independent of temperature at any given shear stress. It was found that the variation of α with temperature can be represented by the equation

$$\alpha = 0.5165 + 0.002855\,T, \qquad [10]$$

where T is the absolute temperature, and the variation of β with F_m by

$$\beta = \frac{1 + 0.00466\,F_m}{0.600 + 0.00317\,F_m}. \qquad [11]$$

Substituting Eqs. [10] and [11] into Eq. [8], we obtain finally

$$\eta_r = \left[1 + \frac{(0.5165 + 0.002855\ T)v}{1 - (1 + 0.00466\ F_m/0.600 + 0.00317\ F_m)}\right]^2 \qquad [12]$$

which is the equation representing the flow behavior of this latex as a function of F_m, T, and v. Furthermore, although Eq. [12] was deduced from the flow data in the non-Newtonian region, it also reproduces very satisfactorily the data for the Newtonian range shown in Table II.

Limiting Conditions of Flow Predicted by Eq. [8]

On taking logarithms of both sides of Eq. [8] we obtain

$$\ln \eta_r = 2 \ln \left(1 + \frac{\alpha v}{1 - \beta v}\right).$$

When $v \rightarrow 0$, βv is negligible compared to unity, and hence

$$\ln \eta_r = 2 \ln (1 + \alpha v).$$

Since as $v \rightarrow 0$, η_r is close to unity, and αv becomes small compared to 1, expansion of the logarithms in series yields

$$\eta_r - 1 = \eta_{sp} = 2\alpha v$$

or

$$\frac{\eta_{sp}}{v} = 2\alpha. \qquad [13]$$

Consequently, on approach to infinite dilution η_{sp}/v should equal 2α, and this, in turn, should be equal to 2.50, in line with the Einstein theory (11) of dilute suspensions of spheres.

Inspection of Table IV shows that in all instances the values of 2α are larger than the expected 2.50, and range in fact from 2.72 to 2.88. However, the values of α were obtained on the basis of v, the volume fraction of rubber only, whereas the actual volume occupied by the particles, v_t, is larger than v because of the adsorbed monolayer of soap. Now, Maron, Madow, and Krieger (2) have shown that

$$\frac{v_t}{v} = 1 + \frac{6\Delta}{D_s}, \qquad [14]$$

where D_s is the volume to surface average diameter of the latex particles, 1388 A. for the latex under study, and Δ is the length of the adsorbed soap molecule, which is 27.5 A. for oleate soap. Inserting these values of D_s and Δ into Eq. [14] we obtain $v = v_t/1.119$, and insertion of this value of v into Eq. [13] yields

$$\frac{\eta_{sp}}{v_t} = \frac{2\alpha}{1.119}, \qquad [15]$$

and hence $2\alpha/1.119$ should be equal to the Einstein 2.50 factor.

The values of $(2\alpha/1.119)$, given in column 5 of Table IV, range now from 2.42 to 2.62, and give an average value of 2.50 ± 0.05, in excellent accord with the predictions of the Einstein equation.

Equation [8] also predicts that η_r will become infinite when $v = 1/\beta$. For rhombohedral close packing of nonuniform spheres the volume fraction at which the viscosity becomes infinite should be 0.74 to 0.78 (12). However, the values of $1/\beta$ listed in column 6 of Table IV are considerably lower than expected, again owing to the fact that no allowance has been made for the adsorbed layer of soap. When this is done, by multiplying $1/\beta$ by the factor given by Eq. [14], we obtain the results shown in the last column of Table IV. These corrected volume fractions are independent of temperature, but increase slightly from $v_t = 0.69$ at $F_m = 50$ to $v_t = 0.75$ at $F_m = 800$ dynes/cm.^{2}. The fact that they are lower than expected for rhombohedral packing of nonuniform spheres suggests that the close packing in this system is tetragonal rather than rhombohedral, with each particle having 10 rather than 12 close neighbors (12). For such a packing v_t should be 0.70 to 0.74, which is very close to the observed values. Furthermore, the results indicate that the packing becomes tighter as F_m increases, and tends to become rhombohedral at higher shearing stresses.

Effect of Temperature on Flow Behavior

The variation of viscosity of a fluid with temperature can be represented by the relation

$$\frac{\partial \ln \eta}{\partial T} = -\frac{E}{RT^2}, \qquad [16]$$

where E is the energy of activation for flow. In terms of relative viscosity, Eq. [16] becomes

$$\frac{\partial \ln \eta_r}{\partial T} = -\left(\frac{E - E_w}{RT^2}\right) \qquad [17]$$

or

$$\frac{\partial \ln \eta_r}{\partial(1/T)} = \frac{(E - E_w)}{R}, \qquad [18]$$

where E_w is the energy of activation for flow of water. Again, by differentiation of Eq. [12] with respect to $(1/T)$ at constant v and F_m we obtain

$$\left[\frac{\partial \ln \eta_r}{\partial(1/T)}\right]_{v,F_m} = \frac{-0.00571\, vT^2}{1 - \beta(F_m)v + \alpha(T)v}, \qquad [19]$$

where $\alpha(T)$ and $\beta(F_m)$ are the functions given by Eqs. [10] and [11]. It follows, therefore, from Eqs. [18] and [19], that

$$E_w - E = \frac{0.00571\, vT^2}{1 - \beta(F_m)v + \alpha(T)v}. \qquad [20]$$

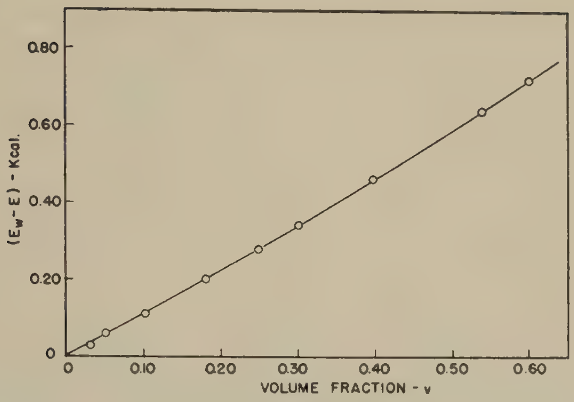

FIG. 4. Variation of $(E_w - E)$ with volume fraction.

Using Eq. [20], values of $(E_w - E)$ were calculated at selected values of v, T, and F_m. The results showed that $(E_w - E)$ varied only slightly and insignificantly with F_m and T, and that the significant variation of $(E_w - E)$ is with v. This variation, shown in Fig. 4, indicates that $(E_w - E)$ is positive and increases almost linearly with v. This means that the energy of activation for flow of the latex is *lower* than that for pure water; and, furthermore, that E is the smaller the more concentrated the latex. It should be emphasized, however, that the biggest difference between E_w and E is only 0.72 kcal. at $v = 0.60$, which amounts to about 20% of E_w in this region (13). From these results it is evident that to a first approximation the variation in the viscosity of the latex with temperature is due primarily to the change in the viscosity of the water. Again, the small observed increase of η_r with temperature at any given v is due to the change in the activation energy of the water caused by dispersion in it of the polymer particles. The direction of the change in E is such as to suggest that with increase in v the medium becomes less polar and associated, and hence that the dispersion of the polymer particles operates to decrease the extent of hydrogen bonding of the water.

Deviation of Latex from Newtonian Behavior

Differentiation of Eq. [12] with respect to F_m at constant v and T leads to

$$\left[\frac{\partial \ln \eta_r}{\partial \ln F_m}\right]_{v,T} = \frac{-0.00075\, v^2 F_m\, \alpha(T)}{(0.600 + 0.00317\, F_m)^2[1 - \beta(F_m)v][1 - \beta(F_m)v + \alpha(T)v]}. \qquad [21]$$

Again, if we consider Eq. [6] as a flow equation with variable N at any given v and T, then differentiation with respect to F_m yields

$$\left[\frac{\partial \ln \eta_r}{\partial \ln F_m}\right]_{v,T} = (1 - N). \qquad [22]$$

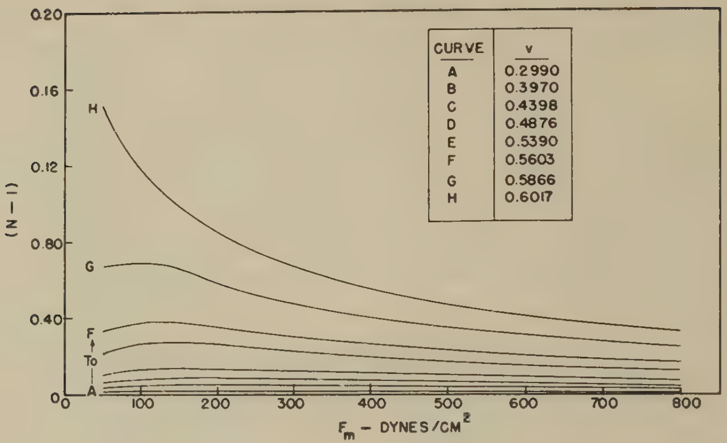

FIG. 5. Dependence of $(N - 1)$ on F_m and v for X-667 latex.

From these two equations it follows, therefore, that

$$(N - 1) = \frac{0.00075\, v^2 F_m \alpha(T)}{(0.600 + 0.00317\, F_m)^2[1 - \beta(F_m)v][1 - \beta(F_m)v + \alpha(T)v]}. \quad [23]$$

Equation [23] expresses the deviation of the latex from Newtonian flow as a function of v, T, and F_m. Using this equation $(N - 1)$ values were calculated at the four temperatures for various values of v and F_m. These proved to be independent of temperature within 1% or less, and to be a function primarily of v and F_m.

The manner in which $(N - 1)$ varies with F_m at various values of v is given in Fig. 5. These curves show that the deviation from Newtonian flow behavior increases with concentration at any given value of F_m. Again, for values of v up to *ca.* 0.44, $(N - 1)$ is only slightly dependent on F_m. Above $v = 0.44$, however, the values of $(N - 1)$ increase with decreasing F_m, and then pass through maxima at F_m's which are the lower the higher the concentration. Although such a maximum was not observed at $v = 0.60$, it is conceivable from the shape of the curve that a maximum may appear below $F_m = 50$ dynes/cm.^{2}.

The results shown in Fig. 5 suggest that it would be of considerable interest to ascertain the dependence of $(N - 1)$ on F_m at shear stresses below those investigated here. Such a study is under way at present in this laboratory.

ACKNOWLEDGMENT

This research was sponsored by the Office of Synthetic Rubber, Federal Facilities Corporation, in connection with the government Synthetic Rubber Program.

SUMMARY

The flow behavior of a GR-S latex prepared at low temperature was studied at volume fractions up to 0.60 over a shear stress region of 50–800

dynes/cm.^{2}, and over a temperature range of 20° to 50°C. The latex was found to be Newtonian below a volume fraction of 0.25, and non-Newtonian above this concentration. Unlike some preceding latices investigated, the dependence of flow of this latex on shear stress could not be represented by the exponential equation, nor could the concentration dependence be expressed by the logarithmic equation employed before.

However, the flow behavior of this latex could be represented by a two-parameter modified Eilers equation in which one of the parameters is a function of the temperature, the other, of shear stress. The limiting form of the expression as the volume fraction v approaches zero yielded $\eta_{sp}/v = 2.50 \pm 0.05$, as against the expected Einstein value of 2.50 for dilute suspensions of spheres. Again, the expression predicted for the volume fractions at which the viscosity becomes infinite values ranging from 0.69 at $F_m = 50$ to 0.75 at $F_m = 800$ dynes /cm.^{2}. These values indicate that the close packing of the nonuniform spheres in the latex is primarily tetragonal, with a transition to rhombohedral packing as F_m increases.

The results also show that the variation of the viscosity of the latex with temperature is due primarily to the change in the viscosity of the water, and only secondarily to the decrease in the energy of activation for flow of the latex with increase in concentration. Finally, it was found that the deviation of the latex from Newtonian behavior is essentially independent of temperature, and dependent only on shear stress and concentration. The dependence on shear stress is more complicated, with maxima occurring in the curves at shear stresses which are the lower the higher the volume fraction of polymer in the latex.

REFERENCES

1. KRIEGER, I. M., AND MARON, S. H., *J. Colloid Sci.* **6,** 528 (1951).
2. MARON, S. H., MADOW, B. P., AND KRIEGER, I. M., *J. Colloid Sci.* **6,** 584 (1951).
3. MARON, S. H., AND MADOW, B. P., *J. Colloid Sci.* **8,** 130, 300 (1953).
4. MARON, S. H., ULEVITCH, I. N., AND ELDER, M. E., *Anal. Chem.* **24,** 1068 (1952).
5. MARON, S. H., ELDER, M. E., AND ULEVITCH, I. N., *J. Colloid Sci.* **9,** 89 (1954).
6. MARON, S. H., KRIEGER, I. M., AND SISKO, A. W., *J. Appl. Phys.* **25,** 971 (1954).
7. KRIEGER, I. M., AND MARON, S. H., *J. Appl. Phys.* **25,** 72 (1954).
8. PORTER, A. W., AND RAO, P. A. M., *Trans. Faraday Soc.* **23,** 311 (1927).
9. FARROW, F., LOWE, G., AND NEALE, S., *J. Textile Inst.* **19,** T18 (1928).
10. EILERS, H., *Kolloid-Z.* **97,** 313 (1941).
11. EINSTEIN, A., *Ann. Physik* **19,** 289 (1906).
12. HEYWOOD, H., *J. Imp. Coll. Chem. Eng. Soc.* **2,** 9 (1946).
13. GLASSTONE, S., LAIDLER, K. J., AND EYRING, H., "The Theory of Rate Processes." McGraw-Hill, New York, 1941.

RHEOLOGY OF SYNTHETIC LATEX

VI. The Flow Behavior of Neoprene Latex

Samuel H. Maron and Arie E. Levy-Pascal

Physical Chemistry Laboratory, Case Institute of Technology, Cleveland, Ohio

Received July 13, 1955

Introduction

Rheologic studies of synthetic rubber latices published to date from this laboratory (1–4) have dealt with systems containing butadiene-styrene copolymers as the disperse phase. In order to ascertain whether the nature of the disperse phase makes any significant difference in the rheology of a latex, a study was made of the flow behavior of Neoprene Type 60 latex, where the disperse phase consists of polychloroprene and hence is quite different from those investigated before.

The variables studied were shear stress and concentration at a constant temperature of 29.94°C. The range of shear stresses covered was 30–800 dynes/cm.^{2}, and the concentration range extended from 0 to 60 % solids.

Experimental

The Neoprene Type 60 latex was obtained from the E. I. du Pont de Nemours and Company of Wilmington, Delaware. This latex was prepared by polymerizing 2-chloro-1,3-butadiene to Neoprene Type 57 latex, and then concentrating the latter by creaming with approximately 0.15 part of ammonium alginate. The product as received contained sodium N-rosinate soap as the emulsifier, had a total solids content of 63.03 %, and a rubber content of 54.21 % by weight. With the use of the conductometric titration technique of Maron, Ulevitch, Elder, and Moore (5–7), this latex was found to have a volume-to-surface average diameter of D_s = 1100 A.

For each concentration investigated a well-agitated sample of latex was withdrawn from the original batch, strained through a nylon stocking, and diluted to the desired concentration with boiled distilled water. The total solids contents of the latter were checked by taking small weighed samples, adding some isopropanol, and drying them to constant weight in a vacuum oven.

All flow measurements were made at 29.94° ± 0.04°C. in the continuously variable pressure head viscometer described and calibrated by Maron, Krieger, and Sisko (8).

TABLE I

Rubber Density Calculated by Means of Eq. [1] at 30°C.

Total solids (%)	Density of latex d (g./c.c.)	Dry rubber content C_r (%)	Rubber density d_r (g./c.c.)
5.04	1.006	4.79	1.257
11.35	1.018	10.79	1.251
14.90	1.026	14.16	1.259
19.93	1.036	18.93	1.254
24.86	1.046	23.62	1.251
29.52	1.057	28.04	1.256
		Avg.	1.255 ± 0.0027 ± 0.22%

RESULTS AND DISCUSSION

Determination of Polymer Density and Volume Fraction

To calculate the volume fraction of rubber in the different latex samples the density of the polymer must be known. This density, d_r, was obtained from the determined densities of the latex solutions, d, by means of the equation (4)

$$d_r = \frac{C_r}{(100/d) - [(100 - C_r)/(d_w)]}, \qquad [1]$$

where C_r is the dry rubber content of the latex in per cent, and d_w is the density of water. In Table I are given the densities of the latices at various concentrations and the values of d_r calculated from these by means of Eq. [1]. It may be seen that up to a total solids of about 30% the values of d_r are constant and equal to 1.255 ± 0.22%.

With d_r known, the volume fraction of contained polymer, v, follows as (4)

$$v = \frac{1}{1 + (d_r/d_w)[(100/C_r) - 1]}. \qquad [2]$$

Since for the latex under investigation $C_r = 0.950$ (total solids), any total solids concentration of latex can be converted into volume fraction by means of Eq. [2].

Flow Results for the Latex

Viscosity measurements showed the Neoprene latex to be Newtonian up to about 25% total solids. Table II gives the total solids concentrations, the volume fractions, and the viscosities relative to water, η_r, observed in this region of Newtonian behavior.

Above 25% total solids the latex gave non-Newtonian flow. In all these cases the data were processed according to the standardized treatment described by Krieger and Maron (9) in order to obtain the relation between shear stress and rate of shear for each concentration investigated. The flow

TABLE II

Relative Viscosity of Neoprene Type 60 Latex in the Newtonian Range at 29.94°C.

Total solids (%)	Volume fraction v	Relative viscosity η_r
0.00	0.0000	1.000
1.20	0.0091	1.009
5.13	0.0391	1.106
10.00	0.0769	1.283
14.94	0.1160	1.513
19.89	0.1560	1.775
24.92	0.1975	2.257

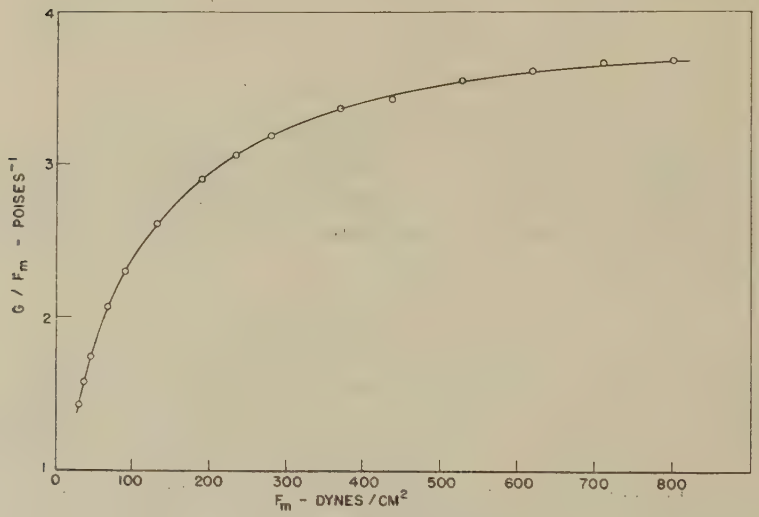

FIG. 1. G/F_m vs. F_m plot for 54.68% solids Neoprene latex type 60.

curves were then plotted as G/F_m vs. F_m, where G is the rate of shear and F_m is the shear stress. Figure 1 shows a typical curve obtained in this manner.

The relative viscosity of the latex in the non-Newtonian range may be defined by the equation

$$\eta_r = \frac{F_m/G}{\eta_w} = \frac{F_m}{G\eta_w}, \qquad [3]$$

where η_w is the viscosity of water at the temperature of measurement. Values of the relative viscosities calculated by Eq. [3] at selected constant shear stresses are given in Table III for all the concentrations studied in the non-Newtonian range.

An attempt was made to represent the above results by means of the exponential equation (10, 11)

$$F_m^N = \eta' G \qquad [4]$$

TABLE III

Relative Viscosities of Neoprene Type 60 Latex in the non-Newtonian Range at 29.94°C.

Total solids (%)	Volume fraction v	F_m (*dynes/cm.*^{2})	G/F_m (*cm.*^{3}*/sec.* × *dynes*)	Relative viscosity η_r
29.89	0.2393	30	43.39	2.888
		50	44.20	2.834
		100	45.10	2.779
		150	45.42	2.759
		200	45.55	2.751
		300	45.64	2.745
		500	45.67	2.744
34.87	0.2821	30	31.45	3.984
		50	32.53	3.851
		100	33.73	3.715
		150	34.17	3.667
		200	34.32	3.651
		300	34.48	3.633
		500	34.61	3.621
39.90	0.3263	30	21.63	5.793
		50	22.62	5.539
		100	23.88	5.247
		150	24.38	5.139
		200	24.65	5.083
		300	24.95	5.023
		500	25.31	4.951
44.92	0.3713	30	12.90	9.712
		50	14.06	8.910
		100	15.49	8.088
		150	16.07	7.799
		200	16.40	7.640
		300	16.80	7.459
		500	17.14	7.311
49.66	0.4147	30	6.48	19.34
		50	7.33	17.09
		100	8.47	14.80
		150	9.08	13.81
		200	9.43	13.29
		300	9.86	12.72
		500	10.26	12.22
		800	10.57	11.85
52.69	0.4429	30	3.44	36.47
		50	4.14	30.29
		100	5.29	23.70
		150	5.86	21.37
		200	6.23	20.12
		300	6.61	18.97
		500	6.99	17.95
		800	7.34	17.08
54.68	0.4617	30	1.41	88.85
		50	1.80	69.61
		100	2.40	52.31
		150	2.73	45.89
		200	2.96	42.40
		300	3.22	38.91
		500	3.50	35.79
		800	3.70	33.88
59.89	0.5115	50	0.260	481.8
		100	0.450	278.4
		150	0.585	214.1
		200	0.673	186.2
		300	0.802	156.2
		500	0.956	131.0
		800	1.108	113.1

which can be written in the form

$$\log \eta_r = (1 - N) \log F_m + \log \eta_r'. \qquad [5]$$

Here N is an index of non-Newtonian behavior ($N = 1$ for Newtonian liquids), and η_r' is the relative viscosity at unit shear stress. However, plots of $\log \eta_r$ vs. $\log F_m$ did not yield straight lines, which signifies that the value of N is not a constant for any given concentration.

Maron and Fok (4) found that for low-temperature GR-S latex the Eilers equation (12), modified to the form

$$\eta_r = \left[1 + \frac{\alpha v}{1 - \beta v}\right]^2, \qquad [6]$$

was capable of representing the flow data satisfactorily. In this equation α and β are constants for any fixed shear stress. This equation can be rearranged to the form

$$\frac{(\eta_r^{1/2} - 1)}{v} = \alpha + \beta(\eta_r^{1/2} - 1), \qquad [7]$$

where by plotting $(\eta_r^{1/2} - 1)/v$ vs. $(\eta_r^{1/2} - 1)$ the constants α and β can be obtained from the intercept and slope of the straight line. Such plots were made for different values of shear stress and were found to be linear, as may be seen from the typical plot shown in Fig. 2. Table IV summarizes the values of these constants obtained at the different shear stresses.

The validity of the constants was tested by using them to calculate the volume fraction, v, by means of Eq. [7]. As shown in the fourth column of

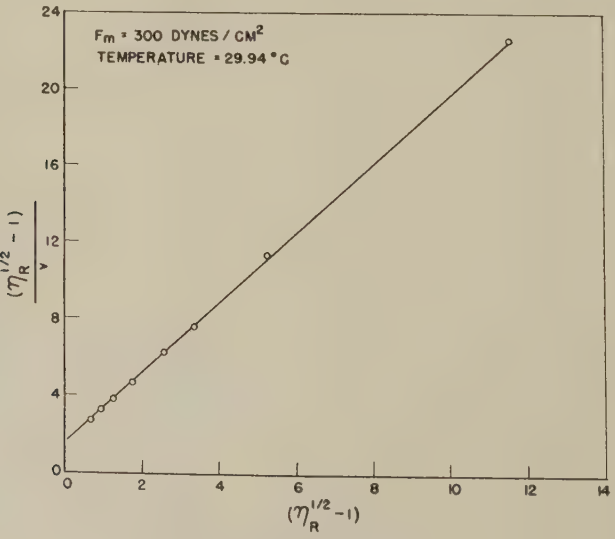

FIG. 2. Modified Eilers equation for Neoprene latex type 60.

TABLE IV

Values of α and β for Neoprene Type 60 Latex at 29.94°C.

F_m (dynes/cm.^{2})	α	β	Avg. error in v (%)	$1/\beta$	v_t
30	1.558	1.981	0.70	0.5048	0.552
50	1.548	1.914	0.58	0.5224	0.571
100	1.549	1.856	0.54	0.5387	0.589
150	1.545	1.842	0.52	0.5430	0.594
200	1.545	1.833	0.57	0.5456	0.596
300	1.549	1.820	0.66	0.5494	0.601
500	1.540	1.808	0.77	0.5532	0.605
800	1.493	1.800	0.88	0.5555	0.607
	Avg. 1.541 ±0.016				

Table IV, the difference between the calculated and observed v's is less than 1%.

Examination of the second column of Table IV indicates that α is practically constant and independent of the shear stress; β, on the other hand, decreases with increase in F_m. A plot of $1/\beta$ vs. F_m showed that the relation between these two quantities could be represented by the equation

$$\frac{1}{\beta} = \frac{1}{\beta_0} + \frac{aF_m}{1 + bF_m}. \quad [8]$$

Here $1/\beta_0$ is the value of $1/\beta$ at $F_m = 0$, while a and b are constants. After the constants were evaluated, the relationship between β and F_m was found to be given by

$$\beta = \frac{1 + 0.02803F_m}{0.4700 + 0.01567F_m}. \quad [9]$$

On substituting Eq. [9] and the average value of α back into Eq. [6], the final relationship

$$\eta_r = \left[1 + \frac{1.541v}{1 - [(1 + 0.02803F_m)v]/(0.4700 + 0.01567F_m)}\right]^2 \quad [10]$$

was obtained. This equation represents the flow behavior of the Neoprene Type 60 latex at 29.94°C. as a function of F_m and v, and is similar to the equation found by Maron and Fok (4) for the flow behavior of GR-S Type X-667 latex.

The validity of Eq. [10] was tested by introducing into it experimental values of η_r and F_m, and calculating the volume fraction v. The values of v thus calculated were found to agree with the observed v's within 1.2% over the entire range of shearing stresses investigated in both the Newtonian and non-Newtonian concentration regions.

Interpretation of Results

Einstein (13) showed that for very dilute suspensions of spheres in a medium $(\eta_r - 1)/v = 2.5$. For the same condition of essentially infinite dilution Eq. [6] predicts that $(\eta_r - 1)/v = 2\alpha$. From the value of α found here $2\alpha = 3.08$. However, this experimental result requires correction owing to the fact that v is the volume fraction of polymer only, and not of polymer plus adsorbed soap, v_t. Maron and Fok (4) showed that this correction involves division of 2α by the factor v_t/v, where this ratio is given by (2)

$$\frac{v_t}{v} = 1 + \frac{6\Delta}{D_s}. \tag{11}$$

Here Δ is the thickness of the adsorbed monolayer of soap, and D_s is the volume-to-surface average diameter. For this latex D_s was found to be 1100 A. Again, if Δ for N-wood rosin is taken to be the same as for K-wood rosin (3), namely, $\Delta = 17$ A, then Eq. [11] yields $v_t/v = 1.093$. On this basis the corrected value of 2α becomes $3.08/1.093 = 2.82$. Although this quantity is larger than the expected 2.50, it is still sufficiently close to indicate that the Einstein equation is obeyed fairly well by the Neoprene latex.

Equation [6] also predicts that η_r will become infinite when $v = 1/\beta$. Values of $1/\beta$ are given in the fifth column of Table IV. However, these quantities again require correction in line with Eq. [11] in order to obtain the volume of polymer plus soap. When this is done we obtain the values of v_t shown in the last column of Table IV as the volumes at which η_r goes to infinity.

These values of v_t for Neoprene latex are considerably lower than those shown by GR-S latices (2–4). The latter give for v_t values ranging from 0.69 to 0.79, whereas v_t here ranges from 0.55 to 0.61. This difference indicates that the packing of the particles when η_r becomes infinite is quite different in the two general classes of latices. Whereas the packing is tetragonal or rhombohedral, with 10 or 12 closest neighbors, in the case of the GR-S latices, the results of this work indicate that the packing in Neoprene latex is cubic, with each particle having only 6 neighbors (14). It should be pointed out, however, that the Neoprene latex studied here was creamed with ammonium alginate, whereas all the GR-S latices investigated were uncreamed. Until information is available on the flow behavior of uncreamed Neoprene latex, it cannot be decided whether the difference in the observed packing characteristics is due to creaming or whether it represents an inherent difference in the packing of the two types of latex particles.

Deviation of Neoprene Latex from Newtonian Behavior

If we consider Eq. [5] to be a flow equation with N variable, then differentiation of $\ln \eta_r$ with respect to $\ln F_m$ at constant v yields

$$\left[\frac{\partial \ln \eta_r}{\partial \ln F_m}\right]_v = -(N - 1). \tag{12}$$

The quantity $(N - 1)$ gives the deviation of a system from Newtonian flow. Again, on differentiation of Eq. [10] we obtain

$$\left[\frac{\partial \ln \eta_r}{\partial \ln F_m}\right]_v = \frac{-0.0025F_m v^2}{(0.4700 + 0.01567F_m)^2[1 - \beta(F_m)v][1 - (\beta(F_m) - 1.541)v]} \tag{13}$$

and hence

$$(N - 1) = \frac{0.0025F_m v^2}{(0.4700 + 0.01567F_m)^2[1 - \beta(F_m)v][1 - (\beta(F_m) - 1.541)v]}, \tag{14}$$

where $\beta(F_m)$ is given by Eq. [8].

Using this equation values of $(N - 1)$ have been calculated at given v's and F_m's, and these are shown graphically in Fig. 3 as plots of $(N - 1)$ vs. F_m at various constant values of v. From this series of curves it may be seen that: (*1*) For a constant value of F_m, the deviation from Newtonian flow increases with the volume fraction; (*2*) up to a volume fraction of about 0.33, the values of $(N - 1)$ decrease very slightly and practically linearly with increasing F_m; (*3*) above a volume fraction of about 0.33, however, values of $(N - 1)$ decrease in a nonlinear way with increasing F_m. The extent of this decrease is always higher at the lower F_m's, and the effect is the more pronounced the higher the volume fraction. In comparing the

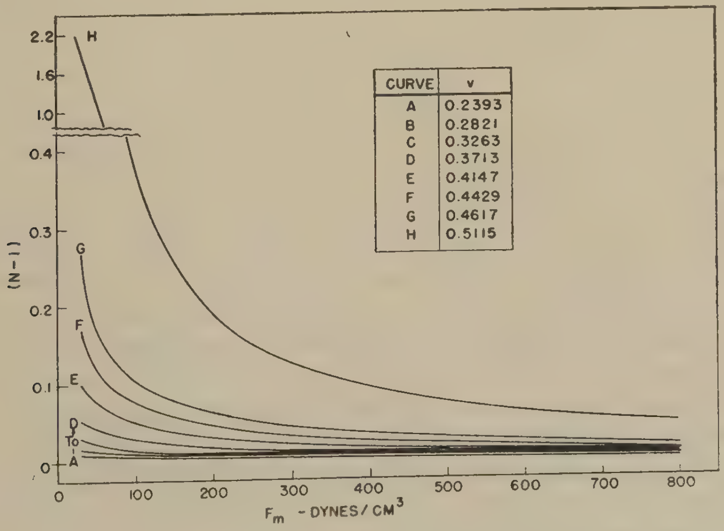

FIG. 3. Plot of $(N - 1)$ vs. F_m for Neoprene latex type 60 at 29.94°C.

curves in Fig. 3 with the corresponding curves of Maron and Fok for GR-S latex Type X-667 (4), it is observed that in the latter case the curves for the lower values of volume fraction are practically horizontal, whereas in the present case, they are not. Furthermore, above a volume fraction of about 0.44 the curves for the GR-S latex passed through maxima in the lower range of F_m, whereas here no maxima were observed. It may well be that the curves for Neoprene latex would also pass through similar maxima, but at shear stresses below the 30 dynes/cm.^{2} attained here. Whether such is the case can be decided only by a study of the flow behavior of Neoprene latex at stresses below those possible in the present investigation.

ACKNOWLEDGMENT

This work was performed as part of a research project sponsored by the Office of Synthetic Rubber, Federal Facilities Corporation, in connection with the government Synthetic Rubber Program.

SUMMARY

The flow behavior of Neoprene Type 60 latex was investigated at 29.94°C. over a concentration range of 0–0.51 rubber volume fraction, v, and a shear stress range of $F_m = 30\text{–}800$ dynes./cm.^{2}. Below $v = 0.20$ the latex was found to be Newtonian, whereas above this concentration it is non-Newtonian. The dependence of the relative viscosity, η_r, on v and F_m could be expressed by the modified Eilers equation

$$\eta_r = \left[1 + \frac{\alpha v}{1 - \beta v}\right]^2$$

where $\alpha = 1.541$ and

$$\beta = \frac{1 + 0.02803\,F_m}{0.4700 + 0.01567\,F_m}.$$

This equation was found to hold well in both the Newtonian and non-Newtonian concentration ranges investigated.

The above equation yields for $(\eta_r - 1)/v$ at infinite dilution 2.82 as against the theoretical Einstein value of 2.50. Again, extrapolation to $\eta_r = \infty$ shows that the viscosity goes to infinity at values of $v = 0.55\text{–}0.61$. These volume fractions are lower than those observed with GR-S latices, and indicate cubical rather than tetragonal or rhombohedral close packing.

The extent of deviation of this latex from Newtonian behavior as a function of v and F_m has also been calculated. The deviations are the more pronounced the higher is the concentration and the lower the shear stress. Futhermore, no maxima have been observed in the curves down to $F_m = 30$ dynes/cm.^{2}. This is another respect in which the flow behavior of Neoprene latex differs from that of GR-S latex.

REFERENCES

1. KRIEGER, I. M., AND MARON, S. H., *J. Colloid Sci.* **6,** 528 (1951).
2. MARON, S. H., MADOW, B. P., AND KRIEGER, I. M., *J. Colloid Sci.* **6,** 584 (1951).
3. MARON, S. H. AND MADOW, B. P., *J. Colloid Sci.* **8,** 130 (1953).
4. MARON, S. H. AND FOK, S. M., *J. Colloid Sci.* **10,** 482 (1955).
5. MARON, S. H., ULEVITCH, I. N., AND ELDER, M. E., *Anal. Chem.* **24,** 1068 (1952).
6. MARON, S. H., ELDER, M. E., AND ULEVITCH, I. N., *J. Colloid Sci.* **9,** 89 (1954).
7. MARON, S. H., ELDER, M. E., AND MOORE, C., *J. Colloid Sci.* **9,** 104 (1954).
8. MARON, S. H., KRIEGER, I. M., AND SISKO, A. W., *J. Appl. Phys.* **25,** 971 (1954).
9. KRIEGER, I. M., AND MARON, S. H., *J. Appl. Phys.* **25,** 72 (1954).
10. PORTER, A. W., AND RAO, P. M., *Trans. Faraday Soc.* **23,** 311 (1927).
11. FARROW, F., LOWE, G., AND NEALE, S. J., *J. Textile Inst.* **19,** T18 (1928).
12. EILERS, H., *Kolloid-Z.* **97,** 313 (1944).
13. EINSTEIN, A., *Ann. Physik* **19,** 289 (1906).
14. HEYWOOD, H., *J. Imp. Coll. Chem. Eng. Soc.* **2,** 9 (1946).

BOOK REVIEWS

Physical Chemistry. By Farrington Daniels and Robert A. Alberty. John Wiley & Sons, New York, 2nd edition, 1955. 671 pp. Price $6.50.

The new edition of Farrington Daniels' well-known treatise on Physical Chemistry has Robert A. Alberty as a co-author. It contains roughly the same material as the previous edition, and the presentation is practically unchanged.

It is, however, somewhat shorter than the earlier edition (671 pages as compared to 712). This is presumably an advantage for a large book that reads so easily as the present. Unfortunately, this condensation means that a large part of the appendix has been omitted. The rigorous derivations of many useful formulas no longer appear.

The important question is, for whom is the book written? If it is addressed to students who are not specializing in physical chemistry, then it is appropriate to omit derivations of more sophisticated equations, but then the book still remains too large for its purpose. If, on the other hand, the book is addressed to students majoring in physical chemistry, then the book is in general too elementary and one needs the appendix.

The brevity of the subject index is unfortunate for students needing the book for reference purposes. There are only about 1.2 references per page of text, with a resulting arbitrary selection of subjects cited. For instance, one finds a reference to "neutrino," although it is mentioned only very briefly in the text, whereas there is no reference to "steady state," which is described more fully but in the awkward place of enzyme kinetics.

The reviewer has found a few mistakes: On page 93 the capacity factor corresponding to the intensity factor temperature is given as heat capacity. It should, of course, be entropy. Also, it is presumably worth while to reconsider the assignment of intensity and capacity factors for kinetic energy.

On page 138 the author apparently hopes that some day it will be possible to prove the validity of the third law. This is, of course, impossible. One can check certain implications of the axiom we call the third law, but this will never lead to a "conclusive proof of the validity of the third law." This may seem to be of minor importance, but, in the reviewer's opinion, it is of importance to stress the axiomatic nature of the laws of thermodynamics.

Finally, one minor point: In fig. 13-5, page 343, a point given in Table IV is missing from the diagram in the present edition, making it difficult to understand why the line is drawn as it is.

Thor A. Bak, New York, New York

The Technology of Solvents and Plasticizers. By Arthur K. Doolittle, John Wiley & Sons, Inc., New York and Chapman & Hall, Ltd., London, 1954. XV + 1056 pages. Price $18.50.

There has been a growing demand among chemists and chemical engineers, working in the paint and plastics fields, for fundamental information based upon sound scientific facts which could be used in determining the correct compositions of resinous mixtures for specific purposes. Therefore Doolittle's new book on "The Technology of Solvents and Plasticizers" should find immediate acceptance and be received with great enthusiasm by workers in those fast developing fields which utilize synthetic resins in combinations with solvents and plasticizers.

The arrangement of the contents is most unique for a book of this type, for it provides specialized as well as general knowledge in both the theoretical and the practical or applied areas of the science. A thorough presentation of the underlying principles in addition to current practices for various type formulations makes it possible for the scientifically trained personnel to extend the technology to lesser known problems for future developments.

This book is designed not only for those working in the field but also for those less familiar with practices of the paint and plastics industries. It will not only provide much needed information to the scientist seriously interested in the fundamentals of this branch of technology but also make it available for ready application in all types of experimental work. Emphasis is on the behavior of the systems over a wide range of variables, rather than on any specific formulations. Therefore, those seeking only to obtain information for the preparation of selected mixtures will find this book somewhat of a disappointment for it is neither a formulary nor an encyclopedia, but rather a book devoted to developing the technological fundamentals for a better understanding of correct methods for the employment of solvents and plasticizers in all types of mixtures. Instead of providing formulas, the reader is afforded sufficient information from which he can arrive at his own answers for a better solution to a great variety of problems in plasticization and solvency.

The author has amassed a great deal of information of both theory and fact into a concise pattern for a clearer understanding of the basic fundamentals of the science. The great amount of material included in this large volume is well integrated into a logical sequence according to the principal fields in which solvents and plasticizers are employed. Included are complete lists of the physical properties of a large group of solvents and plasticizers now commercially available. The applications involve a wide range of products from fluid adhesives and lacquers, on the one hand, to thick, viscous, plastic molding formulations, on the other. It is a valuable reference volume that all commercial laboratories, as well as college and university libraries, should have handy on their shelves for assistance in the solution of problems related to the production of paints, lacquers, varnishes, adhesives, inks, coating compounds, plastic compositions, and synthetic textile fibers.

JAMES M. CHURCH, New York, New York

BIBLIOGRAPHY OF LIESEGANG RINGS (1955)

BY

KURT H. STERN

University of Arkansas Editorial Service

Fayetteville, Arkansas, $1.00.

CHARGE EFFECTS IN LIGHT SCATTERING BY ASSOCIATION COLLOIDAL ELECTROLYTES

Karol J. Mysels

The Department of Chemistry, University of Southern California, Los Angeles 7, California

Received August 29, 1955

ABSTRACT

A simplified treatment of the effect of charge on the light scattering by colloidal solutions is extended to take into account the refractive index contribution of simple electrolyte. It is shown that this effect leads to a reduction of optical efficiencies of fluctuations and to an apparently smaller molecular weight. In case of association colloidal electrolytes the effect of monomeric ions as well as that of added electrolytes is taken into account. The effect of equilibrium between micelles and monomeric ions on the concentration of monomer is examined under idealized conditions and leads to a minor correction. Literature data on micellar weights are recalculated in the light of these ideas.

INTRODUCTION

Since its introduction by Debye (1), light scattering has been widely used in the study of association colloidal electrolytes. In the concentration range of interest the results may be represented always by

$$\frac{H(c - c_0)}{\tau - \tau_0} = A + B(c - c_0), \qquad [1]$$

where H is a constant involving geometrical and refractive index factors of light scattering, and τ the turbidity of a solution of concentration c. The subscript ($_0$) refers to the solution at the critical micelle concentration, cmc, an extrapolated value which may be considered as corresponding to the infinite dilution of micelles. A and B are constants characteristic of the system.

In general A has been interpreted according to Debye to give a micellar weight M' and degree of association n' according to the relations

$$\frac{1}{M'} = \frac{1}{n'M_1} = A \qquad [2]$$

where M_1 is the molecular weight of the monomer. Hutchinson (2) has recently proposed a very different approach. In the present paper I would like to bring out some of the difficulties of Debye's approach and re-examine the question of micellar weights.

Debye treated micelles as if they were uncharged polymers formed by all the solute added above the critical micelle concentration. Hutchinson, while recognizing that the micelle is charged in water, believes that it becomes uncharged in aqueous salt solutions. For uncharged micelles the effect of the monomeric ions may be lumped with that of the solvent and neglected in the calculation of micellar weights. The micelle of ionic surfactants is in fact, however, highly charged both in water and in the presence of salt as shown by its high electrophoretic mobility (16). This requires corrections caused by several effects which we shall examine in order: From the point of view of the fluctuation theory of light scattering (i) the charge tends to reduce the extent of fluctuations, and (ii) the presence of the monomeric ions reduces the optical efficiency of the fluctuations. In general (iii) the equilibrium between monomeric ions and charged micelles affects the concentration of monomer beyond the cmc.

The turbidity causing light scattering may be looked upon as created by submicroscopic inhomogeneities in the refractive index of the solution which are in turn due to fluctuations in concentration of the solute. The extent of these fluctuations is determined by the free energy required to produce them which in turn depends on the change $\partial\pi/\partial c$ of osmotic pressure with concentration. This idea, originating with Einstein (3), is very clearly derived, for example, by Hermans (4). For a single solute this leads without any assumptions to

$$\frac{Hc}{\tau} = \left(\frac{1}{RT}\right)\frac{\partial\pi}{\partial c}. \qquad [3]$$

In case of an ideal solution of a nonelectrolyte one can set $\partial\pi/\partial c = RT/M$ and the familiar formula

$$\frac{Hc}{\tau} = \frac{1}{M} \qquad [4]$$

is obtained.

When several solutes are present simultaneously, the situation is more complicated. Zernike (5) gave a basic statistical mechanical treatment which has been confirmed and extended (6) since. In particular Prins and Hermans (7) showed how it can be readily applied to mixtures of ideal electrolytes. An alternate way, which is less general and rigorous but has the advantage of easier visualization, is based on the detailed consideration of what occurs during a fluctuation in the complex system. I have discussed from the latter point of view the case of a colloidal electrolyte (8) with neglect of the refractive index contribution of the small ions and applied it with Dr. Phillips (9) to association colloids. Prins and Hermans (7) confirmed the results obtained while pointing out correctly the advantages of the more rigorous treatment.

I. THE EXTENT OF FLUCTUATIONS

When the colloid is considered as the only light-scattering species, the effect of charge is solely to reduce the extent of fluctuations (8). This is due to the requirement of electroneutrality that gegenions accompany the colloid during each fluctuation, leading to a Donnan equilibrium between the fluctuating volume and the bulk solution. The osmotic work of changing the concentration of monomeric ions must therefore be added to the osmotic work required by the colloid. If the charge of the colloid is p, this reduces the turbidity $(p + 1)$ times in a pure colloidal electrolyte but leaves it unchanged in the presence of swamping electrolytes. Hence the molecular weight computed by simple formula [4] is $(p + 1)$ times too small in the absence of salt but correct in its swamping excess.

At the cmc, micelles are colloidal ions at infinite dilution while the monomeric ions are a swamping salt. Hence fluctuations of micelles are unimpeded by their charge at the cmc. As the concentration of micelles increases, the fluctuations become impeded, Hc/τ increases linearly according to [1] and from the slope B of this line the charge p' may be calculated (8) by

$$p' = \frac{\sqrt{2Bx}}{A}, \qquad [5]$$

where x is the concentration of monomeric electrolyte at the cmc.

II. THE OPTICAL EFFICIENCY OF FLUCTUATIONS

We shall now include the refractive index contribution of the small ion which introduces a significant correction into the calculated molecular weight of the colloid and a smaller one into the calculated charge. We shall give the detail of the simplified treatment and introduce only the results of applying the statistical treatment.

Normally one assumes in calculating turbidities that as the concentration of colloid fluctuates, the refractive index fluctuates proportionately, the proportionality factor being $\partial\nu/\partial c$, the refractive increment of the solution. This leads to the above result that $1/M = A$. The presence of charge and of small ions invalidates this assumption because as the colloid enters the fluctuating volume, some of the simple electrolyte leaves it to maintain Donnan equilibrium and the optical efficiency of a fluctuation is reduced. This may be visualized as follows: When a colloidal cation with its p anions enters, the escaping tendency of the anions is increased, but to leave they must be accompanied by small cations in order to maintain electroneutrality. When the colloidal electrolyte is pure and there are no small cations, no small anions can leave, and optical efficiency is unimpaired. Under swamping electrolyte conditions, on the other hand, the concentration of small anions is equal to that of small cations and they leave in pairs. This tends to restore the original escaping tendency of the anions but reduces that of the cations below the original. Equilibrium is reached when the two deviations from the original are equal, i.e., when $p/2$ of each have left the volume.[1]

Thus at infinite dilution of colloidal ions (at c_0) the optical effectiveness of each mole of colloid is reduced by the effect of $p/2$ moles of simple electrolyte.

A. Absence of Salt

If we consider first the case of a pure association colloid, each mole of micelles is equivalent optically to n (the degree of association) moles of monomer. Hence the optical effectiveness of fluctuations of micelles is reduced from n to $(n - p/2)$, i.e., by a factor of $(1 - p/2n)$. Turbidity is affected by the square of $\partial\nu/\partial c$ (because it involves intensities and not amplitudes of vibrations); hence the turbidity is reduced by $(1 - p/2n)^2$ and the micellar weight calculated by the Debye method is smaller than the real value by this last factor. Thus we obtain for the corrected micellar weight M

$$\frac{1}{M} = \frac{1}{nM_1} = A\left(1 - \frac{p}{2n}\right)^2 \qquad [6]$$

or in terms of the previously obtained n'

$$n' = n\left(1 - \frac{p}{2n}\right)^2. \qquad [7]$$

When it comes to the slope and its interpretation in terms of charge in analogy to Eq. [5], we may note that the optical efficiency of fluctuations remains substantially constant in the neighborhood of c_0. Therefore all turbidities in this region are affected by it to the same extent by the factor $(1 - p/2n)^2$. In other words, both the intercept A and the slope B of the $H(c - c_0)/(\tau - \tau_0)$ line are increased by this factor. The charge p' calculated by applying Eq. [5] to the data is proportional to $\sqrt{B}/A$ and is

---

[1] More rigorously, if we call δ the fluctuation in m and $-\epsilon$ the corresponding change in x, the Donnan equilibrium condition is

$$x(x + pm) \doteq (x - \epsilon)[x - \epsilon + p(m + \delta)]$$

which gives

$$\epsilon = \frac{\delta p}{2} - \frac{\epsilon m p}{2x} + \frac{\epsilon^2 - \epsilon\delta p}{2x}$$

The last term is always negligible and the penultimate becomes negligible as swamping electrolyte conditions are approached ($m/x \to 0$); hence, only the first right-hand term remains, confirming the previous conclusion.

therefore increased proportionately to $1/(1 - p/2n)$. Hence the real charge p is given by

$$p = \frac{p'}{1 - p/2n} = \frac{\sqrt{2Bx}}{A(1 - p/2n)}. \qquad [8]$$

The approach of statistical mechanics gives, following the procedure of Prins and Hermans (7) for the turbidity due to the solute,

$$\frac{\tau}{H} = \frac{x^2 + xm(p^2 + p + 2n^2 - 2np) + m^2 n^2 p}{2x + mp(p + 1)}. \qquad [9]$$

From this one can obtain exact equations analogous to the ones just derived

$$\frac{1}{M} = A\left[\left(1 - \frac{p}{2n}\right)^2 + \frac{p^2}{4n^2}\right]; \qquad [10]$$

$$p = \frac{\sqrt{2Bx}}{A[1 - p/2n + 1/2n]}. \qquad [11]$$

The difference of the two treatments gives in each case the last fraction within the bracket and amounts to less than 1% for the encountered range of constants.

Thus consideration of charge effects on pure colloidal electrolytes requires that the directly calculated molecular weights be increased, the increase being of the order of 10–20% as shown in the Table.

B. The Presence of Salt

In the presence of salt the micelle at the cmc is surrounded by a mixture of small ions: monomeric micelle-forming ions and those of the added salt. From an electrical point of view these are strictly equivalent (assuming that all are monovalent) so that the expulsion of small ions, which we have seen is required by the Donnan equilibrium, will affect them simply in proportion to their concentration. From an optical point of view the small ions are not equivalent and the reduction in optical efficiency of the fluctuation will depend on their average molar refractive increment.

Quantitatively, if x_1 and x_2 are the molar concentrations of the monomer and the salt, and the molar refractive index increment $\partial\nu/\partial x_2$ of the latter is S times larger than $\partial\nu/\partial x_1$, the effective refractive increment of the mixture is E times larger than that of the monomer where

$$E = \frac{x_1 + Sx_2}{x_1 + x_2}. \qquad [12]$$

The optical efficiency of a fluctuation will therefore be reduced by a factor of $(1 - Ep/2n)$ and the turbidity by the square of this factor. Hence the

TABLE I

Degrees of Aggregation n *and Effective Charges* p *from Light-Scattering Measurements*

System	Added salt $\times 10^2$ M	$C_0 \times 10^2$ M	n' [2]	p' [5]	E^a	n [16]	p [17]	n_a Fig. 5
Sodium C_{12} sulfate and NaCl (9)	0	0.812	80	14.5	1	95.3	16.1	92.5
	.2	0.391	94	12.8	0.431	99.6	13.2	
	.3	0.313	100	12.8	0.374	104.9	13.2	
	10	0.147	112.5	13.4 ± 1	0.333	117 ± .3	13.7	
	20	0.092	118	17 ± 2	0.327	123.5 ± .7	17.5 ± 2	
	40	0.058	126	17 ± 10	0.324	131.5 ± 3.5	17.4 ± 11	
C_{12} amine hydrochloride and NaCl (1)	0	1.31	56	7.0	1	63.5	7.6	61
	1.57	1.04	92	7.9	0.56	96.5	8.1	
	2.37	0.925	101	8.1	0.48	105	8.3	
	4.6	0.722	142	10.9	0.37	146	11.1	
C_{10}TMABr[b] and KBr	0	7.0	36.5	8.9	1	46	10.3	46
	1.3	6.72	38	10.1	0.89	47.5	10.5	
C_{12}TMABr[b] and KBr	0	1.52	50.5	10.5	1	61.5	11.9	61
	1.3	1.05	56.5	9.2	0.61	62.5	10.8	
	3.4	0.848	65.5	10.5	0.44	70	10.9	
C_{14}TMABr[b] and Br	0	0.341	82	11.2	1	93.5	12.2	90.5
	1.3	0.176	95.5	12.0	0.46	101	12.5	
C_{16}TMABr[b] and KBr	1.3		170	15.7	0.26	174	15.9	

[a] Computed using $\delta\nu/\delta c$ values of 0.11 for $NaC_{12}SO_4$ (9), 0.166 for $C_{12}NH_3Cl$ (15), 0.153 for alkyl TMABr (15).

[b] Normal alkyl trimethylammonium bromide.

real micellar weight is given by

$$\frac{1}{M} = A\left(1 - \frac{Ep}{2n}\right)^2 \qquad [13]$$

and

$$n' = n\left(1 - \frac{Ep}{2n}\right)^2. \qquad [14]$$

With respect to the charge p the same reasoning again applies and the real charge p is given by

$$p = \frac{\sqrt{2Bx/A}}{1 - Ep/2n}. \qquad [15]$$

The statistical mechanics treatment shows also that replacement of n by n/E, which occurs in Eqs. [13]–[15], fully accounts for the effects of salt.

The difference between n' and n introduced by the present considerations is usually less in the presence of salt than in pure water because, whereas the refractive increment per gram is larger for the salt than the colloid, the molecular weight of the monomer is generally sufficiently larger to more than compensate for this and to make E less than unity. It should be noted also that in the presence of higher salt concentrations the slope B becomes small and hard to determine from the experimental data whereas p remains approximately constant. Hence the precision in the determination of p and of the correction to n decreases rapidly under these conditions.

C. General Equations

The relations presented above for obtaining n and p must be solved simultaneously to obtain the desired quantities. Fortunately the explicit expressions are reasonably simple and are as follows for the most general case of exact treatment in the presence of salt:

$$n = n' + \frac{Ep'}{1 - (\underline{E/2n'})} + \frac{E^2 p'(p' + \underline{1})}{4n' - \underline{2E}} \qquad [16]$$

$$p = \frac{2(n - n')}{E - p'} = p' \left(\frac{n' + \underline{0.5E}}{n' - \underline{0.5E}} + \frac{p' + \underline{1}}{2n' - \underline{E}} \right) \qquad [17]$$

where underlining indicates the correction introduced by the exact treatment. In the absence of salt E becomes unity. The definition of n' and p' by Eqs. [1] and [5] is directly in terms of experimental quantities.

An approximation sufficient for many purposes is

$$n = n' + Ep'; \qquad [18]$$

$$p = p' + \frac{p'^2}{2n'}. \qquad [19]$$

III. THE EFFECT OF CONCENTRATION OF MONOMERIC IONS

In all previous arguments there is an implied assumption that the concentration x of the simple electrolyte remains constant above the cmc so that the concentration of micellized colloid m increases linearly with the total concentration c. This assumption is quite correct when the concentration of added salt is large compared to the cmc, but must in general be erroneous in the absence of salt because of the equilibrium between micelles and monomeric ions.

It does not seem possible to evaluate the correction for this effect in general terms. We shall therefore attack the problem by calculating as rigorously as possible and without making this assumption the turbidity of solutions having specific values of n_a and p_a, then treating these calculated values as if they were experimental ones, i.e. interpret them according to Debye, apply the corrections developed above, and finally comparing the resulting, calculated n and p with the original n_a and p_a. The difference gives us an estimate of the error introduced by the assumption. Incidental to this process we shall obtain some new results about the meaning of the cmc.

Since all of the previous discussion is in terms of ideal electrolytes we can conduct the present discussion in the same terms. Not only does this seem the only feasible approach, but it does not introduce any fundamental error because the charge p which we use is already not the real charge Q at the shear plane of the micelle but its effective charge, taking into account all deviations from ideality as far as light scattering is concerned. Whereas there is no reason to assume that the charge effective in equilibrium considerations is exactly the same as p, their difference should not be sufficient to invalidate the semiquantitative results which we shall develop.

Total concentration c (moles of monomer/liter) is related to the molar concentrations x of monomer and m of micelles having a degree of association n and a charge p, by

$$c = x + nm. \tag{20}$$

We shall also use explicitly the assumption that there is only one kind of micelle. The equilibrium constant for micellization is then

$$K = \frac{m}{x^n(x + pm)^{n-p}}. \tag{21}$$

As has been pointed out by Murray (10) the concentration x of the small associating ion changes as shown in Fig. 1 and generally passes through a maximum. This maximum may be defined completely as follows. From [20] and [21] the slope of x is given by

$$\frac{dx}{dc} = \frac{x[x + mp(p + 1 - n)]}{x^2 + xm(p + p^2 - 2np + 2n^2) + m^2pn^2}. \tag{22}$$

The condition $dx/dc = 0$ combined with [20] gives for the maximum

$$x_{\max} = \frac{c_{\max}\, p(n - p - 1)}{(n - p)(p + 1)} \tag{23}$$

and

$$m_{\max} = \frac{c_{\max}}{(n - p - 1)(p + 1)}; \tag{24}$$

introducing these two expressions into [21] gives explicitly

$$\log c_{\max} = \frac{\begin{array}{l}[(n+1)\log(n-p) + (2n-p-1)\log(p+1) \\ \qquad - \log K - (2n-p)\log p - n\log(n-p-1)]\end{array}}{(2n-p-1)} \quad [25]$$

When 1 is negligible compared with both n and $n - p$, this simplifies to

$$c_{\max} = \left(\frac{p}{p+1}\right) K^{1/p-2n} \quad [26]$$

and only when p is also large that the first factor can be omitted. Figure 1 shows the locus of the maximum in a particular case. In general this locus moves rapidly to infinity as the micelle becomes neutral or highly charged i.e., as p approaches either 0 or $n - 1$. For fully charged micelles, i.e., within unity of n the maximum disappears, x increasing indefinitely.

Calculation of x is facilitated by using as independent variable $Y = x + pm$. Equations [20] and [21] then give directly

$$n \log x = \log (Y - x) - (n - p) \log Y - \log pK \quad [27]$$

which can be readily solved for x by successive approximations.

It is also permissible to choose $K = 1$ without any loss of generality since values corresponding to any other value K are obtained by changing linearly all concentrations by $K^{1/(1-2n-p)}$.

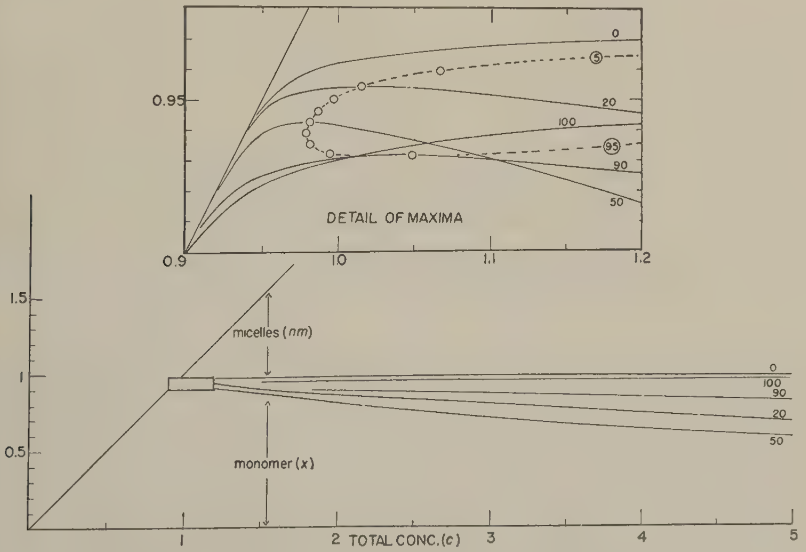

FIG. 1. Calculated concentrations of monomer and micelles for a degree of association $n_a = 100$. Numbers indicate the charge p_a. Dotted line indicates locus of maximum with open circles corresponding to multiples of 10.

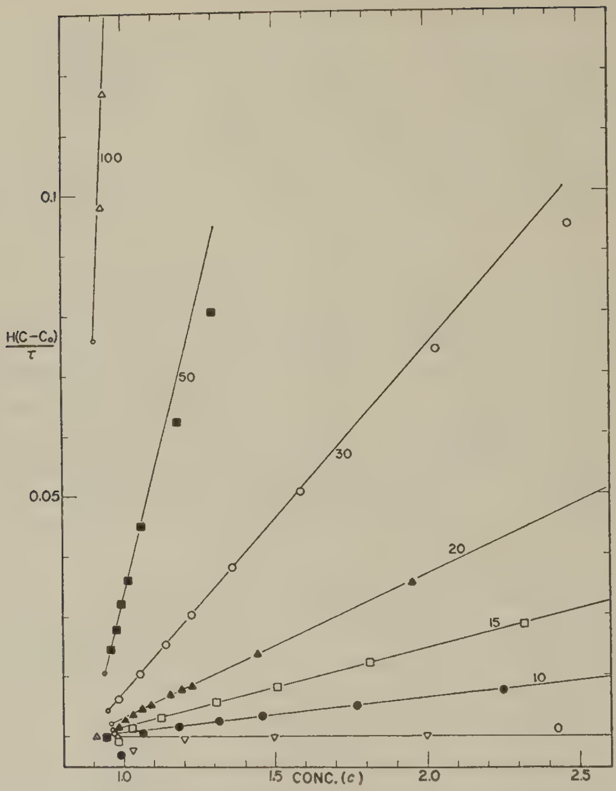

FIG. 2. Calculated Debye plots of light scattering for $n_a = 100$ and indicated values of p_a.

In this way values of x and m were obtained for $n = 100$ and $p = 0$ 10, 15, 20, 30, 50, and 100, as well as for $n = 50$ and $p = 7.5$, and for a large number of c values. A few of the curves obtained for $n = 100$ are shown in Fig. 1. These were used to compute turbidities according to Eq. [9], which follows from Prins and Hermans' treatment, assuming $H = 1$ and $M_1 = 1$.[2]

The turbidities thus obtained were then treated according to Debye to give straight plots of $c - c_0/\tau - \tau_0$. The τ_0 was taken as the turbidity at c_0 extrapolated from lower concentrations, i.e., $\tau_0 = c_0/2$ according to [9]. This treatment involved, as it does always, a certain amount of judgment and presented particularities which I have not noted in treating real experimental data. When c_0 is chosen too high, the curve falls off rapidly at low c values. As c_0 is lowered, a point is reached where an upward bulge and then a maximum appears in the curve; at still lower values the curve increases after a minimum. In the treatment of real data the experimental error would probably overshadow the bulge and maximum. For the sake of consistency c_0 was taken as the highest value which did not give a bulge. At low p values the linear portion extended to several times c_0 but shortened as p increased until for $p = 100$ it extended only between 1.04 and 1.12 c_0. The resulting lines are shown in Fig. 2.

---

[2] Tabulated values of x, m, t, and $c - c_0/\tau - \tau_0$ are available in the Eighth Technical Report, ONR Project NR356-254, and from the author.

We can now consider the meaning of the data thus calculated with respect to the cmc, p, and n.

The Value of the cmc

The critical micelle concentration is generally determined by the point of intersection of lines extrapolating some property of the system from below and from above the region of greatest change. All properties which depend linearly on the concentration of monomeric and micellized solute must in principle give the same result. Since light scattering is a very

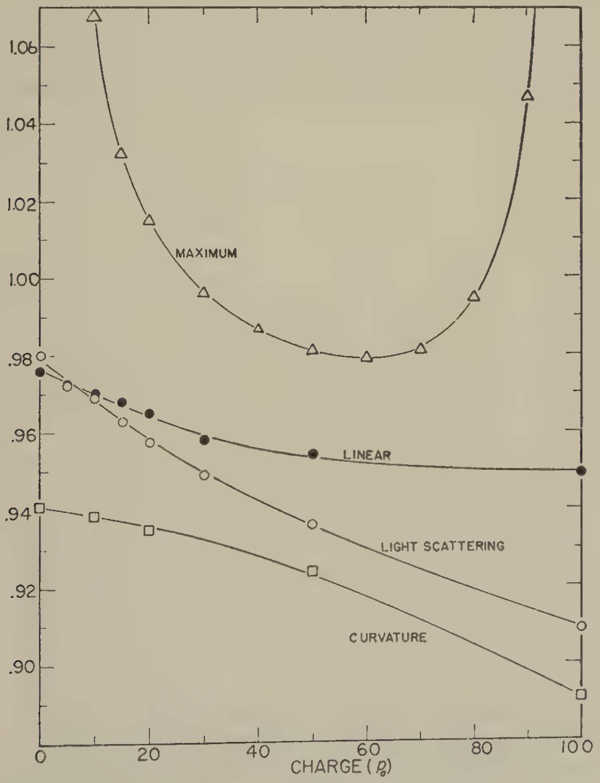

FIG. 3. Calculated critical micelle concentrations for $n_a = 100$ as a function of p_a. Top curve shows position of maximum monomer concentration.

complex function of these two concentrations, it need not give the same results as other properties. Furthermore the nonlinearity of the variation of x and m with c introduces an uncertainty into straight-line extrapolations.

We have seen above how c_0 was obtained from the turbidity and the results are plotted in Fig. 3. To obtain the more conventional value I extrapolated the simplest property related linearly to the concentrations, namely, the concentration x itself. Since x does not vary linearly with c, as Fig. 1 shows clearly, there is again some uncertainty in the extrapolation of this portion. I used a linear extrapolation on a large-scale graph covering the range of c up to 3 and tried to use the most linear part of the plot. This is the type of result expected from conductivity or dye solubilization experiments. The results obtained are also shown in Fig. 3 and indicate close agreement with the turbidity results at low charges (p) but large discrepancies as p increases beyond the range encountered in practice.

Phillips (11) has proposed recently another definition of the cmc which is useful in calculations, namely, the point of maximum curvature of any linear property. Values calculated according to his Eq. [8c] are also shown in Fig. 3 and appear to be slightly but significantly lower than the other two in the practical range. At higher charges they are closer to the turbidity values.

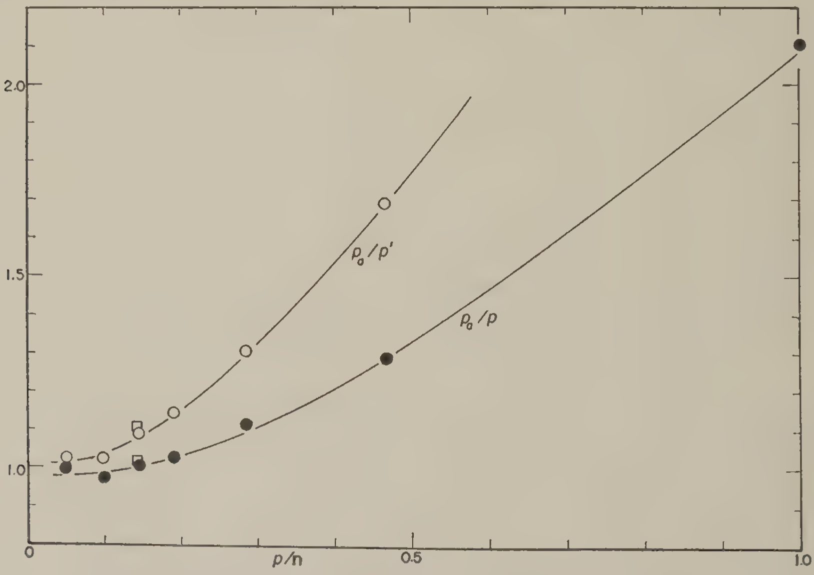

FIG. 4. Effect of assuming constant monomer concentration above the cmc upon the calculated charge. Deviations from unity indicate error. Circles $n_a = 100$, squares $n_a = 50$.

Concentrations at which the maximum of x occurs are also indicated in Fig. 3 to show their lack of simple relation to the cmc.

Thus these calculations confirm the experimentally found agreement (12) between cmc's determined by light scattering, conductivity, and dye solubilization and shows that these values can be used in Phillips' equations in all calculations of reasonable precision. However, if some much more highly charged association colloids are discovered, one may expect significant discrepancies.

The Charge p

From the $c - c_0/\tau - \tau_0$ lines shown in Fig. 2 the charges p' and p have been calculated using Eqs. [5] and [17]. The results are plotted in Fig. 4. It is readily apparent that within the practical range of p values the extrapolation to the cmc introduces no significant error but that at higher charges the results become rapidly meaningless.

The Degree of Aggregation n

From the lines of Fig. 2 the degrees of association n' and n were calculated; n' according to Debye's Eq. [2] and n according to Eq. [16], which takes fully into account the effect of the small ions. Both results are plotted

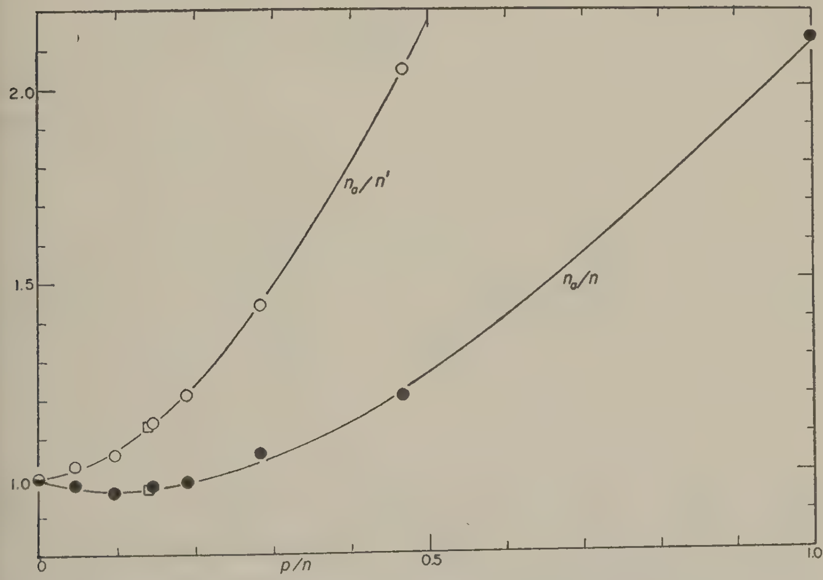

FIG. 5. Effect of assuming constant monomer concentration above the cmc upon the calculated degree of association. Deviations from unity indicate error. Circles $n_a = 100$, squares $n_a = 50$.

in Fig. 5. It may be seen that the ratio of the true, assumed value n_a to the calculated one increases rapidly for n' but stays close to unity for n at practical values of p before increasing also. This last curve gives the correction required by the assumption of constant x above the cmc. In the practical range this correction amounts to 4% or less and is not very dependent on n_a, as shown by results calculated for $n_a = 50$ and $p_a/n_a = 0.15$ which are also indicated in the figure. This correction has been accordingly applied to the recalculated literature data to give the corrected values n_a shown in the last column of the Table. Since this correction is small in the absence of salt, it must be negligible in the presence of salt, where x can vary but little above the cmc. Accordingly, we accept the results of Eq. [16] and the values n of the preceding column remain without change for solutions containing added salt.

Conclusion

The effect of these corrections on the calculated degrees of aggregation and charges is shown in the Table for the data of Debye's and our laboratories. Figure 6 shows in detail the results for sodium lauryl sulfate in the presence of NaCl. It may be seen that whereas the plot of the micellar weight against the total gegenion concentration at the cmc on a log log scale was curved (9) before corrections, it is linear within the experimental

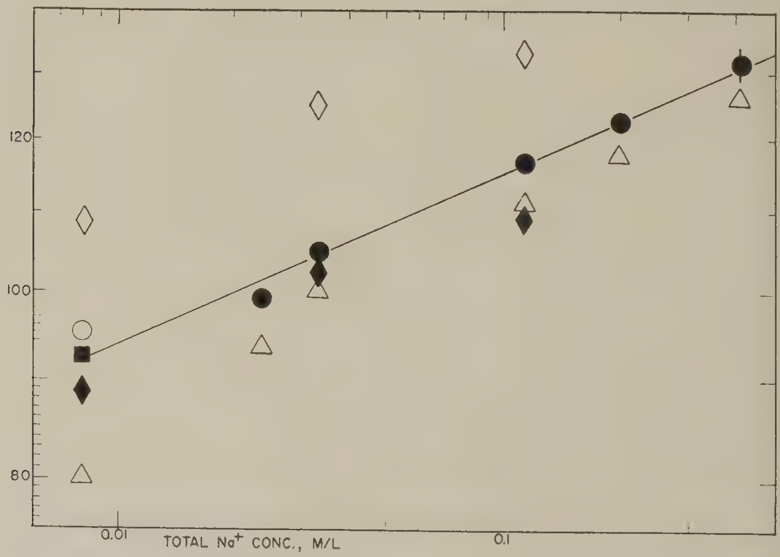

FIG. 6. The degree of association of sodium lauryl sulfate micelles at the cmc. Squares n_a; circles n; triangles n'; diamonds self diffusion, open unhydrated, filled with 1.5 A. of hydration.

error once the present corrections are taken into account. This straight line is given by

$$\log n = 2.152 + 0.091 \log (C + c_0)$$

where c_0 and the concentration of added salt C are both expressed in moles/liter. As has been indicated previously (9) the other compounds suggest a similar linear relationship with similar slopes for the salts of strong bases and acids and a much higher slope for the hydrochloride of the weak base dodecyl amine. These qualitative conclusions remain unchanged.

Figure 6 shows also the published (13) results of self diffusion measurement interpreted in terms of a spherical micelle having a 1.5 A. hydration layer. This corresponds to an average of half a molecule of water (and not one molecule, as stated by mistake previously). The agreement is much better than would be expected from the experimental error and the uncertainty of any assumption about hydration.

It may be noted that light scattering, being proportional to the molecular weight, gives the second moment or weight average of the distribution while self-diffusion being inversely proportional to the cube root gives the 2/3 moment,[3] which is lower than the number average. The agreement of the two sets of data shows therefore that micelles are not highly polydispersed. However, the precision of the self-diffusion data and the accuracy[4] of the light-scattering data do not seem yet to warrant any quantitative conclusions about monodispersity. The fact that the micellar weight increases upon addition of salt is certainly more easily visualized as the gradual shift of distribution of a slightly polydispersed system than as sudden appearance and disappearance of species in a strictly monodispersed system.

[3] It is very likely that all species of micelles are tagged uniformly on a dye/weight basis because the solubilizing power of micelles is substantially independent of the presence of salt, as shown by the slopes of solubilization (12). Because of the rapid equilibrium between micelles the gradient of concentration of any tagged species $dc_i/dx = (c_i/c)(dc/dx)$. The total permeation per unit time m is the sum of the m_i. Hence according to Fick's law

$$m = \frac{D\,dc}{dx} = \Sigma m_i = \Sigma\left(\frac{c_i}{c}\right)\frac{D_i\,dc}{dx},$$

so that $D = \Sigma(c_i/c)D_i$. Since D is inversely proportional to the cube root of M, this gives $cM^{-1/3} = \Sigma c_i M_i^{-1/3}$, or in terms of number of particles, $nM^{2/3} = \Sigma n_i M_i^{2/3}$.

[4] It has been recently suggested (15) that the turbidity standards used in our laboratory in measurements on sodium lauryl sulfate and in Debye's laboratory for the other systems here reported, may have been low by some 25%. If this should be true, all the values for the micellar weight would be increased in almost the same proportion and the charges by some 12%.

ACKNOWLEDGMENTS

I am very grateful to Prof. J. J. Hermans of Leyden for correspondence which eliminated an important misconception from my early thoughts on these matters, to Prof. E. W. Anacker for making available unpublished data, and to Mr. W. A. Forman, who performed most of the computations. This work was supported by the Office of Naval Research Project NR356-254, for which this forms part of the Eighth Technical Report. Reproduction in whole or in part for any purposes of the United States Government is permitted.

REFERENCES

1. DEBYE, P., *J. Phys. & Colloid Chem.* **53,** 1 (1949); *Ann. N. Y. Acad. Sci.* **51,** 575 (1949).
2. HUTCHINSON, E., *J. Colloid Sci.* **9,** 192 (1954).
3. EINSTEIN, A., *Ann. Physik* **33,** 1275 (1910); *in* Alexander, J., ed., "Colloid Chemistry," Vol. 1, p. 323. Chemical Catalog Co., New York, 1926.
4. HERMANS, J. J., *in* H. R. KRUYT, ed., "Colloid Science," Vol. 2, p. 146. Elsevier, New York, 1949; OSTER, G., *Chem. Revs.* **43,** 319 (1948).
5. ZERNIKE, F., *Arch. néerl. sci.* [IIIA], **4,** 74 (1918).
6. BRINKMAN, H. C., AND HERMANS, J. H., *J. Chem. Phys.* **17,** 574 (1949); KIRKWOOD, J. C., AND GOLDBERG, R. J., *ibid.* **18,** 54 (1950); STOCKMAYER, W. H., *ibid.* **18,** 58 (1950).
7. PRINS, W., AND HERMANS, J. J., *J. Phys. Chem.* **59,** 576 (1955).
8. MYSELS, K. J., *J. Phys. Chem.* **58,** 303 (1954).
9. PHILLIPS, J. N., AND MYSELS, K. J., *J. Phys. Chem.* **59,** 325 (1955).
10. MURRAY, R. C., *Trans. Faraday Soc.* **31,** 207 (1935).
11. PHILLIPS, J. N., *Trans. Faraday Soc.* **51,** 561 (1955).
12. WILLIAMS, R. J., PHILLIPS, J. N., AND MYSELS, K. J., *Trans. Faraday Soc.* **51,** 728 (1955).
13. STIGTER, D., WILLIAMS, R. J., AND MYSELS, K. J., *J. Phys. Chem.* **59,** 330 (1955).
14. MARON, S. H., AND LOU, L. H., *J. Phys. Chem.* **59,** 231 (1955).
15. ANACKER, E. W., private communication.
16. STIGTER, D., AND MYSELS, K. J., *J. Phys. Chem.* **59,** 45 (1955).

RHEOLOGY OF SYNTHETIC LATEX

VII. FLOW BEHAVIOR OF SYNTHETIC RUBBER LATEX AT LOW SHEAR STRESS

Samuel H. Maron and Robert J. Belner

Physical Chemistry Laboratory, Department of Chemistry and Chemical Engineering, Case Institute of Technology, Cleveland, Ohio

Received July 18, 1955

INTRODUCTION

Most of the studies made to date on the flow behavior of synthetic rubber latices (1–5) have been made in instruments and under conditions where the lowest shear stress measured was about 20–30 dynes/cm.^{2}. Under such conditions it was found that the latex systems are Newtonian at concentrations below about 0.25 volume fraction of rubber, and non-Newtonian at higher rubber contents. In only one instance (6) were measurements made on a single concentrated latex sample at very low shear stresses. These showed the latex to be Newtonian at 0–0.14 dyne/cm.^{2}, even though the same type and concentration of latex was found to be non-Newtonian at higher shear stresses (1). These observations indicate a need for the clarification of the flow behavior of latices at low shear stresses, and for the definition of the manner in which the flow curve of a non-Newtonian fluid approaches zero shear stress. The present investigation was undertaken, therefore, to obtain data on the basis of which conclusions could be drawn with respect to the behavior of latex systems in the shear stress region between zero and 20 dynes/cm.^{2}.

There are four possible ways in which a non-Newtonian fluid of the pseudoplastic type may approach zero shear stress, and these are indicated in Fig. 1. In plot 1*a* the fluidity G/F_m, where G is the rate of shear and F_m the shear stress, goes to zero as $F_m \rightarrow 0$. In plot *b* of Fig. 1 $G/F_m > 0$ at $F_m = 0$, and the fluid is non-Newtonian over the entire range of shear stresses. In plot *c* the curve intersects the F_m axis at some value other than zero. This situation corresponds to the existence of a yield point, and here $G/F_m = 0$ until a shear stress greater than F_0 is applied. Finally, case *d* indicates that at some definite low shear stress G/F_m becomes constant, and hence that the flow becomes Newtonian. The latter possibility was predicted by Ostwald and Auerbach (7). They also predicted that the com-

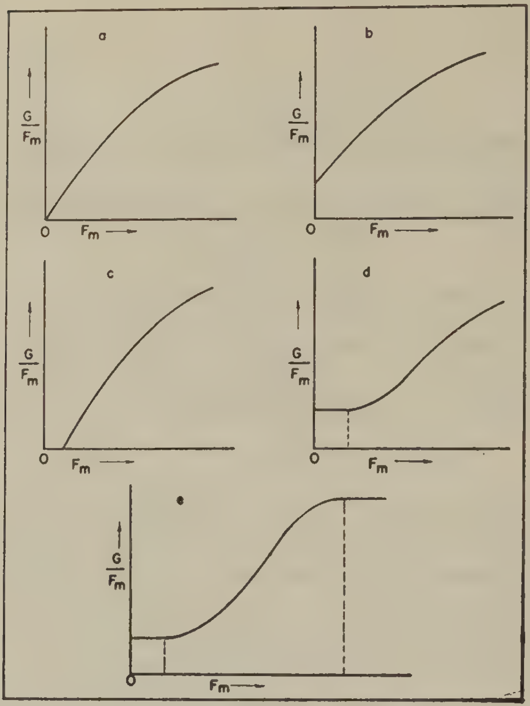

FIG. 1. Possible flow behavior of non-Newtonian fluids.

plete flow curve of a non-Newtonian fluid would show not only a Newtonian limit at low shear stresses but also one in the high shear stress region. A complete flow curve of the type predicted by Ostwald and Auerbach for laminar flow is shown in Fig. 1*e*.

In view of these possibilities, the problem reduces itself in essence to the determination of which of the four cases outlined above corresponds to the actual behavior of the system under investigation.

EXPERIMENTAL

The synthetic rubber latex used throughout this investigation was a low-temperature GR-S X-667 product obtained from the Copolymer Corporation of Baton Rouge, Louisiana. This latex contained an 84:16 butadiene-styrene copolymer, and was emulsified with potassium oleate. The starting concentration was 58.75% solids and 54.59% rubber by weight. By conductometric titration (8, 9) the latex was found to have 0.1487 meq. of soap per gram of latex, and a volume to surface average particle diameter $D_s = 1216$ A.

Lower concentrations of this latex were prepared by the addition of

CO_2-free distilled water. The total solids at each concentration was obtained by drying in a vacuum oven to constant weight.

All flow measurements were made at 30.00° ± 0.01°C. in the low shear capillary viscometer with continuously varying pressure head described by Maron and Belner (10). The δ-method described by these authors was used throughout to obtain the rate of shear-shear stress relation in the non-Newtonian flow regions.

Special handling was found necessary to keep the latex from skinning in the top bulbs of the capillary manometer units. Since skinning was due to surface evaporation, preventive techniques required the raising of the humidity above the latex surface. This was accomplished by suspending a small wad of moistened absorbent cotton in both upper bulbs of the instrument. By this simple means all difficulty due to skinning was removed.

RESULTS

Volume Fraction of Contained Polymer

For handling the data it is necessary to know the density of the latex, d, and the volume fraction of the contained polymer, v. Maron and Fok (4) have shown that the density of the contained polymer, d_r, is given by

$$d_r = \frac{C_r}{100/d - (100 - C_r)/d_w}, \qquad [1]$$

where C_r is the dry rubber content in per cent, and d_w is the density of water. They also found that for X-667 latex $d_r = 0.925$ g./cc. at 30.0°C. Since for the latex studied here $C_r = 0.9292$ (total solids) $= 0.9292$ (T.S.), the latex density follows as

$$d = \frac{92.5}{92.90 + 0.0659(\text{T.S.})}. \qquad [2]$$

Further, the rubber volume fraction is given by

$$v = \frac{V_r}{V_1} = \frac{C_r/d_r}{100/d}, \qquad [3]$$

where V_r is the volume of rubber and V_1 is the volume of latex. On substitution of the values of C_r and d_r, and of Eq. [2] for d, the expression for the volume fraction in terms of total solids for this latex becomes

$$\frac{1}{v} = \frac{99.91}{\text{T.S.}} + 0.0716. \qquad [4]$$

Equation [2] gives thus the density of the latex at any given total solids, while Eq. [4] allows conversion of total solids to volume fraction.

TABLE I

Relative Viscosity of X-667 Latex at 30.0°C. in the Completely Newtonian Concentration Range

Total solids, %	Volume fraction	η_r
5.049	0.0504	1.161
9.854	0.0979	1.357
15.02	0.149	1.626
20.07	0.198	1.998
25.03	0.246	2.488

Flow Behavior of the Latex

The flow properties of the GR-S X-667 latex have been studied at 13 concentrations, in approximately 5% increments, from 5% to 59% solids at 30.00°C. Below 25% solids this latex was found to be completely Newtonian over the entire shear stress range of the instrument. The results of the flow measurements are shown in Table I as relative viscosity, $\eta_r = \eta/\eta_w$, at the various volume fractions; η is the viscosity of the latex, while η_w is the viscosity of water at 30.0°C.

For concentrations above 25% solids the latex was found to be non-Newtonian in the upper shear stress range of the instrument, and Newtonian in the low shear stress region. A typical plot of this behavior is shown in Fig. 2. It was also found that the value of F_m at which the latex shows a transition from Newtonian to non-Newtonian flow is a function of the concentration (Fig. 3). From this figure it may be seen that the shear stress F_0 up to which the latex is Newtonian, obtained from very sensitive large-scale δ plots as described in reference (10), decreases as the concentration goes up, and that the relation between F_0 and v is linear above a v of 0.32. Further, this plot predicts that above a volume fraction of 0.544 the latex should be non-Newtonian over the entire shear stress range. This was actually found to be the case for $v = 0.546$ and $v = 0.564$.

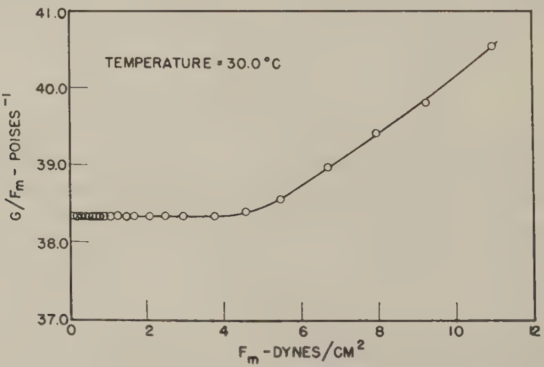

FIG. 2. Plot of G/F_m vs. F_m for 29.93% solids X-667 latex.

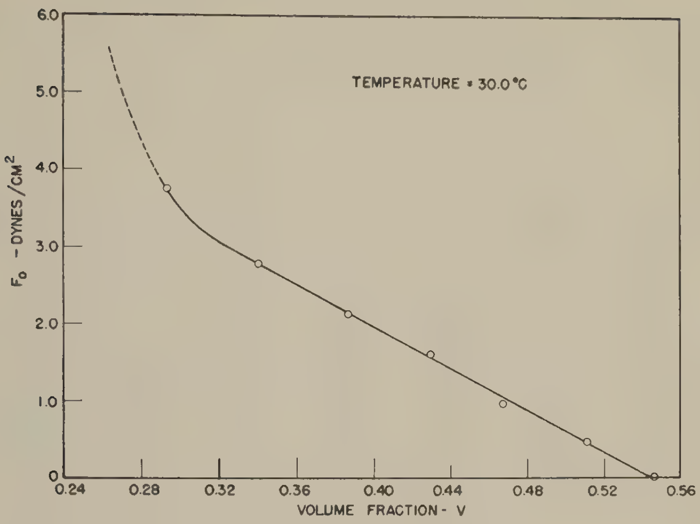

FIG. 3. Dependence of Newtonian shear stress region on volume fraction.

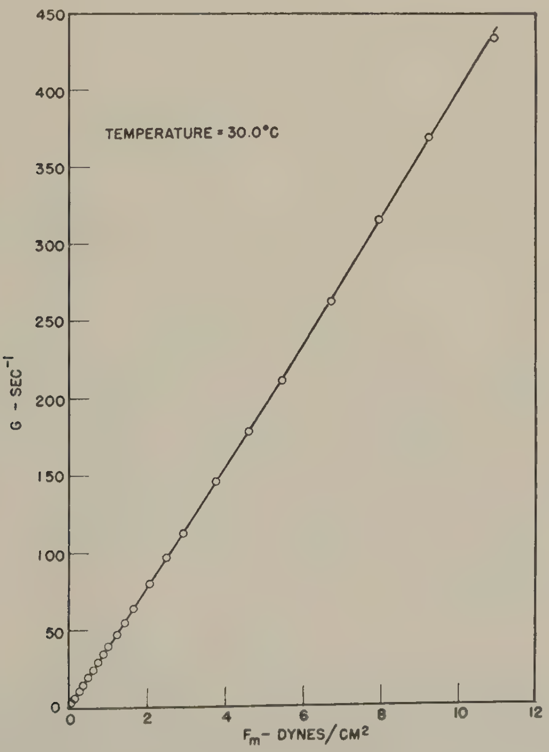

FIG. 4. Rate of shear-shear stress plot for 29.93% solids X-667 latex.

TABLE II

Relative Viscosities of X-667 Latex at 30°C. and Volume Fractions above 0.25

Volume fraction	0.293	0.341	0.387	0.430	0.468	0.511	0.546	0.564
Shear stress	Relative viscosity							
0.08	3.268	4.520	—	—	—	—	—	—
0.25	3.268	4.520	6.945	10.73	17.16	39.48	101.4	202.7
0.50	3.268	4.520	6.945	10.73	17.16	39.48	96.67	186.2
0.75	3.268	4.520	6.945	10.73	17.16	38.55	93.42	174.5
1.00	3.268	4.520	6.945	10.73	17.16	37.71	91.11	167.9
2.00	3.268	4.520	6.945	10.68	16.41	35.64	83.24	149.9
3.00	3.268	4.518	6.721	10.40	15.96	34.16	77.10	137.1
4.00	3.267	4.489	6.587	10.17	15.62	32.86	72.08	127.2
6.00	3.234	4.379	6.425	9.826	15.03	30.75	64.65	112.6
8.00	3.179	4.267	6.324	9.585	14.53	29.05	59.37	102.1
10.00	3.120	4.161	6.248	9.384	14.12	27.53	55.41	93.92
15.00	—	—	6.120	8.930	13.31	25.00	49.58	80.31
20.00	—	—	6.026	8.904	12.83	24.10	45.72	72.00

Below $v = 0.32$ F_0 rises sharply with decrease in v. This behavior may be anticipated, since at approximately $v = 0.25$ the latex is completely Newtonian, and hence F_0 should go theoretically to infinity.

The importance of plotting G/F_m rather than G vs. shear stress can be seen by comparing Fig. 2 with Fig. 4, which is the G vs. F_m plot for the same data as shown in Fig. 2.

The results obtained with latex concentrations above $v = 0.25$, where non-Newtonian behavior is observed, are summarized in Table II. These are given in terms of relative viscosity, defined as

$$\eta_r = \frac{(F_m/G)}{\eta_w}, \qquad [5]$$

corresponding to the various shear stresses and volume fractions of contained polymer.

An attempt was made to apply to these data the exponential flow equation (11, 12)

$$F_m^N = \eta' G, \qquad [6]$$

which can be written as

$$\log \eta_r = (1 - N) \log F_m + \log \eta_r' \qquad [7]$$

where N and η' are constants, and $\eta_r' = \eta'/\eta_w$. On plotting $\log \eta_r$ vs. $\log F_m$, curves rather than straight lines were obtained, indicating that N is not a constant, and that, therefore, Eq. [7] is inapplicable with constant N.

A fit of the data was then attempted using η_r as a function of the volume fraction, v. Maron, Madow, and Krieger (2) had previously used the equation

$$\log \eta_r = \frac{\alpha b v}{1 - \alpha v} \qquad [8]$$

where α and b are constants. This equation also proved inapplicable. Consequently the Eilers (13) equation was tried. The original Eilers equation for suspensions of spheres is

$$\eta_r = \left[1 + \frac{2.5v}{2(1 - (v/b))}\right]^2, \qquad [9]$$

where b is a constant whose value is a function of the packing of spheres, and the 2.5 is the Einstein (14) factor. A more general form of the Eilers equation would read

$$\eta_r = \left[1 + \frac{\alpha v}{1 - \beta v}\right]^2, \qquad [10]$$

where α and β are constants. On rearranging

$$\frac{\eta_r^{1/2} - 1}{v} = \alpha + \beta(\eta_r^{1/2} - 1), \qquad [11]$$

and hence a plot of $(\eta_r^{1/2} - 1)/v$ vs. $(\eta_r^{1/2} - 1)$ at any given value of F_m should yield a straight line of slope β and intercept α. This equation was found to hold at all concentrations, including those in the Newtonian range, and at all shear stresses, as may be seen from the typical plot shown in Fig. 5. The values of α and β evaluated from the data by least squares are given in Table III.

Once values of α and β were available, a volume fraction could be calculated for every η_r. These calculated v's could then be compared with the observed ones as a check on the fit of Eq. [11]. The fourth column in Table III indicates that the agreement between the calculated and observed v's ranged from 0.44% to 1.20%, averaging ±0.88%.

It can be seen from Table III that α is essentially constant, with the average being $\alpha = 1.430 \pm 0.006$. On the other hand, β varies with shear stress. This was also found to be the case by Maron and Fok (4). The variation of β with F_m could be represented by the equation

$$\frac{1}{\beta} = aF_m^{1/2} + c, \qquad [12]$$

where a and c are constants. The least squares evaluation of the constants gave $a = 0.008526$ and $c = 0.5935$. This equation yields β values which agree excellently with the observed ones. Finally, if Eq. [12] is substituted

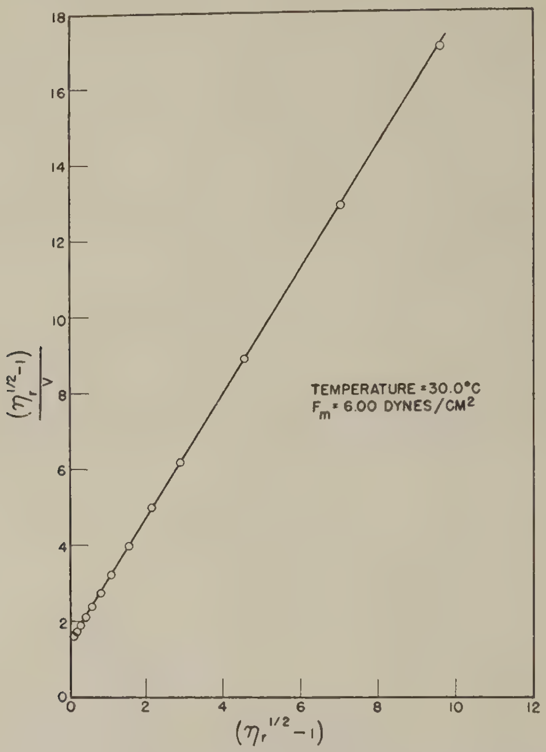

FIG. 5. Modified Eilers equation plot for X-667 latex.

TABLE III

α and β Values Calculated from the Modified Eilers Equation

Shear stress F_m	α	β	Avg. % deviation in v
0.08	1.409	1.683	±0.59
0.25	1.424	1.671	±0.97
0.50	1.429	1.666	±1.06
0.75	1.432	1.663	±1.17
1.00	1.434	1.660	±1.19
2.00	1.437	1.652	±1.20
3.00	1.442	1.644	±1.17
4.00	1.440	1.638	±1.02
6.00	1.434	1.628	±0.81
8.00	1.428	1.620	±0.71
10.00	1.422	1.612	±0.64
15.00	1.432	1.595	±0.45
20.00	1.425	1.584	±0.44
	1.430 ± 0.006		±0.88

into Eq. [10] along with the value of α, we get

$$\eta_r = \left[1 + \frac{1.430v}{1 - \dfrac{v}{0.008526F_m^{1/2} + 0.5935}}\right]^2. \qquad [13]$$

Equation [13] represents the flow behavior of this latex as a function of volume fraction and shearing stress at 30.0°C. in the region of 0.08 to 20 dynes/cm.^{2}.

Discussion of Results

Latex Behavior at Infinite Dilution

Einstein's (14) equation for the viscosity of very dilute suspensions of spherical particles in a medium states that $(\eta_r - 1)/v = 2.50$. The modified Eilers equation predicts in turn for infinite dilution $(\eta_r - 1)/v = 2\alpha = 2.86$, which is higher than the Einstein value of 2.50. However, the α values in the modified Eilers equation are based on the volume fraction of the rubber particles only. Actually, the latex particles consist not only of rubber but also of an adsorbed monolayer of soap. Hence the actual volume fraction v_t is larger than v, and the values of 2α are too large by the factor v/v_t. This ratio can be ascertained from the equation of Maron, Madow, and Krieger (2), who showed that

$$\frac{v_t}{v} = 1 + \frac{6\Delta}{D_s} \qquad [14]$$

where Δ is the thickness of the soap monolayer, 27.5 A. for the oleate ion, and D_s is the volume to surface average diameter of the latex particles, 1216 A. for this latex. On substitution of these values of Δ and D_s into Eq. [14], we obtain $v_t/v = 1.136$. Division of 2α by this correction factor yields the values given in column 3 of Table IV. The average of these, 2.52 ± 0.01 is in excellent agreement with the expected Einstein value of 2.50.

Volume Fraction at Infinite Viscosity

The $1/\beta$ values, which are the volume fractions at which the viscosity of the latex goes to infinity, also have to be corrected to the true volume fraction by multiplication by 1.136. The corrected $1/\beta$ values are given in the last column of Table IV. These vary from 0.68 to 0.72 over the shear stress range covered. With the use of the packing factors given by Heywood (15) for uniform spheres, and with allowance made for the particle size heterogeneity of the latex, it would appear that the packing of this latex at the lower shear stresses is a combination of orthorhombic and tetragonal, with the latter predominating. As the shear stress is increased,

TABLE IV

Corrected Constants for the Modified Eilers Equation

Shear stress	2α	$\frac{2\alpha}{1.136}$	$\frac{1}{\beta}$	$1.136\frac{1}{\beta}$
0.08	2.82	2.48	0.594	0.675
0.25	2.85	2.51	0.598	0.680
0.50	2.86	2.52	0.600	0.682
0.75	2.86	2.52	0.601	0.683
1.00	2.87	2.53	0.602	0.684
2.00	2.87	2.53	0.605	0.688
3.00	2.88	2.54	0.608	0.691
4.00	2.88	2.54	0.611	0.694
6.00	2.87	2.53	0.614	0.698
8.00	2.86	2.53	0.617	0.701
10.00	2.84	2.50	0.620	0.705
15.00	2.86	2.52	0.627	0.712
20.00	2.85	2.51	0.631	0.717

there seems to occur a gradual transition to the densest, or rhombohedral, packing. However, the transition is incomplete, and the dominant packing at the higher shear stresses seems to be the tetragonal. These observations are in agreement with the results of Maron and Fok (4), who found the packing factors for X-667 latex between $F_m = 50$ and $F_m = 800$ dynes/cm.^{2} to vary from 0.69 to 0.74.

Deviation of Latex from Newtonian Flow

Equation [13] may be used to show the manner in which the extent of non-Newtonian behavior of the latex varies with F_m and v. Differentiation of the equation with respect to F_m at constant v yields

$$\left(\frac{\partial \ln \eta_r}{\partial \ln F_m}\right)_{v,T} = \frac{-a\alpha v^2 F_m^{1/2}}{(aF_m^{1/2} + c)^2(1 - \beta(F_m)v)(1 - \beta(F_m)v + \alpha v)}. \qquad [15]$$

Now, if we allow N to be a variable in Eq. [7], then

$$\left(\frac{d \ln \eta_r}{d \ln F_m}\right)_{v,T} = (1 - N) \qquad [16]$$

and hence,

$$(N - 1) = \left[\frac{a\alpha F_m^{1/2}}{(aF_m^{1/2} + c)^2}\right]\left[\frac{v^2}{(1 - \beta(F_m)v)[1 - (\beta(F_m) - \alpha)v]}\right]. \qquad [17]$$

The quantity $(N - 1)$ is a measure of the extent of deviation of the latex from Newtonian behavior, since in the latter instance $N = 1$. Examination of Eq. [17] reveals that $(N - 1)$ has some finite value no matter how small F_m becomes. This cannot be the case, since the latex was found to have a Newtonian limit in the low shear region. Furthermore, the extent of the Newtonian region varies with concentration, as shown in

Fig. 3. It is evident, therefore, that not the entire applied shear stress, F_m, is responsible for producing non-Newtonian flow, but only the part F, where

$$F = F_m - F_0, \tag{18}$$

F_0 being the shear stress up to which the latex is Newtonian at a given volume fraction of rubber. On this basis $(N - 1)$ must be related not to the total shear stress applied, but only to the portion F; i.e., $(1 - N)$ is given not by Eq. [16] but by

$$\left(\frac{\partial \ln \eta_r}{\partial \ln F}\right)_{v,T} = (1 - N). \tag{19}$$

To convert Eq. [16] to Eq. [19] we may proceed as follows. From Eq. [18] at constant T and v $dF = dF_m$, and hence

$$F_m \partial \ln F_m = F \partial \ln F. \tag{20}$$

Consequently,

$$\left(\frac{\partial \ln \eta_r}{\partial \ln F}\right)_{v,T} = \frac{F}{F_m}\left(\frac{\partial \ln \eta_r}{\partial \ln F_m}\right)_{v,T} = (1 - N), \tag{21}$$

and substitution of Eq. [15] yields

$$(N - 1) = \frac{F}{F_m}\left[\frac{a\alpha F_m^{1/2}}{(aF_m^{1/2} + c)^2}\right]\left[\frac{v^2}{(1 - \beta(F_m)v)[1 - v(\beta(F_m) - \alpha)]}\right]. \tag{22}$$

Equation [22] was used to calculate the $(N - 1)$ values corresponding to various values of F_m and v. These are given in Table V. Also listed in the

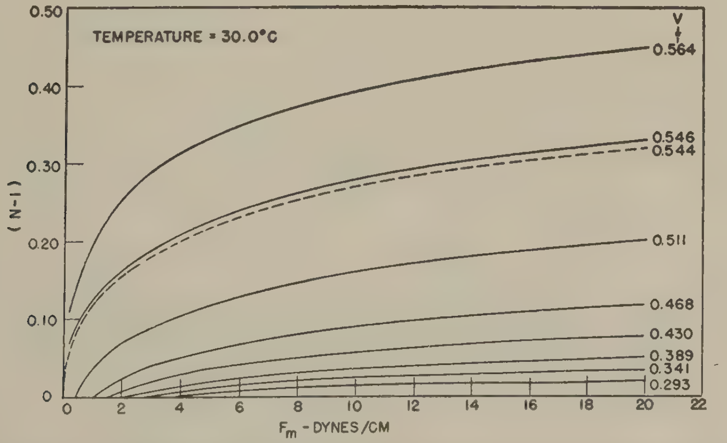

FIG. 6. Degree of non-Newtonian behavior of X-667 latex at various shear stresses and volume fractions.

TABLE V

(N − 1) Values for GR-S X-667 Latex at 30.0°C.

Shear stress dynes/cm²	v = 0.293	0.341	0.387	0.430	0.468	0.511	0.546	0.564
	F_0 = 3.75	2.78	2.15	1.56	1.04	0.45	0	0
	$(N - 1)$							
0.08	0	0	—	—	—	—	—	—
0.25	0	0	0	0	0	0	0.0668	0.110
0.50	0	0	0	0	0	0.00482	0.0908	0.147
0.75	0	0	0	0	0	0.0232	0.109	0.174
1.00	0	0	0	0	0	0.0363	0.122	0.195
2.00	0	0	0	0.00728	0.0242	0.0693	0.163	0.253
3.00	0	0.00119	0.00722	0.0190	0.0392	0.0894	0.188	0.291
4.00	0.000738	0.00564	0.0133	0.0273	0.0502	0.105	0.208	0.312
6.00	0.00529	0.0119	0.0221	0.0394	0.0661	0.127	0.238	0.347
8.00	0.00850	0.0163	0.0285	0.0481	0.0778	0.144	0.260	0.376
10.00	0.0110	0.0199	0.0335	0.0551	0.0871	0.157	0.277	0.393
15.00	0.0156	0.0264	0.0429	0.0681	0.104	0.181	0.305	0.423
20.00	0.0187	0.0313	0.0499	0.0780	0.118	0.200	0.329	0.449

table at the corresponding volume fractions are the F_0 values taken from Fig. 3. Finally, Fig. 6 shows $(N - 1)$ as a function of F_m for various values of v. The dotted curve indicates the dividing line between latices having a measurable Newtonian region in the low shear range, and those which are completely non-Newtonian. The value of v for which this transition occurs is 0.544, and comes from the intersection of the plot with the v-axis in Fig. 3.

The results shown in Fig. 6 agree with those of Maron and Fok (4), whose $(N - 1)$ vs. F_m plots went through maxima at approximately 100 dynes/cm.², and then decreased with decreasing F_m. It was not necessary for them to use the $(N - 1)$ equation corrected for F_0, since as F_m increases, F/F_m approaches unity. The $(N - 1)$ data obtained here decrease with decreasing F_m, and finally intersect the F_m axis at $(N - 1) = 0$, corresponding to $F_m = F_0$. Below F_0 the flow is Newtonian, and $(N - 1)$ remains equal to zero.

ACKNOWLEDGMENT

This work was performed as part of a research project sponsored by the Office of Synthetic Rubber, Federal Facilities Corporation, in connection with the government Synthetic Rubber Program.

SUMMARY

The flow properties of low temperature GR-S X-667 latex have been investigated in a new low shear stress viscometer at 30.0°C. The range of

hear stresses covered was 0.08 to 20.0 dynes/cm.^{2}. The concentration was aried from 5% to 59% solids in approximately 5% increments.

The latex was found to be completely Newtonian below a volume raction of $v = 0.246$. Above $v = 0.246$ the latex flow was Newtonian at ow shear stresses, changing to non-Newtonian as F_m was increased. urthermore, the range of F_m over which the flow was Newtonian proved o be a linear function of the concentration between $v = 0.320$ and $v =$ .544. Above 0.544 the flow behavior was non-Newtonian over the entire ange of F_m covered in this study.

It was found possible to express the flow behavior of this latex as a unction of F_m and v in terms of the modified Eilers equation involving two arameters α and β; α was found to be a constant, while β was a function f F_m. This equation predicts that at infinite dilution 2α should equal the instein 2.50 for suspensions of spheres. When the observed values of 2α ere corrected for the volume occupied by the layer of adsorbed soap on he latex particles, the value obtained for this factor was 2.52 ± 0.01. gain β, which is the volume fraction at which the viscosity becomes nfinite, was found at the lower shear stresses to be of an order of magnitude xpected for spheres with a mixture of orthorhombic and tetragonal packng. With increasing F_m the packing became tighter, and appeared to pproach the densest, or rhombohedral, packing.

The equation was used also to obtain an expression for the deviation of he latex from Newtonian behavior as a function of F_m and v. At any given hear stress the deviation was the greater the higher the volume fraction. gain, at volume fractions above $v = 0.246$, and below $v = 0.544$ the degree f non-Newtonian behavior decreased regularly with decrease in F_m, eaching a Newtonian limit at some low shear stress. However, no Newonian limit was found above $v = 0.544$.

REFERENCES

1. Krieger, I. M., and Maron, S. H., *J. Colloid Sci.* **6,** 528 (1951).
2. Maron, S. H., Madow, B. P., and Krieger, I. M., *J. Colloid Sci.* **6,** 584 (1951).
3. Krieger, I. M., and Maron, S. H., *J. Appl. Phys.* **25,** 72 (1954).
4. Maron, S. H., and Fok, S. M., *J. Colloid Sci.* **10,** 482 (1955).
5. Maron, S. H., and Levy-Pascal, A. E., *J. Colloid Sci.* **10,** 494 (1955).
6. Bergen, J. J., and Patterson, W., *J. Appl. Phys.* **24,** 712 (1953).
7. Ostwald, W., and Auerbach, R., *Kolloid-Z.* **38,** 261 (1926).
8. Maron, S. H., Ulevitch, I. N., and Elder, M. E., *Anal. Chem.* **24,** 1068 (1952).
9. Maron, S. H., Ulevitch, I. N., and Elder, M. E., *J. Colloid Sci.* **9,** 89 (1954).
0. Maron, S. H., and Belner, R. J., *J. Appl. Phys.*, in press.
1. Porter, A. W., and Rao, P. A. M., *Trans. Faraday Soc.* **23,** 311 (1927).
2. Farrow, F., Lowe, G., and Neale, S., *J. Textile Inst.* **19,** T18 (1928).
3. Eilers, H., *Kolloid-Z.* **97,** 313 (1941).
4. Einstein, A., *Ann. Physik* **19,** 289 (1906).
5. Heywood, H. J., *J. Imp. Coll. Chem. Eng. Soc.* **2,** 9 (1946).

KINETIC CONSTANTS FOR METHYL METHACRYLATE POLYMERIZATION

T. E. Ferington and A. V. Tobolsky

Frick Chemical Laboratory, Princeton University, Princeton, New Jersey

Received June 1, 1955

ABSTRACTS

Values for A' and $C_{tr,m}$ for methyl methacrylate polymerization betwen 20°C. and 98°C. are presented. These are important for accurate calculation of rates of initiation.

The general relation between number-average degree of polymerization, $\bar{P}_n$, and the initial rate of polymerization, R_p, in the presence of varying amounts of a given catalyst is (1):

$$\frac{1}{\bar{P}_n} = C_{tr,m} + \frac{A'R_p}{[M]^2} + \frac{C_{tr,cat}R_p^{\ 2}}{B_I[M]} \qquad [1]$$

where: $C_{tr,cat}$ is the chain transfer to catalyst constant;
$C_{tr,m}$ is the chain transfer to monomer constant;
$[M]$ is the initial monomer concentration;
B_I is defined by the relation

$$R_p^{\ 2} = B_I[\mathrm{cat}] + R^2_{p,th}\,. \qquad [2]$$

For certain catalysts, the plot of $1/\bar{P}_n$ versus R_p is a straight line. This is clearly a necessary and sufficient condition for the absence of chain transfer to catalyst. In these cases the value of A' can be obtained from the slope of $1/\bar{P}_n$ vs. R_p line, which we have termed the monoradical line.

The quantity A' is a combination of the kinetic constants for propagation and for termination by combination and disproportionation.

$$A' = \frac{2k_{td} + k_{tc}}{k_p^{\ 2}}. \qquad [3]$$

The importance of A' lies in its role in relating the rate of initiation of polymer chains, R_i, to the rate of polymerization, R_p.

$$R_i(1 + x) = \frac{2A'}{[M]^2}R_p^{\ 2} \qquad [4]$$

where x is the ratio of disproportionation to over-all termination and can

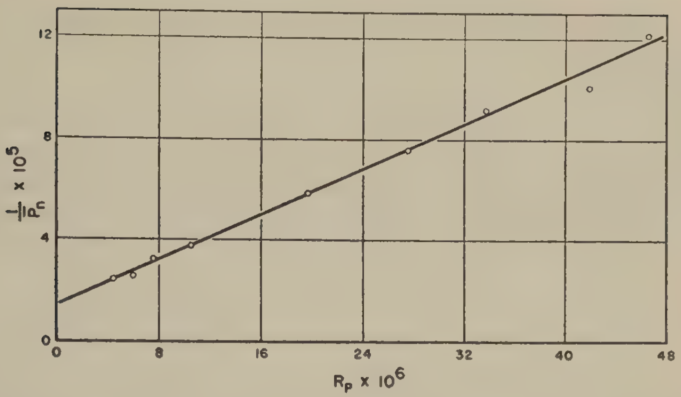

FIG. 1. $1/\bar{P}_n$. versus R_p for methyl methacrylate initiated by 2-azobisisobutyronitrile at 30° C.

vary between zero and unity. If A' is known, a measurement of R_p is thus essentially a measurement of R_i.

In the earlier reference (1), A' values for methyl methacrylate at various temperatures compiled from various literature sources were tabulated. In this paper we have supplemented these with A' values obtained over a much wider range of temperature in our own laboratories. These A' values were all obtained from plots of $1/\bar{P}_n$ versus R_p using initiator systems which gave straight lines. The values of $\bar{P}_n$ were obtained by measurements of

TABLE I

A' and $C_{tr,m}$ for Methylmethacrylate at Various Temperatures

T, °C.	$\frac{1}{T}$, (°K.)$^{-1}$	A'	$C_{tr,m}$	Initiator*	Ref.
20	3.42×10^{-3}	311	3×10^{-6}	Azo	*a*
25	3.35 "	292	1.5×10^{-5}	Azo	*b*
30	3.30 "	176	1.2 "	Azo	*a*
30	3.30 "	193	1.5 "	Azo	*c*
50	3.10 "	103	4 "	Bz_2O_2	*d*
60	3.00 "	67.3	1 "	Bz_2O_2 & Azo	*e*
60	3.00 "	65.3	—	Azo	*f*
70	2.92 "	44	6 "	Bz_2O_2	*d*
98	2.70 "	16.4	3.1 "	DTBP	*g*

* Azo = 2-azobisisobutyronitrile.
Bz_2O_2 = dibenzoylperoxide.
DTBP = di-*t*-butylperoxide.

a. J. A Levy, Senior Thesis, Princeton University (1954).

b. H. Hsieh, unpublished results, this Laboratory.

c. T. E. Ferington, unpublished results.

d. G. V. Schulz and G. Haborth, *Makromol. Chem.* **1**, 106 (1947).

e. B. Baysal and A. V. Tobolsky, *J. Polymer Sci.* **8**, 529 (1952).

f. J. L. O'Brien and F. Gornick, presented at Philadelphia Meeting of the American Chemical Society, January 29, 1953.

g. J. A. Offenbach, unpublished results, this Laboratory.

the intrinsic viscosities of the unfractionated polymer samples using the equation (2)

$$\text{Log } P_n = 3.2485 + 1.250 \log [\eta] \qquad [5]$$

A typical linear plot of $1/\bar{P}_n$ versus R_p is shown in Fig. 1 for the system methyl methacrylate-2-azobis-isobutyronitrile at 30°C. The values of A' obtained from the slopes of this and similar plots are given in Table I.

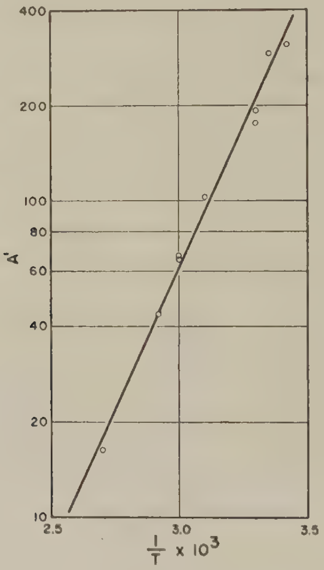

FIG. 2. Log A' versus $1/T$ for methyl methacrylate.

The values of log A' are plotted as a function of $1/T$ in Fig. 2 and the best straight line drawn through these points. The best fit to the data is given by the equation

$$A' = 3.00 \times 10^{-4} \exp \frac{8.18 \text{ kcal.}}{RT} \qquad [6]$$

This result modifies the previous result set forth by Tobolsky and Baysal (1)

$$A' = 5.02 \times 10^{-5} \exp \frac{9.35 \text{ kcal.}}{RT} \qquad [7]$$

which was based on results over a much more limited temperature range.

The equation calculated from the absolute rate constants of Matheson *et al.* (3) is:

$$A' = 2.59 \times 10^{-5} \exp \frac{9.78 \text{ kcal.}}{RT}$$

We have also tabulated the intercepts of the $1/\bar{P}_n$ vs. R_p graphs in Table I. This intercept, as shown by Eq. [1], is equal to $C_{tr,m}$ and is defined by $k_{tr,m}/k_p$ where $k_{tr,m}$ is the specific rate constant for the transfer of growing radical chains to the monomer and k_p is the specific rate constant for the growth step. Since $C_{tr,m}$ is rather small, its experimental determination by our methods is not too precise. The values obtained are of the order of 10^{-5} and show only a small increase with temperature. The older literature values of Schulz and Haborth appear to be somewhat high.

REFERENCES

1. TOBOLSKY, A. V., AND BAYSAL, B., *J. Polymer Sci.* **11,** 471 (1953).
2. BAYSAL, B., AND TOBOLSKY, A. V., *J. Polymer Sci.* **8,** 529 (1952).
3. MATHESON, M. S., AUER, E. E., BEVILACQUA, E. B., AND HART, E. J., *J. Am. Chem. Soc.* **71,** 497 (1949).

THE INFLUENCE OF PACKING DENSITY ON THE SMALL-ANGLE X-RAY SCATTERING OF A POLYDISPERSE COLLOID SYSTEM[1]

Katarina Kranjc

Physical Institute, Faculty of Science, University of Zagreb, Zagreb, Yugoslavia

Received June 6, 1955

INTRODUCTION

Small-angle X-ray scattering depends on the shape and size of structural elements, on their size distribution, and on their mutual arrangement. The arrangement of structural elements affects the scattering in the case of dense systems because of the interference between the rays scattered from the individual elements. The influence of the "inter-particle interference" has been experimentally proved and theoretically investigated on different models of specimen structure.

There is a field of application of the small-angle scattering method where the opinions of various authors do not agree with regard to the necessity of taking into account the inter-particle interference. Polydisperse systems of irregular structure, such as various adsorbents and catalysts, were—owing to their industrial importance—often investigated by the small-angle scattering method. In order to obtain some information about the degree of dispersion, the scattering curves of such materials have been evaluated by methods used for dilute systems neglecting the phenomenon of inter-particle interference (1, 2). In several cases the results were confirmed by independent methods (2, 3). An early experiment (4) showed that colloidal silver in dilute solution and after flocculation had almost equal scattering curves. The question whether neglecting interference is justified in the case of polydisperse systems is the main point of a discussion by Hosemann and Kratky (5) and continued by Hosemann and Porod (6–10). In the course of this discussion two methods of analysis of scattering curves were elaborated, both applicable to rather irregular polydisperse systems. One method is due to Hosemann (6) and the other to Porod (10, 11).

The purpose of this investigation was to study the influence of increasing packing density of a polydisperse system on the trend of the scattering curve and on the intensity of scattered radiation, and to compare Hosemann's method both with that of Porod and with the electron micrograph method.

---

[1] Presented at the Third International Congress of the International Union of Crystallography in Paris, July 21–28, 1954.

EXPERIMENTAL

1. Material

Finely divided hydrated alumina obtained by spontaneous oxidation of pure aluminum activated with mercury seemed to be a material suitable for the intended investigation. This substance was obtained by exposing aluminum plates to oxidation in air after purifying them in 50% caustic soda (50°C.) and immersing in a saturated solution of $HgCl_2$. The white powder formed on the surface of the aluminum plates was used as the initial material for preparing the specimens of various packing densities.

The physical and chemical properties of the material were investigated. The X-ray powder diffraction analysis showed the material to be the aluminum hydroxide called bayerite (12). The chemical analysis gave: 59.5% Al_2O_3; loss on ignition 40.5%; mercury in traces (13). The density measured with a pycnometer was 2.2 $g.cm.^{-3}$. The mass absorption coefficient calculated—and also verified experimentally—was 24 $cm.^2g.^{-1}$ for the CuK_α radiation.

The electron micrograph of the material is given in Fig. 1. The structural elements are visible at the edges of the nontransparent clusters, and have the form of filaments of various thicknesses and various lengths. Most filaments consist of a row of knots and seem to be composed of globular particles. Since the thickness of the filaments probably corresponds to the size of elementary particles, the thicknesses of filaments with the sharpest edges were measured by means of a micrometer. The mean thickness of 165 filaments was 77 A.

2. Preparation of Specimens

If ρ' is the average density, i.e., the ratio of the mass to the volume of the specimen, and ρ is the true density of the substance, then the ratio

$$p = \frac{\rho'}{\rho} \qquad [1]$$

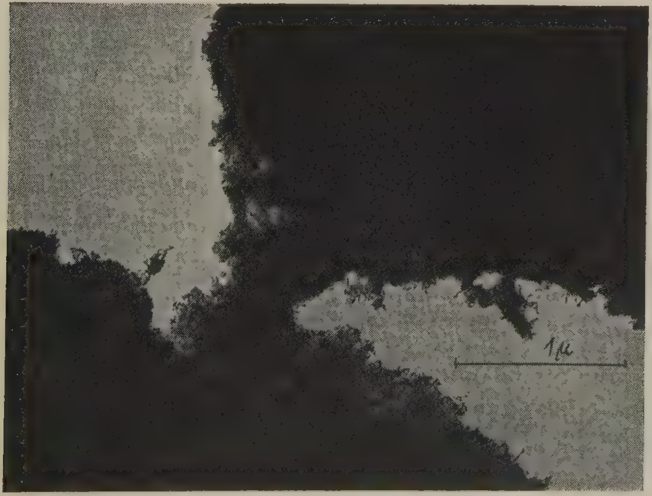

FIG. 1. Electron micrograph of the examined alumina hydrate.

describes the so-called packing density or the relative volume of the specimen, occupied by the substance.

We desired to prepare a set of specimens of various packing densities but of the same thickness so that the volume irradiated by X-rays would remain constant for each specimen. This thickness cannot be optimal for all specimens with respect to the intensity of scattered radiation because the optimal thickness—being $1/\mu$ (μ is the linear absorption coefficient)—depends on the average density. We, therefore, considered as most favorable the thickness for which the total exposure time for all specimens would be a minimum. In order to estimate this thickness we had to derive an expression which could be a measure for the total exposure time. We started from the relation giving the intensity of scattered radiation I:

$$I \sim I_0 d e^{-\mu d}, \tag{2}$$

where I_0 is the intensity of incident radiation, and d is the thickness of the specimen whose density is ρ. For a specimen of average density ρ' and thickness d' the condition

$$\rho d = \rho' d' \tag{3}$$

must be fulfilled if we wish to obtain the same intensity of scattered radiation with both specimens. By substituting [3] in [2] we obtain:

$$I \sim I_0 \frac{\rho' d'}{\rho} e^{-(\mu/\rho)\rho' d'}. \tag{4}$$

Hence the optimal thickness is given by

$$d'_{\text{opt}} = \frac{\rho}{\mu\rho'} = \frac{1}{\mu p}. \tag{5}$$

The exposure time t is inversely proportional to the intensity of scattered radiation; thus we can write:

$$t \sim \frac{1}{(\rho' d'/\rho) e^{-(\mu/\rho)\rho' d'}}. \tag{6}$$

The demand that the total exposure time be minimum may be written as

$$\sum \frac{1}{(\rho' d'/\rho) e^{-(\mu/\rho)\rho' d'}} = \text{minimum}, \tag{7}$$

the sum being taken over all specimens prepared for examination.

By selecting in advance the values of ρ' for twelve specimens (these values are indicated on the abscissa in Fig. 3), the expression [7] was computed for different values of d'. The minimum exposure time would be given by the specimens of thickness 0.6 mm., if, of course, the intensity of scattered radiation were affected only by absorption and not by the inter-particle interference.

The specimens of low average density in the form of powder were exposed to X-rays in a demountable cell between two foils of mica. Specimens of average densities higher than 0.5 g.cm.$^{-3}$ were tableted in a steel mold; the inside tube had to be very smooth to make possible the extrusion of tablets without breaking them. The pressure used for tableting the specimens of greatest densities exceeded 15,000 atmospheres. The highest obtained average density was 1.96 g.cm.$^{-3}$, but the tablet fell to pieces; however, one piece of it was exposed to X-rays.

With the specimens prepared for examination denoted by numbers 1 to 12, the

TABLE I

The Data on the Examined Specimens

Specimen	Thickness d (*mm.*)	Average density ($g.cm^{-3}$)	Packing density, p	Computed exposure time	Observed exposure time
1	0.60	0.057	0.026	4.76	4.17
2	0.60	0.11	0.052	2.65	2.76
3	0.60	0.23	0.10	1.51	0.83
4	0.60	0.46	0.21	1.05	0.71
5	0.58	0.59	0.27	1.01	0.80
6	0.59	0.81	0.37	1.00	1.00
7	0.62	0.99	0.45	1.08	1.14
8	0.59	1.21	0.55	1.16	1.96
9	0.62	1.38	0.64	1.35	2.64
10	0.62	1.62	0.73	1.64	3.67
11	0.64	1.82	0.83	2.10	6.91
12	0.50	1.96	0.89	2.61	7.51

second column of Table I shows their thicknesses and the third and fourth columns refer to their average and packing densities. The average densities ranged from 0.057 to 1.96 g.cm.$^{-3}$ and the packing densities from 0.026 to 0.89.

3. Registration of Small-Angle Scattering

The specimens were irradiated by the nickel-filtered copper radiation in an evacuated camera as described by Kiessig (14). The specimen-film distance was 200 mm. The smallest registered scattering angle was 21′. Four diagrams of each specimen were registered photographically with various exposure times and developed under strictly the same conditions. The photometering was performed by means of a Chalonge-Laffineur self-registering microphotometer.

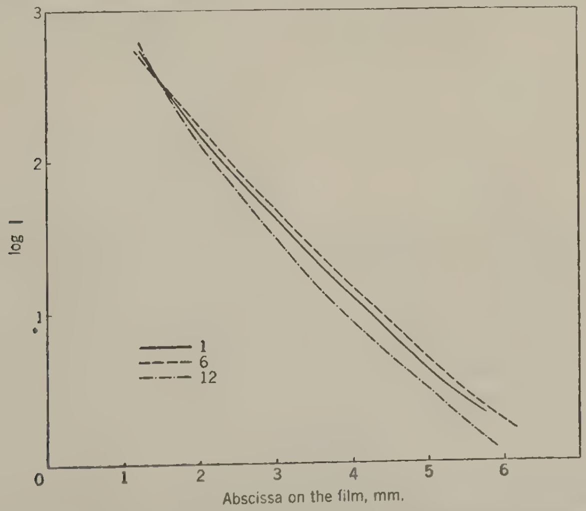

FIG. 2. The scattering curves corresponding to the specimens 1, 6, and 12 of average densities 0.057, 0.81, and 1.96 g.cm.$^{-3}$, respectively.

By arranging the scattering curves to intersect in a point, a pencil is obtained bounded on one side by the steepest scattering curve corresponding to the specimen of the highest average density (1.96 $g.cm.^{-3}$) and on the other side by the curve of smallest slope, given by the specimen of the average density 0.81 $g.cm.^{-3}$ (Fig. 2). Comparison of the twelve scattering curves revealed the imperfection of the photographic method of registration. Because of the uncertainty in the measurement of the background blackening it was difficult to observe the subtle differences between the shapes of the curves. Figure 2 represents the scattering curves corresponding to specimens 1, 6, and 12. Curves 6 and 12 are extremes in the slope and 1 and 12 in the average density of the corresponding specimens.

THE INTERPRETATION OF EXPERIMENTAL DATA

1. The Influence of Packing Density on the Intensity of Scattered Radiation

By considering the exposure times used for detecting the small-angle scattering of different specimens and the resulting blackening some conclusions can be drawn about the relation between the packing density and the intensity of the scattered radiation.

Relative exposure times as computed by means of relation [6] and related to specimen 6 are given in column 5 of Table I. The experimental exposure times giving the same blackening in a fixed direction (scattering angle 0.007 rad. was chosen) were found from scattering curves and were related to the same specimen. These values are given in column 6 of Table I; they differ greatly from the theoretical set of values in column 5.

It is remarkable that specimen 4 showed the strongest scattering and not specimen 6, as would be expected from consideration of the absorption only. Such a behavior would correspond to a material of greater mass absorption coefficient. To see whether the apparent increase of absorption

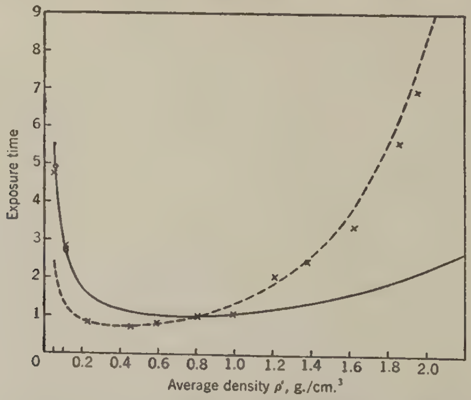

FIG. 3. The observed exposure times giving the same intensity of scattered radiation in a fixed direction for specimens of various average densities (crosses) compared with exposure times computed by help of the expression [6], substituting $\mu/\rho = 24$ (full line) and 42 (broken line).

coefficient could account for all the differences between the theoretical and experimental exposure times we tried to derive the mass absorption coefficient from the experimental scattering curves. We applied the relation [6] to the two specimens adjacent with respect to the average density. Dividing the corresponding values:

$$\frac{(\rho_1'\, d_1'/\rho)e^{-(\mu/\rho)\rho_1' d_1'}}{(\rho_2'\, d_2'/\rho)e^{-(\mu/\rho)\rho_2' d_2'}} = \frac{t_2}{t_1}, \tag{8}$$

the constant of proportionality disappears and μ/ρ can be determined. Substituting d' and ρ' for several pairs of specimens in relation [8] we found the mean value of μ/ρ to be 42.

Then the exposure times were computed by help of relation [6] substituting for μ/ρ the value 42 (instead of 24). These computed values for exposure times were in rather good accordance with the experimental ones. Figure 3 illustrates the exposure time as a function of the average density for specimens of thickness 0.6 mm. and mass absorption coefficient 24 (full line) and 42 (broken line), as computed by means of relation [6]. The crosses represent the experimentally obtained exposure times corrected to the thickness 0.6 mm.

It is seen that the absorption alone accounts only for the scattering of the two specimens of smallest packing densities; the others scatter approximately as if the mass absorption coefficient were increased. This behavior could be attributed to the influence of inter-particle interference on the intensity of scattered radiation, if we supposed that the variation of shape of scattering curves could be neglected. Hence, this interference effect can be described approximately by an exponential law.

2. The Analysis of Scattering Curves

The scattering curves represented in Fig. 2 were analyzed by the methods of Hosemann (6) and Porod (10, 11).

Hosemann supposes that the specimen consists of individual particles, each particle with its surrounding space forming one sphere and the packing density of all spheres being constant. The curves obtained by plotting k^2I vs. $k(k = 2\pi\epsilon/\lambda$, ϵ being the scattering angle) have a maximum; the part of the curve from the maximum toward greater scattering angles is of interest for interpretation. This part is not affected by inter-particle interference if the mean relative statistic fluctuation g is not smaller than the packing density p:

$$g \geqq p. \tag{9}$$

In a simple way g can be found and therefrom the parameters of the assumed Maxwell particle mass distribution.

Evaluating the scattering curves of specimens 1, 6, and 12 by this method, we obtained the mean particle diameters 91, 116, and 194 A., respectively. The statistic fluctuation increased with increasing packing density. The condition [9] was fulfilled only for the first two specimens. Thus in the case of specimen 12 one can expect that the position of maximum on the (Ik^2, k) curve is affected by inter-particle interference. However, the calculation showed that the value of 194 A. would not change much if the maximum was shifted toward smaller scattering angles.

Porod investigated the scattering from a system of "gel structure." In such a system the concept of individual particles becomes senseless owing to their close contact. With regard to the scattering, the dispersed phase is treated as a whole. As to the parameters obtainable from scattering curves there is some inconsistency within the papers of Porod himself. We shall therefore describe the way we obtained them.

None of the scattering curves of the three specimens showed the decrease of the intensity with the fourth power of the corresponding scattering angle. The slope of all three curves represented in system log I vs. log ϵ was -5 in the range of greater scattering angles. This disagreement with Porod's theory could be explained by the deformation of the scattering curves due to the collimation error of circular apertures used in the collimating system (15). Thus it was impossible to obtain the characteristic parameter of the colloid system, called by Porod the "reduced range of inhomogeneity" l_r (11). The other size parameter l_c, called the "range of coherence," was found using Porod's formula derived for an ideal collimating system (10)

$$l_c = \frac{D\lambda}{2} \frac{\int_0^\infty I(x)x\,dx}{\int_0^\infty I(x)x^2\,dx}; \qquad [10]$$

D is the specimen-film distance, x is the abscissa on the film, measured from the center of the diffraction pattern. This parameter, found for specimens 1, 6, and 12, was 84, 91, and 122 A., respectively. Having set $l_c = 2l_r$, we assumed (11) that the system is built of irregular particles forming clusters.

Without theoretical justification Porod (11) generalized a formula derived for micellar systems (10):

$$\frac{1}{a} + \frac{1}{b} = \frac{1}{l_r}, \qquad [11]$$

where a—called "the range of inhomogeneity"—is the mean section of all sections occupied by the substance on the straight lines drawn through the specimen, and b is the mean section of all free sections on the same lines. Porod related a and b to p by the equations

$$aq = bp = l_r, \qquad [12]$$

where $q = 1 - p$. We preferred to find a and b using the relation [11] and the following relation:

$$\frac{a}{b} = \sqrt[3]{\frac{p}{q}}, \qquad [13]$$

where p/q is the ratio of relative volumes of the substance and the interstices in the specimen. The values for a were found to be 55, 83, and 183 A., respectively.

From l_r the specific surfaces were obtained: 423, 254, and 32 $\text{m.}^2\text{g.}^{-1}$ for specimens 1, 6, and 12, respectively.

Discussion and Conclusions

In considering the results of the experiment just described, the first conclusion is that the trend of scattering curves is not much modified by the increase of packing density. This fact is in accordance with the predictions of Guinier (4, 16), Hosemann (17), and Fournet (18) in the case of irregular polydisperse systems.

As to the packing density influence on the intensity of scattered radiation Guinier (16) stated that the inter-particle interference would destroy the intensity the more, the greater the packing density. By a rough theoretical estimation he found also the rate of intensity decrease. If the system is composed of irregular particles and is not too compact, the intensity would diminish in the ratio $(1 - d'/d)$, d being the electron density of the substance and d' the mean electron density of the specimen.

The performed experiment has outlined an approximate law describing the relative intensity of scattered radiation as a function of packing density. By separating this expression into two factors:

$$\frac{I}{I_0} \sim \frac{\rho' d'}{\rho} e^{-42\rho' d'} = \frac{\rho' d'}{\rho} e^{-24\rho' d'} \cdot e^{-18\rho' d'} \qquad [14]$$

we have separated the effect caused by absorption as given by [4] and the interference effect. Representing graphically the isolated parts of [14], three curves in Fig. 4 illustrate the packing density influence on the intensity of scattered radiation as caused by the absorption alone (curve A), by the inter-particle interference alone (curve B), and by both effects together (curve C).

The trend of curve B in Fig. 4 confirms qualitatively Guinier's statement about the intensity-destroying influence of packing density. A theoretical explanation of the quantitative behavior of intensity in our experiment is hardly attainable owing to the complicated structure of the investigated substance.

There is another view of the same question taken by several authors (17, 9); they suppose that the strongest intensity of scattered radiation could be expected if the packing density were about 0.5. This statement is not as yet experimentally proved, and it is not clear how proof could be obtained. In our experiment the thickness of the specimens being constant, the strongest scattering was given by the specimen of packing density about 0.2 (see curve *C* in Fig. 4), but this optimal density obviously depends on the specimen thickness. On the other hand, we could imagine the specimens prepared in such a way that a constant amount of the material occupies the irradiated volume. This condition would require the thickness of the specimens to diminish with increasing packing density, or the product $\rho'd'$ to be constant for all specimens. In case our previous experience could be applied, both factors in [14] would not depend on packing density, and thus the intensity of scattered radiation would be constant for all specimens.

Of course, the entire question could be answered more precisely if we knew the course of the whole scattering curve including the zero scattering angle. However, we may conclude that, for registering the small-angle scattering of various powders and gels, the specimen thickness smaller than that given by [5] would be optimal.

The mathematical analysis of the scattering in polydisperse systems is necessarily based on simplified models which do not describe real materials. Owing to this fact and to the experimental errors (collimation and chromatic error) we cannot expect more than a rough estimation of the parameters characterizing the substance. It is therefore always of interest to compare

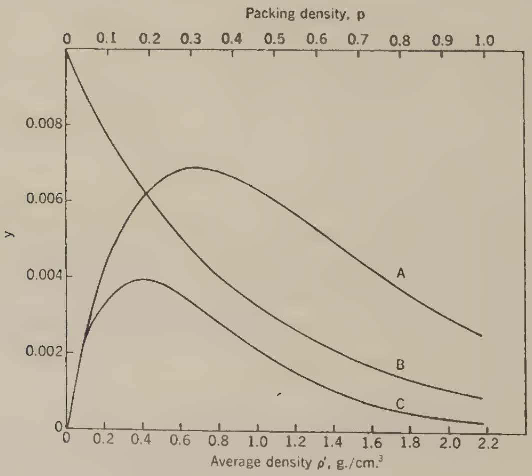

FIG. 4. The approximate influence of packing density on the intensity of scattered X-rays, as caused by the absorption (curve *A*, given by the relation $y = (\rho'd'/\rho)e^{-24\rho'd'}$), by inter-particle interference (curve *B*, representing the relation $y = e^{-18\rho'd'}.10^{-2}$), and by both effects together (curve *C* given by $y = (\rho'd'/\rho)e^{-42\rho'd'}$).

the data obtained by small-angle scattering with that obtained by other methods.

We shall compare the data obtained by Hosemann's method with the electron micrograph data of specimen 1. First, the average values obtained by both methods do not describe the same physical quantity. Knowing the thicknesses of a number of structural elements seen in the electron micrograph, and supposing that these elements have spherical form, we can in a simple way compute their mean diameter with regard to the mass distribution. This value being 98 A., we can compare it with 91 A. obtained by Hosemann's method. The agreement is rather good, though the specimen does not fulfill the assumptions underlying Hosemann's theory.

We obtained also an increase of the average size with packing density. This result is quite reasonable, because the more material is packed into the same volume, the more structural elements will associate together and thus the average size will become greater. The decrease of the degree of polydispersity could be explained by the disappearance of the smallest particles owing to their association into greater units.

One more conclusion could be drawn from the obtained data. The fact that the average size increases with packing density proves that, in the case of the very dense systems also, this average size, as obtained by Hosemann's method, describes the size of the particles and not of the interstices. If the predictions about this point were fulfilled (4, 9), the maximum average size would be reached for specimens of packing density about 0.5; at greater densities the holes penetrating the substance would be responsible for the scattering.

The theoretical basis of Porod's method was seriously critized by Hosemann (8). However, a number of substances were investigated by the gel-structure method (10, 11) and the data obtained were in accordance with known properties of the specimens. The physical picture of the size obtained by Porod's method is not clear enough to compare it with that obtained by the electron micrograph. But its increase with increasing packing density proves that we are dealing with a size parameter which could describe the state of dispersion of matter. The decrease of specific surface with increasing packing density, as shown by this method, is also a reasonable result.

We wish to thank Professor M. Paić for his continued interest and frequent advice in the course of this work, which has been performed in his laboratory. We thank also the Ruđer Bošković Institute for the loan of the microphotometer and for material support.

SUMMARY

The influence of packing density of a polydisperse colloid system on the shape of the small-angle scattering curve and on the intensity of scattered

radiation was studied experimentally. Twelve specimens of a finely divided alumina hydrate were prepared, their thickness being constant and their packing density increasing from 0.026 to 0.89. The shape of scattering curves did not vary much from one specimen to the other, as predicted by several authors. The intensity of scattered radiation was destroyed by the inter-particle interference as if the mass absorption coefficient was increased by a constant value. The average particle size of structural elements, as obtained from scattering curves by methods of Hosemann and Porod, increased with the packing density; this could be explained by the association of the particles in the process of pressing the material. The average size as obtained by the X-ray method is in rather good agreement with the average size of structural elements as shown by electron micrograph.

References

1. Biscoe, J., and Warren, B. E., *J. Appl. Phys.* **13,** 364 (1942); Roess, L. C., and Shull, C. G., *J. Appl. Phys.* **18,** 308 (1947).
2. Jellinek, M. H., Solomon, E., and Fankuchen, I., *Ind. Eng. Chem., Anal. Ed.* **18,** 172 (1946); Shull, C. G. and Roess, L. C., *J. Appl. Phys.* **18,** 295 (1947).
3. Elkin, P. B., Shull, C. G., and Roess, L. C., *Ind. Eng. Chem.* **37,** 327 (1945); Jellinek, M. H., and Fankuchen, I., *Ind. Eng. Chem.* **37,** 158 (1945); Smith, A. E., *Phys. Rev.* **71,** 277 (1947); Ritter, H. L., and Erich, L. C., *Anal. Chem.* **20,** 665 (1948).
4. Guinier, A., *Ann. phys.* **12,** 161 (1939).
5. Hosemann, R., *Z. Elektrochem.* **46,** 535 (1940); Kratky, O., Sekora, A., and Treer, R., *Z. Elektrochem.* **48,** 587 (1942); Kratky, O., and Porod, G., *J. Colloid Sci.* **4,** 35 (1949).
6. Hosemann, R., *Kolloid-Z.* **117,** 13 (1950).
7. Hosemann, R., *Ergebn. exakt. Naturw.* **24,** 142 (1951).
8. Hosemann, R., *Z. Elektrochem.* **58,** 271 (1954).
9. Porod, G., *Z. Naturforsch.* **4a,** 401 (1949).
10. Porod, G., *Kolloid-Z.* **124,** 83 (1951); *Kolloid-Z.* **125,** 51, 109 (1952).
11. Kahovec, L., Porod, G., and Ruck, H., *Kolloid-Z.* **133,** 16 (1953).
12. Kranjc, K., *Arhiv Kem.* **26,** 95 (1954).
13. Težak, S., *Arhiv Kem.* **24,** 45 (1952).
14. Kiessig, H., *Kolloid-Z.* **98,** 213 (1942).
15. Kranjc, K., *Glasnik mat.-fiz.astr.* **9,** 179 (1954).
16. Guinier, A., *J. chim. phys.* **40,** 133 (1943).
17. Hosemann, R., *Z. Physik* **113,** 751 (1939).
18. Fournet, G., Thèses, Ser. A. Nr. 2384. Paris (1951).

A NEW EQUATION BETWEEN THE TIME OF COAGULATION AND ELECTROLYTE CONCENTRATION-STUDIES ON COPPER FERROCYANIDE SOL

Amal K. Bhattacharya, Ram Kumar, and Abani K. Bhattacharya

Department of Chemistry, Agra College, Agra, India

Received June 14, 1955

Abstract

A new relation between the concentration of the coagulating electrolyte and the time of coagulation of copper ferrocyanide sol has been studied. The observations have been found to agree with the new equation, $C = a + (m \cdot 1/t)/(n + 1/t)$, where C and t are electrolyte concentration and time of coagulation, respectively; a, m, and n are constants.

Extensive studies have been made on the coagulation of colloids and various suggestions have been advanced by well-known workers in this field to explain the mechanism of rapid and slow coagulations. Smoluchowski (6), on a mathematical basis, derived his ingenious equation $\Sigma\nu = \nu_0/(1 + t/T)$, which has been tested by many authors and has been found to be consistent with experiment for rapid coagulation but to fail in the region of slow coagulation. The process of coagulation by the charge neutralization of colloidal particles is so complicated that no one has been sure of the exact mechanism of the phenomenon that follows after the addition of the flocculating electrolyte to a particular sol at various stages. In spite of the extensive amount of work that has been done so far in order to elucidate the phenomenon of coagulation, it will be of much interest to study the relationship between the concentration of the electrolyte and the corresponding time of coagulation.

Mathews and Murphy (4), Boutaric (2), and Dumanski and Scherschnev (3) investigated the relation between the electrolyte concentration and the stability of sols. Their studies brought out the important fact that the time of coagulation was a function of the electrolyte concentration which, as expressed by Dumanski, was of the form $t = aC^n$, when t is the time of coagulation and C the number of cubic centimeters of the electrolyte added, a and n being constants for the given system. Mathews and Murphy, and Boutaric also, observed that for every electrolyte there was a limiting concentration below which coagulation was not possible. Bhattacharya and Ram Kumar (1) studied the variation of the time of coagulation with the electrolyte concentration with arsenious sulfide, chromium hydroxide, and ferric hydroxide sols. By plotting the concentration of the electrolyte C with the reciprocal of the corresponding time of coagulation $1/t$ they obtained hyperbolic curves in the majority of cases but in a very few cases the plots were straight lines. On these grounds, a general equation $C = a + (m \cdot 1/t)/(n + 1/t)$, where a, m, and n are constants, has been suggested. This equation represents a hyperbola between C and $1/t$ but when the constant n becomes very large as compared to t, the equation takes the form $C = a + m \cdot 1/nt$, which is linear between C and $1/t$. In this paper we communicate our results on the slow coagulation of copper ferrocyanide sol by electrolytes.

EXPERIMENTAL

Preparation of Copper Ferrocyanide Sol

A number of preliminary experiments were made to find a proper proportion of copper sulfate and potassium ferrocyanide solutions which would result in the formation of a stable copper ferrocyanide sol. These experiments suggested that copper sulfate and potassium ferrocyanide solutions must be mixed in the ratio 4/5 in order to yield a stable sol. The sol thus prepared was dialyzed against distilled water until it was free from potassium ferrocyanide.

Reagents used were of "Analar" (B. D. H) quality.

The method of determining the time of coagulation was based upon the visible separation of clear liquid at the surface. Five cleaned and dried test tubes, each containing v c.c. of the electrolyte of known concentration, $(5-v)$ c.c. of water, and 5 c.c. of sol, were allowed to stand undisturbed. The time at which the coagulam just began to leave the surface of the liquid was noted carefully. The mean of the readings for the five test tubes was taken as the time of coagulation corresponding to v c.c. of the electrolyte. The above method has been found to be satisfactory for determining the comparative values of the time of coagulation for different concentrations of the electrolyte.

Experiments were performed with three different concentrations of the sol, viz., A, $3A/4$, and $A/2$ using different electrolytes.

TABLE I

Values of the Constants, a, m, and n, for Copper Ferrocyanide Sol

(Concentration A = 3.38 g. of copper ferrocyanide per liter.)

Electrolyte used	a (*millimoles/liter*)			m (*millimoles/liter*)			n (*min.*$^{-1}$)		
	Sol A	Sol $3A/4$	Sol $A/2$	Sol A	Sol $3A/4$	Sol $A/2$	Sol A	Sol $3A/4$	Sol $A/2$
1. Li_2SO_4	400	300	200	2174	1667	1250	0.0304	0.036	0.035
2. $MgSO_4$	0.75	0.70	0.50	8.333	1.923	1.316	0.0666	0.0269	0.0237
3. $AlCl_3$	0.18	0.09	0.02	0.9091	0.6250	0.4348	0.4091	0.3125	0.2391

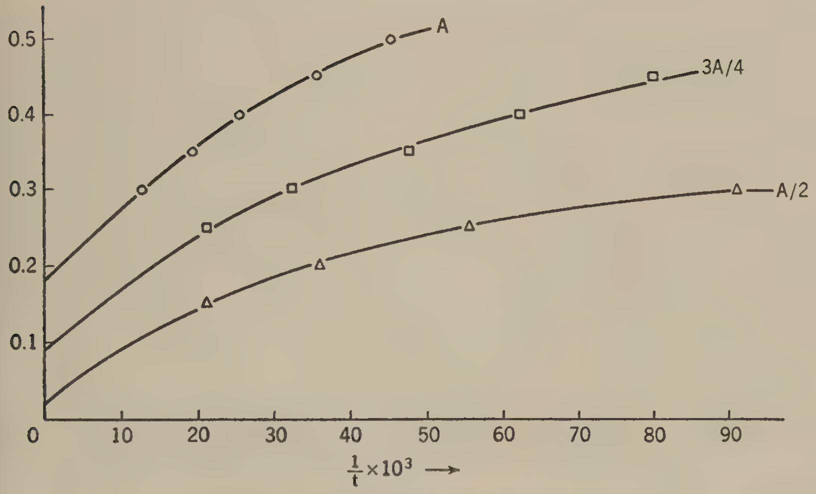

FIG. 1. Coagulation with lithium sulfate.

In order to verify the applicability of the new equation,

$$C = a + \frac{m \cdot 1/t}{n + 1/t} \qquad [1]$$

it was put in the form

$$\frac{1}{C - a} = \frac{nt}{m} + \frac{1}{m} \qquad [2]$$

which shows that the plot of $1/(C - a)$ against t should be a straight line. By knowing the concentrations of the electrolyte (C) and the corresponding

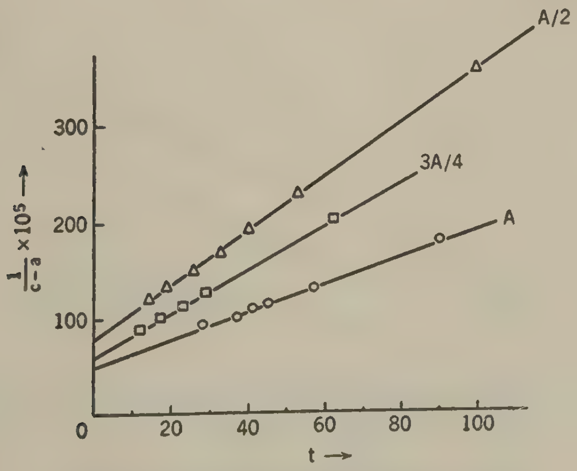

FIG. 2. Coagulation with lithium sulfate.

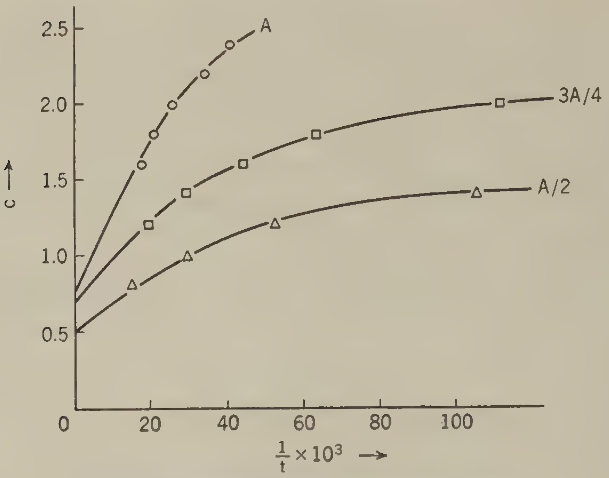

FIG. 3. Coagulation with magnesium sulfate.

times of coagulation (t), C–$1/t$ curves were plotted. The intercepts on the C-axis of the C–$1/t$ curves gave the values of "a". Knowing "a", $1/(C - a)$ was plotted against t and the curves were found to be straight lines in all cases, showing the validity of the new equation.

A few typical curves obtained by using lithium sulfate, magnesium sulfate, and aluminum chloride as the coagulating electrolytes are given below and the constants a, m, and n have been evaluated from these curves as shown in the following table. As evident from Eq. [2], m is the reciprocal of the intercept on the $1/(C - a)$ axis and n/m can be obtained from the slope of the straight line to the t-axis. From the known values n/m and m, n was evaluated.

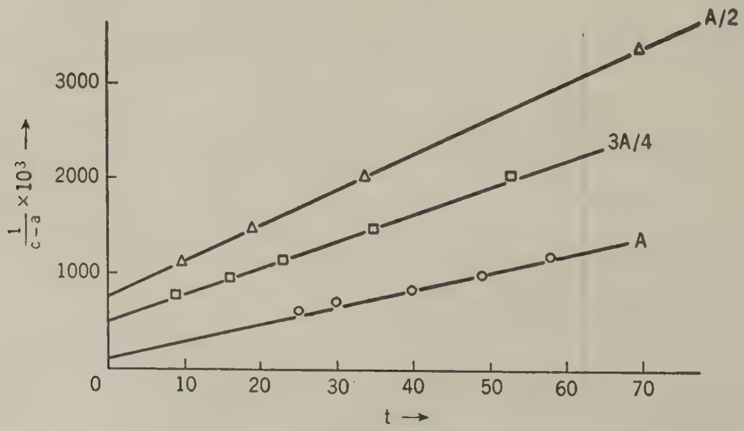

FIG. 4. Coagulation with magnesium sulfate.

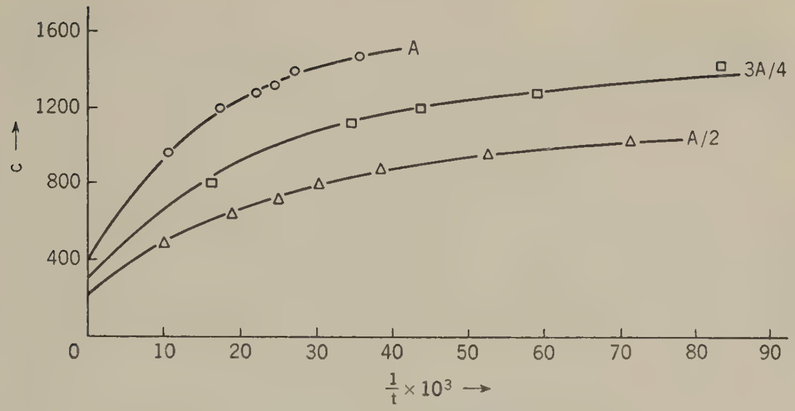

FIG. 5. Coagulation with aluminum chloride.

OBSERVATIONS

DISCUSSION

Since in all cases the plots of $1/(C - a)$ and t are straight lines, it follows that Eq. [2] and consequently Eq. [1] agree with our results obtained in the study of slow coagulation of copper ferrocyanide sol.

It is of much interest to interpret the constants a, m, and n in our new equation, $C = a + m \cdot 1/t/n + 1/t$.

The Constant "a"

If $1/t$ is put equal to zero in the above equation, we obtain C equal to a. It therefore follows that a is the concentration of the electrolyte which will coagulate the sol in infinite time. In other words, we may say that the sol

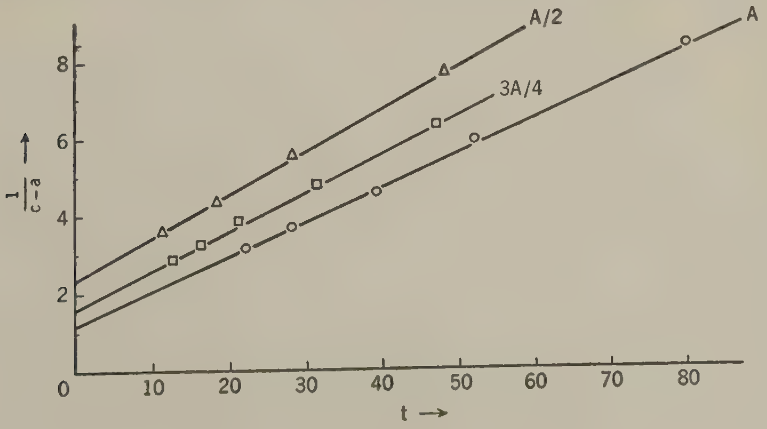

FIG. 6. Coagulation with aluminum chloride.

can remain stable up to a concentration given by a and hence a may be designated as the critical stability concentration of the electrolyte for the sol.

The Constant m

If $1/t$ is made infinitely large as compared to n in the new equation stated above, we get $C = a + m$. This means that m is the excess of the electrolyte that should be added above the critical stability concentration in order to cause the immediate coagulation of the sol. It may be said that at $C = a + m$, the region of slow coagulation merges into that of rapid coagulation.

The Constant n

Let us consider the equation, $C - a = m/nt + 1$, which is an alternative form of our new equation. It is evident that n has the dimension t^{-1}. Hence putting $n = k/t$, we get $C - a = m/k + 1$. This means that n is a constant characteristic for the sol which shows that the sol will be coagulated in time interval t by $1/k + 1$th-fraction of m (the quantity for instantaneous coagulation). Hence we finally connect n with the susceptibility or sensitiveness of the sol to the electrolyte which becomes equal to k when $t = 1$.

It will be interesting to examine critically the variations in the values of the constants a and m. From the table given above it is evident that the variation of the constants a and m with the dilution of the sol is quite normal in the sense that less of an electrolyte is necessary to coagulate the diluted sol for mono-, bi-, and ter-valent precipitating ions. Further the variation in the values of a and m with the valency of the cation of the electrolyte used suggests that the coagulating power of the cation increases with the increase in its valency. But the values of the constant n, however, vary normally or abnormally with dilution, specifically with the nature of the precipitating ion. In the case of lithium sulfate the value of "n" increases with the dilution of copperferrocyanide sol, whereas with magnesium sulfate and aluminum chloride the values are in decreasing order with dilution.

The normal and abnormal behavior of various sols had been extensively studied by previous workers (Weiser, Mukherji, Dhar, Ghosh, and others). It was established by their work that the precipitation concentration of the electrolyte is fundamentally governed by three factors: (*1*) number of the particles per c.c., (*2*) the distance between the particles; and (*3*) surface adsorption. According to the view of Mukherji (5) the increased distance on dilution tends to increase the stability of the sol and increase the adsorption of the precipitating ion per unit surface due to decrease in the number of particles. Hence the normal or abnormal behavior of the sol on dilution, or, in other words, the decrease or increase in stability, will be due to the predominating influence of one factor over the other. It is interesting to note that the values of n also vary normally or abnormally with dilution, as had been observed for the values of the precipitation concentrations of the electrolytes. It can thus be concluded that the value of n is an index of the stability and hence represents the susceptibility of the sol to the electrolyte, as has been already interpreted from the new equation.

Further work in this line is in progress.

References

1. Bhattacharya, A. K., and Kamur, R., *J. Indian Chem. Soc.* **28,** 179 (1951); *ibid.* **28,** 638 (1951); *ibid.* **29,** 687 (1952); *ibid.* **29,** 759 (1952).
2. Boutaric, A., *Bull. soc. chim. France* **43,** 146 (1928).
3. Dumanski, A. V., and Scherschnev, P. A., *J. Russ. Phys.-Chem. Soc.* **62,** 187 (1930).
4. Mathews, J. M., and Murphy, R. V., *Science* **53,** 581 (1921).
5. Mukherji, J. N., and Sen, N. N., *J. Chem. Soc.* **115,** 461 (1919).
6. Smoluchowski, Von, *Z. Physik* **92,** 129 (1917).

A NOTE ON THE FILTRATION OF AEROSOLS BY A SIMPLIFIED FILTER MODEL[1, 2]

Isaiah Gallily

Tel-Aviv, Israel

Received June 21, 1955

The filtration of aerosols by fiber mats has been treated theoretically by the use of a simplified model consisting of a long cylindrical wire (1, 2). The theoretical approaches differ regarding the relative importance of the mechanisms by which the deposition of particles occurs. However, the same conclusion was reached by the various authors, *viz.*, that filtration should have a minimum value for a certain particle size. Experiments with commercial filters have not confirmed this prediction (3). Furthermore, filtration by inertial impaction has been found experimentally to depend on the inter-fiber distance (4), although this was not taken into account by some theories (1).

It is most likely that the complicated paths followed by particles through the meshes of a real filter are remote from the flow route discussed in the simple theories. In order to check the validity of the theoretical conclusions it seemed desirable to construct a filter which would be intermediate between the single wire and the complicated system of the fiber mat. To deal with mechanical mechanisms only, the filter had to be free of electrostatic charges.

The filter consisted of a metallic pipe (5 cm. diameter) containing an array of 76 grids set in planes perpendicular to its geometric axis. Each grid was composed of parallel, equally spaced metallic wires wound on metallic frames (Fig. 1). The diameter of the wires as well as their interdistance could be changed within wide limits. On the other hand, the spacing between the grids was calculated and fixed so that the flow near the axis would be practically repeated in front of every one of them. The calculations were based on the equations of Kovasznay (5). In the present series of experiments the wire used was 0.0050 cm. in diameter, the interdistance was 0.0270 cm., and the grids were spaced 0.550 cm. apart. The

---

[1] This work has been carried out under the auspices of the Scientific Department, Israeli Ministry of Defence.

[2] This note forms part of a thesis submitted to the Hebrew University, Jerusalem, in partial fulfillment of the requirements for the degree of Ph.D.

number of grids was chosen so as to obtain filtration with a reasonable experimental accuracy. This was determined by applying the equations of Davies (2) to the calculation of the efficiency of a single grid and allowing for the limitation imposed on the length of the filter by the sedimentation of the particles and their diffusion to the walls of the pipe.

The performance of this filter was investigated by passing through it an homogeneous aerosol at different laminar velocities of flow (Reynolds numbers, based on the diameter of the wire, ranging from 0.3 to 0.6). To attain such flows it was necessary to place a suitable calming pipe before the grid array (6).

The aerosol, consisting of liquid spherical particles of dioctyl phthalate, was formed by the LaMer-Sinclair generator (7) and had the usual degree of homogeneity. The radii of its particles were 0.5 to 0.9 micron and their concentration[3] varied independently between 10^4 and 10^5 particles/cm^3. Under these conditions coagulation, sedimentation and evaporation could be ignored. It was observed to contain a small but significant fraction of electrically charged particles (approximately 3 % or 12 %, depending on the bubbler used within the generator). These were removed almost completely by means of a small electrostatic precipitator.

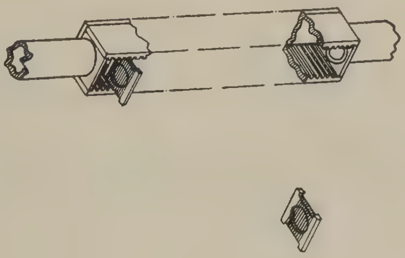

FIG. 1. The grid array. Diameter of pipe—5.00 cm., diameter of wire—0.0050 cm.; inter-wire distance—0.0270 cm.; spacing between grids—0.550 cm.; number of grids—76.

As the experimental work demanded a strict control of the properties of the aerosol, special attention was paid to the operation of the generator itself. Within experimental limits, the radius of the particles [measured in a convection-free ultramicroscope cell with a standard error of the mean of 0.007 μ and by the "owl" (8)] was found to increase linearly with the temperature of the boiler (Fig. 2) and to decrease slightly with the temperature of the reheater (Fig. 3). Likewise, as the temperature of the ionizer—a small quartz tube containing fused sodium chloride and heated by a small electric oven—was lowered, the particle size increased almost exponentially

---

[3] Measured in a transmissiometer (optical path—50,5 cm.; wavelength of light—546 mμ) built by Mr. S. Weinstock.

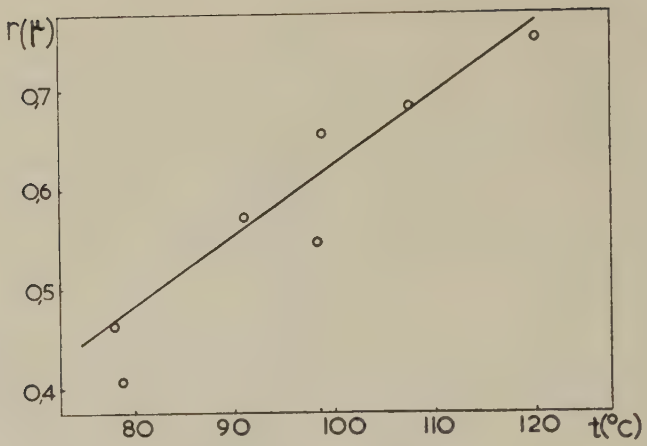

Fig. 2. Radius of aerosol vs. temperature of boiler.

Temperature of ionizer—333°C.; temperature of reheater—130°C. (room temperature—26.5°C.).

Rate of flow through boiler—0.95 l./min., rate of flow through ionizer—0.39 l./min. (For dimensions of boiler, reheater and condensing chimney, see *Chem. Revs.* **44,** 262 (1949), Fig. 11; ionizer—a small quartz tube containing fused NaCl and heated by a small electric oven).

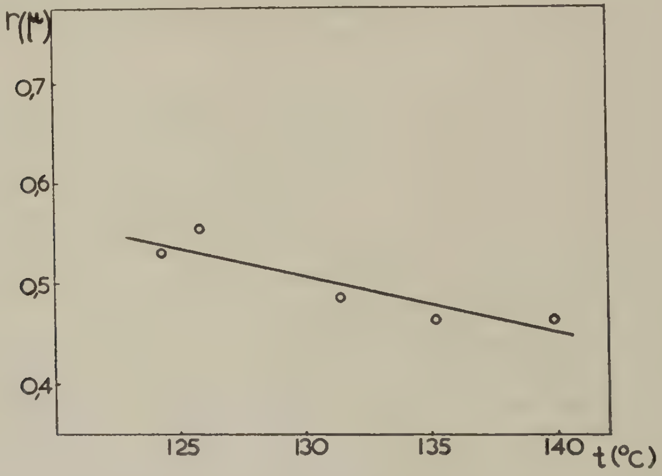

Fig. 3. Radius of aerosol vs. temperature of reheater.

Temperature of boiler—111.8°C.; temperature of ionizer—343°C.; room temperature—23.5°C.

Rate of flow through boiler—0.96 l./min.; rate of flow through ionizer—0.39 l./min. (For dimensions of boiler, reheater, and condensing chimney, see *Chem. Revs.* **44,** 262 (1949), Fig. 11; ionizer—a small quartz tube containing fused NaCl and heated by a small electric oven).

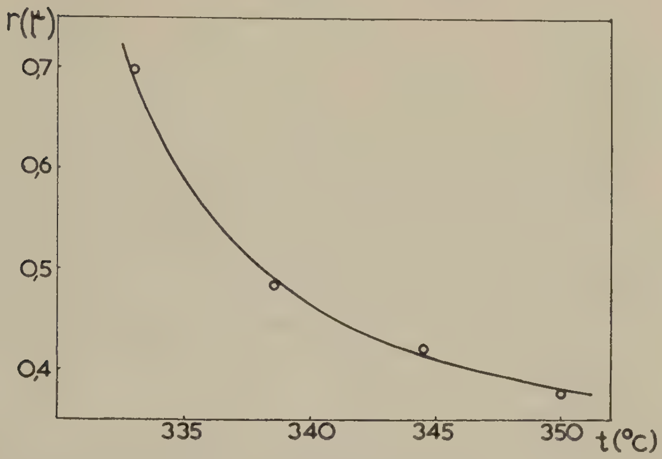

FIG. 4. Radius of aerosol vs. temperature of ionizer.

Temperature of boiler—97.4°C.; temperature of reheater—132°C. (room temperature—26°C.).

Rate of flow through boiler—0.96 l./min.; rate of flow through ionizer—0.39 l./min.

(For dimensions of boiler, reheater, and condensing chimney, see *Chem. Revs.* **44,** 262 (1949), Fig. 11; ionizer—a small quartz tube containing fused NaCl and heated by a small electric oven).

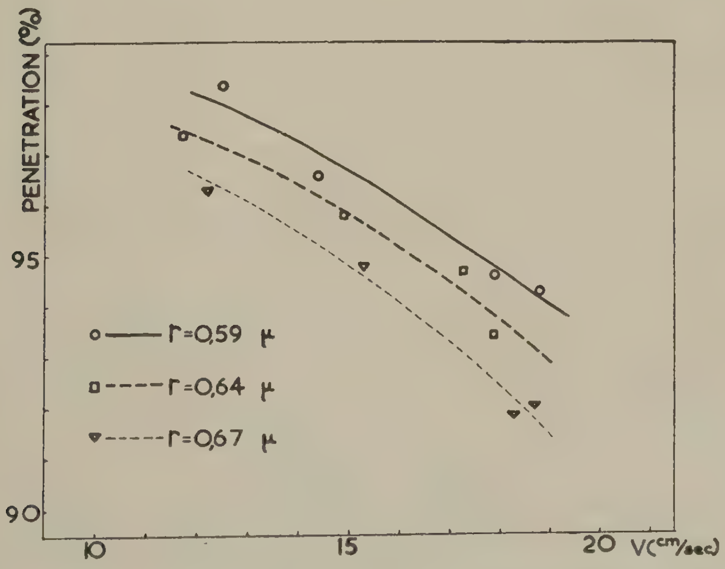

FIG. 5. Penetration vs. average linear velocities. Diameter of wire—0.0050 cm.; inter-wire distance—0.0270 cm.; spacing between grids—0.550 cm.

up to a certain limit (Fig. 4). Beyond this limit, the generator produced smaller and more heterogeneous aerosols which might have been formed by self-nucleation.

Aerosol of a constant radius was passed through the filter at variable velocities of flow, the latter being controlled by a sideline introduced before the calming pipe. The filter efficiency, measured by the ratio between the effluent and influent concentration of the particles, was determined by a light-scattering method. This determination was carried out by a modified Zimm apparatus (9)[4] fitted as a "right angle penetrometer." Some extra stops were added to the optical parts of the instrument to measure the filtration near the geometric axis of the pipe, where homogeneity of flow could be assumed.

Within limits determined mainly by the filter's low efficiency, the penetration (defined as the fraction of aerosol passing through the filter) decreased steadily with increasing particle radius and with increasing velocity of flow (Fig. 5). According to the present theories of filtration (1, 4) it appears that such a dependence between penetration and velocity of flow is due mainly to the inertial mechanism. The values of the parameter $\psi(\sqrt{\psi} = 0.14\text{–}0.20)$, which owing to the present "idealized" experimental conditions could be calculated exactly, were found to be smaller than the critical value given by Langmuir and others (10).

Detailed experimental results containing data of filtration by grids of different inter-wire distance and a comparison with theories will be published later.

The author expresses his thanks to Mr. G. Volinez for his helpful suggestions and criticism during this work.

REFERENCES

1. LANGMUIR, I., O.S.R.D. Report No. 865 (1942).
2. DAVIES, C. N., *Inst. Mech. Engrs. Proc.* (*London*) (b) **1B,** 185 (1952).
3. LAMER, V. K., GENDRON, P., AND GRUEN, R. S., A.E.C. Progress Report NYO-511.
4. RAMSKILL, E. A., AND ANDERSON, W. L., *J. Colloid Sci.* **6,** 416 (1951).
5. KOVASZNAY, L. I. G., *Proc. Cambridge Phil. Soc.* **44,** 58 (1948).
6. GOLDSTEIN, S., "Modern Developments in Fluid Dynamics," pp. 299. Oxford University Press, 1950.
7. SINCLAIR, D., AND LAMER, V. K., *Chem. Revs.* **44,** 245 (1949).
8. "Handbook on Aerosols," p. 106. A.E.C., Washington, D. C., 1950.
9. ZIMM, B., *J. Chem. Phys.* **16,** 1093 (1948).
10. RANZ, W. E., Technical Report No. 3, SO-1004 (1951).

---

[4] Built by the electrical engineers of these laboratories.

VERIFICATION OF THE FREE ENERGY EQUATION FOR ELECTRICALLY POLARIZED DROPLETS[1]

C. T. O'Konski[2] and R. L. Gunther

Department of Chemistry and Chemical Engineering, University of California, Berkeley, California

Received May 16; revised July 29, 1955

Abstract

By measurements from microphotographs of small hanging drops, it was found that liquid droplets polarized in a homogeneous electric field become prolate spheroids if elongations are small or moderate. Experimental values for the eccentricities were compared with values predicted by a previous theoretical treatment, which was verified within a few per cent. The conclusions are discussed with reference to earlier work, and a brief review of the related literature is presented.

Introduction

Interest arose in the problem of the deformation of liquid droplets by an external homogeneous field when considering the possible use of the Kerr electrooptic effect for studies of molecular association and nucleation phenomena in gases. The nucleation embryos postulated in the quasi-equilibrium theory (1) may be treated approximately as small droplets.

Recently an equation was obtained by O'Konski and Thacher (2) for the static deformation of droplets to spheroids, by minimizing the free energy of the spheroid in the external field, where the shape-dependent part of the energy was taken as the sum of an electrical and a surface term. Eccentricities were computed for various cases of interest. From these it may be concluded that the deformations are too small to serve as a practical basis for electrooptic studies of the small (ca. 10^{-7} cm. radius) nucleation embryos. However, the deformation may be of interest in devising new techniques (2) for the study of dynamic surface tension, droplet diameters, size distributions in liquid sprays, or for radar meteorology.

In the previous work, the treatment was not verified experimentally. Certain questions might be raised regarding (*a*) the limits imposed by the assumption of a spheroidal shape, (*b*) the constancy of the surface tension

---

[1] This research was supported by the Office of Naval Research.

[2] John Simon Guggenheim Memorial Foundation Fellow, University of Leiden, Holland, February to August, 1955.

in the external field, and (*c*) the possible effect of surface charges. Since irregular shapes are difficult to treat analytically, question (*a*) seems of a nature best to explore experimentally. From a consideration of the magnitude of molecular orientation energies and interaction energies, it would appear that the assumption of a constant surface tension (*b*) would be adequate for most experimental studies. Regarding (*c*), it appears evident that since the equation obtained by Stratton (3) and employed in the previous work (2) gives the total electrostatic energy of the system, the mutual and external effects of surface charges are implicitly included when the dielectric constants are properly chosen (e.g., infinity for a conducting droplet in an insulating medium with static field). Nevertheless, it might be well to subject (*b*) and (*c*) to experimental test under conditions such that the shape is essentially spheroidal.

There were a number of early studies where deformations of liquid surfaces by intense electric fields were observed.[3] Zeleny (4) studied electrical discharges between liquid "points" and metal planes. He observed that under certain conditions the liquid surface became cone-shaped, and a fine liquid thread which broke into a spray of very fine droplets issued from the point. Droplet deformation by a homogeneous electric field was considered as a possible source of error by Millikan in his oil drop experiments (5), but it was shown to be negligible in that work. In fact no indication was given that such an effect (in a homogeneous field) was definitely known to exist at that time. Wilson and Taylor (6) studied the deformation of hemispherical soap bubbles placed on one of two plane parallel electrodes, recognizing the difficulties of studying liquid drops. In increasing fields, the bubbles first became distorted into hemi-spheroids, then took on less simple forms, becoming cones with a spray from the point, like the drops observed by Zeleny. They presented a general equation for for the equilibrium condition for each surface element of a charged bubble, and concluded that "for bubbles of given shape but different sizes, the surface density of charge at corresponding points is proportional to the field but independent of the linear dimensions. The field therefore which produces a given shape should be proportional to $(\gamma/\text{linear dimensions})^{\frac{1}{2}}$, and in particular the field which causes the bubble . . . to become just unstable should be inversely proportional to the square root of the radius of the undistorted bubble." They found experimentally that the product of the bursting field intensity and the square root of radius, for bubbles of various radii, was a constant, and calculated that the largest stable water drop, at the breakdown field in air, 30,000 v./cm., would be 0.02 cm. radius. Nolan (7) in observing the breaking of falling water drops by horizontal electrical fields, confirmed the field-radius relationship. Macky

---

[3] The authors are happy to acknowledge that the earlier studies were called to our attention by V. G. Drozin. See ref. 10.

(8) repeated some of the experiments on breaking soap bubbles and falling water drops with vertical fields, observing glow and spark discharges at the higher fields, and also confirmed the field-radius relation.

Elongations along the electric field were observed, but a quantitative comparison of this work with the previous calculations (2) could not be made for two reasons. In the first place, eccentricities were not reported, and second, the falling drops were partially distorted by vibrations and hydrodynamic forces.

Recently, interest in the discharge and spray phenomena was revived by Vonnegut and Neubauer (9) and by Drozin (10) in connection with attempts to produce uniform droplets by electrical techniques. In this connection it should be noted that Zeleny (4) (1917) observed that "the brush spray appears colored both by transmitted light and by reflected light . . ." and thus reported the first indications of higher order Tyndall spectra. Furthermore he observed that there were two groups of droplets, each with some spread of sizes, and inferred that the smaller ones originated from the "satellites." The satellites are small droplets produced between the main drops and should be well known from the classic works of Rayleigh on the break-up of liquid jets. It would appear that they must be separated from the main droplets if a relatively homogeneous aerosol is to be obtained.

In this research a method was devised for making direct measurements of the electrical deformation on droplets large enough to give a readily observable effect; eccentricities were measured under conditions where the theoretical treatment was applicable, and results are compared with the predictions of the theory. It was found that the complicated theoretical equation, [7], of reference (2), can be approximated very closely by a simple relation for a considerable range of eccentricities. The same relation is shown to be in accord with the earlier experimental observations regarding the fields required to rupture droplets and bubbles.

EXPERIMENTAL METHODS

Because the experimentally realizable eccentricities for aerosol droplets are very small (2), we chose to do experiments on small hanging drops.

Water droplets were suspended from special tips on vertically aligned fine glass rods. They were illuminated from the side, and photographed from the bottom. By means of this technique, a circular outline of the droplet was obtained in the absence of electric field, in spite of small elongations produced by the gravitational field. The gravitational distortion was visible in a side view of larger droplets as a slight (ca. 1%) vertical asymmetry. In strong electric field relatively large *horizontal* elongations were obtained.

The electric fields were produced between parallel metal plates, 5 × 10 cm. wide, and separated 0.81 cm. Applied potentials up to 10,000 v. d.c., from a conventional power supply, were measured with a calibrated vacuum tube voltmeter and high-voltage probe.

The droplets were illuminated by means of a ribbon filament tungsten source and a two-piece double convex achromatic lens system, essentially identical to the auxiliary condensing lens system of a previously described instrument (11), and so disposed that the droplet and source were at conjugate foci.

Photographs were taken on Super Panchro Press type B sheet film with a Leitz Makam Microscope Camera, mounted in one section of a binocular microscope. The camera was calibrated by photographing the scale of an optical micrometer. A prismatic beam-splitter and eye-piece facilitated visual observations of the droplets. To reduce heating of the droplets, the light source was turned on just before each photographic exposure. Care was exercised to minimize vibrations. As a possible procedure, flash photography was considered but was rejected because of the possibility of misleading results due to vibrational deformations of the droplets.

Best results were obtained with a thin (ca. 0.02 mm.) suspending rod, which flared at the tip to about 0.05 mm. diameter. This arrangement minimized the tendency of the drop to climb up the rod. Water was applied in small increments by means of a very fine hypodermic-type applicator fabricated from glass.

Charges on the droplets caused difficulties because of the resulting force on the droplet along the applied field. Attempts to discharge the droplets by means of an electrical ground lead were unsuccessful, but difficulties were considerably reduced by covering all but the tip of the supporting rod with ceresin wax.

Experimental Results

Photographs were taken of electrically polarized droplets in a number of separate experiments. Five more experiments were performed on suspended droplets in zero electric field, to aid in evaluating the precision of the measurements, and to determine whether distortions might occur from extraneous causes. The droplet contained a dilute suspension of $BaSO_4$, freshly precipitated from equivalent quantities of Na_2SO_4 and $BaCl_2$ solutions, to improve sharpness of outline in the photographs.

In each case with an applied field, the droplets became elongated along the direction of the field, as predicted by the theory (2). Maximum and minimum dimensions of the droplets, 2a and 2b, were determined from measurements on the film and the optical calibration mentioned above. Magnifications were in the range 22× to 32×.

Table I summarizes the experimental results in order of decreasing eccentricities. Only results obtained at eccentricities in excess of 0.4 are

TABLE I

Summary of Experimental Results

r (*mm.*)	Eccentricities	
	Measured	*Calculated*
0.943	0.633	0.634
0.928	0.626	0.628
0.902	0.622	0.616
0.905	0.618	0.618
0.911	0.595	0.620
0.813	0.595	0.578
0.834	0.580	0.587
0.598	0.490	0.484
0.463	0.459	0.425

Applied field was 11.4 kv./cm. First five experiments with 0.025 M, last four with 0.01 M, $BaSO_4$ suspension.

given, as lower eccentricities were difficult to measure accurately. Column one contains values of r computed from the relation $r = a^{1/3}\, b^{2/3}$. Thus r is the radius of the water droplet, which, when distorted into an ellipsoid of revolution, has a semimajor axis a and a semiminor axis b. Column two contains eccentricities, e, obtained from the experimentally determined values of a and b by the usual relation for an ellipsoid of revolution. Column three contains theoretical values of e. Since the droplets were very good conductors and the medium was an insulator, ϵ_2 was set equal to infinity in equation [7′] of reference 2. Then, for water droplets in saturated vapor at 25°C.,

$$rE^2 = 2\,\frac{\gamma B^2 C}{\epsilon_1} = 1795\, B^2 C. \qquad [1]$$

The notation is that employed previously (2). Values of rE^2 were computed for $e = 0.45$, 0.55, 0.60, and 0.65, to extend Table I of the cited reference. (A misprint was found in Eq. [16] of reference (2), in which the denominator should be the same as the numerator of the expression below the line in [7].) These, together with corresponding values of B and C are given in Table II. It was found that the theoretical values of e are remarkably linear in rE^2 in the region $0.45 \leq e \leq 0.70$, and can be obtained from the relation

$$e = 0.003\, rE^2 + 0.223, \qquad [2]$$

TABLE II

Computed Eccentricities of Polarized Water Droplets, 25°C.

e	rE^3 (*cgs*)	B	C
0.45	75.6	0.3037	0.457
0.55	108.3	0.2866	0.734
0.60	125.4	0.2760	0.917
0.65	142.1	0.2635	1.140

with an average deviation under 0.2% for the six available points. This greatly facilitated getting the values of ε for column three of Table I.

The shape of the vertical projection of one of the most elongated drops ($\varepsilon > 0.6$) was compared to that of an accurately constructed ellipse of the same axes by superposing the film negative upon the figure. The two coincided at all points within the experimental accuracy, which was about 1% of r.

DISCUSSION

Because the shape of the vertical projection was elliptical, it appears that polarized droplets will closely approximate prolate spheroids in the absence of forces other than surface tension and electric polarization by a homogeneous field. Thus, the treatment given earlier can not be significantly in error because of the shape assumption if $\varepsilon \lesssim 0.6$.

The electric field situation around the drop was altered somewhat by the gravitational elongation at the suspending tip, and the presence of the suspending rod. Because the insulated suspending rod was of very small diameter, and was oriented normal to the field, its effect on the electric field was considered negligible. The slight deformation of the upper part of the suspended droplet was first of all relatively remote from the elements of surface giving rise to the vertically projected outline, so the field effects produced were second-order. Secondly, the volume of liquid of the distorted section, in excess of that of a perfect sphere (or spheroid) having the same outline, was a very small fraction of the total. Thus no corrections were considered necessary within the experimental precision realized.

The probable error in measuring b/a from a given photograph was around 1%, as determined from a number of measurements by separate observers. The product εE^2 was experimentally determined within 3%. Other possible sources of error were the effect of vibrations, evaporation of the droplet, and surface tension variations. The surface tensions of the suspensions were compared with pure water by means of the capillary rise method, and were found to be the same within a few per cent. As all measurements were made on the same photograph, evaporation did not introduce errors. The major difficulties were believed to arise from vibrations, and were of a magnitude which could account for the deviations between experiment and theory. Thus, for applications of the sort suggested previously (2) the theory may be considered adequate.

The accuracy was not enough to permit an experimental choice between the values infinity and 80 for the effective dielectric constant of water in the computation of the distortion of water droplets in air. It appears that at least an order of magnitude greater accuracy would be required for experimental support of our choice. If such accuracy could be achieved, corrections would probably become necessary for the electric field disturbances mentioned above, and considered unimportant compared to the experimental errors in this study.

It should be noted that the essentially linear dependence of rE^2 upon e discussed above is a property of the function B^2C since γ and ϵ_1 are constants in Eq. [1]. Hence, Eq. [2] can be transformed into

$$B^2C = 0.1856\,e - 0.0414; 0.45 \leq e \leq 0.70 \qquad [3]$$

which may be employed in Eq. [1] for any conducting liquid sphere with interfacial tension γ in an insulating medium characterized by ϵ_1.

From Eq. [1] we may deduce the relation between the radius and the homogeneous field intensity required to rupture a conducting droplet or bubble which was experimentally observed by several workers (4, 6, 7, 8) and deduced from dimensional arguments (6). We make use of the observation that instability commences (12) in mechanically deformed cylindrical soap bubbles when the length of the bubble becomes larger than its circumference, independent of its size. Then instability will be expected to occur when B^2C of Eq. [1], the function characterizing the elongation (or the corresponding function for any shapes other than perfectly spheroidal) becomes equal to a certain value. Then

$$\frac{rE_c^2}{\gamma} = K, \qquad [4]$$

where E_c is the critical field intensity for rupture, and K is a constant. This is in accord with the experimental observations.

With all but the best insulators, the relaxation times for redistribution of charges (3) in an applied external field will be short compared to the usual time of exposure to the field in which the observation is made. Therefore Eq. [1] should nearly always be applicable for moderate eccentricities and Eq. [4] for rupture, for liquid droplets in an unionized gas.

It appears evident that the complex dynamic phenomena involved in the production of sprays (4–10) cannot be explained by any static theoretical treatments. In particular the effect of conductivity of the dispersed liquid on the spray mechanism has not been explained by the authors concerned with this phenomenon. This is probably connected with the redistribution of charges which must occur as each droplet is broken from the liquid.

REFERENCES

1. See, for example, VOLMER, "Kinetic der Phasenbildung." Edward Bros., Ann Arbor, Michigan, 1945.
2. O'KONSKI, C. T., AND THACHER, H. C., *J. Phys. Chem.* **57**, 955 (1953).
3. STRATTON, J. A., "Electromagnetic Theory." McGraw-Hill, New York, 1941.
4. ZELENY, J., *Proc. Cambridge Phil. Soc.* **18**, 71 (1914); *Phys. Rev.* **3**, 69 (1914); *ibid.* **10**, 1 (1917); *ibid.* **16**, 102 (1920).

5. Millikan, R. A., *Phys. Rev.* **2**, 109 (1913).
6. Wilson, C. T. R., and Taylor, G. I., *Proc. Cambridge Phil. Soc.* **22**, 728 (1925).
7. Nolan, J. J., *Proc. Roy. Irish Acad.* **37**, 28 (1926).
8. Macky, W. A., *Proc. Cambridge Phil. Soc.* **26**, 421 (1930); *Proc. Roy. Soc. (London)* **133**, 565 (1931).
9. Vonnegut, B., and Neubauer, R. L., *J. Colloid Science* **7**, 616 (1952).
10. Drozin, V. G., *J. Colloid Science* **10**, 158 (1955).
11. Gucker, F. T., Jr., and O'Konski, C. T., *J. Colloid Science* **4**, 541 (1949).
12. Lawrence, A. S. C., "Soap Films," p. 29. G. Bell and Sons, London, 1929.

THE RATE OF EVAPORATION OF MICRO-DROPS IN THE PRESENCE OF INSOLUBLE MONOLAYERS

R. S. Bradley

Department of Inorganic and Structural Chemistry, The University of Leeds, England

Received July 11, 1955

ABSTRACT

Based on the writer's experimental work an analysis is given of the effect of monolayers on the rate of evaporation of small drops in air. In contrast to the effect on large plane surfaces of water evaporating in air, monolayers may reduce the rate of evaporation of water drops by factors of the order 10^4.

The persistence of small drops in the atmosphere is remarkable, notably in phenomena such as haze and smog. It is the purpose of this paper to show that the rate of evaporation of such drops is enormously reduced by "insoluble" monolayers, whereas such layers may reduce the rate of evaporation of a plane surface of water by much smaller factors.

Early work on the rate of evaporation of drops of diameter circa 1 mm. in an absorbent enclosure of diameter a few centimeters, in the presence of air at atmospheric pressure, showed that the process was controlled by diffusion (1), since, in the steady state

$$-\frac{dM}{dt} = 4\pi r^2 D m_2\, dC/dr, \qquad [1]$$

where M is the drop mass evaporating in time t, r is a radius of a geometrical surface taken with the drop as center, D is the diffusion coefficient, m_2 the molecular mass of the vapor molecules, and C the number of molecules of vapor per cubic centimeter. On integrating with respect to r we obtain

$$-\frac{dM}{dt} = 4\pi a D m_2 C_0, \qquad [2]$$

where the enclosure is taken with a radius large compared with that of the drop, and where C_0 is the concentration of vapor molecule per cubic centimeter in the saturated vapor and a is the drop radius. The absorbent is supposed for simplicity to exert no back pressure.

Equation [2] breaks down when the air pressure p is sufficiently reduced, since it predicts an infinite rate when $p \to 0$. Likewise the rate of evaporation per unit area is DmC_0/a, which tends wrongly to infinity when $a \rightarrow 0$ at constant p.

The writer and co-workers have shown (2) that these difficulties can be overcome by supposing that droplet evaporation proceeds by a two-stage process. As a crude but sufficiently accurate approximation the drop is imagined to be surrounded by a virtually vacuous space, of thickness of the order of the mean free path of the diffusing molecules. Across this space of thickness Δ vapor passes by Knudsen flow or molecular distillation. A shell of vapor is built up round the drop, of concentration C_1, which is less than C_0, and this value C_1 is set by the balancing of supply of vapor from the drop and loss by diffusion. Similar arguments were used by Langmuir (3) to describe the loss of heat from a wire, which was imagined to be surrounded by a cylindrical vacuous space. Using Chapman and Cowling's formula for diffusion (4) the value of Δ is given by

$$\Delta = \frac{8D}{3\pi\nu}\left(\frac{m_1}{m_2}\right)^{1/2},$$

where $\nu = (kT/2\pi m_2)^{1/2}$, and m_1 and m_2 are the masses of the molecules of air (the mean) and of the diffusing vapor, respectively.

This gives

$$4\pi a^2\nu\alpha(C_0 - C_1) = 4\pi(a + \Delta)DC_1, \tag{3}$$

where α is the so-called evaporation or condensation coefficient.

Hence

$$C_1 \doteq \frac{C_0 a^2 \nu\alpha}{(a + \Delta)D + a^2\nu\alpha},$$

and

$$-\frac{dM}{dt} = \frac{4\pi a D C_0 m_2}{D/(a\nu\alpha) + a/(a + \Delta)}. \tag{4}$$

Unlike Eq. [2] Eq. [4] gives the correct extrapolation to the limits $p \rightarrow 0$ for $-dM/dt$, and $a \rightarrow 0$ for $(-dM/dt)/(4\pi a^2)$. Equation [4] has been abundantly tested experimentally in drops of diameter of the order 1 mm. in air and other gases at a range of pressures (2).

The study of micro-drops is more difficult, and the rate of evaporation can be found only by observing the rate of fall as was done by Whytlaw-Gray and Patterson (5) and by Monchick and Reiss (6). The latter authors have verified that an equation similar to [4] applied to the rate of evaporation of drops of diameter of order 10^{-4} cm. in air. These authors use the formulation of Chapman and Cowling (4) and give a result which is equivalent to

$$-\frac{dM}{dt} = \frac{4\pi a D C_0 m_2}{D(1 - \alpha/2)/(a\nu\alpha) + 1}. \tag{5}$$

It may be of interest at this point to comment on apparent differences between formulas [4] and [5]. Equation [5] is not intended (unlike [4]) to cover the whole range of pressure down to $p \rightarrow 0$, and it gives as it stands an incorrect limit, owing to the deliberate omission of higher terms of a series. Monchick and Reiss compare their result with the writer's by putting $\Delta = 0$ in Eq. [4]. Since Eq. [4] may be rewritten

$$-\frac{dM}{dt} = \frac{4\pi a^2 \nu \alpha C_0 m_2}{1 + a^2 \nu \alpha / [(a + \Delta) D]}. \qquad [6]$$

This gives

$$-\frac{dM}{dt} = \frac{4\pi a^2 \nu \alpha C_0 m_2}{1 + a \nu \alpha (1 - \Delta / a \cdots) / D} \quad \text{if} \quad a > \Delta. \qquad [7]$$

Now

$$\Delta = \frac{8D}{3\pi\nu} \left(\frac{m_1}{m_2} \right)^{1/2} = \beta \frac{D}{\nu}, \text{ say.}$$

Hence

$$-\frac{dM}{dt} = \frac{4\pi a^2 \nu \alpha C_0 m_2}{1 + (a \nu \alpha / D) - \alpha \beta \cdots} \qquad [8]$$

which agrees with [5] if $\beta = \frac{1}{2}$. According to the writer's views the value of β depends on the masses of diffusing molecules, but it is clear that for large vapor molecules there is less difference between Eqs. [4] and [5] than might be supposed. It should be emphasized that the work of Monchick and Reiss covers a smaller range than that of the writer, and over this range the two formulations are more alike than might be supposed.

It is reasonable therefore to suppose that Eq. [4], or possibly some variant which differs only slightly, applies to droplets of diameter 10^{-4} cm. evaporating in air at atmospheric pressure; for much smaller droplets Eq. [4] is probably nearly correct. It may be noticed that, per unit area,

$$\left(-\frac{dM}{dt} \right) \frac{1}{4\pi a^2} = \frac{D C_0 m_2}{D/(\nu \alpha) + a^2/(a + \Delta)} \qquad [9]$$

and when

$$a \rightarrow 0, \qquad \left(-\frac{dM}{dt} \right) \frac{1}{4\pi a^2} \rightarrow \nu \alpha C_0 m_2,$$

the vacuum rate, even although the pressure is atmospheric.

It is now possible to understand the effect of insoluble monolayers on the rate of evaporation of droplets, since the rate for small enough drops is mainly controlled by the evaporation coefficient rather than by the diffusion coefficient. For a drop of water of radius 10^{-4} cm. evaporating in an absorbent enclosure of the type discussed above, taking $D = 0.249$ cm.^{2} sec.$^{-1}$ at 1 atmosphere, $\alpha = 0.034$ (7), $-dM/dt$ according to Eq. [4] is 9.29×10^{-10} g. sec.$^{-1}$. Now suppose α is reduced to 10^{-6} by the presence of a virtually insoluble monolayer. According to Eq. [4] $-dM/dt$ becomes 3.19×10^{-14} g. sec.$^{-1}$. The lifetime of a drop, if Δ is neglected, is given by

$$t = \frac{a\rho}{\alpha\nu C_0 m_2} + \frac{a^2\rho}{2Dm_2C_0}, \qquad [10]$$

where ρ is the density, as may readily be proved by integration; it is the sum of the lifetimes for a drop evaporating in a vacuum and by simple diffusion according to Eq. [2]. If $\alpha = 10^{-6}$ the lifetime of a drop of water evaporating in an enclosure of the type discussed is approximately 400 sec. In practice this could be increased by the presence of neighboring drops, by the fact that the drop evaporates in air which is not completely dry, and by the presence of soluble impurities, which will concentrate as the drop evaporates.

This large reduction in rate may be contrasted with the much smaller effect of a film on a plane water surface. The application of the theory above to plane surfaces was discussed by the writer (8) and gives results similar to those deduced by Langmuir and Schaefer (9) and by Archer and LaMer (10). These latter authors have shown that much of the previous work on surface planes is erroneous, but support the result that very large reductions in α may occur owing to such films.

The writer's treatment for drops may be applied to plane surfaces as follows. Suppose we have a plane surface of water with an absorbent a distance Δ above the surface and suppose for simplicity that there is no back pressure from the absorbent; this simplification is not critical and is for convenience of formulation only. As before there will be a concentration of vapor molecules C_1, at a distance Δ above the liquid surface, given by

$$\nu\alpha(C_0 - C_1) = \frac{DC_1}{b - \Delta}. \qquad [11]$$

The rate of evaporation per centimeter is therefore

$$-\frac{dM}{dt} = \frac{DC_1 m_2}{b - \Delta} \qquad [12]$$

$$= \frac{DC_0 m_2}{D/(\nu\alpha) + (b - \Delta)}. \qquad [13]$$

In the presence of a film we may use accented symbols and write

$$\left(-\frac{dM}{dt}\right)' = \frac{DC_0 m_2}{D/(\nu\alpha') + (b - \Delta)}. \qquad [14]$$

Hence

$$\frac{m_2 C_0}{(-dM/dt)'} - \frac{m_2 C_0}{(-dM/dt)} = \frac{1}{\nu}\left(\frac{1}{\alpha'} - \frac{1}{\alpha}\right), \tag{15}$$

which is Langmuir and Schaefer's result if $1/\alpha$ is neglected in comparison with $1/\alpha'$.

As an example, if $b = 10$ cm., Δ is negligible in atmospheric air and if $\alpha = 0.034$, $-dM/dt = 4.30 \times 10^{-7}$ g. sec.$^{-1}$ cm.$^{-2}$. In the presence of a film with $\alpha = 10^{-6}(-dM/dt)' = 1.59 \times 10^{-7}$ g. sec.$^{-1}$ cm.$^{-2}$, a much smaller reduction than with the drop.

REFERENCES

1. MORSE, H. W., *Proc. Am. Arts & Science* **45,** No. 14 (1910); LANGMUIR, I., *Phys. Rev.* **12,** 368 (1918).
2. BRADLEY, R. S., EVANS, M. G., AND WHYTLAW-GRAY, R. W., *Proc. Roy. Soc. (London)* **A186,** 368 (1946); BIRKS, J., AND BRADLEY, R. S., *ibid.* **A198,** 226, (1949); BRADLEY, R. S., AND SHELLARD, A. D., *ibid.* **A198,** 239 (1949); BRADLEY, R. S., AND WAGHORN, G. C. S., *ibid.* **A206,** 65 (1951).
3. LANGMUIR, I., *J. Am. Chem. Soc.* **37,** 417 (1915); cf. p. 426.
4. CHAPMAN, S., AND COWLING, T. G., "The Mathematical Theory of Non-uniform Gases." Cambridge University Press, Cambridge, 1939.
5. WHYTLAW-GRAY, R. W., AND PATTERSON, H. S., "Smoke," Arnold, London, 1932.
6. MONCHICK, L., AND REISS, H., *J. Chem. Phys.* **22,** 831 (1954).
7. ALTY, T., *Proc. Roy. Soc. (London)* **A131,** 554 (1931); BARANAEV, M., *J. Phys. Chem. (U.S.S.R.)* **11,** 484 (1938).
8. *cf.* BIRKS, J., AND BRADLEY, R. S., *Proc. Roy. Soc. (London)* **A198,** 237 (1949).
9. LANGMUIR, I., AND SCHAEFER, V. J., *J. Franklin Inst.* **235,** 119, (1943).
10. ARCHER, R. T., AND LA MER, V. K., *J. Phys. Chem.* **59,** 200 (1955).

THE KINETICS OF ELECTROLYTE PRECIPITATION

Arne E. Nielsen

Københavns universitets fysisk-kemiske institut, Copenhagen, Denmark

Received July 18, 1955

Abstract

The law that the incubation period of precipitation, for a certain electrolyte, is proportional to some (negative) power of the ionic product (1–4) is found to be valid for AgCl, Ag_2CrO_4, CaC_2O_4, CaF_2, and $KClO_4$, but not for $BaSO_4$.

The equation of Johnson and O'Rourke (8) for the rate of precipitation

$$\frac{d\alpha}{dt} = K\alpha^q(1 - \alpha)^p,$$

where α = the degree of reaction, t = time, and K, q, and p are constants which can be determined experimentally ($q = \frac{2}{3}$; $p = 3$ or 4), is integrated and found to be valid for precipitation of $BaSO_4$, $SrSO_4$, Ag_2CrO_4, and CaC_2O_4, whereas it is only partly valid for CaF_2.

The agreement seems to indicate that the precipitation rate is controlled by a chemical reaction in the surface of the growing crystals rather than by diffusion.

The Incubation Period

The incubation period t may be defined as the period of time between the preparation of the supersaturated solution and the occurrence of visible turbidity or the first measurable decrease in concentration of the solute. These two definitions are often equivalent within a factor of 2 or less (1, 2).

With only one known clear exception ($BaSO_4$), t and the concentration of the supersaturated solution c are related by

$$t = \text{const.} \times c^{-n} \qquad [1a]$$

or

$$\log t = -n \log c + \text{a constant.} \qquad [1b]$$

If the reactants are not present in equivalent concentrations c must be replaced by the ionic product or the (geometric) mean ionic concentration $\bar{c}$ (1–4). With CaF_2, for example, $\bar{c}$ is equal to $([Ca^{++}][F^-]^2)^{1/3}$.

Figure 1 shows that the incubation time t for calcium oxalate does not depend on the ratio of the ionic concentration for a constant value of $\bar{c} = ([Ca^{++}][C_2O_4^{--}])^{1/2}$. Even better constancy was found by van Hook (2) with Ag_2CrO_4.

In Fig. 2 $\log t$ has been plotted against $\log \bar{c}$ for different substances all of which show a straight-line relationship.

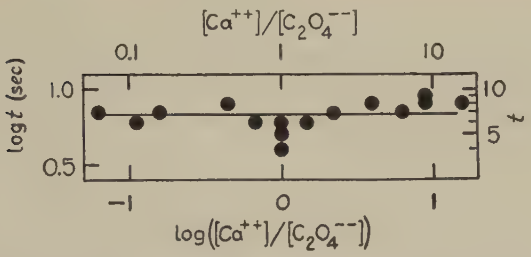

FIG. 1. t is the period of time elapsed between the mixing of two equally large volumes (50 or 70 ml.) of solutions of calcium acetate and ammonium oxalate, and the occurrence of visible turbidity. Both solutions contained 0.5 mole NaCl per liter. Just after mixing $[Ca^{++}][C_2O_4^{--}] = 2.5 \times 10^{-5}$, i.e., $\bar{c} = 5.0 \times 10^{-3}$ for all points. Temperature 22°C.

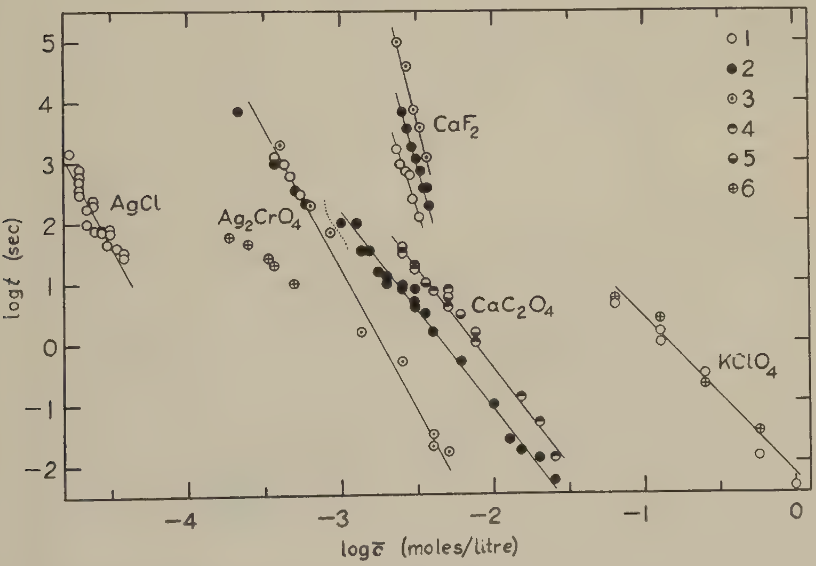

FIG. 2. Log (incubation period) against log (geometric mean concentration).

Silver chloride: Kobayashi (3).

Silver chromate: 1. See Table 2 in Van Hook (2); *2.* see Fig. 1 in Van Hook (2); *3.* see Fig. 2 in Christiansen and Nielsen (4); *6.* see Table p. 344, Fischer (5).

Calcium fluoride: $Ca(OH)_2 + 2HF$; all data by Tovborg Jensen (1); *1.* Table 6, (ionic strength 0.1 with NaCl; 18°C.); *2.* Table 2, (no salt added, 18°C.); *3.* Table 7, (no salt added, 23°C.)

Calcium oxalate: Nielsen, unpublished data; *2.* calcium acetate + ammonium oxalate, 23°C., no salt added; *4.* same reactants but with 0.5 mole NaCl per liter, 23°C.; *5.* $CaCl_2 + Na_2C_2O_4$, 0.5 mole NaCl per liter, 6°C.

Potassium perchlorate: Nielsen, unpublished data; $KCl + NaClO_4$, 23°C.; *1.* no salt added; *6.* ionic strength 2.0 by means of NaCl.

Kobayashi (3) measured the incubation period for silver chloride following the potential of a silver electrode. Unfortunately he investigated only a rather small range of concentrations, with the result that the linear dependency is not as clear as in most of the other cases. In Eqs. [1*a*] and [1*b*] $n = 5$ for AgCl.

Van Hook (2) measured t for Ag_2CrO_4 potentiometrically and Christiansen and Nielsen (4) measured it visually. Their data agree very closely with each other and with a straight line; $n = 4.7$. Fischer (5) measured the time for the appearance of a Tyndall beam and found incubation times only 0.010 to 0.014 times as long as were found by van Hook and by Christiansen and Nielsen at the same concentrations. Tovborg Jensen's (1) data on CaF_2 show dependence on ionic strength (negative salt effect) and on temperature (t is shorter at higher temperatures); $n = 9$. With calcium oxalate the present author found a negative salt effect but could not detect any temperature dependence; $n = 3.3$.

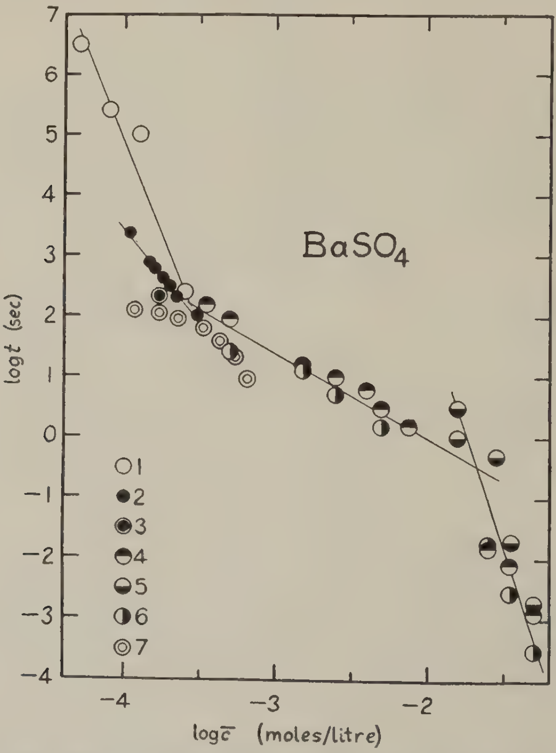

FIG. 3. Log (incubation period) against log (geometric mean concentration) for $BaSO_4$ at room temperature.

1. Von Weimarn (6) $Ba(CNS)_2 + MnSO_4$; *2.* La Mer and Dinegar (7) $Ba(NO_3)_2 + H_2SO_4$; *3.* Johnson and O'Rourke (8), $BaCl_2 + Na_2SO_4$; *4.* Nielsen, unpublished data, $BaCl_2 + H_2SO_4$; *5.* Christiansen and Nielsen (4), $BaCl_2 + H_2SO_4$; *6.* Nielsen, unpublished data, $BaCl_2 + K_2SO_4$; *7.* Fischer (5), $BaCl_2 + Na_2SO_4$.

A few measurements on potassium perchlorate by the present author also satisfy the Eqs. [1*a*] and [1*b*], with $n = 2.6$.

$BaSO_4$, however, makes an exception to the rule, as is seen from Fig. 3, where data from several authors, covering a wide concentration range, are plotted in one diagram. The points approach a single curve, but not a single straight line.

The Kinetics of Precipitation

The rate of precipitation or crystallization is sometimes controlled by diffusion, and this mechanism has also been tried on sparingly soluble electrolyte precipitates, e.g., by Odén and Werner (9) and Turnbull (10). In order to get agreement with experiment both Odén and Werner, and Turnbull were led to assume, however, that the growth of very small barium sulfate particles is limited not by diffusion but by a process occurring at the crystal-solution interface. In this way Turnbull gets agreement for small particles, i.e., when the degree of reaction $\alpha < 0.04$, but not when $\alpha > 0.05$, even though his experiments show reproducibility and simple behavior up to $\alpha = 0.40$ (Fig. 4, *loc. cit.*).

The Diffusion Theory

All investigations of the final precipitate agree in finding it rather monodisperse (1, 10, 11). Therefore it is usually assumed (as we shall assume) that the number of crystals does not change during the process and that the total surface of the precipitate is proportional to $\alpha^{2/3}$, i.e., r^2, where the radius is proportional to the cube root of the volume of precipitated matter.

If the rate of precipitation is controlled by diffusion of matter through the solution, the rate of change of the degree of reaction $d\alpha/dt$ must be proportional to $\alpha^{2/3}(dc/dx)_{x=r}$, where x is the distance from the center of a particle. From the diffusion laws follows (see, e.g., Smoluchowski (12), p. 140)

$$\left(\frac{dc}{dx}\right)_{x=r} = \frac{c - c_r}{r}, \qquad [2]$$

and since r is proportional to $\alpha^{1/3}$

$$\frac{d\alpha}{dt} = k\alpha^{1/3}(c - c_r). \qquad [3]$$

If diffusion is the only rate-determining phenomenon c_r equals the solubility s. We then have

$$\frac{d\alpha}{dt} = k\alpha^{1/3}(c_0(1 - \alpha) - s), \qquad [4]$$

or

$$\frac{d(\alpha^{2/3})}{dt} = k'(c_0(1 - \alpha) - s). \qquad [5]$$

This is equation (8) of LaMer and Dinegar's paper (13) although with different symbols.

We now introduce the new variable $\alpha' = \alpha c_0/(c_0 - s_\infty)$, where s_∞ is the solubility of large crystals; α' runs from 0 to 1 during the experiment and if we approximate $s = s_\infty$ we obtain

$$\frac{d\alpha'}{dt} = k''\alpha'^{1/3}(1 - \alpha') \qquad [6]$$

$$k''t = \int_0^{\alpha'} \alpha'^{-1/3}(1 - \alpha')^{-1}\, d\alpha' \equiv I_D. \qquad [7]$$

In Fig. 4 the "diffusion integral" I_D, from numerical calculation, is shown together with some other kinetic integrals to be introduced below.

If a precipitation process is diffusion-controlled (and the approximation $s = s_\infty$ holds) we should get a straight line if we plot I_D corresponding to experimentally determined values of α' against the time.

In Fig. 5, the data by LaMer and Dinegar (13) on the precipitation of sulfur (through addition of water to solutions in ethanol or acetone) give almost straight lines when plotted in this way. The small deviations are

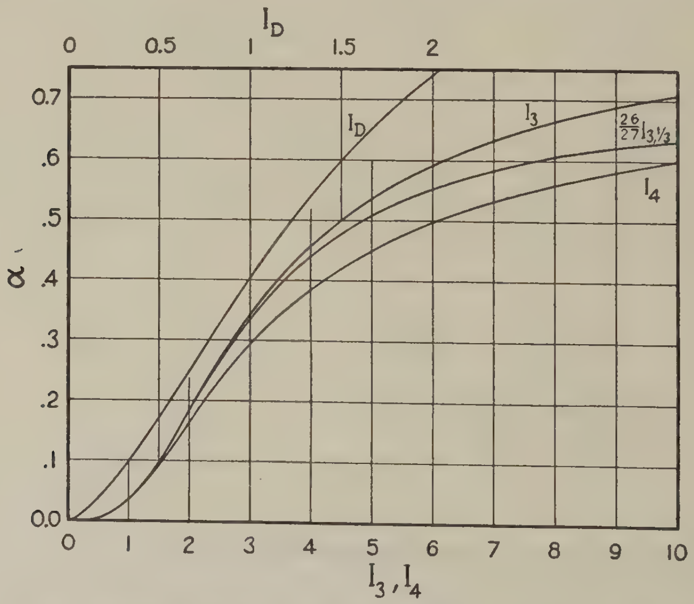

FIG. 4. Some kinetic integrals obtained through numerical integration. For definitions, see Eqs. [7], [9], and [10].

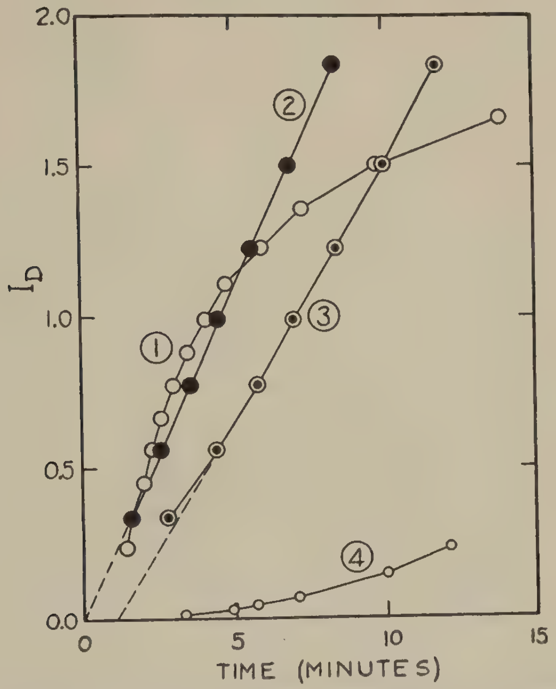

FIG. 5. I_D as a function of time at round values of α (the degree of reaction). *1*. $BaSO_4$, see Fig. 3 in Turnbull (10); *2*. sulfur from acetone through addition of water; and *3*. from ethanol, La Mer and Dinegar (13); *4*. $BaSO_4$, see Fig. 8 in Turnbull (10). In *1*. times are divided by 5.

due to $s \neq s_\infty$ for small particles as accounted for by the more elaborate calculations in the original paper.

Figure 5 also shows that the data of Turnbull (10) on $BaSO_4$ do not agree with the diffusion theory. The curve displays a very strong S-shape, with the point of inflection in the neighborhood of $I_D = 0.3$, corresponding to $\alpha' = 0.1$, as seen from Fig. 4.

THE SURFACE REACTION THEORY

Johnson and O'Rourke (8) assumed the precipitation to be controlled by a reaction in the surface proportional to the area and to some power of the activity, or concentration, of the reacting ions,

$$\frac{d\alpha}{dt} = k\alpha^{2/3}(1 - \alpha)^p. \qquad [8]$$

The integrals

$$kt = \int_0^\alpha \alpha^{-2/3}(1 - \alpha)^{-p}\, d\alpha \equiv I_p. \qquad [9]$$

are shown in Fig. 4 for $p = 3$ and 4.

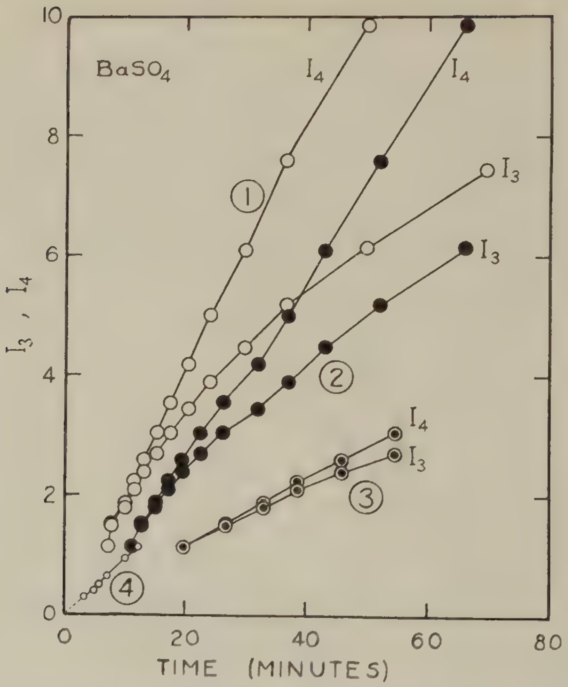

FIG. 6. Barium sulfate. *1*. See Fig. 3 in Turnbull (10); *2*. and *3*. see Fig. 1 in Turnbull (10). In *2*. times are multiplied by 2. *4*. See Fig. 8 in Turnbull (10). Experiments *1* and *4* are the same as experiments *1* and *4* in Fig. 5.

If the solubility s is not negligible I_p must be replaced by

$$\int_0^{\alpha} \alpha^{-2/3}\left[(1-\alpha)^p - \left(\frac{s}{c_0}\right)^p\right]^{-1} d\alpha \equiv I_{p,s/c_0} \qquad [10]$$

in order to give $d\alpha/dt = 0$ for $c = s$. The deviation from I_p is not great, as can be seen from Fig. 4 (the factor 26/27 makes the integrals coincide, for $\alpha \cong 0$). In the following we shall not use $I_{p,s/c_0}$.

In Fig. 6 Turnbull's data on BaSO$_4$ show a straight-line dependence on time with I_4 but not with I_3. [In Figs. 6–9 all data are plotted for round values of α both as I_3 and I_4 (I_4 having larger values than I_3 for the same value of α).] The equally numbered curves 1 and 4 in Fig. 5 and Fig. 6 are derived from the same two experiments.

We see that for $I < 1.5 (\alpha < 0.10)$ the integrals I_3 and I_4 are practically identical. The integrals obey a common limiting law

$$\alpha = \text{const.} \times t^3 \qquad (\alpha \to 0) \quad [11]$$

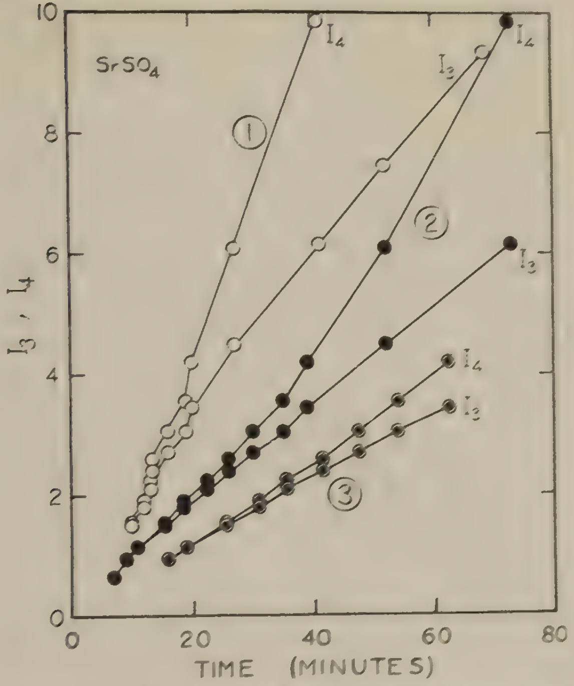

FIG. 7. Strontium sulfate, Odén (11). The numbering follows that of the original paper. In *1* times are multiplied by 4.

which may be derived from the differential equation. When $1 - \alpha \cong 1$

$$\frac{d\alpha}{dt} \cong k\alpha^{2/3} \qquad [11a]$$

$$t \cong \text{const.} \times \int \alpha^{-2/3}\, d\alpha = \text{const.} \times \alpha^{1/3} \qquad [11b]$$

This limiting law was derived by Turnbull and verified by him through very exact measurements on $BaSO_4$.

Figures 7 and 8 show that strontium sulfate and calcium oxalate also agree with Johnson and O'Rourke's theory, although it cannot be said from these experiments whether I_3 or I_4 is best, but any of these is much better than I_2 or I_5.

All the concentration measurements used for Figs. 6–8 were made by conductometry. In Fig. 9 is used van Hook's (2) measurement of the potential of a silver electrode during precipitation of silver chromate. The use of I_3 gives straight lines which, however, do not go through the origin. This may be due to an "incubation period effect" or to a depend-

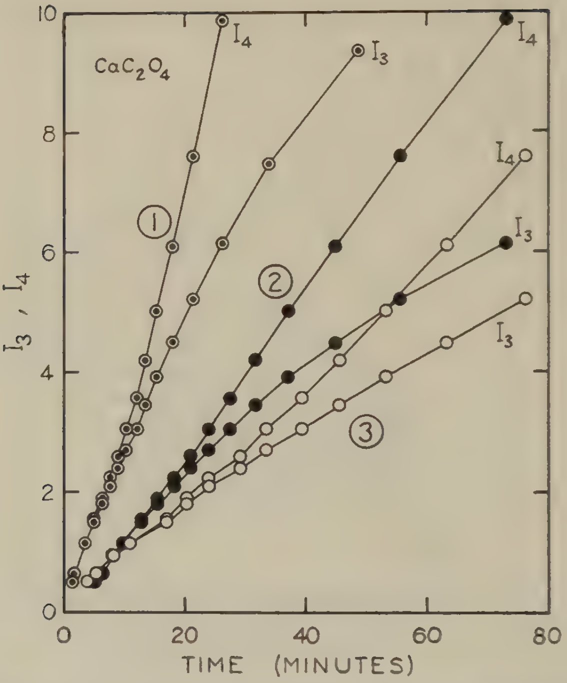

FIG. 8. Calcium oxalate, Nielsen, unpublished data. Equivalent amounts of $CaCl_2$ and $Na_2C_2O_4$ in equal volumes of water were placed for some time in a thermostated water bath at 25.00°C. and mixed. The solutions were before mixing: *1.*: 0.0015 *M*, *2.*: 0.0010 *M*; and *3.*: 0.0008 *M*. The electric conductivity was measured with a Kohlrausch bridge plus an amplifier. The readings were converted into terms of the degree of reaction by means of a calibration curve found through direct measurements on solutions containing $CaCl_2$, $Na_2C_2O_4$, and NaCl.

ence of solubility on the magnitude of the particles, as with sulfur (Fig. 5). Perhaps these two explanations are virtually identical.

The surface reaction theory was first mentioned by Christiansen and Nielsen (14) (in a slightly more complicated form), but it was only tried on Tovborg Jensen's (1) data on calcium fluoride, and this substance agrees with Eq. (9) only in the later part of the experiment (see Fig. 3, loc. cit.). The deviations are rather complicated and invite further experiments.

CHRISTIANSEN'S THEORY OF HOMOGENEOUS NUCLEATION

Recently Christiansen (15) showed that Eq. (9) can also be derived from quite different assumptions, among which the more essential ones may be stated thus:

a. The nuclei are formed homogeneously during the reaction.

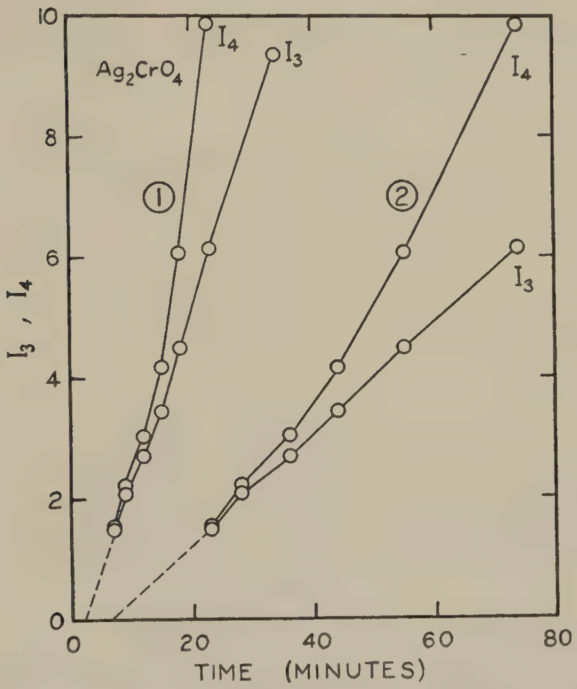

FIG. 9. Silver chromate, see Fig. 1 in van Hook (2). *1.* $H_0 = 1.25 \times 10^{-10}$; *2.* $H_0 = 0.50 \times 10^{-10}$; ($H_0 = [Ag^+]^2\,[CrO_4^{--}]$ at zero time).

b. The growth of crystals is quasi-stationary from the nuclei almost to the largest crystals, containing n ions per crystal.

c. The distribution curve is given by

$$x_i = \text{const.} \times i^{-\sigma}(1 - \alpha)^{\nu-\gamma}, \qquad [12]$$

where x_i is the concentration of crystals containing i ions, σ, ν, and γ are characteristic parameters, ν being the value of i for the nucleus and γ the order of the single stages of the growth reaction (corresponds rather closely to p in Johnson and O'Rourke's theory). From these and some auxiliary assumptions Christiansen found

$$\frac{d\alpha}{dt} = \text{const.} \times \alpha^q(1 - \alpha)^p, \qquad [13]$$

where $q = 1/(2 - \sigma)$; $p = \nu(1 - 1/(2 - \nu)) + \gamma/(2 - \sigma)$. Inserting $q = \frac{2}{3}$ (from experiment, as mentioned previously) we find $\sigma = \frac{1}{2}$ and with $p = 4$ (as found with $BaSO_4$) we obtain $\nu - (\nu - \gamma) \times \frac{2}{3} = \frac{1}{3}\nu + \frac{2}{3}\gamma = 4$; $\nu = 12 - 2\gamma$. Christiansen assumed $\nu = 8$, which gives $\gamma = 2$.

In order to make experiments decide between the two theories we may extract from Christiansen's theory the magnitude of a crystal as a function of α. The theory assumes that the distribution is given by (c) up to the largest crystals containing n ions. Now it follows from Christiansen's Eq. III that

$$n + 1 = \text{const.} \times \frac{d\alpha/dt}{(1 - \alpha)^{\nu}} = \text{const.} \times \alpha^{q}(1 - \alpha)^{p-\nu}. \qquad [14]$$

With $q = 2/3$, $p = 4$, $\nu = 8$ we obtain

$$n \cong n + 1 = \text{const.} \times \alpha^{2/3}(1 - \alpha)^{-4}. \qquad [15]$$

But according to Johnson and O'Rourke's theory, where the number of crystals is constant,

$$n = \text{const.} \times \alpha. \qquad [16]$$

It should therefore be possible to decide between these fundamentally different theories through measuring the size of the largest particles during the precipitation.

Experiments of this kind are planned in this laboratory.

REFERENCES

1. TOVBORG JENSEN, A., *Z. physik. Chem.* **180A,** 93 (1937).
2. HOOK, A. VAN, *J. Phys. Chem.* **44,** 751 (1940).
3. KOBAYASHI, K., *Science Repts. Tôhoku Imp. Univ. First Ser.* **37,** 125 (1953).
4. CHRISTIANSEN, J. A., AND NIELSEN, A. E., *Acta Chem. Scand.* **5,** 673 (1951).
5. FISCHER, W. M., *Z. anorg. u. allgem. Chem.* **145,** 311 (1925).
6. WEIMARN, P. P. VON, *Kolloid-Z.* **3,** 282 (1906).
7. LAMER, V. K., AND DINEGAR, R. H., *J. Am. Chem. Soc.* **73,** 380 (1951).
8. JOHNSON, R. A., AND O'ROURKE, J. D., *J. Am. Chem. Soc.* **76,** 2124 (1954).
9. ODÉN, S., AND WERNER, D., *Ark. Kemi, Mineral. Geol. 9,* No. 32 (1926).
10. TURNBULL, D., *Acta Metallurgica* **1,** 684 (1953).
11. ODÉN, S., *Ark. Kemi, Mineral. Geol. 9,* No. 23 (1925).
12. SMOLUCHOWSKI, M. VON, *Z. physik. Chem.* **92,** 129 (1918).
13. LAMER, V. K., AND DINEGAR, R. H., *J. Am. Chem. Soc.* **72,** 4847 (1950).
14. CHRISTIANSEN, J. A., AND NIELSEN, A. E., *Z. Elektrochem.* **56,** 465 (1952).
15. CHRISTIANSEN, J. A., *Acta Chem. Scand.* **8,** 1665 (1954).

DETERMINATION OF THE DIAMETER OF THE COILED MACROMOLECULE FROM VISCOSITY, SEDIMENTATION, AND DIFFUSION

Anton Peterlin[1]

Department of Chemistry, Wayne University, Detroit, Michigan

Received August 5, 1955

ABSTRACT

The existing theories of viscosity and sedimentation (diffusion) of the coiled macromolecule with hydrodynamic interaction yield formulas which, in the case of a Gaussian coil, can be easily applied to the determination of the diameter R of the coil and of the hydrodynamic radius a_h of the monomer unit, from either $[\eta]$ or $[s]$ or D, together with the derivative with respect to M. This method fails in all the cases where the actual macromolecular coil is not Gaussian. By combining the data for viscosity and sedimentation (diffusion), however, the coil diameter and the hydrodynamic radius can be determined regardless of the actual relation between R and the degree of polymerization. The method is illustrated for polymethylmethacrylate in acetone and on polyacrylonitrile in dimethylformamide.

I. INTRODUCTION

All the advanced theories of Brinkman (1), Debye-Bueche (2), Kirkwood-Riseman (3), Kuhn-Kuhn (4), and Peterlin (5), taking into consideration the hydrodynamic interaction of the chain elements in flow, assume a constant hydrodynamic radius a_h of the monomer unit and the linear relation

$$R^2 = Pl^2 \qquad [1]$$

for the mean square of the end-to-end distance R of the coiled macromolecule. The apparent length l is proportional to the actual length l_0 of the monomer unit, and P is the degree of polymerization. In the validity range of Eq. [1] the theories can be applied to the determination of the dimensions of a macromolecule from viscosity or sedimentation (diffusion) alone. Two parameters, the values of R and of a_h, have to be determined. Therefore not only $[\eta]$, or $[s]$, or D values of one sample but in addition the slope of a log-log plot (1–3) or of a $M/[\eta]$, or a $[s]$, or a MD vs. $M^{1/2}$ plot (4, 5) must be known.

The agreement between the molecular parameters thus derived from

---

[1] On leave from Jožef Stefan Institute, Ljubljana, Yugoslavia. This work was supported by the Office of Ordnance Research in connection with a research project of W. Heller.

$[\eta]$ and $[s]$ or D is rather poor. This is due partly to the limitations inherent in a hydrodynamic treatment of macromolecules, and mainly to the use of the simple Gaussian statistics (Eq. [1]), which do not apply to actual macromolecules owing to the excluded volume effect and to long-range interactions of the chain elements. Consideration of the latter leads to a more general law for R. In a first approximation (6) one has

$$R^2 = l^2P(1 + AP^{1/2} + \cdots). \qquad [2]$$

Equation [2] including also higher terms, could in principle, be introduced into the basic formulation of the hydrodynamic problem. Although this would be difficult to do, practically all the theories mentioned above could be modified accordingly, thus yielding equations of probably more general significance for $[\eta]$, $[s]$, and D for the determining of molecular dimensions.

A simple alternate possibility exists, however. In the existing theories the assumption of any particular relationship between R and P can be eliminated. By combining data on viscosity and sedimentation (diffusion) the diameter R and the hydrodynamic radius a_h can be determined for any sample without ambiguity, regardless of the actual relation between R and P. This is easiest to do in the very general theory of Brinkman and Debye-Bueche, which supposes a uniform distribution of the P chain elements in a sphere of diameter $d_s = 1.054\ R$.

The situation is less simple with the other theories (3–5), which use the necklace model. Here the knowledge of all distances between any two chain elements is required for the calculation of intrinsic viscosity and sedimentation (diffusion) constant. An essential simplification, mainly supported by the practical identity of the fundamental relationship resulting from the Debye-Bueche, Kirkwood-Riseman, and Peterlin treatments, consists of replacing the actual coil by a model with the true R, assuming that all the distances between any two chain elements obey the same Eq. [1] with the effective length $l = R/P^{1/2}$, i.e., the actual difference between Eqs. [1] and [2] amounts to a matter of l becoming a function of P. This assumption allows the application of the necklace theories to the determination of the molecular dimensions also in the case of a nonlinear relationship between R^2 and P.

II. Theory

a. Brinkman and Debye-Bueche replace the coiled linear macromolecule by a sphere of diameter d_s uniformly filled with chain elements each of them having the same hydrodynamic resistance coefficient $\Lambda = 6\pi a_h$. They obtain, after rigorously solving the pertinent hydrodynamical problem,

$$[\eta] = \frac{\pi N d_s^3}{6M} \cdot \frac{2.5}{1/[1 - 3(\coth \sigma/\sigma) + 3/\sigma^2] + 10/\sigma^2} = \frac{\pi N d_s^3}{6M}\, \Phi(\sigma) \qquad [3]$$

$$[s] = \frac{s_0 \eta}{1 - \bar{v}\rho} = \frac{M}{3\pi d_s N}\left(\frac{1}{1 - (\mathrm{tgh}\sigma/\sigma)} + 3/\sigma^2\right) = \frac{M}{3\pi d_s N}\frac{1}{\psi(\sigma)} \tag{4}$$

$$D = \frac{kT}{3\pi\eta\, d_s}\frac{1}{\psi(\sigma)}, \tag{5}$$

with $d_s = 1.054\ R$ and the parameter

$$\sigma = \frac{d_s}{2k^{1/2}}. \tag{6}$$

The permeability k is given by Debye-Bueche as

$$k = \frac{d_s^3}{36Pa_h} \tag{7}$$

and by Brinkman as

$$k = \frac{d_s^3}{36Pa_h}\left\{1 + 6x - 6[x(9 - 3x)]^{1/2}\right\}, \tag{8}$$

with $x = Pa_h^3/d_s^3$. Since in most cases, as will be seen later, the parameter x is very small, both definitions practically coincide, yielding

$$\sigma = 3\left(\frac{Pa_h}{d_s}\right)^{1/2}. \tag{9}$$

For the determination of the molecular parameters d_s and a_h any of the Eqs. [3], [4], [5], together with its logarithmic derivative

$$\frac{d \log [\eta]}{d \log M} = \alpha = -1 + \frac{1}{2}\frac{d \log \phi}{d \log \sigma} + \left(3 - \frac{1}{2}\frac{d \log \phi}{d \log \sigma}\right)\frac{d \log d_s}{d \log M} \tag{10a}$$

$$\frac{d \log [s]}{d \log M} = 1 - \beta = \left(1 - \frac{1}{2}\frac{d \log \psi}{d \log \sigma}\right)\left(1 - \frac{d \log d_s}{d \log M}\right) \tag{10b}$$

$$\frac{d \log D}{d \log M} = -\beta \tag{10c}$$

has to be used. As long as R is proportional to $P^{1/2}$ in the considered range of DP, one has $d \log d_s/d \log M = \frac{1}{2}$ and Eqs. [10a, b, c] reduce to the well-known expressions

$$\alpha_{1/2} = \frac{1}{2} + \frac{1}{4}\frac{\sigma}{\phi}\frac{d\phi}{d\sigma}; \tag{11a}$$

$$\beta_{1/2} = \frac{1}{2} + \frac{1}{4}\frac{\sigma}{\psi}\frac{d\psi}{d\sigma}. \tag{11b}$$

From the tabulated functions $\alpha_{1/2}$ and $\beta_{1/2}$ the parameter σ can be derived from the measured slope in the log-log plot of the experimental values $[\eta]$, $[s]$, or D. But this easy method is not applicable in the case of deviations

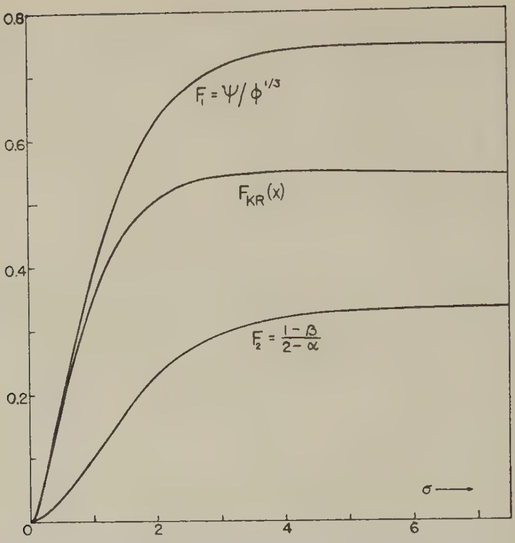

FIG. 1. The functions $F_1(\sigma)$, $F_2(\sigma)$, and $F_{KR}(x)$ defined in Eqs. [12], [13], and [24], respectively.

from Eq. [1] and hence yields incorrect values for R in most actual macromolecular systems.

By combining Eq. [4] with Eq. [5] or [6], however, the parameter σ is obtained without any additional assumption

$$3\pi\left(\frac{6N^2}{\pi}\right)^{1/3}\frac{[s]}{M}([\eta]M)^{1/3} = 3\pi\left(\frac{6}{\pi N}\right)^{1/3}\frac{D\eta}{kT}([\eta]M)^{1/3} \qquad [12]$$
$$= \Phi^{1/3}/\psi = 1/F_1(\sigma).$$

The function F_1 is plotted in Fig. 1 and tabulated in Table I. For small values of σ the series expansion

$$F_1(\sigma) = \left(\frac{2 \times 10^{1/3}}{9}\right)\sigma^{4/3}\left(1 - \frac{26\sigma^2}{105} - \cdots\right). \qquad [12a]$$

TABLE I

σ	$F_1(\sigma)$	$F_2(\sigma)$
0	0.000	0.000
1	0.386	0.102
2	0.627	0.228
3	0.712	0.292
4	0.738	0.319
5	0.746	0.328
8	0.746	0.336
10	0.744	0.337
∞	0.739	0.333

may give an idea of the behavior at the origin. The function reaches very early a nearly constant value 0.75, which limits its usefulness for determining σ. For both systems to which Eq. [12] was applied, the values are located within the useful range.

A little better is the combination of the exponents α and β to

$$\frac{1-\beta}{2-\alpha} = \frac{2-(\sigma/\psi)(d\psi/d\sigma)}{6-(\sigma/\Phi)(d\Phi/d\sigma)} = F_2(\sigma). \qquad [13]$$

This ratio becomes constant at a slightly higher value of σ as F_1 (Fig. 1, Table I), but the difference is hardly significant and is very likely more than outweighed by the usually lower precision in the determination of the exponents α and β.

The diameter of the coil and the hydrodynamic radius of the monomer follow in the usual way from Eqs. [3], [4], [5], and [9].

$$d_s = \frac{(6[\eta]M)^{1/3}}{\pi N\,\phi(\sigma)} = \frac{M}{3\pi N[s]\psi(\sigma)} = \frac{kT}{3\pi\eta D\psi(\sigma)}; \qquad [14]$$

$$a_h = d_s\,\frac{\sigma^2}{9P}. \qquad [15]$$

b. As a result of experiments on large-scale wire models Kuhn and Kuhn give the following formulas for the intrinsic viscosity

$$[\eta] = \frac{Nl_0^2 A_m}{M_0}\cdot\frac{0.43P}{-1.6+2.3\log_{10}(A_m/d_h)+(Pl_0/A_m)^{1/2}} \qquad [16]$$

and for the intrinsic sedimentation constant or the diffusion constant, respectively,

$$[s] = \frac{\eta MD}{NkT} = \frac{M_0}{Nl_0}\left[-0.03+0.16\log_{10}\left(\frac{A_m}{d_h}\right)+0.136\left(\frac{Pl_0}{A_m}\right)^{1/2}\right]. \qquad [17]$$

The numerical constants are those given by Kuhn, Kuhn, and Silberberg (7). The length A_m of the "preferential" segment is determined by the two definitions

$$L = Pl_0 = ZA_m \qquad R^2 = ZA_m^2 \qquad [18]$$

yielding

$$A_m = \frac{R^2}{L} \qquad [19a]$$

and

$$\left(\frac{Pl_0}{A_m}\right)^{1/2} = Z^{1/2} = \frac{R}{A_m}. \qquad [19b]$$

According to the definition given by Eq. [18] the segments are completely independent in their orientation. The hydrodynamic parameter d_h represents the diameter of the cylindrical segment. According to Eqs. [16] and [17], this parameter influences the viscosity and sedimentation values but slightly.

Setting

$$x^2 = \frac{A_m}{Pl_0} \text{ and } y = \log_{10}\frac{A_m}{d_h}, \qquad [20]$$

one obtains

$$\begin{aligned} \frac{0.43NP^2l_0^3}{M_0[\eta]}x^2 &= Bx^2 = \frac{1}{x} + 2.3y - 1.6 \\ \frac{Nl_0[s]}{0.136M_0} &= C = \frac{1}{x} + 1.176y - 0.22, \end{aligned} \qquad [21]$$

and, by eliminating y, the cubic equation in x,

$$x^3 - (1.954C - 1.17)Bx + 0.954B = 0. \qquad [22]$$

Only the largest positive root has a physical meaning yielding $d_h < A_m$ One has

$$\begin{aligned} R = xPl_0; \qquad A_m &= x^2Pl_0; \\ \log_{10}\frac{A_m}{d_h} &= \frac{C + 0.22 - 1/x}{1.176}. \end{aligned} \qquad [23]$$

c. The formulas of Kirkwood-Riseman (KR) can also be easily transformed to a form suitable for the determination of molecular dimensions by introducing $R = lP^{1/2}$ and $\zeta = 6\pi a\eta$, $x = \lambda_0 P^{1/2} = (6/\pi)^{1/2}a_hP/R$. One obtains, in complete analogy to Eq. [12],

$$3\pi\left(\frac{6N^2}{\pi}\right)^{1/3}\cdot\frac{[s]}{M}([\eta]M)^{1/3} = 0.62[xF(x)]^{1/3}\left(\frac{8}{3} + \frac{1}{x}\right) = \frac{1}{F_{\mathrm{KR}}(x)}. \qquad (24)$$

The function $F_{\mathrm{KR}}(x)$ is very similar to $F_1(\sigma)$, as may be seen from Fig. 1, where it is plotted over $\sigma = 2.486x^{1/2}$, but its maximum value 0.55 is appreciably smaller than 0.75 in $F_1(\sigma)$. Since the experimental data for polymethylmethacrylate and polyacrylonitrile yield larger values, viz., 0.625–0.731 and 0.610 ÷ 0.630, it seems that the numerical factors in the KR formulas are not able to reproduce the simultaneous measurements of intrinsic viscosity and sedimentation or diffusion. Also, the recently reported corrections in the numerical coefficients of the viscosity expression replacing the factor 3.60 at complete solvent immobilization

$$[\eta]_{x=\infty} = 3.60 \times 10^{23}\frac{R^3}{M}$$

by 3.36 (9), 2.90, and 2.84 (10) can not remove this discrepancy, since they increase the maximum of $F_{\mathrm{KR}}(x)$ only from 0.55 to 0.56, 0.59, and 0.60, respectively. Very likely it is due to the oversimplification in the model and especially to the assumption that the r.m.s. distances between any two elements j and k can be represented as $l\,|\,j - k\,|^{1/2}$ with $l = R/P^{1/2}$, i.e., as in a Gaussian coil, although the relation between R and P is definitely non-Gaussian (see Section IV).

In the evaluation of the experimental data by the method proposed above a careful choice is necessary for the molecular weight which enters Eqs. [12], [14], [22]. The most appropriate average is that derived from the ratio of the sedimentation and diffusion constants, since it very closely agrees with the viscosity average, $M_{S,D} \sim M_\eta$.

There is of course no discrepancy between the molecular parameters derived from viscosity or from sedimentation or diffusion, since only one value is obtained. The diameter d_s or R has only to be compared with the light-scattering value. The latter is calculated on the basis of a necklace model with all distances between any two chain elements being given by Eq. [1]. The deviations from the Gaussian character of the coil actually influence the value for the diameter since they change the relationship between R and the gyration radius (8).

On the other side according to the basic assumptions in the theoretical treatment, the hydrodynamic radii a_h and d_h ought to be constant in the same polymer series (the same solvent, constant temperature).

III. EVALUATION OF EXPERIMENTAL DATA

There are very few simultaneous measurements of viscosity and sedimentation or diffusion for a wide range of molecular weights to which the proposed method can be applied. Possibly, the most reliable data are those for polymethylmethacrylate (PMMA) in acetone, for which Schulz and collaborators (11) have determined a consistent set of data on diffusion, sedimentation, viscosity, and light scattering and with M ranging from some thousand to several million. There is further a new investigation of Bisschops (12) on the viscosity sedimentation and diffusion of polyacrylonitrile (PAN) solutions in dimethyl formamide in a much narrower range of molecular weights (M = 47,000–270,000). In both cases the molecular weight was determined from the ratio of the sedimentation and diffusion constants.

Since the experimental data inevitably show a random scattering which in many cases may overshadow the actual trend in the calculated molecular parameters, every set of data was first smoothed out by the simplest possible interpolation which still reproduces the main features of the respective molecular weight dependence. In the case of PMMA the wide range of M requires a quadratic interpolation

$$\log\,[\eta] = A + B \log M + C\,(\log M)^2, \qquad [25]$$

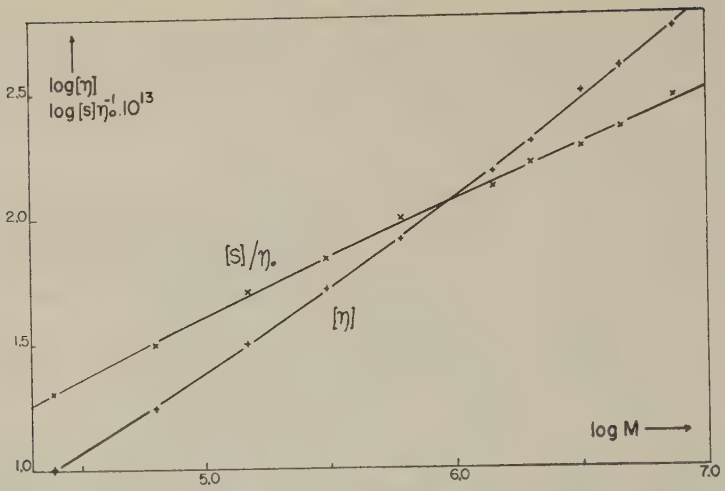

FIG. 2. The experimental data of $[\eta]$ (+) and $[s]/\eta$ (×) for PMMA in acetone and the quadratic interpolation curve used in the determination of the molecular parameters.

whereas in the case of PAN a linear equation is sufficient. The amount of the small corrections can be estimated from Fig. 2, where the original data and the smoothed-out interpolation curves were plotted for PMMA. For PAN the agreement is still better. The resulting molecular parameters d_s, a_h, R_K, and A_m/d_h are listed in Table II for PMMA and in Table IV for PAN.

a. *Polymethylmethacrylate in Acetone.* The diameter of the sphere d_s and the r.m.s. end-to-end distance R_K of the Kuhn's (K) model agree rather well in the whole range of M. The situation is the same in the case of PAN and indicates a less good agreement in the diameters R_{BDB} (diameter based on Brinkman, Debye-Bueche model) and R_K (Tables III and V). The increase of A_m with M indicates a deviation of the molecule from the random coil model without long-range interaction. A correct measure of

TABLE II

PMMA

M	$F_1(\sigma)$	σ	$\phi(\sigma)$	$d_s(A.)$	$a_h(A.)$	$A_m(A.)$	$\log_{10} A_m/d_h$
14.02×10^6	0.620	1.94	0.311	5220	0.016	78.7	54.4
6.50	0.632	2.02	0.331	3210	0.022	64.7	38.7
3.02	0.644	2.12	0.360	1970	0.033	53.8	26.5
1.40	0.657	2.22	0.387	1220	0.048	45.0	18.1
0.65	0.670	2.36	0.426	760	0.071	38.2	12.2
0.30	0.685	2.52	0.467	476	0.111	32.6	8.0
0.14	0.699	2.73	0.526	298	0.176	28.1	5.2
0.065	0.714	3.04	0.612	186	0.294	22.2	2.9
0.030	0.731	3.59	0.755	115	0.546	20.6	1.9

TABLE III

PMMA

M	$R_\lambda (A.)$	$R_{BDB} (A.)$	$R_K (A.)$	$R_F (A.)$	$R_\eta (A.)$	$l = R_{BDB}/P^{1/2}$ (A.)
14.02×10^6	4880	4950	5274	4000	3435	15.65
6.50	2840	3040	3251	2503	2148	11.92
3.02	1705	1870	2023	1581	1352	10.80
1.40	1056	1160	1261	1006	859	9.80
0.65	674	721	791	645	551	8.94
0.30	444	452	498	417	356	8.25
0.14		283	315	272	232	7.56
0.065		176	191	178	152	6.90
0.030		109	125	118	101	6.29

these deviations is the increase of the parameter $l = R/P^{1/2}$ from 6.29 A. to 15.65 A., indicating that the molecule at $M = 14 \times 10^6$ is $15.65/6.29 = 2.5$ times more stretched than it ought to be in the case of simple Gaussian statistics on the basis of the dimensions at $M = 30{,}000$. Of course, also the difference between $l = 6.29$ A. and $l_0 = 2.52$ A., mostly due to the steric and energetic limitations of the free rotation of the monomer units, includes some effect of long-range interaction and of the volume requirement of the chain elements.

Rather surprising is the decrease of σ with increasing M. The coil seems to be more permeable the larger the molecule. That is only partly due to the widening of the coil where R increases more than proportionally to $P^{1/2}$ (Table III). The main cause, however, is the appreciable decrease of the fractional resistance of the chain element, the hydrodynamic radius decreasing from 0.546 A. to 0.01 A. in contradiction to the basic assumptions of the hampered flow theory. At first sight this fact is hard to understand and will be discussed in more detail a little later.

The hydrodynamic parameter d_h of Kuhn's theory, however, has quite unrealistic values, strongly indicating that the resistance of the coil to translational and rotational motion cannot depend on the frictional resistance of the monomer in the manner suggested by Eqs. [16] and [17], since, e.g., it yields for the hydrodynamic radius of the segment at $M = 14 \times 10^6$ the value $d_h = 10^{-52}$ A.

Table III and Fig. 3 show the r.m.s. end-to-end distances of the molecules calculated according to the single viscosity theories. The smoothed-out light scattering diameter[2] (11) is denoted by R_λ; R_{BDB} and R_K are the values derived from the parameters in Table II; R_η is the value which

---

[2] The non-Gaussian character of the PMMA chain yields a correction of 10% in the diameter of the coil. The light scattering value R_λ calculated on the assumption of a Gaussian coil has to be increased by this amount (8). By this correction the experimental points in Fig. 3 are just shifted on the R_{BDB} curve. All the estimates in the text of this paper were corrected according to this shift. (Note added in proof).

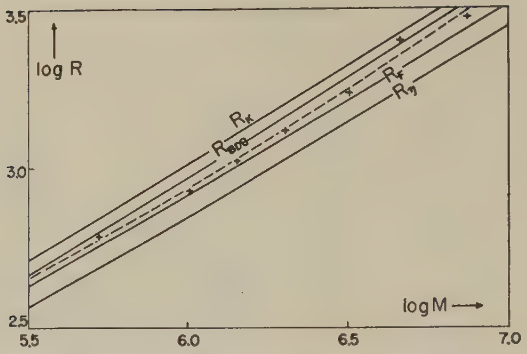

FIG. 3. The coil diameter of PMMA in acetone. Experimental data from light scattering (+) and the interpolation curve (R_λ —) used in Table III. The upper curves are determined from [η] and [s] according to Kuhn (R_K) and Brinkman, Debye-Bueche (R_{BDB}), the lower ones from [η] only, according to Flory (R_F) and Debye-Bueche (R_η).

Schulz and collaborators (11) obtained from the intrinsic viscosity by applying the Debye-Bueche Eqs. [4] and [11*a*]. R_F is calculated according to Flory with $\phi_F = 2.1 \times 10^{23}$. The agreement between R_λ and R_{BDB} is so good—the differences being less than 5%—that it substantially supports the model used in the hydrodynamic treatment by Brinkman and Debye-Bueche, but it is impossible, owing to the variation of a_h and to the deviation of the actual R^2 from the simple linear law (Eq. [1]), to derive the molecular dimensions from viscosity or sedimentation alone. The resulting values of R_η actually deviate so much from those obtained from light-scattering data that they cannot be used for any precise characterization of the macromolecular system.

In the special case of PMMA in acetone the validity of Flory's relation $[\eta] = \phi_F R^3/M$ can be very roughly understood by the fact that in that range of molecular weights where the available light-scattering data for the diameter are still reliable enough, i.e., from $M = 0.5 \times 10^6$ upwards, the function $\phi(\sigma)$ changes rather slowly from 0.426 at $M = 0.65 \times 10^6$ to 0.311 at $M = 14 \times 10^6$, hence yielding for the Flory constant the value

$$\phi_F = \frac{\pi 1.054^3 N}{6} \phi(\sigma) = 1.57 \div 1.15 \times 10^{23},$$

which actually changes so little that it can be considered as a constant in most practical applications where very precise values of R are not required.

The diameters R_K are always larger than the light-scattering values and also larger than R_{BDB}, the differences between R_K and R_λ being possibly as large as 10%. The deviations between R_{BDB}, R_F, R_K, R_λ are not very serious, however, and do not prevent, by any means, the use of the respective

TABLE IV

PAN

M	$F_1(\sigma)$	σ	$\phi(\sigma)$	$d_s(A.)$	$a_h(A.)$	$A_m(A.)$	$\log_{10} A_m/d_h$
270×10^3	0.630	2.01	0.329	1096	0.092	88.4	9.84
155	0.624	1.96	0.317	760	0.111	79.8	8.11
113	0.620	1.94	0.311	633	0.124	77.0	7.25
48	0.610	1.88	0.296	385	0.167	63.8	5.36

TABLE V

PAN

M	$R_{BDB}(A.)$	$R_K(A.)$	$R_F(A.)$	$l = R_{BDB}/P^{1/2}$
270×10^3	992	1065	817	13.90
155	721	767	585	13.33
113	601	651	480	13.01
48	365	381	291	12.12

methods for the determination of the coil diameter. The more elaborate method using Eq. [12], requiring the simultaneous measurement of $[\eta]$ and of $[s]$ or D, seems to yield the most accurate R.

b. Polyacrylonitrile in Dimethyl Formamide. In the much smaller range of M the effects of the single parameters and especially the deviations from the simple linear relations are much less apparent and hence general conclusions concerning the behavior of the molecular parameters as a function of M cannot be obtained. Nevertheless there seem to be differences between the PMMA and PAN. For instance, σ increases slightly with M. This may be due to the lesser deviation from the simple Gaussian statistics, as indicated by the fact that in the same range of P the parameter l increases only by a factor 1.15 as compared with 1.25 in the case of PMMA. It is most likely a consequence of a substantially smaller hydrodynamic interaction as shown in Eqs. [30] and [31] resulting from a smaller ratio a_h/l. The practical constancy of $\phi(\sigma)$ yields an equally constant value for $\phi_F = 1.09/1.21 \times 10^{23}$. A comparison of R with R_λ which could be determined rather precisely for all but the lowest fraction, would be very desirable. In the case of PAN also, the hydrodynamic radius a_h decreases rather quickly with M and the Kuhn radius d_h assumes physically impossible values of 10^{-3} to 10^{-7} A., supporting the view that the radius d_h is not included in a proper fashion in Eqs. [16] and [17].

IV. The Hydrodynamic Radius

The large decrease of a_h with M—it varies from 0.546 A. at $M = 30{,}000$ to 0.016 A. at $M = 14 \times 10^6$—is incompatible with the basic assumption of the Brinkman, Debye-Bueche theory requiring a constant a_h. A better understanding of the situation, however, can be achieved by the necklace theory. The latter also attributes to every monomer unit a constant a_0, which is then substantially reduced by the hydrodynamic influence of the neighbors moving on the average in the same direction. According to Burgers (13), who introduced Oseen's approximation in the hydrodynamic treatment of flow through the coiled macromolecule, the increase in the velocity of a sphere (1) by the presence of a second sphere (2) at a distance $\mathbf{r}$ can be represented by the series expansion

$$\delta\mathbf{v}_1 = \mathbf{v}_2 \frac{3a_0}{4}\left(\frac{1 + \cos^2\theta}{r} + \frac{2a_0^2(1 - 3\cos^2\theta)}{3r^2}\right) + \cdots \qquad [26]$$

where θ is the angle between $\mathbf{r}$ and $\mathbf{v}$. For a random distribution of the chain elements, moving all in the same direction, the second term vanishes. The influence of the remaining first term results according to the simplified treatment of Peterlin (5*a*) in a reduction of the apparent fractional resistance

$$\begin{aligned} \frac{1}{a_h} &= \frac{1}{a_0}\left(1 + \gamma a_0 < \sum_{j\neq k}\sum \frac{1}{r_{jh}} > A_v\right) \\ &= \frac{1}{a_0}\left(\alpha + \beta a_0 \frac{P}{R} + \cdots\right) = A + B\frac{P}{R} + \cdots \end{aligned} \qquad [27]$$

where the coefficients depend on the special conditions of the flow (uniform flow in sedimentation, flow with a constant gradient in viscosity). The coefficient A may become negative at high values of the ratio a_0/l when the mutual influence of the monomer unit is large. For a non-Gaussian distribution of the chain elements requiring Eq. [2] for R, the average of the double sum of all the inverse distances in the coil is no longer proportional to P/R. In a first approximation a linear correction term has to be added, yielding

$$\frac{1}{a_h} = A + B\frac{P}{R} + C\left(\frac{P}{R}\right)^2 \qquad [28]$$

instead of Eq. [27]. By introducing it in the expressions (5*a*) for $[\eta]$ and $[s]$ one obtains

$$[\eta] = \frac{\pi N}{6}\frac{R^2}{M_0}\Big/\left[A + B\frac{P}{R} + C\left(\frac{P}{R}\right)^2\right]$$

and [29]

$$[s] = \frac{M_0}{6\pi N_2}\left[A' + B'\frac{P}{R} + C'\left(\frac{P}{R}\right)^2\right].$$

The experimental data obtained on PMMA can be reproduced as follows:

$$\begin{aligned} [\eta] &= \frac{\pi N}{6}\frac{R^2}{M_0}\Big/\left[-3.7 \times 10^8 + 2.34\frac{P}{R} + 2.33 \times 10^{-10}\left(\frac{P}{R}\right)^2\right] \\ [s] &= \frac{M_0}{6\pi N}\left[-3.7 \times 10^8 + 3.55\frac{P}{R} + 2.50 \times 10^{-10}\left(\frac{P}{R}\right)^2\right] \end{aligned} \qquad [30]$$

with $R = R_{\mathrm{BDB}}$. The coefficient of P/R is smaller in $[\eta]$ than in $[s]$ according to the theoretical requirement. The negative value of the first term is not surprising since it includes zero order terms of the sum average. Such negative values were already found in the calculation of $[\eta]$ and $[s]$ for short-chain models (5*b*) resulting in negative intercepts with the abscissa in a plot of $M/[\eta]$ and $[s]$ against $M^{1/2}$. In the case of PAN with the low range of M the experiments can be reproduced by a linear approximation

$$[\eta] = \frac{\pi N}{6}\frac{R^2}{M_0}\Big/\left(1.47 \times 10^8 + 2.44\,\frac{P}{R}\right)$$

$$[s] = \frac{M_0}{6\pi N}\left(1.58 \times 10^8 + 4.24\,\frac{P}{R}\right). \qquad [31]$$

The positive value of A is in agreement with a larger l and a smaller a_h as compared with PMMA (in the same range of P). Both representations Eq. [30] and [31] support the assumption of a constant hydrodynamic radius of the monomer unit, all apparent deviations as shown in Tables III and V, being due to hydrodynamic interaction of the segments in the non-Gaussian coil. This interaction cannot be represented, however, by writing the a_h from Tables III and V in the form of Eq. [28], since the BDB treatment, by virtue of σ, already partly considers the reduction of the resistivity of the single monomer unit by its neighbors. Of course, Eqs. [30] and [31] do not yield numerical values for a_0 as long as the function $A(a_0/l)$ is not explicitly known. They are, therefore, only good interpolation formulas reflecting the actual mechanism involved in the hydrodynamics of the problem.

The quadratic function of P/R in Eq. [30] and the difference between the coefficients A and A' in Eqs. [30] and [31] yield also an understanding of the rather surprising fact that the Kirkwood-Riseman formulas cannot be easily adapted to the case of a non-Gaussian coil. The actual r.m.s. distances between any two segments j and k of the coiled macromolecule cannot be satisfactorily expressed as $l\,|\,j - k\,|^{1/2}$ with $l = R/P^{1/2}$ when l varies with P, i.e., in the case of a non-Gaussian coil. Therefore Eq. [24] does not represent the correct result of the necklace model in that case and has to be replaced by a more complicated function.

V. Conclusions

When simultaneous values of the intrinsic viscosity and the sedimentation or diffusion constant for the same polymer system are available, the coil diameter and the hydrodynamic radius of the monomer unit can, in principle, be calculated unambiguously on the basis of any of the existing theories or the hindered flow through a coiled macromolecule, but as far as can be concluded from considering two systems, the Brinkman, Debye-Bueche formalism seems to be most suitable and yields the best results.

In the case of PMMA in acetone and of PAN in dimethyl formamide both parameters were calculated according to the Brinkman, Debye-Bueche, and the Kuhn-Kuhn theories. The coil diameters do not differ appreciably when determined by the first or the second theory, but in the first case the agreement with the light-scattering data is much better. On the other hand, the diameters obtained from the viscosity or sedimentation alone are incorrect mainly owing to the decrease of the apparent radius a_h and to the more than proportional increase of R with $P^{1/2}$. The success of Flory's empirical formula for the intrinsic viscosity seems to be based on the fact that in the whole range of molecular weights where the diameter can be independently determined by light scattering, the changes in the coil permeability and hence in the proportionality factor—which measures the deviation of the viscosity from the Einstein value 2.5—are very small, much smaller than could be expected on the basis of the model assuming a constant a_h and a strict proportionality between R and $P^{1/2}$.

Very suprisingly the permeability of the coil increases with M at least in the case of PMMA. That is due not so much to the widening of the coil as to the sharp decrease of the apparent hydrodynamical radius of the monomer unit. The explanation for such a behavior which deviates from the basic assumptions in the treatment of the hindered flow through a coil, can be understood by considering the more realistic necklace model. The average sum over all reciprocal distances cannot be expressed by a single term proportional to the ratio P/R in the entire range of molecular weights, especially when the deviations from the simple square-root law for R become more and more pronounced. By considering the pertinent correction terms a quadratic interpolation formula for $[\eta]$ and $[s]$ can be established, reflecting the actual hydrodynamic behavior of the coil and also the influence of an increasing departure of its dimensions from that of the random coil model.

References

1. Brinkman, H. C., *Physica* **13,** 447 (1947); *Appl. Sci. Research* **1,** 27, 81 (1947); *Proc. Intern. Rheol. Congr. 1948*, p. 58; *Appl. Sci. Research* **2,** 190 (1949).
2. Debye, P., and Bueche, A. M., *J. Chem. Phys.* **16,** 573 (1948).
3. Kirkwood, J. G., and Riseman, J., *J. Chem. Phys.* **16,** 565 (1948).
4. Kuhn, H., and Kuhn, W., *Helv. Chim. Acta* **30,** 1233 (1947); *J. Chem. Phys.* **16,** 838 (1948); *J. Polymer Sci.* **5,** 519 (1950); *ibid.* **9,** 1 (1952); Kuhn, H., Habilitationsschrift, Basel, 1946; *J. Colloid Sci.* **5,** 331 (1950).
5. (*a*) Peterlin, A., Intern. Congr. "Les grosses molécules en solution," Paris, 1948, p. 70; *Diss. Acad. Ljubljana* (3A) **1,** 48 (1950); *J. Polymer Sci.* **5,** 473 (1950).

   (*b*) Peterlin, A., *J. chim. phys.* **47,** 669 (1950); *ibid.* **48,** 13 (1951); *J. Polymer Sci.* **8,** 173 (1952).
6. Teramoto, E., Yamamoto, M., and Matsuda, H., various papers in *Busseiron-Kenkyu* **39–51** (1951, 1952); summary in English by P. J. Flory, *J. Polymer*

Sci. **14,** 1 (1954). Grimley, B., *J. Chem. Phys.* **21,** 185 (1953); Bueche, F., *J. Chem. Phys.* **21,** 205 (9953); James, H. M., *J. Chem. Phys.* **21,** 1628 (1953); Zimm, B. H., Stockmayer, W. H., and Fixman, M., *J. Chem. Phys.* **21,** 1716 (1953).

7. Kuhn, H., Kuhn, W., and Silberberg, A., *J. Polymer Sci.* **10,** 79 (1953).
8. Peterlin, A., *J. Chem. Phys.*, in press.
9. Kirkwood, J. G., Zwanzig, R. W., and Plock, R. J., *J. Chem. Phys.* **23,** 213 (1955).
10. Zimm, B. H., "The dynamics of polymer molecules in dilute solution: viscoelasticity, flow birefringence and dielectric loss" (to appear in *J. Chem. Phys.*) I am very much indebted to Dr. Zimm for letting me see the manuscript before its publication. The figure 2.90 was derived by P. L. Auer and is cited by Zimm, whereas 2.84 is the result of Zimm's theory as presented in the cited paper.
11. Schulz, G. V., and Meyerhoff, G., *J. Polymer Sci.* **10,** 79 (1953); *Z. Elektrochem.* **56,** 545 (1952); *Makromol. Chem.* **7,** 294 (1952).
12. Bisschops, J., *J. Polymer Sci.* **17,** 81 (1955).
13. Burgers, J. M., *Proc. Acad. Sci. Amsterdam* **44,** 1045 (1941).

Book Reviews

Introduction to Thermodynamics of Irreversible Processes. By I. Prigogine, D.Sc., Professor University of Brussels. Charles C Thomas, Springfield, Illinois, 1955. 114 pp. Price $4.75.

At long last we have a situation where we can complain about too little advertising from a publisher. One would think that when Prigogine writes a book on the thermodynamics of irreversible processes in English it would be a significant event for American chemists, but few know of its existence.

This small book (102 pages text) is an excellent introduction to a new branch of science and could serve as a textbook for a course in advanced thermodynamics. The book is self-contained in the sense that the first chapters give an outline of equilibrium thermodynamics. Although this introduction is hardly sufficient for a reader not acquainted with classical thermodynamics, it certainly facilitates the reading of the book.

The introduction, which takes the first third of the book, is followed by a chapter on general theorems including Onsager's reciprocity relations. The chapter is arranged in what now seems to be the canonical way, that is, so that the reader may skip the derivation of the reciprocity relations and take them as a new axiom if he is interested only in the applications. The reviewer has the pious hope that most readers will swallow the bitter pill and work through this part of the chapter. In this way we could possibly avoid in this new subject the confusion about the fundamental axioms which has been so common in textbooks on classical thermodynamics.

The last two chapters give a few important examples of applications of the thermodynamics of irreversible processes and deal with Prigogine's theorem on minimum entropy production in stationary states. Nonlinear problems are treated in an appendix which also serves as a survey of recent Belgian literature on the subject.

The book is written with constant reference to chemical reactions and has in this way an exceptional position among the textbooks on the subject. Its only disadvantage—if any—is one it shares with many books and papers on thermodynamics: the huge number of queer symbols. Although the present author partly makes up for this with an extensive list of symbols, it is still very much to be hoped that an agreement regarding use of symbols will be reached in the near future.

Thor A. Bak, Columbia University, New York

Methoden der Organischen Chemie (Houben-Weyl). 4th edition. Edited by Eugen Müller, Tübingen. Vol. VII, Part 1 xxii + 556: Vol. VIII: xviii + 775 Georg Thieme Verlag, Stuttgart, 1955. Prices $19.55 and $23.30.

The 4th edition of the famous "Houben-Weyl," under the editorship of Eugen Müller, has now reached considerable proportions. Four extremely handsome volumes (II, 1953; IV–2, 1955; VII–1, 1954; VIII, 1952) are available as of this writing; of these, Vol. VII, Part 1, covering aldehydes, and Vol. VIII, covering peroxides and carboxylic acids, will be considered here.

Certainly, all the characteristic elements of the massive, monumental tradition of German book making in the organic field are present in this series. In Vol. VII, Part 1, one finds, for example, a lucid and compact survey of the Oxo-reaction (over 90 references), along with detailed directions for the preparation of Adkin's zinc-nickel-barium-copper chromite "kontakt" (or even of carbon monoxide!). One finds a 50-reference review of the Darzens-Erlenmeyer jr.-Claisen (*sic*) glycidic ester synthesis, and one can obtain also detailed directions for the preparation of 1-formyl-2,3-dihydroxypropane ("glycerolaldehyde") published as recently as 1953 (E. Waldmann and V. Pray, *Monatsh. Chem.* **84,** 543 (1953)). In keeping with the original character of the series, theoretical aspects of the reactions treated are not included.

It will come as no surprise to users of previous editions of Houben-Weyl to find, for example, that a review on aldehyde syntheses by means of Friedel-Crafts type of reactions is leisurely—although economically—initiated with a reference to L. Gattermann and J. A. Koch, *Ber.* **30,** 1622 (1897) and carried through references such as A. Robertson and W. B. Whalley, *J. Chem. Soc.*, p. 3355 (1951). Yet an up-to-date treatment of aldehyde synthesis *via* free radicals (references include A. Mondon, *Angew. Chem.* **64,** 224 (1952)) also finds its proper place. Whether the promised 18 volumes will suffice, at the present pace, appears doubtful.

Volume VIII contains a 75-page monograph on peroxides by R. Criegee, which undoubtedly will become one of the outstanding features of the series. An excellent chapter on derivatives of carbonic acids gathers material of considerable value (the interesting class of carbodiimides are treated, although new methods based on them are post-publication developments). The generally unfamiliar chemistry of dimeric and trimeric carbonic acid derivatives is carefully and exhaustively treated. The rest of the volume is devoted to nitriles, isonitriles, and carboxylic acids and their derivatives.

This reviewer considers superfluous a recommendation of this series, in particular to those who have not benefited from a thorough preparative training. The physical aspects of these books can hardly be improved, although the very excellence of the paper has resulted in heavy volumes. It can be added that in reviewing this work it becomes apparent that the epoch of cumulative topical surveys as part of a single comprehensive treatise on organic chemistry, is, of necessity, coming to an end. This may, in fact, be one of the last, and certainly one of the most distinguished, representatives of the period.

FAUSTO RAMIREZ, Columbia University, New York

Statistical Mechanics of Irreversible Change. RICHARD T. COX. The Johns Hopkins Press, Baltimore, 1955. 126 pp. and index. Price $5.00.

This monograph treats the subject of irreversible processes from a somewhat different viewpoint than in the phenomenological approach adopted in the recent monographs of Prigogine, of de Groot, and of Denbigh.

A thermodynamic system has microscopic detail in structure, and its processes have microscopic detail in time. Kinetic theory attempts both kinds of detail, whereas the phenomenological theory ignores the molecular structure of matter and the molecular processes which underlie microscopic change.

Cox's treatment is intermediate; it employs the statistical methods of Willard Gibbs, which ignores the molecular details of structure but recognizes the microscopic details of change.

This is a clearly written book. The author makes a good case for his viewpoint. All students of energetics interested in new developments should study it.

VICTOR K. LA MER, Columbia University, New York

Lehrbuch der organischen Chemie. By P. KARRER. Georg Thieme, Stuttgart, 1954, 12th ed. 949 pp. Price $14.20.

Since 1927, twelve German and four English editions of this text have appeared, attesting to its popularity. The present German edition offers some points of departure from previous ones. For example, a few attempts have been made to introduce some needed theoretical background (*cf.* page 48 on the subject of double bonds). Some of the general references have been brought up to date, although few beyond 1951 were noted. In the excellent treatment of alcoholic fermentation, the latest reference to enzymes is to 1951. The treatment of alcoholic fermentation, incidentally, serves well to illustrate the mixed objective of Professor Karrer in this work. On the one hand, the book is a "text," inasmuch as each subject is approached from its most elementary level. On the other hand, the author is not unduly bound by pedagogical developments, as is apparent from the discussion of the details of fermentation at an early point (page 90) in the book.

A number of topics which in this reviewer's opinion were accorded a somewhat cursory and perhaps obsolete treatment in the fourth English edition do not appear to have been re-examined. For example: (*1*) the section on aliphatic hydrocarbons, (*2*) reduction of aromatic nuclei, (*3*) dynamic stereochemistry and conformational analysis. Some new material appears on certain subjects (*cf.* ketenes, page 183; tropolones, page 718; morphine, page 865).

The extent of the coverage is, of course, one of the outstanding features of this text. This reviewer was surprised to find no mention of the application of pyridinium salts in synthesis, for example, of α-keto acids and aldehydes. The index is very well prepared and the book is beautifully printed and bound. It is of interest to note that the numerous tables at the end ("estimate of world sugar," "classification of odors," etc.) have been deleted, although Professor Karrer's personal selection of the outstanding dates of organic chemistry remains a characteristic feature of this Treatise.

As a well-organized description of the facts of organic chemistry which have been uncovered in a definite span in the development of the science, this book has few peers.

FAUSTO RAMIREZ, Columbia University, New York

AUTHOR INDEX

A

Andrews, A. C. See Lyons, T. D., 370

B

Baer, Eric. See Topper, Leonard, 226
Ballou, E. Vernon. Electroosmotic flow in homoionic kaolinite, 450
Basu, Sadhan, and Sircar, Anil K. Studies on polyelectrolytes. VII. gum tragacanth, 263
Belner, R. J. See Maron, S. H., 523
Bhattacharya, Abani K. See Bhattacharya, Amal K., 551
Bhattacharya, Amal K., Kumar, Ram, and Bhattacharya, Abani K. A new equation between the time of coagulation and electrolyte concentration-studies on copper ferrocyanide sol., 551
Bierman, Arthur. Electrostatic forces between nonidentical colloidal particles, 231
Bisschop, M. C. See Tollenaar, D., 151
Blocker, H. G. See Orr, Clyde, Jr., 24
Bolt, G. H. Analysis of the validity of the Gouy-Chapman theory of the electric double layer, 206
Bradley, R. S. The rate of evaporation of micro drops in the presence of insoluble monolayers, 571
Brass, P. D. See Roe, Charles P., 194

C

Catsiff, E., and Tobolsky, A. V. Stress-relaxation of polyisobutylene in the transition region (1, 2), 375
Chandler, Ray C., and Shelberg, Wesley E. The role of colloidal electrolytes in decontamination studies, 393
Chepeswick, Carol. See Goring, D. A. I., 440
Cox, A. Lucile. See Kerker, Milton, 413

D

DeWitt, T. W. See Markovitz, H., 165
DeWitt, T. W., Markovitz, H., Padden, F. J., Jr., and Zapaz, L. J. Concentration dependence of the rheological behavior of the polyisobutylene-decalin system, 174
Drozin, Vadim G. The electrical dispersion of liquids as aerosols, 158
Dulin, Cyril I. See Mysels, Karol J., 461

E

Elyash, L. J. See Markovitz, H., 165
Erikson, J. A., and Lingafelter, E. C. Primary salt effects with some paraffin-chain salt solutions, 71

F

Ferington, T. E., and Tobolsky, A. V. Kinetic constants for methyl methacrylate polymerization, 536
Ferry, John D. See Williams, Malcolm L., 1
Ferry, John D. See Williams, Malcolm L., 474
Fok, Shiu Ming. See Maron, Samuel H., 482
Fuller, George W. The osmotic properties of tetradecylsulfonic acid, 403

G

Gallily, Isaiah. A note on the filtration of aerosols by a simplified model, 558
Gillespie, T. On the adhesion of drops and particles on impact at solid surfaces. I, 266
  Rideal, Sir Eric. On the adhesion of drops and particles on impact at solid surfaces. II, 281
  The role of electric forces in the filtration of aerosols by fiber filters, 299
Goring, D. A. I., and Chepeswick,

CAROL. Sedimentation of naturally occurring polyelectrolytes, 440
GUCKER, FRANK T., JR., AND PETERSON, AXEL H. A comparison photometer to measure light scattering of aerosols and gases, using the latter as light-scattering standards, 12
GUNN, ROSS. The statistical electrification of aerosols and small cloud droplets by the diffusion of ions, 107
GUNTHER, R. L. See O'konski, C. T., 563

H

HARMSEN, G. J., VAN SCHOOTEN, J., AND OVERBEEK, J. TH. G. Errata to 'viscosity and electroviscous effect of the agI sol II. influence of the concentration of AgI and of electrolyte on the viscosity, 120
HARRAP, B. S. The molecular weight of insulin, determined by the surface balance technique, 351
HARTUNG, HOMER A., AND RICE, O. K. Some studies of spontaneous emulsification, 436
HERMONAT, W. A. See Mooney, M., 121
HUBBARD, WILLARD D. See Kushner, Lawrence M., 428

K

KAUFMAN, SAMUEL, AND SINGLETERRY, CURTIS R. Micelle formation by sulfonates in a non-polar solvent, 139
KERKER, MILTON, COX, A. LUCILE, AND SHOENBERG, MELVIN D. Maximum particle sizes in polydispersed aerosols, 413
KIPLING, J. J. Molecular areas of adsorbates, 156
KRANJC, KATARINA. The influence of packing density on the small-angle X-Ray scattering of a polydisperse colloid system, 540
KUMAR, RAM. See Bhattacharya, Amal K., 551
KUSHNER, LAWRENCE M., AND HUBBARD, WILLARD D. Light scattering and micelle structure in the system sodium dodecyl sulfate-sodium chloride-water, 428

L

LEVY-PASCAL, ARIE E. See Maron, Samuel H., 494
LINGAFELTER, E. C. See Erikson, J. A., 71
LODGE, JAMES P., AND TUFTS, BARBARA J. An electron microscope study of sodium chloride particles as used in aerosol generation, 256
LOWER, G. W. See Zettlemoyer, A. C., 29
LYONS, T. D., AND ANDREWS, A. C. Phenylsulfonic acid as a mediating agent in histamine-human gamma globulin interactions, 370

M

MATALON, R., AND PACKTER, A. The Liesegang phenomenon. I. Sol protection and diffusion, 46
MANDEL, JOHN. See Rothman, S., 338
MANLEY, DON R., AND STERN, KURT H. Liesegang rings in inhomogenous media, powdered glass, 409
MARKOVITZ, H., ELYASH, L. J., PADDEN, F. J., JR., AND DEWITT, T. W. A cone-and-plate viscometer, 165
  See DeWitt, T. W., 174
MARON, S. H., AND BELNER, R. J. Rheology of synthetic latex. VII. Flow behavior of synthetic rubber latex at low shear stress, 523
MARON, SAMUEL H., AND FOK, SHIU MING. Rheology of synthetic latex. V. flow behavior of low-temperature GR-S latex, 482
  LEVY-PASCAL, ARIE E. Rheology of synthetic latex VI. the flow behavior of neoprene latex, 494
MCBAIN, M. E. L. Properties of sodium abietate from American colophony from experiments of J. W. McBain's students, 219
  Note on the conductivity of dilute solutions of myristyl acid, 223
MCCANN, FLORENCE R., See Rothman, S., 338
MOONEY M., AND HERMONAT, W. A. Effect of swelling or of an adsorbed layer on the viscosity of a suspension of spherical particles, 121

MYSELS, KAROL J. Charge effects in light scattering by association colloidal electrolytes, 507

MYSELS, KAROL J., AND DULIN, CYRIL I. Tracer electrophoresis. III. the mobility of the Na^+ constituent in sodium lauryl sulfate solutions, 461

N

NIELSON, ARNE E. The kinetics of electrolyte precipitation, 576

O

O'KONSKI, C. T., AND GUNTHER, R. L. Verification of the free energy equation for electrically polarized droplets, 563

ORR, CLYDE, JR., AND BLOCKER, H. G. The viscosity of suspensions of spheres, 24

OVERBEEK, J. TH. G. See Harmsen, G. J., 120

OVERBEEK, J. TH. G. See Verwey, E. J. W., 225

P

PACKTER, A. See Matalon, R., 46

PADDEN, F. J., JR., See Markovitz, H., 165

See DeWitt, T. W., 174

PETERLIN, ANTON. Determination of the diameter of the coiled macromolecule from viscosity, sedimentation and diffusion, 587

PETERSON, AXEL H. See Gucker, Frank T., Jr., 12

R

RICE, O. K. See Hartung, Homer A., 436

RIDEAL, SIR ERIC. See Gillespie, T., 299

ROE, CHARLES P., AND BRASS, P. D. The effect of aliphatic detergents on the mechanical stability of polystyrene latex, 194

ROSANO, HENRI L. Measurement of the molecular weight of a polyester and evaluation of its molecular volume, 362

ROSS, SYDNEY, AND WINKLER, WERNER. On physical adsorption. VIII. monolayer adsorption of argon and nitrogen on graphitized carbon, 319

WINKLER, WERNER. On physical adsorption. IX. sub-critical and supracritical adsorption isotherms for krypton monolayers on graphitized carbon black, 330

ROTHMAN, S., MANDEL, JOHN, MCCANN, FLORENCE R., AND WEISSBERG, S. G. Sorption of macromolecules to solid surfaces: sorption of dextran to cellulose nitrate membranes in the presence of serum albumin and surface-active agents, 338

S

SHELBERG, WESLEY E. See Chandler, Ray C., 393

SHER, IRVING H., AND SOBOTKA, HARRY. Interaction of serum albumin with built-up monomolecular layers of fatty acids, 125

SHERMAN, P. Studies in water-in-oil emulsions. IV. the influence of the emulsifying agent on the viscosity of water-in-oil emulsions of high water content, 63

SHOENBERG, MELVIN D. See Kerker, Milton, 413

SINGLETERRY, CURTIS R. See Kaufman, Samuel, 139

SIRCAR, ANIL K. See Basu, Sadhan, 263

SOBOTKA, HARRY. See Sher, Irving H., 125

STERN, KURT H. See Manley, Don R., 409

T

THOMAS, JESS W. The diffusion battery method for aerosol particle size determination, 246

TOBOLSKY, A. V. See Catsiff, E., 375

TOBOLSKY, A. V. See Ferington, T. E., 536

TOLLENAAR, D., AND BISSCHOP, M. C. The bar viscometer, 151

TOPPER, LEONARD, AND BAER, ERIC. Dropwise condensation of vapors and heat transfer rates, 226

TUFTS, BARBARA J. See Lodge, James P., 256

V

van Schooten, J. See Harmsen, G. J., 120

Verwey, E. J. W., and Overbeek, J. Th. G. Theory of the stability of lyophobic colloids, 225

W

Weissberg, S. G. See Rothman, S., 338

Williams, Malcolm L., and Ferry, John D. Dynamic mechanical properties of plasticized polyvinyl acetate, 1

Williams, Malcolm L., and Ferry, John D. Dynamic mechanical properties of polymethyl acrylate, 474

Winkler, Werner. See Ross, Sydney, 319, 330

Winsor, P. A. The structure of "viscoelastic solutions" of colloidal electrolytes, 88
  Electrical-optical effects in liquid crystalline solutions containing amphiphilic salts, 101

Y

Yamaguchi, Shigeto. On the 'active centres' found on metal surfaces, 189

Z

Zapas, L. J. See DeWitt, T. W., 174

Zettlemoyer, A. C., and Lower, G. W. The rheology of printing inks III. Studies of simple dispersions, 29

SUBJECT INDEX

A

Abietate, from colophony, McBain, 219

Adhesion, to solid surfaces, filtration of aerosols, Gillespie, 266, 299; Gillespie and Rideal, 281

Adsorbates, molecular areas, Kipling, 156

Adsorption (see also *Sorption*), of argon, nitrogen, and krypton on carbon, Ross and Winkler, 319, 330

Aerosols (see also *Filtration*, *Photometer*, *Sodium*), polydispersed, Kerker *et al.*, 413

Albumin, and fatty acids, Sher and Sobotka, 125

Atmosphere, ionic diffusion, Gunn, 107

C

Coiled macromolecules, Peterlin, 587

Colloids, stability of lyophobic, Verwey and Overbeek, 224; electrostatic forces between nonidentical particles, Bierman, 231; colloidal electrolytes and decontamination, Chandler and Shelberg, 393; x-ray scattering of a polydisperse system, Kranjc, 540

Copper ferrocyanide sol, coagulation, Bhattacharya *et al.*, 551

D

Diffusion battery, for particle size determination, Thomas, 246

Dispersion, electrical, of liquids, Drozin, 158

Droplets, electrically polarized, O'Konski and Gunther, 563

Drops, evaporation of small, Bradley, 571

E

Electric double layer, and the Gouy-Chapman theory, Bolt, 206

Electrical-optical effect, in liquid crystalline solution, Winsor, 101

Electrolytes (see also *Precipitation*), association colloidal, Mysels, 507

Electrophoresis, ionization of micelles, Mysels and Dulin, 461

Electroviscous, see *Viscosity*

Emulsification, spontaneous, Hartung and Rice, 436

Emulsions, water-in-oil emulsions, Sherman, 63

F

Filtration, of aerosols, Gallily, 558

G

Gum tragacanth, viscosity, Basu and Sircar, 263

H

Histamine, binding to proteins, Lyons and Andrews, 370

I

Ink, rheology, Zettlemoyer and Lower, 29

Insulin, molecular weight, Harrap, 351

International symposium on polymers, announcement, 318

K

Kaolinite, electroosmotic flow in clay, Ballou, 450

L

Latex, aliphatic detergents and polystyrene latex, Roe and Brass, 194; rubber microscopy, Schoon and Phoa, 226; rheology of GR-S latex, Maron and Fok, 482; of Neoprene latex, Maron and Levy-Pascal, 494; rheology of synthetic, Maron and Belner, 523

Liesegang, phenomenon, Matalon and Packter, 46

Liesegang rings, in powdered glass, Manley and Stern, 409

M

Metal surfaces, active centers, Yamaguchi, 189

Methyl methacrylate, polymerization, Ferington and Tobolsky, 536

Micelle weight, and light scattering, Kushner and Hubbard, 428

Myristyl sulfonic acid, conductivity, McBain, 223

P

Paraffin-chain, solutions of salts, Erikson and Lingafelter, 71

Photometer, for aerosols and gases, Gucker and Peterson, 12

Polyelectrolytes, sedimentation, Goring and Chepeswick, 440

Polyester, molecular weight, Rosano, 362

Polyisobutylene, stress-relaxation, Catsiff and Tobolsky, 375

Polyisobutylene-decalin, system, rheology, DeWitt *et al.*, 174

Polymethyl acrylate, dynamic mechanical properties, Williams and Ferry, 474

Polyvinyl acetate, plasticized, Williams and Ferry, 1

Precipitation, kinetics of electrolyte, Nielsen, 576

R

Rubber, see *Latex*

S

Sodium chloride, in aerosol generation, Lodge and Tufts, 256

Sorption (see also *Adsorption*), of macromolecules to solid surfaces, Rothman *et al.*, 338

Sulfonates, micellar properties, Kaufman and Singleterry, 139

T

Tetradecylsulfonic acid, osmotic properties, Fuller, 403

V

Vapor, condensation, Topper and Baer, 225

Viscometer, bar viscometer, Tollenaar and Bisschop, 151; cone-and-plate viscometer, Markovitz *et al.*, 165

Viscosity, of suspensions of spheres, Orr and Blocker, 24; viscoelastic solutions, Winsor, 88; and electroviscous effect of AgI sol, Harmsen *et al.*, 120; of spherical particles, Mooney and Hermonat, 121; electroviscous effect, Harmsen *et al.*, 315

INDEX OF BOOK REVIEWS

Bennett, C. A., and Franklin, N. L., Statistical Analysis in Chemistry and the Chemical Industry (Mandel, J.), 123

Boell, E. J. (ed.), Dynamics of Growth Processes (Steinhardt, J.), 406

Clark *et al.* (ed.)., Adhesion and Adhesives. Fundamentals and Practice (Bikerman, J. J.), 229

Cox, R. T., Statistical Mechanics of Irreversible Change (La Mer, V. K.), 603

Daniels, F., and Alberty, R. A., Physical Chemistry (Bak, T. A.), 504

Doolittle, A. K., The Technology of Solvents and Plasticizers (Church, J. M.), 504

Jellinek, H. H. G., Degradation of Vinyl Polymers (Mesrobian, R. B.), 317

Karrer, P., Lehrbuch der organischen Chemie (Ramirez, F.), 603

Müller, E. (ed.), Methoden der Organischen Chemie (Houben-Weyl) (Ramiro, F.), 602

Neurath, H., and Bailey, K. (ed.), The Proteins. Chemistry, Biological Activity, and Methods (Steinhardt, J.), 407

Prigogine, I., Introduction to Thermodynamics of Irreversible Processes (Bak, T. A.), 602

Simons, J. H. (ed.), Fluorine Chemistry, Vol. II (Roberts, C. W.), 406

Sobotka, H. (ed.), Monomolecular Layers (Rosano, H. L.), 123

Whitby, G. S., *et al.* (ed.), Synthetic Rubber (Walling, C.), 229

JOURNAL OF
COLLOID SCIENCE

Editor-in-Chief
Victor K. La Mer, Columbia University, New York

Advisory Board

C. O. Beckmann
K. F. Bonhoeffer
J. A. Christiansen
M. L. Corrin
P. J. W. Debye
John T. Edsall
I. Fankuchen
John D. Ferry
Wilfried Heller
John G. Kirkwood
E. C. Lingafelter
L. G. Longsworth
S. G. Mason
J. Th. G. Overbeek
R. Ruyssen
E. K. Rideal
William Seifriz
Leo Shedlovsky
Theodore Shedlovsky
Robert Simha
R. H. Smellie
Jacinto Steinhardt
The Svedberg
Hugh S. Taylor
Arne Tiselius
Robert D. Vold
Bernard Vonnegut
Ralph W. G. Wyckoff
Bruno H. Zimm

VOLUME 10
1955

ACADEMIC PRESS INC.—PUBLISHERS
NEW YORK, N. Y.

Copyright 1955, by Academic Press Inc.
Made in United States of America

CONTENTS OF VOLUME 10

Number 1, February, 1955

Malcolm L. Williams and John D. Ferry. Dynamic Mechanical Properties of Plasticized Polyvinyl Acetate.................... 1

Frank T. Gucker, Jr., and Axel H. Peterson. A Comparison Photometer to Measure Light Scattering of Aerosols and Gases, Using the Latter as Light-Scattering Standards................ 12

Clyde Orr, Jr., and H. G. Blocker. The Viscosity of Suspensions of Spheres.. 24

A. C. Zettlemoyer and G. W. Lower. The Rheology of Printing Inks. III. Studies of Simple Dispersions.......................... 29

R. Matalon and A. Packter. The Liesegang Phenomenon. I. Sol Protection and Diffusion.................................... 46

P. Sherman. Studies in Water-in-Oil Emulsions. IV. The Influence of the Emulsifying Agent on the Viscosity of Water-in-Oil Emulsions of High Water Content............................ 63

J. A. Erikson and E. C. Lingafelter. Primary Salt Effects with Some Paraffin-Chain Salt Solutions............................ 71

P. A. Winsor. The Structure of "Viscoelastic Solutions" of Colloidal Electrolytes.. 88

P. A. Winsor. Electrical-Optical Effects in Liquid Crystalline Solutions Containing Amphiphilic Salts.......................... 101

Ross Gunn. The Statistical Electrification of Aerosols and Small Cloud Droplets by the Diffusion of Ions...................... 107

LETTERS TO THE EDITORS:

G. J. Harmsen, J. van Schooten, and J. Th. G. Overbeek. Errata to "Viscosity and Electroviscous Effect of the AgI Sol. II. Influence of the Concentration of AgI and of Electrolyte on the Viscosity".. 120

M. Mooney and W. A. Hermonat. Effect of Swelling or of an Adsorbed Layer on the Viscosity of a Suspension of Spherical Particles.. 121

BOOK REVIEWS:

John Mandel. Statistical Analysis in Chemistry and the Chemical Industry.. 123

Henri L. Rosano. Monomolecular Layers.......................... 123

NUMBER 2, APRIL, 1955

IRVING H. SHER AND HARRY SOBOTKA. Interaction of Serum Albumin with Built-up Monomolecular Layers of Fatty Acids ... 125
SAMUEL KAUFMAN AND CURTIS R. SINGLETERRY. Micelle Formation by Sulfonates in a Nonpolar Solvent ... 139
D. TOLLENAAR AND M. C. BISSCHOP. The Bar Viscometer ... 151
J. J. KIPLING. Molecular Areas of Adsorbates ... 156
VADIM G. DROZIN. The Electrical Dispersion of Liquids as Aerosols ... 158
H. MARKOVITZ, L. J. ELYASH, F. J. PADDEN, JR., AND T. W. DEWITT. A Cone-and-Plate Viscometer ... 165
T. W. DEWITT, H. MARKOVITZ, F. J. PADDEN, JR., AND L. J. ZAPAS. Concentration Dependence of the Rheological Behavior of the Polyisobutylene-Decalin System ... 174
SHIGETO YAMAGUCHI. On the 'Active Centres' Found on Metal Surfaces ... 189
CHARLES P. ROE AND P. D. BRASS. The Effect of Aliphatic Detergents on the Mechanical Stability of Polystyrene Latex ... 194
G. H. BOLT. Analysis of the Validity of the Gouy-Chapman Theory of the Electric Double Layer ... 206
M. E. L. McBAIN. Properties of Sodium Abietate from American Colophony. From Experiments of J. W. McBain's Students (1923–1926) ... 219

LETTERS TO THE EDITOR

M. E. L. McBAIN. Note on the Conductivity of Dilute Solutions of Myristyl Acid ... 223
E. J. W. VERWEY AND J. TH. G. OVERBEEK. Theory of the Stability of Lyophobic Colloids ... 225
LEONARD TOPPER AND ERIC BAER. Dropwise Condensation of Vapors and Heat Transfer Rates ... 226
TH. G. F. SCHOON AND K. L. PHOA. Phase Contrast of Natural Rubber Latices (Morphology of the Rubber Particles in Natural Latices) ... 227

BOOK REVIEWS

J. J. BIKERMAN. Adhesion and Adhesives. Fundamentals and Practice ... 229
CHEVES WALLING. Synthetic Rubber ... 229

NUMBER 3, JUNE, 1955

ARTHUR BIERMAN. Electrostatic Forces Between Nonidentical Colloidal Particles ... 231
JESS W. THOMAS. The Diffusion Battery Method for Aerosol Particle Size Determination ... 246
JAMES P. LODGE AND BARBARA J. TUFTS. An Electron Microscope Study of Sodium Chloride Particles as Used in Aerosol Generation ... 256

Sadhan Basu and Anil K. Sircar. Studies on Polyelectrolytes. VII. Gum Tragacanth 263
T. Gillespie. On the Adhesion of Drops and Particles on Impact at Solid Surfaces. I. 266
T. Gillespie and Sir Eric Rideal. On the Adhesion of Drops and Particles on Impact at Solid Surfaces. II. 281
T. Gillespie. The Role of Electric Forces in the Filtration of Aerosols by Fiber Filters 299

LETTER TO THE EDITOR:

G. J. Harmsen, J. van Schooten, and M. van der Waarden. Electroviscous Effect 315

BOOK REVIEW:

R. B. Mesrobian. Degradation of Vinyl Polymers 317
Announcement 318

Number 4, August, 1955

Sydney Ross and Werner Winkler. On Physical Adsorption. VIII. Monolayer Adsorption of Argon and Nitrogen on Graphitized Carbon 319
Sydney Ross and Werner Winkler. On Physical Adsorption. IX. Sub-critical and Supracritical Adsorption Isotherms for Krypton Monolayers on Graphitized Carbon Black 330
S. Rothman, John Mandel, Florence R. McCann, and S. G. Weissberg. Sorption of Macromolecules to Solid Surfaces: Sorption of Dextran to Cellulose Nitrate Membranes in the Presence of Serum Albumin and Surface-Active Agents 338
B. S. Harrap. The Molecular Weight of Insulin, Determined by the Surface Balance Technique 351
Henri L. Rosano. Measurement of the Molecular Weight of a Polyester and Evaluation of Its Molecular Volume 362
T. D. Lyons and A. C. Andrews. Phenylsulfonic Acid as a Mediating Agent in Histamine-Human Gamma Globulin Interactions 370
E. Catsiff and A. V. Tobolsky. Stress-Relaxation of Polyisobutylene in the Transition Region (1, 2) 375
Ray C. Chandler and Wesley E. Shelberg. The Role of Colloidal Electrolytes in Decontamination Studies 393
George W. Fuller (communicated by M. E. L. McBain). The Osmotic Properties of Tetradecylsulfonic Acid 403

BOOK REVIEWS

Jacinto Steinhardt. Dynamics of Growth Processes 406
C. W. Roberts. Fluorine Chemistry, Volume II 406
Jacinto Steinhardt. The Proteins, Volume II. Part B 407

NUMBER 5, OCTOBER, 1955

DON R. MANLEY AND KURT H. STERN. Liesegang Rings in Inhomogenous Media. Powdered Glass 409
MILTON KERKER, A. LUCILE COX, AND MELVIN D. SHOENBERG. Maximum Particle Sizes in Polydispersed Aerosols 413
LAWRENCE M. KUSHNER AND WILLARD D. HUBBARD. Light Scattering and Micelle Structure in the System Sodium Dodecyl Sulfate-Sodium Chloride-Water 428
HOMER A. HARTUNG AND O. K. RICE. Some Studies of Spontaneous Emulsification 436
D. A. I. GORING AND CAROL CHEPESWICK. Sedimentation of Naturally Occurring Polyelectrolytes 440
E. VERNON BALLOU. Electroosmotic Flow in Homoionic Kaolinite 450
KAROL J. MYSELS AND CYRIL I. DULIN. Tracer Electrophoresis. III. The Mobility of the Na^+ Constituent in Sodium Lauryl Sulfate Solutions 461
MALCOLM L. WILLIAMS AND JOHN D. FERRY. Dynamic Mechanical Properties of Polymethyl Acrylate 474
SAMUEL H. MARON AND SHIU MING FOK. Rheology of Synthetic Latex. V. Flow Behavior of Low-Temperature GR-S Latex 482
SAMUEL H. MARON AND ARIE E. LEVY-PASCAL. Rheology of Synthetic Latex. VI. The Flow Behavior of Neoprene Latex 494

BOOK REVIEWS

THOR A. BAK. Physical Chemistry 504
JAMES M. CHURCH. The Technology of Solvents and Plasticizers 504
ANNOUNCEMENT 506

NUMBER 6, DECEMBER, 1955

KAROL J. MYSELS. Charge Effects in Light Scattering by Association Colloidal Electrolytes 507
S. H. MARON AND R. J. BELNER. Rheology of Synthetic Latex. VII. Flow Behavior of Synthetic Rubber Latex at Low Shear Stress 523
T. E. FERINGTON AND A. V. TOBOLSKY. Kinetic Constants for Methyl Methacrylate Polymerization 536
KATARINA KRANJC. The Influence of Packing Density on the Small-Angle X-Ray Scattering of a Polydisperse Colloid System 540
AMAL K. BHATTACHARYA, RAM KUMAR, AND ABANI K. BHATTACHARYA. A New Equation Between the Time of Coagulation and Electrolyte Concentration-Studies on Copper Ferrocyanide Sol 551
ISAIAH GALLILY. A Note on the Filtration of Aerosols by a Simplified Model 558
C. T. O'KONSKI AND R. L. GUNTHER. Verification of the Free Energy Equation for Electrically Polarized Droplets 563

R. S. BRADLEY. The Rate of Evaporation of Micro Drops in the Presence of Insoluble Monolayers.......................... 571
ARNE E. NIELSON. The Kinetics of Electrolyte Precipitation.......... 576
ANTON PETERLIN. Determination of the Diameter of the Coiled Macromolecule from Viscosity, Sedimentation and Diffusion..... 587

BOOK REVIEWS

THOR A. BAK. Introduction to Thermodynamics of Irreversible Processes.. 602
FAUSTO RAMIREZ. Methoden der organischen Chemie.............. 602
VICTOR K. LA MER. Statistical Mechanics of Irreversible Change. 603
FAUSTO RAMIREZ. Lehrbuch der organischen Chemie............... 603
AUTHOR INDEX.. 605
SUBJECT INDEX.. 609
INDEX OF BOOK REVIEWS..................................... 610